AFML-TR-68-391

FEASIBILITY OF JOINING ADVANCED COMPOSITE FLIGHT VEHICLE STRUCTURES

D. Kutscha
K. E. Hofer, Jr.

FOREWORD

This technical report summarizes the study performed by the Mechanics of Materials Research Division of IIT Research Institute under USAF Contract No. AF33(615)-3962 during the period from 1 May 1966 through 1 July 1967. This contract was initiated under Project No. 7381 "Materials Application, Task 738106 "Engineering and Design Data." The initial phases of the study were conducted under the technical direction of Capt. W. Schulz and the study was completed under the direction of Mr. T. J. Reinhart of the Materials Support Division of the Air Force Materials Laboratory. The manuscript was released by the authors March 1969 for publication.

The following personnel made major contributions to the program.

Program Management - D. Kutscha
Mechanical Joints - K. E. Hofer, Jr.
Bonded Joints Analysis and Design - D. Kutscha, R. M. Chaney and M. Salmon
Bonded Joints Fabrication and Testing - C. Mayhew, R. Szuch and J. Sullivan

The fatigue testing of joints was carried out at the USDA Forest Products Laboratory by Mr. K. Boller.

This technical report has been reviewed and is approved.

Albert Olevitch

Albert Olevitch, Chief
Materials Engineering Branch
Materials Support Division
Air Force Materials Laboratory

ABSTRACT

A combined analytical-experimental study was carried out to establish the feasibility of developing rational design techniques for bonded and mechanical joints in advanced composite structures. Available stress analyses were compared for their predictions of maximum stresses in joints and these results were compared to experimental data.

The static strengths were measured for three adhesives bonded to fiberglass, steel, and titanium, and the fatigue strengths were measured for the optimum joint designs. A direct relationship was shown between joint behavior and adhesive modulus.

The load distribution and joint strength was studied for fiberglass bolted joints. These results were also compared to analytical predictions. An extensive literature survey was made for design procedures in mechanical joints.

Recommendations were made for specific additional work required both in joints analysis and characterization of materials.

TABLE OF CONTENTS

PART I - INTRODUCTION AND ADHESIVE BONDED JOINTS

TABLE OF CONTENTS (CONTD)

TABLE OF CONTENTS (Contd)

PART II - MECHANICALLY FASTENED COMPOSITE JOINTS

TABLE OF CONTENTS (Contd)

ILLUSTRATIONS

ILLUSTRATIONS (Contd)

ILLUSTRATIONS (Contd)

ILLUSTRATIONS (Contd)

ILLUSTRATIONS (Contd)

ILLUSTRATIONS (Contd)

ILLUSTRATIONS (Contd)

ILLUSTRATIONS (Contd)

ILLUSTRATIONS (Contd)

ILLUSTRATIONS (Contd)

ILLUSTRATIONS (Contd)

ILLUSTRATIONS (Contd)

ILLUSTRATIONS (Contd)

ILLUSTRATIONS (Contd)

TABLES

TABLES (Contd)

TABLES (Contd)

TABLES (Contd)

TABLES (Contd)

TABLES (Contd)

TABLES (Contd)

TABLES (Contd)

PART I - INTRODUCTION AND ADHESIVE BONDED JOINTS

1.0 INTRODUCTION

1.1 OBJECTIVE

The purpose of this study was to establish the feasibility of developing a design method, based on rational engineering concepts, for bonded and mechanically fastened joints to be used in advanced flight vehicles fabricated from fiberglass composites and fiberglass composite-metal materials combinations. The thesis of the study was that if a stress analysis for a joint is available, this can be combined with materials properties and failure criteria to predict the strength and deflection characteristics of a joint. The study utilized already available stress analyses and to some extent available materials properties. Predictions of joint behavior made from the analyses were then compared with experimental test results.

The general approach of the study was to first investigate in detail the analyses now available for relatively simple joint geometries. For the bonded configurations, these included the single lap joint, double lap joint and scarf type lap joints. For the mechanically fastened joints, these include single and double fasteners, both in line with the load and side by side. Once these simpler joints are understood analytically, the analyses can be extended to more complex configurations of geometry and materials, such as stepped lap joints and multiple riveted joints.

Since any stress analysis method requires the mechanical properties of the materials involved as input to the problem, it was necessary to identify these properties for the joints under study. Measurements of strength and modulus were made for the composite adherends and for free films of the adhesive materials used. With this information available, along with the behavior of the joints tested, the joint data would become more meaningful and would provide for more thorough interpretation of the results from the standpoint of joint mechanics.

A body of strength data for typical bonded and mechanical joints was obtained to satisfy three criteria.

a. Provide joints data for comparison with existing analysis predictions.
b. Provide joints data for use in empirical design schemes.
c. Provide joints data which can be compared with the predictions from new analysis schemes as their development continues.

This data was obtained for joints loaded both statically and in fatigue.

Finally, a literature survey was conducted for both bonded and mechanical joints to place the present study in proper relationship to the logical development of joints technology. From this literature review and the results of this study, suggestions are made for further research on problems which require solution before joint design can be placed on a completely rational basis.

1.2 PROGRAM PLAN

This study was divided into the following major task areas:

1.2.1 Literature Survey

A literature survey was carried out for pertinent documents covering primarily the period from 1961 to date. The major works in adhesive bonding prior to this date have already been reviewed by Kutscha (1.1)*. At present there is no similar review for mechanically fastened joints, therefore, a more extensive review was required.

1.2.2 Design of Adhesive Bonded Joints

The purpose of this task was to select candidate joint geometries for adhesive bonding and establish the required stress analyses and materials properties.

1.2.3 Design of Mechanically Fastened Joints

The purpose of this task was to select candidate joint geometries for mechanical fasteners and establish the required stress analyses and materials properties.

1.2.4 Fabrication and Testing of Selected Joints

Joints were fabricated and tested to provide experimental data for comparison with predictions made in sections 1.22 and 1.23, and to provide data for empirical design schemes.

---

* All references in each section are placed at the end of that section.

REFERENCES

1.1 Kutscha, D., "Mechanics of Adhesive-Bonded Lap-Type Joints: Survey and Review", ML-TDR-64-298, December 1964.

2.0 LITERATURE SURVEY OF ADHESIVE BONDED JOINTS

2.1 INTRODUCTION

The survey of the literature concerned with the mechanics of adhesive bonded joints has concentrated on the period, 1961 to date. Work prior to this period has been reviewed by Kutscha (Ref. 2.15). This earlier review was concerned primarily with joints involving isotropic, homogeneous adherends such as metals, which have received the bulk of attention applied in the area of mechanics of joints. It has only been recently that the renewed interest in structural composites has created the requirement for a better understanding of joints formed with anisotropic materials.

All the work in bonded isotropic materials provides an important base from which to approach composite joints. In a sense they represent a simpler model of the composite joint and for certain composite constructions actually represent a usable model. It is important then for one to have well in hand the basic fundamentals of bonded joints with isotropic adherends.

Once begun it is evident in reviewing the literature that the material applied to composite joints is very meager. One is forced to continue with the literature on isotropic materials and attempt to abstract whatever techniques one can and generalize these to composites. This is the same approach which has been applied to other areas of mechanics of composites such as test methods and generation of design-allowable stresses. This is perfectly acceptable as long as one is aware of the basic anisotropic structure of composites and how this will effect the possible modes of failure and the variation of other properties with the working direction in the composite.

A review was made of the following abstract services and in addition three separate report searches on design of joints were requested from the Scientific and Technical Information Center (DDC).

- Technical Abstract Bulletin
- AIAA Aerospace Abstracts
- STAR
- Applied Mechanics Reviews
- Engineering Index
- Solid Propellant Structural Integrity Abstracts

The literature obtained and reviewed from these sources has been divided into the following three areas.

1. Mechanical Properties of Adhesive

   Includes studies made to characterize the basic mechanical properties of adhesives, elastic, time dependent or failure in joints or in some free film or bulk form.

2. Analytical and Experimental Stress Analyses

   This includes any work concerned with studying or measuring the stress distribution in typical bonded joints.

3. Design Methods for Bonded Joints and Test Results

   This includes any empirical or rational methods of designing joints based on existing analysis methods and the results of tests relating joint strength to the major parameters of joint geometry and adherend-adhesive properties.

Each of these topics is discussed in a separate section which is immediately followed by an annotated bibliography arranged by author, alphabetically. All references used for this section are cited in a list of references at the end of the section.

2.2 MECHANICAL PROPERTIES OF ADHESIVES

2.2.1 Technical Review

The analysis of any bonded configuration can only be successfully carried out if the mechanical properties of all the joint components are known in detail. One of the greatest difficulties hindering the solution of this problem has been the lack of any body of data on mechanical properties of common structural adhesives and the variation of these properties with environment. The one classic reference cited continually is the work of Kuenzi and Stevens (2.14). In this study the shear properties of a series of adhesives were characterized using a thin wall torsion specimen. The first significant study to extend this work has recently been reported by Rutherford et al (2.6, 2.7, 2.19).

Rutherford and his co-workers have developed a set of capacitance transducers which are used in conjunction with a butt joint to measure tensile and compressive properties and a torsion tube to measure shear behavior of an adhesive film in a joint. The transducers have a sensitivity of 5×10^{-7} in. and 6.1×10^{8} radians respectively.

Several adhesives were bonded to type 303 stainless steel and aluminum and their mechanical behavior characterized. The properties obtained are summarized in Table 2.1. In addition to general properties, the effects of temperature, load cycle, film thickness and aging on these properties were evaluated. The instrumentation and test method yielded very reproducible results and successfully resolved the influence of these parameters.

The one criticism of the study is related to the reduction of the data from the tensile butt joints tests. It was assumed that the state of stress in the thin film of adhesive under tension was uniaxial and that the joint strength and stresses calculated for the modulus of elasticity was simply the load divided by the bonded area. In actuality the adhesive is under

Table 2.1

MECHANICAL PROPERTIES OF ADHESIVES DETERMINED BY RUTHERFORD, et al
BONDED TO TYPE 303 STAINLESS STEEL

Adhesive	Tensile Modulus (ksi)	Tensile Strength (ksi)	Shear Modulus (ksi)	Shear Strength (ksi)
Epon 828, Versamid 140	620*	4.5-8.6	388	
CIBA 6005	1100	>35		
AF-111		2.5	109-124	1900
Epon 9601	585-685		73.3-95	4.1-5.3

* Compressive Modulus = 620,000 psi
Free Tensile Modulus = 330,000 psi
Same results bonded to aluminum.

a nonuniform three dimensional state of strain which is a function of the adherend properties, adhesive properties and the adhesive film thickness. The stresses and joint strength resulting from this state of strain cannot be calculated assuming a uniform uniaxial distribution. It is inconclusive then whether the joint strength is a function of film thickness as concluded by this study and similarly the conclusions concerning the variation in adhesive properties through the thickness of the bond may be open to question.

The second significant advance in recent years is the work of Ju and Baker (2.13) and Iosipescu (2.12). The purpose of both of these studies was to develop a specimen for measuring the shear strength of materials. The problem here has always been to design a specimen other than a bar in torsion which will subject a material to a uniform state of pure shear. Iosipescu discusses this problem very well and then describes the development of the test specimen shown in Fig. 2.1.

The specimen is complicated to fabricate and could not be used to test a thin free film of material. It could be used, however, to study a film in a joint or to measure the shear strength of the adhesive polymer cast into a thicker plate.

One final reference is the study by Miller et al (2.16) in which the complex shear modulus was measured using a forced vibration technique. This work is of interest because as more sophisticated analysis methods become available, it will be necessary to characterize the viscoelastic properties of adhesive materials, especially when a thermal environment is included in the analysis. The majority of adhesives are viscoelastic but as yet attempts are still being made just to characterize their elastic behavior.

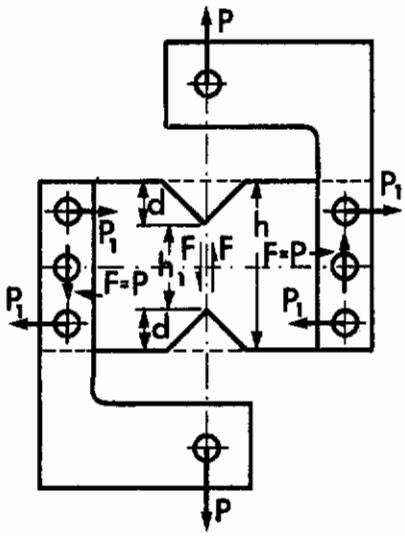

Fig. 2.1 SPECIMEN FOR ZERO-MOMENT-SECTION SHEAR TEST

2.2.2 Annotated Bibliography

Franzblau, M. C., and Rutherford, J. L., General Precision, Inc. (2.6)

"Study of Micromechanical Properties of Adhesive Bonded Joints" First Quarterly Progress Report, Contract No. DAAA 21-67-C-0500, Pictanny Arsenal, October 1967.

This is a continuation of the fine work by Rutherford et al (2.19) in which the measurement of joint tensile properties has been extended to shear properties, the effects of joint thickness and other adhesive types.

The shear specimen used to obtain the shear strength and modulus of rigidity was a thin walled tube containing a single joint in the center of its length. The angular rotation of one adherend relative to the other was sensed with capacitance type transducer and was capable of resolving 6.1 by 10^{-8} radians. This is sufficient to measure the modulus of an adhesive with a rigidity of 250,000 psi bonded in a single glue line of thickness 0.005 in.

The following adhesives and their properties were evaluated:

- Epon 828, Versamid 140-70 percent/30 percent
  Bulk Tensile Modulus = 330,000 psi
  Joint Tensile Modulus = 620,000 psi
  Joint Tensile Strength = 4,500-8,600 psi
  Joint Compressive Modulus = 620,000 psi
  Joint Shear Modulus = 388,000 psi

All the properties determined in the adhesive joint showed elastic behavior to failure while the free bulk behavior was strongly time dependent. All joints were bonded to type 303 stainless steel.

A separate test series utilizing an ultra pure form of Epon 828 showed that this adhesive formulation had an electrical capacitance which was frequency dependent.

- CIBA 6005
  Joint Tensile Modulus = 1,100,000 psi
  Joint Tensile Strength = 735,000 psi

The capacitance of this adhesive was strain sensitive.

- AF-111
  Joint Tensile Strength = 2,500 psi
  Joint Shear Modulus = 109,000 psi
  Joint Shear Strength = 1,900 psi

The capacitance of this material was also strain sensitive.

One series of tests were made with the Epon 828, Versamid 140 system which indicated that both the tensile modulus and strength were a function of adhesive film thickness. Generally, strengths were higher and moduli higher for lower film thicknesses. It is felt that these results have again failed to take into account the complex three dimensional state of stress in this type of butt joint specimen and it is erroneous to assume a uniform state of stress when calculating these results.

Franzblau, M. C. and Rutherford, General Precision Inc. (2.7)
"Study of Micromechanical Properties of Adhesive Bonded Joints," Second Quarterly Progress Report, Contract No. DAAA 21-67-C-0500, Picatinny Arsenal, January 1968.

The second progress report has extended the work on characterization of adhesives to additional materials and included the effect of temperature on its properties. The following properties were obtained:

- Epon 9601
  Joint Tensile Modulus = 685,000 psi
  with cycling reduced to 585,000 psi
  Joint Shear Modulus = 73,300 to 95,000 psi
  depending on film thickness

Joint Shear Strength = 4,100 to 5,300 psi
depending on film thickness

- Epon 828, Versamid 140
  Joint Tensile Modulus = 620,000 psi
  bonded to aluminum

Iosipescu, N. (2.12)

"New Accurate Procedure for Single Shear Testing of Metals," Journal of Materials, Vol. 2, No. 3, September 1967.

Iosipescu clearly and succinctly reviews all the problems associated with obtaining the shear strength of homogeneous materials. He describes all the major specimens used in the past for generating shear stresses in overlap configurations, torsion bars and thin plate specimens of the type developed by Ju and Baker (2.13). With this background in hand, he goes on to describe the development of a specimen in which a uniform state of pure shear stress was achieved.

The specimen is based on the configuration of a simple beam containing a section with zero moment. From the theory of beam flexure it is known that the zero moment section will be subject to a simple shear stress. Based on this simple criteria the beam geometry is further modified to obtain failure in a designated section by reducing the beam cross section at one point. A fixture suitable for loading the specimen in a conventional test machine was designed. Photoelastic studies were made of the specimen geometry and these did indeed show the presence of a uniform state of pure shear. Figure 2.1 shows a sketch of the test specimen and fixture.

Iosipescu goes on to describe the use of the method to determine the shear strength of several metallic alloys and sections of welded joints.

This technique as described has potential application for both the measurement of shear strength of joints and the shear strength of adhesives in significant bulk forms. The specimens

for joint strength would be difficult to fabricate but less so than tubular torsion specimens. Bulk adhesive data would still be open to question as to whether it corresponded to data for material in the joint. With proper instrumentation the specimen could also be used for shear modulus determination.

Ju, F. D. and Baker, J. G. (2.13)

"Preliminary Study of Pure Shear Fracture Model" AFOSR Scientific Report 65-1195, May 1965.

This report is a survey of the types of specimens which have been designed to obtain the shear strength of materials. Previous specimens have included torsion, short beam shear, and plate twist specimens. The purpose of the study was to design a specimen suitable for thin sheet materials. Since the problem of generating a uniform pure shear stress in thin film adhesive materials is still unresolved it is felt that the specimens designed here might be useful.

The specimen was designed to meet the following requirements:

1. A pure shear state should exist in the specimen up to failure.
2. No specimen rotation.
3. Shear should be limited to a narrow band along the line of shear fracture.
4. Fracture should be insensitive to specimen thickness.

The final specimen design is shown in Fig. 2.2. The shear strain in the gage length was measured with moiré grids and was found to be uniform up to failure throughout the section.

It should be possible to fabricate specimens of this type either in plastic plates or in relatively thin adhesive films. The specimen should also be applicable to FRP composites.

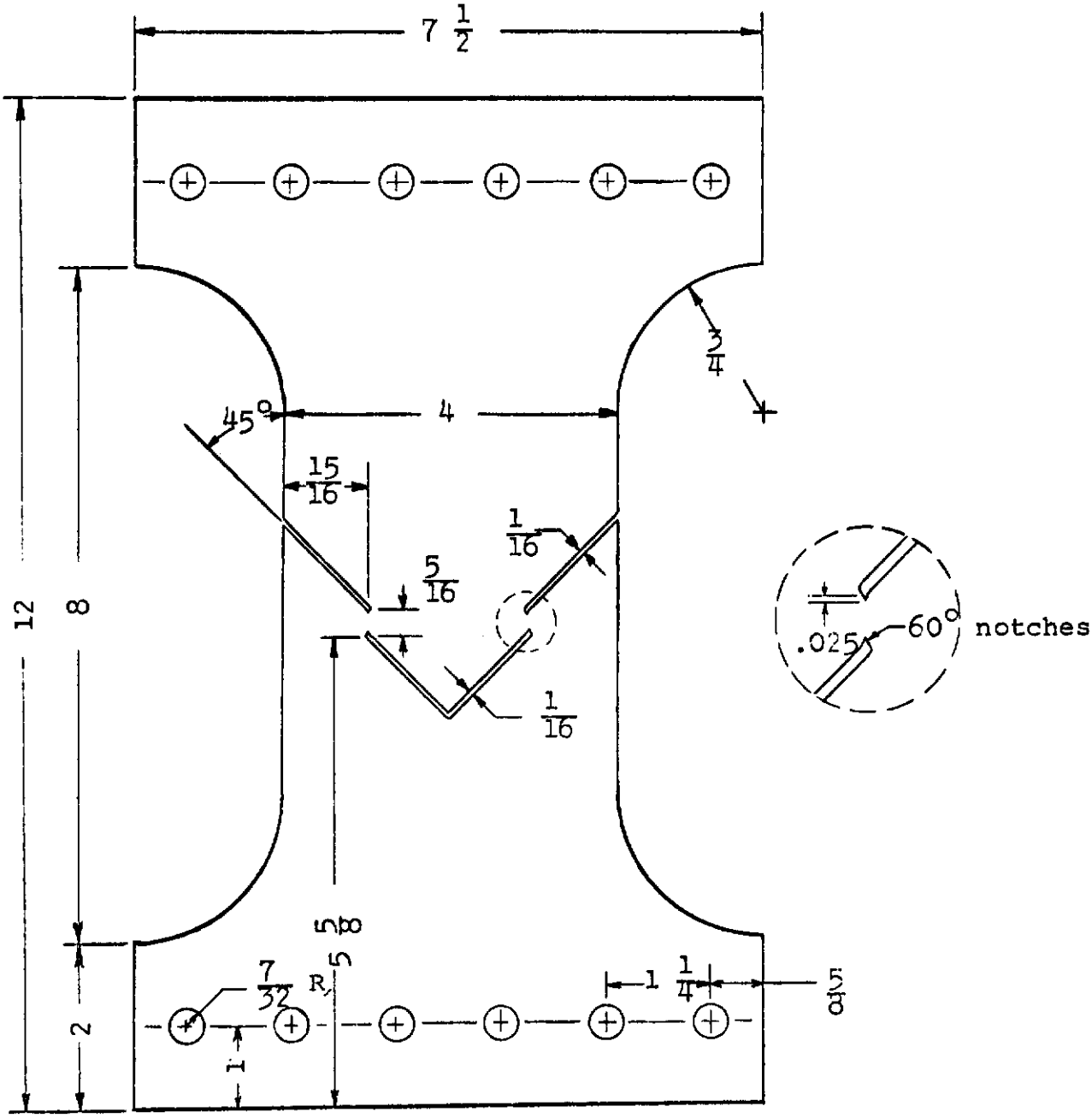

Fig. 2.2 THIN PLATE SHEAR SPECIMEN

Miller, H. E., Jergens, J. L. and Plunkett, R. (2.6)

"Measurement of Complex Shear Modulus of Thin Viscoelastic Layers," University of Minnesota, Institute of Technology, TR-65-4, October 1965.

A technique was developed to measure the complex shear modulus of an adhesive film while present in a joint. The specimen consists of a small steel block bonded in place between two large masses. The block is driven by a sinusoidal force and the driving force and acceleration of the mass are measured.

Two low modulus adhesives, 3M #465, #466, were studied over the frequency range from 400 to 5000 cycles. The complex modulus was found to be frequency dependent but only slightly dependent on film thickness. An objection to this technique is that it assumes the shear stress to be constant over the overlap length. This is probably acceptable for low modulus materials but may not be reasonable for more stiff adhesives.

Rutherford, J. L., Bossler, F. C. and Hughes, E. J. (2.19)

"Capacitance Methods for Measuring Properties of Adhesives in Bonded Joints," Rev. Scientific Inst., Vol. 39, No. 5, May 1968, pp. 666-671.

A simple butt joint specimen, circular in cross-section, was used to measure the tensile properties of an adhesive film while it was present in the joint. Two techniques were used to measure the total deformation of the film in the direction normal to the plane of the film. Knowing the adhesive film thickness the strain in the adhesive could be calculated. The specimen allowed the adhesive to be measured in both tension and compression.

In the first technique an external capacitance type extensometer was developed to measure the motion of one adherend relative to the other. It consisted of two annular copper rings

mounted externally and concentric with the butt joint. The plate spacing was 0.25 mm initially and the change in capacitance of this air gap was measured as load was applied to the specimen. The sensitivity of the extensometer is 0.5 microinches which for a 0.005 in. glue line would equal a strain of 1 by 10^{-8} in. per in.

The second technique involved the use of the metal adherends themselves as the capacitor plates and measuring their change in capacitance with load. This method assumes that the capacitance of the adhesive is a constant and does not vary with strain. This assumption was checked by comparing the results of the first method with this second technique. It was found that the capacitance of the adhesives used was strain sensitive.

Both methods were used to measure the modulus and strength of three adhesives bonded to type 303 stainless steel. The following results were reported:

Adhesives	Test Velocity (in./min)	Film Thickness (in.)	Tensile Secant Modulus (ksi)
Epon 828, Thiokol LP-3 28 pph, DETA 6.5 pph	0.02	0.005	752
Epon 828, Versamid 140, 43 pph	0.02	0.0045	620
Hysol 1-C, Epoxy patch	0.02	0.008	2900

A separate measurement of tensile modulus was made for the Epon 828-Versamid 140 material in a free film form and this material had a modulus of 334,000 psi which is only one half the value obtained from the joint data. This discrepancy was attributed to physical restraints offered by the adherends or perhaps a change in the molecular structure of the film.

The true reason for the discrepancy is related to the factor that is listed above. It was assumed in this experiment

that the thin layer of adhesive was in a uniaxial state of stress. Actually, the adhesive is subject to a nonuniform polyaxial state of stress which contains a small area of uniaxial stress only at the center of the specimen. In order to make a true comparison of the free film and joint data the analysis for the above state of stress would have to be utilized.

The real contribution of this work was the development of the fine instrumentation and specimen fabrication methods which have resulted in good reproducible adhesive properties for joints.

2.3 STRESS ANALYSES

2.3.1 Technical Review

The application of experimental stress analysis techniques to bonded joints has remained essentially static with only a small advance in the area of elastic behavior. Gnapp (2.9) instrumented some composite joints with strain gages and obtained a measure of the moment in lap joints within 20% of that predicted by Goland and Reissner (2.8). These results would encourage the use of their analysis for at least elastic behavior.

Durelli and Parks (2.4) investigated residual stresses from thermal effects in some photoelastic joint models but did not compare them with any analysis. Their work is available for comparison with an analytical model when it is developed.

Under analytical studies Filippi (2.5) has generalized the shear lag modeling method to a layered structure in an attempt to predict the transfer of load through a bonded pad into a tensile specimen but the greatest change in this area has been the increase in use of finite element techniques to analyze bonded joints. AVCO (2.2) and Cost and Parr (2.3) have both applied this method to the double overlap joint geometry. AVCO analyzed the ply by ply stress distribution in the composite and adhesive and showed that in a boron composite to titanium joint 2.0 in. long all the load was transferred through only 0.60 in. of the overlap.

Cost and Parr analyzed the stress distribution in the adhesive only and found excellent agreement with experimental results obtained by photoelastic stress analysis. Their paper is a good example of the current state of analysis in composites in general and particularly bonded joints. The analyst has available to him a powerful tool, in finite element analysis, for prediction of elastic behavior. He can attack any combination of geometry, elements or material provided he has material properties available. The problem is how to extend this to prediction of inelastic and finally fracture behavior in joints.

2.3.2 Annotated Bibliography

AVCO Corporation, "Evaluation of Test Techniques for Advanced Composite Materials" Quarterly Report No. 2, Contract F33 (615)-67-C-1719, Air Force Materials Laboratory, January 1968 (2.2)

A stress analysis was made of a double overlap joint of unidirectional boron composite bonded to two skins of titanium. The material arrangement was titanium-boron-titanium with the boron containing sixteen plies of unidirectional filament. A finite element technique was used to obtain the distribution of stresses throughout the adhesive and adherends and the following properties were used to characterize the components, which were assumed to have linear behavior.

	Titanium	Boron	Epoxy	Adhesive
Tensile Modulus (E) $\times 10^{-6}$ psi	16	57.5	0.46	0.18
Poisson's Ratio (μ)	0.33	0.16	0.30	0.30
Thickness (t)	0.63	0.108		0.006

The joint geometry and finite element grid are shown in Fig. 2.3.

For this particular joint the relative adherend stiffness $(Et)_B/(Et)_T = 3.4$ and the joint parameter $L/t = 20$ based on the thickness of the boron. The tensile modulus of 180,000 psi places the adhesive in a intermediate stiffness category with a computed shear modulus of 69,000 psi.

Two particular stresses are of interest to this study, the shear distribution along the length of overlap in the adhesive, and the shear distribution between plies as one moves from the bondline into the composite.

The adhesive distribution was compared with the results obtained from the Volkersen analysis of the same joint. The Volkersen analysis predicted shear stresses 2.5 times larger than the finite element method at the end of the joint where the load is carried into the titanium.

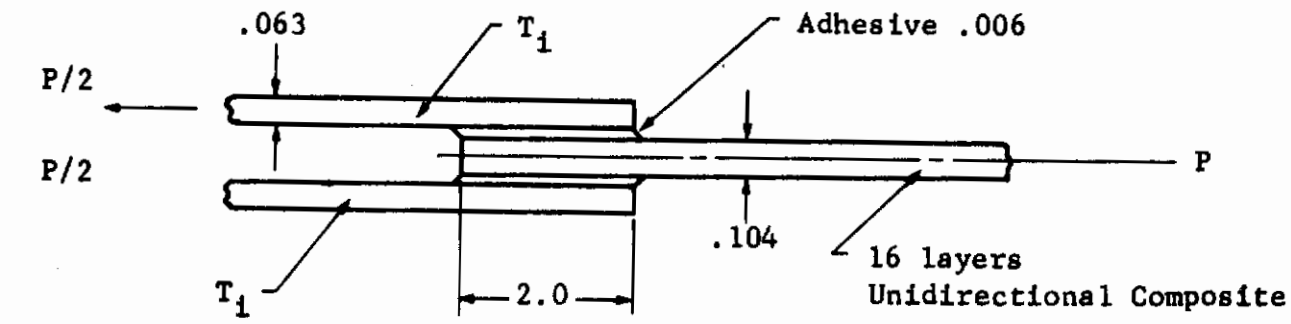

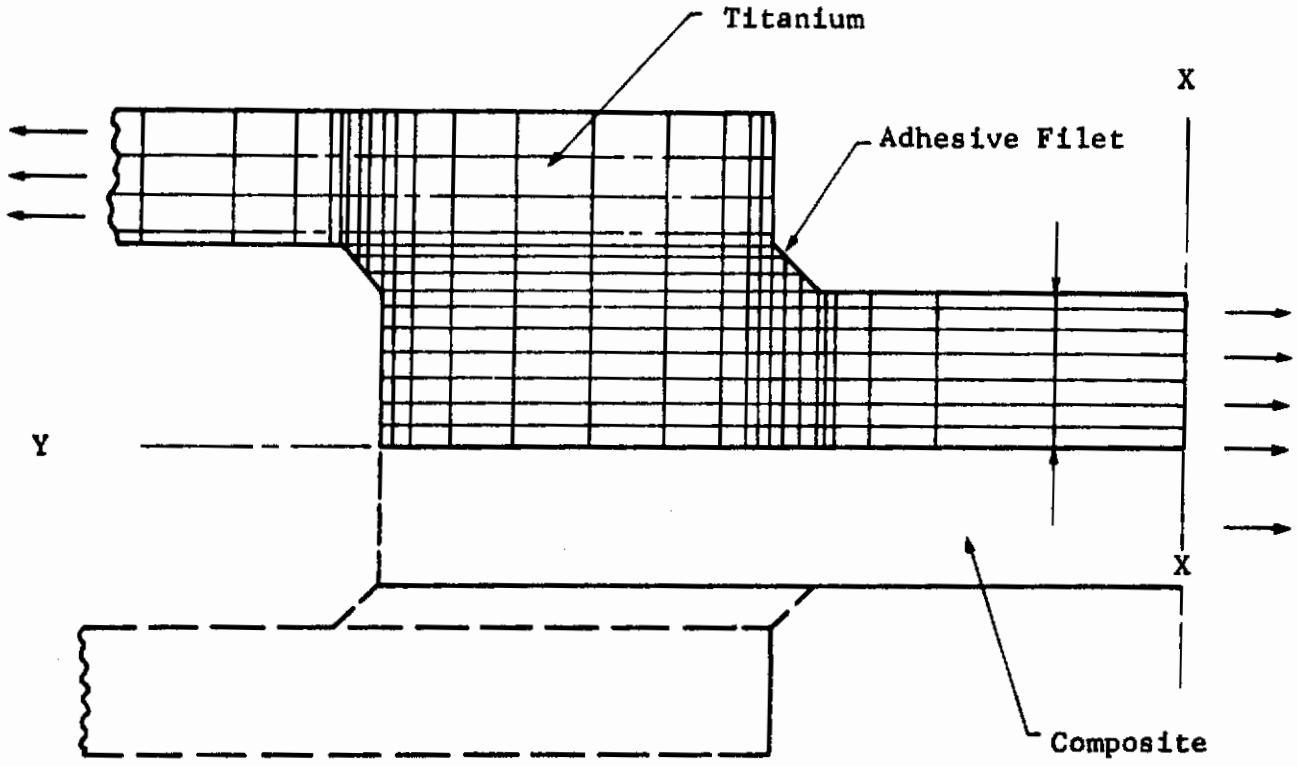

Fig. 2.3 JOINT GEOMETRY AND FINITE ELEMENT MODEL ANALYZED BY AVCO (2.2)

The ply by ply distribution showed a definite decrease in shear as one moves away from the bond line which results in a very high tensile stress in the filaments directly at the end of the overlap. This filament stress was 1.3 times the average filament stress at the surface and this decreased to almost zero within 25 percent of the length into the bonded area. The stress in all the filaments was essentially zero within 30 percent of the overlap length or in other words all the load from the boron was transferred to the titanium within 0.6 in. of the 2.0 in. bonded length.

The code developed by AVCO is readily adaptable to studying the effects of overlap length, material properties, bond thickness and variations in joint taper.

Cost, T. L. and Parr, C. H. (2.3)

"Analysis of the Biaxial Strip and Shear Lap Tests for Solid Propellant Characterization" Rohm and Haas Company, Redstone Research Laboratories, Report No. S-73, May 1967.

A combined finite element analysis and photoelastic analysis was carried out for a double lap joint configuration in which the adhesive was modeled with the finite element technique. All behavior was assumed elastic and the adhesive thickness (t_a) was relatively thick compared to the adherends (t), $(t_a/t) \approx 1$. The length of overlap parameter (L/t_a) for the adhesive was equal to the range from 2 to 10. These were thick adhesive joints with very short lengths of overlap.

In addition to the above variations in geometry several joints were investigated in which the exposed end of the adhesive ran at some acute angle to the adherend, giving the appearance of a joint in a state of large shear strain.

The numerical and experimental isochromatics showed very good agreement. The following results were obtained:

a. For a joint with $L/t_a = 6$ the ratio of the maximum shear stress at the center of the adhesive to that at the interface was 10.
b. The joints with the "scarfed" adhesive at the ends of the bond did not improve the stress distribution towards a more uniform distribution.
c. The most uniform shear stress distribution was obtained for an L/t_a equal to 10, at the midplane of the adhesive. No uniform distribution could be obtained along the interface for any of the geometries selected.

Durelli, A. J. and Parks, V. J. (2.4)

"Experimental Stress Analysis of Loaded Boundaries in Two Dimensional Second Boundary Value Problems" Report No. 11, Contract No. 2249(06), School of Engineering and Architecture, The Catholic University of America, February 1967.

This is a study of the residual stresses occurring in several joint configurations due to thermal stresses and external load. The joint configurations are applicable to lap shear and butt joint types and also transfer of load from a loaded filament to a surrounding matrix. The stress distribution in these geometries were analyzed using photoelastic stress analysis.

Relationships were developed for the maximum stresses as a function of the thermal expansion coefficients in the bonded adhesive and for the butt joint geometries the shear stresses at the interface were compared to that at the center of the bondline. The results of this work should be compared with some analytical model.

Filippi, F. J. (2.5)

"Analysis of Axial Stresses in a Multi-Ply Laminate Loaded in Shear on the Outer Ply" in AFML TR-66-209, Contract No. AF-33(616)-3288, August 1966.

Filippi has used the shear lag analysis to determine the stress distribution in a composite material as the load is

introduced into the faces by shear and then alternately through each fiber and resin layer. The problem is analogous to that of load transfer through a series of stepped lap joints.

A matrix of linear differential equations are obtained where each equation is similar to that developed by Volkersen (2.24). A solution is carried out for a two-ply composite and the stresses are obtained for the fiber and matrix as a function of distance into the composite.

The limiting case of the stresses in the filaments directly at the bond line was checked and the analysis correctly predicted these to be equal to the average axial stress away from the bonded area.

Gnapp, Julius I. (2.9)

"Measurements of Moments at Edges of Adhesive Lap Joints Between Glass-Reinforced Plastic Laminates," Picatinny Arsenal, Technical Memorandum 1932, September 1965.

Measurements were made of the moment being applied to the ends of the overlap of a simple lap joint fabricated from glass-reinforced plastic adherends bonded with FM-1000. The moment was determined by mounting strain gages along the joint on both sides of the adherends and measuring the surface strains.

The moments measured experimentally were compared to those predicted by Goland and Reissner (2.8) in their analysis of the loads applied to a simple lap joint. The experimental results were generally 20 percent lower than those predicted analytically, indicating that use of this analysis for design would be conservative, but should be acceptable for bonded joints in glass reinforced plastics.

2.4 DESIGN METHODS AND STRENGTH OF JOINTS

2.4.1 Technical Review

The design procedures available at present for bonded joints fall into two categories. These are the pragmatic and the empirical with some support from an analysis. Both procedures have been used in the recent literature with success.

The pragmatic design procedure is based on building typical joints of a simple geometry and testing them to failure, and using the average strengths as a guide in more complex joint geometries. A modification of this is to go directly to the complex part, build it with different adhesives and test it to failure. Data and results of this method are given in references 2.1, 2.11, 2.17, 2.18, 2.20, 2.22 and 2.23.

In the empirical or semi-analytical technique an analysis is assumed for a simple geometry, joints of the geometry are fabricated and tested and some curvefitting procedure is applied to correlate the analytical and experimental results. The analysis may be used only to identify a set of geometric variables such as the joint parameter (L/t) which should have a strong functional relationship with the joint strengths. Again a transition must be made from the simple geometries to a complex structure but if the results have some analytical basis this can be accomplished usually with more insight and less testing. Szepe (2.21) has developed this method for both fatigue and thermal effects with reasonable success and Hartman and deJonge (2.10) attempted to use the Volkersen (2.24) and Goland and Reissner (2.8) analyses but with less success.

The present state of design in bonded joints is simply that there is no rational procedure available and it must now wait on further developments in analysis and materials characterization. Until this occurs design techniques must remain empirical and rely heavily on testing and experimental results.

2.4.2 Annotated Bibliography

Anonymous (2.1)

"Design Manual on Adhesive Bonded Glass Reinforced Plastic Joints," New York Naval Shipyard, Lab Proj. 5616-1, June 1958

This is a short general manual which covers the bonding of FRP structural joints. The manual discusses the characteristics of FRP relative to bonding, common joint geometries, and includes some strength data for these joints bonded with an epoxy room temperature curing adhesive.

Joint geometries discussed include variations of these three basic types: lap joints, scarf joints, and butt joints. No actual design calculations or stress analyses are included but from the strength data given, a judgment as to the optimum configuration can be made. Some of the test results are shown in Fig. 2.4.

Some information is also included on repair of FRP panels using adhesives in wet lay ups. This manual is a good introduction to simple joint designs for FRP structures.

Hartman, A. and de Jonge, J. B. (2.10)

"Non-destructive and Destructive Tests on Redux Bonded Single and Double Lap Joints with Various Glue Line Thicknesses," National Aero- and Astronautical Research Institute, Amsterdam, 1960.

A series of Redux bonded joints were tested nondestructively with the Fokker Bond Tester and then destructively under static load. The strength of double lap joints was independent of adhesive thickness but strength of single lap joints was dependent on film thickness. An analysis of the results was discussed in light of the Volkersen and Goland and Reissner analyses for shear stress distribution in lap joints. It was concluded that these analyses were inadequate for explaining the results.

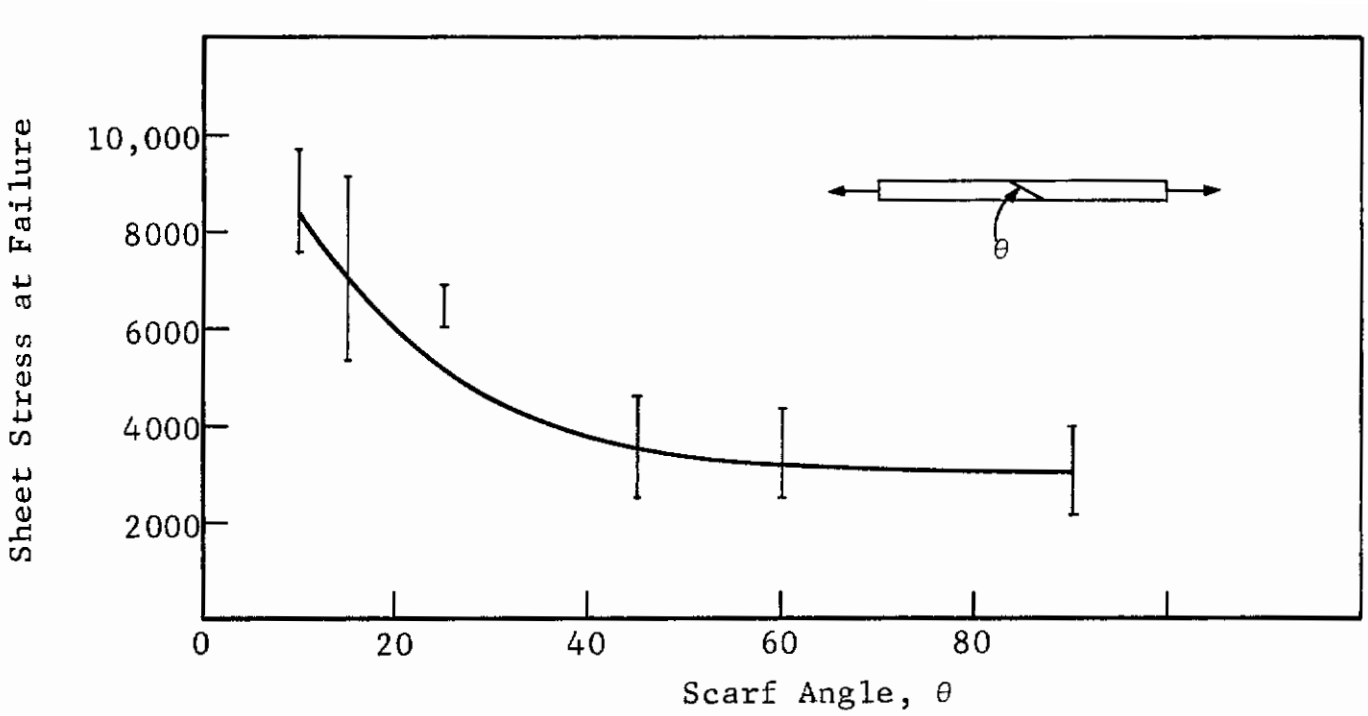

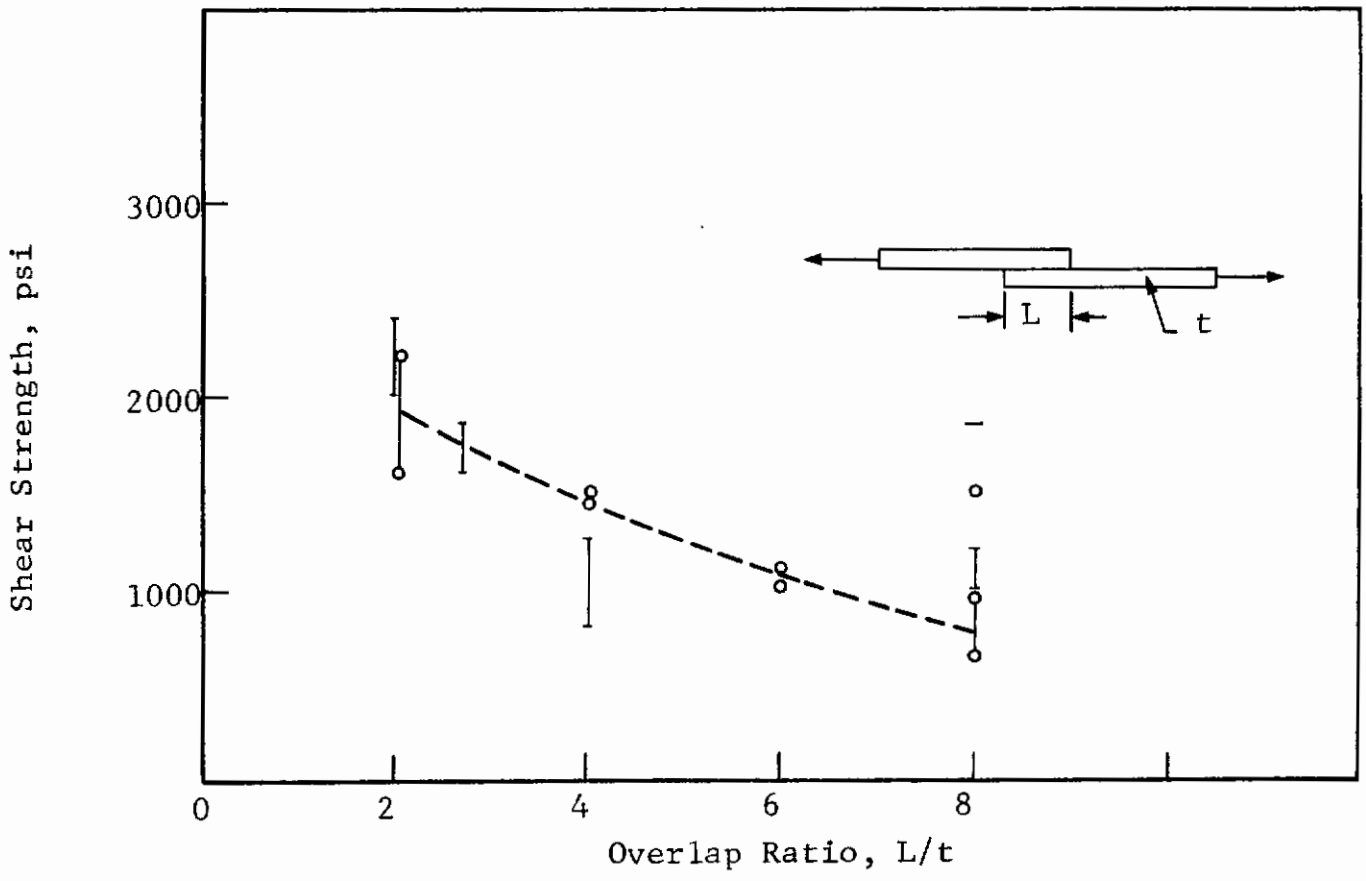

Fig. 2.4 STRENGTH OF BONDED COMPOSITE JOINTS (2.1)

It was emphasized that inelastic behavior of the adhesive and adherends must be introduced to obtain a better understanding of joint strengths. It was also stated that application of fracture mechanics to joints should result in more fruitful results.

Hartman, A. and De Rijk, P. (2.11)

"The Effect of the Rigidity of the Glue Line on the Fatigue Strength of 2024-T Aluminum Alloy Specimens with an Adhesive-Bonded Reinforcing Plate on Both Sides" National Aero- and Astronautical Research Institute, Amsterdam, NLR-TN M2096, February 1962.

Fatigue tests were conducted for tensile strips of aluminum which were reinforced in their central length by bonding on a doubler strip to each side of the sheet. The doublers were bonded with Redux adhesive (Shear Modulus = 5000 psi). The presence of the bonded doublers causes a stress concentration in the aluminum sheet which should effect the fatigue life of that sheet.

It was found that for the Metlbond 4021 bonded doublers the fatigue strength reduction factor (K_f) was (1.0) indicating no change in fatigue behavior and for the Redux K_f was (1.1), indicating a slight reduction in fatigue strength. The K_f values were measured at 10^5 cycles.

These results are in agreement with those of Wang (2.25) who has shown that bonded joints with lower moduli adhesives have better fatigue strength.

Prokhorov, B. F. (2.17)

"Joints Used in Plastic and Composite Shipboard Super Structures, Deckhouses, Light Bulkheads, and Enclosures" Sudostroyeniye, #9 p. 44-51, 1965, U. S. Dept. of the Navy Translation No. 2076-b.

This is one of the few Russian references obtained concerning design of joints particularly for FRP structures.

It is a general summary article presenting guidelines and comments on joint design covering both adhesive bonded and mechanically fastened joints.

Reference is made to the standard analyses for lap joints using shear lag methods, but no real designs based on these methods are described. Some work was referenced in which it was suggested that by varying the rigidity of the adherends throughout the bonded lap length a uniform shear stress distribution would be obtained. This variable rigidity was to be achieved by reducing the thickness of the adherends according to a hyperbolic function.

In order to achieve a uniform shear stress distribution, the doubler strips should be reduced in section at the ends of the overlap. But in order to decrease the peeling stresses, the doubler rigidity should be increased in this area. An attempt was made to resolve this dilemma by designing a combination doubler as shown in Fig. 2.5.

For practical design of double overlap joints with constant thickness doublers, a length to thickness ratio of (30) was suggested. This was for adherend thicknesses up to 0.20 in. thick.

For the design of riveted joints tests were conducted of joints with variable rivet to plate edge distance. For $a \geqq 3d$ crushing at the rivet occurred. For $a \leqq 3d$ rivet pull out occurred, where

a = distance from center of rivet to plate edge

d = rivet diameter.

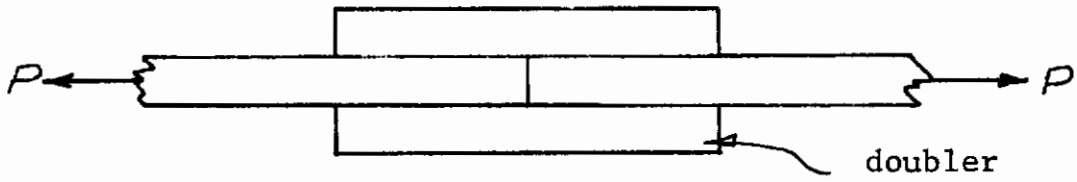

Constant rigidity doubler

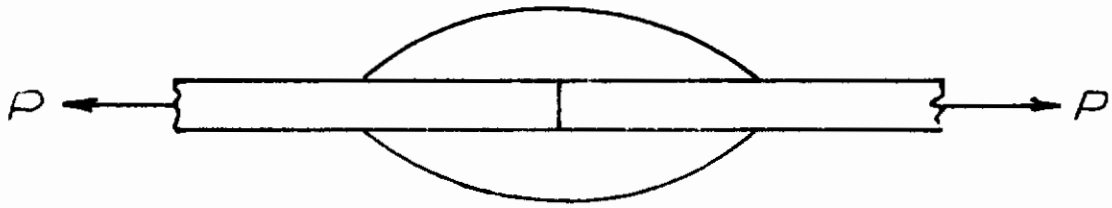

Doubler with rigidity a hyperbolic function of position for uniform shear stress

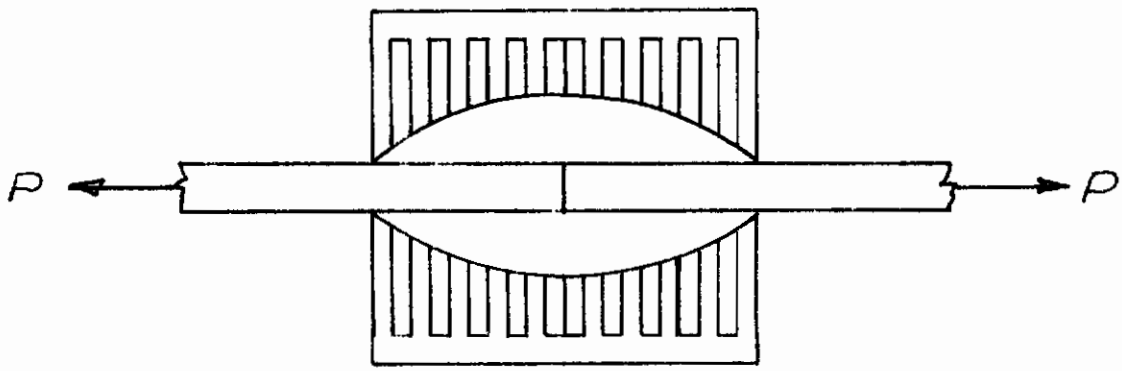

Combined doubler for both uniform shear and normal stress distribution

Fig. 2.5 VARIOUS DOUBLER DESIGNS FOR DOUBLE OVERLAP TYPE BONDED JOINTS

Reed, R. and Marano, D. (2.18)

"Research to Determine Mechanical Properties of Polybenzimidazole Metal to Metal Adhesives," AFML-TR-65-136, Air Force Materials Laboratory, April 1965.

This extensive study covers the development of PBI adhesives to bond PH15-7Mo stainless steel, 2219-T81 aluminum alloy and GA1-4V titanium, and included surface treatments for the adherends, strength and fatigue behavior under extreme environments and effects of joint geometry on efficiency.

One important variable investigated was the effect of adhesive film thickness on shear strength of double overlap joints. The results of this data was graphed as a function of the parameter (L/t_a) where L is overlap length and t_a is adhesive thickness. An attempt was made to fit the data to the function

$$\tau = \frac{cG\gamma}{\sqrt{L/t_a}}$$

where

τ = average shear strength
G = adhesive shear modulus
γ = joint shear deformation at failure
c = film thickness constant.

The results were a poor fit but could have been improved if the data was plotted as a function of the more usual parameter (L/t) where (t) is adherend thickness. This was done and a family of curves obtained each for a different thickness indicating it was a major variable. Actually, a variation in adhesive thickness is equivalent to a change in modulus since adhesive shear strain is directly proportional to the product, thickness times modulus.

Using the above relationship with measurements of total joint deformation, an attempt was made to characterize the shear modulus of the PBI. Values in the range from 10 to 20,000 psi were obtained at room temperature which would appear to be low for this material.

Strauss, E. L. (2.20)

"The Strength of Bolted and Bonded Attachments of Glass-Reinforced Polybenzimidazole and Phenolic Laminates to Metal" Society of the Plastics Industry, Annual Meeting, 1966.

The strength of several bonded and bolted joints of polybenzimidazole and phenolic laminates were measured with the following specimens: (1) standard tensile, (2) stress concentration, (3) bolted double shear, (4) bolted single shear, (5) bonded double shear and (6) bonded single shear. The laminates were bonded or bolted to Inconel metal doublers. Some of the data is presented below to indicate the range of joint efficiencies obtained.

Polybenzimidazole Laminate

Specimen	Tensile Strength*	Strength Efficiency
Standard Tensile	80,700	100.0
Bolted Double Shear	30,300	28.4
Bolted Single Shear	30,400	28.6
Bonded Double Shear	19,400	24.4
Bonded Single Shear	16,200	19.7

Phenolic Laminate

Standard Tensile	70,500	100.0
Bolted Double Shear	20,400	31.8
Bolted Single Shear	22,300	30.4
Bonded Double Shear	22,400	56.8
Bonded Single Shear	18,600	37.8

*Tensile load per inch of specimen width.

This data indicates some of the potential increases in strength possible through improvements in joint design.

Szepe, F. (2.21)

"Strength of Adhesive-Bonded Lap Joints with Respect to Change of Temperature and Fatigue," Exp. Mech. 6 pp. 280-286, 1966.

A simplified form of the shear lag analysis for lap type joints is utilized to develop a design method based on lap shear strength data. In the complete shear lag analysis the axial loads in the adherends and the resultant shear stress distribution are a hyperbolic function of joint position. Szepe has simplified the problem by assuming the adherend load to be a linear function of position. This assumption results in a parabolic shear stress distribution.

The maximum shear stresses at the ends of the overlap are now given by

$$\tau_{max} = \tau_{avg}\left[1 + \frac{CL^2}{3E}\left(\frac{1}{t_1} - \frac{1}{2t_2}\right)\right]$$

where

τ = shear stress
L = length of overlap
E = adherend modulus
t_1, t_2 = adherend thickness
C = G/d
G = adhesive shear modulus
d = adhesive thickness

For the special case of equal adherends

$$\tau_{max} = \tau_{avg}\left[1 + \frac{CL^2}{GEt}\right]$$

When failure occurs in the joint, τ_{max} must be equal to the shear strength of the adhesive and τ_{avg} equals τ_{ult}, the maximum average shear stress for a given joint. Therefore, there are two unknowns (τ_o) and (C). These can be simply determined by carrying out two joint tests with length of overlap and solving two simultaneous equations.

This analysis was applied to two different types of adhesives, and a reasonably good fit to the experimental data was obtained. The method was also extended to include the effect of temperature and fatigue loading on (τ_o) and (C).

Thomason, D. P. (2.22)

"Adhesive Bonding of End Closures for High Strength and Reliability in Rocket Motor Cases: Borg-Warner Corporation, Contract NOrd 15719, Final Report, July 1963.

Studies were carried out to design a 15,000 pounds per peripheral inch tensile strength bonded joint for attaching end closures to steel cylinders. Final design was achieved by testing simple lap joints and small model cylinders. The adhesive used was FM-1000 manufactured by Bloomingdale Rubber Company.

The interesting aspect of this study is that the joint geometry chosen was a scarf joint which produces no offset in wall geometry as a lap joint would. Cylinder wall thickness was 0.10 in. and the joint was scarfed over a 1.125 in. length giving a scarf slope of 1:11. The required design load was achieved with adhesive bonding.

Underwood, W. F. (2.23)

"Filament Wound Joint Design Study" ACF Industries, Albuquerque Division, ACF-412-256, 1965.

The purpose of this program was to provide data on the type of joints suitable for joining filament wound structures. Joint geometries considered were (1) double lap, (2) scarfed and (3) stepped single lap joints. The adherends were fiberglass to fiber glass and fiberglass to aluminum.

Figure 2.6 shows some of the shear strength data obtained for the double overlap joints. Uniaxial fiberglass bonded to uniaxial fiberglass gave the highest shear strength followed by biaxial bonded to biaxial FRP and then biaxial FRP bonded to aluminum.

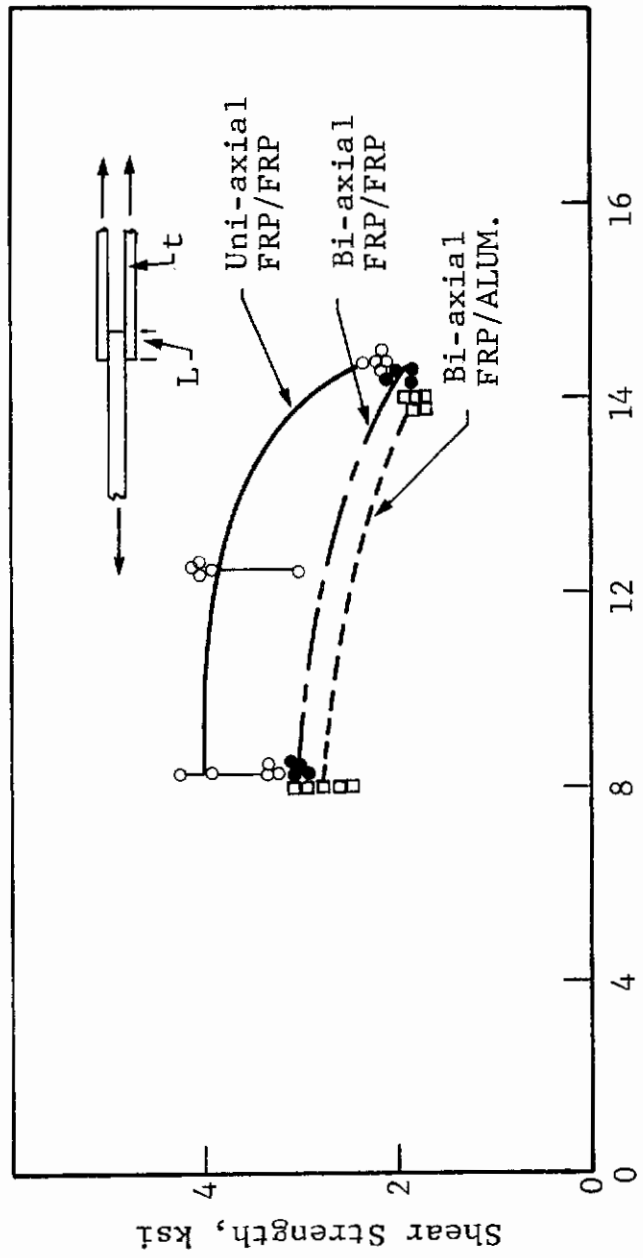

Fig. 2.6 SHEAR STRENGTH OF DOUBLE OVERLAP JOINTS OF FIBERGLASS REINFORCED PLASTIC AND ALUMINUM

Biaxial laminate bonded with a 15° scarf angle gave a strength of 3237 psi which is stronger than the double-overlap joint design for the same material.

Also included in the report are detailed process specifications for building filament wound flat laminates and for preparation of bonded specimens.

The data generated in this and similar programs would be ideal for further analytical interpretation if the properties of the adhesives used were available. In this study the adhesive used was an epoxy resin ERL 0510, cured with ZZL 0803.

References (Section 2.0)

2.1 Anonymous, "Design Manual on Adhesive Bonded Glass Reinforced Plastic Joints," New York Naval Shipyard, Lab Project 5616-1, June 1958.

2.2 AVCO Corporation, "Evaluation of Test Techniques for Advanced Composite Materials," Quarterly Report No. 2, Contract F33(615)-67-C-1719, Air Force Materials Laboratory, Jan. 1968.

2.3 Cost, T. L. and Parr, C. H., "Analysis of the Biaxial Strip and Shear Lap Tests for Solid Propellant Characterization," Rohm and Haas Co., Redstone Research Laboratories, Report No. S-73, May 1967.

2.4 Durelli, A. J. and Parks, V. J., "Experimental Stress Analysis of Loaded Boundardies in Two-Dimensional Second Boundary Value Problems," Report No. 11, Contract Nonr 2249(06), School of Architecture and Engineering, The Catholic University of America, Febr. 1967.

2.5 Filippi, F. J., "Analysis of Axial Stresses in a Multi-Ply Laminate Loaded in Shear on the Outer Ply," in AFML TR-66-209, Contract No. AF33(616)-3288, Aug. 1966.

2.6 Franzblau, M. C. and Rutherford, J. L., (General Precision, Inc.) "Study of Micromechanical Properties of Adhesive Bonded Joints," First Quarterly Progress Report, DAAA-21-67-C-0500, Picatinny Arsenal, Oct. 1967.

2.7 Franzblau, M. C. and Rutherford, J. L., (General Precision, Inc.) "Study of Micromechanical Properties of Adhesive Bonded Joints," Second Quarterly Report, DAAA-21-67-C-0500, Picatinny Arsenal, Jan. 1968.

2.8 Goland, M. and Reissner, E., "Stresses in Cemented Joints," J. Applied Mechanics (ASME), 11 pp. A17-A27, 1944.

2.9 Grapp, Julius, I., "Measurement of Moments at Edges of Adhesive Lap Joints between Glass-Reinforced Plastic Laminates," Picatinny Arsenal T. M. 1932, Sept. 1965.

2.10 Hartman, A. and deJonge, J. B., "Nondestructive Tests on Redux Bonded Single and Double Lap Joints with Various Glue Line Thicknesses," National Aeronautical and Astronautical Research Institute, Amsterdam, 1960.

References (Cont)

2.11 Hartman, A. and de Rijk, R., "The Effect of the Rigidity of the Glue Line on the Fatigue Strength of 2024-T Aluminum Alloy Specimens with an Adhesive Bonded Reinforcing Plate on Both Sides," National Aeronautical and Astronautical Research Institute, Amsterdam NLR TN M2096, Febr. 1962.

2.12 Iosipescu, N., "New Accurate Procedure for Single Shear Testing of Metals," Journal of Materials, Vol. 2, No. 3, Sept. 1967.

2.13 Ju, F. D. and Baker, J. G., "Preliminary Study of Pure Shear Fracture Model," AFOSR Scientific Report G5-1195, May 1965.

2.14 Kuenzi, E. and Stevens, G. H., "Determination of Mechanical Properties of Adhesives for Use in the Design of Bonded Joints," U.S. Forest Service Res., Note FPL-011, 1963.

2.15 Kutscha, D., "Mechanics of Adhesive Bonded Lap-Type Joints, Survey and Review," MLTDR-64-298, AFML, Oct. 1964.

2.16 Miller, H. E., Jergens, J. L. and Plunkett, R., "Measurement of Complex Shear Moduli of Thin Viscoelastic Layers," Univ. of Minn., Institute of Technology, TR.65-4, Oct. 1965.

2.17 Prokhorov, B. F., "Joints Used in Plastic and Composite Shipboard Super Structures, Deckhouses, Light Bulkheads, and Enclosures," Sudostroyeniye, #9, pp. 44-51, 1965, U.S. Dept. of the Navy Translation No. 2074-b.

2.18 Reed, R. and Marano, D., "Research to Determine Mechanical Properties of Polybenzimidazole Metal to Metal Adhesives," AFML TR-65-136, AFML, Apr. 1965.

2.19 Rutherford, J. L., Bossler, F. C. and Hughes, E. J., "Capacitance Methods for Measuring Properties of Adhesives in Bonded Joints," Rev. Scient. Inst. Vol. 39, No. 5, pp. 666-671.

2.20 Strauss, E. L., "The Strength of Bolted and Bonded Attachments of Glass-Reinforced Polybenzimidazole and Phenolic Laminates to Metal, Soc. of the Plastics Ind. Annual Mtg., 1966.

2.21 Szepe, F., "Strength of Adhesive-Bonded Lap Joints with Respect to Change of Temperature and Fatigue," Exp. Mech. 6 pp. 280-286, 1966.

References (Cont.)

2.22 Thomason, D. P., "Adhesive Bonding of End Closures for High Strength and Reliability in Rocket Motor Cases," Borg-Warner Corp., Contract NOrd 15719, Final Report, July 1963.

2.23 Underwood, W. F., "Filament Wound Joint Design Study," ALF Industries, Albuquerque Div. ALF 412-256, 1965.

2.24 Volkersen, O., "Die Niet Kraftverteilurg in Zugbeanspruchten Nietverbindungen mit Konstanten Laschenguerschnitten," Luftfahrtforschung, 15, pp. 41-47, 1938.

2.25 Wang, D. Y., "The Effect of Stress Distribution on the Fatigue Behavior of Adhesive Bonded Joints," ASD-TDR-63-93, AFML, July 1963.

3.0 STRESS ANALYSIS OF BONDED JOINTS

3.1 INTRODUCTION

A study was made of available stress analyses for bonded joints in order to determine the following:

- The generality of the analysis, to what type of joints could it be applied.
- The difficulty in using the analysis, its requirements for computational aids and its applicability to use in a design manual.
- The type of stress distributions which resulted from its use and how they varied with different joint parameters and how they compared with predictions from other analysis methods.

The study was restricted to available methods which would cover as wide a range of joints as possible. Four analyses shown in Table 3.1 were selected, ranging from the most simple to the most complex. The joint type indicates the type of joint geometry to which they are applicable. Material behavior is the type of stress-strain curve which must be known or assumed for the adhesive and the adherends. The material variation indicates whether it is possible to vary the properties of the adhesive or adherend along the length of the joint. The finite element is the most general and it also allows property variation through the thickness of the joint components. The computational tools indicate whether the analyses can be done by hand calculation or require the use of a high-speed computer.

Each one of these methods is discussed in the following section.

Table 3.1

STRESS ANALYSIS METHODS FOR BONDED JOINTS

Analysis	Joint Type	Material Behavior	Material Properties along Joint	Stress Predicted	Computation Tools
Volkersen	Supported Lap Joint Double Overlap	Linear Elastic	Constant	Shear - Adhesive	Hand or Simple Program
Goland and Reissner	Unsupported Lap Joint Single Overlap	Linear Elastic	Constant	Shear and Normal Adhesive	Hand or Simple Program
Numerical Shear Lag	Supported Lap Joint	Linear Elastic	Variable	Shear - Adhesive	Hand or Program
Finite Element	Any Joint	Linear Elastic Nonlinear by Iteration	Variable, Length and Thickness	Shear and Normal at any Point	Complex Computer Program

3.2 ANALYSIS OF THE SUPPORTED LAP JOINT

The following sample calculation and computer program for the shear stress distribution along the adhesive film, in a simple lap joint without bending, is based on the analysis originally carried out by Volkersen (3.1) and then extended by DeBruyne(3.2). The analysis applies to joints with the adherends of equal thickness or unequal thickness. It does not account for adherends tapering in thickness. It assumes that both adherend and adhesive behave elastically.

3.2.1 Analysis and Sample Calculation

Schematically the joint can be represented as

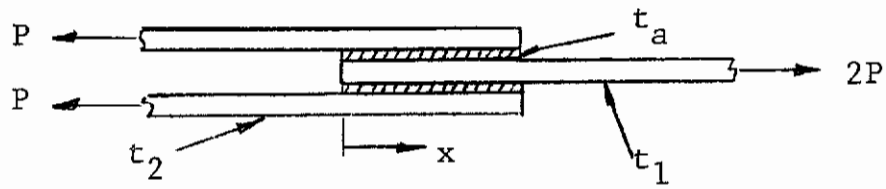

and the final result for the shear stress as a function of (x) is as follows:

$$\tau_{(x)} = \frac{P}{wl} \frac{(\Delta/K)^{1/2}}{\sinh (\Delta \cdot K)^{1/2}} \left[(K-1) \cosh \left[(\Delta \cdot K)^{1/2} \cdot \frac{x}{L} \right] + \cosh \left[(\Delta \cdot K)^{1/2} \quad (1 - \frac{x}{L}) \right] \right]$$

where

$$\Delta = \frac{G_a L^2}{E \cdot t_2 t_a} \qquad K = \frac{t_1 t_2}{t_1} \quad , \quad t_1 > t_2$$

Table 3.2 defines the various symbols, shows a typical value for each variable and the range of values of each variable which the computer program was written to include.

The following calculation uses the values given in Table 3.2 to illustrate use of the equations for a typical

Table 3.2

DEFINITION OF SYMBOLS FOR VARIABLES AND THEIR VALUE FOR THE VOLKERSEN ANALYSIS

Symbol	Variable	Typical Value	Range of Values
P	Applied Load	1 lb	1 → 9,999 lb
W	Joint Width	1 in.	0.250 → 10.00 in.
L	Length of Overlap	0.500 in.	0.125 → 10.00 in.
t_a	Adhesive Thickness	0.010 in.	0.005 → 0.10 in.
t_1, t_2	Adherend Thickness	0.032 in.	0.020 → 1.00 in.
G_a	Shear Modulus - Adhesive	50,000	500 → 100,000 psi
E	Young's Modulus - Adherend	10.5×10^6	3.1×10^6 → 60×10^6 psi
X	Distance from Edge of Joint of Thicker Adherend	0.1 L	0.01 → 0.1 L

joint. The sample calculation was given for two reasons. The first is that a hand computation is useful to check a computer program and it provides a feeling for the size of the numbers involved in the computation. The second is that for the many times in the literature that this analysis is referenced the writer has yet to find a sample calculation carried out in detail. It was felt that an example given here would help guide others who are faced with the problem of actually making numerical computations.

Determine the shear stress at the center of the overlap ($x = L/2$).

$$\frac{P}{wL} = \frac{1}{1\ (1/2)} = 2 \text{ psi}$$

$$K = \frac{(0.032) + (.064)}{(0.064)} = 1.5$$

$$\Delta = \frac{G_a L^2}{E\ t_2 t_a}$$

$$= \frac{5(10)^4\ (0.5)^2}{10.5(10)^6(0.032)(0.01)} = 3.72$$

$$(\Delta/K)^{1/2} = \left[\frac{3.72}{1.5}\right]^{1/2} = 1.57$$

$$(\Delta \cdot K)^{1/2} = ((3.72)\ 1.5)^{1/2} = 2.36$$

$$\sinh\ (\Delta \cdot K)^{1/2} = \frac{e^{2.36} - e^{-2.36}}{2} = \frac{10.6 - 0.094}{2} = 5.253$$

$$\cosh\left[(\Delta \cdot K)^{1/2} \cdot \frac{x}{L}\right] = \cosh\ (2.36)(0.5) = \cosh\ (1.18)$$

$$= \frac{e^{1.18} + e^{-1.18}}{2} = \frac{3.25 + 0.307}{2} = 1.778$$

$$\tau(0.5L) = \frac{2(1.57)}{5.253}\ (1.5\text{-}1)(1.778 + 1.778) = 1.53 \text{ psi}$$

Stress Concentration Factor

$$n = \frac{\tau(x)}{\tau_{avg}} \qquad \tau_{avg} = \frac{P}{wL}$$

$$= \frac{1.53}{2} = 0.76$$

Similarly the calculation can be carried out to determine the maximum shear stresses in the joint which must occur at the ends of the joint (x=0, x=L).

At	x = 0	$\tau(0) = 3.48$	n = 1.74
	x = L	$\tau(L) = 2.19$	n = 1.09

Note that the maximum stress in a joint with unequal adherends will always occur at (x = 0), which by definition for the analysis is the point where load enters the joint from the thinner adherend. In a joint with equal thickness adherends the stress is the same at both ends of the overlap.

In the sample calculation only a unit load (1#) was applied to the joint. For this analysis the load (P) is explicitly factorable and therefore the stress at any load is equal to the load times the stress for a unit load.

3.2.2 Computer Program

The computer program for calculating the shear stress distribution was written in Fortran IV. The program can be used to compute $\tau(x)$ for specific values of (x), or by having the program generate increment values for (x). This option is controlled in statement 42 depending on the value assigned to (S) in statement 7. For $S \geq 0$ the program computes the number (k) of (x) values read in at statement 140, for S = 0 the desired values of (x) must be read in individually.

Two types of output are available from this program, tabular and graphical. Graphical output requires the use of a Calcomp plotting machine. The program listing is given in

Table 3.3 and the tabular output from a sample problem is shown in Table 3.4. The graphical plotted results are shown in Fig. 3.1.

3.2.3 Parametric Problems

In order to become thoroughly familiar with the analyses, and to study the effect of joint geometry and materials properties on the shear stress distribution, a series of sample joints have been analyzed by the Volkersen analysis. Table 3.5 summarizes the joints for which the shear stress distribution was calculated.

The results of the caluclations have been summarized in Figs. 3.2, 3.3 and 3.4. The figures show graphs of the shear stress distribution in the joint and the maximum shear stress concentration factor (n) where

$$n = \frac{\tau(L)}{P/wL} \qquad \tau(L) = \text{maximum stress in the joint}$$

as a function of a single parameter. In all cases the joints were a unit width (w) and loaded by a unit load (P = 1 lb.). In the Volkersen analysis the load P is explicitly factorable and therefore the stress at any load is directly proportional to the stress for a unit load.

Figure 3.2 shows the effect of simply increasing the length of the overlap. The stress concentration factor increases linearly but the maximum stress does not.

Figure 3.3 shows the effect of changing the shear modulus. In the range of 1,000 to 5,000 psi the shear stress is almost uniform throughout the joint. At 150,000 psi, which is the modulus range of most conventional phenolic or epoxy adhesives, the distribution is drastically non-uniform.

Figure 3.4 shows the effect of increasing the thickness of the adhesive film for a 50,000 psi shear modulus adhesive. The graph indicates that one would have to use a 0.10 in film thickness to approach a uniform shear stress throughout the joint. A thickness of this order would only be practical in very selective cases.

Table 3.3

PROGRAM LISTING FOR THE VOLKERSEN ANALYSIS

```
      SCDPLT                                                          04/27/67
          MAIN        -  FEN    SOURCE STATEMENT  -  IFN(S)  -

C       VOLKERSEN ANALYSIS
        DIMENSION SV(200),X(200),SCON(200),XBAR(200),ASHEAR(200)
        DIMENSION DATA(476)
        CALL PLOTS (DATA,476,16)                                          2
      1 I = 0
        FDC=0.
      2 I = I + 1
C       ADHERENT PROPERTIES
      3 READ (5,4) T1, T2, W, OL, E                                       6
      4 FORMAT (2X,4F6.3,E10.2)
        IF(T1.EQ.999.) GO TO 100
C       ADHESIVE PROPERTIES
      5 READ (5,6) TA, GA                                                10
      6 FORMAT (2X,F6.3,F8.0)
C       APPLIED LOAD
      7 READ (5,8) P, S                                                  11
      8 FORMAT (2X,F8.2,F4.1)
     10 WRITE (6,11) I                                                   12
     11  FORMAT (13H1 CASE NUMBER,I3 ,32X,19H VOLKERSEN ANALYSIS )
     12 WRITE (6,13)                                                     13
     13 FORMAT (21H0 ADHERENT PROPERTIES)
     14 WRITE (6,15) T1, T2, W, OL, E                                    14
     15 FORMAT (2X,6H T1 = ,F6.3,4H IN.,5X,6H T2 = ,F6.3,4H IN.,5X,5H W =
       2,F7.3,4H IN.,5X,5H L = ,F7.3,4H IN.,5X,5H E = ,2PE10.2,4H PSI)
     16 WRITE (6,17)                                                     15
     17 FORMAT (21H0 ADHESIVE PROPERTIES)
     18 WRITE (6,19) TA, GA                                              16
     19 FORMAT (2X,6H TA = ,F6.3,4H IN.,5X,6H GA = ,F8.0,4H PSI//)
     20 WRITE (6,21) P                                                   17
     21 FORMAT (3X,18H APPLIED LOAD P = ,F6.0,5H  LB.//)
    211 AVESHE=P/(W*OL)
     22 WRITE(6,23) AVESHE                                               19
     23 FORMAT  (28H0 AVERAGE SHEAR STRESS TAU =,F9.4,3HPSI//)
     30 DO 36 J=1,200
     31 X(J) = 0.0
     32 SV(J) = 0.0
     33 SCON(J)=0.0
     34 XBAR(J)=0.0
     35 ASHEAR(J)=AVESHE
     40 READ (5,41) K                                                    36
     41 FORMAT (I4)
     42 IF (S) 50,50,43
     43 AK = K
     44 BK = K - 1
     45 DELX = OL / BK
     46 DO 47 L = 2,K,1
     47 X(L) = X(L-1) + DELX
     48 GO TO 60
     50 READ (5,51) ( X(J), J = 1,K )                                    53
     51 FORMAT (10F7.3)
     60 CK = (T1 + T2) /T1
     61 DEL = (GA * DI * OL) / (E * T2 * TA)
     70 DO 83 J=1,K
     71 Y = X(J)
     72 B1 = (DEL * CK) ** 0.5                                           69
```

Table 3.3 (contd)

PROGRAM LISTING FOR THE VOLKERSEN ANALYSIS

```
    SCDPLT                                                          04/27/67
        MAIN        -  EFN   SOURCE STATEMENT  -  IFN(S)  -

 73 B2 = B1 * Y / OL
 74 B3 = B1 * (OL - Y) / OL
 75 B4 = (DEL / CK) ** 0.5                                                  73
 76 S1 = 0.5 *(EXP(B1) - (1.0/EXP(B1)))                                     75
 77 C1 = 0.5 * (EXP(B2) + (1.0/EXP(B2)))                                    77
 78 C2 = 0.5* (EXP(B3) + (1.0/EXP(B3)))                                     79
 80 SVT = (((CK - 1.0)*(C1)) + (C2)) / S1
 81 SV(J) = (P *B4 * SVT) / (W * OL)
 82 XBAR(J)=X(J)/OL
 83 SCON(J)=SV(J)/AVESHE
 90 WRITE (6,91)                                                            91
 91 FORMAT(2X,4HSTA.,5X,5HJOINT,11X,8HRELATIVE,14X,5HSHEAR,22X,
   15HSHEAR / 2X,3HNO.,5X,8HPOSITION,9X,8HPOSITION,14X,6HSTRESS,17X,
   113HCONCENTRATION / 11X,5H(IN.),34X,5H(PSI)  ///)
 92 WRITE (6,93)  (J,X(J), XBAR(J), SV(J), SCON(J),J=1,K)                   92
 93 FORMAT (2X,I2,4X,4H X =,F8.4,6X,8HX BAR = ,F5.2,8X,6HTAU = ,E12.4,
   1 9X,4HN = ,F7.3)
 94 GO TO 2
100 CALL PLOT(1.,1.,-3)                                                    104
    FNC=FNC+1.
    XBAR(K+1)=0.0
    XBAR(K+2)=0.10
    SV(K+1)=50.00
    SV(K+2)=50.00
    ASHEAR(K+1)=50.00
    ASHEAR(K+2)=50.00
    CALL AXIS  (0.,0.,33HSHEAR STRESS/UNIT LOAD TAU(X) PSI,33,6.,90.,
   2SV(K+1),SV(K+2))                                                       114
    CALL AXIS (0.,0.,29HRELATIVE JOINT POSITION (X/L),-29,10.,0.,
   2XBAR(K+1),XBAR(K+2))                                                   118
    CALL AXIS (10.,0.,1H ,-1,6,0.90,,SV(K+1),SV(K+2))                      122
    CALL LINE (XBAR,SV,K,1,1,4)                                            124
    ASHEAR(K+1)=SV(K+1)
    ASHEAR(K+2)=SV(K+2)
    CALL LINE (XBAR,ASHEAR,K,1,0)                                          130
    CALL SYMBOL (11.5,4.5,.15,8HCASE NO.,0.,8)                             132
    CALL NUMBER (12.75,4.5,.15,FNC,0.,-1)                                  134
    CALL SYMBOL (11.,.4,,.13,15,0.,-1)                                     136
    CALL SYMBOL (11.5,4.,,13,18HAVER. SHEAR STRESS,0.,18)                  138
    CALL SYMBOL (11.,3.5,.13,4,0.,-1)                                      140
    CALL SYMBOL (11.5,3.5,.13,12HSHEAR STRESS,0.,12)                       142
    CALL SYMBOL (11.5,3.,,13,18HSHEAR STRESS CONC.,0.,18)                  144
    CALL SYMBOL (11.,.3,,.13,0.0,,-1)                                      146
    CALL PLOT (0.,.3,,-3)                                                  148
    SCON(K+1)=0.00
    SCON(K+2)=1.00
    CALL AXIS (-.75,0.,27HSTRESS CONCENTRATION FACTOR, 27,3.,90.,SCON(
   2K+1),SCON(K+2))                                                        154
    CALL LINE (XBAR,SCON,K,1,1,0)                                          156
    CALL PLOT (15.0,-4.0,-3)                                               158
    GO TO 3
    END
```

Table 3.4

SAMPLE PROBLEM OUTPUT - VOLKERSEN ANALYSIS

CASE NUMBER 1 VOLKERSEN ANALYSIS

ADHERENT PROPERTIES
T1 = 0.064 IN. T2 = 0.064 IN. W = 1.000 IN. L = 0.500 IN.

ADHESIVE PROPERTIES
TA = 0.005 IN. GA = 50000. PSI E = 10.60E 06 PSI

APPLIED LOAD P = 64. LB.

AVERAGE SHEAR STRESS TAU = 128.0000PSI

STA. NO.	JOINT POSITION (IN.)	RELATIVE POSITION	SHEAR STRESS (PSI)	SHEAR CONCENTRATION
1	X = 0.0000	X BAR = 0.00	TAU = 0.1984E 03	N = 1.550
2	X = 0.0250	X BAR = 0.05	TAU = 0.1766E 03	N = 1.379
3	X = 0.0500	X BAR = 0.10	TAU = 0.1580E 03	N = 1.234
4	X = 0.0750	X BAR = 0.15	TAU = 0.1423E 03	N = 1.112
5	X = 0.1000	X BAR = 0.20	TAU = 0.1293E 03	N = 1.010
6	X = 0.1250	X BAR = 0.25	TAU = 0.1187E 03	N = 0.927
7	X = 0.1500	X BAR = 0.30	TAU = 0.1102E 03	N = 0.861
8	X = 0.1750	X BAR = 0.35	TAU = 0.1038E 03	N = 0.811
9	X = 0.2000	X BAR = 0.40	TAU = 0.9931E 02	N = 0.776
10	X = 0.2250	X BAR = 0.45	TAU = 0.9664E 02	N = 0.755
11	X = 0.2500	X BAR = 0.50	TAU = 0.9576E 02	N = 0.748
12	X = 0.2750	X BAR = 0.55	TAU = 0.9664E 02	N = 0.755
13	X = 0.3000	X BAR = 0.60	TAU = 0.9931E 02	N = 0.776
14	X = 0.3250	X BAR = 0.65	TAU = 0.1038E 03	N = 0.811
15	X = 0.3500	X BAR = 0.70	TAU = 0.1102E 03	N = 0.861
16	X = 0.3750	X BAR = 0.75	TAU = 0.1187E 03	N = 0.927
17	X = 0.4000	X BAR = 0.80	TAU = 0.1293E 03	N = 1.010
18	X = 0.4250	X BAR = 0.85	TAU = 0.1423E 03	N = 1.112
19	X = 0.4500	X BAR = 0.90	TAU = 0.1580E 03	N = 1.234
20	X = 0.4750	X BAR = 0.95	TAU = 0.1766E 03	N = 1.379
21	X = 0.5000	X BAR = 1.00	TAU = 0.1984E 03	N = 1.550

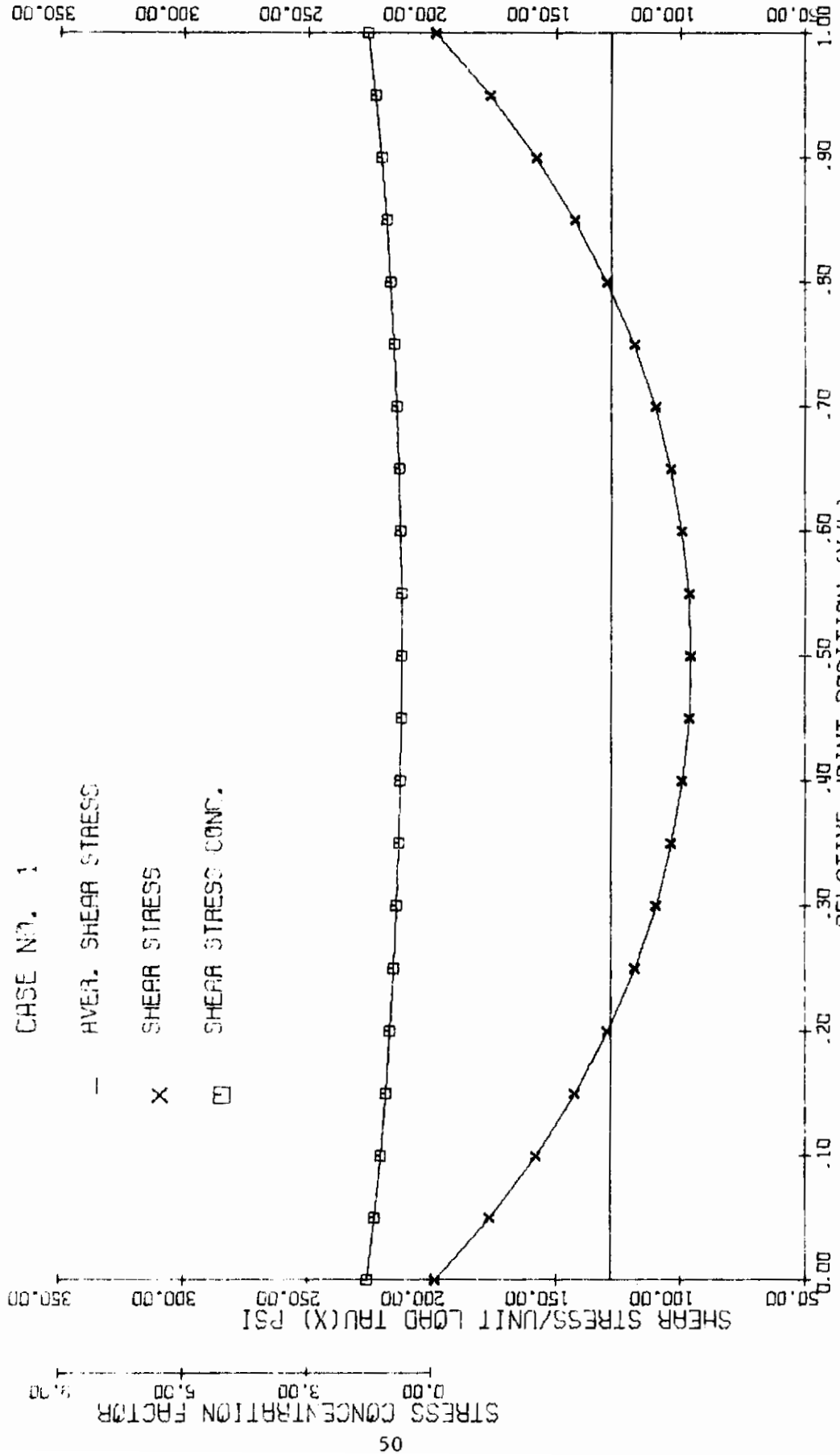

Fig. 3.1 SAMPLE PROBLEM OUTPUT - VOLKERSEN ANALYSIS

Table 3.5

SUMMARY OF JOINTS FOR ANALYZED VOLKERSEN METHOD, LOAD = 1.0 LB., WIDTH = 1.0 IN.

Identification	Adherend t_1 (in.)	Adherend t_2 (in.)	Length of Overlap L (in.)	Adherend Modulus $10^6 E$ psi	Adhesive Thickness (in.)	Adhesive Modulus (psi)	Maximum Shear Stress (psi)	Shear Stress Concentration
1 - 1	0.032	0.032	0.8	10.60	0.005	1,000	1.32	1.05
1 - 2						5,000	1.62	1.29
1 - 3						50,000	3.85	3.08
1 - 4						150,000	6.65	3.34
3 - 1	0.032	0.032	0.8	10.60	0.005	50,000	3.85	3.08
3 - 2					0.010		2.78	2.22
3 - 3					0.025		1.95	1.56
3 - 4					0.050		1.62	1.29
3 - 5					0.100		1.44	1.15
4 - 1	0.064	0.064	0.5	10.60	0.005	50,000	3.10	1.55
4 - 2			1.0				2.74	2.74
4 - 3			1.5				2.71	4.11
4 - 4			2.0				2.71	5.42
4 - 5			2.5				2.71	6.78
4 - 6			3.0				2.71	8.13
5 - 1	0.020	0.020	0.5	10.60	0.005	50,000	4.93	2.46
5 - 2	0.032	0.032	0.8				3.87	3.10
5 - 3	0.064	0.064	1.60				2.72	4.35
5 - 4	0.081	0.081	2.02				2.41	4.88
5 - 5	0.125	0.125	3.12				1.94	6.03
5 - 6	0.250	0.250	6.25				1.37	8.56

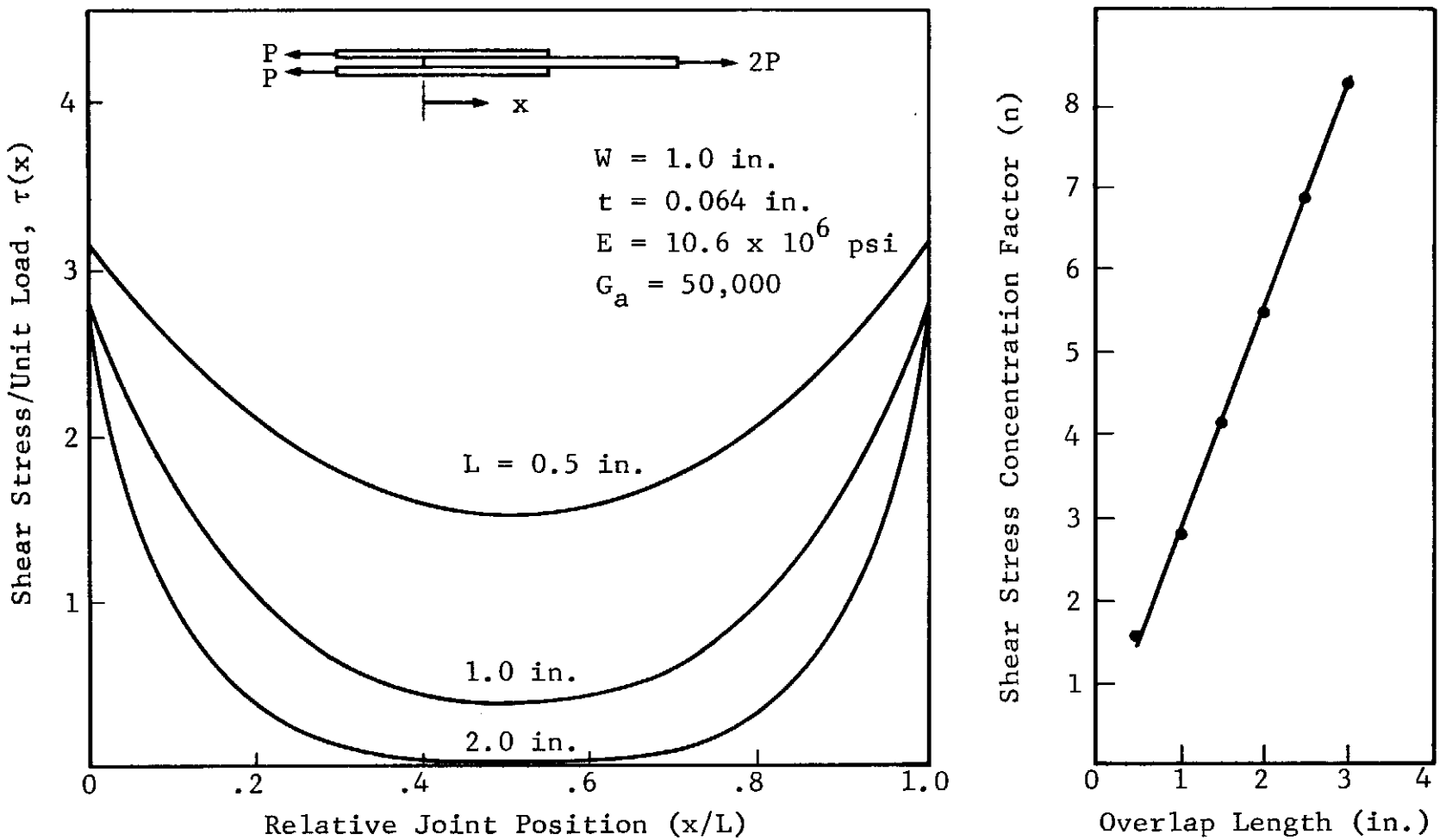

Fig. 3.2 SHEAR STRESS AND STRESS CONCENTRATION AS A FUNCTION OF LENGTH OF OVERLAP

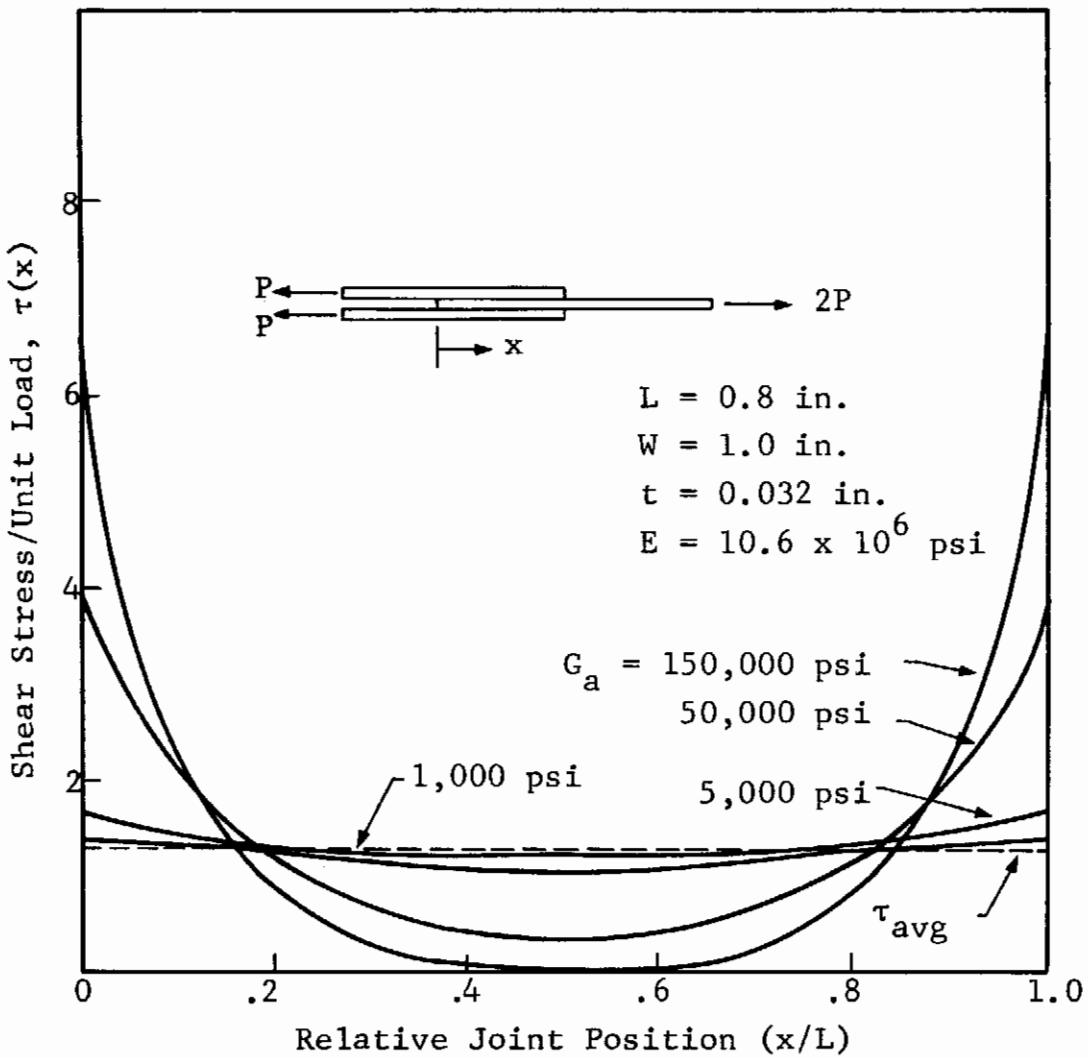

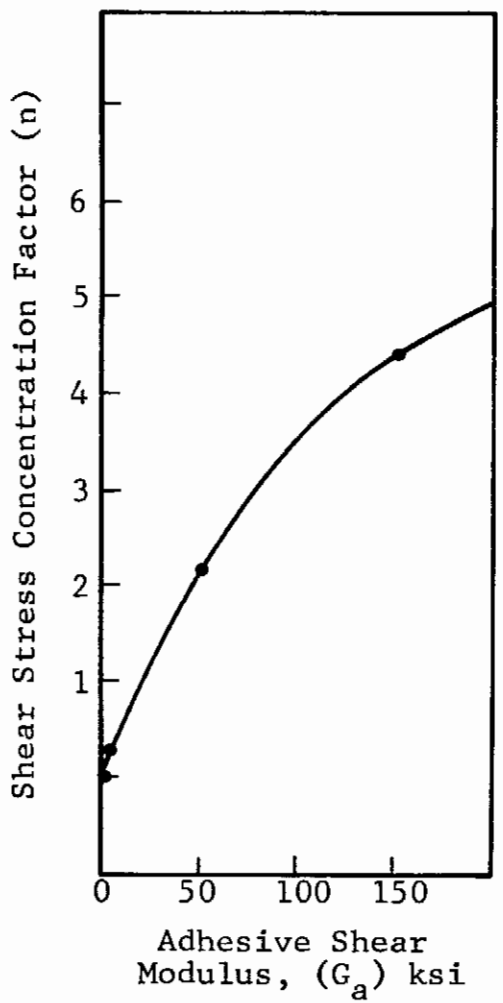

Fig. 3.3 SHEAR STRESS AND STRESS CONCENTRATION AS A FUNCTION OF SHEAR MODULUS

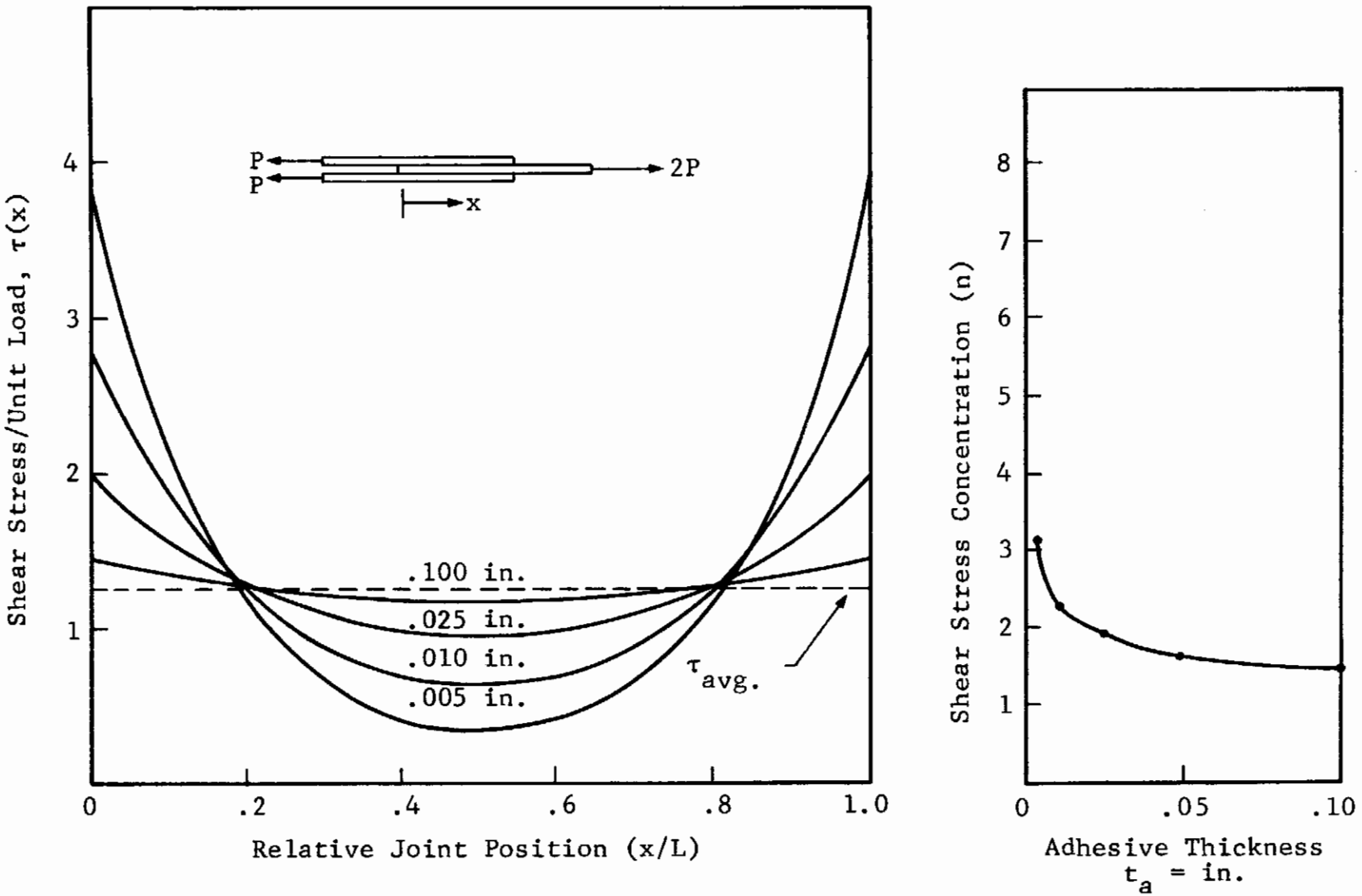

Fig. 3.4 SHEAR STRESS AND STRESS CONCENTRATION AS A FUNCTION OF ADHESIVE THICKNESS

3.3 ANALYSIS OF THE UNSUPPORTED LAP JOINT

The analysis of the unsupported lap type joint was carried out by Goland and Reissner (3.3) and expressions were developed for both the shear stress distribution and the normal stress (peeling stress) distribution in the adhesive. Their analysis assumes equal thickness adherends, elastic behavior of all the materials, and is further restricted to joints for which the following ratios are satisfied:

$$\frac{t}{E} \geq \frac{1}{10} \frac{t_a}{E_a} \qquad \text{or} \qquad \frac{t}{G} \geq \frac{1}{10} \frac{t}{G_a}$$

In the original paper by Goland and Reissner, a mistake was made in deriving the expressions for the normal stress distribution. Kuenzi (3.4) in his work has rederived the expression and algebraically simplified the results. The corrected expression is used in this study.

3.3.1 Analysis and Sample Calculation

The supported joint is represented schematically as shown below.

Table 3.6 gives the definition of variables and their range of values used to format the computer program.

Table 3.6

DEFINITION OF SYMBOLS AND RANGE OF VARIABLES

Symbol	Variable	Typical Value	Range of Values
P	Applied Load	1 lb	1 → 9,999 lb
w	Joint Width	1 in.	0.250 → 10.00 in.
L	Length of Overlap	0.500 in.	0.125 → 10.00 in.
t_a	Adhesive Thickness	0.010 in.	0.005 → 0.10 in.
t	Adherend Thickness	0.064 in.	0.020 → 1.00 in.
G_a	Shear Modulus - Adhesive	50,000	500 → 100,000 psi
E	Young's Modulus - Adherend	10.5×10^6	3.1×10^6 → 60×10^6 psi
ν	Poisson's Ratio	0.30	0.10 → 0.50
x	Distance from Center of Joint	0.1 L	0.01 → 0.1 L

3.3.1.1 Shear Stress Distribution

The shear stress in the adhesive as a function of position in the joint (x) is given as follows.

$$\tau(x) = \frac{P}{wL4}\left[\frac{\beta L}{2t}(1 + 3K)\frac{\cosh \beta x/t}{\sinh \beta L/2t} + 3(1-K)\right]$$

where

$$K = 1/\left[1 + 2\sqrt{2}\tanh\left[\frac{L}{2t}\left(\frac{3\lambda P}{2Etw}\right)^{1/2}\right]\right]$$

$$\beta = \left[\frac{8G_{at}}{E\,t_a}\right]^{1/2} \qquad \lambda = 1 - \nu^2$$

Note that in this case the load (P) is not explicitly factorable since it appears in the expression for (K). Therefore even though the sample computation is carried out for a unit load (P), the stress at any other load is not directly proportional to the stress at unit load.

Using the typical values from Table 3.6, the stress is calculated for (x = 0) the center of the joint.

$$\frac{P}{wL4} = \frac{1}{1(.5)4} = .5$$

$$\lambda = 1 - \nu^2 = 1 - (.3)^2 = .91$$

$$\beta = \left[\frac{8\ G_a\ t}{Et_a}\right]^{1/2}$$

$$= \left[\frac{8\ (5)\ 10^4\ (.064)}{(10.5)\ 10^6\ (.010)}\right]^{1/2} = \left[\frac{8(6.4)}{210}\right]^{1/2} = .244^{1/2}$$

$$= .494$$

$$\cosh \frac{\beta x}{t} = \cosh \frac{(.494)(0)}{.064} = 1$$

$$\sinh \frac{\beta L}{2t} = \sinh \frac{(.494).5}{2\ (.064)} = \sinh 1.93$$

$$= \frac{e^{1.93} - e^{-1.93}}{2} = \frac{6.90 - 1.45}{2} = 3.377$$

$$\left(\frac{3\lambda P}{2Etw}\right)^{1/2} = \left(\frac{1.5(.91)1}{(10.5)10^6(.064)1}\right)^{1/2} = \left((2.31)10^{-6}\right)^{1/2} = (1.52)10^{-3}$$

$$\tan \frac{L}{2t}\left(\frac{3\lambda P}{2Etw}\right)^{1/2} = \tanh \frac{.5}{2(.064)}\ (1.52)10^{-3} = \tanh\ (5.94)10^{-3}$$

$$= .00594$$

$$\left(\tanh\ (x) \quad x \approx \text{ for small } (x)\right)$$

$$K = 1/\left[1 + 2\ 2\ \ (.00594)\right] = .985$$

$$\tau\ (x=0) = .5\ \frac{.494(.5)}{2\ (.064)}\ \ 1 + 3(.985)\ \ \frac{1}{3.377} +$$

$$3(1.985) = 1.153 \text{ psi}$$

Stress concentration Facton $n = \dfrac{\tau(x)}{\tau_{avg}}$

$$n = \frac{\tau(x)}{P/wL} = \frac{1.153}{2} = .576$$

The maximum shear stress occurs at the end of the overlap or (x = L/2) for this analysis.

Using the same procedure:

$x = L/2 \quad \tau(x) = 3.987 \text{ psi} \quad n = 1.993$

When the Volkersen analysis was used for the same joint, the maximum shear stress was slightly lower.

$\tau(x) = 2.58 \quad n = 1.29$

3.3.1.2 Normal Stress Distribution

The normal stress distribution in the adhesive is given in the corrected form by Kuenzi as follows:

$$\sigma(x) = \frac{P\gamma K}{wt\,\Delta}\left[\left[R_2\gamma - 2\sqrt{2}\,\alpha\cosh\lambda\cos\lambda\right]\left[\cosh\frac{\gamma x}{t}\cos\frac{\gamma x}{t}\right] + \left[R_1\gamma - 2\sqrt{2}\,\alpha\sinh\lambda\sin\lambda\right]\left[\sinh\frac{\gamma x}{t}\sin\frac{\gamma x}{t}\right]\right]$$

where;

$$\gamma = \left[\frac{6\,E_\alpha\,t}{E\,t_a}\right]^{1/4} \qquad \alpha = \left[\frac{3}{2}(1-\nu^2)\frac{P}{twE}\right]^{1/2}$$

$$\lambda = \frac{\gamma L}{2t} \qquad K = 1/\left(1 + 2\sqrt{2}\tanh\frac{L\gamma}{2t}\right)$$

$$\Delta = \sinh 2\lambda + \sin 2\lambda$$

$$R_1 = \cosh\lambda\sin\lambda + \sinh\lambda\cos\lambda$$

$$R_2 = \sinh\lambda\cos\lambda - \cosh\lambda\sin\lambda$$

Using the typical values given in Table 3.6 the sample calculation is carried out for $x = .25L$

The analysis assumes that,

$$\frac{t}{E} \leq \frac{1}{10} \quad \frac{t_a}{E_a}$$

$$\frac{.064}{10.5 \times 10^6} \leq \frac{1}{10} \cdot \frac{.010}{1.4 \times 10^5}$$

$6.1 \times 10^{-9} \leq 7.1 \times 10^{-8}$ $\therefore$ assumption is satisfied.

$$\gamma = \left[\frac{6 E_a t}{E t_a} \right]^{1/4}$$

$$= \left[\frac{6 (1.4) 10^5 (.064)}{(10.5) 10^6 (.010)} \right]^{1/4} = .846$$

$$\alpha = \left[3/2 (1-\nu^2) \frac{P}{twE} \right]^{1/2}$$

$$= \left[1.5 (1 - .09) \frac{1}{(.604) 1 (10.5) 10^6} \right]^{1/2} = .00142$$

$$\lambda = \frac{\gamma L}{2t}$$

$$= \frac{.846(.5)}{2 (.064)} = 3.31$$

$$K = {}^{1}\!/\!_{1 + 2\sqrt{2} \tanh \frac{L\alpha}{2t}} \qquad \frac{L\alpha}{2t} = \frac{.5(.00142)}{2(.064)}$$

$$= {}^{1}\!/\!_{1 + 2\sqrt{2} \tanh(.0056)} = .00555$$

$$\tanh x \approx x \qquad x << 1$$

$$\therefore \quad K = \frac{1}{1.0157} = .985$$

$$\Delta = \sinh 2\lambda + \sin 2\lambda$$

$$\sinh 2(3.31) = \frac{e^{6.62} - e^{-6.62}}{2} = \frac{650 - \sim 0}{2} = 325$$

$$\sin 2\lambda = \sin\left[\frac{2(3.31)}{2\pi} \times 360°\right] = \sin 19° = .325$$

$$\Delta = 325 + .325 = 325.325$$

$$R_1 = \cosh \lambda \sin \lambda + \sinh \lambda \cos \lambda$$

$$\cosh \lambda = \frac{e^{3.31} + e^{-3.31}}{2} = \frac{27.4 + .0462}{2} = 13.77$$

$$\sinh \lambda = \frac{e^{3.31} - e^{-3.31}}{2} = \frac{27.5 - .0462}{2} = 13.68$$

$$\sin \lambda = \sin\left[\frac{3.31}{2\pi} \times 360°\right] = -\sin 9.6° = -.1668$$

$$\cos \lambda = \cos\left[\frac{3.31}{2\pi} \times 360°\right] = -\cos 9.6° = -.9860$$

$$R_1 = 13.77\ (-.1668) + 13.68\ (-.9860)$$

$$= -2.295 - 13.50 = -15.795$$

$$R_2 = \sinh \lambda \cos \lambda - \cosh \lambda \sin \lambda$$

$$= 13.68(-.986) - 13.77(-.1668)$$

$$= -13.50 + 2.295 = -11.205$$

$$\sinh \frac{\gamma x}{t} = \sinh \frac{.846(.125)}{.064}$$

$$= \sinh 1.652 = \frac{e^{1.652} - e^{-1.652}}{2} = \frac{5.23-.192}{2} = 2.519$$

$$\cosh \frac{\gamma x}{t} = \frac{e^{1.652} + e^{-1.652}}{2}$$

$$= \frac{5.23 + .192}{2} = 2.711$$

$$\sin \frac{\gamma x}{t} = \sin \left[\frac{1.652}{2\pi} \times 360°\right]$$

$$= \sin 95° = + \sin 85° = .995$$

$$\cos\frac{\gamma x}{t} = \cos 95° = -\sin 5° = -.0872$$

$$\sigma(x) = \frac{1(.846).985}{1(.064)325}\Big[\Big[-11.205(.846) - 2\sqrt{2}(13.77)\cdot (-.9860)\Big]\cdot\Big[2.711(-.0872)\Big] + \Big[(-15.795)(.846) - 2\sqrt{2}\cdot (.00142)\ 13.68\ (-.1668)\Big]\cdot\Big[2.52(.995)\Big]\Big] = 11.05 \text{ psi}$$

3.3.2 Computer Program

The following program for computing the shear stress and normal stress distribution is written in Fortran IV. The program can be used to compute $\tau(x)$ and $\sigma(x)$ for specific values of (x) or by having the program generate increment values of (x). This option is controlled by statement 142, depending on the value of assigned to (S) in statement 107. For $S \geq 0$ the program conputes the number (K) of (x) values read in at statement 140, for S = 0 the desired values of (x) must be read in individually.

This program also contains the option for graphical output which requires the use of a Calcomp plotter. A program listing is given in Table 3.7.

The capability of the program was illustrated by using it to analyze the two lap joints discussed by Kuenzi (3.4). Both joints have identical geometry and load but one uses an adhesive with a shear modulus of 180,000 psi, the other a shear modulus of 1,530 psi. The data output for these joints are shown in Tables 3.8 and 3.9, and the stress distributions obtained with a Cal-Comp Plotter are shown in Figs. 3.5 and 3.6.

The data for these joints have been given here because the work by Kuenzi (3.4) is well known in the industry and it is felt that the actual data points would be an aid to anyone wishing to use the Goland and Reissner analysis. These data are the same results obtained by Kuenzi.

Table 3.7

PROGRAM LISTING FOR THE GOLAND AND REISSNER ANALYSIS

```
       SCOPLT                                                          04/10/67
          MAIN       -  EFN   SOURCE STATEMENT  -  IFN(S)  -

C       GOLAND - REISSNER ANALYSIS
      DIMENSION SY(200),SN(200),XBAR(200),X(200),SCON(200),ASHEAR(200)
      DIMENSION DATA(476)
      CALL PLOTS (DATA,476,16)                                                  2
  101 I = 0
 1011 EOC=0
  102 I = I + 1
C       ADHERENT PROPERTIES
  103 READ (5,104) T, W, OL, E, AMU                                             6
  104 FORMAT (2X,3F6.3,1PE10.2,0PF5.2)
      IF(T.EQ.999.) GO TO 301
C       ADHESIVE PROPERTIES
  105 READ (5,106) TA, GA, EA                                                  10
  106 FORMAT (2X,F6.3,F8.0,E10.2)
C       APPLIED LOAD
  107 READ (5,108) P,S                                                         11
  108 FORMAT (2X,F8.2,F4.1)
  110 WRITE (6,111) I                                                          12
  111 FORMAT (13H1 CASE NUMBER,I3,6X,27H GOLAND - REISSNER ANALYSIS)
  112 WRITE (6,113)                                                            13
  113 FORMAT (21HO ADHERENT PROPERTIES)
  114 WRITE (6,115) T, W, OL, E, AMU                                           14
  115 FORMAT (2X,5H T = ,F6.3,9X,5H W = ,F7.3,9X,5H L = ,F7.3,9X,
     1 5H E = ,2PE10.2,6X,3HMU=,0PF6.2)
  116 WRITE (6,117)                                                            15
  117 FORMAT (21HO ADHESIVE PROPERTIES)
  118 WRITE (6,119) TA, GA , EA                                                16
  119 FORMAT (2X,6H TA = ,F6.3,9X,6H GA = ,F8.0,9X,6H EA = ,2PE10.2///)
  120 WRITE (6,121) P                                                          17
  121 FORMAT (19HO APPLIED LOAD P = ,F6.0)
  122 AVESH=P/(W*OL)
  123 WRITE(6,124)AVESH                                                        19
  124 FORMAT(28HO AVERAGE SHEAR STRESS TAU =,  F8.2,3H PSI///)
C       SHEAR   STRESS  COMPUTATION
  130 DO 136 J = 1,200,1
  131 X(J) = 0.0
  132 SY(J) = 0.0
  133 SN(J) = 0.0
  134  XBAR (J) =  0.0
  135  SCON (J) =  0.0
  136 ASHEAR(J)=AVESH
  140 READ (5,141) K                                                           38
  141 FORMAT (I4)
  142 IF (S) 150,150,143
  143 AK = K
  144 BK = K - 1
  145 DELX = OL /(2. * BK )
  146 DO 147 L = 2,K,1
  147 X(L) = X(L-1) + DELX
  148 GO TO 160
  150 READ (5,151) ( X(J), J = 1,K)                                            55
  151 FORMAT (10F7.3)
  160 BE = ((8.0 * GA * T) / (E *TA))**0.5                                     63
  161 AL = 1.0 - (AMU*AMU)
  162 D1 = (OL/(2.0*T)) * ((1.5*AL*P/(E*T*W))**0.5)                            66
```

Table 3.7 (contd)

PROGRAM LISTING FOR THE GOLAND AND REISSNER ANALYSIS

```
      SCOPE 7                                                          04/10/67
          MAIN       - EFN   SOURCE STATEMENT  -  IFN(S)  -

  163 TANHE= ((EXP(D1) - (1.0/EXP(D1)))/(EXP(D1) + (1.0/EXP(D1))))                  68
  164 DK = 1.0 / (1.0 + ((8.0**0.5)*(TANHE)))                                       70
  165 EB = (0.5*BE*DL) / T
  166 F1 = (1.0 + (3.0*DK))
  167 F2 = 3.0 * (1.0 - DK)
  168 SINHE= 0.5 * (EXP(EB) - (1.0/EXP(EB)))                                        75
  169  DO 175  J  = 1,K
 1169  XBAR (J)= X(J)/DL
  170 Y = X(J)
  171 G1 = BE * Y / T
  172 COSHE= 0.5 * (EXP(G1) + (1.0/EXP(G1)))                                        87
  173 G2 = (BE * F1 * COSHE) / SINHE
  174 SY(J) = ((0.25 * P)/(W * DL)) * (G2 + F2)
  175  SCON(J) = SY(J) / AVESH
C      NORMAL  STRESS  COMPUTATION
       GAMMA = ((6.*EA*T) / (E*TA))** 0.25                          JOIN0010    96
       ALAMBD = GAMMA * DL / (2.*T)                                 JOIN0020
       ARG3   = 2.* ALAMBD                                          JOIN0025
       DELTA  = SINH(ARG3) + SIN(ARG3)                              JOIN0030    97    98
       R1     = COSH(ALAMBD) * SIN(ALAMBD) + SINH(ALAMBD) * COS(ALAMBD)  JOIN0040  99   100   101   102
       R2     = SINH(ALAMBD) * COS(ALAMBD) - COSH(ALAMBD) * SIN(ALAMBD)  JOIN0050  103  104   105   106
       ALPHA  = ((1.5*(1.-AMU*AMU)* P) /(T * W * E))**0.5          JOIN0060    107
       ARG1   = (DL* ALPHA)/(2.* T)                                 JOIN0070
       CONSTK = 1. / (1.+ (2.* 2.**.5) * TANH(ARG1))                JOIN0080    108   109
       S1     = COSH(ALAMBD) * COS(ALAMBD)                          JOIN0090    110   111
       S2     = SINH(ALAMBD) * SIN(ALAMBD)                          JOIN0100    112   113
       TERM1  = P * GAMMA * CONSTK / (W * T * DELTA)                JOIN0110
       TERM2  = R2 * GAMMA - 2.*2.**0.5 * ALPHA* S1                 JOIN0120    114
       TERM4  = R1 * GAMMA - 2.*2.**0.5 * ALPHA* S2                 JOIN0130    115
       DO 208  J=1,K                                                JOIN0140
       ARG2   = GAMMA* X(J) / T                                     JOIN0150
       TERM3  = COSH(ARG2) * COS(ARG2)                              JOIN0160    120   121
       TERM5  = SINH(ARG2) * SIN(ARG2)                              JOIN0170    122   123
  208  SN(J)  = TERM1*(( TERM2 * TERM3) + (TERM4 * TERM5))          JOIN0180
  215 WRITE(6,220)                                                             128
  220 FORMAT(2X,4HSTA.,5X,5HJOINT,11X,8HRELATIVE,14X,5HSHEAR,22X,
     15HSHEAR,19X,6HNORMAL / 2X,3HNO.,5X,8HPOSITION,9X,8HPOSITION,
     114X,6HSTRESS,17X,13HCONCENTRATION,15X,6HSTRESS / 11X,5H(IN.),
     134X,5H(PSI),45X,5H(PSI)//)
  212 WRITE(6,213) (J,X(J),XBAR(J),SY(J),SCON(J),SN(J),J= 1,K)                 129
  213 FORMAT (2X,I2,4X,4H X =,0PF8.4,6X,8HX BAR = ,F5.2,8X,6HTAU = ,
     1 1PE12.4,9X,4HN = ,0PF7.3,8X,10HSIGMA N = ,1PE12.4)
      GO TO 102
  301 CALL PLOT (1.0,1.0,-3)                                                   142
      EOC=EOC+1.
      CALL SCALE(SY,6.0,K,1)                                                   144
      CALL SCALE(SN,6.0,K,1)                                                   146
      CALL SCALE (SCON,3.0,K,1)                                                148
      ASHEAR(K+1)=SY(K+1)
      ASHEAR(K+2)=SY(K+2)
      CALL SCALE(XBAR,5.0,K,1)                                                 154
      CALL AXIS (0.0,0.0,33HSHEAR STRESS/UNIT LOAD TAU(X) PSI,33,6.0,90.,
     2,SY(K+1),SY(K+2))                                                        158
      CALL AXIS (5.0,0.0,36HNORMAL STRESS/UNIT LOAD SIGMA(X) PSI,-36,6.0
     2,90.,SN(K+1),SN(K+2))                                                    162
      CALL AXIS (0.0,0.0,29HRELATIVE JOINT POSITION (X/L),-29,5.0,0.0,
```

Table 3.7 (contd)

PROGRAM LISTING FOR THE GOLAND AND REISSNER ANALYSIS

```
  SCDPLT                                                          04/10/67
      MAIN        -  EFN    SOURCE STATEMENT  -  IFN(S)  -

2 XBAR(K+1),XBAR(K+2))                                                    166
 CALL AXIS (5.75,3.0,20HSTRESS CONCENTRATION,-20,3.0,90.,SCON(K+1),
2SCON(K+2))                                                               170
 CALL LINE (XBAR,SY,K,1,1,4)                                              172
 CALL LINE (XBAR,SN,K,1,1,2)                                              174
 CALL LINE (XBAR,ASHEAR,K,1,0)                                            176
 CALL SYMBOL (6.5,4.,.13,15,0.,-1)                                        178
 CALL SYMBOL (6.5,3.5,.13,4,0.,-1)                                        180
 CALL SYMBOL (6.5,3.,.13,2,0.,-1)                                         182
 CALL SYMBOL (6.5,2.5,.13,0,0.,-1)                                        184
 CALL SYMBOL (7.,4.,.13,18HAVER. SHEAR STRESS,0.,18)                      186
 CALL SYMBOL (7.,3.5,.13,12HSHEAR STRESS,0.,12)                           188
 CALL SYMBOL (7.,3.,.13,13HNORMAL STRESS,0.,13)                           190
 CALL SYMBOL (7.,2.5,.13,18HSHEAR STRESS CONC.,0.,18)                     192
 CALL PLOT (0.,3.,-3)                                                     194
 CALL LINE (XBAR,SCON,K,1,1,0)                                            196
 CALL PLOT (15.0,-4.0,-3)                                                 198
 GO TO 103
 END
```

Table 3.8

STRESS ANALYSIS OF A LAP JOINT FROM KUENZI (3.4) - LOW MODULUS ADHESIVE

CASE NUMBER 1 GOLAND - REISSNER ANALYSIS

ADHERENT PROPERTIES
T = 0.064 w = 1.000 L = 0.500 E = 10.60E 06 MU= 0.33

ADHESIVE PROPERTIES
TA = 0.007 GA = 1530. EA = 52.00E 02

APPLIED LOAD P = 300.

AVERAGE SHEAR STRESS TAU = 600.00PSI

STA. NO.	JOINT POSITION (IN.)	RELATIVE POSITION	SHEAR STRESS (PSI)	SHEAR CONCENTRATION	NORMAL STRESS (PSI)
1	X = 0.0000	X BAR = 0.00	TAU = 5.8669E 02	N = 0.978	SIGMA N = -1.3151E 02
2	X = 0.0125	X BAR = 0.02	TAU = 5.8679E 02	N = 0.978	SIGMA N = -1.3083E 02
3	X = 0.0250	X BAR = 0.05	TAU = 5.8709E 02	N = 0.978	SIGMA N = -1.2878E 02
4	X = 0.0375	X BAR = 0.07	TAU = 5.8758E 02	N = 0.979	SIGMA N = -1.2532E 02
5	X = 0.0500	X BAR = 0.10	TAU = 5.8828E 02	N = 0.980	SIGMA N = -1.2041E 02
6	X = 0.0625	X BAR = 0.12	TAU = 5.8917E 02	N = 0.982	SIGMA N = -1.1397E 02
7	X = 0.0750	X BAR = 0.15	TAU = 5.9026E 02	N = 0.984	SIGMA N = -1.0593E 02
8	X = 0.0875	X BAR = 0.17	TAU = 5.9155E 02	N = 0.986	SIGMA N = -9.6155E 01
9	X = 0.1000	X BAR = 0.20	TAU = 5.9304E 02	N = 0.988	SIGMA N = -8.4540E 01
10	X = 0.1125	X BAR = 0.22	TAU = 5.9473E 02	N = 0.991	SIGMA N = -7.0942E 01
11	X = 0.1250	X BAR = 0.25	TAU = 5.9663E 02	N = 0.994	SIGMA N = -5.5209E 01
12	X = 0.1375	X BAR = 0.27	TAU = 5.9872E 02	N = 0.998	SIGMA N = -3.7178E 01
13	X = 0.1500	X BAR = 0.30	TAU = 6.0102E 02	N = 1.002	SIGMA N = -1.6677E 01
14	X = 0.1625	X BAR = 0.32	TAU = 6.0352E 02	N = 1.006	SIGMA N = 6.4701E 00
15	X = 0.1750	X BAR = 0.35	TAU = 6.0623E 02	N = 1.010	SIGMA N = 3.2444E 01
16	X = 0.1875	X BAR = 0.37	TAU = 6.0914E 02	N = 1.015	SIGMA N = 6.1423E 01
17	X = 0.2000	X BAR = 0.40	TAU = 6.1226E 02	N = 1.020	SIGMA N = 9.3581E 01
18	X = 0.2125	X BAR = 0.42	TAU = 6.1558E 02	N = 1.026	SIGMA N = 1.2908E 02
19	X = 0.2250	X BAR = 0.45	TAU = 6.1912E 02	N = 1.032	SIGMA N = 1.6807E 02
20	X = 0.2375	X BAR = 0.47	TAU = 6.2287E 02	N = 1.038	SIGMA N = 2.1069E 02
21	X = 0.2500	X BAR = 0.50	TAU = 6.2683E 02	N = 1.045	SIGMA N = 2.5702E 02

Table 3.9

STRESS ANALYSIS OF A LAP JOINT FROM KUENZI - HIGH MODULUS ADHESIVE

CASE NUMBER 2 GOLAND - REISSNER ANALYSIS

ADHERENT PROPERTIES

T = 0.064 W = 1.000 L = 0.500 E = 10.60E 06 MU= 0.33

ADHESIVE PROPERTIES

TA = 0.003 GA = 180000. EA = 50.00E 04

APPLIED LOAD P = 300.

AVERAGE SHEAR STRESS TAU = 600.00PSI

STA. NO.	JOINT POSITION (IN.)	RELATIVE POSITION	SHEAR STRESS (PSI)	SHEAR CONCENTRATION	NORMAL STRESS (PSI)
1	X = 0.0000	X BAR = 0.00	TAU = 1.0375E 02	N = 0.173	SIGMA N = 2.1964E 01
2	X = 0.0125	X BAR = 0.02	TAU = 1.0423E 02	N = 0.174	SIGMA N = 2.3490E 01
3	X = 0.0250	X BAR = 0.05	TAU = 1.0574E 02	N = 0.176	SIGMA N = 2.7672E 01
4	X = 0.0375	X BAR = 0.07	TAU = 1.0844E 02	N = 0.181	SIGMA N = 3.3275E 01
5	X = 0.0500	X BAR = 0.10	TAU = 1.1264E 02	N = 0.188	SIGMA N = 3.8082E 01
6	X = 0.0625	X BAR = 0.12	TAU = 1.1879E 02	N = 0.198	SIGMA N = 3.8710E 01
7	X = 0.0750	X BAR = 0.15	TAU = 1.2760E 02	N = 0.213	SIGMA N = 3.0465E 01
8	X = 0.0875	X BAR = 0.17	TAU = 1.4093E 02	N = 0.233	SIGMA N = 7.3414E 00
9	X = 0.1000	X BAR = 0.20	TAU = 1.5748E 02	N = 0.262	SIGMA N = -3.7648E 01
10	X = 0.1125	X BAR = 0.22	TAU = 1.8190E 02	N = 0.303	SIGMA N = -1.1162E 02
11	X = 0.1250	X BAR = 0.25	TAU = 2.1601E 02	N = 0.360	SIGMA N = -2.2020E 02
12	X = 0.1375	X BAR = 0.27	TAU = 2.6361E 02	N = 0.439	SIGMA N = -3.6489E 02
13	X = 0.1500	X BAR = 0.30	TAU = 3.3002E 02	N = 0.550	SIGMA N = -5.3924E 02
14	X = 0.1625	X BAR = 0.32	TAU = 4.2264E 02	N = 0.704	SIGMA N = -7.2379E 02
15	X = 0.1750	X BAR = 0.35	TAU = 5.5182E 02	N = 0.920	SIGMA N = -8.8008E 02
16	X = 0.1875	X BAR = 0.37	TAU = 7.3196E 02	N = 1.220	SIGMA N = -9.4439E 02
17	X = 0.2000	X BAR = 0.40	TAU = 9.8316E 02	N = 1.639	SIGMA N = -8.2258E 02
18	X = 0.2125	X BAR = 0.42	TAU = 1.3335E 03	N = 2.222	SIGMA N = -3.8842E 02
19	X = 0.2250	X BAR = 0.45	TAU = 1.8219E 03	N = 3.037	SIGMA N = 5.1139E 02
20	X = 0.2375	X BAR = 0.47	TAU = 2.5031E 03	N = 4.172	SIGMA N = 2.0411E 03
21	X = 0.2500	X BAR = 0.50	TAU = 3.4529E 03	N = 5.755	SIGMA N = 4.3432E 03

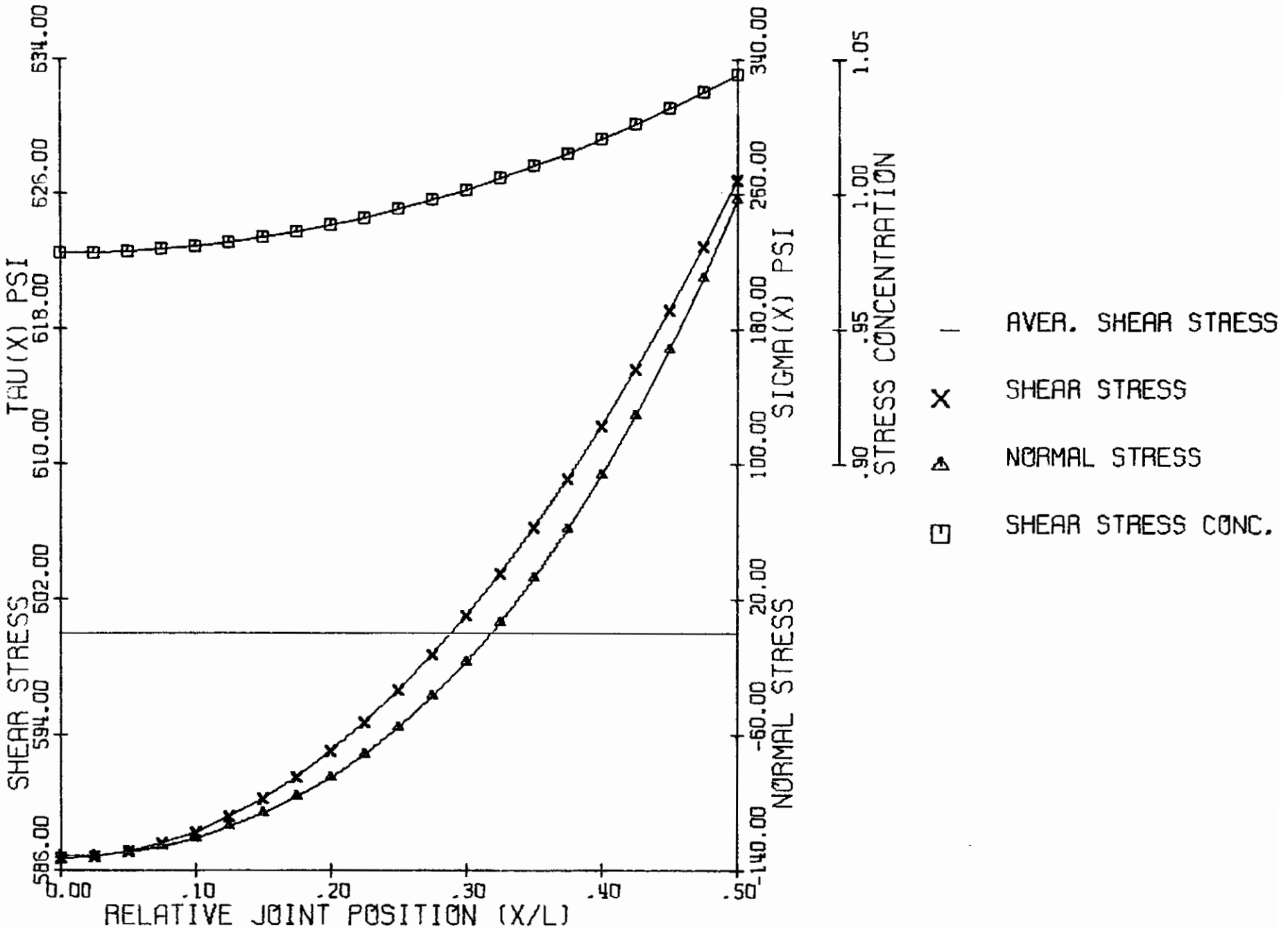

Fig. 3.5 STRESS DISTRIBUTION OF A LAP JOINT FROM KUENZI (3.4) - LOW MODULUS ADHESIVE

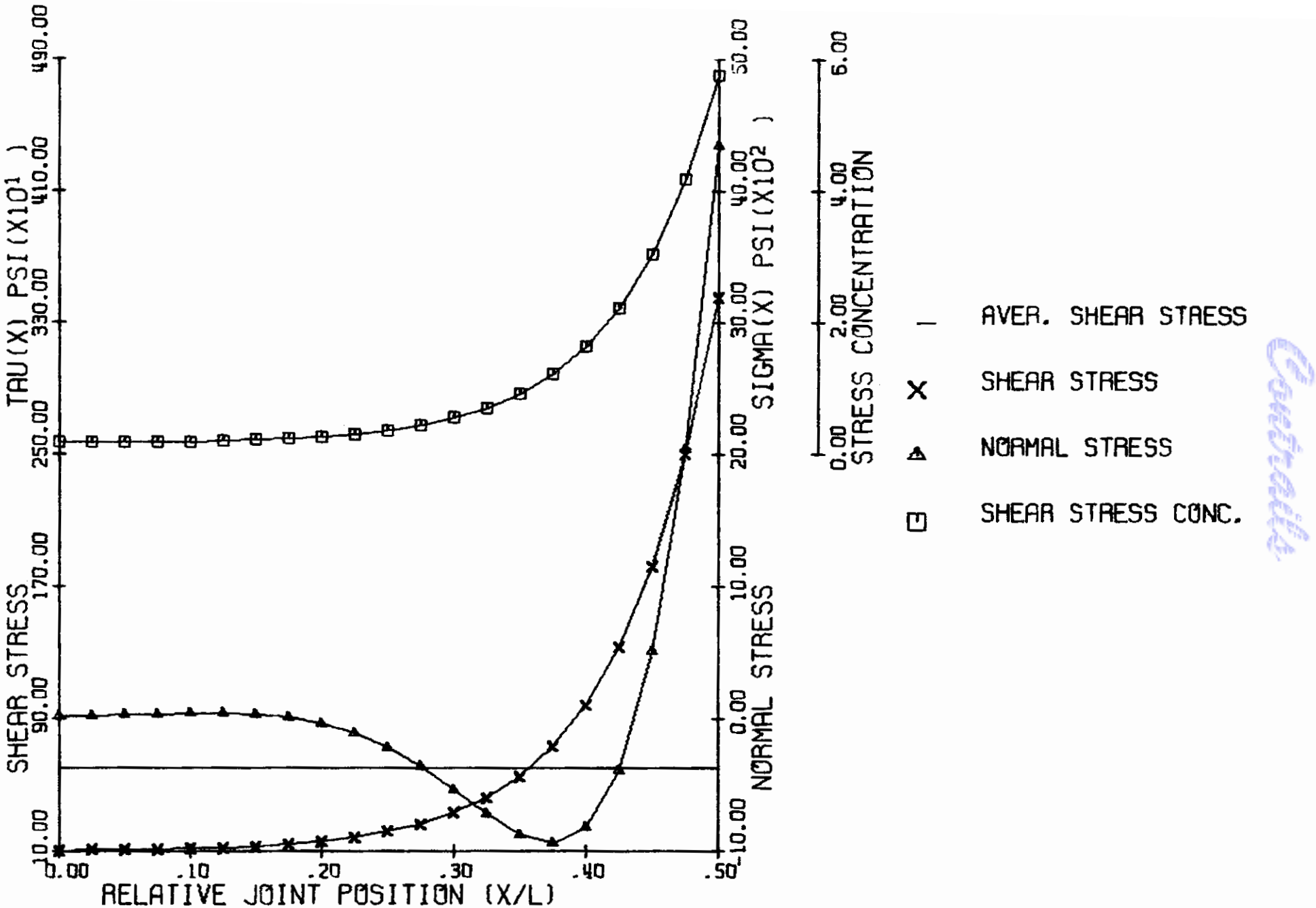

Fig. 3.6 STRESS DISTRIBUTION OF A LAP JOINT FROM KUENZI (3.4) - HIGH MODULUS ADHESIVE

References

3.1 Volkersen, O., "Die Nietkraftverteilung in Zugbeanspruchten Nietverbindungen mit Konstanten Laschenquerschnitten," Luftfahrtforshung 15, pp. 4.-47, 1938.

3.2 DeBruyne, H. A., "The Strength of Glued Joints," Aircraft Engineering 16, pp. 115-118, 1944.

3.3 Goland, M. and Reissner, E., "Stresses in Cemented Joints," J. Applied Mechanics (ASME), 11, pp. A17-A27, 1944.

3.4 Kuenzi, E. and Stevens, G. H., "Determination of Mechanical Properties of Adhesives for Use in the Design of Bonded Joints," US-FPL Res. Note FPL-011.

3.3.3 Parametric Studies

A series of forty joints were analyzed to study the variation of joint and material parameters on the maximum shear and normal (peel) stresses in the joint. The basic joint analyzed was a single lap one inch overlap of two composite adherends 0.050 in. thick, bonded with a medium stiffness adhesive in a film thickness of 0.005 in. The variations on this joint were load, joint width, length of overlap, adhesive film thickness, adherend thickness, adhesive modulus and adherend modulus. The joints and the results for maximum stresses are summarized in Table 3.10 and plotted graphically in Figs. 3.7 through 3.13.

3.3.3.1 Applied Load

The effect of applied load on the predicted stress per unit load is shown in Fig. 3.7. It was pointed out earlier that load is not explicitly factorable from the functions for shear and normal stress. If it was factorable the stress per unit load would remain constant with applied load rather than decreasing by a factor of two over the range from zero to 400 lb as is shown in Fig. 3.7. This means that if one develops a predictive scheme based on this analysis, joints involving maximum loads less than 400 lb should be treated individually rather than on a unit load basis.

The remainder of the parametric studies to be discussed are all based on a unit load applied to each joint. The predicted stresses can be corrected for larger applied loads simply by interpolating from Fig. 3.7.

3.3.3.2 Joint Width

It is usually assumed in bonded joints that joint strength is directly proportional to joint width and that wider joints can be scaled directly from one in. wide specimens. The analytical prediction for width scaling is shown in Fig. 3.8, which shows the stresses to decrease with increasing width. This effect continues up to widths of 4.0 in. beyond which the

Table 3.10
SUMMARY OF PARAMETRIC STUDIES - GOLAND AND REISSNER ANALYSIS

Case No.	Load (in.)	Joint Width (in.)	Adherend Thickness (in.)	Adherend Modulus (10^6 psi)	Poisson's Ratio	Length of Overlap (in.)	Thickness (in.)	Shear Modulus (psi)	Tensile Modulus (psi)	Shear Stress (psi)	Shear Concentration	Peel Stress (psi)
1	1	1.0	0.05	5	0.40	1.00	0.005	150,000	420,000	14.84	14.8	21
2	10									136.7	13.7	184
3	100									1131	11.3	1323
4	1000									8608	8.6	7128
5	1	0.5	0.05	5	0.40	1.00	0.005	150,000	420,000	29.2	14.6	40.95
6		1.0								14.8	14.8	21.02
7		5.0								3.0	15.2	4.36
8		10.0								1.5	15.3	2.19
9	1	1.0	0.05	5	0.40	0.25	0.005	150,000	420,000	15.4	3.8	21.95
10						0.50				15.2	7.6	21.67
11						1.00				14.8	14.8	21.02
12						1.500				14.5	21.8	20.41
13						2.00				14.2	28.4	19.83
14						4.00				13.2	52.7	--
15						5.00				12.7	63.68	--
16	1	1.0	0.05	5	0.40	1.00	0.001	150,000	420,000	33.1	33.13	47.06
17							0.002			23.4	23.44	33.26
18							0.005			14.8	14.84	21.02
19							0.010			10.5	10.50	14.85
20							0.050			4.7	4.72	6.62
21	1	1.0	0.05	5	0.40	1.00	0.005	150,000	420,000	14.84	14.84	21.02
22			0.10							10.79	10.79	15.48
23			0.20							7.70	7.70	11.12
24			0.50							4.89	4.89	7.19
25	1	1.0	0.05	5	0.40	1.00	0.005	250,000	700,000	19.2	19.14	27.15
26								200,000	560,000	17.1	17.13	24.27
27								150,000	420,000	14.84	14.84	21.02
28								100,000	280,000	12.12	12.12	17.15
29								50,000	140,000	8.58	8.58	12.12
30								10,000	28,000	3.87	3.87	5.40
31								5,000	14,000	2.76	2.76	3.82
32								500	1,400	1.24	1.24	1.19
33	1	1.0	0.05	0.5	0.45	1.00	0.005	150,000	420,000	43.10	43.10	58.95
34				5	0.40					19.80	19.80	27.51
35				10	0.33					10.62	10.62	15.11
36				30	0.15					6.21	6.21	8.88
37				5	0.50					14.87	14.87	21.09
38				5	0.40					14.84	14.84	21.02
39				5	0.30					14.81	14.81	20.96
40				5	0.20					14.80	14.80	20.92

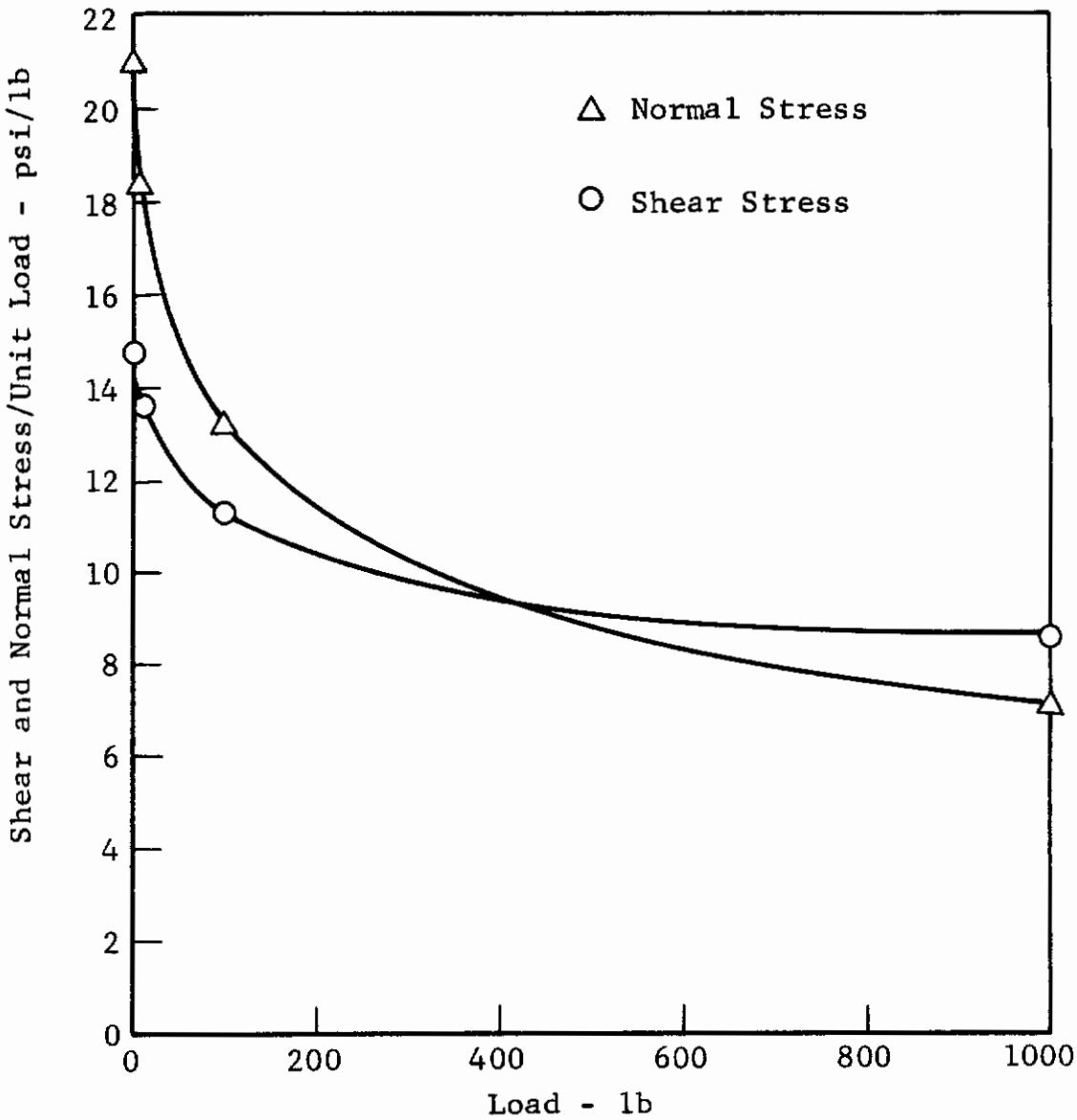

Fig. 3.7 JOINT STRESSES VS. APPLIED LOAD

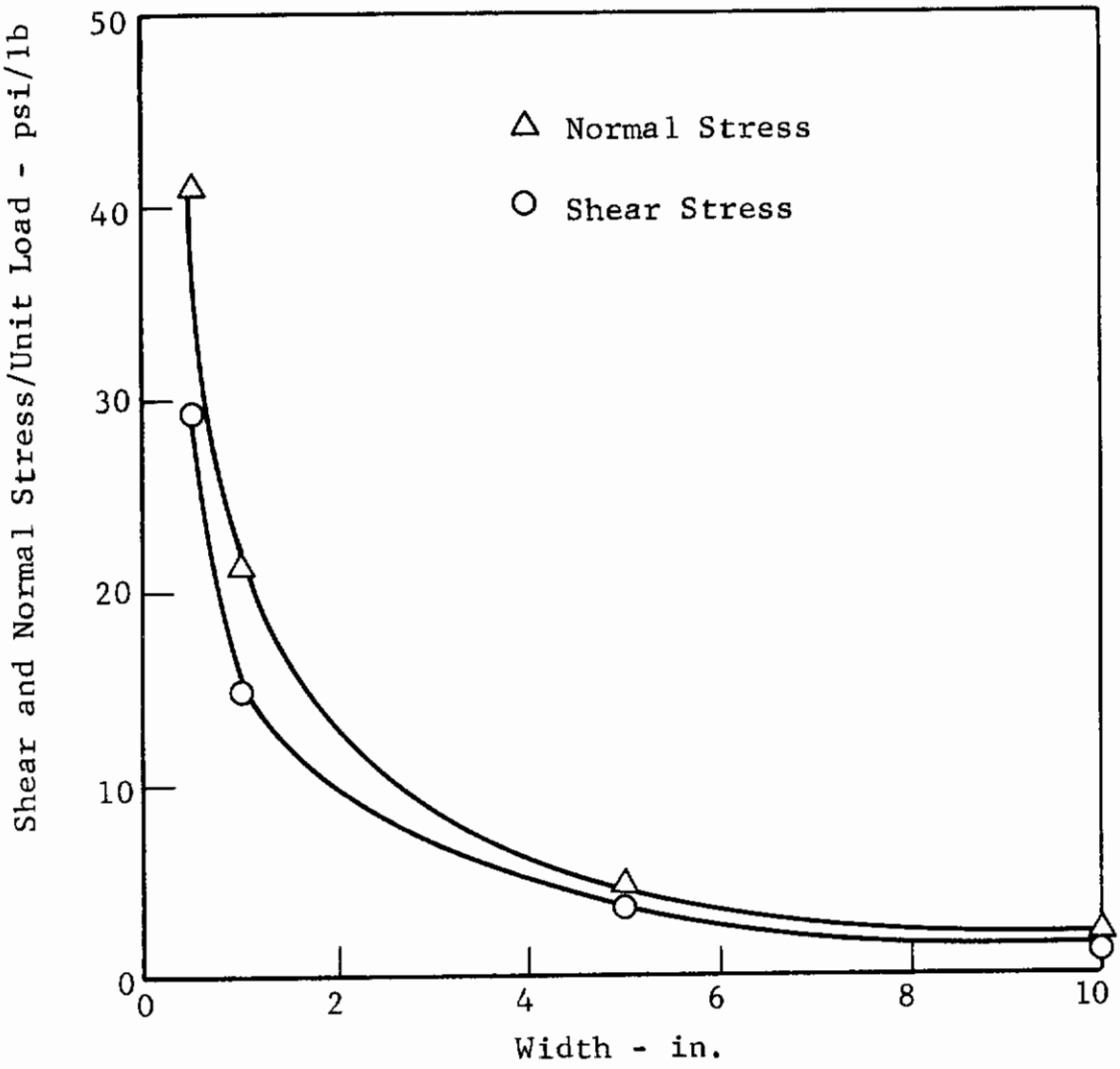

Fig. 3.8 JOINT STRESSES VS. JOINT WIDTH

stresses are essentially constant. This means that wider joint strengths based on one in. widths should be conservative and the wider joints should be stronger than predicted.

3.3.3.3 Length of Overlap and Joint Parameter

The effect of increasing the length of overlap is shown in Fig. 3.9. This clearly indicates that the maximum stresses in the joint do not decrease significantly as the bonded area increases. This is also an experimentally observed result that load carrying capacity does increase but not proportionately with the change in bonded length.

3.3.3.4 Adhesive Thickness and Modulus

The effect of the two most important adhesive variables are shown in Figs. 3.10 and 3.11. As adhesive film thickness increases, more material is available to absorb differential straining and the stresses decrease. The unit strain at any point is lower and subsequently the stresses decrease.

Both shear and normal stress are a strong function of adhesive modulus. As modulus increases so do the stresses. In the range from 50,000 psi to 250,000 psi for shear modulus, which is the behavior range of conventional structural adhesives, the stresses increase almost linearly with shear modulus.

3.3.3.5 Adherend Thickness, Modulus and Poisson's Ratio

The effect of adherend properties are shown in Figs. 3.12 and 3.13. In general, as the stiffness of the adherend increases, e.g., becomes thicker or its modulus increases, the resistance of the joint to bending increases and the stresses decrease. For moduli greater than 30 by 10^6 psi the stresses become constant with increasing modulus. Up to this value, which is an upper bound on modulus for conventional structural materials, the stresses are highly nonlinear with modulus. These results indicate that FPP-FRP joints should be weaker than steel-steel bonded joints.

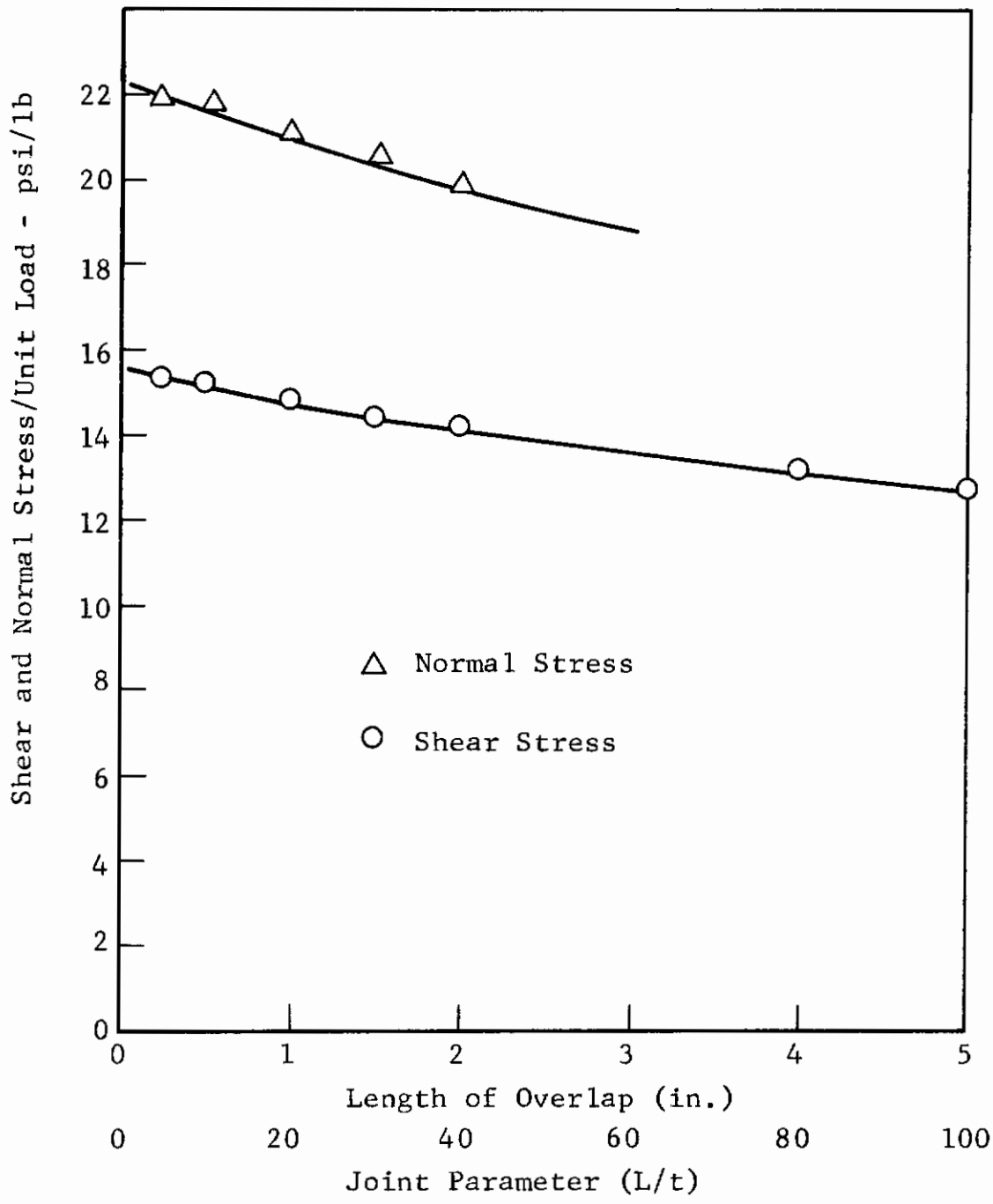

Fig. 3.9 JOINT STRESSES VS. JOINT PARAMETER AND LENGTH OF OVERLAP

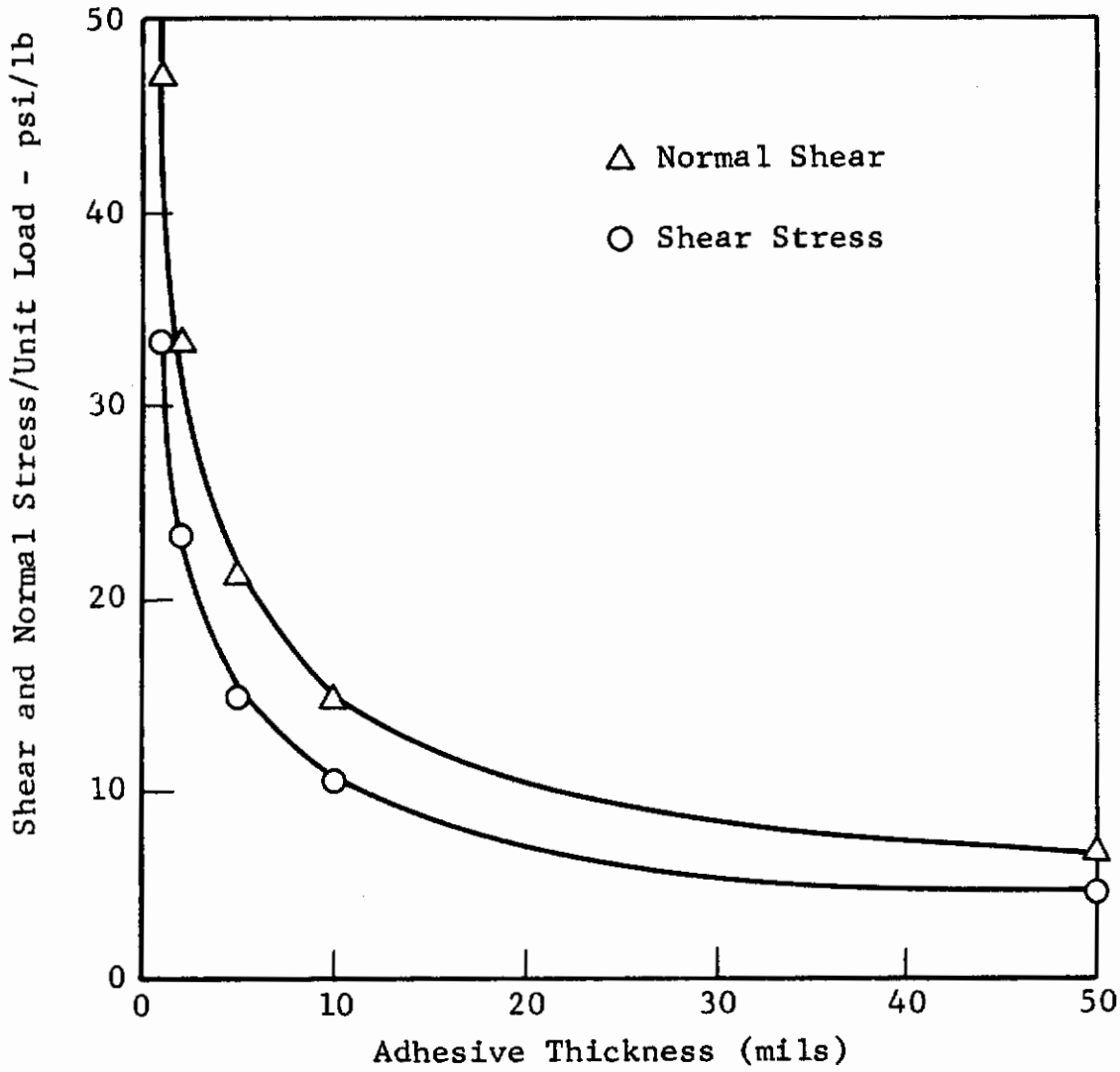

Fig. 3.10 JOINT STRESSES VS. ADHESIVE THICKNESS

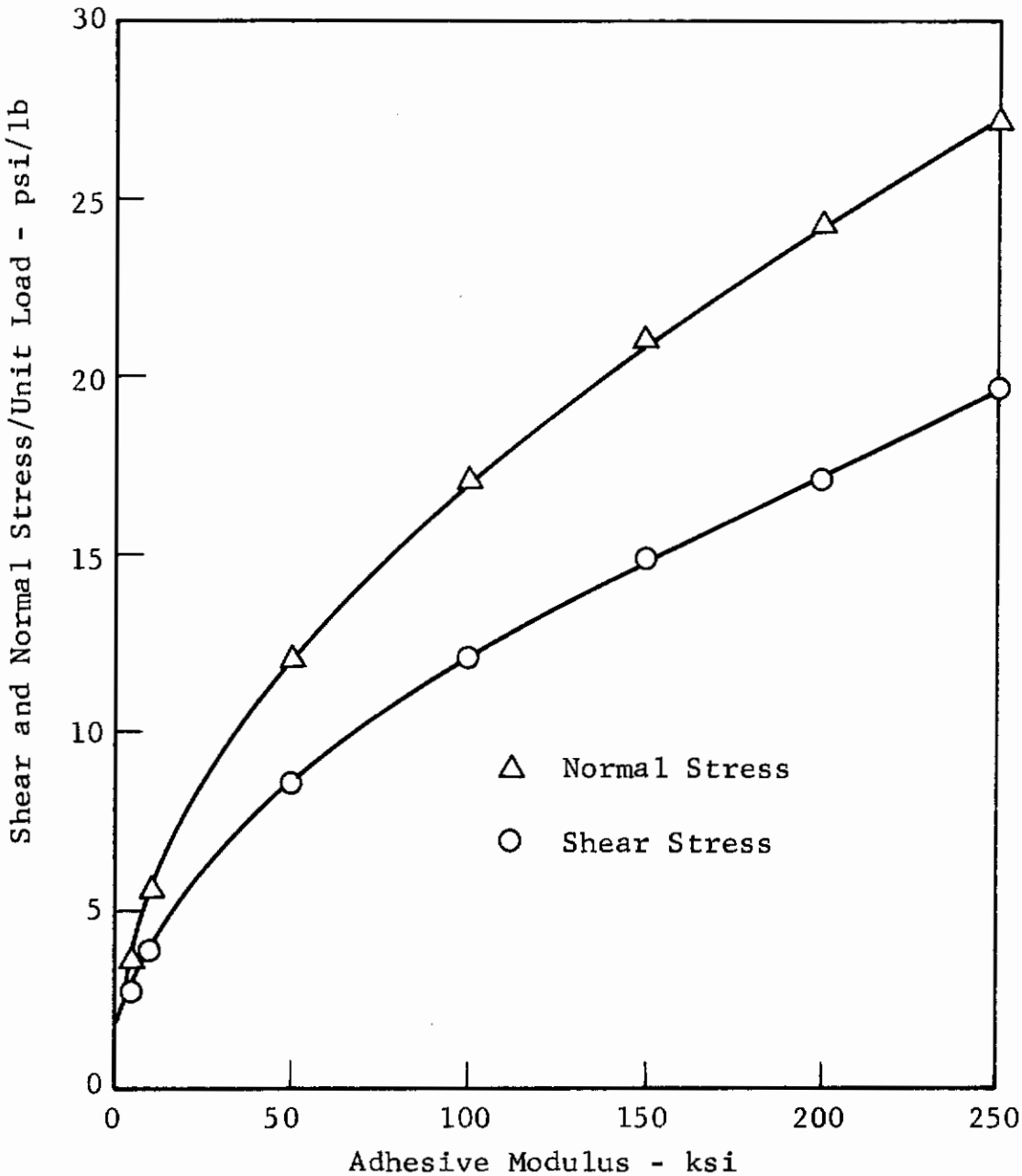

Fig. 3.11 JOINT STRESSES VS. ADHESIVE MODULUS

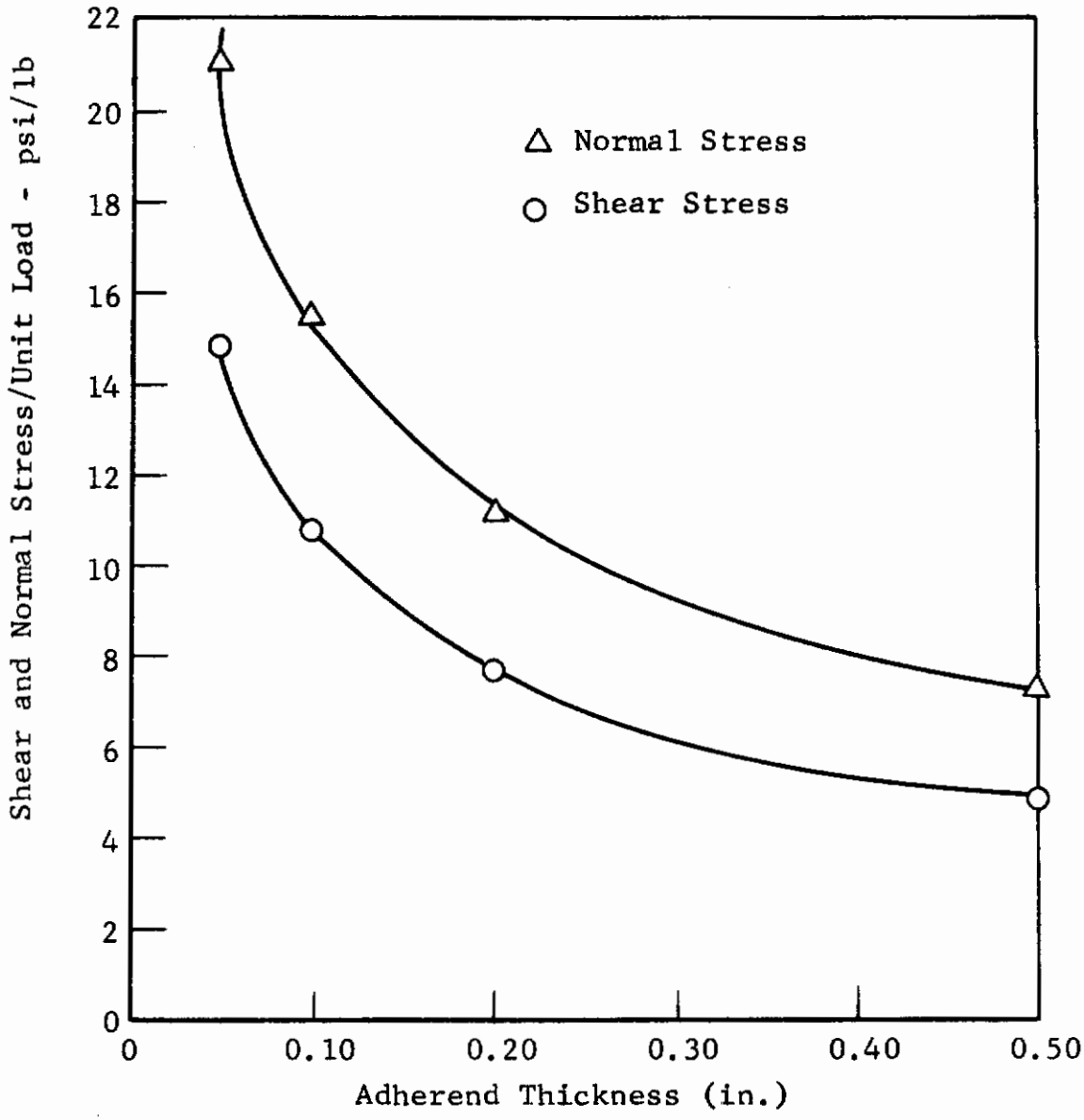

Fig. 3.12 JOINT STRESSES VS. ADHEREND THICKNESS

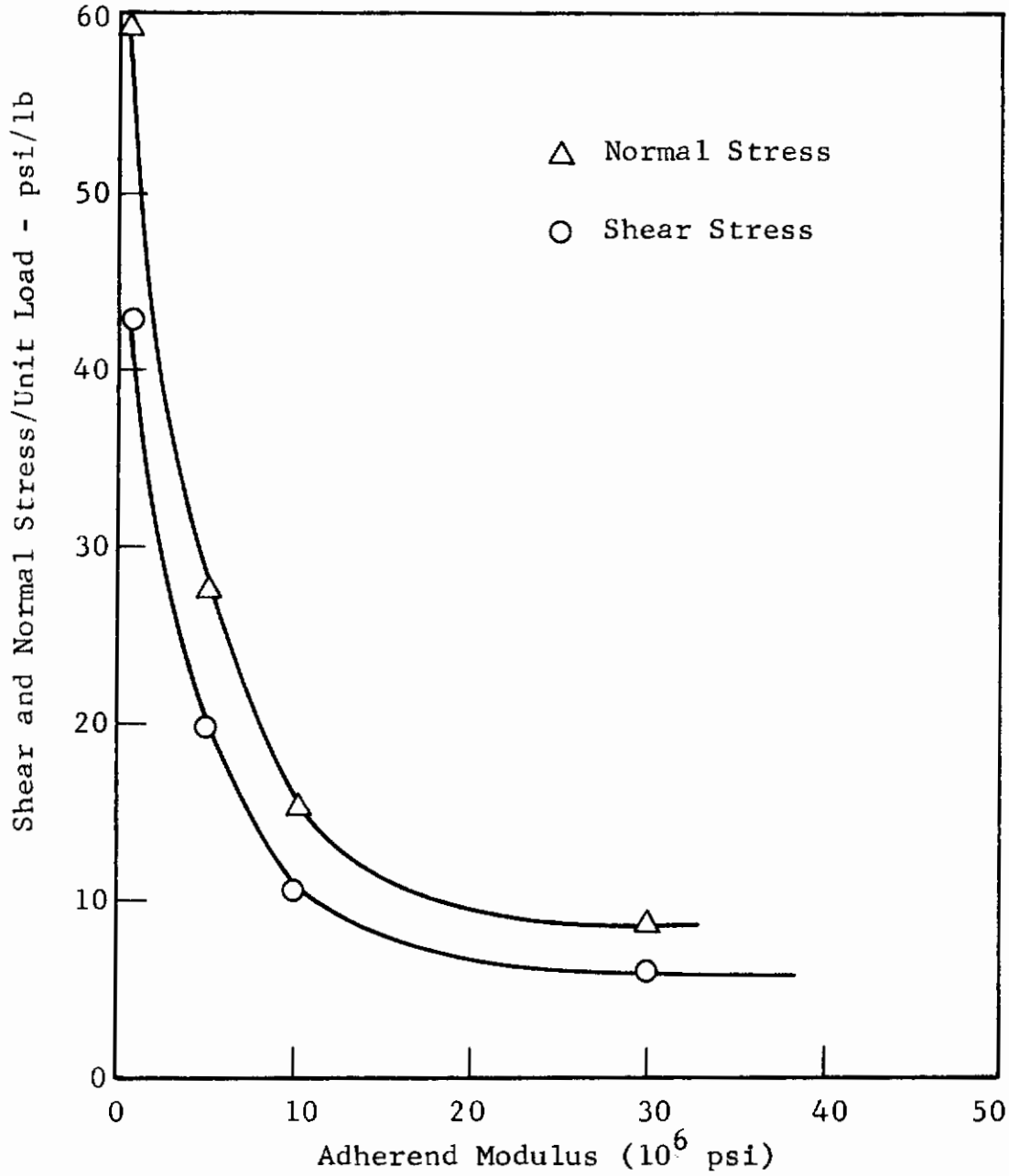

Fig. 3.13 JOINT STRESSES VS. ADHEREND MODULUS

The effect of Poisson's ratio of the adherend on the predicted stresses was checked because the value of this material property is not always well established especially for composite materials. In Table 3.10 cases 37 to 40 showed the stresses to be relatively insensitive to this property. This means that if Poisson's ratio is unknown, a value of 0.45 could be assumed and the stresses obtained would be correct within one percent error.

3.4 NUMERICAL SHEAR LAG ANALYSIS

The application of a combined graphical-numerical shear lag analysis to bonded ahdesive joints was first carried out by Jacobson (3.5). The method is based on assuming:

1. Static equilibrium between the load applied to the joint and the shear stress distribution in the adhesive.
2. Strain compatibility between the adherends and the adhesive.
3. Boundary conditions on the joint do not involve any peeling forces.
4. The shear stress is a function of the relative adherend deformations at a given point and the adhesive modulus and thickness.

The problem is to obtain a unique shear stress distribution in the adhesive which will meet the above constraints. The shear stress in the adhesive will be a function of the several joint variables,

$$\tau(x) = f\left[t_1(x),\ t_2(x),\ E_1(x),\ E_2(x),\ P(x),\ G(x),\ t_a(x),\ A(x),\ L\right]$$

where

$\tau(x)$ = shear stress at any position (x).

$t_1(x)$, $t_2(x)$ = thickness adherend No. 1 and No. 2.

$E_1(x)$, $E_2(x)$ = modulus adherend No. 1 and No. 2.

$P(x)$ = load in the adherend, P(o) = applied load.

$G(x)$ = adhesive modulus.

$t_a(x)$ = adhesive thickness.

L = length of overlap.

$A(x)$ = cross sectional area of the adherends.

It is important to note that all these factors are a function of joint position (x) and theoretically can be taken into account by this method. If one attempts to solve the differential equation for this general case, the problem is a difficult one. The Volkersen analysis is the solution to this problem when all the joint parameters are constant with position. The method described here involves a numerical finite difference solution to the general problem which can be solved using hand computation. The general procedure is as follows:

1. Diagram the joint and divide the length of the bond into an arbitrary number of elements.

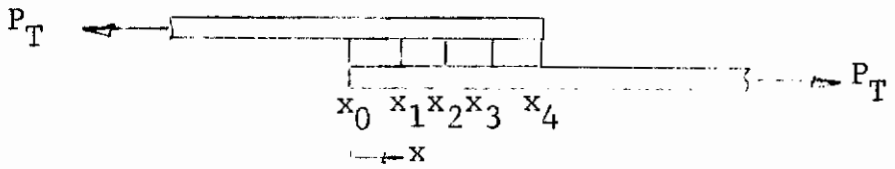

2. Assume an arbitrary shear stress distribution to the adhesive. Theoretically, any distribution can be selected, but it is suggested for convenience and ease of calculation, that a triangular distribution be assumed.

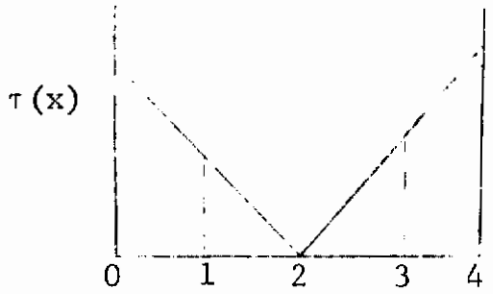

Again for convenience of computation, it is suggested that the integral of the shear stress be equal to the applied load. This will satisfy the first requirement for static equilibrium.

$$P_t = \int_o^L \tau(x)dx$$

In this step, one is assuming a distribution of load transfer across the joint. It is convenient to do this by assuming a reasonable shear stress distribution and working in reverse to obtain P(x). The actual $\tau(x)$ equivalent to P(x) will be computed in a later step.

3. Compute the load distribution in each adherend. This will have the boundary conditions

Adherend No. 1	$P(o) = P_t$	$x = o$
	$P(L) = o$	$x = L$
Adherend No. 2	$P(o) = o$	$x = o$
	$P(L) = P_t$	$x = L$

and is obtained by integrating the shear stress over each increment in the joint.

$$P(x_i) = P(x_{i-1}) - \int_{x_{i-1}}^{x_i} \tau(x)dx$$

Numerically this is computed as

$$P(x_i) = P(x_{i-1}) - \left[\frac{\tau(x_i) + \tau(x_{i-1})}{2} \quad \Delta x\right]$$

For the first increment above

Adherend 1

$$P(x_o) = P_t$$

$$P(x_1) = P_t - \left[\frac{\tau(x_1) + \tau(x_o)}{2} \quad \Delta x\right]$$

Adherend 2

$$P(x_o) = P_t$$

$$P(x_1) = \left[\frac{\tau(x_1) + \tau(x_o)}{2}\right] \Delta x$$

4. Compute the distribution of deformations $\delta(x)$ in each adherend.

$$\delta(x_i) = \int_{x_{i-1}}^{x_i} \frac{P(x)}{A(x)E(x)} \, dx$$

Numerically, average values are used for the load distribution $P(x)$, which was computed above; the modulus distribution $E(x)$ would be known for any given adherend and also the distribution of area $A(x)$. For example, area would vary linearly in a scarf joint.

$$\delta(x_i) = \left[\frac{P(x_i) + P(x_{i-1})}{\left[E(x_i) + E(x_{i-1})\right] \left[A(x_i) + A(x_{i-1})\right]}\right] \Delta x$$

For the first increment above

$$\delta(x_1) = \frac{P(x_1) + P(x_2)}{\left[E(x_1) + E(x_2)\right] \left[A(x_1) + A(x_2)\right]} \Delta x$$

5. Compute the shear stress distribution required in the adhesive to make the strains in the two adherends compatible.

Assume shear strain (γ) is constant through the adhesive thickness

$$\gamma(x_i) = \frac{\delta_1(x_i) - \delta_2(x_i)}{t}$$

δ_1 = deformation Adherend No. 1

δ_2 = deformation Adherend No. 2

Assuming linear elastic behavior for the adhesive and knowing the shear modulus

$$\tau(x_i) = G \, \gamma(x_i)$$

If the adhesive modulus is variable along the joint, then its proper value for (x_i) must be used. If the shear stress-shear strain behavior is nonlinear, then the shear stress can be obtained from the nonlinear shear stress-strain curve.

6. Integrate the new shear stress distribution and test it for static equilibrium with the applied load.

$$P' = \int_o^L \tau'(x_i)\, dx$$

Numerically

$$P' = \sum_{x_o}^{x_i} \frac{\tau(x_i) + \tau(x_{i-1})}{2} \Delta x$$

If $P' \neq P_t$, then the new distribution must be adjusted by applying a uniform shear stress to each increment.

7. The new distribution $\tau(x_i)$ is again carried through another iteration of the above process until P' agrees with P_t within some acceptable error. When this error is reached, the maximum value of shear stress is picked from the curve at the ends of the overlap. If this value exceeds the known shear strength of the adhesive, a lower value of applied load must be selected. If all material behavior is assumed to be elastic, the problem can be solved for a unit load and the resultant shear stress for any other load will be on integral value of the stress/unit load.

An example of this method was carried out for a single lap joint with the following data:

Length of Overlap (L)	= 0.50 in.
Joint Width (w)	= 1.00 in.
Adherend Thickness ($t_1 = t_2$)	= 0.064 in.
Adherend Modulus (E)	= 10.6×10^6 psi
Adhesive Modulus (G)	= 5.0×10^4 psi
Adhesive Thickness (t_a)	= 0.005 in.
Applied Load (P)	= 64 lb

Table 3.11 shows the detailed calculations for the joint using four increments. Figure 3.14 shows the development of the shear stress distributions. The comparison of the results of this solution with that obtained using the Volkersen analysis, which this method should approach, is given in Fig. 3.15. Assuming the Volkersen value of maximum shear stress is correct, the numerical shear lag prediction is in error by

$$\frac{200-180}{200} \times 100 = 10\%$$

This error was obtained after two iterations and the final shear distribution was still 2.5 percent in error compared to total applied load.

The attractive feature of this method, as pointed out earlier, is that it allows one to numerically include all the joint variables using hand computation and it does not require the use of a digital computer. The method can be programmed for computer solution which would allow one to handle a larger number of mesh points and increase the accuracy of the final result.

Table 3.11

NUMERICAL EXAMPLE FOR THE SHEAR LAG ANALYSIS

Station Number	Position (x) (in.)	Shear Stress $\tau(x)$ (psi)	Load $P_1(x)$ (lb)	Load $P_2(x)$ (lb)	Deformation $\delta_1(x)$ (10^{-6} in.)	Deformation $\delta_2(x)$ (10^{-6} in.)	Relative Deformation $\delta_1 - \delta_2$ (10^{-6} in.)	Shear Stress $\tau(x)$ (psi)	Shear + Shift Stress (psi)	Load $P_1(x)$ (lb)	
Iteration No. 1											
0	0	256	64	0	11.81	0	11.81	118			
		(192)*	(52)	(12)				(75)		9.4	
1	0.125	128	40	24	7.38	4.43	2.95	29			Error = 64-22.4
		(64)	(36)	(28)				(15)		1.8	= 41.6 lb
2	0.250	0	32	32	5.91	5.91	0	0			Shift Stress = $\frac{41.6}{(.50)1.0}$
		(64)	(28)	(36)				(15)		1.8	
3	0.375	128	24	40	4.43	7.38	2.95	29			= 80 psi
		(192)	(12)	(52)				(75)		9.4	
4	0.500	256	0	64	0	11.81	11.81	118			
										22.4 = ΣP	
Iteration No. 2											
0	0	200	64	0	10.00	0	10.00	100	180		
		(155)	(54)	(10)					(156)	19.5	
1	0.125	110	44	20	7.02	1.85	5.17	52	132		Error = 65.6-64
		(95)	(38)	(26)					(106)	13.3	= 1.6 lb
2	0.250	80	32	32	4.81	4.81	0	0	80		
		(95)	(26)	(38)					(106)	13.3	$\frac{1.6}{64}$ x 100 = 2.5%
3	0.375	110	20	44	1.85	7.02	5.17	52	132		
		(155)	(10)	(54)					(156)	19.5	
4	0.500	200	0	64	0	10.00	10.00	100	180		
										65.6 = ΣP	

* Values in parentheses represent averages for each joint interval.

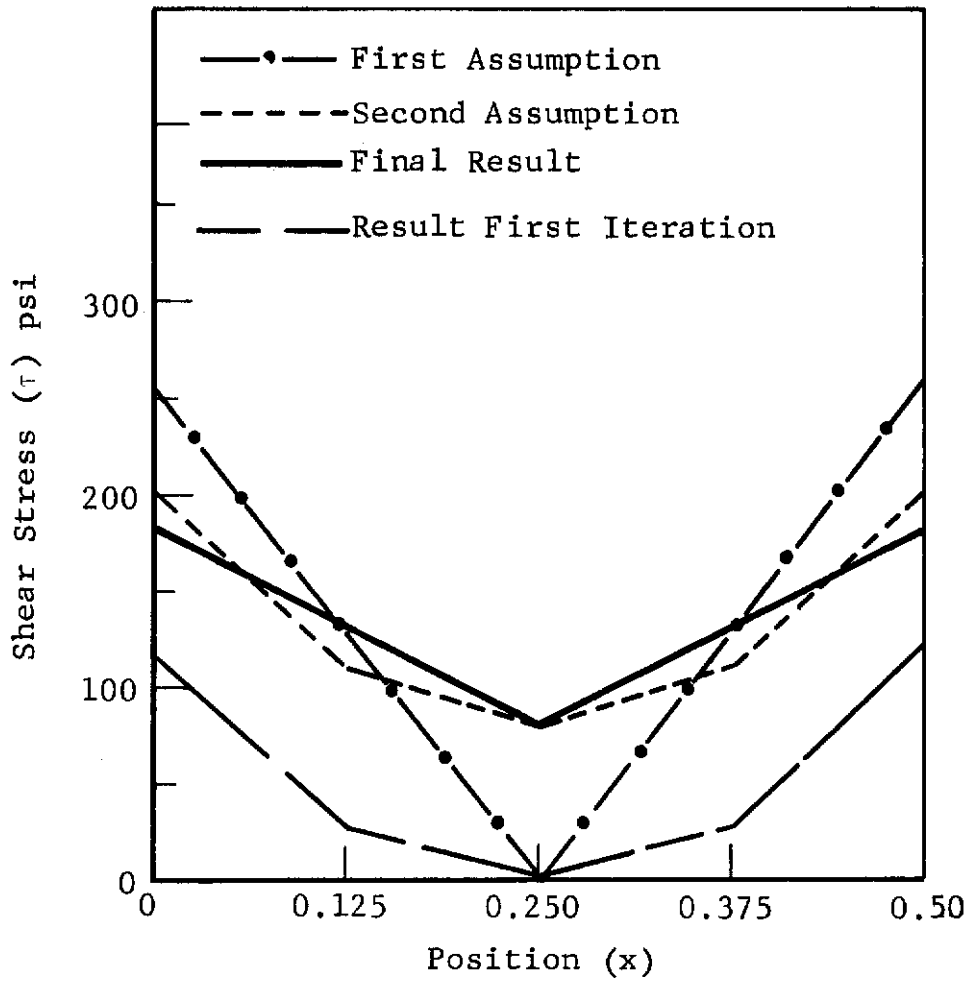

Fig. 3.14 DEVELOPMENT OF THE SHEAR STRESS BY NUMERICAL SHEAR LAG ANALYSIS

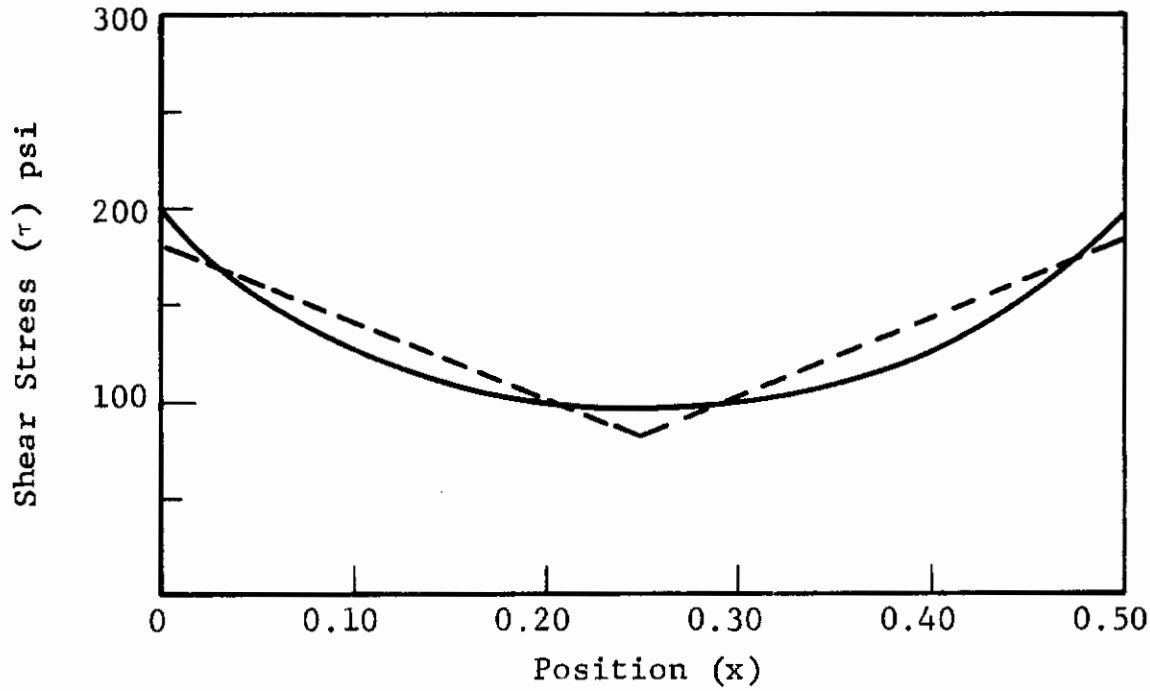

Fig. 3.15 COMPARISON OF VOLKERSEN AND SHEAR LAG ANALYSES

3.5 FINITE ELEMENT ANALYSIS

In the finite element method of analysis, the structure to be investigated is idealized by a two-dimensional physical model consisting of quadrilateral elements. These elements can be assigned various sizes, moduli of elasticity, loads and specific coordinates in space to achieve any desired structure. The mesh size used for the structure is dependent on the degree of accuracy desired from the model. Generally one decreases the mesh size in the area of anticipated high stress concentration. The analysis was made using a computer program developed by Becker and Brisbane (3.6) at Redstone Arsenal. This program can handle problems of plane stress or generalized plane strain.

Two different models with different degrees of support along the adherend were analyzed. Figure 3.16 shows the finite element model with a point support at the end of the adherend. The magnitude of the reaction at this support is not specified; this value is solved for in the analysis. The result of placing a support at this point is to specify this as a point of zero deflection. This joint would compare to the type of support assumed in the Goland and Reissner analysis. Figure 3.16 also shows the major mesh points for the model.

Figure 3.17 shows the model for the supported lap joint which coincides to the joint for the Volkersen analysis. Figure 3.18 shows the detail of the mesh grid in the critical area near the end of the overlap where the highest stresses do occur.

Note that both of these models result in a matrix of 27 rows by nine columns which yields 234 elements whose initial loads, position, and properties must be specified. It is the specification of all the initial and boundary conditions which require the longest amount of time when using this type of analysis. If one carries out a series of parametric studies using this technique, each parametric change requires a new

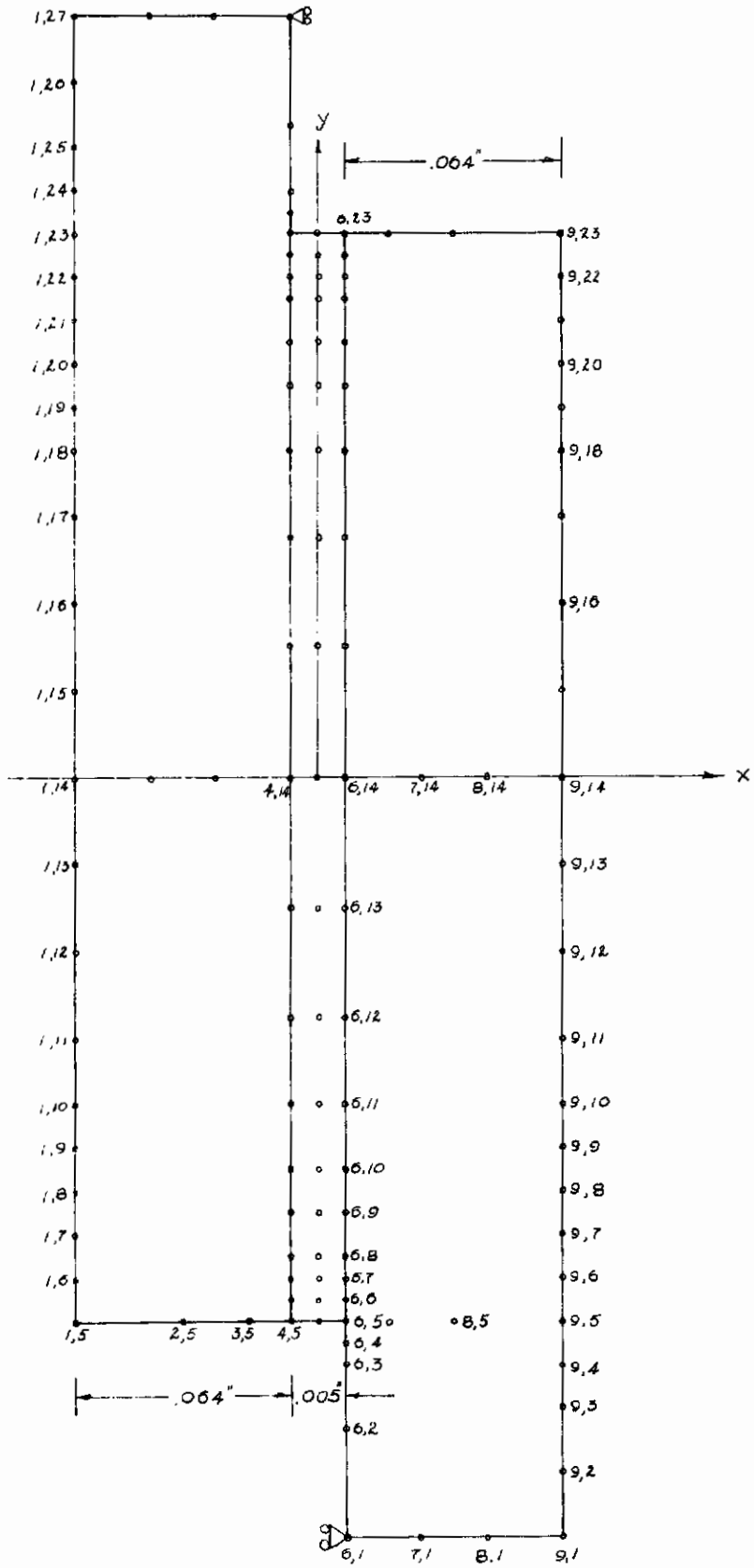

Fig. 3.15 FINITE ELEMENT MODEL OF A LAP JOINT, POINT SUPPORTED ADHEREND, MAJOR MESH POINTS

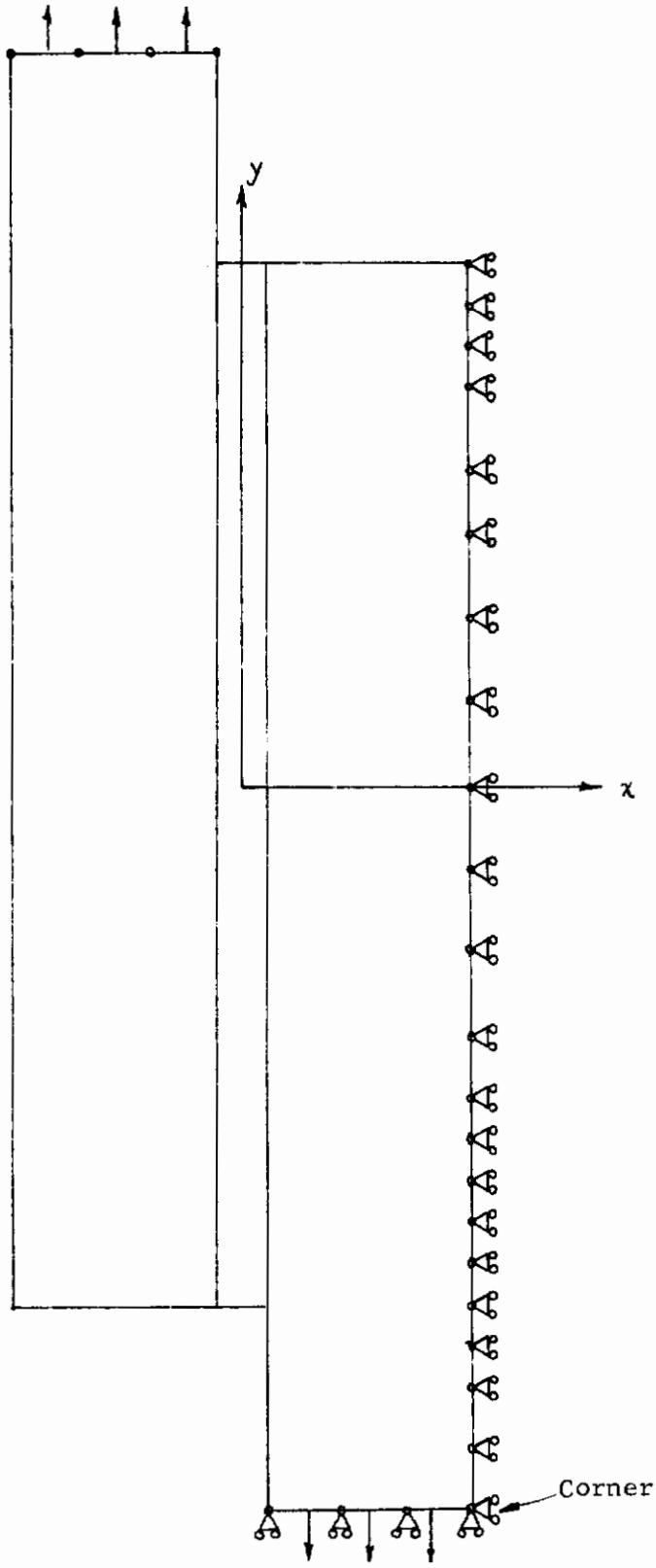

Fig. 3.17 FINITE ELEMENT MODEL OF A LAP JOINT WITH A UNIFORMLY SUPPORTED ADHEREND

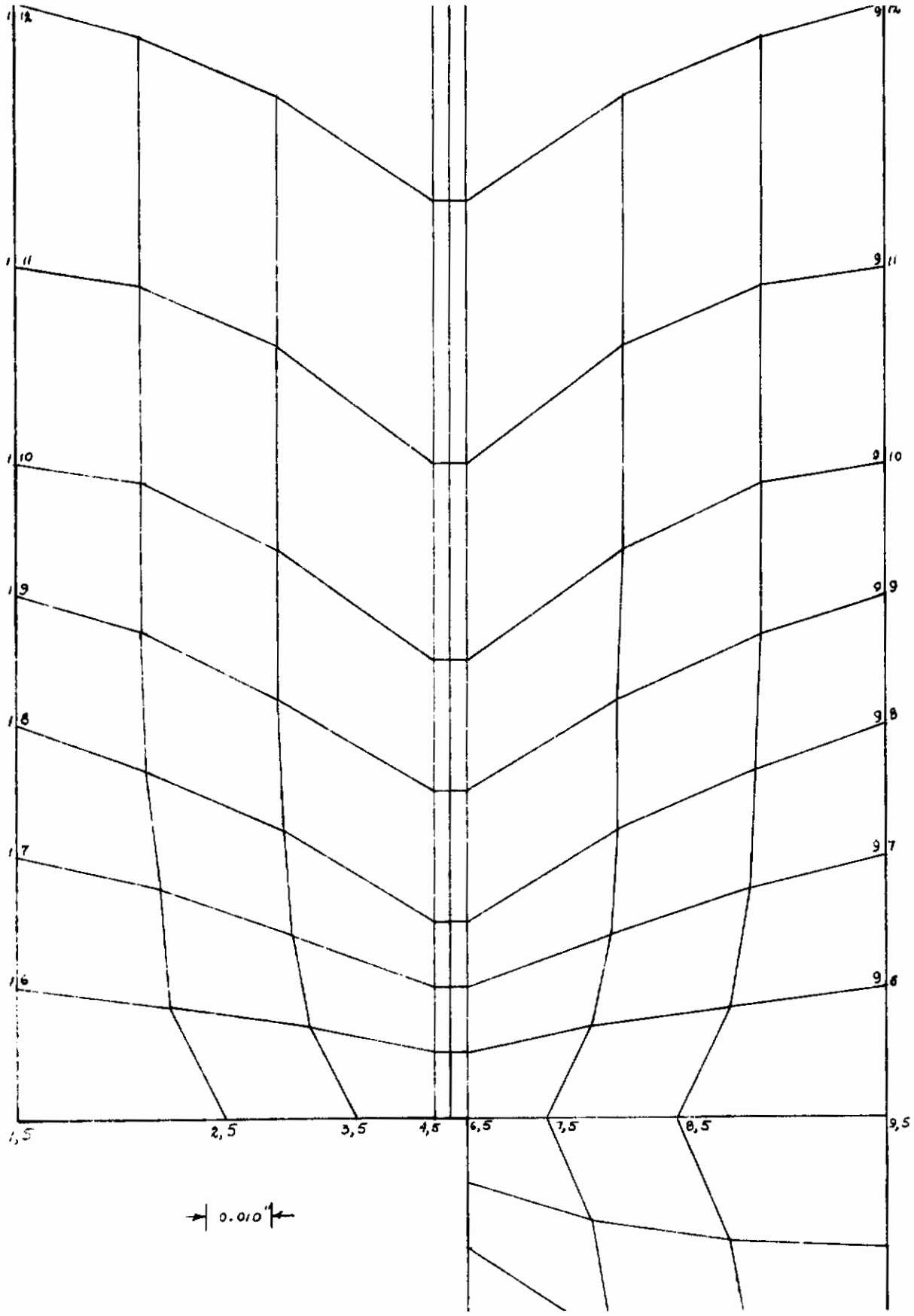

Fig. 3.18 FINITE ELEMENT GRID AT THE END OF THE OVERLAP

detailed input. These changes can be carried out more efficiently if the parameters are selectively varied so that a minimum of changes are necessary for the program input.

Table 3.12 includes sample input and output for the supported joint analyzed. It is important to note the complete detail which is available from the output. This complete detail of the state of stress, strain, and deformation is the powerful advantage of this method and none of the other analysis methods allow one to obtain this degree of discrimination.

The results of the two joints analyzed are summarized in Section 3.6.

Table 3.12

SAMPLE INPUT-OUTPUT, FINITE ELEMENT ANALYSIS OF THE SUPPORTED LAP JOINT

AMG033 SUPPORTED LAP JOINT(4-1) PLANE STRAIN ANALYSIS-COARSE MESH PLANE STRAIN SOLUTION

BOUNDARY CONDITION ARRAY - SUPPORT CONDITIONS ON BOUNDARY

NODAL PT		X		Y		ROTATIONAL		SLIDING	
I	J	CODE	VALUE	CODE	VALUE	CODE	VALUE	CODE	VALUE
6	1	-0	-0.0000000E-39	1	-0.0000000E-39	-0	-0.0000000E-39	-0	-0.0000000E-39
7	1	-0	-0.0000000E-39	1	-0.0000000E-39	-0	-0.0000000E-39	-0	-0.0000000E-39
8	1	-0	-0.0000000E-39	1	-0.0000000E-39	-0	-0.0000000E-39	-0	-0.0000000E-39
9	1	1	-0.0000000E-39	1	-0.0000000E-39	-0	-0.0000000E-39	-0	-0.0000000E-39
9	2	1	-0.0000000E-39	-0	-0.0000000E-39	-0	-0.0000000E-39	-0	-0.0000000E-39
9	3	1	-0.0000000E-39	-0	-0.0000000E-39	-0	-0.0000000E-39	-0	-0.0000000E-39
9	4	1	-0.0000000E-39	-0	-0.0000000E-39	-0	-0.0000000E-39	-0	-0.0000000E-39
9	5	1	-0.0000000E-39	-0	-0.0000000E-39	-0	-0.0000000E-39	-0	-0.0000000E-39
9	6	1	-0.0000000E-39	-0	-0.0000000E-39	-0	-0.0000000E-39	-0	-0.0000000E-39
9	7	1	-0.0000000E-39	-0	-0.0000000E-39	-0	-0.0000000E-39	-0	-0.0000000E-39
9	8	1	-0.0000000E-39	-0	-0.0000000E-39	-0	-0.0000000E-39	-0	-0.0000000E-39
9	9	1	-0.0000000E-39	-0	-0.0000000E-39	-0	-0.0000000E-39	-0	-0.0000000E-39
9	10	1	-0.0000000E-39	-0	-0.0000000E-39	-0	-0.0000000E-39	-0	-0.0000000E-39
9	11	1	-0.0000000E-39	-0	-0.0000000E-39	-0	-0.0000000E-39	-0	-0.0000000E-39
9	12	1	-0.0000000E-39	-0	-0.0000000E-39	-0	-0.0000000E-39	-0	-0.0000000E-39
9	13	1	-0.0000000E-39	-0	-0.0000000E-39	-0	-0.0000000E-39	-0	-0.0000000E-39
9	14	1	-0.0000000E-39	-0	-0.0000000E-39	-0	-0.0000000E-39	-0	-0.0000000E-39
9	15	1	-0.0000000E-39	-0	-0.0000000E-39	-0	-0.0000000E-39	-0	-0.0000000E-39
9	16	1	-0.0000000E-39	-0	-0.0000000E-39	-0	-0.0000000E-39	-0	-0.0000000E-39
9	17	1	-0.0000000E-39	-0	-0.0000000E-39	-0	-0.0000000E-39	-0	-0.0000000E-39
9	18	1	-0.0000000E-39	-0	-0.0000000E-39	-0	-0.0000000E-39	-0	-0.0000000E-39
9	19	1	-0.0000000E-39	-0	-0.0000000E-39	-0	-0.0000000E-39	-0	-0.0000000E-39
9	20	1	-0.0000000E-39	-0	-0.0000000E-39	-0	-0.0000000E-39	-0	-0.0000000E-39
9	21	1	-0.0000000E-39	-0	-0.0000000E-39	-0	-0.0000000E-39	-0	-0.0000000E-39
9	22	1	-0.0000000E-39	-0	-0.0000000E-39	-0	-0.0000000E-39	-0	-0.0000000E-39
9	23	1	-0.0000000E-39	-0	-0.0000000E-39	-0	-0.0000000E-39	-0	-0.0000000E-39

COORDINATES CALCULATED AFTER 53 ITERATIONS

I	J	X	Y	CODE
6	1	0.0025	-0.3500	21000100
7	1	0.0240	-0.3500	31000100
8	1	0.0450	-0.3500	21000100
9	1	0.0665	-0.3500	25001100
6	2	0.0025	-0.3000	20000000
7	2	0.0233	-0.3134	0
8	2	0.0445	-0.3185	0
9	2	0.0665	-0.3200	25001000
6	3	0.0025	-0.2700	20000000
7	3	0.0221	-0.2850	0
8	3	0.0433	-0.2907	0
9	3	0.0665	-0.2900	25001000
6	4	0.0025	-0.2600	20000000
7	4	0.0192	-0.2661	0
8	4	0.0403	-0.2692	0
9	4	0.0665	-0.2700	25001000
1	5	-0.0665	-0.2500	20000000
2	5	-0.0320	-0.2500	20000000
3	5	-0.0120	-0.2500	20000000
4	5	-0.0025	-0.2500	21000000
5	5	-0.0000	-0.2500	20000000
6	5	0.0025	-0.2500	21000000
7	5	0.0120	-0.2500	20000000
8	5	0.0320	-0.2500	20000000
9	5	0.0665	-0.2500	25001000

ORIGINAL COORDINATES OF EACH ELEMENT
LOWER LEFT CORNER

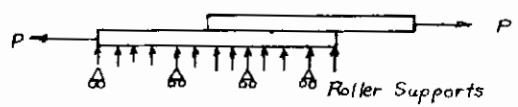

Table 3.12 (cont)

SAMPLE INPUT-OUTPUT, FINITE ELEMENT ANALYSIS OF THE SUPPORTED LAP JOINT

MATERIAL PROPERTIES AND LOADING

I	J	X	Y	E	NU	THERM	BFX	BFY	PRESSURE	SHEAR	FACE NO.
6	1	0.0131	-0.3283	10600000.	0.30000	0.000E-39	0.000E-39	0.000E-39	0.000E-39	0.000E-39	0
7	1	0.0342	-0.3336	10600000.	0.30000	0.000E-39	0.000E-39	0.000E-39	0.000E-39	0.000E-39	0
8	1	0.0556	-0.3346	10600000.	0.30000	0.000E-39	0.000E-39	0.000E-39	0.000E-39	0.000E-39	0
6	2	0.0124	-0.2921	10600000.	0.30000	0.000E-39	0.000E-39	0.000E-39	0.000E-39	0.000E-39	0
7	2	0.0338	-0.3019	10600000.	0.30000	0.000E-39	0.000E-39	0.000E-39	0.000E-39	0.000E-39	0
8	2	0.0552	-0.3048	10600000.	0.30000	0.000E-39	0.000E-39	0.000E-39	0.000E-39	0.000E-39	0
6	3	0.0116	-0.2703	10600000.	0.30000	0.000E-39	0.000E-39	0.000E-39	0.000E-39	0.000E-39	0
7	3	0.0327	-0.2777	10600000.	0.30000	0.000E-39	0.000E-39	0.000E-39	0.000E-39	0.000E-39	0
8	3	0.0542	-0.2800	10600000.	0.30000	0.000E-39	0.000E-39	0.000E-39	0.000E-39	0.000E-39	0
6	4	0.0091	-0.2565	10600000.	0.30000	0.000E-39	0.000E-39	0.000E-39	0.000E-39	0.000E-39	0
7	4	0.0259	-0.2588	10600000.	0.30000	0.000E-39	0.000E-39	0.000E-39	0.000E-39	0.000E-39	0
8	4	0.0513	-0.2598	10600000.	0.30000	0.000E-39	0.000E-39	0.000E-39	0.000E-39	0.000E-39	0
1	5	-0.0513	-0.2407	10600000.	0.30000	0.000E-39	0.000E-39	0.000E-39	0.000E-39	0.000E-39	0
2	5	-0.0259	-0.2423	10600000.	0.30000	0.000E-39	0.000E-39	0.000E-39	0.000E-39	0.000E-39	0
3	5	-0.0090	-0.2441	10600000.	0.30000	0.000E-39	0.000E-39	0.000E-39	0.000E-39	0.000E-39	0
4	5	-0.0013	-0.2450	50000.	0.30000	0.000E-39	0.000E-39	0.000E-39	0.000E-39	0.000E-39	0
5	5	0.0013	-0.2450	50000.	0.30000	0.000E-39	0.000E-39	0.000E-39	0.000E-39	0.000E-39	0
6	5	0.0090	-0.2441	10600000.	0.30000	0.000E-39	0.000E-39	0.000E-39	0.000E-39	0.000E-39	0
7	5	0.0259	-0.2423	10600000.	0.30000	0.000E-39	0.000E-39	0.000E-39	0.000E-39	0.000E-39	0
8	5	0.0513	-0.2407	10600000.	0.30000	0.000E-39	0.000E-39	0.000E-39	0.000E-39	0.000E-39	0
1	6	-0.0541	-0.2221	10600000.	0.30000	0.000E-39	0.000E-39	0.000E-39	0.000E-39	0.000E-39	0
2	6	-0.0317	-0.2267	10600000.	0.30000	0.000E-39	0.000E-39	0.000E-39	0.000E-39	0.000E-39	0
3	6	-0.0116	-0.2321	10600000.	0.30000	0.000E-39	0.000E-39	0.000E-39	0.000E-39	0.000E-39	0
4	6	-0.0013	-0.2350	50000.	0.30000	0.000E-39	0.000E-39	0.000E-39	0.000E-39	0.000E-39	0
5	6	0.0013	-0.2350	50000.	0.30000	0.000E-39	0.000E-39	0.000E-39	0.000E-39	0.000E-39	0
6	6	0.0116	-0.2321	10600000.	0.30000	0.000E-39	0.000E-39	0.000E-39	0.000E-39	0.000E-39	0
7	6	0.0317	-0.2267	10600000.	0.30000	0.000E-39	0.000E-39	0.000E-39	0.000E-39	0.000E-39	0
8	6	0.0541	-0.2221	10600000.	0.30000	0.000E-39	0.000E-39	0.000E-39	0.000E-39	0.000E-39	0
1	7	-0.0552	-0.2032	10600000.	0.30000	0.000E-39	0.000E-39	0.000E-39	0.000E-39	0.000E-39	0
2	7	-0.0332	-0.2103	10600000.	0.30000	0.000E-39	0.000E-39	0.000E-39	0.000E-39	0.000E-39	0
3	7	-0.0125	-0.2196	10600000.	0.30000	0.000E-39	0.000E-39	0.000E-39	0.000E-39	0.000E-39	0
4	7	-0.0013	-0.2250	50000.	0.30000	0.000E-39	0.000E-39	0.000E-39	0.000E-39	0.000E-39	0
5	7	0.0013	-0.2250	50000.	0.30000	0.000E-39	0.000E-39	0.000E-39	0.000E-39	0.000E-39	0
6	7	0.0125	-0.2196	10600000.	0.30000	0.000E-39	0.000E-39	0.000E-39	0.000E-39	0.000E-39	0
7	7	0.0332	-0.2103	10600000.	0.30000	0.000E-39	0.000E-39	0.000E-39	0.000E-39	0.000E-39	0
8	7	0.0552	-0.2032	10600000.	0.30000	0.000E-39	0.000E-39	0.000E-39	0.000E-39	0.000E-39	0
1	8	-0.0556	-0.1835	10600000.	0.30000	0.000E-39	0.000E-39	0.000E-39	0.000E-39	0.000E-39	0
2	8	-0.0340	-0.1917	10600000.	0.30000	0.000E-39	0.000E-39	0.000E-39	0.000E-39	0.000E-39	0
3	8	-0.0129	-0.2032	10600000.	0.30000	0.000E-39	0.000E-39	0.000E-39	0.000E-39	0.000E-39	0
4	8	-0.0013	-0.2100	50000.	0.30000	0.000E-39	0.000E-39	0.000E-39	0.000E-39	0.000E-39	0
5	8	0.0013	-0.2100	50000.	0.30000	0.000E-39	0.000E-39	0.000E-39	0.000E-39	0.000E-39	0
6	8	0.0129	-0.2032	10600000.	0.30000	0.000E-39	0.000E-39	0.000E-39	0.000E-39	0.000E-39	0
7	8	0.0340	-0.1917	10600000.	0.30000	0.000E-39	0.000E-39	0.000E-39	0.000E-39	0.000E-39	0
8	8	0.0556	-0.1835	10600000.	0.30000	0.000E-39	0.000E-39	0.000E-39	0.000E-39	0.000E-39	0
1	9	-0.0557	-0.1625	10600000.	0.30000	0.000E-39	0.000E-39	0.000E-39	0.000E-39	0.000E-39	0
2	9	-0.0343	-0.1699	10600000.	0.30000	0.000E-39	0.000E-39	0.000E-39	0.000E-39	0.000E-39	0
3	9	-0.0131	-0.1824	10600000.	0.30000	0.000E-39	0.000E-39	0.000E-39	0.000E-39	0.000E-39	0
4	9	-0.0013	-0.1900	50000.	0.30000	0.000E-39	0.000E-39	0.000E-39	0.000E-39	0.000E-39	0
5	9	0.0013	-0.1900	50000.	0.30000	0.000E-39	0.000E-39	0.000E-39	0.000E-39	0.000E-39	0
6	9	0.0131	-0.1824	10600000.	0.30000	0.000E-39	0.000E-39	0.000E-39	0.000E-39	0.000E-39	0
7	9	0.0343	-0.1699	10600000.	0.30000	0.000E-39	0.000E-39	0.000E-39	0.000E-39	0.000E-39	0
8	9	0.0557	-0.1625	10600000.	0.30000	0.000E-39	0.000E-39	0.000E-39	0.000E-39	0.000E-39	0
1	10	-0.0558	-0.1365	10600000.	0.30000	0.000E-39	0.000E-39	0.000E-39	0.000E-39	0.000E-39	0
2	10	-0.0344	-0.1428	10600000.	0.30000	0.000E-39	0.000E-39	0.000E-39	0.000E-39	0.000E-39	0
3	10	-0.0131	-0.1564	10600000.	0.30000	0.000E-39	0.000E-39	0.000E-39	0.000E-39	0.000E-39	0
4	10	-0.0013	-0.1650	50000.	0.30000	0.000E-39	0.000E-39	0.000E-39	0.000E-39	0.000E-39	0
5	10	0.0013	-0.1650	50000.	0.30000	0.000E-39	0.000E-39	0.000E-39	0.000E-39	0.000E-39	0
6	10	0.0131	-0.1564	10600000.	0.30000	0.000E-39	0.000E-39	0.000E-39	0.000E-39	0.000E-39	0
7	10	0.0344	-0.1428	10600000.	0.30000	0.000E-39	0.000E-39	0.000E-39	0.000E-39	0.000E-39	0

Table 3.12 (cont)

SAMPLE INPUT-OUTPUT, FINITE ELEMENT ANALYSIS OF THE SUPPORTED LAP JOINT

OUTPUT ELEMENTS DISPLACEMENTS

I	J	X-COORDINATE	Y-COORDINATE	X-DISPLACEMENT	Y-DISPLACEMENT
6	1	0.0025	-0.3500	2.3643E-06	0.0000E-39
7	1	0.0240	-0.3500	1.5721E-06	0.0000E-39
8	1	0.0450	-0.3500	7.9538E-07	0.0000E-39
9	1	0.0665	-0.3500	0.0000E-39	-0.0000E-39
6	2	0.0025	-0.3000	2.2954E-06	4.2389E-06
7	2	0.0233	-0.3134	1.5644E-06	3.1388E-06
8	2	0.0445	-0.3185	7.9423E-07	2.7102E-06
9	2	0.0665	-0.3200	-0.0000E-39	2.5847E-06
6	3	0.0025	-0.2700	2.1955E-06	6.8316E-06
7	3	0.0221	-0.2850	1.5083E-06	5.5770E-06
8	3	0.0433	-0.2907	7.8505E-07	5.0846E-06
9	3	0.0665	-0.2900	-0.0000E-39	5.1293E-06
6	4	0.0025	-0.2600	2.0204E-06	7.7490E-06
7	4	0.0192	-0.2661	1.4444E-06	7.2211E-06
8	4	0.0403	-0.2692	8.0413E-07	6.8855E-06
9	4	0.0665	-0.2700	-0.0000E-39	6.7688E-06
1	5	-0.0665	-0.2500	-5.3502E-06	5.3633E-05
2	5	-0.0320	-0.2500	-5.4460E-06	5.0766E-05
3	5	-0.0120	-0.2500	-5.6056E-06	4.8800E-05
4	5	-0.0025	-0.2500	-5.6644E-06	4.7587E-05
5	5	-0.0000	-0.2500	-4.3666E-06	2.9718E-05
6	5	0.0025	-0.2500	1.8379E-06	8.7475E-06
7	5	0.0120	-0.2500	1.5281E-06	8.6572E-06
8	5	0.0320	-0.2500	9.5146E-07	8.4746E-06
9	5	0.0665	-0.2500	-0.0000E-39	8.3382E-06
1	6	-0.0665	-0.2300	-3.6923E-06	5.3599E-05
2	6	-0.0403	-0.2330	-3.9246E-06	5.1489E-05
3	6	-0.0192	-0.2363	-4.2036E-06	4.9600E-05
4	6	-0.0025	-0.2400	-4.5168E-06	4.7681E-05
5	6	-0.0000	-0.2400	-6.0986E-07	2.8416E-05
6	6	0.0025	-0.2400	1.7901E-06	9.7158E-06
7	6	0.0192	-0.2363	1.2404E-06	9.7124E-06
8	6	0.0403	-0.2330	6.8234E-07	9.7532E-06
9	6	0.0665	-0.2300	0.0000E-39	9.8757E-06
1	7	-0.0665	-0.2100	-2.1024E-06	5.3492E-05
2	7	-0.0433	-0.2155	-2.4893E-06	5.1760E-05
3	7	-0.0220	-0.2221	-2.9915E-06	4.9932E-05
4	7	-0.0025	-0.2300	-3.6764E-06	4.7823E-05
5	7	-0.0000	-0.2300	-1.0982E-06	2.9092E-05
6	7	0.0025	-0.2300	1.7715E-06	1.0609E-05
7	7	0.0220	-0.2221	1.1861E-06	1.0807E-05
8	7	0.0433	-0.2155	6.0826E-07	1.1048E-05
9	7	0.0665	-0.2100	0.0000E-39	1.1366E-05
1	8	-0.0665	-0.1900	-7.3454E-07	5.3356E-05
2	8	-0.0445	-0.1972	-1.1715E-06	5.1903E-05
3	8	-0.0231	-0.2064	-1.8251E-06	5.0175E-05
4	8	-0.0025	-0.2200	-2.8463E-06	4.7996E-05
5	8	-0.0000	-0.2200	-4.6803E-07	2.9612E-05
6	8	0.0025	-0.2200	1.7747E-06	1.1454E-05
7	8	0.0231	-0.2064	1.1789E-06	1.1999E-05
8	8	0.0445	-0.1972	5.9499E-07	1.2399E-05
9	8	0.0665	-0.1900	-0.0000E-39	1.2820E-05
1	9	-0.0665	-0.1700	3.6291E-07	5.3251E-05
2	9	-0.0449	-0.1767	2.3108E-08	5.2051E-05
3	9	-0.0236	-0.1865	-5.8030E-07	5.0486E-05
4	9	-0.0025	-0.2000	-1.4962E-06	4.8434E-05
5	9	-0.0000	-0.2000	1.5725E-07	3.0635E-05
6	9	0.0025	-0.2000	1.7896E-06	1.3025E-05
7	9	0.0236	-0.1866	1.1899E-06	1.3473E-05

Table 3.12 (cont)

SAMPLE INPUT-OUTPUT, FINITE ELEMENT ANALYSIS OF THE SUPPORTED LAP JOINT

OUTPUT - STRESS/STRAINS

I J / ANGLE	COORDINATES X / Y	σ_x / ϵ_x	σ_y / ϵ_y	STRESSES / STRAINS AXIAL σ_z, ϵ_z	SHEAR X-Y τ_{xy}, γ_{xy}	MAXIMUM σ_1, ϵ_1	MINIMUM σ_2, ϵ_2	MAX SHEAR τ_{max}, δ_{max}
6 1	0.013 -0.325	1.6574E 00	9.9355E 02	2.9833E 02	-6.6467E-01	9.9355E 02	1.6570E 00	4.9595E 02
-89.96	1.2196E-04	-3.6385E-05	8.5262E-05	-0.0000E-39	-1.6308E-07	8.5262E-05	-3.6385E-05	1.2165E-04
7 1	0.034 -0.333	2.2850E 00	1.0017E 03	3.0114E 02	-1.7697E 00	1.0017E 03	2.2819E 00	4.9971E 02
-89.90	1.2512E-04	-3.6655E-05	8.5915E-05	-0.0000E-39	-4.3406E-07	8.5915E-05	-3.6655E-05	1.2257E-04
8 1	0.056 -0.335	4.0533E 00	1.0050E 03	3.0271E 02	-8.7258E-01	1.0050E 03	4.0526E 00	5.0045E 02
-89.95	1.2375E-04	-3.6628E-05	8.6125E-05	-0.0000E-39	-2.1403E-07	8.6125E-05	-3.6628E-05	1.2275E-04
6 2	0.013 -0.292	4.8956E 00	1.0047E 03	3.0334E 02	-9.0372E 00	1.0068E 03	4.8140E 00	5.0098E 02
-89.48	1.2401E-04	-3.6602E-05	8.6260E-05	-0.0000E-39	-2.2167E-06	8.6270E-05	-3.6612E-05	1.2288E-04
7 2	0.033 -0.302	1.3420E 01	1.0034E 03	3.0506E 02	-1.0757E 01	1.0036E 03	1.3303E 01	4.9513E 02
-89.38	1.2471E-04	-3.5768E-05	8.5651E-05	-0.0000E-39	-2.6386E-06	8.5665E-05	-3.5782E-05	1.2145E-04
8 2	0.055 -0.305	1.9579E 01	9.9974E 02	3.0670E 02	-5.0208E 00	9.9926E 02	1.9553E 01	4.8986E 02
-89.71	1.2497E-04	-3.5090E-05	8.5057E-05	-0.0000E-39	-1.2315E-06	8.5060E-05	-3.5094E-05	1.2015E-04
6 3	0.012 -0.270	7.6287E 00	1.0421E 03	3.1349E 02	-2.6645E 01	1.0427E 03	6.9429E 00	5.1790E 02
-88.53	1.2616E-04	-3.7512E-05	8.9353E-05	-0.0000E-39	-6.5356E-06	8.9437E-05	-3.7596E-05	1.2703E-04
7 3	0.031 -0.278	3.5037E 01	1.0037E 03	3.1141E 02	-3.1027E 01	1.0047E 03	3.4044E 01	4.8531E 02
-88.17	1.2730E-04	-3.3894E-05	8.4899E-05	-0.0000E-39	-7.6104E-06	8.5021E-05	-3.4016E-05	1.1904E-04
8 3	0.054 -0.280	4.6384E 01	9.8459E 02	3.0960E 02	-1.2487E 01	9.8476E 02	4.6218E 01	4.6927E 02
-89.24	1.2657E-04	-3.2281E-05	8.2782E-05	-0.0000E-39	-3.0629E-06	8.2802E-05	-3.2302E-05	1.1510E-04
6 4	0.009 -0.257	5.4974E 01	1.1122E 03	3.4554E 02	-7.7152E 01	1.1178E 03	4.9375E 01	5.3420E 02
-85.85	1.4126E-04	-3.5635E-05	9.4020E-05	-0.0000E-39	-1.8924E-05	9.4707E-05	-3.6322E-05	1.3103E-04
7 4	0.026 -0.259	7.0049E 01	9.9935E 02	3.2006E 02	-5.7646E 01	1.0029E 03	6.6486E 01	4.6821E 02
-86.46	1.3084E-04	-3.0661E-05	8.3310E-05	-0.0000E-39	-1.4140E-05	8.3747E-05	-3.1098E-05	1.1485E-04
8 4	0.051 -0.263	7.4356E 01	9.6437E 02	3.1199E 02	-2.1982E 01	9.6491E 02	7.3814E 01	4.4555E 02
-88.59	1.2754E-04	-2.9144E-05	8.0009E-05	-0.0000E-39	-5.3918E-06	8.0075E-05	-2.9211E-05	1.0929E-04
1 5	-0.051 -0.241	-1.3717E 01	-1.1201E 00	-5.5291E 00	1.6566E 01	1.0304E 01	-2.5141E 01	1.7723E 01
55.41	-2.2603E-06	-1.0042E-06	5.4072E-07	-0.0000E-39	4.0633E-06	1.9418E-06	-2.4053E-06	4.3471E-06
2 5	-0.026 -0.242	-3.2506E 01	1.9948E 01	-4.4723E 00	-1.5122E-01	1.9949E 01	-3.2506E 01	2.6228E 01
-89.83	-1.8283E-05	-3.4381E-06	2.9950E-06	-0.0000E-39	-3.7092E-08	2.9950E-06	-3.4382E-06	6.4332E-06
3 5	-0.009 -0.244	1.1844E 01	3.4786E 01	1.6159E 01	-5.2211E 01	7.6771E 01	-3.0141E 01	5.3456E 01
-51.20	6.6059E-06	-5.2918E-07	2.2844E-06	-0.0000E-39	-1.2806E-05	7.4335E-06	-5.6783E-06	1.3112E-05
4 5	-0.001 -0.245	6.8321E 01	2.5960E 01	7.8284E 01	-1.3811E 02	1.8686E 02	-9.2582E 01	1.3972E 02
-40.64	2.4513E-03	1.0410E-03	-6.0429E-05	-0.0000E-39	-7.1816E-03	4.1231E-03	-3.1425E-03	7.2656E-03
5 5	0.001 -0.245	1.1535E 02	4.8518E 01	4.9160E 01	-1.4901E 02	2.3465E 02	-7.0780E 01	1.5271E 02
-38.68	4.2605E-03	1.7209E-03	-1.6681E-05	-0.0000E-39	-7.7486E-03	4.8226E-03	-3.1184E-03	7.9411E-03
6 5	0.009 -0.244	9.9435E 01	1.1002E 03	3.5898E 02	-7.6463E 01	1.1060E 03	9.3627E 01	5.0618E 02
-85.66	1.4675E-04	-3.1831E-05	9.0902E-05	-0.0000E-39	-1.8755E-05	9.1615E-05	-3.2543E-05	1.2416E-04
7 5	0.024 -0.242	9.6222E 01	9.8322E 02	3.2372E 02	-5.4973E 01	9.8662E 02	9.2827E 01	4.4689E 02
-86.47	1.3234E-04	-2.7901E-05	8.0883E-05	-0.0000E-39	-1.3484E-05	8.1279E-05	-2.8317E-05	1.0962E-04

3.6 COMPARISON OF ANALYSES

A comparison has been made of the stress distribution predicted by the finite element analysis and that predicted by the Volkersen (3.1) and the Goland and Reissner (3.3) analyses. The two joints analyzed using the finite element technique were the supported joint which most closely matches the assumptions of the Volkersen analysis and the second was the unsupported joint which is analogous to the Goland and Reissner model.

The comparison for the supported joint is shown in Figs. 3.19 and 3.20. Table 3.13 gives the point by point results from the Volkersen analysis. The average shear stress in this joint is 128 psi. The shear stress (τ_{xy}) predicted at the end of the overlap by the finite element analysis was 149 psi. This occurred along the line for x = 0.001 in. which is slightly off the centerline of the adhesive. This results in a shear stress concentration factor of 1.16. The principal stresses at this point give a maximum shear stress of 152 psi which is only slightly higher than the plane shear value.

The Volkersen analysis predicts a maximum shear stress of 198 psi with a resultant stress concentration of 1.55. This is 33 percent higher than the finite element. Assuming a maximum shear stress theory of failure, the finite element analysis would predict 33 percent stronger joints than the Volkersen analysis.

The results for the unsupported joint can be seen in Figs. 3.21 and 3.22. Table 3.14 gives the results of the point stresses from the Goland and Reissner analysis. The results are summarized below.

Stress	Finite Element	Goland & Reissner	Percent Change
Average Shear Stress - psi	128	128	--
Maximum Shear Stress - psi	175	332	90
Shear Concentration	1.4	2.6	90
Normal Stress	187	432	131
Principal Normal Stress	317	432	36

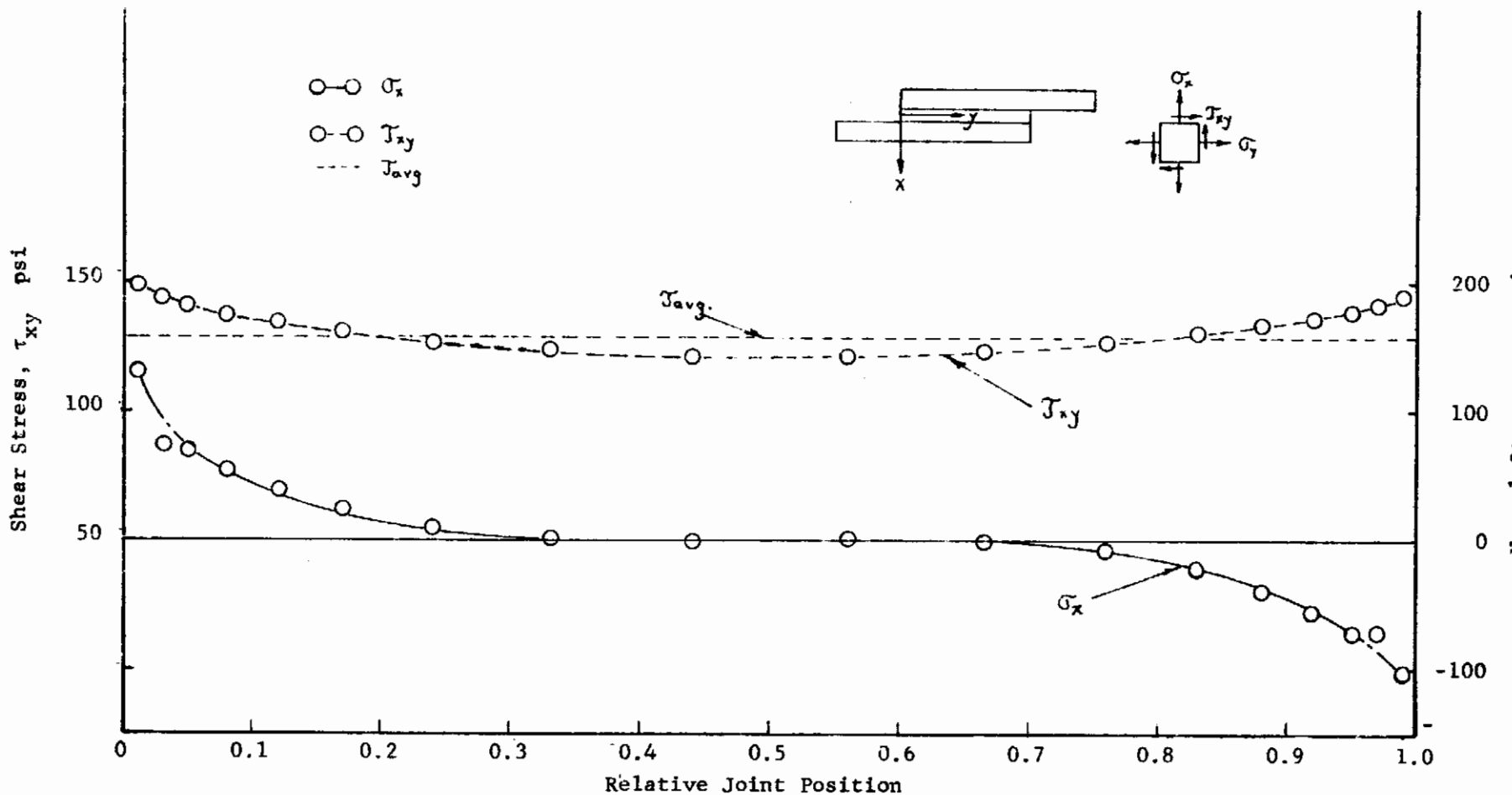

Fig. 3.19 STRESS DISTRIBUTION FROM FINITE ELEMENT ANALYSIS - SUPPORTED LAP JOINT

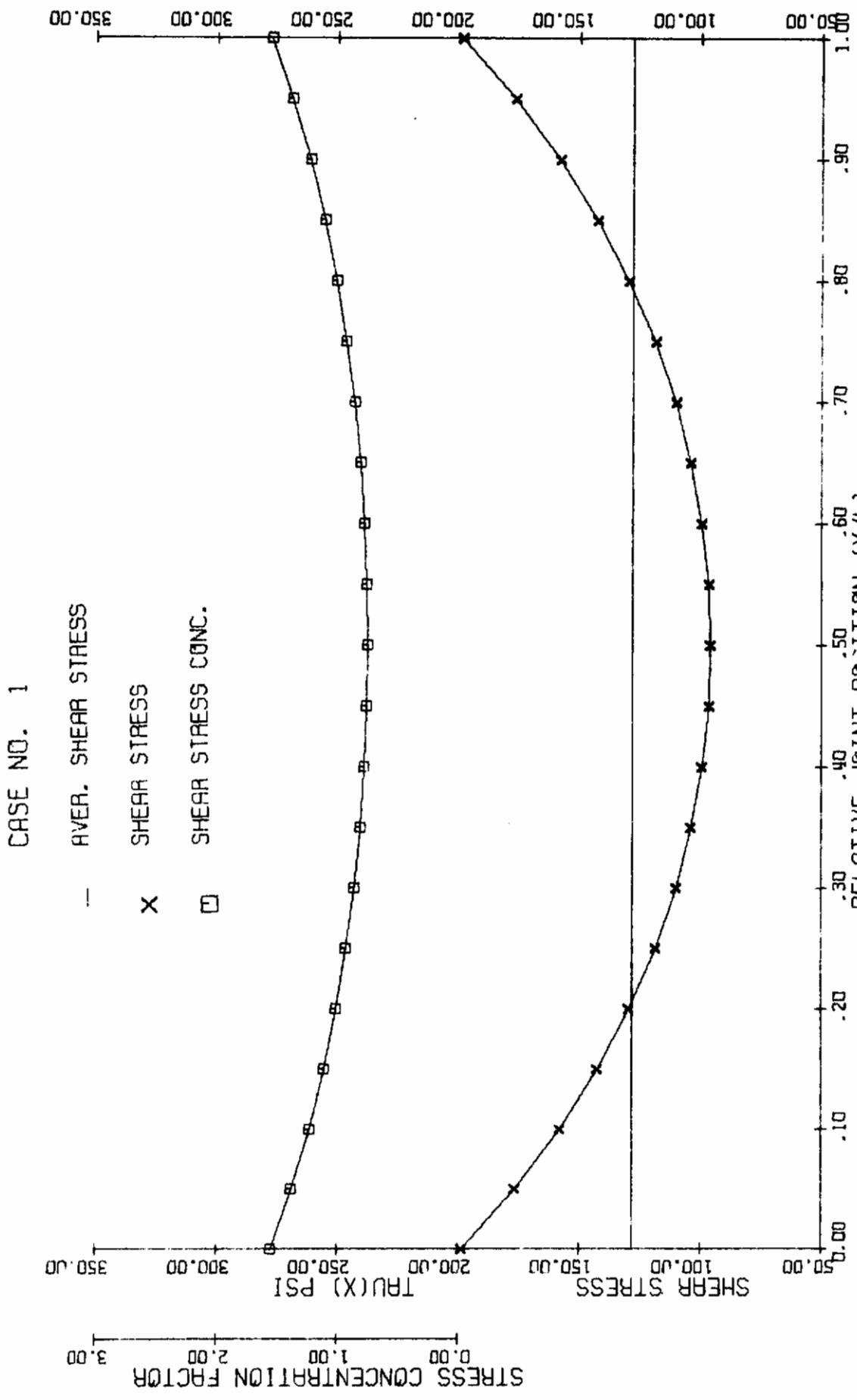

Fig. 3.20 STRESS ANALYSIS OF THE SUPPORTED LAP JOINT USING THE VOLKERSEN ANALYSIS

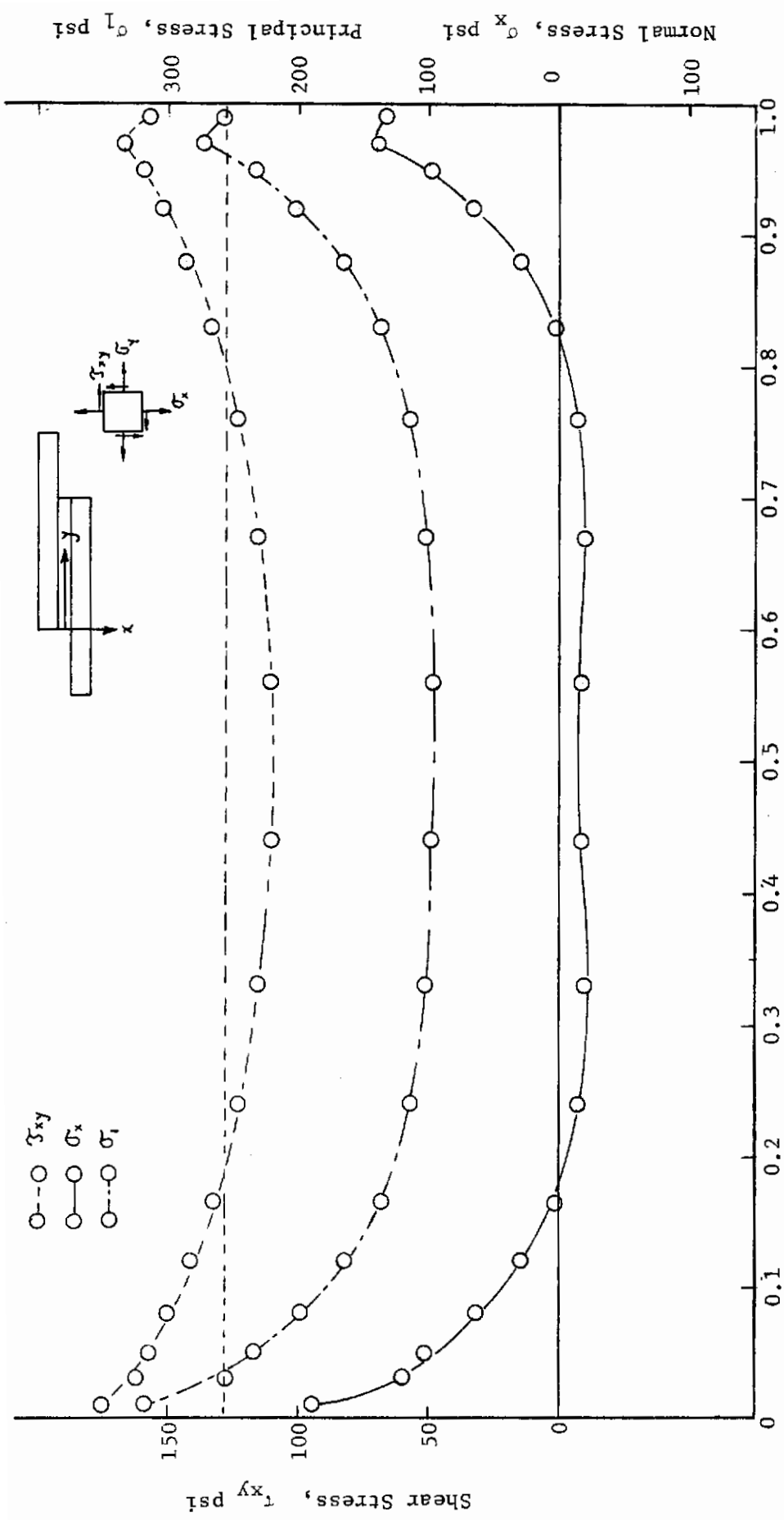

Fig. 3.21 STRESS DISTRIBUTION FROM INFINITE ELEMENT ANALYSIS - UNSUPPORTED LAP JOINT

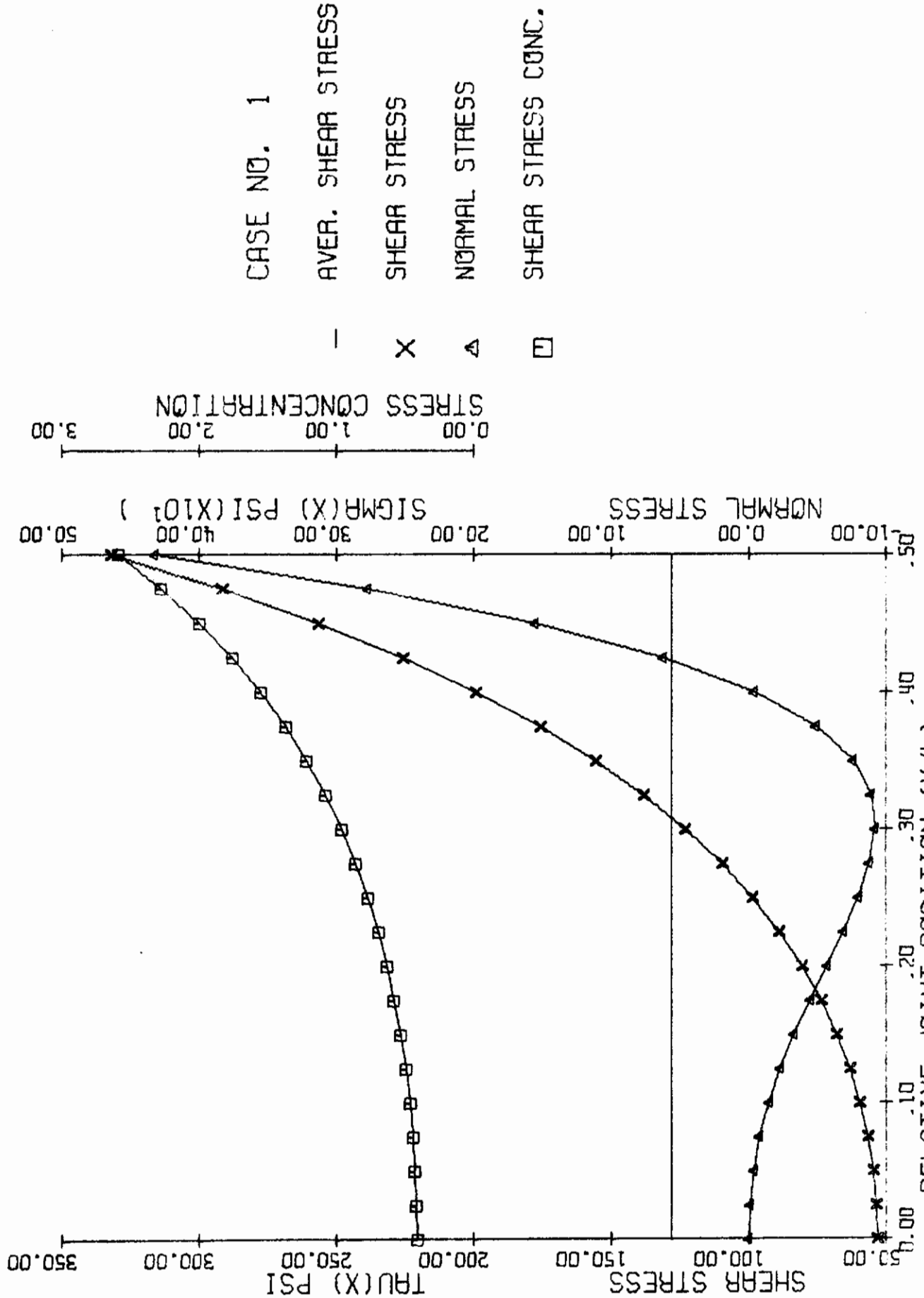

Fig. 3.22 STRESS ANALYSIS OF THE UNSUPPORTED JOINT USING THE GOLAND AND REISSNER ANALYSIS

Table 3.13

STRESS ANALYSIS OF THE SUPPORTED JOINT USING THE VOLKERSEN ANALYSIS

CASE NUMBER 1 VOLKERSEN ANALYSIS

ADHERENT PROPERTIES
T1 = 0.064 IN. T2 = 0.064 IN. W = 1.000 IN. L = 0.500 IN. E = 0.11E 08 PSI

ADHESIVE PROPERTIES
TA = 0.005 IN. GA = 50000. PSI

APPLIED LOAD P = 64. LB.

AVERAGE SHEAR STRESS TAU =********PSI

STA. NO.	JOINT POSITION (IN.)	RELATIVE POSITION	SHEAR STRESS (PSI)	SHEAR CONCENTRATION
1	X = 0.0000	X BAR = 0.00	TAU = 0.1984E 03	N = 1.550
2	X = 0.0250	X BAR = 0.05	TAU = 0.1766E 03	N = 1.379
3	X = 0.0500	X BAR = 0.10	TAU = 0.1580E 03	N = 1.234
4	X = 0.0750	X BAR = 0.15	TAU = 0.1423E 03	N = 1.112
5	X = 0.1000	X BAR = 0.20	TAU = 0.1293E 03	N = 1.010
6	X = 0.1250	X BAR = 0.25	TAU = 0.1187E 03	N = 0.927
7	X = 0.1500	X BAR = 0.30	TAU = 0.1102E 03	N = 0.861
8	X = 0.1750	X BAR = 0.35	TAU = 0.1038E 03	N = 0.811
9	X = 0.2000	X BAR = 0.40	TAU = 0.9931E 02	N = 0.776
10	X = 0.2250	X BAR = 0.45	TAU = 0.9664E 02	N = 0.755
11	X = 0.2500	X BAR = 0.50	TAU = 0.9576E 02	N = 0.748
12	X = 0.2750	X BAR = 0.55	TAU = 0.9664E 02	N = 0.755
13	X = 0.3000	X BAR = 0.60	TAU = 0.9931E 02	N = 0.776
14	X = 0.3250	X BAR = 0.65	TAU = 0.1038E 03	N = 0.811
15	X = 0.3500	X BAR = 0.70	TAU = 0.1102E 03	N = 0.861
16	X = 0.3750	X BAR = 0.75	TAU = 0.1187E 03	N = 0.927
17	X = 0.4000	X BAR = 0.80	TAU = 0.1293E 03	N = 1.010
18	X = 0.4250	X BAR = 0.85	TAU = 0.1423E 03	N = 1.112
19	X = 0.4500	X BAR = 0.90	TAU = 0.1580E 03	N = 1.234
20	X = 0.4750	X BAR = 0.95	TAU = 0.1766E 03	N = 1.379
21	X = 0.5000	X BAR = 1.00	TAU = 0.1984E 03	N = 1.550

Table 3.14

STRESS ANALYSIS OF THE UNSUPPORTED JOINT USING THE GOLAND AND REISSNER ANALYSIS

CASE NUMBER 1 GOLAND - REISSNER ANALYSIS

ADHERENT PROPERTIES
T = 0.064 IN. = 1.000 IN. L = 0.500 IN. E = 10.60E 06 PSI MU= 0.30

ADHESIVE PROPERTIES
TA = 0.005 IN. GA = 50000. PSI EA = 14.00E 04 PSI

APPLIED LOAD P = 64. LB.

AVERAGE SHEAR STRESS TAU = 128.00PSI

STA. NO.	JOINT POSITION (IN.)	RELATIVE POSITION	SHEAR STRESS (PSI)	SHEAR CONCENTRATION	NORMAL STRESS (PSI)
1	X = 0.0000	X BAR = 0.00	TAU = 5.2052E 01	N = 0.414	SIGMA N = 2.4306E-01
2	X = 0.0125	X BAR = 0.02	TAU = 5.3443E 01	N = 0.418	SIGMA N = -7.0557E-01
3	X = 0.0250	X BAR = 0.05	TAU = 5.4623E 01	N = 0.427	SIGMA N = -3.5512E 00
4	X = 0.0375	X BAR = 0.07	TAU = 5.6613E 01	N = 0.442	SIGMA N = -8.2877E 00
5	X = 0.0500	X BAR = 0.10	TAU = 5.9451E 01	N = 0.464	SIGMA N = -1.4886E 01
6	X = 0.0625	X BAR = 0.12	TAU = 6.3189E 01	N = 0.494	SIGMA N = -2.3266E 01
7	X = 0.0750	X BAR = 0.15	TAU = 6.7896E 01	N = 0.530	SIGMA N = -3.3258E 01
8	X = 0.0875	X BAR = 0.17	TAU = 7.3659E 01	N = 0.575	SIGMA N = -4.4555E 01
9	X = 0.1000	X BAR = 0.20	TAU = 8.0583E 01	N = 0.630	SIGMA N = -5.6649E 01
10	X = 0.1125	X BAR = 0.22	TAU = 8.8797E 01	N = 0.694	SIGMA N = -6.8771E 01
11	X = 0.1250	X BAR = 0.25	TAU = 9.8453E 01	N = 0.769	SIGMA N = -7.9817E 01
12	X = 0.1375	X BAR = 0.27	TAU = 1.0973E 02	N = 0.857	SIGMA N = -8.8277E 01
13	X = 0.1500	X BAR = 0.30	TAU = 1.2283E 02	N = 0.960	SIGMA N = -9.2172E 01
14	X = 0.1625	X BAR = 0.32	TAU = 1.3810E 02	N = 1.078	SIGMA N = -8.9009E 01
15	X = 0.1750	X BAR = 0.35	TAU = 1.5553E 02	N = 1.215	SIGMA N = -7.5755E 01
16	X = 0.1875	X BAR = 0.37	TAU = 1.7572E 02	N = 1.373	SIGMA N = -4.8861E 01
17	X = 0.2000	X BAR = 0.40	TAU = 1.9896E 02	N = 1.554	SIGMA N = -4.3477E 00
18	X = 0.2125	X BAR = 0.42	TAU = 2.2568E 02	N = 1.763	SIGMA N = 6.2039E 01
19	X = 0.2250	X BAR = 0.45	TAU = 2.5636E 02	N = 2.003	SIGMA N = 1.5456E 02
20	X = 0.2375	X BAR = 0.47	TAU = 2.9157E 02	N = 2.278	SIGMA N = 2.7707E 02
21	X = 0.2500	X BAR = 0.50	TAU = 3.3197E 02	N = 2.594	SIGMA N = 4.3250E 02

Again the finite element analysis is much more conservative in predicting maximum stresses. The two analyses are closest in predicting the principal normal stress. If one were to assume a shear stress failure criteria for the adhesive the finite element predicts a joint almost twice as strong as that by the Goland and Reissner. Assuming a maximum tensile stress criteria the finite element joint would be 36 percent stronger.

The real question which must now be answered is which analysis method most closely predicts actual joint behavior. The finite element method makes the least number of assumptions concerning the joint model and should be closest to reality. Next is the Goland and Reissner, third is the Volkersen. The numerical shear lag method falls close to the Volkersen method.

From the problem examples given it can now be seen what type of detail is involved in actually using the analyses. The finite element method obviously requires the most sophistication but also yields the greatest detail. It is also the only method which would allow one to actually model the composite as a layered structure and include different ply properties. The method does require access to a digital computer.

The numerical shear lag method allows one to vary joint geometry as much as the finite element method but does become tedious when all parameters are varied. The two closed form methods are limited to more uniform conditions.

Analytically, the largest contribution could be made by extending the finite element method to nonlinear elastic, plastic and finally ultimate behavior of the joint. This will, of course, be tied to the availability of materials property data of the joint components. As the general area of composite analysis develops this will be reflected by parallel advances in joints analysis.

4.0 STRENGTH OF BONDED JOINTS

The purpose of this portion of the program was to generate a body of data on the strength of bonded joints for which the mechanical properties of the joint constituents were known in detail. The group of data were to provide the basis for a set of general design guidelines for bonded construction in FRP and also a set of data for which various analytical methods could be compared. This latter point is very important since the general development of tools for analyzing bonded joints will continue and the experimental data from this program can always be used to evaluate the newer methods as they become available.

The important mechanical properties selected as variables were the modulus of the adherends and the modulus of the adhesives used to fabricate the joints. The effect of joint geometry were studied by varying the relative thickness of the adherends, the length of bonded overlap, and the thickness of the adherend within the bonded area by scarfing the adherend throughout the bonded length.

The basic joint geometry studied was the double overlap joint. The joints were tested for their static strength and several selected designs were tested in fatigue. A total of 522 joints specimens were fabricated and tested. For every variable chosen, six replicate specimens were tested, this resulted in eighty-seven groups of six specimens each. In addition, supporting studies were carried out to determine adhesive and adherend properties and surface preparation techniques.

4.1 SELECTION OF ADHESIVES AND THEIR PROPERTIES

4.1.1 Criteria for Adhesive Selection

The major thesis of this study was that the mechanical properties of adhesive in the joint have a direct effect on the stress distribution in the joint and subsequently the strength of the joint. To test this hypothesis. it was required to obtain a group of materials with a variation in at least their elastic

moduli. Kuenzi and Stevens (Ref. 4.1) have shown that materials are available with shear moduli in the ranges of 5000 psi, 50,000 psi, and 100 to 150,000 psi. Assuming a Poisson's ratio of 0.4 for materials of this type, these would be equivalent to elastic tensile moduli of 14,000 psi, 140,000 psi, and 280 to 420,000 psi.

A series of five materials were selected for evaluation as possible adhesives. These were:

1. FM 1000 (Polyamide-epoxy, American Cyanamid)
2. FM 47, Type 2 (Bloomingdale Rubber Co.)
3. Metlbond 040C (Whitaker-Narmco)
4. AF-131 (3M Co.)
5. Epon 422 (Shell Chemical Co.)
6. E 787 (Epon 828-1031, BDMA, NMA)

It was assumed that the tensile modulus of these materials as obtained from their behavior in film form could be used to characterize their general behavior. This assumes that their behavior in film form will be the same as that in a joint and that the general shape of their stress-strain curve will be the same in shear as in tension.

The materials finally selected for use in fabricating joints were the following:

Adhesive	IITRI Material Number	Tensile Modulus (psi)
FM-1000	80	160,000
Metlbond 400	90	292,000
FM-47, Type II	81	621,000

No material was found for the low tensile modulus class of 15,000 psi.

4.1.2 Film Properties of Adhesives

The primary guideline in preparing adhesive films for generating mechanical properties data is to use the same adhesive material and as near as possible the same cure conditions during film preparation as in curing the joints. It is inevitable that in either process there will be some differences. One problem that exists is that following cure of the adhesive film, flaws that might exist are easily detected and the film discarded and remade. In the bonded joint, the adhesive must be tested first and then the results interpreted accordingly. Attempts were made during the course of this work to not only establish a workable process for producing good film but to simulate the type film which might occur within the confines of the joint.

Since films of the adhesives employed had not been previously made, it was necessary to explore the previously proposed methods and conditions to establish a workable process for fabrication of each different adhesive film. Conditions of time, temperature, and pressure recommended by the manufacturer for the adhesive were followed. After several experimental trials, it was possible to make uniform films with few irregularities such as wrinkles or bubbles from adhesives with less than 2 percent volatiles. These adhesives were FM-1000, AF-131, (100 percent) solids, and Metlbond 400.

Attempts to prepare thin films from AF-131, 65 percent solids in M.E.K., on glass plates using a calibrated doctor blade yielded uniform but very fragile films. These films contained a series of edge fractures induced during cutting of the test specimens. Thus it became necessary to press thicker sheets from the AF-131 directly from 100 percent solids material.

Of the remaining adhesive materials which contained greater than 2 percent volatiles, films were prepared from both FM-47, Type II and Epon 422. However, only film from FM-47 was considered good enough for testing. Epon 422, which contains plyophen, liberates up to 15 percent volatiles during curing

which results in a porous foam type bond. Test films were excessively porous with large bubbles and appeared like the surfaces of adhesively failed metal to metal peel specimens observed in the past.

It was felt this material could not be characterized with sufficient accuracy for this program and therefore was not used for further joint fabrication.

A schematic diagram showing the layup for fabricating films is shown in Fig. 4.1.

The tensile mechanical properties of the adhesive films were measured using a clip-gage extensometer and an Instron Test Machine equipped with an area compensator. With this instrumentation it was possible to obtain stress-strain curves directly. All the specimens were of uniform width and thickness and approximately 4.0 in. long. The tests were conducted at 0.05 in./min unless otherwise noted. Figure 4.2 shows a film specimen under test.

The purpose of these tests was to categorize the materials as to modulus of elasticity and to provide some measure of their variability of strength. The modulus for all tests was taken as the initial tangent modulus of the stress-strain curve.

The specific details of film fabrication and test results are described for each adhesive in the following sections.

4.1.2.1 FM-1000

Adhesive films of FM-1000 (polyamide-epoxy unsupported film, manufactured by the American Cyanamid Co., Bloomingdale Division) were prepared from Batch No. B-2070, Roll No. 6-23934. This same batch of material was later used for fabrication of bonded joints.

Two plies of adhesive, 6 in. by 8 in., were cut and placed as a laminate between two sheets of Capran fill pretreated with Ram 225 mold release. This assembly was sandwiched between two

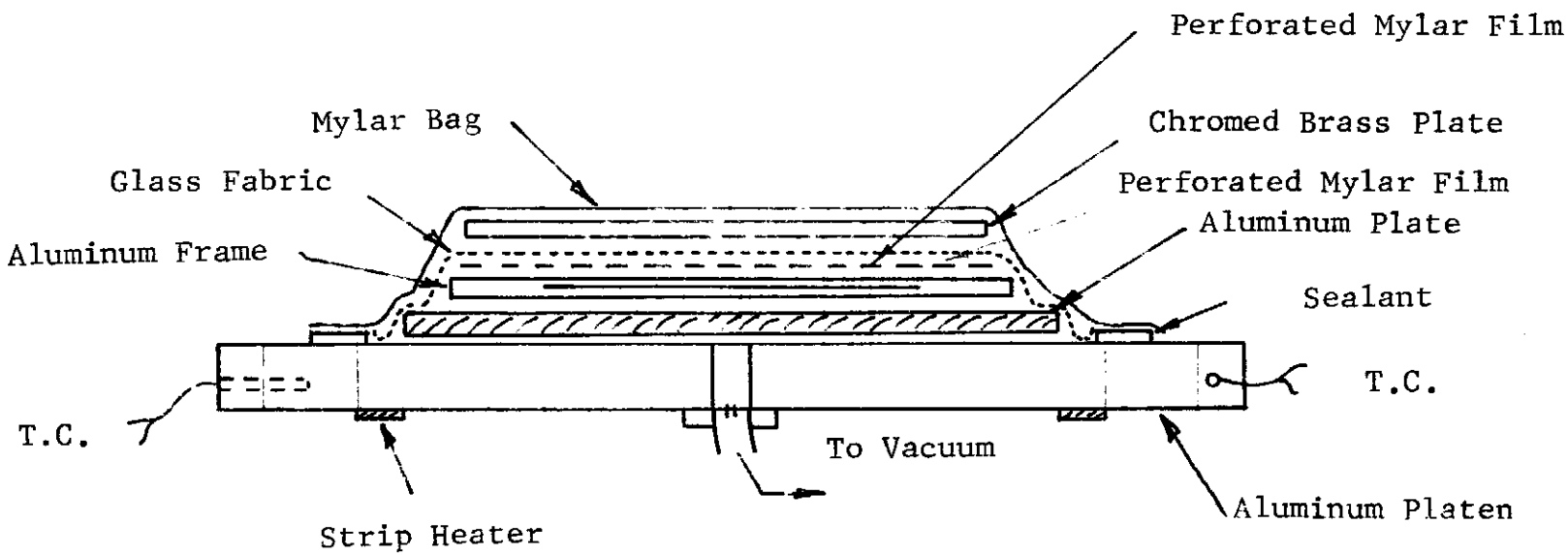

Fig. 4.1 VACUUM BAG SYSTEM FOR FILM FABRICATION

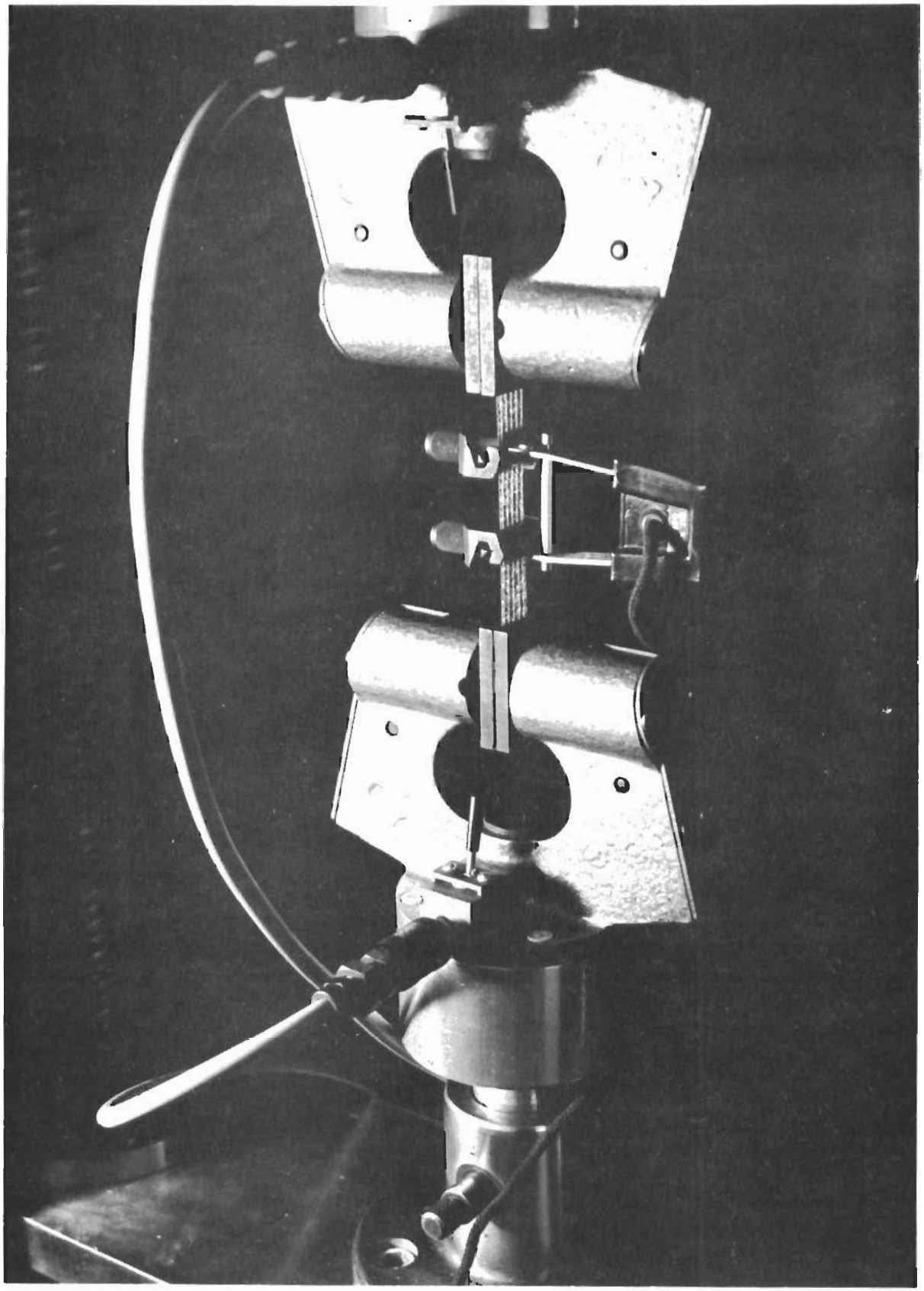

Fig. 4.2 TENSILE TEST OF AN ADHESIVE FILM USING A CLIP GAGE EXTENSOMETER

1/16 in. aluminum plates, resting on a 1/2 in. aluminum base plate with electric heaters attached underneath. The plate was fitted with a vacuum line and instrumented with thermocouples. A vacuum diaphragm of Mylar film was placed over the assembly and sealed to the base plate with zinc chromate putty.

The adhesive film was cured by drawing enough vacuum to just seal the diaphragm during elevation of temperature from R.T. to 340°F in 60 min in an autoclave. Temperature was held at 340°F under a total pressure of 20 psi for 60 min then cooled to R.T. under pressure.

This same technique was used to prepare seven different films. A total number of forty-five specimens were tested, and these were used to evaluate the effects of strain rate and film age on the mechanical properties.

In general the FM-1000 material exhibited a larger degree of time dependent behavior than was initially anticipated when it was selected for this program. The results of the first film prepared are shown in Table 4.1. The material had an average modulus of 123,000 psi, an undefined fracture strength, and a greater than 50 percent elongation. It exhibited a marked amount of yielding and time dependent behavior. The average yield stress was 1940 psi. None of the specimens actually fractured, but continued to flow plastically at the deflection rate of 0.05 in./min. A typical stress-strain is shown in Fig. 4.3. There was also some evidence that the film was changing with age. The material would be classed as an aging non-linear viscoelastic material.

In an attempt to further investigate the above effects, six new films were prepared and tested. These films yielded 38 specimens and their test results are shown in Tables 4.2 and 4.3.

Table 4.2 shows the results of 22 specimens all tested at 2.0 in./min and made from three separate films. The average tensile strength of each film compares well with each other film but the range of scatter for each does vary.

Table 4.1

TENSILE PROPERTIES OF FM-1000 ADHESIVE FILM AT 0.05 IN./MIN

Specimen Number	Thickness (in.)	Width (in.)	Maximum Strain (%)	Tensile[b] Strength (psi)	Modulus (10^5 psi)	Deflection Rate (in./min)
80-5-1	0.025	0.50	a	2900	1.32	0.05
80-5-2	0.023	0.50	a	2900	1.25	0.05
80-5-3	0.013	0.50	a	1700	-	0.05
80-5-4	0.023	0.50	a	1500	-	0.05
80-5-5	0.023	0.50	a	2275	1.13	0.05
80-5-6	0.022	0.50	a	1600	-	0.05
80-5-7	0.028	0.50	a	700	-	0.05
		Average		1940	1.23	

[a] None of the specimens fractured, all yielded continuously to greater than 300% strain.

[b] Stress at yield.

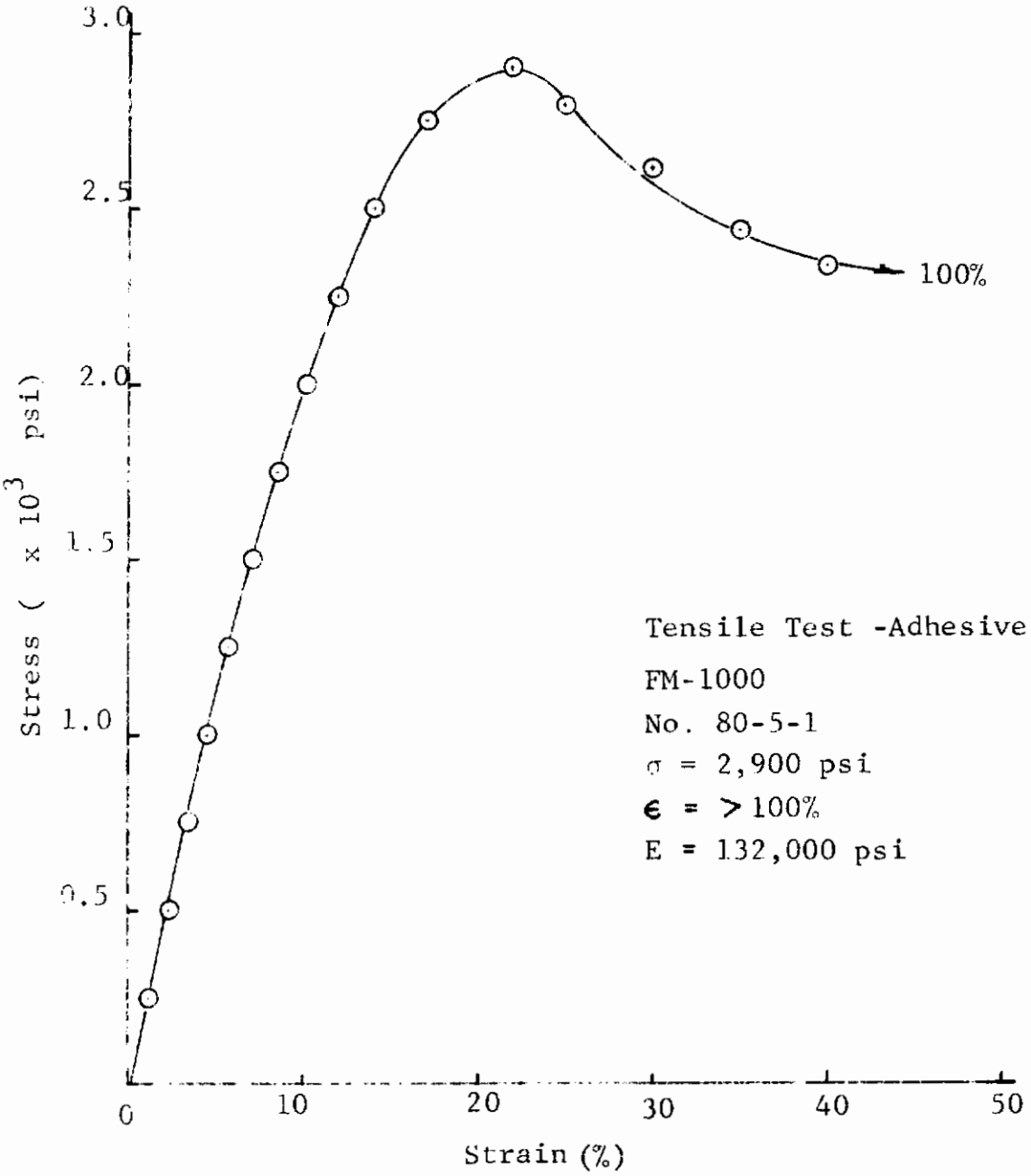

Fig. 4.3 TENSILE PROPERTIES OF FM-1000 ADHESIVE AT 0.05 IN./MIN

Table 4.2

TENSILE PROPERTIES OF FM-1000 ADHESIVE FILM AT 2.0 IN./MIN

Specimen Number	Thickness (in.)	Width (in.)	Maximum Strain (%)	Tensile Strength (psi)	Modulus (10^5 psi)	Deflection Rate (in./min)
80-30-1	0.010	0.50	-	7400	-	2.0
80-30-2	0.010	0.50	42	6200	-	2.0
80-30-3	0.010	0.50	50	7800	-	2.0
80-30-4	0.010	0.50	44	6600	-	2.0
80-30-5	0.010	0.50	44	6600	-	2.0
80-30-6	0.010	0.50	45	5600	-	2.0
		Average	45	6700		
80-31-1	0.010	0.50		7040	2.74	2.0
80-31-2	0.010	0.50		6510	2.32	2.0
80-31-3	0.010	0.50		8010		2.0
80-31-4	0.010	0.50		6030		2.0
80-31-5	0.010	0.50		6900		2.0
80-31-6	0.010	0.50		4760[a]		2.0
		Average		6500	2.53	
80-36-1	0.009	0.5	116	5870	2.33	2.0
80-36-2	0.009	0.5	154	6080	1.64	2.0
80-36-3	0.009	0.5	a	5480	2.53	2.0
80-36-4	0.009	0.5	121	5220	1.49	2.0
80-36-5	0.009	0.5	116	5020	1.51	2.0
80-36-6	0.009	0.5	155	7300	2.67	2.0
80-36-7	0.009	0.5	153	7190	a	2.0
80-36-8	0.009	0.5	146	5670	a	2.0
80-36-9	0.009	0.5	159	6590	2.12	2.0
80-36-10	0.009	0.5	123	5540	2.18	2.0
		Average		6000	2.06	

[a]Incomplete record

Table 4.3

TENSILE PROPERTIES OF FM-1000 ADHESIVE FILM AT VARIOUS DEFLECTION RATES

Specimen Number	Thickness (in.)	Width (in.)	Maximum Strain (%)	Tensile Strength (psi)	Modulus (10^5 psi)	Deflection Rate (in./min)
80-37-1	0.010	0.50	314	5800	a	0.05
80-37-2	0.010	0.50	272	5600	a	0.50
80-37-3	0.010	0.50	386	6560	a	2.0
80-37-4	0.010	0.50	308	6840	a	2.0
80-38-1	0.010	0.50	> 400	3200[c]	1.77	0.05
80-38-2	0.010	0.50	> 400	6000[c]	1.45	0.05
80-38-3	0.010	0.50	203	6370		0.50
80-38-4	0.010	0.40	214	6510		0.50
80-38-5	0.010	0.50	176	5570		2.0
80-38-6	0.010	0.50	210	7780		2.0
80-40-1	0.010	0.50	37	6170[c]	2.52	2.0
80-40-2	0.010	0.50	d	6900[c]	2.58	2.0
80-40-3	0.010	0.50	49[d]	5080[c]	2.30	0.5
80-40-4	0.010	0.50	223	5450[c]	2.36	0.5
80-40-5	0.010	0.50	> 400	3480[c]	1.76	0.05
80-40-6	0.010	0.50	> 400	3690	1.83	0.05

[a] Specimen length 0.50 in. between grips. All other data for 4.0 in. grip length.

[c] Yield Stress

[d] Premature Failure

All the data obtained at 2.0 in./min has been treated as coming from the same population and the tensile strength as a function of cumulative probability of failure has been computed and is shown in Fig. 4.4. The data ranged from 5,000 to 8,000 psi with an average of 6,400 psi.

The cumulative probability (Sn) is obtained by first ordering all the data from the lowest to the highest value and assigning each value a rank (n) ranging from (1) to (N) the total number of values in the group. By definition then:

$$S_n = \frac{n}{N+1}$$

The cumulative probability then indicates what percentage of the total population will have failed at any given stress level. For the FM-1000 at a stress of 6,400 psi, 50 percent of the population of specimens will have failed.

The modulus of elasticity of the first films showed a variation of 149,000 to 274,000 psi. This range would be unacceptable to obtain a design value for joint analysis; therefore, three more films were prepared and their properties determined. For the results shown in Table 4.3, difficulties were encountered in measuring the moduli and no firm conclusions could be reached. The results shown in Table 4.3 though show a definite relationship between strength, modulus, and deflection rate. Both strength and modulus increase with test velocity over the range from 0.05 to 2.0 in./min. At the lowest rate the material yields continuously without fracture and at the highest rate actual fracture does occur. All the stress calculations made for these specimens are based on the original area of the specimen prior to load and are not correct after the specimen exceeds the small deflection range. As an indication of how far off these values can be, the true engineering stress at failure was computed for one of the specimens tested at 0.5 in./min and was found to be over 20,000 psi.

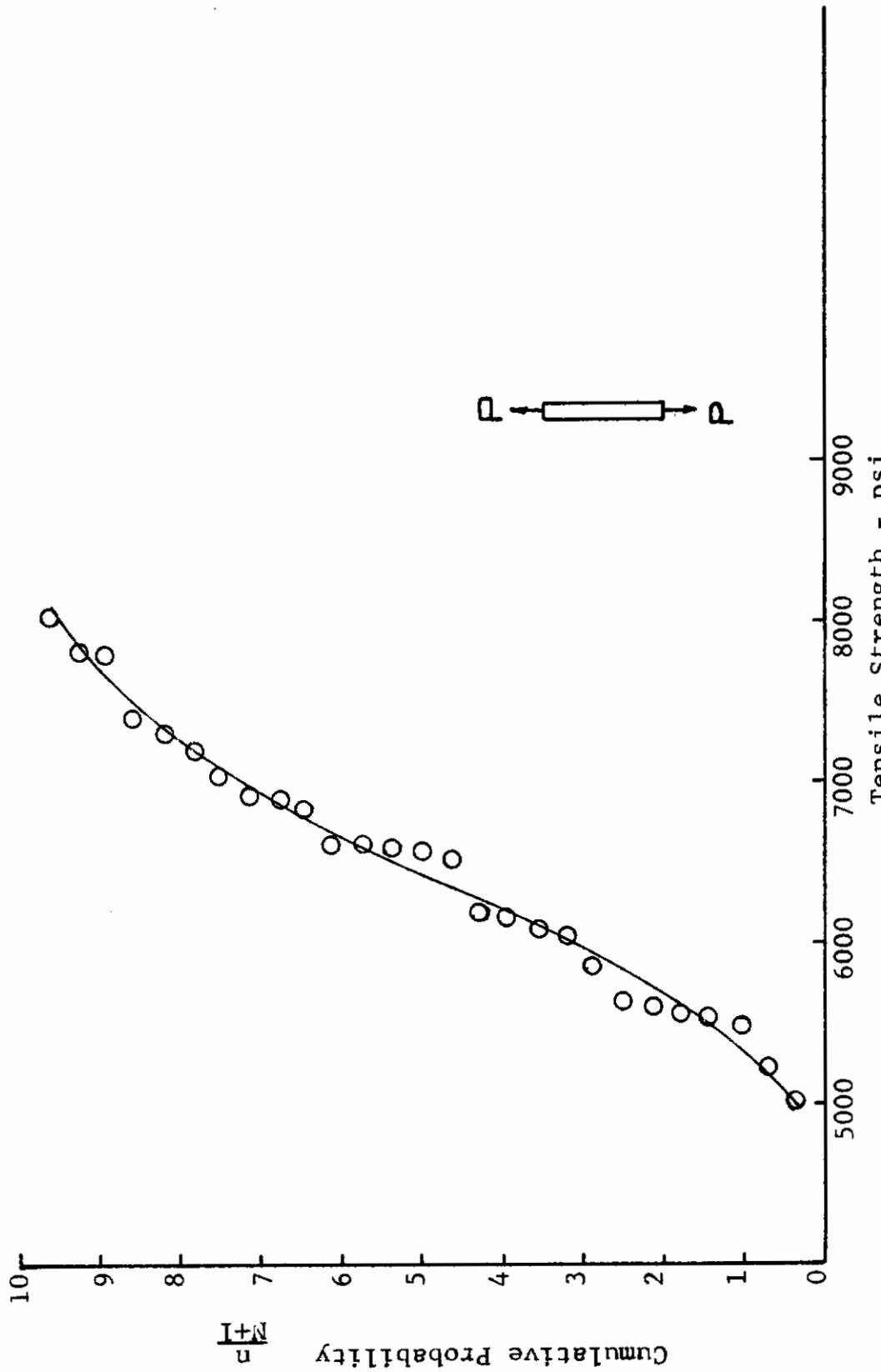

Fig. 4.4 STATISTICAL DISTRIBUTION OF TENSILE STRENGTH OF FM-1000 ADHESIVE FILM AT 2.0 IN./MIN

Two major conclusions can be drawn thus far concerning this material.

1. The material has a modulus in the intermediate range between the conventionally high modulus adhesives and the low (E) 15,000 psi materials.

2. At slow rates of deformation, the material has a large amount of plastic behavior which should allow it to relieve itself in areas of high strain concentrations and should reach a more uniform state of strain when used in a shear condition in a joint. This should result in very strong joints.

A summary of the average properties is given in Table 4.4.

4.1.2.2 Metlbond 400

Two films of Metlbond 400 (manufactured by Whittaker-Narmco) were prepared from unsupported film, Batch No. 386. The procedure established was to lay up a single ply of adhesive film, 4.0 by 8.0 by 0.10 in. within a flat aluminum picture frame of approximately the same internal dimensions. The layup sequence is shown in Fig. 4.1. All materials, aluminum and perforated Mylar, in contact with the adhesive film were pretreated with Ram 225 release agent. Assembly of the thermocouple instrumented vacuum diaphragm assembly was completed in an autoclave. The film was cured according to the cycle which follows:

The layup was evacuated to 29 in. ca., 14 psi, and temperature raised to 350°F in 60 min (4 to 5 deg/min). Temperature was held 60 min at 350°F and 14 psi. Film was cooled under pressure to room temperature.

The results of fourteen tests of Metlbond 0400 are shown in Table 4.5. This material has an average modulus of 292,000 psi based on all the data at 2.0 in./min. The tensile strength was 7310 psi. At the higher rates of deflection the material showed the

Table 4.4

SUMMARY OF TENSILE PROPERTIES OF FM-1000 ADHESIVE

Deflection Rate (in./min)	Tensile Yield Strength (psi)	Maximum Strain (%)	Elastic Modulus (ksi)
0.05	3400	~400	1.60
0.50	5250	~ 150	2.33
2.0	6530	~ 100	2.55

Table 4.5

TENSILE STRENGTH OF METLBOND 400 ADHESIVE FILM

Specimen Number	Thickness (in.)	Width (in.)	Maximum Strain (%)	Tensile Strength (psi)	Modulus (10^5 psi)	Deflection Rate (in./min)
90-11-1	0.013	0.50	250	7080	-	2.00
90-11-2	0.012	0.50	225	7080	-	2.00
90-11-3	0.012	0.50	225	5670	-	20.00
90-11-4	0.011	0.50	220	5920	-	20.00
90-11-5	0.013	0.50	245	6620	-	20.00
90-11-6	0.012	0.50	85	3840	-	20.00
90-16-1	0.012	0.50	50	6900	2.90	0.05
90-16-2	0.012	0.50	-	8800	3.45	0.05
90-16-3	0.012	0.50	100+	7900	3.23	0.2
90-16-4	0.011	0.50	100+	5600	2.32	0.2
90-16-5	0.012	0.50	100+	5300	2.30	0.2
90-16-6	0.013	0.50	100+	6000	2.47	2.0
90-16-7	0.012	0.50	100+	8000	3.06	2.0
90-16-8	0.009	0.50	190	6900	2.69	2.0
		Average[a]	200	7310	2.92	2.0

[a]Averages of the results at 2.0 in./min

formation of a true neck with resultant yielding and then finally increased to a fracture stress. For all of these film tests, the stress is based on original cross sectional area. A typical stress-strain curve is shown in Fig. 4.5. This material appears to be stiffer than the FM-1000 and to have a lesser value for maximum elongation.

4.1.2.3 Adhesive AF-131

Three film samples of AF-131 (manufactured by 3M Company) were prepared from chunks of 100 percent solids material. The material was broken into small pieces and placed between 10 mil Mylar film pretreated with Ram 225 release agent. The adhesive film sandwich was placed between 3/8 in. thick aluminum plates and heated to 230°F for 15 min in an oven to melt the adhesive to a continuous layer. The assembly was then removed from the oven and, with the top aluminum plate removed, film formation was assisted by running a roller over the fluid adhesive within the Mylar films. The top Mylar film was replaced with a perforated prereleased Mylar film which was covered with Type 181 glass cloth. This sandwich was placed between aluminum plates and sealed within a Mylar vacuum diaphragm to the electrically heated aluminum base plate located in the autoclave. Temperature was controlled by instrumented thermocouples.

The cure cycle was started after evacuation of the diaphragm and sealing the autoclave as is shown in the following schedule:

> Raised temperature from 77 to 350°F under 14 psi in 40 min. Held 350°F for 60 min at 64 psi (absolute). Cooled under pressure.

The resulting films were 0.040 to 0.080 in. thick with a few scattered bubbles.

Thirty-two tests were run for the AF-131 material at a deflection rate of 0.05 in./min. These results are shown in Table 4.6. The average modulus for this material is 482,000 psi, which places it in the category of the stiffer adhesives.

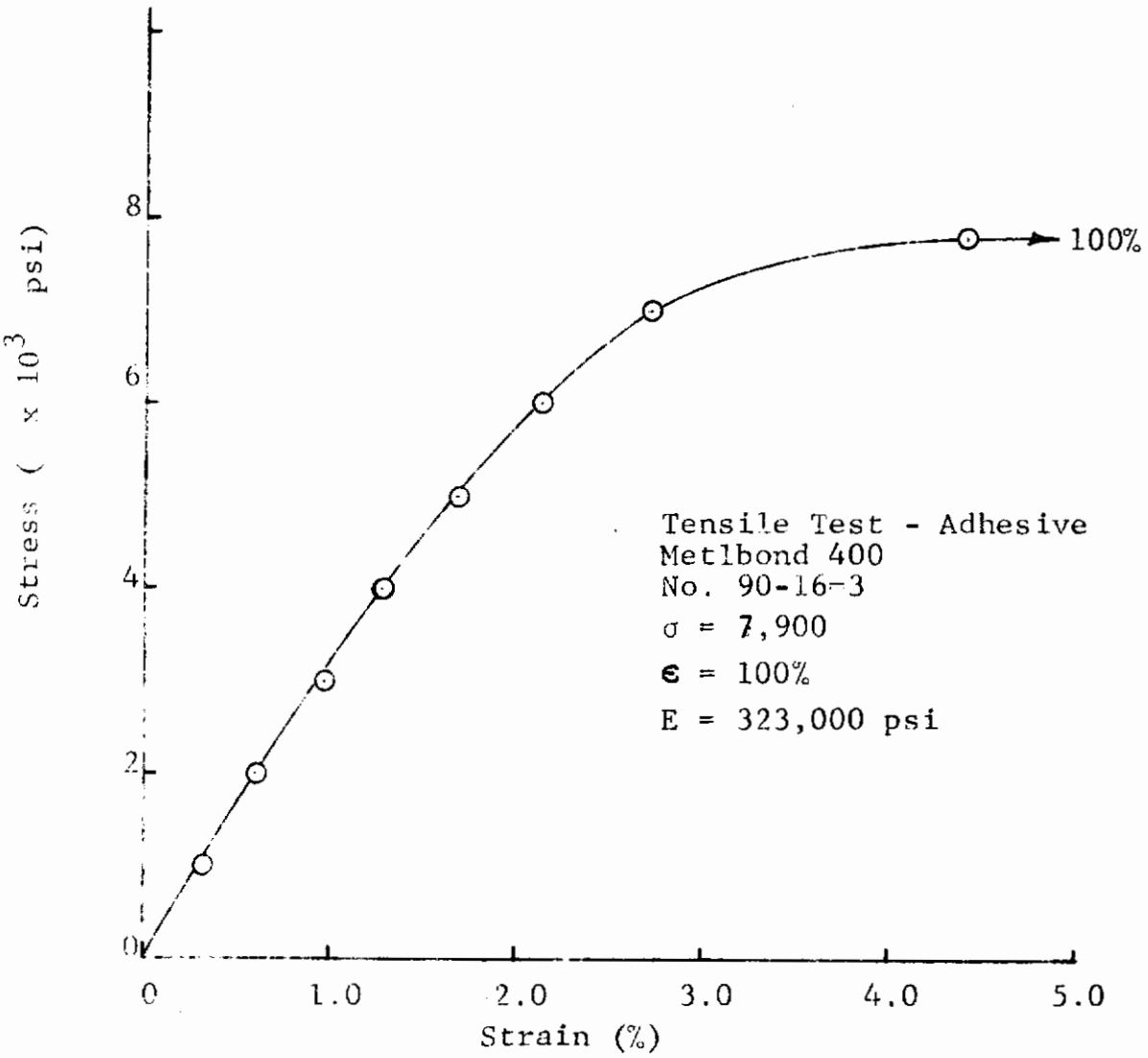

Fig. 4.5 TENSILE STRESS-STRAIN CURVE OF METLBOND 400 ADHESIVE FILM

Table 4.6

TENSILE PROPERTIES OF AF 131 ADHESIVE FILM

Specimen Number	Thickness (in.)	Width (in.)	Maximum Strain (%)	Tensile Strength (psi)	Modulus (10^5 psi)	Deflection Rate (in./min)
82-7-1	0.075	0.440	1.40	6100	4.89	0.05
82-7-2	0.073	0.447	1.60	6800	4.67	0.05
82-7-3	0.077	0.443	1.45	6300	4.62	0.05
82-7-4	0.071	0.451	2.10	9200	5.06	0.05
82-7-5	0.066	0.446	1.25	5500	4.72	0.05
82-7-6	0.057	0.435	2.25	8500	4.32	0.05
82-7-7	0.075	0.444	1.72	7200	4.56	0.05
82-7-9	0.056	0.454	2.13	9100	4.88	0.05
82-7-10	0.065	0.443	1.80	7200	4.44	0.05
82-7-11	0.067	0.448	2.10	8500	4.53	0.05
		Avg.	1.78	7400	4.67	
82-8-1	0.040	0.510	0.9	3900	-	0.05
82-8-2	0.050	0.510	1.15	5000	4.65	0.05
82-8-3	0.046	0.510	1.33	5500	4.52	0.05
82-8-4	0.052	0.510	2.00	8000	4.60	0.05
82-8-5	0.053	0.504	1.50	6600	4.30	0.05
82-8-6	0.052	0.506	1.65	7000	4.68	0.05
82-8-7	0.050	0.504	1.30	6300	5.30	0.05
82-8-8	0.044	0.453	1.25	5400	4.71	0.05
82-8-9	0.046	0.443	1.25	5900	5.48	0.05
82-8-10	0.042	0.439	1.25	5600	4.94	0.05
82-8-11	0.051	0.408	2.03	6000	4.52	0.05
82-8-12	0.050	0.360	1.33	6100	4.90	0.05
		Avg.	1.41	5950	4.80	
82-9-1	0.046	0.544	1.78	7500	5.29	0.05
82-9-3	0.040	0.548	1.03	4900	5.43	0.05
82-9-4	0.044	0.548	1.50	6300	4.71	0.05
82-9-5	0.038	0.550	0.73	3300	4.51	0.05
82-9-6	0.031	0.546	1.43	7400	5.80	0.05
82-9-7	0.045	0.497	1.15	5600	5.33	0.05
82-9-8	0.043	0.535	1.35	6100	5.00	0.05
82-9-9	0.040	0.545	0.80	3900	-	0.05
82-9-10	0.047	0.542	0.88	4100	4.88	0.05
82-9-11	0.043	0.546	0.85	4000	4.51	0.05
		Avg.	1.15	5300	5.05	

The stress-strain curve for this material is almost linear up to failure and shows no yielding or flow behavior. The tensile strength varied from 3,330 psi to 9,200 psi with the lower strengths usually due to the presence of small air bubbles. A typical stress-strain curve is shown in Fig. 4.6.

4.1.2.4 Adhesive FM-47

Three free films of FM 47, Type II (vinyl phenolic on glass cloth, manufactured by American Cyanamid, Bloomingdale Division) were prepared from Batch No. 1141. A single ply of adhesive film cut to 4 x 8 in. size was laid up as described previously mounted in an autoclave and cured according to the schedule which follows:

Time (min)	Temp °F	Pressure (psi)
30	R.T. to 200	14(29 in. Hg)
30	200 to 340	64
30	340	64

Cooled from 340°F to R.T. under pressure.

Seventeen tests were run on the cast films and these are summarized in Table 4.7. This material showed the highest modulus of all the materials tested with an average value of 621,000 psi. The highest average value was obtained for film 81-14. This value may be slightly inaccurate since no extensometer was used and the modulus was taken from the load-deflection record. If there was any grip slippage present, this would have reduced the modulus by increasing the deflection at any load, consequently, if the modulus value is incorrect, the true modulus would be higher yet. Films 81-32 and 81-33 were tested using a clip gage extensometer for measuring the strain. The modulus results for these films were slightly lower than for 81-14 indicating a low error probability for the uninstrumented specimens.

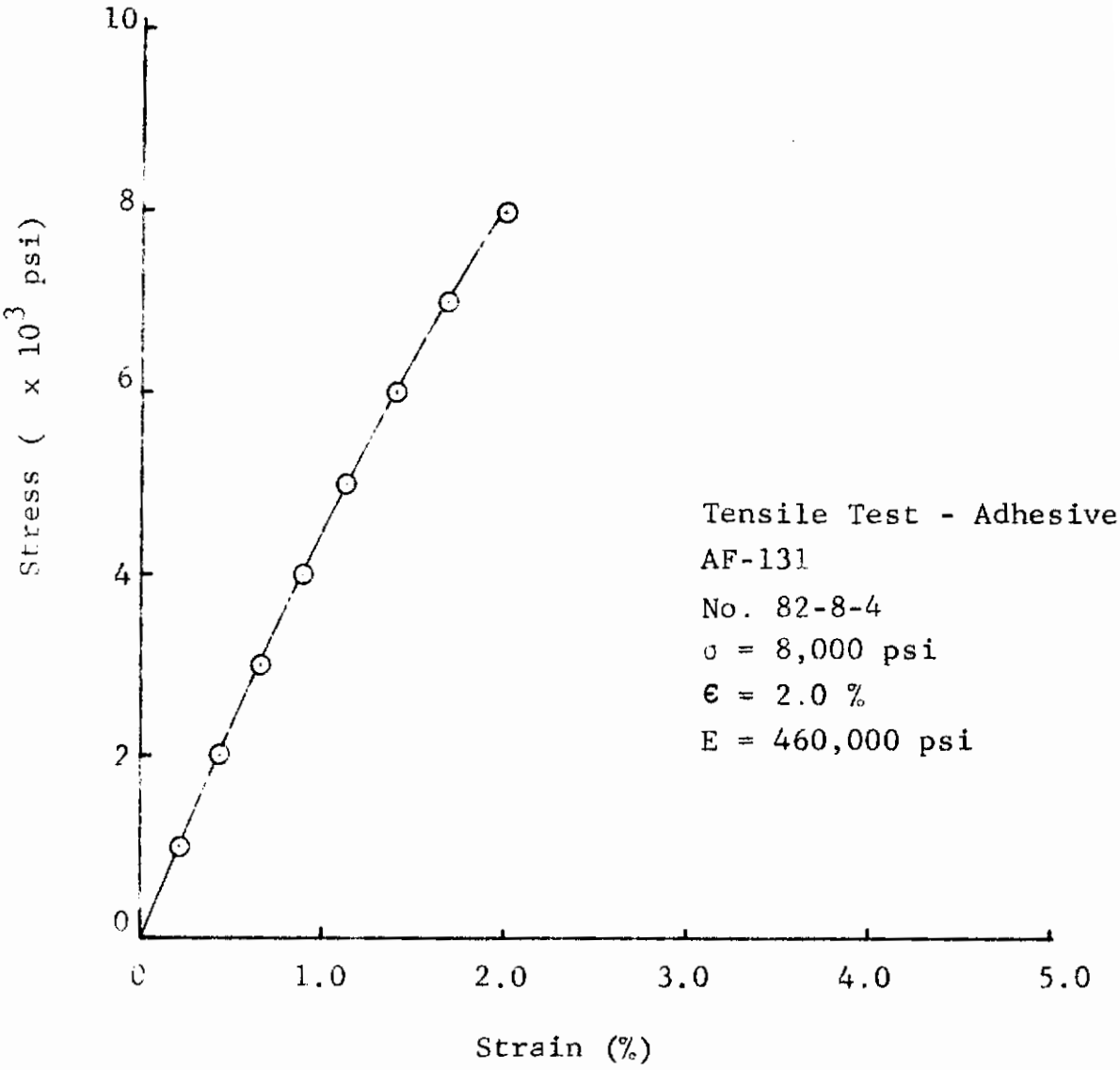

Fig. 4.6 TENSILE STRESS STRAIN CURVE OF AF-131 ADHESIVE

Table 4.7

TENSILE PROPERTIES OF FM-47 ADHESIVE FILM

Specimen Number	Thickness (in.)	Width (in.)	Maximum Strain (%)	Tensile Strength (psi)	Modulus (10^5 psi)	Deflection Rate (in./min)
81-14-1	0.012	0.50	-	7,750	-	0.5
81-14-2	0.012	0.50	2.2	10,200	6.64	0.5
81-14-3	0.013	0.50	1.6	8,000	6.30	0.5
81-14-4	0.012	0.50	1.8	9,740	6.33	0.5
81-14-5	0.012	0.50	1.3	6,670	6.11	0.5
81-14-6	0.012	0.50	1.2	6,870	6.73	0.5
81-14-7	0.012	0.50	1.5	8,160	6.18	0.5
		Avg.	1.6	8,200	6.38	
81-32-2	0.016	0.500	1.62	8,800	5.85	0.5
81-32-3	0.016	0.500	1.16	6,400	5.74	0.5
81-32-4	0.016	0.500	1.47	8,700	6.46	0.5
81-32-5	0.016	0.500	1.71	9,400	5.93	0.5
81-32-6	0.016	0.500	1.45	8,200	6.07	0.5
		Avg.	1.48	8,300	6.00	
81-33-1	0.016	0.500	1.55	8,600	6.05	0.5
81-33-2	0.016	0.500	1.40	7,200	5.55	0.5
81-33-3	0.016	0.500	1.34	7,900	6.31	0.5
81-33-4	0.016	0.500	1.48	9,200	6.50	0.5
81-33-5	0.016	0.500	1.33	9,000	6.92	0.5
		Avg.	1.42	8,400	6.26	

This film showed an almost linear load-deflection record similar to the AF-131 material with no indication of yielding or flow. A typical stress-strain curve is shown in Fig. 4.7.

4.1.2.5 Summary of Adhesive Film Properties

Table 4.8 summarizes the final materials properties selected to characterize the final four adhesives tested. All the joints finally made from these materials were tested at 0.05 in./min which is equivalent to the rates at which the adhesives were tested.

4.1.3 Shear Moduli of Bulk Adhesive Materials

The shear modulus of rigidity has been measured for AF-131 (3 M Co.) and Epon 828-1031-MNA-BDMA resins using the plate shear method and also by using data for modulus of elasticity and Poisson's ratio obtained from strain-gage instrumented tensile bars. These tests were carried out to determine if the plate shear method could be used as an alternative method for determining shear modulus. The specimens for this method are easier to prepare and test than those for the torsion testing of a right circular cylinder which is the conventional test specimen used.

4.1.3.1 Specimen Preparation

Five flat plate specimens approximately 4.5 in. square by 0.125 in. thick were fabricated for both materials. The AF-131 was obtained from the 3 M Co. in the form of large solid resin chunks. These pieces were broken to a smaller size and were then placed in a steel compression mold coated with RAM 225 mold release. The following cure schedule was used.

Time (hr)	Temp (°F)	Pressure (psi)
1	R.T. to 350	200
2	350	220
As required	350 to 200	220

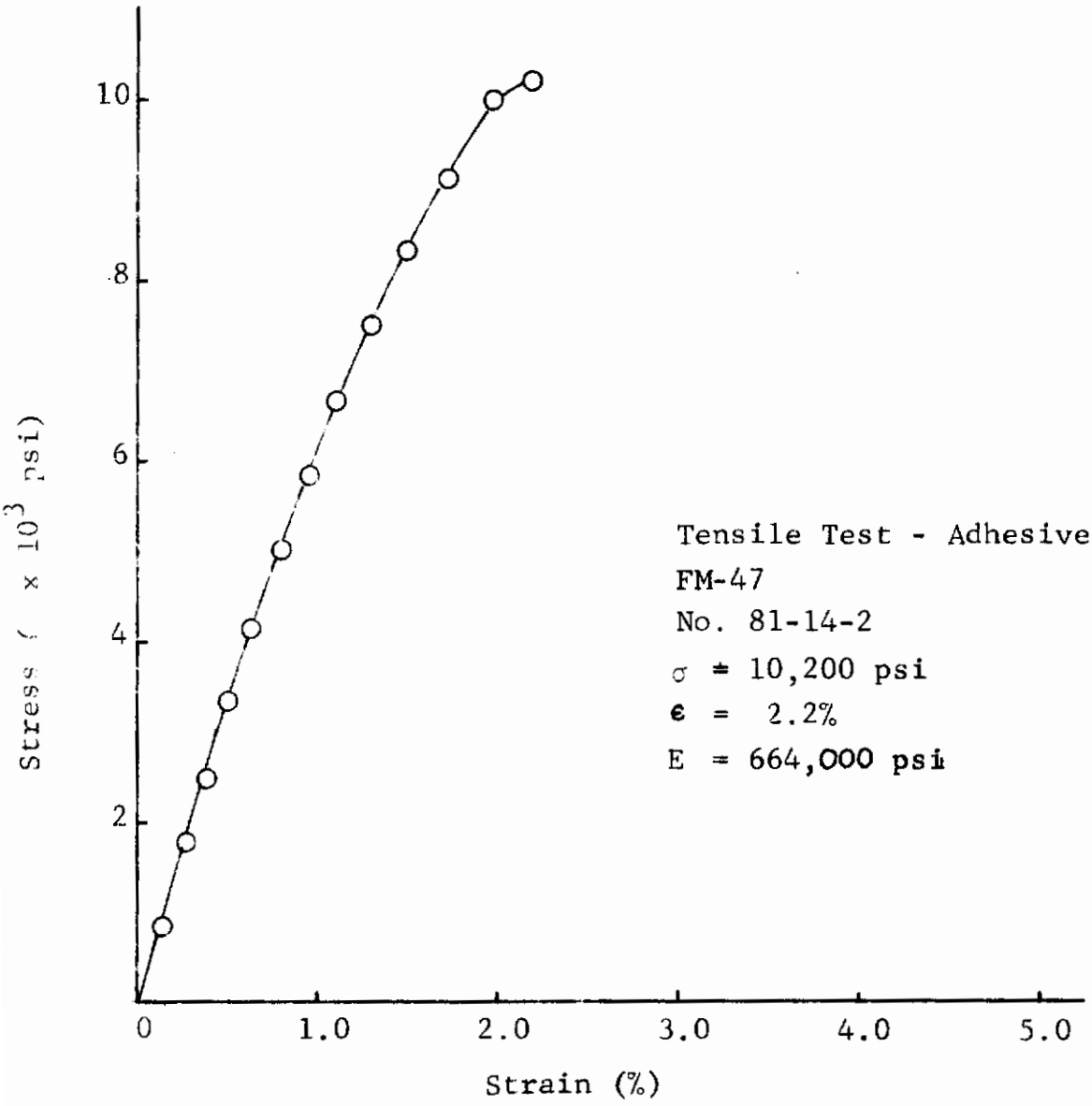

Fig. 4.7 TENSILE STRESS STRAIN CURVE OF FM-47 ADHESIVE FILM

Table 4.8

SUMMARY OF MECHANICAL PROPERTIES OF ADHESIVE FILMS

Adhesive	Chemical Type Manufacturer	Tensile Strength (psi)	Maximum Strain (%)	Modulus (10^5 psi)	Deflection Rate (in./min)
FM 1000	Polyamide Epoxy American Cyanamid, Bloomingdale Division	3400	> 300	1.60	0.05
Metlbond 400	Nylon Epoxy Whittaker Corp. Narmco Materials Div.	7310	200	2.92	2.0 *
AF 131	Modified Epoxy 3 M Co.	5300	1.15	4.82	0.05
FM 47	Vinyl Phenolic American Cyanamid, Bloomingdale Division	8300	1.50	6.21	0.5 *

* No strain rate effect on modulus.

The plates obtained were flat, homogeneous and void free. They did show the presence of flow lines from the melting of the material but it was not felt that these affected the behavior of the plates. The plate edges did not require any further machining prior to test.

The Epon 828-1031-BDMA-MNA material was prepared from the following formulation.

Shell Epon 828	50	gms
Shell Epon 1031-B80	62.5	gms
Nadic Methyl Anhydride	90	gms
N, N Benzyl Dimethylamine	0.55	gms

The resins and the NMA were mixed at room temperature and then let stand for one and one-half hours before adding the BDMA. The resulting mix was cast between glass plates coated with RAM 225 mold release using rubber gaskets to control the plate shape. The following cure schedule was used.

Time (hr)	Temp (°F)	Pressure (psi)
2	180	14.7
2	350	14.7

The plates obtained were clear, void free and homogeneous. They were cut to final size using a wet diamond wheel.

The tensile specimens for these tests were cut from the same plates used for the plate shear test after the shear test was completed. The specimens were 0.50 in. wide with a uniform width throughout their length. These were also cut off using the diamond saw.

4.1.3.2 Plate-Shear Tests

According to St. Venant's principle, a homogeneous square plate loaded in opposite directions on the diagonal corners is equivalent to a plate loaded with a constant twisting moment. A linear elastic analysis of a plate subject to this type of

loading shows that the shear modulus of the material can be related to the load-deflection characteristics of the plate with the following expression:

$$G = \frac{3\,u^2\,P}{2\,t^3\,w}$$

where:

G = shear modulus
P = load applied at any plate corner
t = plate thickness
u = distance from the center of the plate to the point at which the deflection is measured
w = deflection at (u) relative to the center of the plate

The test fixture for the plate measurements is shown in Fig. 4.8. A deflectometer was built using a 0.0001 in. dial gage which measured the deflection of the quarter point between the load reactions on one diagonal relative to the center of the plate. A load deflection-curve was obtained using an Instron machine equipped with a trace marker. The load record was "marked" for every 0.002 in. of plate deflection. All plates were tested at a deflection rate of 0.05 in./min.

A load-deflection record was obtained with both increasing and decreasing load to check for material creep. No difference in behavior was observed. One plate for each material was rotated 90° to its original orientation and retested and also turned over the retested. No anomalous behavior was noted. After each test the flatness of the plates was checked and no variation from original geometry was observed.

A load-deflection curve for each material is shown in Figs. 4.9 and 4.10 respectively. All the plates showed an initially linear behavior followed by an apparent stiffening of

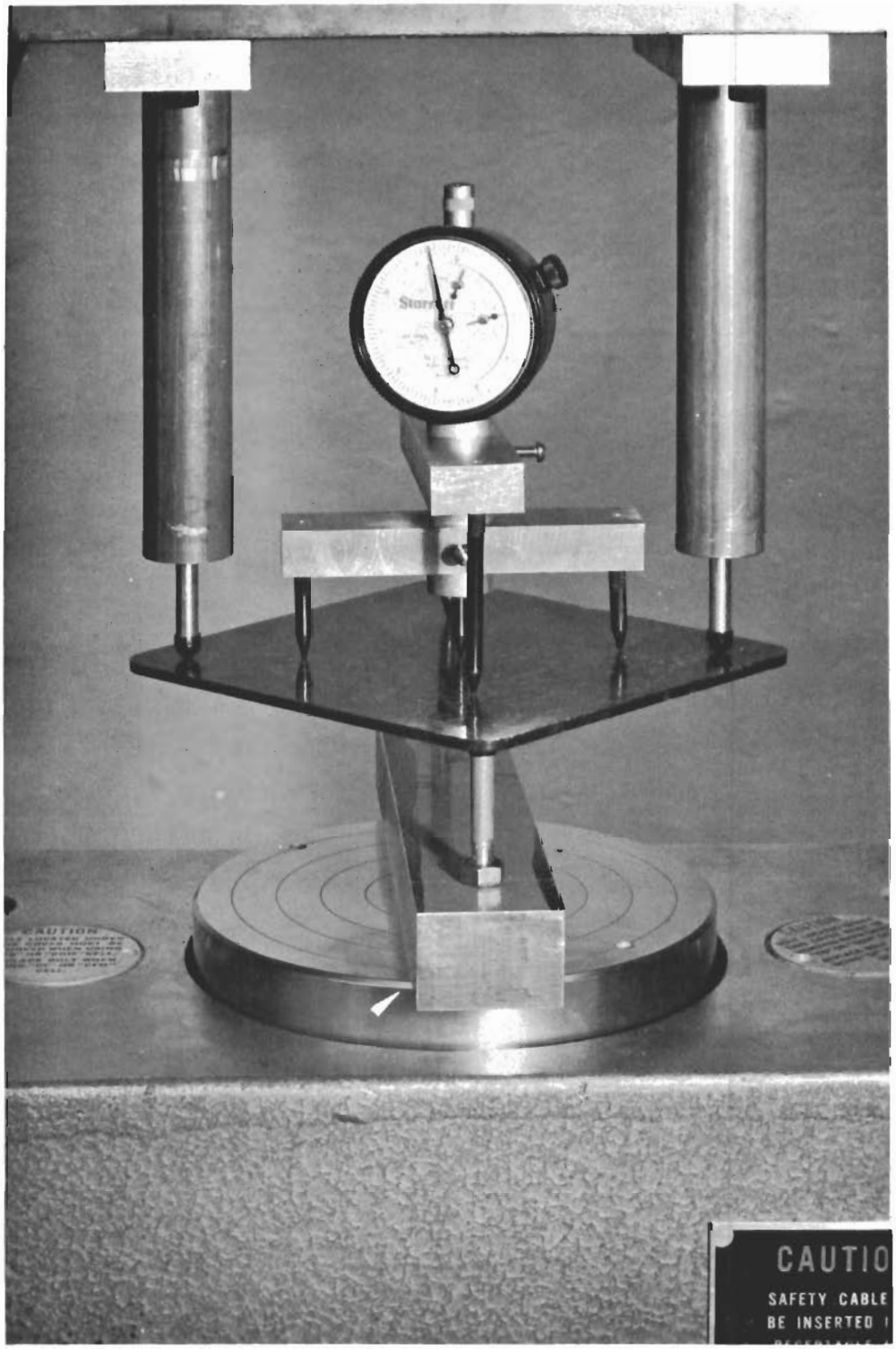

Fig. 4.8 TEST FIXTURE AND DEFLECTOMETER FOR THE PLATE SHEAR TESTS

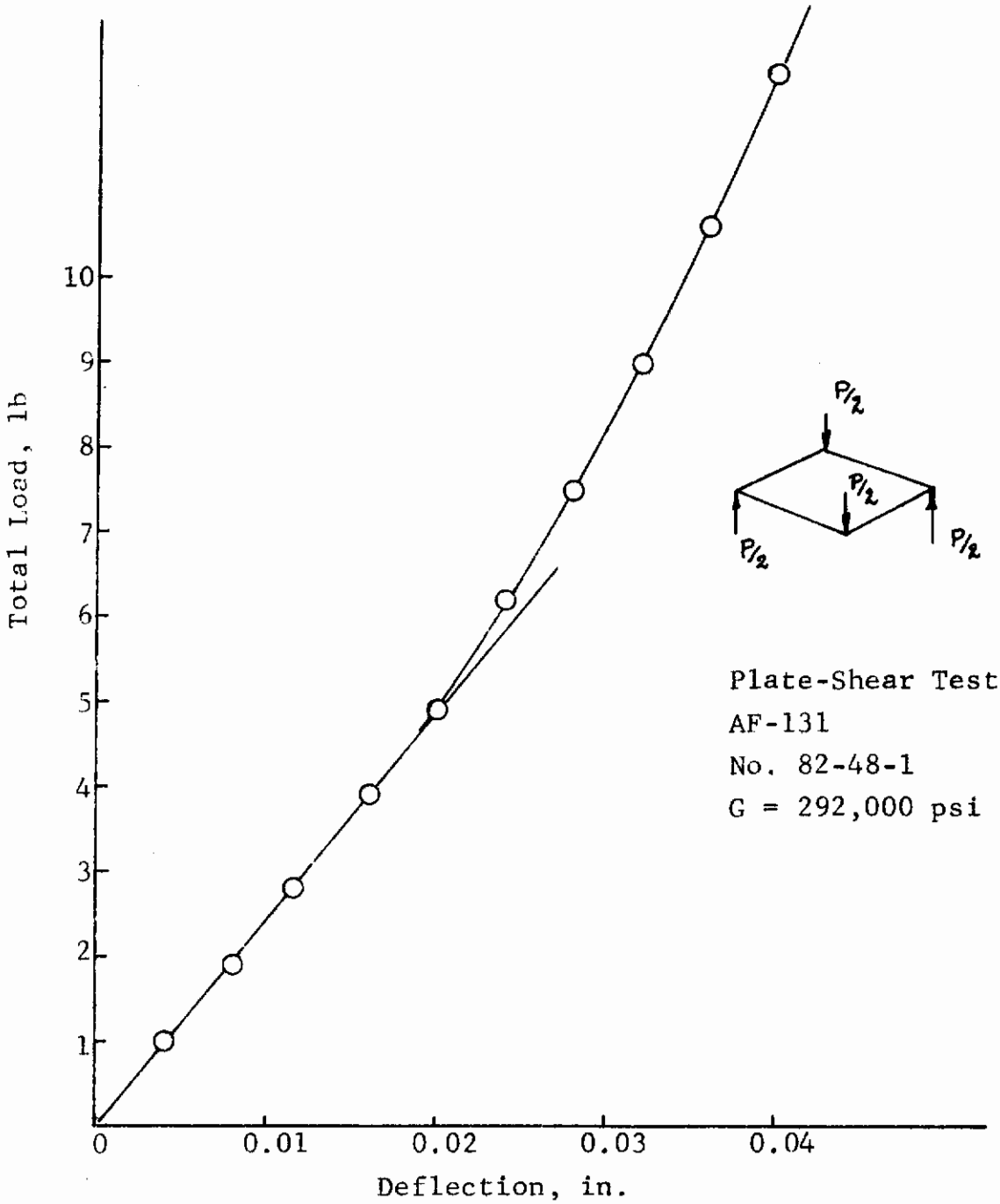

Fig. 4.9 LOAD-DEFLECTION, PLATE SHEAR TEST, RESIN AF-131

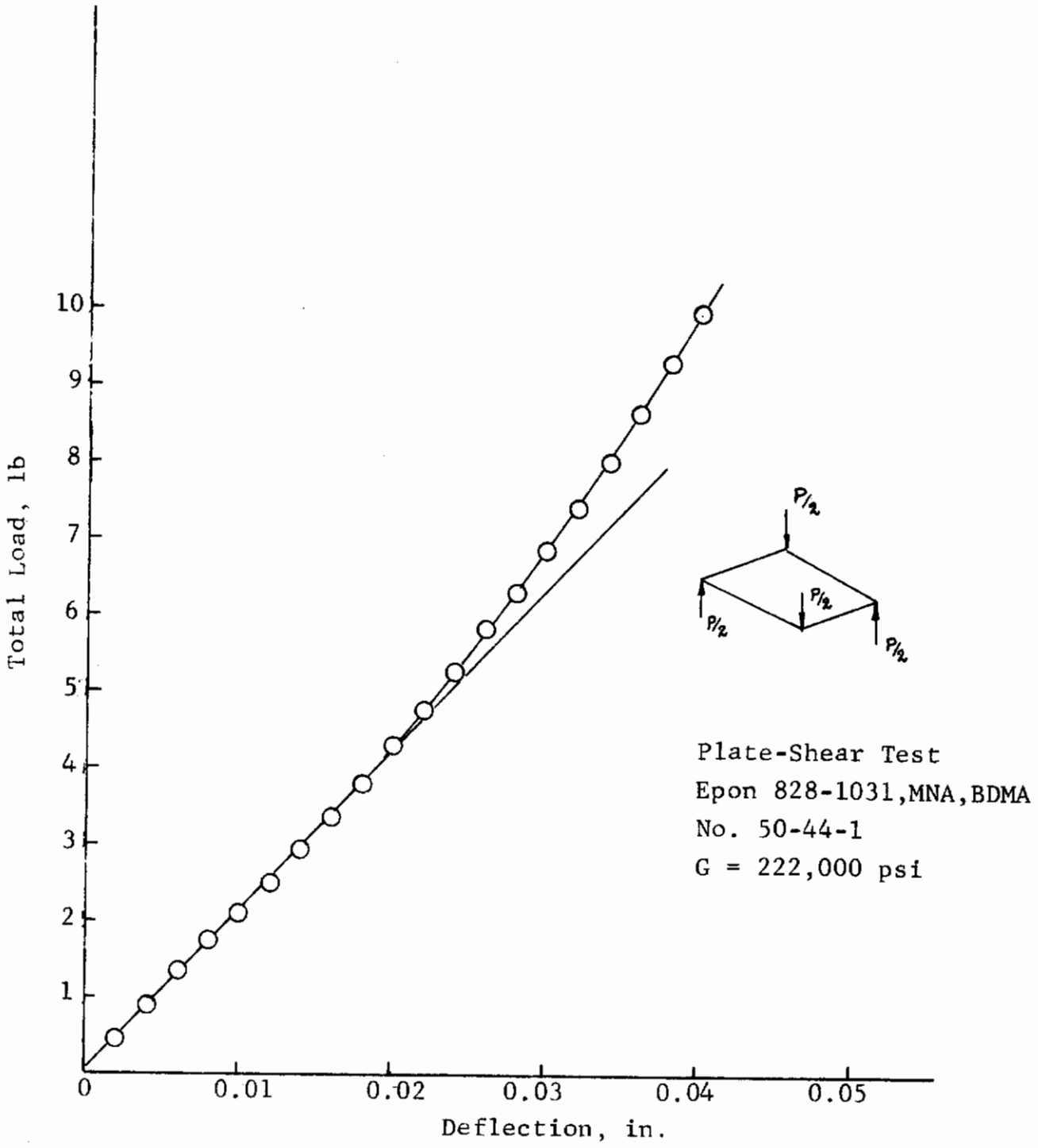

Fig. 4.10 LOAD-DEFLECTION, PLATE SHEAR TEST, EPON 828-1031, MNA, BDMA

the plate. Only the linear region was used to determine the shear modulus. The results of the tests are shown as follows:

Shear Modulus-Bulk Resins

Specimen Number	AF-131 (psi)	Specimen Number	Epon 828-1031-MNA,BDMA (psi)
82-46-1	236,000	50-44-1	222,000
82-47-1	287,000	50-44-2	194,500
82-48-1	292,000	50-44-3	202,200
82-49-1	264,000	50-44-4	189,500
82-50-1	288,000	50-44-5	215,500
82-51-1	305,000	Avg.	204,600
Avg.	278,600		

4.1.3.3 Tensile Properties - Bulk Resins

The tensile behavior of uniform cross-section specimens cut from the saddle shear plates were measured using a clip-gage extensometer and adhesive bonded strain gages. The strain gage layout utilized one longitudinal and one transverse gage on each side of the specimens. By averaging the two longitudinal and the two transverse gages, it was possible to correct for any bending in the specimens.

From the clip-gage extensometer data, it was possible to calculate the modulus of elasticity (E). Then using this value in conjunction with the shear modulus (G) from the plate shear specimen, Poisson's (μ) ratio was calculated using

$$\mu = \frac{E}{2G} - 1$$

From the strain gage data, Poisson's ratio and modulus of elasticity were measured directly and then a value of shear modulus was computed.

4.1.3.4 Results of Resin-Property Determination

All the data obtained on E, G and μ are summarized in Table 4.9. All of the data on modulus of elasticity shows good

Table 4.9

MECHANICAL PROPERTIES OF BULK ADHESIVE RESINS, AF 131, AND EPON 828-1031

Data Source	Modulus of Elasticity (E)	Poisson's Ratio (μ)	Shear Modulus (G)
Resin - Epon 828-1031-MNA, BDMA			
Tensile-Strain Gaged	446,000	0.446	154,000[a]
Plate Shear	431,000	0.052[a]	204,600
Tensile-Extensometer	495,000	-	-
Tensile-Extensometer[b]	526,000	-	-
Torsion Cylinder[b]	-	-	316,000
Resin - AF-131			
Tensile-Strain Gaged	470,000	0.406	168,000[a]
Plate Shear	500,000	-0.105[a]	278,000
Tensile-Extensometer	482,000	-	-

a. Calculated Value

b. Ref. 4.2

agreement regardless of the method of test. The marked differences occur when comparing the shear modulus values. For both materials the shear moduli appear to be much too high. The most realistic value is that obtained from the strain-gaged specimen. In this case the $\mu = 0.446$ is a commonly quoted value for epoxy resins and the test is the least complicated of the three. The torsion test as performed by Noyes and Jones (Ref. 4.2) does involve direct uniform shear strain of the material and should be the most realistic but even a Poisson's ratio of zero then implies that the material modulus (E) would be 632,000 which is high for this material based on other tests conducted at IITRI on related programs. It was concluded that the most realistic value of shear modulus is obtained from the strain-gaged tensile specimens used to measure E and μ directly and then to calculate G.

4.2 ADHEREND PROPERTIES, FABRICATION AND TESTING OF BONDED JOINTS

4.2.1 Selection of Adherends

A series of adherends were selected for this program which would provide as wide a range of relative stiffnesses as possible and still provide data for practical design use. The composite material selected for study was crossplied reinforced fiberglass. This was bonded to itself, to steel, and to titanium to provide the following range of relative moduli in the adherends:

Adherend	Modulus (E) (psi)	E/E frp
FRP	4.1×10^6	1.0
Titanium 6Al-4V	16.4×10^6	4.0
Steel AISI 1025	29×10^6	7.1

The relative adherend stiffnesses were further varied by making joints with different adherend thicknesses. Fiberglass was fabricated in sheet thicknesses of 0.05, 0.10, and 0.20 in. The steel and titanium were always used at a sheet thickness of 0.10 in. This resulted in the following tensile stiffnesses of the sheet:

Adherend	Thickness (in.)	Stiffness per Unit Width (Et) (lb/in.)	Relative Stiffness
FRP	0.05	2.0×10^5	1
	0.10	4.1×10^5	2
	0.20	8.2×10^5	4
Titanium	0.10	16.4×10^5	8
Steel	0.10	29.0×10^5	13

4.2.2 Production of Fiberglass Laminate

The fiberglass laminate material selected to be used throughout the program for joint fabrication was Scotchply XP-251S manufactured by the 3 M Company. The material was purchased as

12 in. wide unidirectional prepreg tape coated with an epoxy resin at 25 percent resin content. The material was obtained in several lots during the program and there was no indication of variation in properties between lots except for scattered amounts of low resin content material.

This material was laidup and cured into plates as they were required during the course of the program. The plates were press-laminated followed by an oven postcure. The following fabrication procedure (as suggested by the supplier) was used:

1. Cut tape lamina to size and bring to room temperature for layup.
2. Layup lamina with backing sheet and use slight pressure to remove air bubbles.
3. Remove backing sheet and place next lamina.
4. Raise press to 300°F and place lamina in the warm press.
5. Apply contact pressure for two min to begin resin flow.
6. Increase pressure to 100 psi over a 2 min period.
7. Cure at 100 psi and 300°F for 30 min.
8. Remove laminate and place in 350°F oven for 4 hr.

The average room temperature properties for Scotchply were quoted by the supplier as follows:

	Crossply (psi)	Unidirectional (psi)
Tensile Strength	130,000	270,000
Modulus	5.2×10^6	8.4×10^6
Flexural Strength	170,000	200,000
Modulus	5×10^6	8×10^6
Beam Shear		11,200

A series of five tensile specimens of rectangular geometry, constant cross section were tested to measure the strength of the crossply composite and a strength of 115,000 psi was obtained. These tests were made from the first plates fabricated in the program. A second series of instrumented specimens were tested from later plates, these results are summarized in Table 4.10. Based on these results, a modulus of 4.10×10^6 psi was used to characterize the Scotchply composite.

4.2.3 Surface Cleaning of Adherends

4.2.3.1 Fiberglass Surface Treatment

Two methods of cleaning reinforced plastics for adhesive bonding were investigated to determine an optimum method for surface preparation. The methods follow the following procedures:

Method A

1. Sand bonding area uniformly with 240 grit paper extending 0.5 in. beyond the overlap area.
2. Dust the sanded area with a vacuum.
3. Swab off the abraded area with clean gauze pad saturated with M.E.K.
4. Rinse the abraded area with distilled water.
5. Dry adherends in circulating air oven at 150°F for 60 min.
6. Bond adherends immediately.

Method B

1. With a stiff brush and a 2 % aqueous solution of Tide at 104 to 122°F, scrub entire surface of panels.
2. Thoroughly rinse in tap water followed by immersion in distilled water.
3. Dry in forced air oven at 150°F for 30 min.
4. With 240 grit sandpaper abrade bonding area plus 0.5 in. margin.

Table 4.10

TENSILE PROPERTIES OF SCOTCHPLY XP-251S

Specimen Number	Orientation Outer Lamina (deg)	Thickness (in.)	Width (in.)	Total Strain to Fracture	Tensile Strength ($\times 10^5$ psi)	Modulus of Elasticity ($\times 10^6$ psi)
1	90	0.114	0.489	3.3	1.16	3.85
2	0	0.119	0.484	3.1	1.26	4.13
3	90	0.111	0.490	3.2	1.27	3.81
4	0	0.052	0.231	3.5	1.34	4.07
			Avg.	3.3	1.26	3.97

Note: Specimens 1-3 were ASTM D638-61T size, 8 1/2 in. long with 2 in. gage length. Specimen 4 was of similar shape but of reduced size with 1 in. gage length.

5. Dust abraded area with vacuum.
6. Swab off abraded area with acetone wet clean gauze.
7. Rinse generously in distilled water (entire panel).
8. Dry in forced air oven at 212°F 60 min, then bond parts immediately.

Scotchply XP234 adherends, 0.10 in. thick, were cleaned by Methods A and B and then bonded in 0.5 and 0.1 in. overlap lengths using Metlbond 400 adhesive. The cure cycle was as follows:

Time (min)	Temperature (°F)	Pressure (ksi)
30	R.T. to 340	14 (29 in. Hg)
60	340 ± 10	14

Cooled to about 100°F before releasing pressure.

Test specimens were cut from the panels and tested for shear strength as described in the following section. Results are summarized in Tables 4.11 and 4.12, and plotted as a function joint parameter in Fig. 4.11. The average shear strengths for joint parameter L/t = 5 by cleaning Methods A and B were 1800 and 2700 psi. Cleaning Method B produced a significantly higher apparent shear strength. There were two process factors which may have contributed to these results. First, cleaning was done by two operators; and second, the panel holes were somewhat tight for the panels cleaned by Method A. This may have resulted in a nonuniform bond pressure on the joint. These results were further checked with another series of tests which are summarized in Fig. 4.12 for Scotchply XP-251S. Based on these results, Method B was still slightly better than Method A and was selected to be used for all further joints fabrication.

Table 4.11

SHEAR STRENGTH OF DOUBLE OVERLAP JOINTS OF SCOTCHPLY XP-234 BONDED WITH METLBOND 0400-CLEANING METHOD A

Specimen Number	Length of Overlap (in.)	Width of Joint (in.)	Load at Failure (lb)	Adherend Stress (ksi)	Shear Strength (psi)	Joint Efficiency (%)	Joint Parameter (L/t)
1090-17-1	0.50	0.534	1310		2460		5
1090-17-2	0.50	0.542	1640		3030		5
1090-17-3	0.50	0.560	1340		2390		5
1090-17-4	0.50	0.525	1290		2460		5
1090-17-5	0.50	0.532	1380		2600		5
1090-17-6	0.50	0.510	1430		2810		5
1090-17-7	1.0	0.525	1860		1770		10
1090-17-8	1.0	0.527	1750		1660		10
1090-17-9	1.0	0.545	2050		1880		10
1090-17-10	1.0	0.515	1970		1910		10
1090-17-11	1.0	0.541	1940		1800		10

Table 4.12

SHEAR STRENGTH OF DOUBLE OVERLAP JOINTS OF SCOTCHPLY XP-234 BONDED WITH METLBOND 0400-CLEANING METHOD B

Specimen Number	Length of Overlap (in.)	Width of Joint (in.)	Load at Failure (lb)	Adherend Stress (ksi)	Shear Strength (psi)	Joint Efficiency (%)	Joint Parameter (L/t)
1090-18-1	0.500	0.532	3100		5830		5
1090-18-2	0.500	0.528	2950		5600		5
1090-18-3	0.500	0.510	2500		4900		5
1090-18-4	0.500	0.531	3000		5880		5
1090-18-5	0.500	0.516	2190		5640		5
1090-18-6	0.500	0.572	3200		5600		5
1090-18-7	1.00	0.537	3750		3500		10
1090-18-8	1.00	0.537	2990		2790		10
1090-18-9	1.00	0.524	2830		2700		10
1090-18-10	1.00	0.524	2250		2140		10
1090-18-11	1.00	0.523	2380		2270		10
1090-18-12	1.00	0.517	2880		2800		10

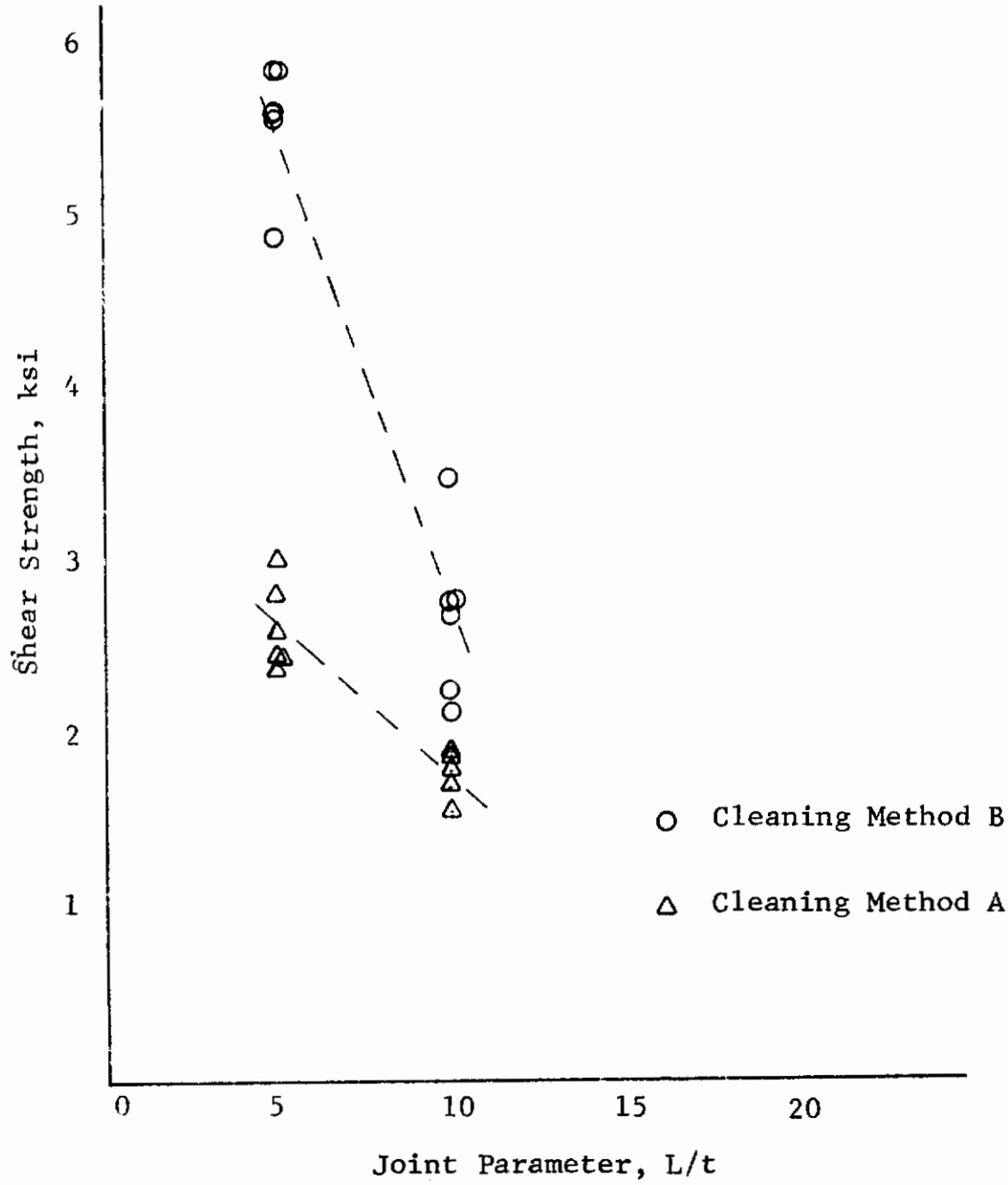

Fig. 4.11 COMPARISON OF CLEANING METHODS FOR SCOTCHPLY XP-234, METLBOND ADHESIVE 400

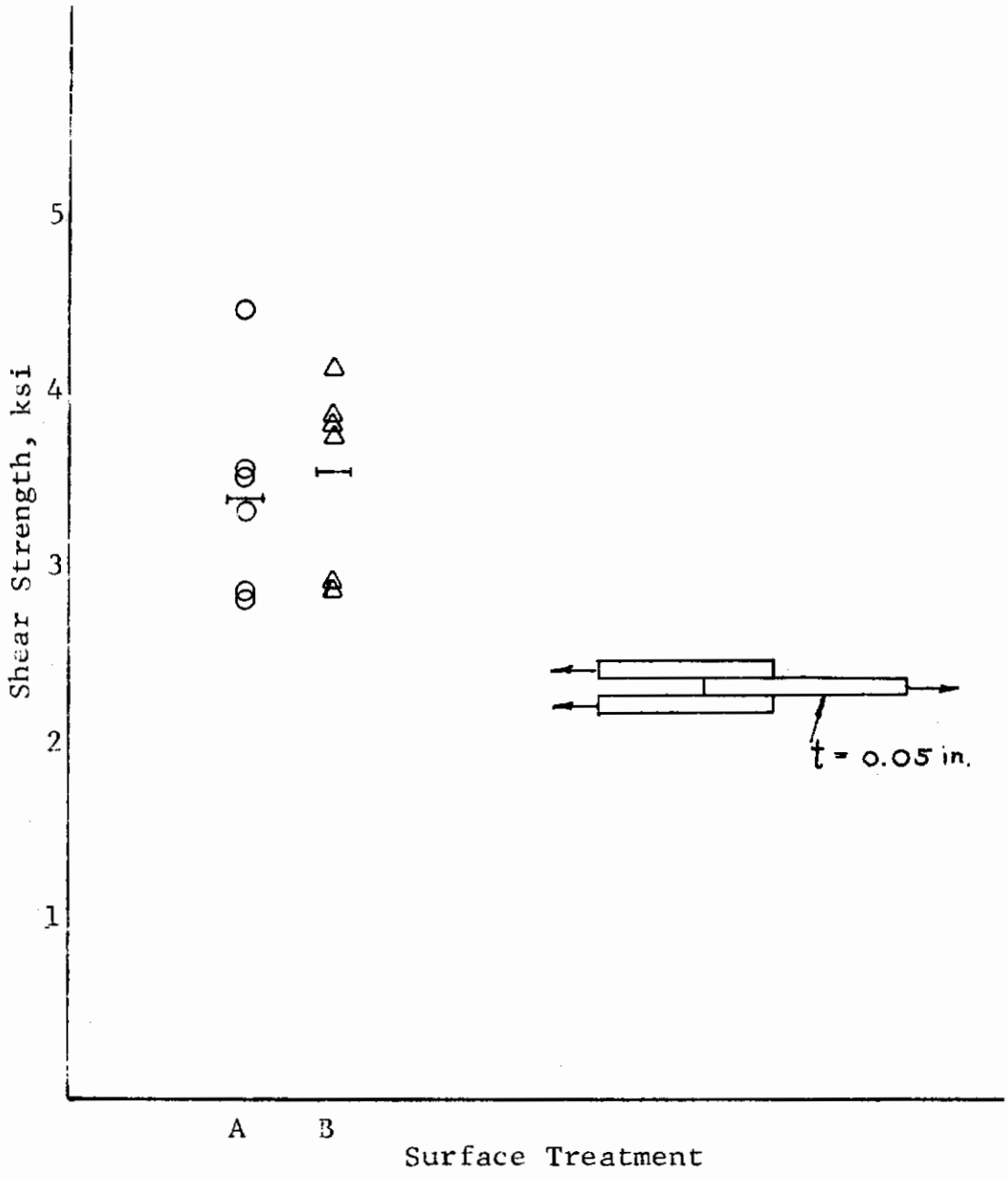

Fig. 4.12 EFFECT OF SURFACE TREATMENT ON SHEAR STRENGTH OF SCOTCHPLY XP-251S - METLBOND 400 JOINTS

4.2.3.2 Metal Surface Treatment

The steel and titanium metals were prepared for adhesive bonding using standard surface treatments for these materials. These methods were as follows:

Steel

1. Vapor degrease with trichloroethylene.
2. Sand blast with virgin sand.
3. Vapor degrease with new trichloroethylene.

Titanium

1. Vapor degrease with trichloroethylene.
2. Immerse for 15 minutes at 150±10°F in a solution of

Triton X-200 (Rohm and Haas Co.)	3.6 parts by wt.
Sodium metasilicate	2.0 parts by wt.
Distilled water	94.4 parts by wt.

3. Rinse thoroughly with tap water and dry at 150-200°F.

4.2.3 Joints Fabrication

All the adhesive bonded joints for this program were fabricated with vacuum-oven conditions. The adherend materials of proper thickness were cut into panels 4.0 in. wide x 4.5 in. long. Holes 0.125 in. diameter were drilled 3.75 in. apart and 0.125 in. in from the panel edge and at selected distances to provide 0.5, 1.0, 1.5 or 2.0 in. overlap joints when fitted to slip-fit pins mounted at the same distance in an aluminum plate. Two sets of overlap panels were prepared and adhesive bonded per lay up as shown in Fig. 4.13.

The detailed procedure was as follows:

1. All joints were bonded with the fibers in the face ply running parallel to the direction of load.

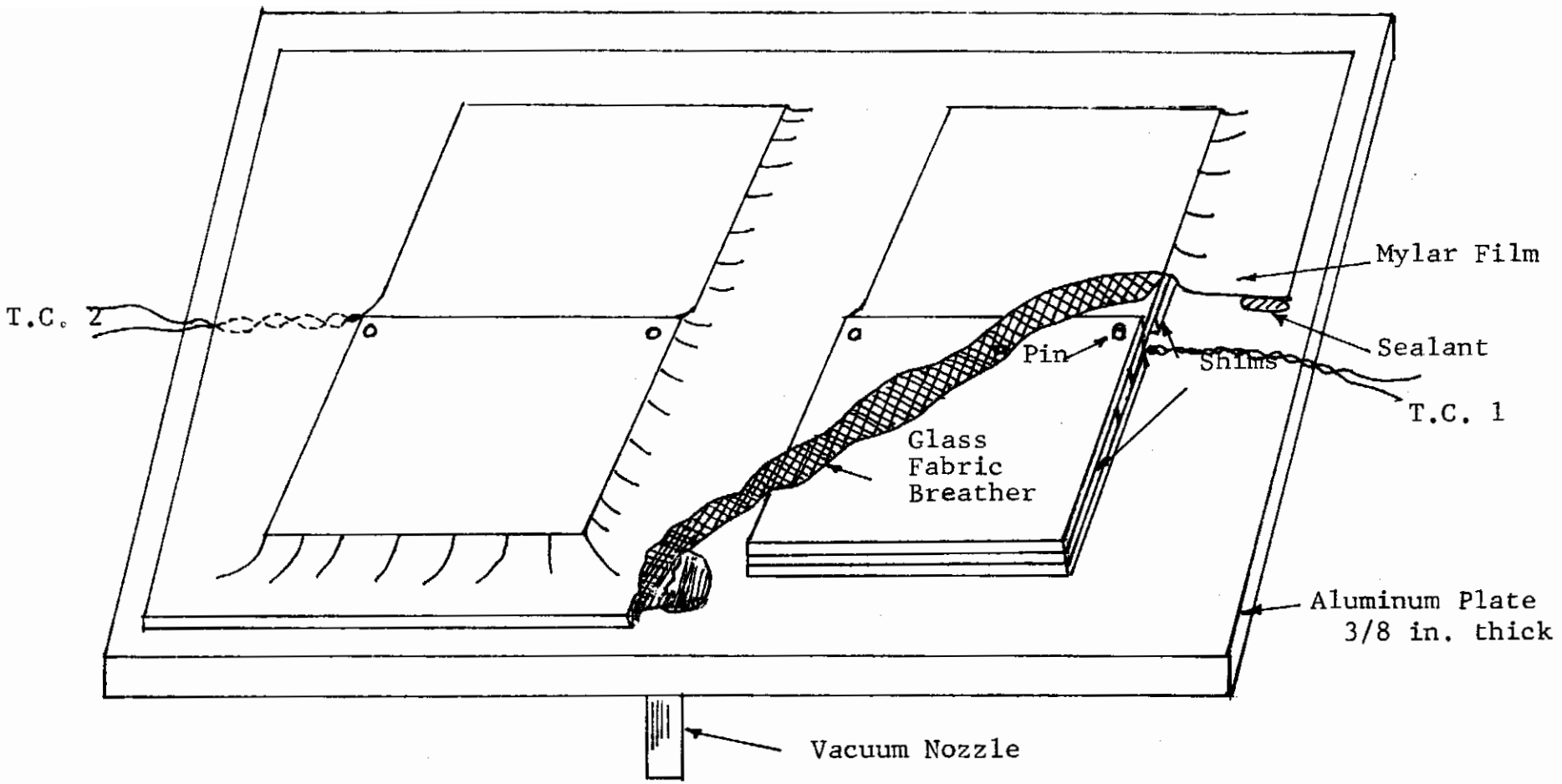

Fig. 4.13 VACUUM DIAPHRAGM LAYUP OF DOUBLE LAP JOINT ADHESIVE BONDED PANELS

2. The adherend bonding surface was cleaned by Method B.

3. Adhesive film was cut to the overlap size and laid up in double overlap style between the prepared surfaces. The adherends were assembled by placing shims beneath the single adherend and between the double adherends to obtain uniform adhesive thickness when cured. Each set of panels were instrumented with thermocouples at the bond line, and the assembly completed by placing a glass cloth breather over the panels followed by a Mylar diaphragm sealed to the aluminum plate at periphery with a zinc chromate putty.

4. The instrumented assembly was placed in a circulating air oven and connected to a vacuum pump and gage system.

5. The assembly was exposed to an established cure cycle. Temperature was checked and controlled by use of a potentiometer and an oven thermostat.

6. The bonded panels were sectioned into 0.5 in. wide specimens by first scribing and cutting with a diamond circular saw as indicated in Fig. 4.14. All metal bonded joints were cut with a band saw.

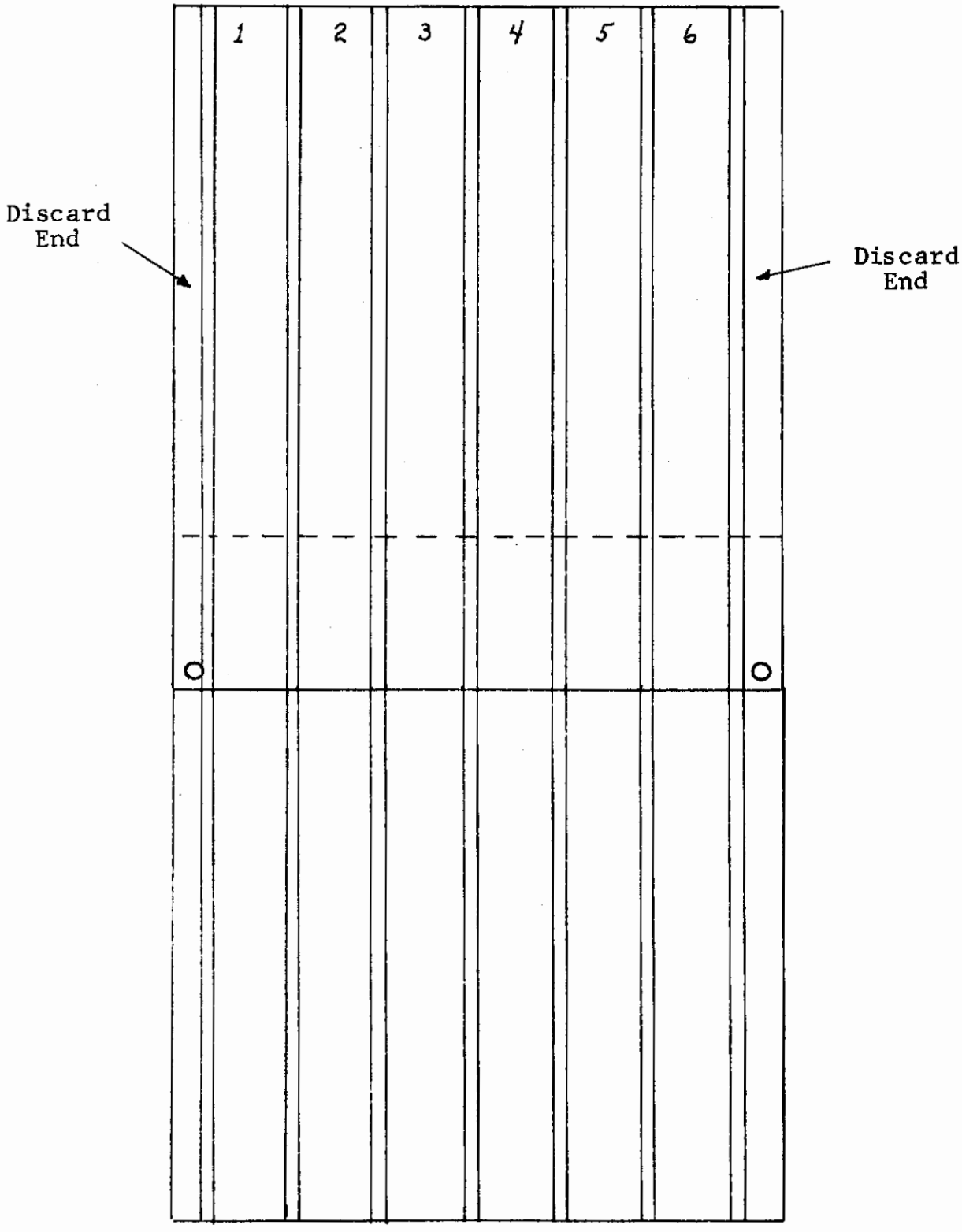

Fig. 4.14 SECTIONED DOUBLE LAP JOINT BONDED PANEL

4.3 STATIC STRENGTH OF BONDED JOINTS

Measurements were made of the static strength of bonded joints in a double overlap geometry for composite to composite joints, composite to metal joints and composite scarfed joints. The major variables were the adhesive, joint overlap length (L) and adherend thickness (t) which resulted in variation of the joint parameter over the range from 5 to 40. All the joints were fabricated in replicates of six specimens and all joints were tested in a universal testing machine at 0.05 in./min, at 75°F, 50% R. H. A long-deflection record was obtained for each joint. A joint under test is shown in Fig. 4.15.

The experimental results for each joint tested are given in tabular and graphical format in Section 4.5. The summary of these results and details of each group of tests are discussed separately in the following section. The intent here is simply to present the data in a form suitable for engineers who need results for the specific joints, and may not be interested in the details of a design procedure for these joints. This data will serve as the body of information suitable for checking out the design procedures discussed in later section and for evaluating future design methods as they become available.

4.3.1 Composite to Composite Joints

Twenty-eight different groups of composite to composite joints were bonded and tested using adhesives FM-1000, Metlbond 400, and FM-47. The joints were double overlap type with constant thickness adherends. Table 4.13 summarizes the joint configurations tested. The actual test results are given in Section 4.5.1.

4.3.1.1 Shear Strength and Joint Efficiency vs. Joint Parameter

The two parameters used to characterize joint behavior at failure were average shear strength and joint efficiency. The average shear strength (τ) is defined as the load at failure

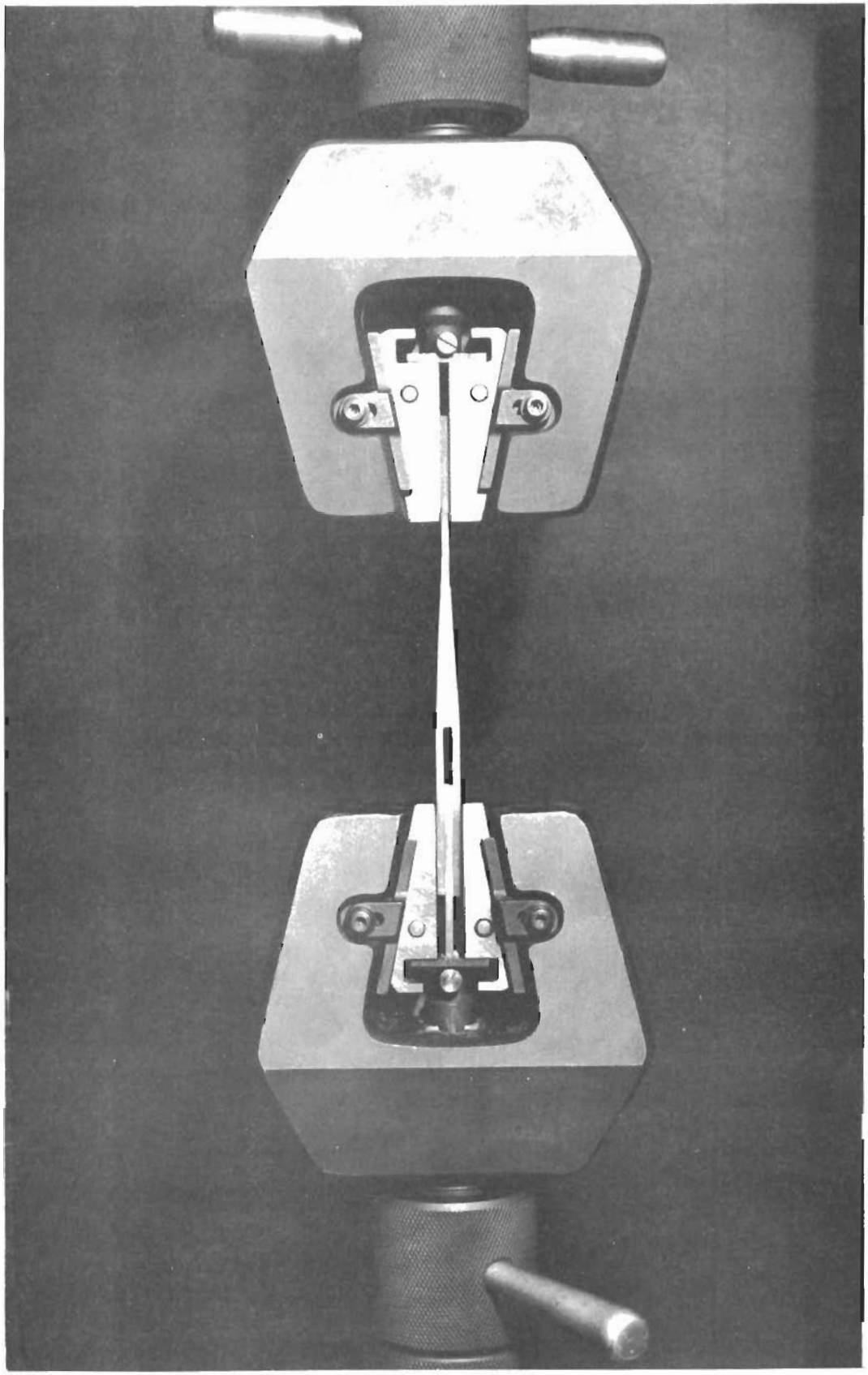

Fig. 4.15 STATIC STRENGTH TEST OF AN ADHESIVE BONDED DOUBLE SCARFED JOINT

Table 4.13

SUMMARY OF FIBERGLASS - FIBERGLASS DOUBLE OVERLAP JOINTS FOR STATIC STRENGTH TESTS

Adhesive	Adherend Thicknesses (in.)	Length of Overlap (in.)	Joint Parameter L/t	Fabrication Number	Number of Joints
FM-1000	0.05-0.05-0.05	0.5	10.0	1080-27	6
FM-1000	0.05-0.05-0.05	1.0	20.0	1080-27	6
FM-1000	0.05-0.05-0.05	1.5	30.0	1080-27	6
FM-1000	0.05-0.05-0.05	2.0	40.0	1080-27	6
FM-1000	0.10-0.10-0.10	0.5	5.0	1080-28	6
FM-1000	0.10-0.10-0.10	1.0	10.0	1080-28	6
FM-1000	0.10-0.10-0.10	1.5	15.0	1080-28	6
FM-1000	0.10-0.10-0.10	2.0	20.0	1080-28	6
FM-1000	0.20-0.20-0.20	1.0	5.0	1080-29	6
FM-1000	0.20-0.20-0.20	2.0	10.0	1080-29	6
Metlbond 400	0.05-0.05-0.05	0.5	10.0	1090-22	6
Metlbond 400	0.05-0.05-0.05	1.0	20.0	1090-22	6
Metlbond 400	0.05-0.05-0.05	1.5	30.0	1090-22	6
Metlbond 400	0.05-0.05-0.05	2.0	40.0	1090-22	6
Metlbond 400	0.10-0.10-0.10	0.5	5.0	1090-20	6
Metlbond 400	0.10-0.10-0.10	1.0	10.0	1090-20	6
Metlbond 400	0.10-0.10-0.10	1.5	15.0	1090-20	6
Metlbond 400	0.10-0.10-0.10	2.0	20.0	1090-20	6
Metlbond 400	0.20-0.20-0.20	1.0	5.0	1090-26	6
Metlbond 400	0.20-0.20-0.20	1.5	7.5	1090-26	6
Metlbond 400	0.20-0.20-0.20	2.0	10.0	1090-26	6
FM-47	0.05-0.05-0.05	0.5	10.0	1081-36	6
FM-47	0.05-0.05-0.05	1.0	20.0	1081-36	6
FM-47	0.05-0.05-0.05	1.5	30.0	1081-36	6
FM-47	0.05-0.05-0.05	2.0	40.0	1081-36	6
FM-47	0.10-0.10-0.10	1.0	10.0	1081-25	6
FM-47	0.10-0.10-0.10	1.5	15.0	1081-25	6
FM-47	0.10-0.10-0.10	2.0	20.0	1081-25	6
				Total Joints	168

(P) divided by the total bonded area. For the 0.5 in. wide double overlap joints the shear strength is

$$\tau = \frac{P}{L}$$

where (L) is the length of overlap. The joint efficiency is a measure of the ability of the joint to transfer load up to the maximum load capacity of the weakest adherend present in the joint. For these joints the adherend most highly stressed is the single fiberglass adherend. This was assumed to have a failure stress of 110,000 psi. Efficiency (e) then is defined as

$$\%e = \frac{P_{max} / A_{min}}{110,000} \times 100$$

where

P_{max} = load at failure

A_{min} = nominal area of the weakest adherend combination present.

The parameter used to characterize each joint is the ratio of length of overlap to minimum adherend thickness present in the joint. This (L/t) parameter is a measure of the bending stiffness of the adherends.

Figures 4.16, 4.17 and 4.18 summarize the average results for the three adhesives FM-1000, FM-47 and Metlbond 400.

For FM-1000, the lowest modulus adhesive, the data falls into two distinct groups. The most efficient joints and the strongest bonds are obtained with the 0.05 in. material for any specified joint parameter. The data for the 0.10 in. and 0.20 in. thick joints fall on the same curve and are significantly reduced in magnitude. For the thinnest material joint efficiencies of 80-100 percent were obtained, while for the two thicker materials the efficiencies were 40-50 percent, an exact reduction of one half. This data would indicate that the 0.10 in. and 0.20 in.

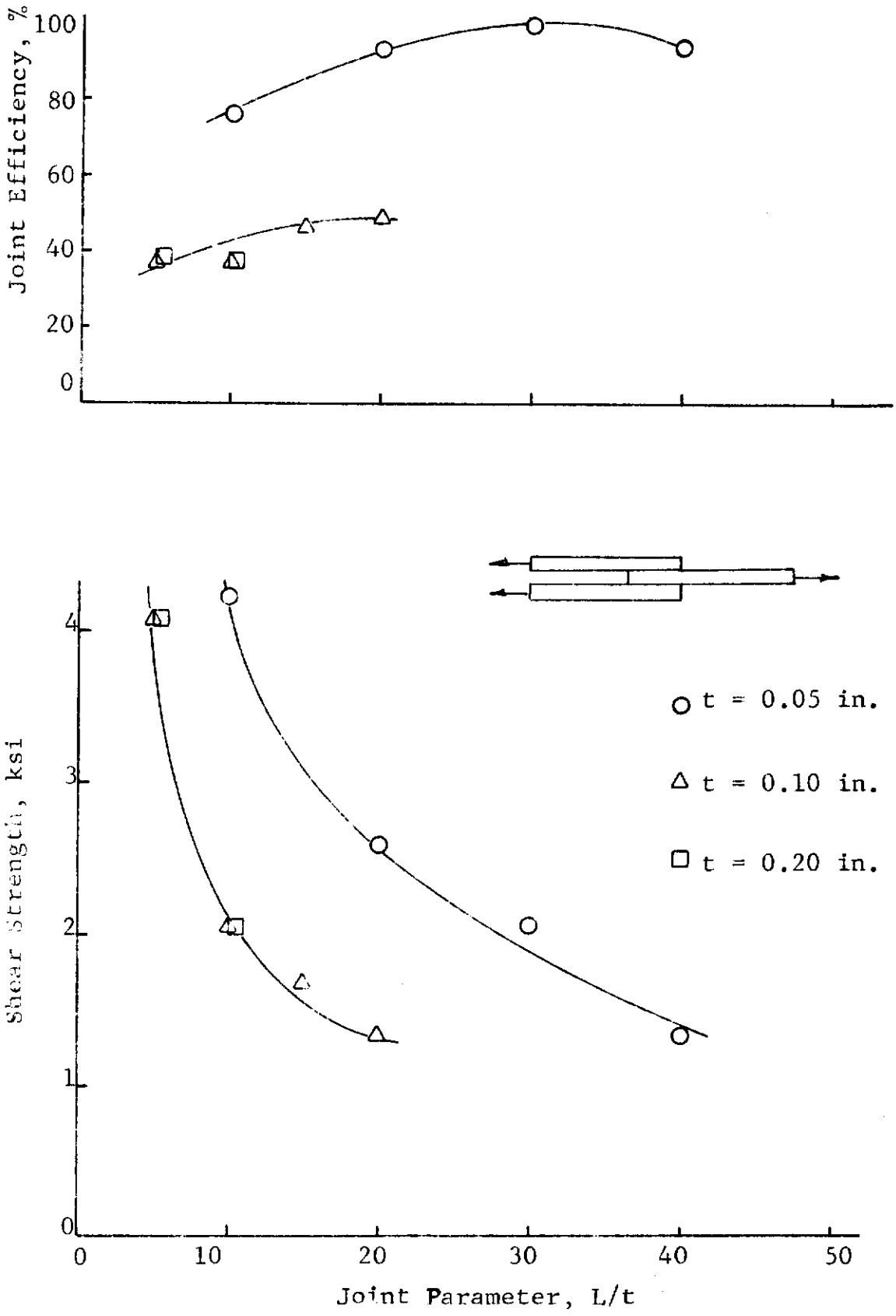

Fig. 4.16 SHEAR STRENGTH AND JOINT EFFICIENCY OF SCOTCHPLY XP-251S BONDED WITH FM-1000

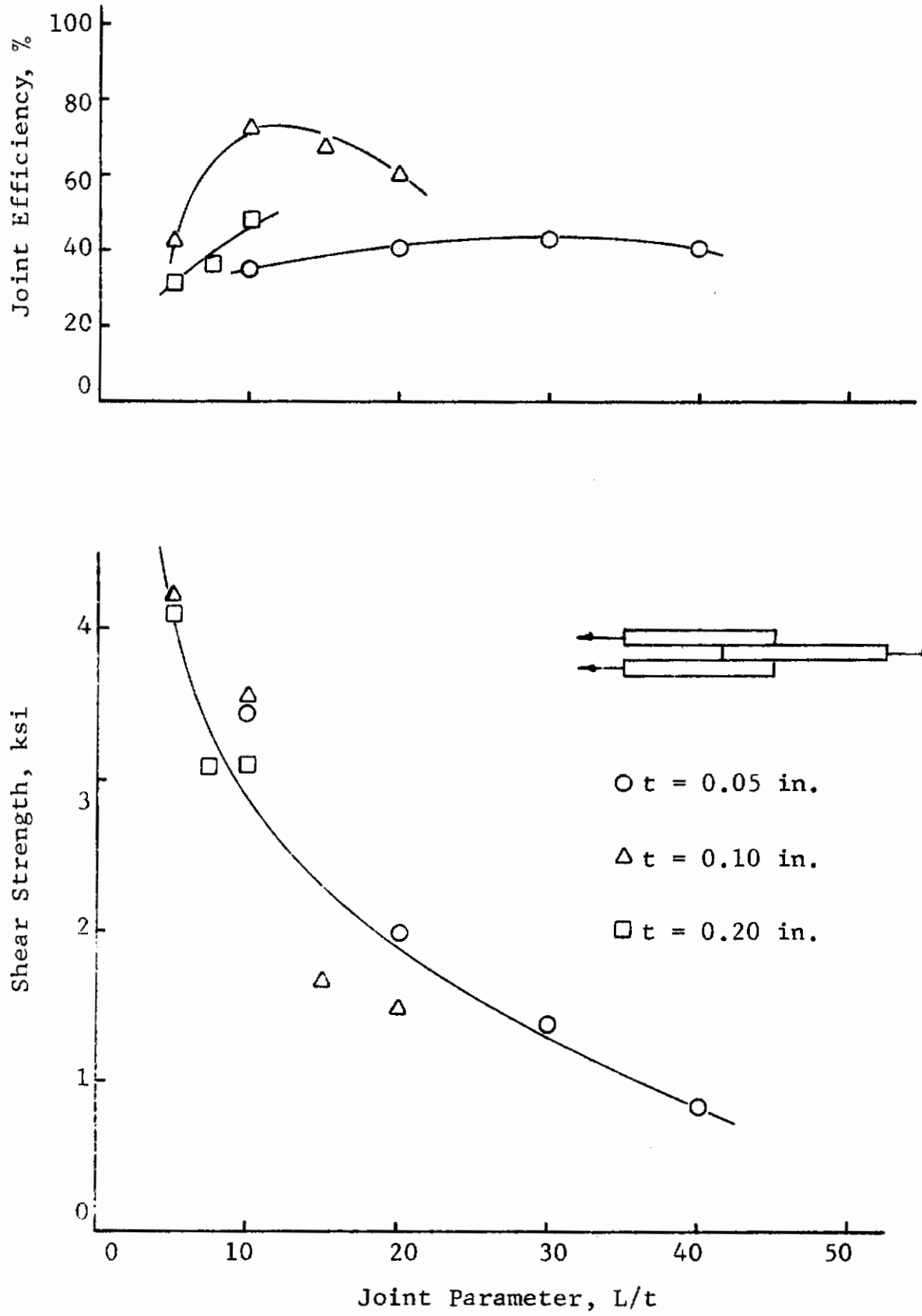

Fig. 4.17 SHEAR STRENGTH AND JOINT EFFICIENCY OF SCOTCHPLY XP-251S BONDED WITH METLBOND 400

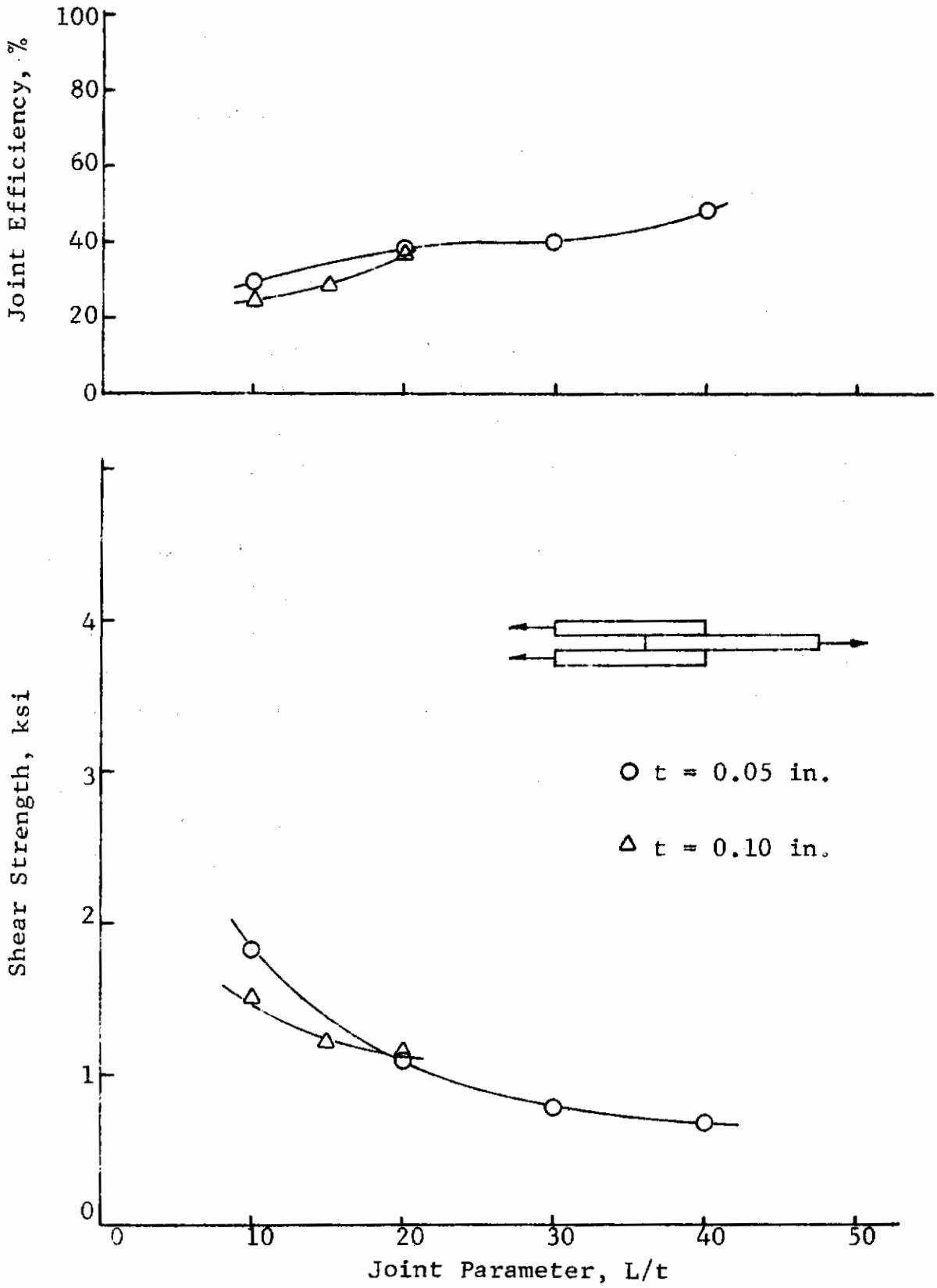

Fig. 4.18 SHEAR STRENGTH AND JOINT EFFICIENCY OF SCOTCHPLY XP-251S BONDED WITH FM-47

materials were behaving in the same manner. A possible explanation is that any material 0.10 in. and larger in thickness is essentially a rigid adherend relative to the low modulus plastic type behavior of FM-1000.

In the case of the Metlbond 400 and the FM-47 the shear strength data for each adhesive tends to fall on the same curve. There is no significant difference as occurred with the FM-1000 material. The only significantly more efficient joints are the 0.10 in. material bonded with Metlbond 400. For this geometry efficiency reached 40-75 percent while all other designs were in the range from 25-50 percent. This data indicates that all these joints are failing in the same manner regardless of the adhesive used.

In all cases the data shows a curvilinear relationship with joint parameter and demonstrates the dramatic reduction in shear strength of the joint as the length of overlap increases. This shows the influence of a nonuniform shear stress distribution present in the joints. It should be noted that if these curves are extrapolated to $L/t = 0$, this implies no overlap length and a uniform shear distribution, the joint strength at this point should represent the pure shear strength of the adhesive. For the three adhesives tested this results in the following shear strengths.

Adhesive	Maximum Shear Strength
FM-100	6800 psi
Metlbond 400	6500 psi
FM-47	3300 psi

These values are obtained by extrapolation of the test results and some judgement is involved as to where the curves are drawn. The values appear to represent a common intercept for all the adherend thicknesses for a given adhesive.

The results for joint efficiency show a relative maximum for each adherend thickness which again indicates that beyond a certain length of overlap no further increase in joint load carrying capacity is obtained. For t = 0.05 in. the optimum L/t was equal to 30 for all three adhesives. For the two thicker adherends the optimum value was in the range from L/t = 10 to 20.

When all the results are considered together, it appears that there is distinct difference in behavior between the 0.05 in. material and the two thicker adherends. It appears that beyond some thickness between 0.05 in. and 0.10 in. any increase in adherend thickness will yield the same results. It appears that the joints become failure critical in the composite and may no longer be influenced by the adhesive present.

Figure 4.19 shows all the results for the 0.10 in. and 0.20 in. adherends. For FM-1000 and Metlbond 400 the strengths fall together quite well. The strengths for FM-47 appear distinctly different which may be the result of adhesive modulus discussed in the following section.

4.3.1.2 Shear Strength and Joint Efficiency vs. Adhesive Modulus

One of the important objectives of this program is to demonstrate the role of the mechanical properties of the adhesive in determining the strength of a joint. This concept has been successfully demonstrated for the first time with the data obtained for the 0.05 in. thickness joints. These results are shown in Fig. 4.20.

The highest modulus material (FM-47) shows the lowest joint strengths followed by an increase to the intermediate modulus (Metlbond 400) and the highest strengths with the lowest modulus (FM-1000). We know from the stress analyses that the elastic stresses increase with adhesive modulus and if one assumes the films to have approximately the same material strength the highest modulus material should produce the weakest joints. In this case the strengths are not the same but they are directly

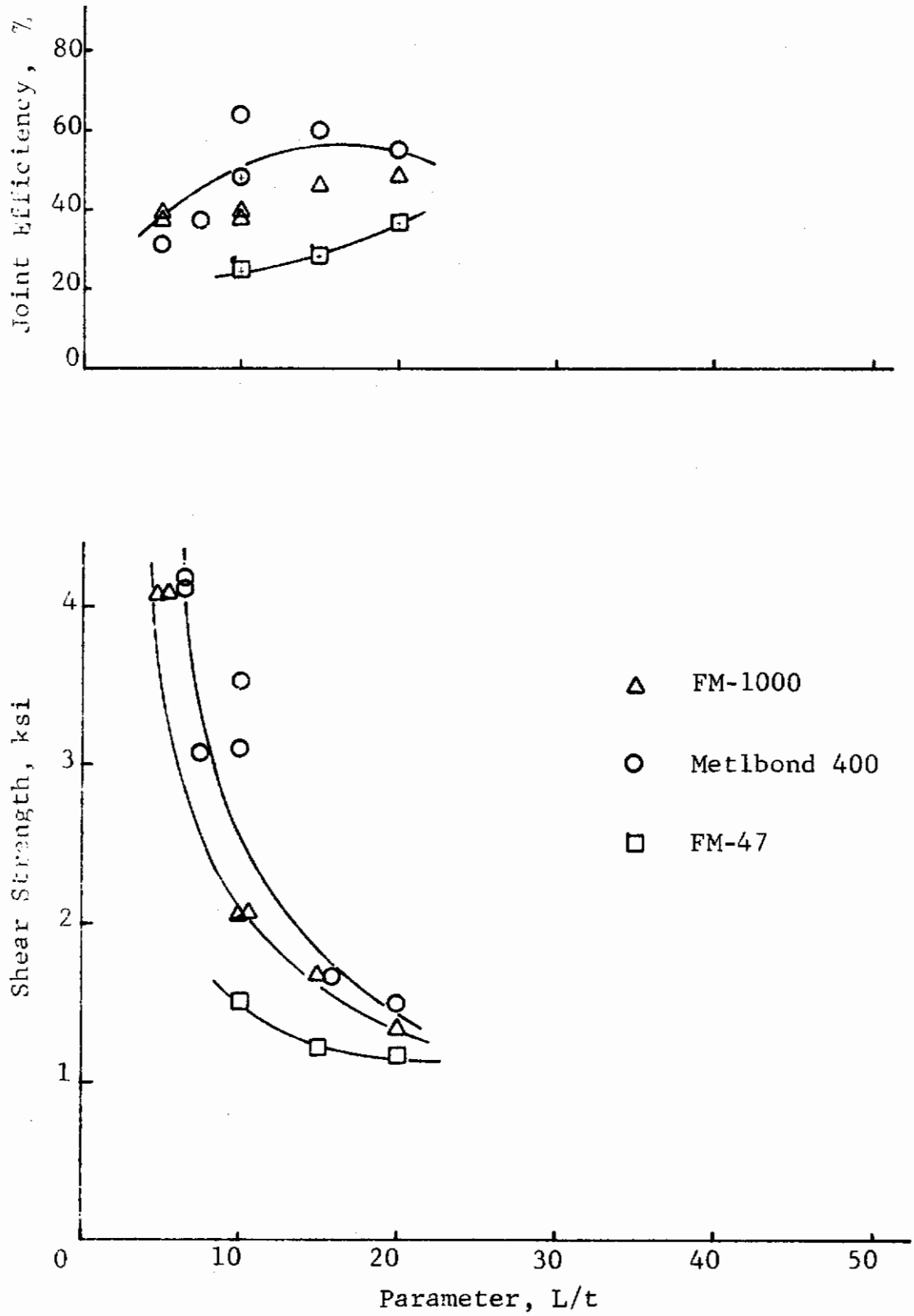

Fig. 4.19 SHEAR STRENGTH AND JOINT EFFICIENCY FOR ALL 0.10 and 0.20 IN. ADHEREND JOINTS

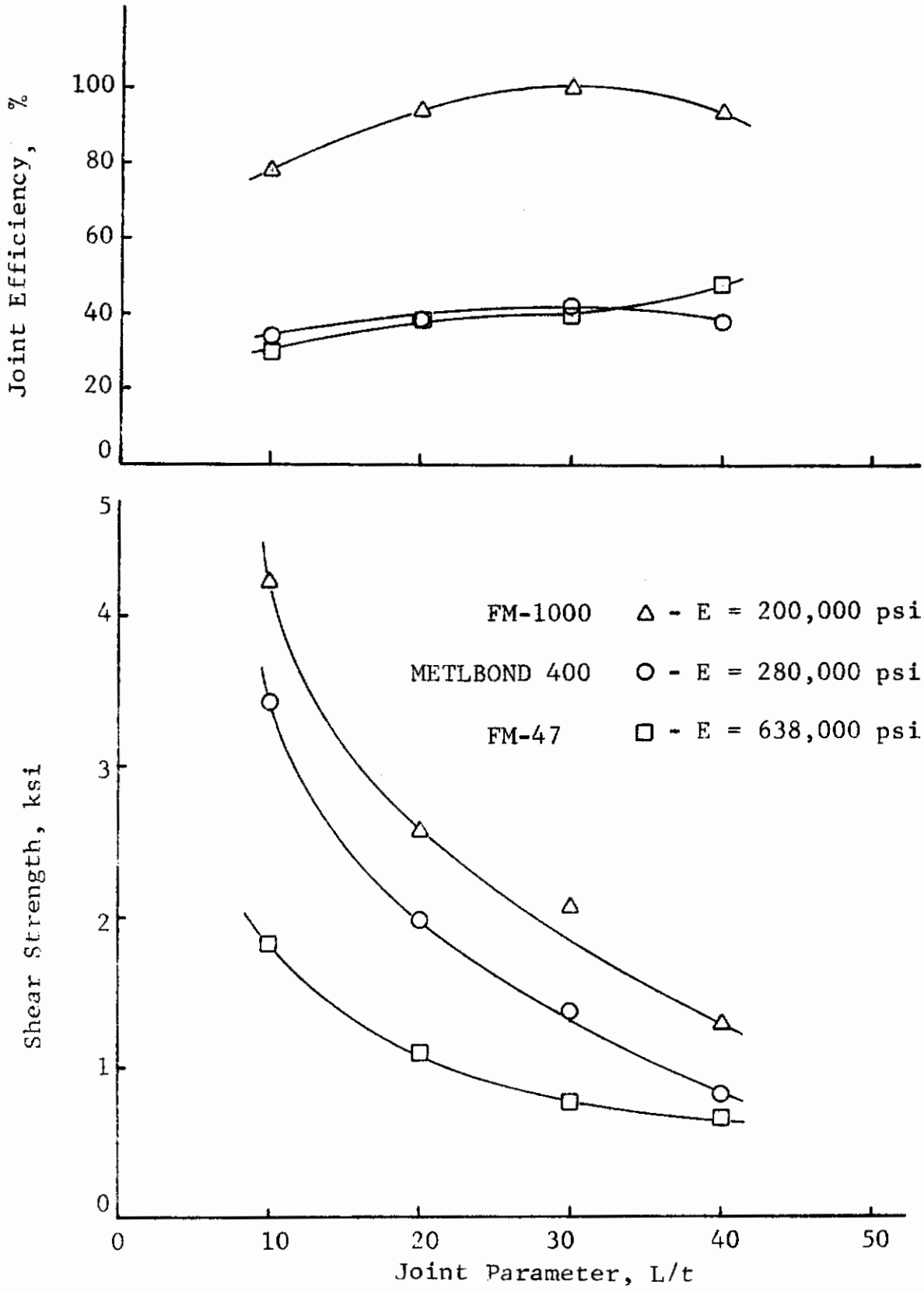

Fig. 4.20 SHEAR STRENGTH AND JOINT EFFICIENCY AS A FUNCTION OF ADHESIVE MODULUS FOR SCOTCHPLY XP-251S, 0.05 IN. THICKNESS

related to the modulus, therefore, the stiffest strongest adhesive produced the weakest joints.

There is one indication that elastic modulus alone does not completely explain the results. This can be observed from the joint efficiencies obtained. The low modulus FM-1000 gave efficiencies 100 percent greater than either the intermediate or high modulus materials. A possible explanation is the high elongation of the FM-1000 which allows it to reach a more uniform state of strain throughout the joint than either of the other two materials.

4.3.1.3 Effect of Composite Construction on Shear Strength and Joint Efficiency

One series of measurements were made to determine what effect the direction of the filaments directly at the bond line had on joint strength. All the panels fabricated in this program contained an odd number of plies parallel (0°) to the load direction at the bond line and an even number perpendicular (90°) to the load. This means both surface plies of the adherend were parallel to the load. Table 4.10 showed the tensile properties for this composite both at 0° and 90° orientation. Note at the 90° orientation the stiffness and strength are lower since for this construction there are a smaller percentage of the total number of fibers acting parallel to the principal stress.

Two sets of panels at 0.20 in. adherend thickness were bonded with FM-1000 with the surface plies perpendicular to the direction of load. These results are summarized in Table 4.14. The 90° orientation resulted in joint strengths almost 50% lower in strength than the 0° orientation. The fracture surfaces were also markedly different.

The lower strength construction showed local in depth failure in the composite within the bonded area. The higher strength 0° construction contained long failures extending well beyond the bonded area. This data indicates that even though

Table 4.14

EFFECT OF COMPOSITE CONSTRUCTION ON JOINT STRENGTH OF FM-1000

Fabrication Number	Outerply Fiber Orientation	Length of Overlap (in.)	Adherend Thickness (in.)	Joint Parameter (L/t)	Shear Strength (psi)	Joint Efficiency (%)
1090-29	Parallel to Load	1.0	0.20	5	4030	39.6
		2.0	0.20	10	2020	39.2
1090-34	Perpendicular to Load	1.0	0.20	5	2130	20.9
		2.0	0.20	10	1250	25.1

the average plate properties of the composite are not markedly anisotropic along the principle axes the construction of the composite locally at the bonded area has a marked effect on joint strength. In this case the joints are subjected locally to a "rolling shear" condition which does not allow the load to reach the important longitudinal load carrying fibers.

The real implication of these results is that any stress analysis or design technique for joints would have to be able to incorporate local perturbations of this type, local ply properties and cannot simply be based on average plate properties.

4.3.2 Scarfed Composite Joints

The shear strength of selected double overlap scarfed joints of Scotchply XP-251S bonded with FM-1000 and FM-47 was determined for a range of joint parameter (L/t) from (5) through (40). The purpose of the scarf joint geometry was to obtain a variable stiffness adherend along the length of overlap which will reduce the stress concentrations. The variable sheet stiffness is designed to reduce the amount of differential straining induced in the adhesive with a resultant more uniform shear stress distribution in the joint. Table 4.15 summarizes all of the joints fabricated and tested. The strength results are given in Section 4.5.2.

4.3.2.1 FM-1000

The experimental scatter of the data is low except for the 0.10 in. joints with the 0.5 in. overlap (L/t = 5). At this overlap length, which was the smallest that was scarfed, it was difficult to maintain a smooth slope of scarf and as uniform a bonding pressure as was possible with the longer overlaps. All the scarfed joints were prepared by scarfing the adherends prior to bonding.

The average results for FM-1000 are shown in Fig. 4.21. All the data for the 0.05 in. and 0.10 in. thickness material fell on one curve, and the 0.20 in. results were only slightly

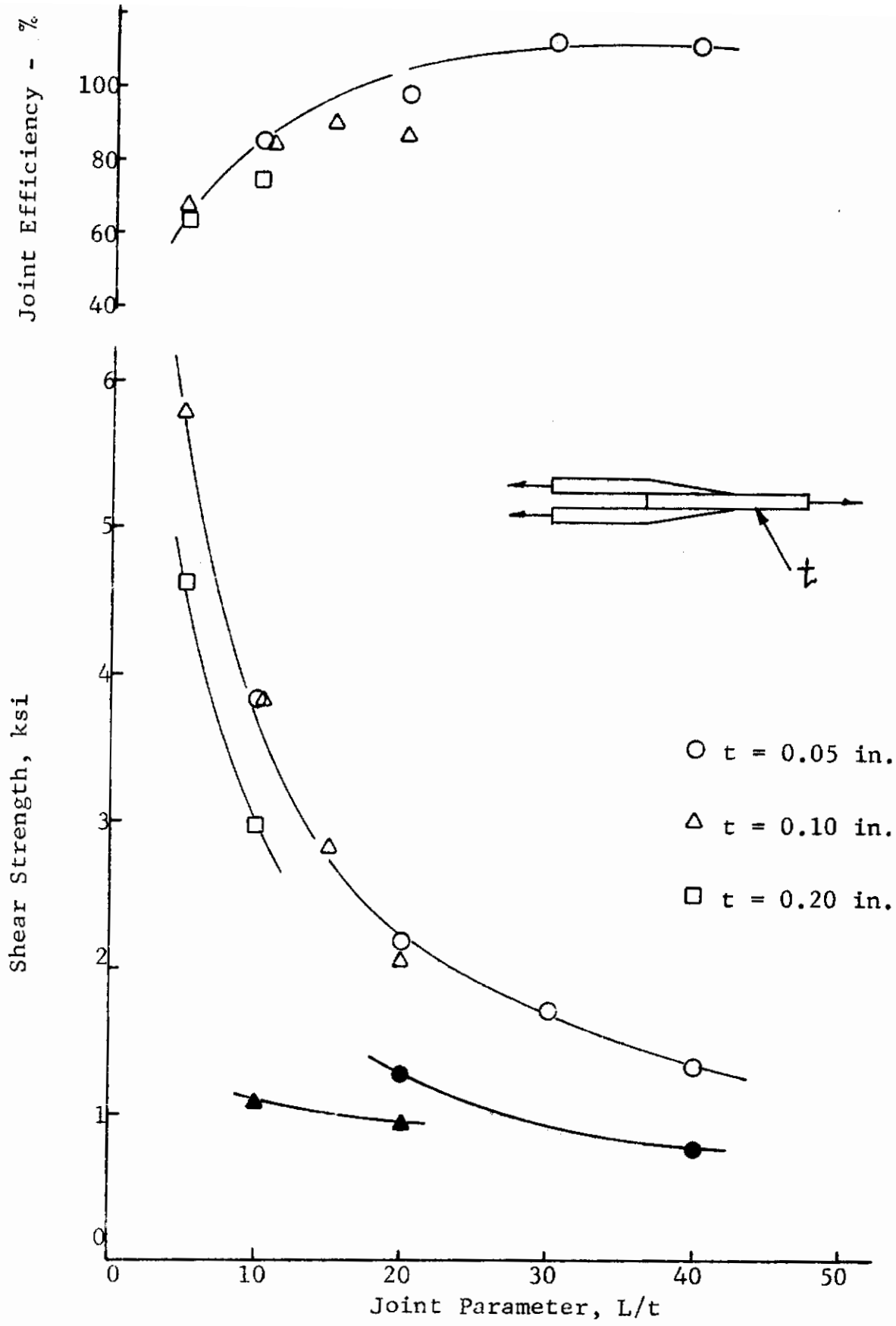

Fig. 4.21 SHEAR STRENGTH AND JOINT EFFICIENCY OF SCOTCHPLY XP-251S SCARFED JOINTS BONDED WITH FM-1000 AND FM-47

Table 4.15

SUMMARY OF FIBERGLASS - FIBERGLASS DOUBLE OVERLAP SCARFED JOINTS FOR STATIC STRENGTH TESTS

Adhesive	Adherend Thicknesses (in.)	Length of Overlap (in.)	Joint Parameter L/t	Fabrication Number	Number of Joints
FM-1000	0.05-0.05-0.05[a]	0.5	10	1080-56	6
FM-1000	0.05-0.05-0.05	1.0	20	1080-56	6
FM-1000	0.05-0.05-0.05	1.5	30	1080-56	6
FM-1000	0.05-0.05-0.05	2.0	40	1080-56	6
FM-1000	0.10-0.10-0.10	0.5	5	1080-55	6
FM-1000	0.10-0.10-0.10	1.0	10	1080-55	6
FM-1000	0.10-0.10-0.10	1.5	15	1080-55	6
FM-1000	0.10-0.10-0.10	2.0	20	1080-55	6
FM-1000	0.20-0.20-0.20	1.0	5	1081-59	6
FM-1000	0.20-0.20-0.20	2.0	10	1081-59	6
FM-47	0.05-0.05-0.05	1.0	20	1081-58	6
FM-47	0.05-0.05-0.05	2.0	40	1081-58	6
FM-47	0.10-0.10-0.10	1.0	10	1081-57	6
FM-47	0.10-0.10-0.10	2.0	20	1081-57	6
				Total Joints	84

a. Outside adherends scarfed uniformly throughout the length of overlap.

below this curve. These results are different from those obtained for the double overlap full thickness joints, where a family of curves, each for a different adherend thickness, was obtained. A second major difference between the two types of joints is that scarfing slightly reduced the strength and efficiency of the 0.05 in. material joints, but increased strength and efficiency of the thicker bonded materials. This data seems to indicate that changing the relative stiffness (EA) of the 0.05 in. material by scarfing does not aid much in improving joint performance since the joints may be close to the optimum strength of the materials involved. For the large thicknesses changing the stiffness does help performance, but not as significantly as might be expected.

Scarfing of the joints generally shifts the joint parameter curves towards the behavior of a thinner adherend. The results for 0.10 in. adherend is superimposed on that for 0.05 in. The results for 0.20 in. are approximately 1000 psi lower at the smaller joint parameter.

Extrapolating the shear strength data to L/t = 0 resulted in a shear strength of 7600 psi for FM-1000. This is 12 percent higher than the value obtained from constant thickness joints.

4.3.2.2 FM-47

The results for FM-47 show very little change in behavior due to the effect of scarfing compared with full thickness joints. The only advantage to be gained by scarfing these joints is their increase in weight efficiency since their strengths were not reduced with the removal of the scarfed material. For this particular adhesive, the stress concentration factors must be so large that scarfing alone is insufficient to make any large change in joint strength.

If one compares Fig. 4.21 with Fig. 4.20, it can be seen that the scarfed results show the same trend as full thickness joints as to the effect of adhesive modulus. The results for the low modulus, high elongation FM-1000 are significantly greater

than those for the high modulus FM-47. This data again illustrates the important role mechanical properties of the adhesive play in joint behavior.

4.3.2.3 Failure Analysis of the Scarfed Joints

Several major conclusions were made based on observations of the failed specimens.

- There is a marked difference between the FM-47 (stiff) and the FM-1000 (plastic) adhesive specimens. None of the FM-47 bonded material showed any composite failure in the adherends. All joints failed in the adhesive layer even though the joints were well bonded. The FM-1000 joints all contained failures in the composite.
- For the FM-1000 in every case there was extensive failure in the scarfed adherends and no composite failure in the full thickness center adherend. Only in three joints did a shallow failure, one to two plies in depth, occur within the bonded area of the full thickness adherend.
- For FM-1000, generally longer overlaps showed more extensive composite damage. For the short 0.5 in. overlap, the failure would occur only in two or three major planes rather than having interlaminar failure occur at each lamina. A major failure would usually occur at the mid-thickness ply.
- For the FM-1000, $t = 0.05$, $L/t = 30, 40$, the failures occured in the composite near the grip area. In these cases the joints had sufficient strength to make the structure critical at the grips. The adherend stresses

at failure were lower than the design allowable for the composite indicating a stress concentration factor of 1.2 due to the grips.

4.3.3 Composite to Metal Joints

Thirty-four different geometries of Scotchply XP-251S were bonded in double overlap joints to titanium and steel using FM-1000 as the low modulus adhesive and FM-47 for the high modulus material. Table 4.16 summarizes the joints tested. The actual test results are given in Section 4.5.3.

In all these joints the metal thickness was always 0.10 in. and relative deformation between adherends was varied by changing the FRP thickness. One variable introduced between the metal joints was that the steel joints were bonded using steel for the outer two adherends and a single FRP adherend. This was necessary since the bond strengths of the joints were strong enough in the FRP-Steel-FRP configuration to cause failure of the steel adherend. In other words, all the joints for this configuration (Fabrication No. 1080-64) were strong enough to develop the full strength of the steel or they were 100 percent efficient based on the tensile strength of the steel, which is less than half that of the FRP.

For the titanium joints a FRP-Ti-FRP configuration was used since both materials had approximately the same tensile strength. This configuration still placed the joints critical in tension, in the titanium adherend, provided that the joint strengths were high enough. This only occured in two geometries.

4.3.3.1 Steel to FRP Joints

The results for FM-1000 and FM-47 are shown in Figs. 4.22 and 4.23. The following conclusions were based on these results:

- All the joint strength results for FM-1000 fall on one curve when plotted vs. joint

Table 4.16

SUMMARY OF METAL-FIBERGLASS DOUBLE OVERLAP JOINTS FOR STATIC STRENGTH TESTS

Adhesive	Adherend Thicknesses (in.)	Length of Overlap (in.)	Joint Parameter L/t	Fabrication Number	Number of Joints
	Steel-FRP-Steel				
FM-1000	0.1-0.05-0.1	1.0	20.0	1080-66	6
FM-1000	0.1-0.05-0.1	1.5	30.0	1080-66	6
FM-1000	0.1-0.05-0.1	2.0	40.0	1080-66	6
FM-1000	0.1-0.10-0.1	1.0	10.0	1080-67	6
FM-1000	0.1-0.10-0.1	2.0	20.0	1080-65	6
FM-1000	0.1-0.20-0.1	1.0	5.0	1080-68	6
FM-1000	0.1-0.20-0.1	1.5	7.5	1080-68	6
FM-1000	0.1-0.20-0.1	2.0	10.0	1080-68	6
	FRP-Steel-FRP				
FM-1000	0.1-0.10-0.1	1.25	12.5	1080-64	6
	Steel-FRP-Steel				
FM-47	0.1-0.05-0.1	1.0	20.0	1081-77	6
FM-47	0.1-0.05-0.1	1.5	30.0	1081-77	6
FM-47	0.1-0.05-0.1	2.0	40.0	1081-77	6
FM-47	0.1-0.10-0.1	1.0	10.0	1081-87	6
FM-47	0.1-0.10-0.1	1.5	15.0	1081-78	6
FM-47	0.1-0.10-0.1	2.0	20.0	1081-78	6
	Steel-FRP-Steel				
FM-47	0.1-0.20-0.1	1.0	5.0	1081-76	6
FM-47	0.1-0.20-0.1	1.5	7.5	1081-76	6
FM-47	0.1-0.20-0.1	2.0	10.0	1081-76	6
	FRP-Ti-FRP				
FM-1000	0.05-0.10-0.05	1.0	20.0	1080-71	6
FM-1000	0.05-0.10-0.05	1.5	30.0	1080-71	6
FM-1000	0.05-0.10-0.05	2.0	40.0	1080-71	6
FM-1000	0.10-0.10-0.10	1.0	10.0	1080-83	6
FM-1000	0.10-0.10-0.10	1.5	15.0	1080-72	6
FM-1000	0.10-0.10-0.10	2.0	20.0	1080-69	6
FM-1000	0.20-0.10-0.20	1.0	5.0	1080-82	6
FM-1000	0.20-0.10-0.20	1.5	7.5	1080-82	6
FM-1000	0.20-0.10-0.20	2.0	10.0	1080-82	6
	FRP-Ti-FRP				
FM-47	0.10-0.10-0.10	1.0	10.0	1081-86	6
FM-47	0.10-0.10-0.10	1.5	15.0	1081-81	6
FM-47	0.10-0.10-0.10	2.0	20.0	1081-81	6
FM-47	0.20-0.10-0.20	1.0	5.0	1081-79	6
FM-47	0.20-0.10-0.20	1.5	7.5	1081-79	6
FM-47	0.20-0.10-0.20	2.0	10.0	1081-79	6
				Total Joints	198

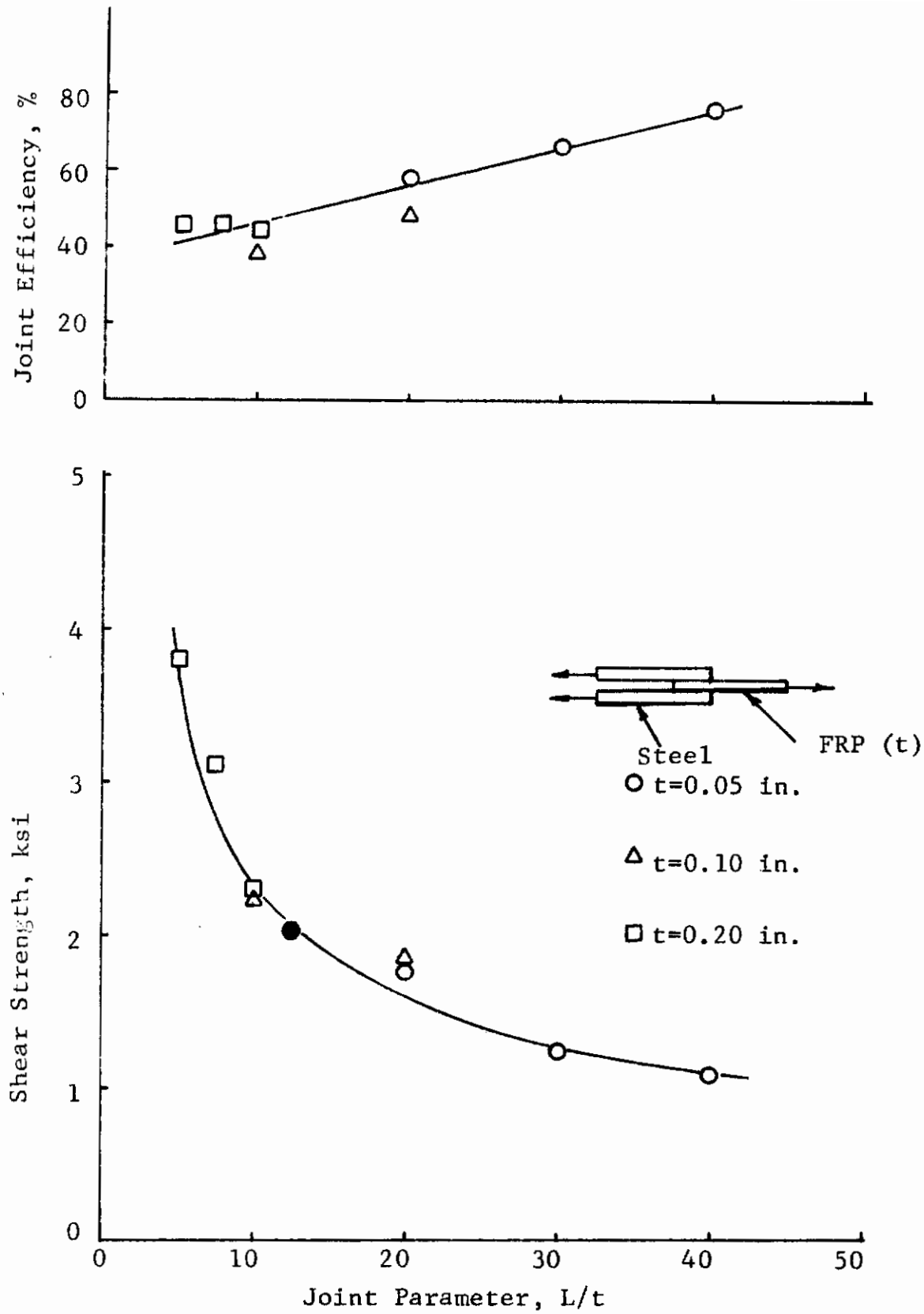

Fig. 4.22 SHEAR STRENGTH AND JOINT EFFICIENCY OF STEEL BONDED TO SCOTCHPLY XP-251S WITH FM-1000 ADHESIVE

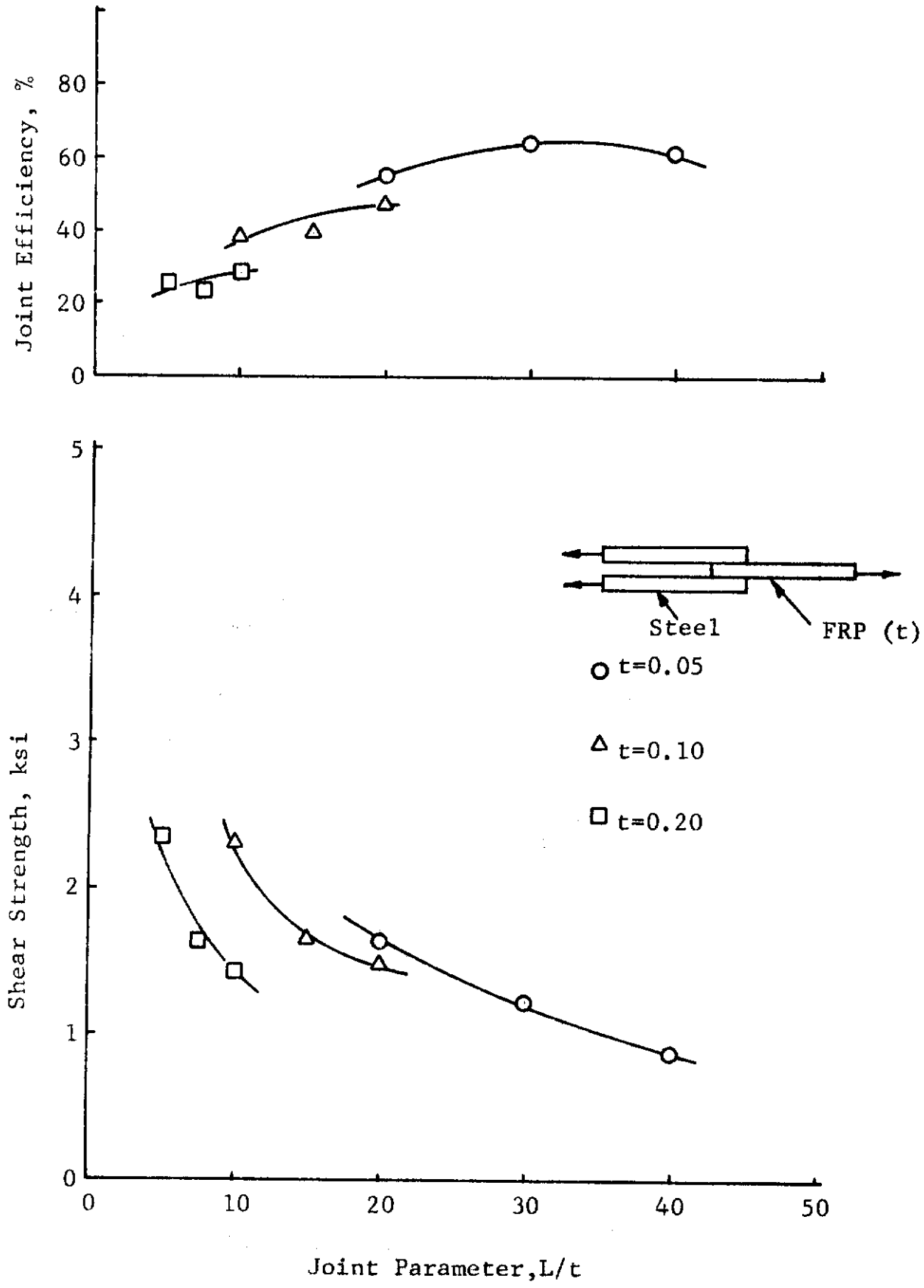

Fig. 4.23 SHEAR STRENGTH AND JOINT EFFICIENCY OF STEEL BONDED TO SCOTCHPLY XP-251S WITH FM-47 ADHESIVE

parameter (L/t). For FM-47 the results for the two thinnest adherends, 0.05 and 0.10 in. thick, almost lie on one curve while the 0.20 in. thick adherend data is definitely displaced. The same results hold true for joint efficiency. All the joint strengths are curvilinear with joint parameter.

- All the joint strengths for both adhesives at 0.05 and 0.10 in. lie on a common curve. This means that the effect of adhesive modulus does not play a strong role in these geometries. The same result holds true for joint efficiencies. The points overlay each other identically except at L/t = 40 where the FM-1000 joint is 20 percent stronger than the FM-47 bonded joint.

- The joint strengths for the 0.20 in. adherends bonded with FM-1000 are significantly stronger (35 to 85 percent) and 20 percent more efficient than the FM-47 results. These data support the thesis of effect of modulus on joint strength.

There is one extra result given in Fig. 4.22, the dark data point, which is the strength result for Fabrication No. 1080-64, FRP-Steel-FRP, t = 0.10/0.10/0.10 in. configuration. The shear strength data point falls on the same curve as the other results but the joint efficiency would be 100 percent based on the tensile strength of the steel, and 20 percent efficient based on the stress reached in each of the FRP adherends.

- The maximum joint efficiencies obtained were 60 percent for the FM-47 and 78 percent for the FM-1000.

- Review of the fractured specimens showed that none of the FM-47 contained any fractures in the FRP. Failure occurred in the adhesive film between the adherends. The FM-47 showed good adhesion to both the FRP and steel.
- All the FM-1000 bonded joints contained fractures two to three plies deep into the FRP, initiating in the bond area and then extending beyond the joint. The 0.05 in. material was generally fractured throughout the thickness. The FM-1000 showed good adhesion to the steel.

4.3.3.2 Titanium to FRP Joints

The results of the FRP-Ti-FRP joints bonded with FM-1000 and FM-47 are given in Figs. 4.24, and 4.25. It should be noted that the efficiencies for these joints are all based on the tensile strength of the single titanium adherend. This is different from all the other joints tested where efficiencies are based on FRP tensile strength. The following conclusions are drawn from the results:

- All the joint strengths are curvilinear with joint parameter (L/t) and the results for each adherend thickness fall on a separate curve.
- Comparing FM-1000 with FM-47, the joint strengths for the thickest adherend 0.20 in. are almost colinear. The strengths with the thinner adherends are 30 percent greater and the joint efficiencies 20 to 40 percent greater for the FM-1000 adhesive. These results support the modulus-strength hypothesis.

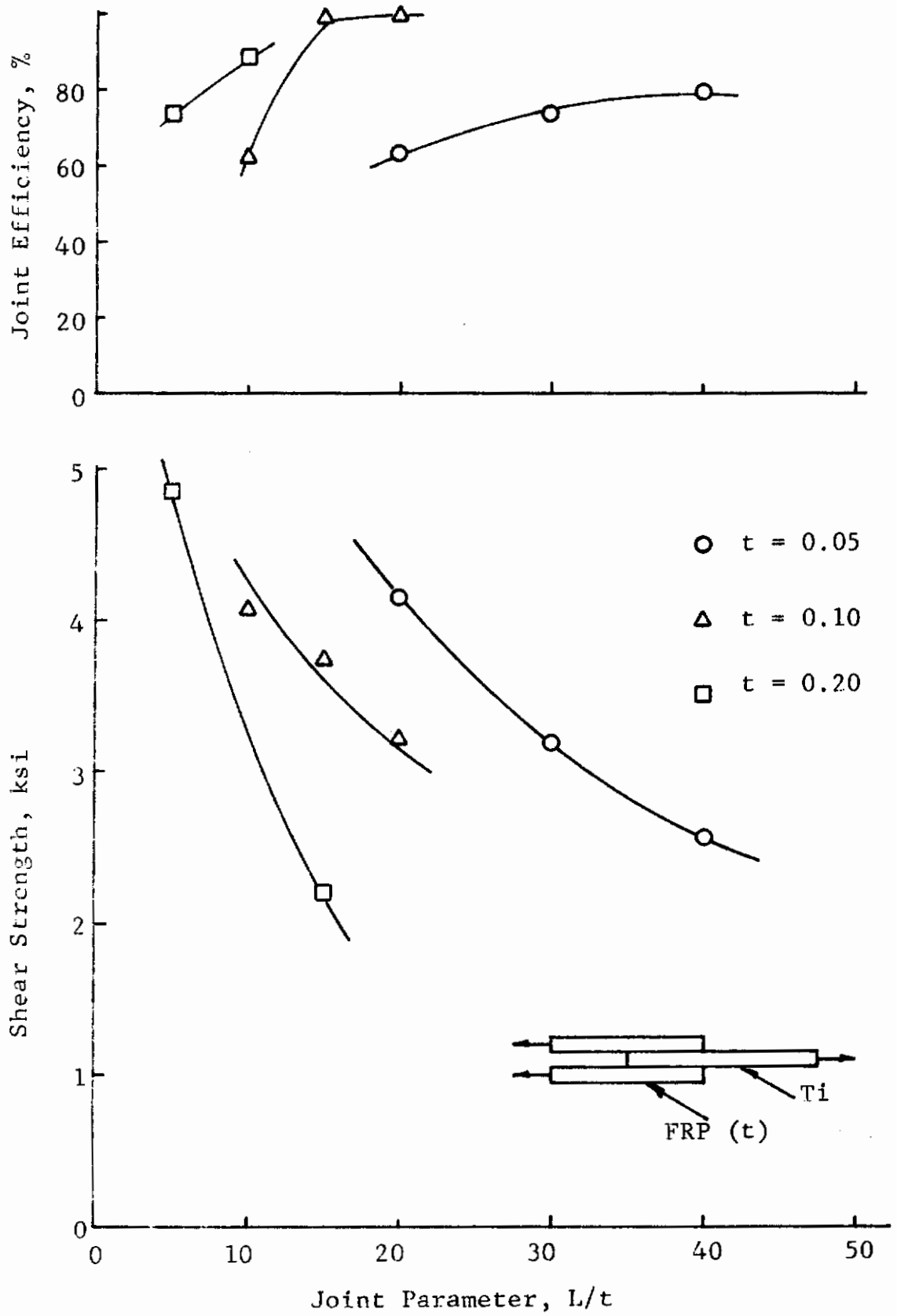

Fig. 4.24 SHEAR STRENGTH AND JOINT EFFICIENCY OF TITANIUM BONDED TO SCOTCHPLY XP-251S WITH FM-1000 ADHESIVE

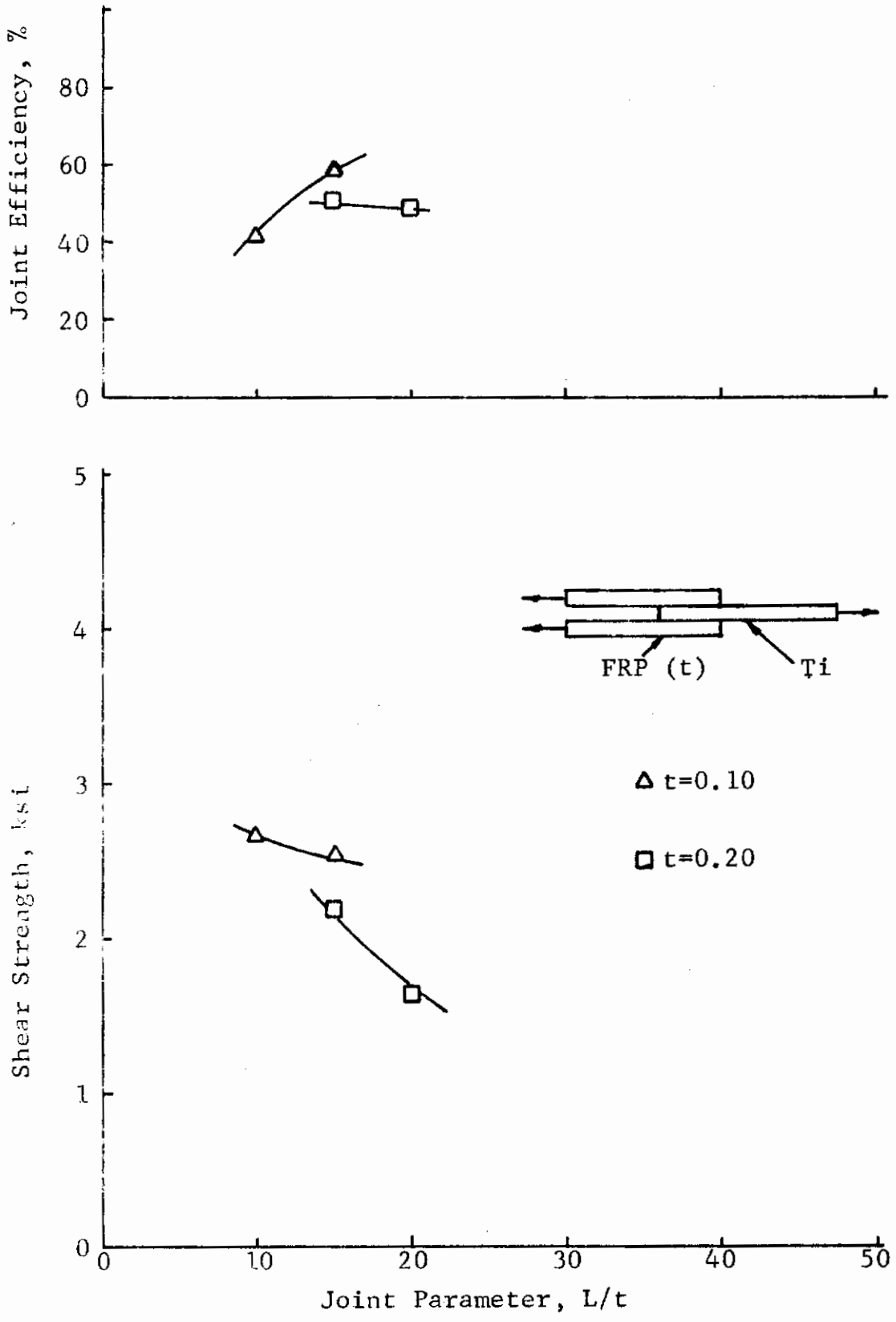

Fig. 4.25 SHEAR STRENGTH AND JOINT EFFICIENCY OF TITANIUM BONDED TO SCOTCHPLY XP-251S BONDED WITH FM-47 ADHESIVE

- The highest joint efficiencies obtained were 100 percent for the FM-1000 and 60 percent for the FM-47.
- Comparing the strengths of the FRP-Ti-FRP (Figs. 4.24, 4.25) joints with the FRP-FRP-FRP (Figs. 4.16, 4.18) joints of the same geometry for both FM-1000 and FM-47, the metal-composite joints have higher strengths than the composite-composite joints. This may be due to the introduction of the single metal adherend. The titanium has a higher shear strength than the composite, and we have just removed one low-strength component of the joint.
- Comparing the titanium joints to the steel joints, all the titanium joint strengths are higher for both adhesives.
- All the FM-1000 joints showed composite failure two to three plies into the adherend beginning in the bonded area. The FM-47 joints showed no composite failures present. Again failure occured through the adhesive film.
- The FM-1000, 0.05 in. thick joints contained almost total composite failure generally increasing with length of overlap.

4.4 FATIGUE STRENGTH OF ADHESIVE BONDED JOINTS

The fatigue was measured for three adhesives bonded in the double overlap geometry with two different lengths of overlap. The purpose of this series of joints was to establish the relationship between fatigue behavior of these joints with adhesive modulus and the joint parameter (L/t). The joint geometries chosen had shown either optimum or close to optimum efficiency based on the static strength results.

4.4.1 Fatigue Testing

All the fatigue testing for this study was done by the U.S.D.A. Forest Products Laboratory. Table 4.17 summarizes the joints tested and the stress levels selected for testing. All joints were 0.5 inches wide, 0.05 inches thick and L was variable.

Two specimens were tested at each stress level where the static strength for each geometry was obtained by averaging the strength of the two specimens tested at the U.S.D.A. Forest Products Laboratory with the results of the six specimens tested for the same geometry by IITRI as described under the static testing in this section.

All specimens were tested at a cyclic rate of 900 cycles per minute with a tension-zero-tension cycle. The stress ratio was

$$R = \frac{\tau_{min}}{\tau_{max}} = 0.1.$$

All fatigue results are given in Section 4.5.4.

4.4.2 Fatigue Results

Shear strength as a function of cycles to failure was graphed from the experimental results of each adhesive and are shown in Figs. 4.26, 4.27, and 4.28. The residual strength for each adhesive at 10 million cylcles are shown on the following page.

Table 4.17

SUMMARY OF FIBERGLASS - FIBERGLASS DOUBLE OVERLAP JOINTS TESTED IN FATIGUE[a]

Adhesive	Adherend Thicknesses (in.)	Length of Overlap (in.)	Joint Parameter L/t	Fabrication Number	Number of Joints
FM-1000	0.05-0.05-0.05	0.5	10	1080-73	12
FM-1000	0.05-0.05-0.05	1.5	30	1080-73	12
Metlbond 400	0.05-0.05-0.05	0.5	10	1081-75	12
Metlbond 400	0.05-0.05-0.05	1.5	30	1081-75	12
FM-47	0.05-0.05-0.05	0.5	10	1090-74	12
FM-47	0.05-0.05-0.05-	1.5	30	1090-74	12
				Total Joints	72

a.

Stress Level at Test	Number
% τ_{ult}	
100%	2
55%	2
45%	2
A	2
B	2

Stress Cycle Tension-Zero-Tension, $R = \frac{\tau_{min}}{\tau_{max}} = 0.1$

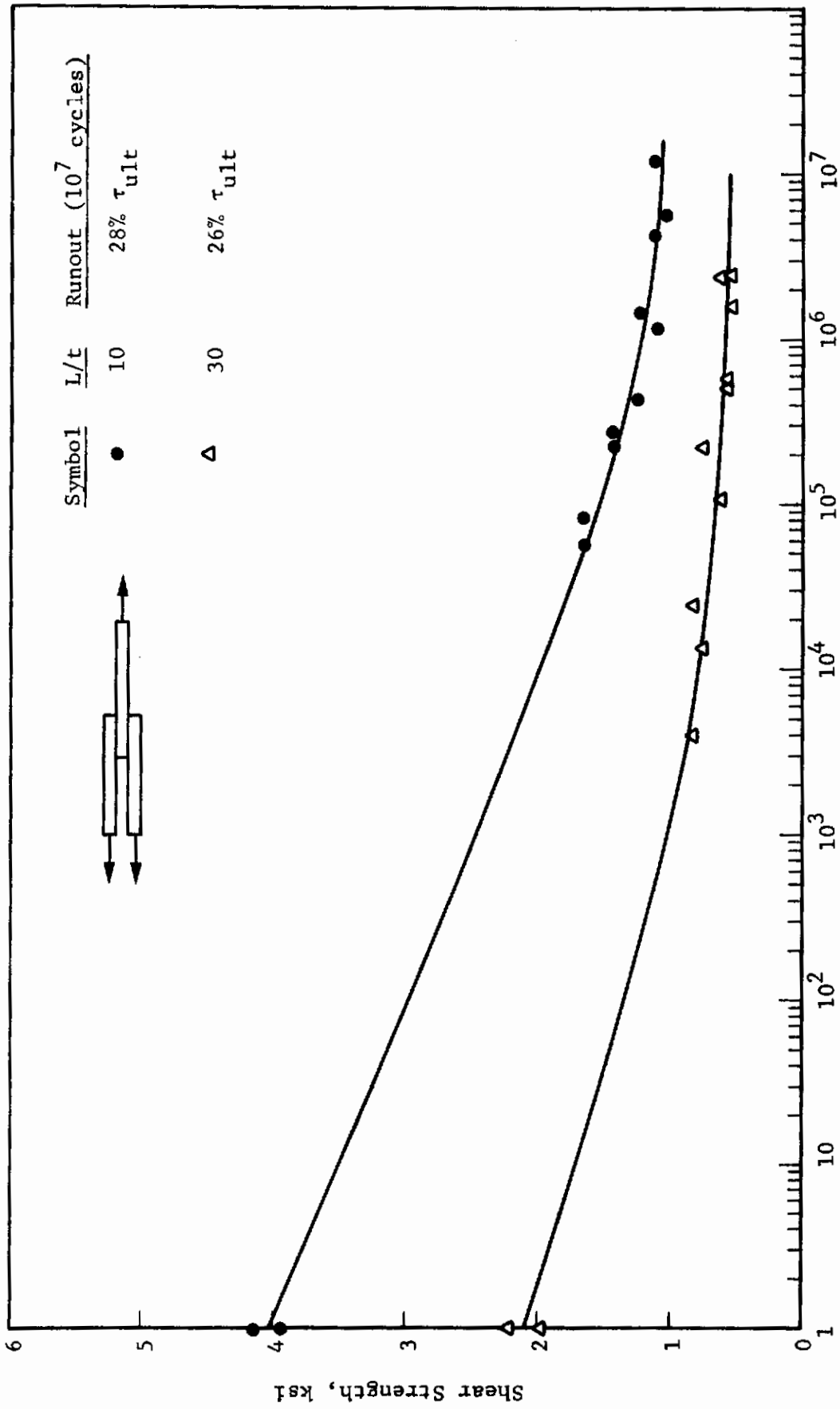

Fig. 4.26 FATIGUE STRENGTH OF DOUBLE OVERLAP JOINTS BONDED WITH FM-1000

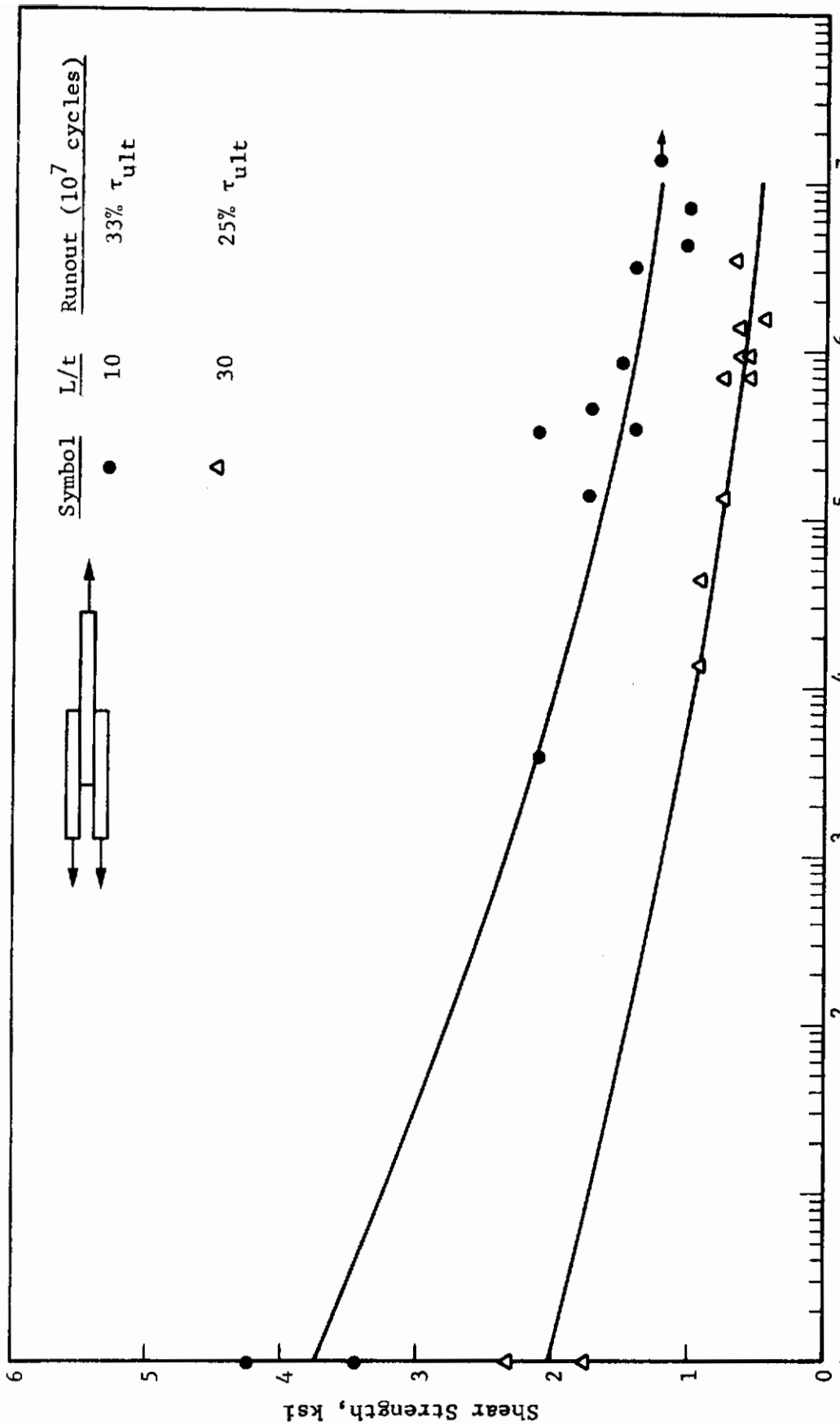

Fig. 4.27 FATIGUE STRENGTH OF DOUBLE OVERLAP JOINTS BONDED WITH METLBOND 400

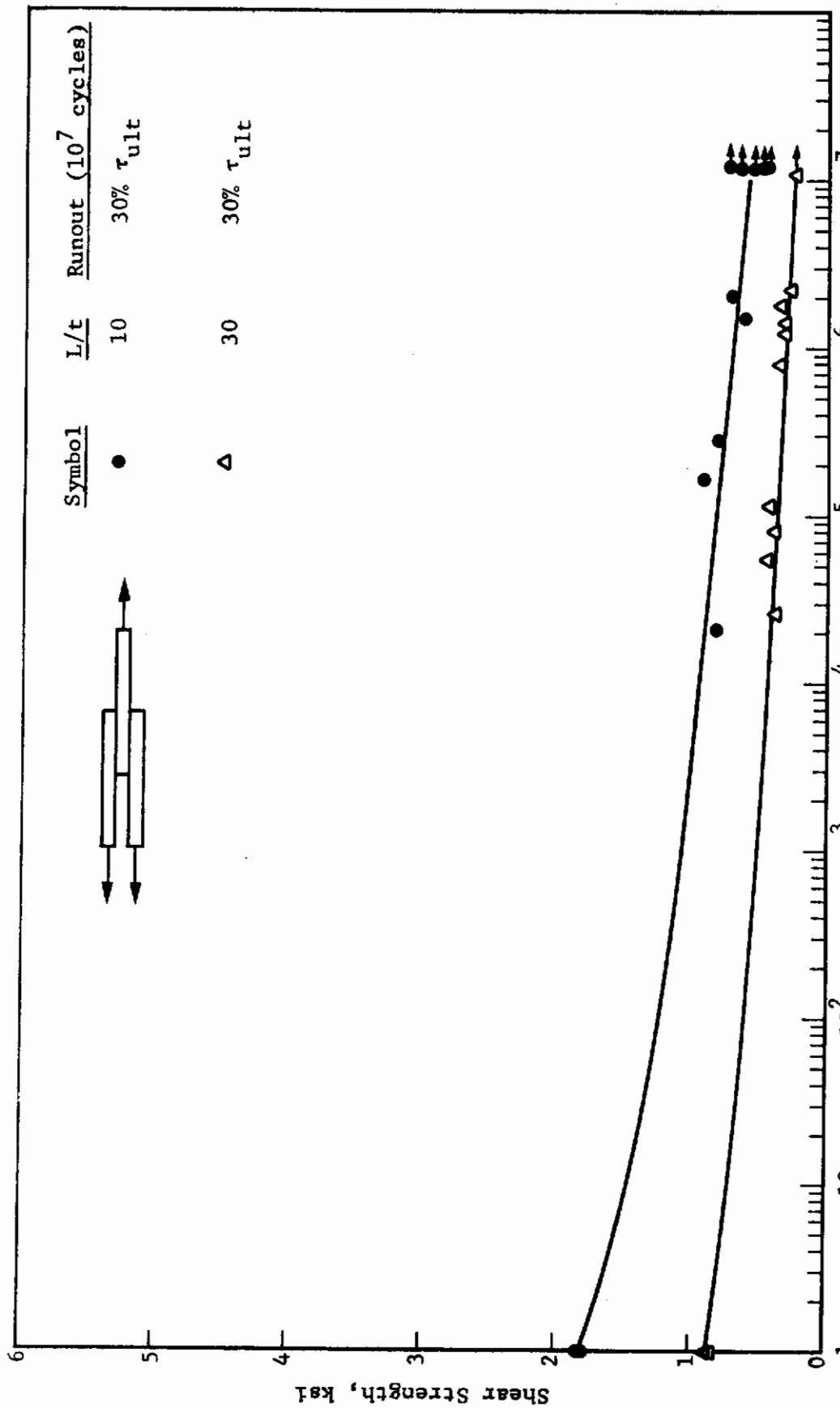

Fig. 4.28 FATIGUE STRENGTH OF DOUBLE OVERLAP JOINTS BONDED WITH FM-47

Adhesive	Joint Parameter	Relative Strength 10^7 Cycles	Adherend Stress 10^7 Cycles	Fatigue Efficiency %
FM-1000	10	0.27	21,600	0.86
	30	0.26	33,000	1.32
Metlbond 400	10	0.32	24,400	0.97
	30	0.25	30,000	1.20
FM-47	10	0.33	12,000	0.48
	30	0.31	15,600	0.62

The relative strength at 10^7 cycles is the ratio of the residual shear strength of each geometry to the static shear strength. The adherend stress at 10^7 cycles is the stress in the single adherend of the joint and the fatigue efficiency is the ratio of this stress to the fatigue limit of the Scotchply XP-251S composite material at 10^7 cycles. This fatigue limit is 25,000 psi. The following conclusions are based on these results.

1. The relative joint strength at 10^7 cycles of each adhesive is approximately the same, with a slight indication that L/t = 10 degrades less from the L/t = 30 geometry.

2. Based on joint efficiency or the ability of the joint to develop the fatigue life of the composite, the L/t = 30 joint geometry is the most efficient. This is further supported by the failure analyses of the joint. The least efficient adhesive FM-47 yielded all bond failures. The most efficient joints, L/t = 30, for the other two adhesives were all laminate failure. The two intermediate designs FM-1000 and Metlbond 400 at L/t = 10 failed in a mixed mode of both laminate and composite failure.

3. The highest fatigue efficiencies were obtained for FM-1000 and Metlbond 400. These are both the lower

modulus higher elongation materials compared to the stiff, brittle FM-47. This result again supports the thesis proposed by the study that a lower modulus adhesive significantly improves joint performance.

4. Figure 4.29 shows the fatigue results for the three adhesives at the joint parameter L/t = 10. This shows the close grouping of the data for the two tougher adhesives compared to the stiffer more brittle FM-47.

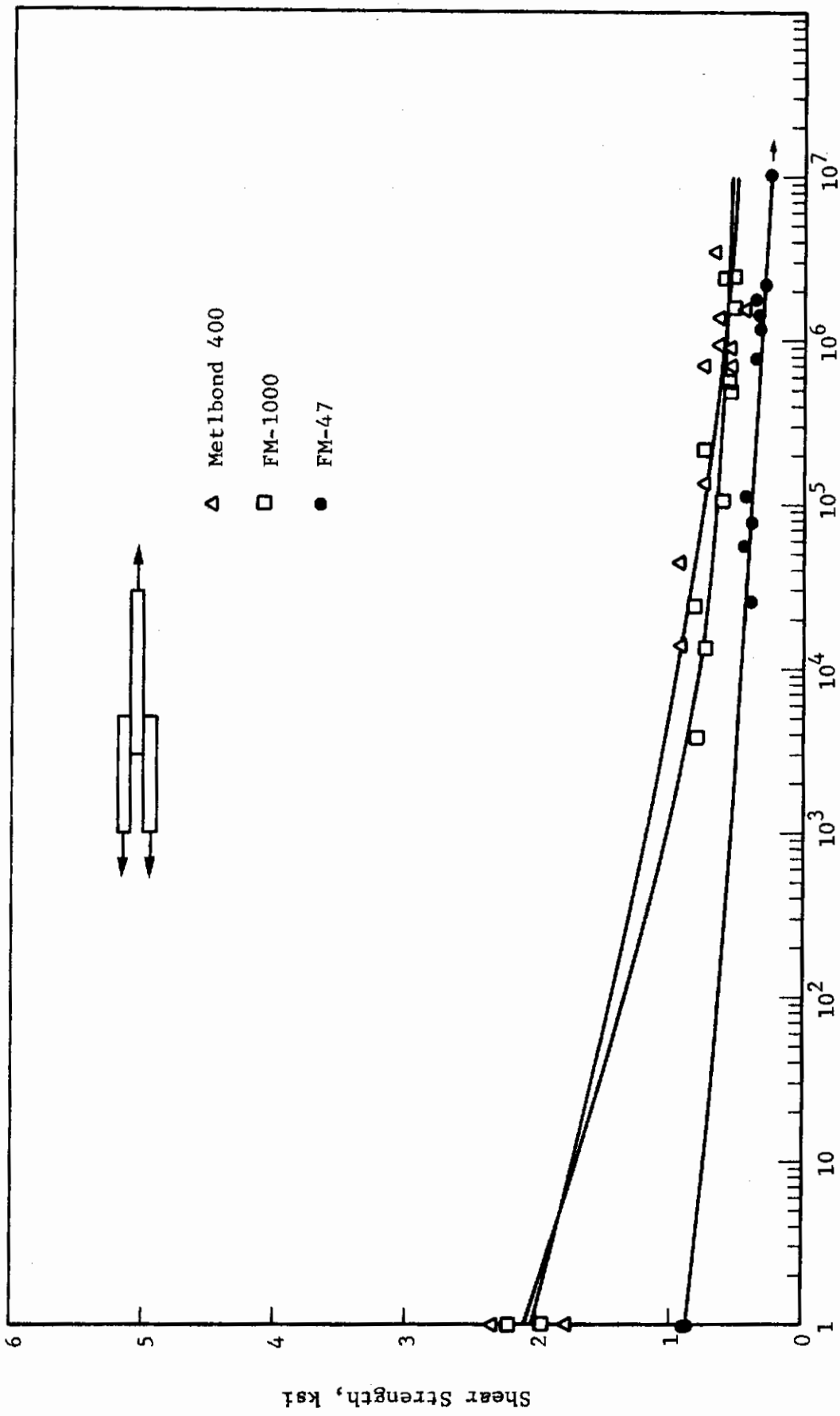

Fig. 4.29 FATIGUE STRENGTH OF SEVERAL ADHESIVES AT CONSTANT JOINT PARAMETER

4.5 EXPERIMENTAL DATA FOR STATIC AND FATIGUE STRENGTH JOINT PROPERTIES

4.5.1 STRENGTH OF FRP-FRP BONDED JOINTS

This section contains the static strength results for the double-overlap joints of Scotchply XP-251S bonded with Metlbond 400, FM-1000 and FM-47 adhesives. Each table of data is followed by a graph of joint strength and joint efficiency as a function of the joint parameter L/t.

Table 4.18

SHEAR STRENGTH OF DOUBLE OVERLAP JOINTS OF SCOTCHPLY XP-251S BONDED WITH FM-1000, ADHEREND THICKNESS 0.05 IN.

Specimen Number	Length of Overlap (in.)	Width of Joint (in.)	Load at Failure (lb)	Adherend Stress (ksi)	Shear Strength (psi)	Joint Efficiency (%)	Joint Parameter (L/t)
1080-27-1	0.5	0.531	2080	78.2	3920	71.1	10
1080-27-2	0.5	0.534	2370	88.8	4450	80.7	10
1080-27-3	0.5	0.529	2220	84.2	4200	76.6	10
1080-27-4	0.5	0.547	2480	90.5	4540	82.3	10
1080-27-5	0.5	0.555	2280	82.2	4110	74.8	10
1080-27-6	0.5	0.529	2130	80.7	4030	73.5	10
				Average	4210	76.5	
1080-27- 7	1.0	0.522	2650	101.0	2550	91.8	20
1080-27- 8	1.0	0.540	2970	110.0	2750	100.0	20
1080-27- 9	1.0	0.528	2750	104.0	2590	94.5	20
1080-27-10	1.0	0.575	2930	102.0	2550	92.8	20
1080-27-11	1.0	0.510	2680	105.0	2630	95.5	20
1080-27-12	1.0	0.493	2330	94.4	2360	85.8	20
				Average	2570	93.4	
1080-27-13	1.5	0.554	3330	120.0	2000	109.0	30
1080-27-14	1.5	0.535	3520	132.0	2180	120.0	30
1080-27-15	1.5	0.537	3510	131.0	2180	119.0	30
1080-27-16	1.5	0.509	3170	125.0	2070	114.0	30
1080-27-17	1.5	0.485	2870	119.0	1980	108.0	30
1080-27-18	1.5	0.554	3250	118.0	1960	107.0	30
				Average	2060	112.8	
1080-27-19	2.0	0.545	2850	105.0	1300	95.5	40
1080-27-20	2.0	0.524	2800	107.0	1330	97.3	40
1080-27-21	2.0	0.514	2440	90.0	1130	81.8	40
1080-27-22	2.0	0.548	3210	117.0	1460	106.0	40
1080-27-23	2.0	0.513	2760	108.0	1350	98.3	40
1080-27-24	2.0	0.532	2460	92.5	1150	84.0	40
				Average	1290	93.8	

* Joint efficiency should not exceed 100% efficiency. These results were based on the 110 ksi ultimate tensile strength of the Scotchply XP-251S laminates determined by testing prior to preparing double overlap specimens for this study.

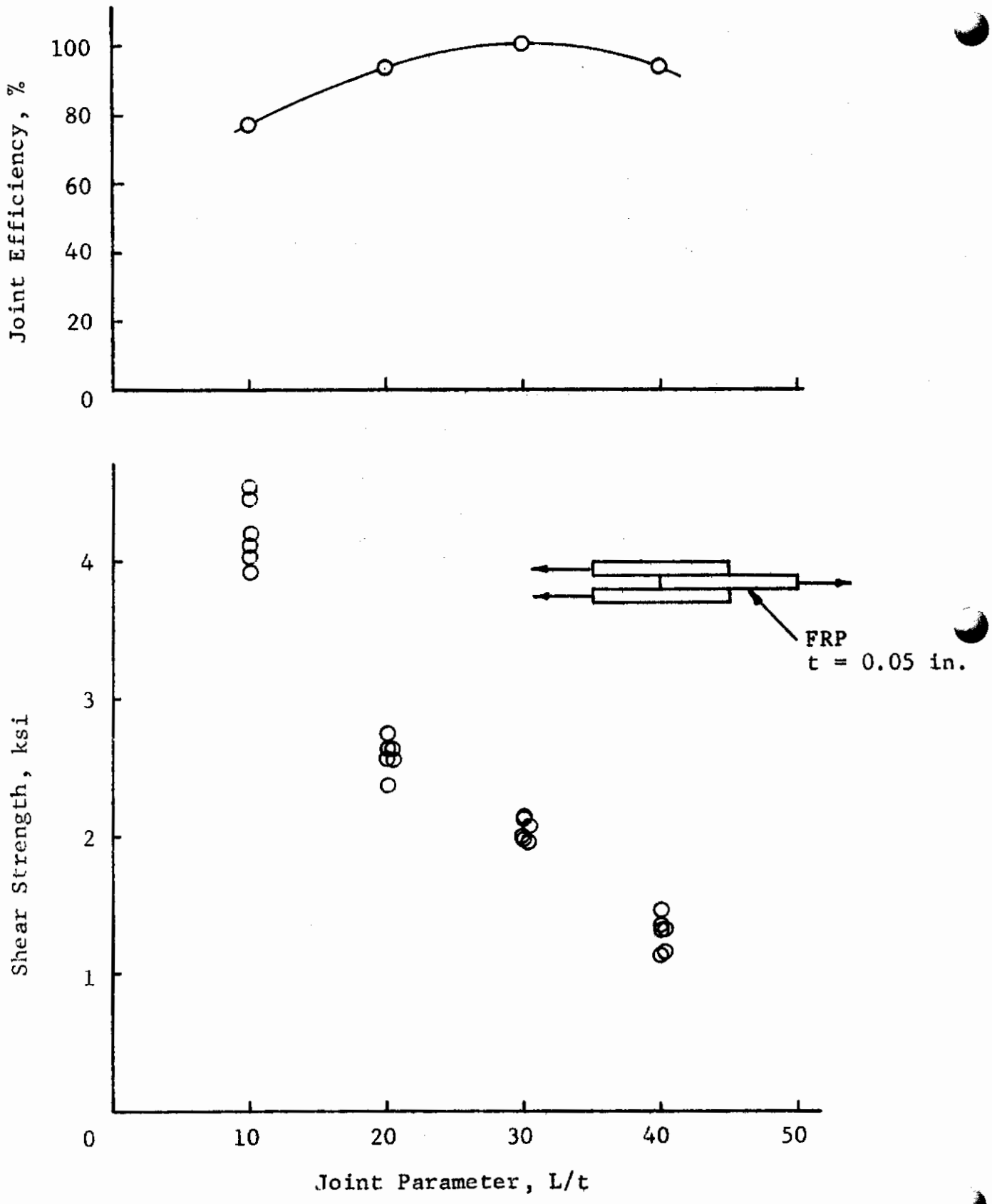

Fig. 4.30 SHEAR STRENGTH AND JOINT EFFICIENCY OF SCOTCHPLY XP-251S BONDED WITH FM-1000, t = 0.05 in.

Table 4.19

SHEAR STRENGTH OF DOUBLE OVERLAP JOINTS OF SCOTCHPLY XP-251S BONDED WITH FM-1000, ADHEREND THICKNESS 0.10 IN.

Specimen Number	Length of Overlap (in.)	Width of Joint (in.)	Load at Failure (lb)	Adherend Stress (ksi)	Shear Strength (psi)	Joint Efficiency (%)	Joint Parameter (L/t)
1080-28-37	0.5	0.507	1960	38.7	3870	35.2	5
1080-28-38	0.5	0.520	2130	41.0	4090	37.3	5
1080-28-39	0.5	0.525	2210	42.0	4210	38.2	5
1080-28-40	0.5	0.526	2300	43.8	4370	39.8	5
1080-28-41	0.5	0.524	2100	40.1	4010	36.4	5
1080-28-42	0.5	0.527	2030	38.6	3850	35.1	5
				Average	4070	37.0	
1080-28-31	1.0	0.517	2130	41.3	2070	37.6	10
1080-28-32	1.0	0.528	2100	39.8	1980	36.2	10
1080-28-33	1.0	0.498	2110	42.4	2110	38.6	10
1080-28-34	1.0	0.545	2100	38.5	1930	35.0	10
1080-28-35	1.0	0.536	2200	41.0	2060	37.2	10
1080-28-36	1.0	0.500	2140	42.8	2140	38.9	10
				Average	2050	37.2	
1080-28-25	1.5	0.519	2970	57.7	1910	52.4	15
1080-28-26	1.5	0.507	2060	40.6	1350	36.9	15
1080-28-27	1.5	0.517	2550	49.4	1650	44.8	15
1080-28-28	1.5	0.522	3020	57.8	1920	52.6	15
1080-28-29	1.5	0.551	3040	55.2	1840	50.2	15
1080-28-30	1.5	0.518	2310	44.6	1490	40.6	15
				Average	1690	46.2	
1080-28-19	2.0	0.518	2350	45.4	1130	41.2	20
1080-28-20	2.0	0.520	2560	49.2	1230	44.7	20
1080-28-21	2.0	0.522	2850	54.6	1360	49.6	20
1080-28-22	2.0	0.494	2560	51.5	1290	46.8	20
1080-28-23	2.0	0.538	3250	60.4	1510	55.0	20
1080-28-24	2.0	0.535	3130	58.6	1460	53.3	20
				Average	1330	48.4	

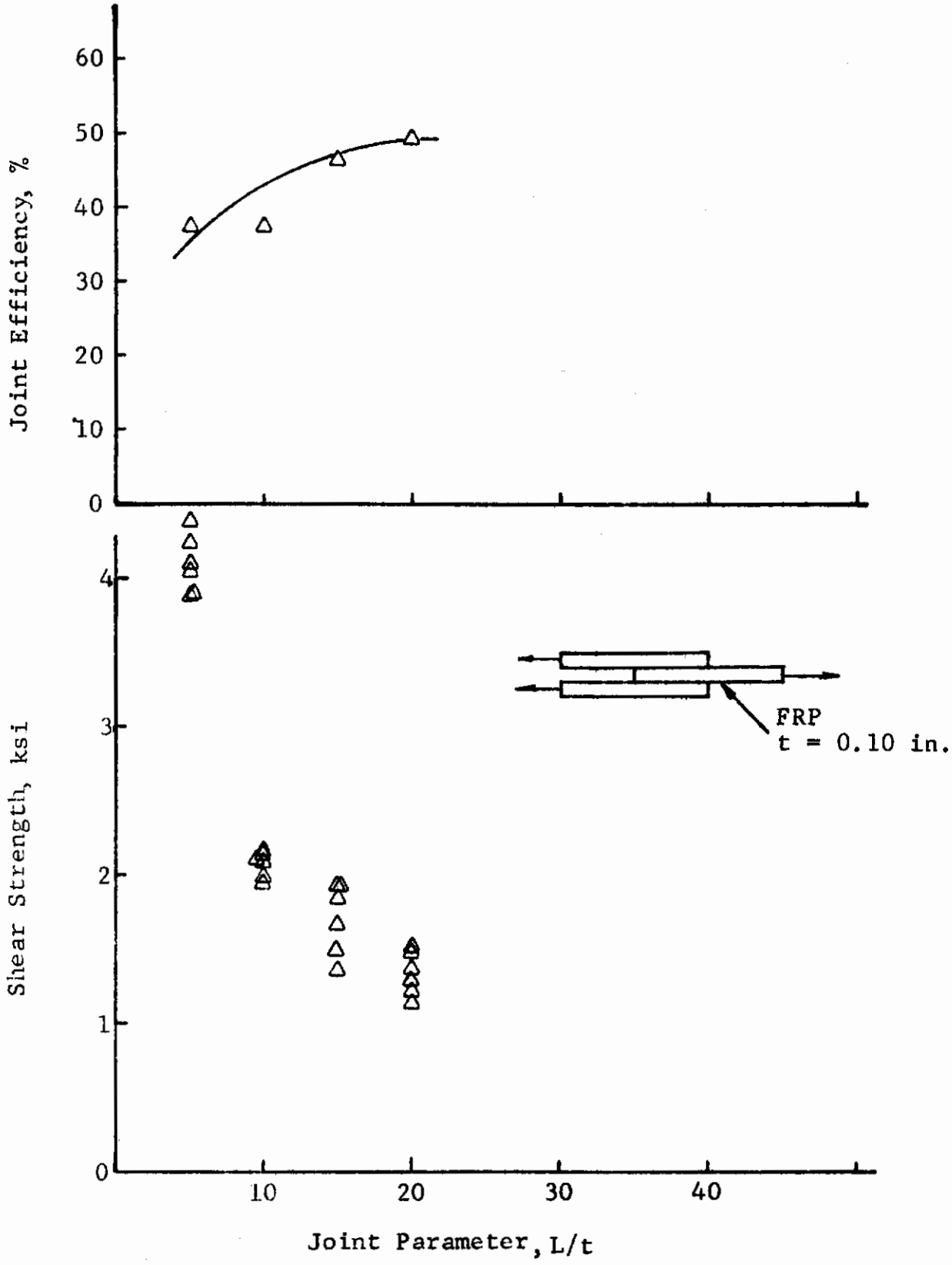

Fig. 4.31 SHEAR STRENGTH AND JOINT EFFICIENCY OF SCOTCHPLY XP-251S BONDED WITH FM-1000, t = 0.10 in.

Table 4.20

SHEAR STRENGTH OF DOUBLE OVERLAP JOINTS OF SCOTCHPLY XP-251S BONDED WITH FM-1000, ADHEREND THICKNESS 0.2 IN.

Specimen Number	Length of Overlap (in.)	Width of Joint (in.)	Load at Failure (lb)	Adherend Stress (ksi)	Shear Strength (psi)	Joint Efficiency (%)	Joint Parameter (L/t)
1080-29-1	1.0	0.515	4330	45.5	4200	41.4	5
1080-29-2	1.0	0.524	3760	38.6	3580	35.1	5
1080-29-3	1.0	0.504	3920	42.0	3880	38.2	5
1080-29-4	1.0	0.544	4210	41.7	3860	37.9	5
1080-29-5	1.0	0.510	4270	45.1	4180	41.0	5
1080-29-6	1.0	0.469	4200	48.2	4480	43.8	5
				Average	4030	39.6	
1080-29- 7	2.0	0.453	3220	38.2	1780	34.7	10
1080-29- 8	2.0	0.541	4040	40.0	1870	36.4	10
1080-29- 9	2.0	0.491	3960	43.0	2020	39.1	10
1080-29-10	2.0	0.528	4470	45.6	2120	41.5	10
1080-29-11	2.0	0.545	4570	44.8	2100	40.7	10
1080-29-12	2.0	0.522	4580	47.0	2200	42.7	10
				Average	2020	39.2	

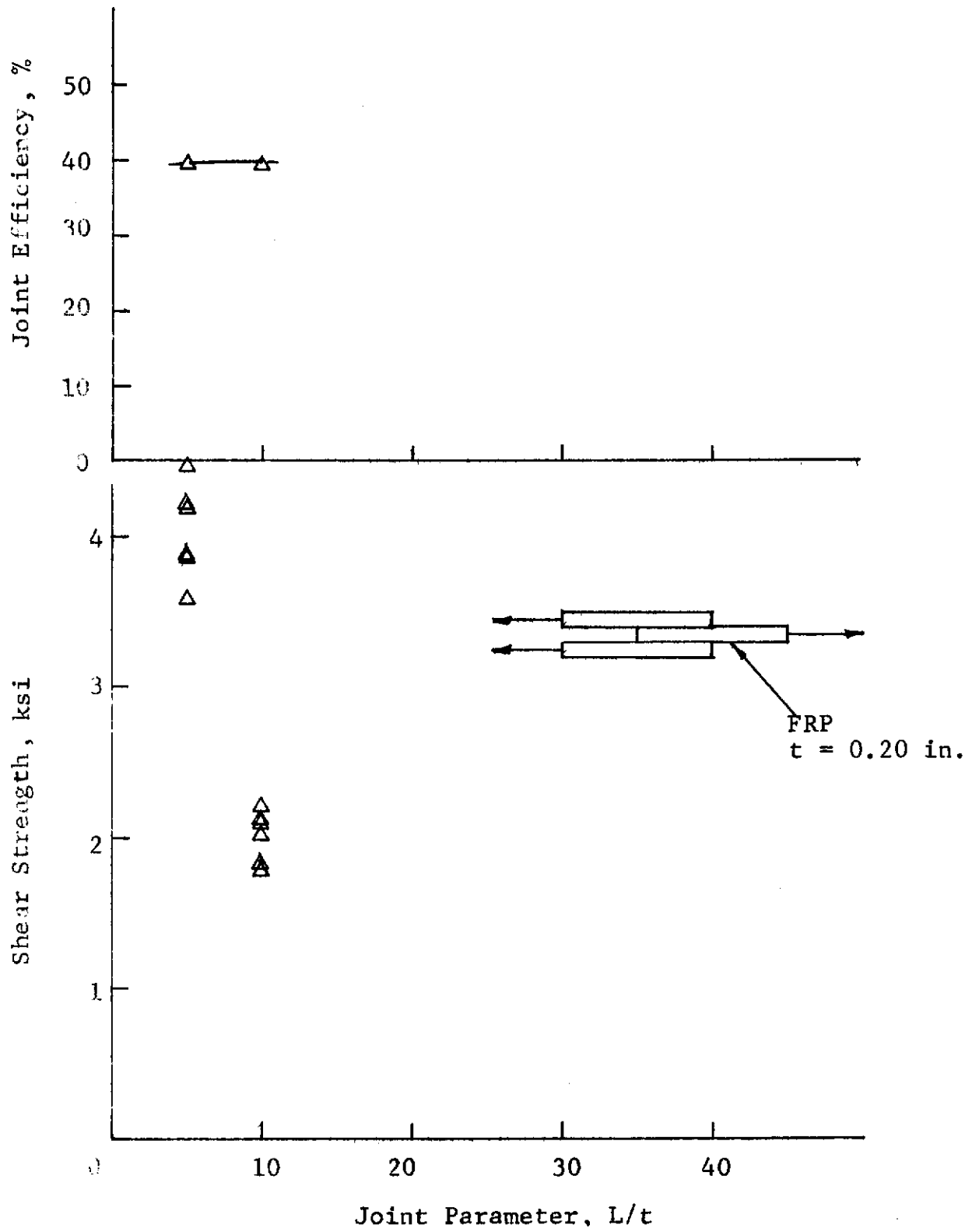

Fig. 4.32 SHEAR STRENGTH AND JOINT EFFICIENCY OF SCOTCHPLY XP-251S BONDED WITH FM-1000, t = 0.20 in.

Table 4.21

SHEAR STRENGTH OF DOUBLE OVERLAP JOINTS OF SCOTCHPLY XP-251S*
BONDED WITH FM-1000, ADHEREND THICKNESS, 0.2 INCHES

Specimen Number	Length of Overlap (in.)	Width of Joint (in.)	Load at Failure (lb)	Adherend Stress (ksi)	Shear Strength (psi)	Joint Efficiency (%)	Joint Parameter (L/t)
1080-34-1	1.0	0.504	2250	24.1	2220	21.9	5
1080-34-2	1.0	0.510	2070	21.9	2030	19.9	5
1080-34-3	1.0	0.511	2210	23.4	2170	21.2	5
1080-34-4	1.0	0.503	1940	20.9	1920	19.0	5
1080-34-5	1.0	0.513	2340	24.7	2300	22.5	5
				Average	2130	20.9	
1080-34- 6	2.0	0.509	2680	28.9	1310	26.3	10
1080-34- 7	2.0	0.516	2330	25.0	1130	22.7	10
1080-34- 8	2.0	0.520	2620	27.7	1260	25.2	10
1080-34- 9	2.0	0.517	2820	30.0	1360	27.3	10
1080-34-10	2.0	0.513	2600	27.9	1270	25.4	10
1080-34-11	2.0	0.519	2430	26.0	1170	23.6	10
				Average	1250	25.1	

* Outer ply perpendicular to load direction.

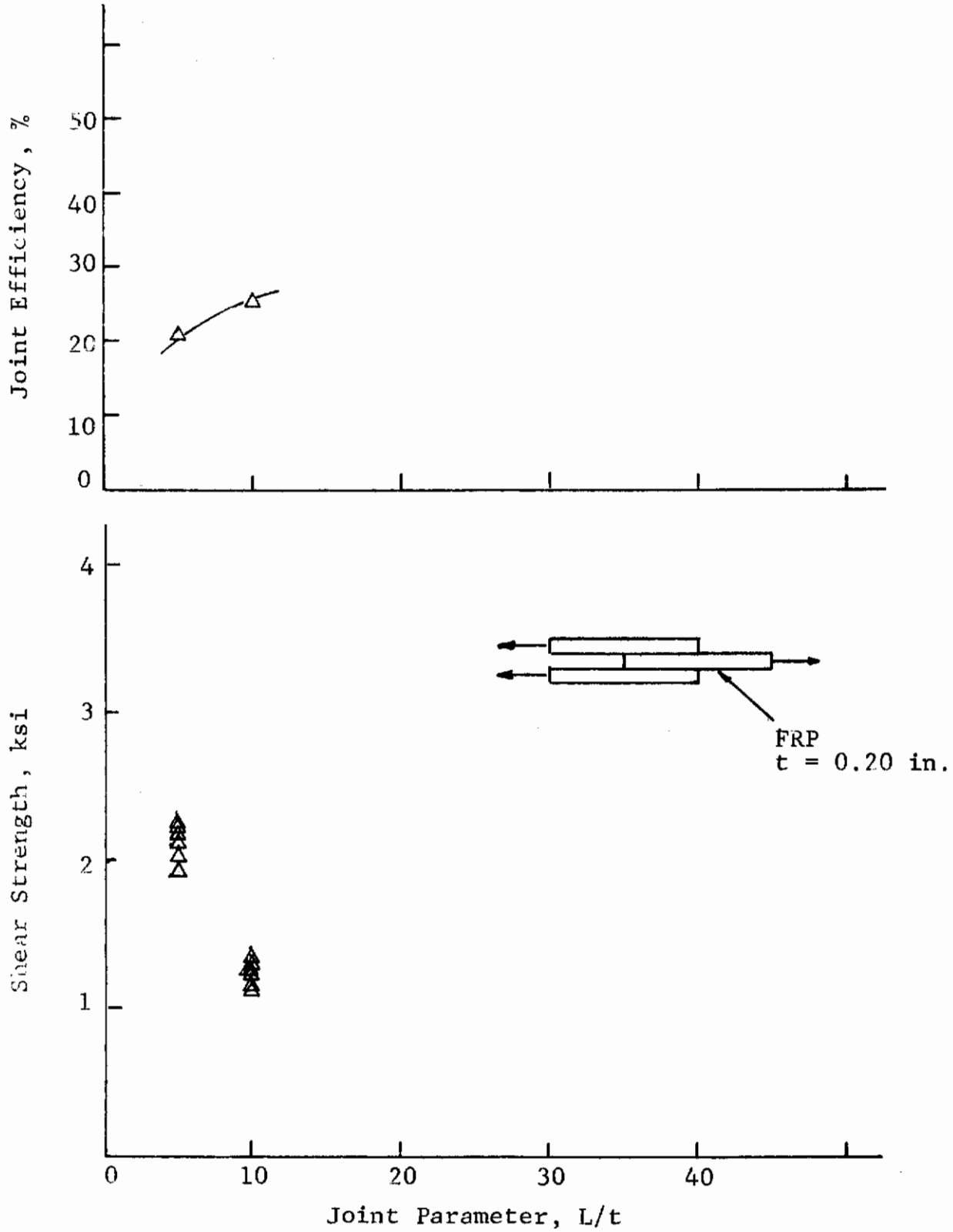

Fig. 4.33 SHEAR STRENGTH AND JOINT EFFICIENCY OF SCOTCHPLY XP-251S BONDED WITH FM-1000, OUTER PLY PERPENDICULAR TO THE JOINT LOAD, t = 0.20 in.

Table 4.22

SHEAR STRENGTH OF DOUBLE OVERLAP JOINTS OF SCOTCHPLY XP-251S BONDED WITH METLBOND 0400, ADHEREND THICKNESS, 0.05 IN.

Specimen Number	Length of Overlap (in.)	Width of Joint (in.)	Load at Failure (lb)	Adherend Stress (ksi)	Shear Strength (psi)	Joint Efficiency (%)	Joint Parameter (L/t)
1090-22-19	0.5	0.526	1750	33.3	3320	36.7	5
1090-22-20	0.5	0.513	2260	44.0	4410	43.6	5
1090-22-21	0.5	0.559	1460	26.3	2620	34.1	5
1090-22-22	0.5	0.536	1320	24.6	2460	38.6	5
1090-22-23	0.5	0.527	1300	24.6	2420	34.6	5
1090-22-24	0.5	0.523	2680	51.0	5120	38.8	5
				Average	3390	37.7	
1090-22-13	1.0	0.546	2250	41.0	2060	69.1	10
1090-22-14	1.0	0.539	1810	33.6	1680	73.6	10
1090-22-15	1.0	0.541	2250	41.5	2080	57.6	10
1090-22-16	1.0	0.556	2180	39.2	1960	53.2	10
1090-22-17	1.0	0.531	2080	39.1	1960	79.5	10
1090-22-18	1.0	0.542	2070	38.2	1920	49.6	10
				Average	1940	63.7	
1090-22-7	1.5	0.538	2320	43.4	1440	61.0	15
1090-22-8	1.5	0.543	2220	41.0	1360	59.1	15
1090-22-9	1.5	0.530	2420	45.6	1520	50.0	15
1090-22-10	1.5	0.532	2250	42.5	1410	91.8	15
1090-22-11	1.5	0.554	2270	41.2	1370	49.6	15
1090-22-12	1.5	0.528	1630	31.0	1030	49.1	15
				Average	1355	60.1	
1090-22-1	2.0	0.539	1760	32.8	815	47.7	20
1090-22-2	2.0	0.566	2480	44.0	1100	57.5	20
1090-22-3	2.0	0.526	1470	28.0	700	45.6	20
1090-22-4	2.0	0.538	2130	40.0	990	59.3	20
1090-22-5	2.0	0.538	2230	41.5	1040	52.3	20
1090-22-6	2.0	0.528	1900	36.1	900	55.6	20
				Average	809	53.0	

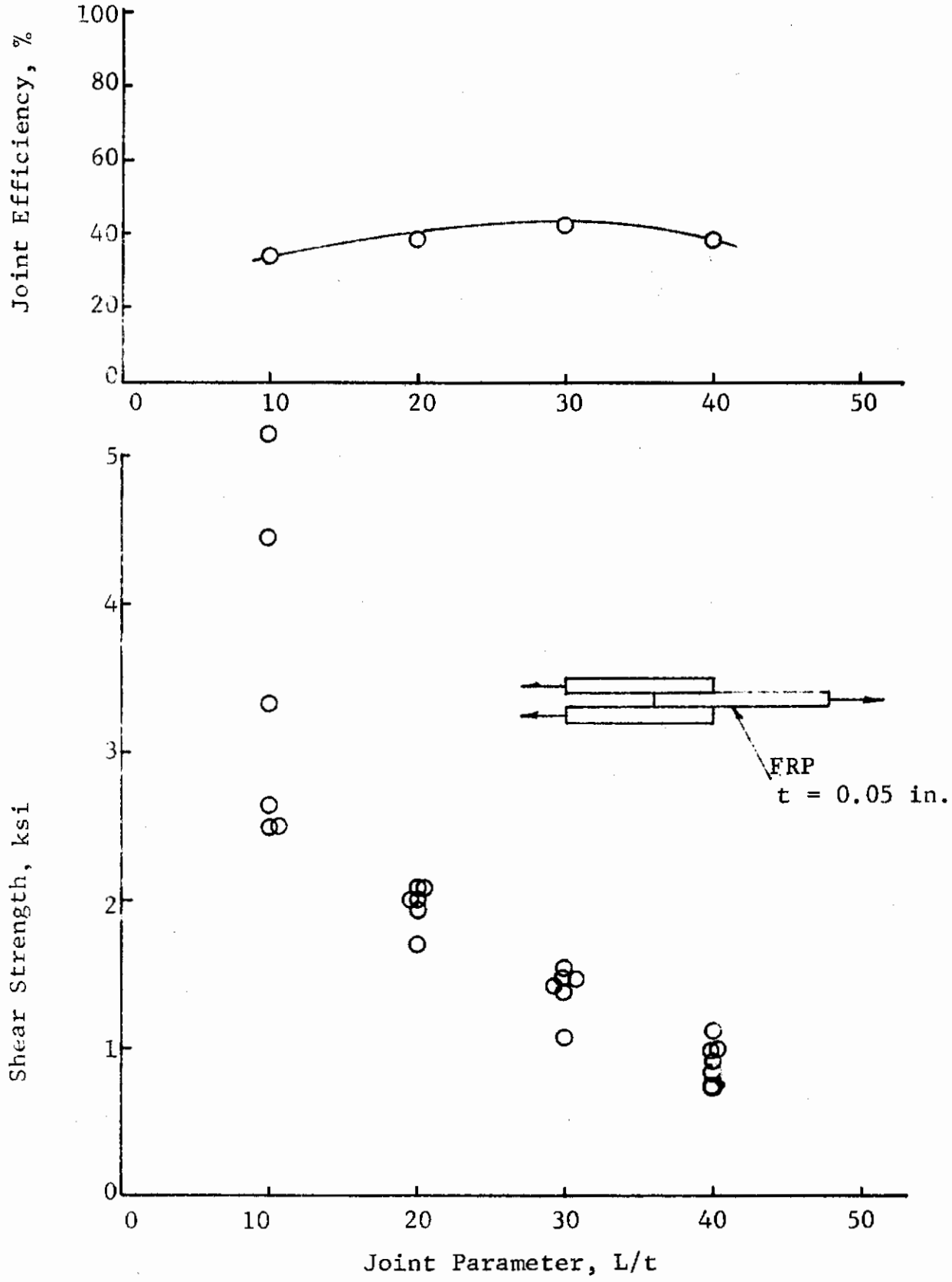

Fig. 4.34 SHEAR STRENGTH AND JOINT EFFICIENCY FOR SCOTCHPLY XP-251S BONDED WITH METLBOND 400, t = 0.05 in.

Table 4.23

SHEAR STRENGTH OF DOUBLE OVERLAP JOINTS OF SCOTCHPLY XP-251S
BONDED WITH METLBOND 0400 ADHEREND THICKNESS 0.10 IN.

Specimen Number	Length of Overlap (in.)	Width of Joint (in.)	Load at Failure (lb)	Adherend Stress (ksi)	Shear Strength (psi)	Joint Efficiency (%)	Joint Parameter (L/t)
1090-20-19	0.5	0.520	2100	40.4	4200		5
1090-20-20	0.5	0.531	2550	48.0	4800		5
1090-20-21	0.5	0.520	1950	37.5	3750		5
1090-20-22	0.5	0.506	2150	42.5	4250		5
1090-20-23	0.5	0.530	2010	38.0	3800		5
1090-20-24	0.5	0.545	2320	42.6	4260		5
				Average	4180		
1090-20-13	1.0	0.544	4150	76.0	3800		10
1090-20-14	1.0	0.541	4380	81.0	4050		
1090-20-15	1.0	0.550	3500	63.4	3180		10
1090-20-16	1.0	0.527	3090	58.5	2940		10
1090-20-17	1.0	0.517	4540	87.5	4400		10
1090-20-18	1.0	0.501	2750	54.5	2750		10
				Average	3520		
1090-20-7	1.5	0.527	3540	67.2	1680		15
1090-20-8	1.5	0.510	3320	65.0	1630		15
1090-20-9	1.5	0.517	2840	55.0	1370		15
1090-20-10	1.5	0.524	5300	101.0	2520		15
1090-20-11	1.5	0.565	3070	54.6	1360		15
1090-20-12	1.5	0.532	2870	54.0	1350		15
				Average	1650		
1090-20-1	2.0	0.536	2820	52.5	1340		20
1090-20-2	2.0	0.516	3260	63.2	1580		20
1090-20-3	2.0	0.537	2700	50.2	1260		20
1090-20-4	2.0	0.520	3400	65.2	1630		20
1090-20-5	2.0	0.521	3000	57.5	1440		20
1090-20-6	2.0	0.517	3180	61.2	1540		20
				Average	1470		

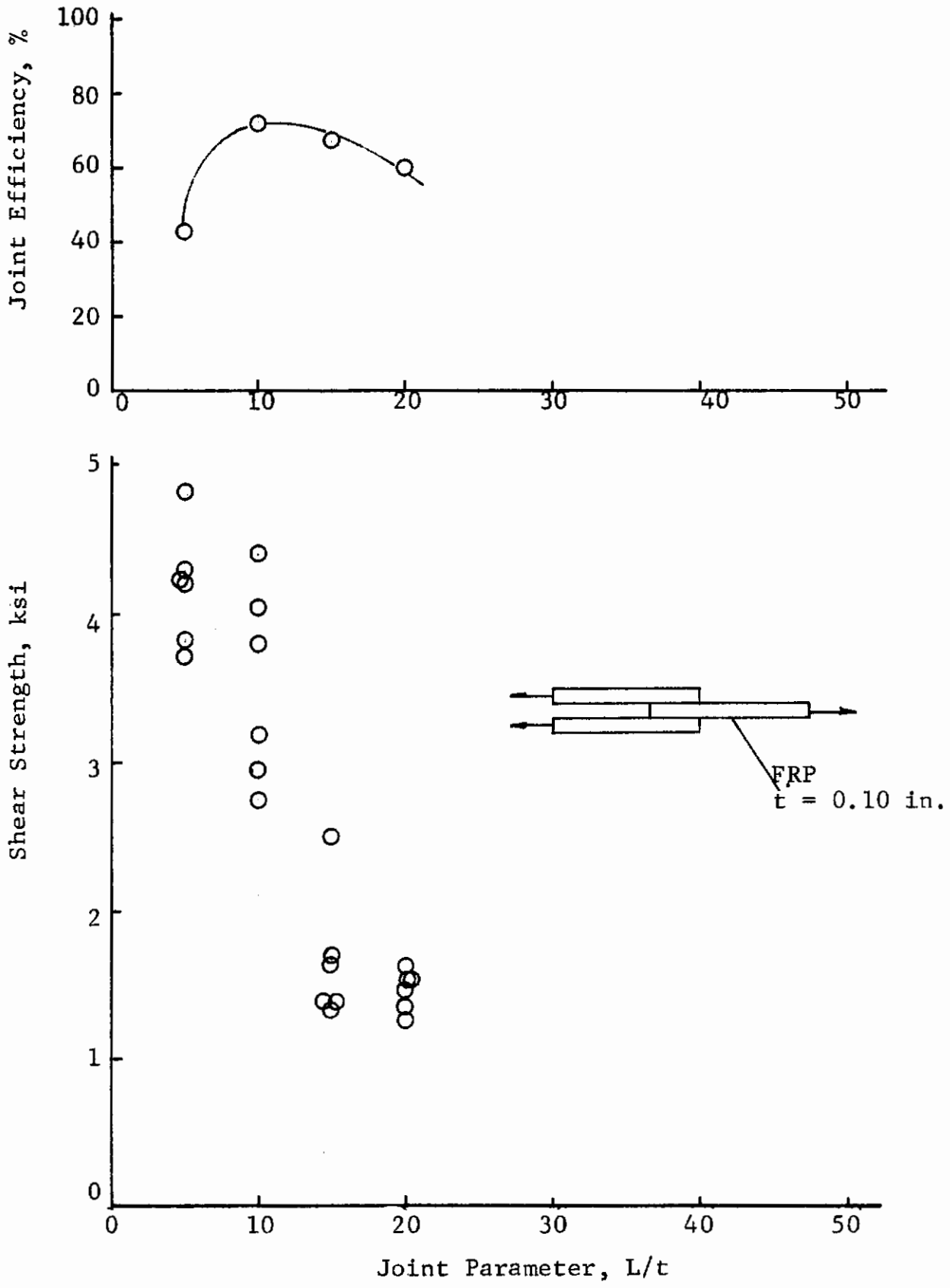

Fig. 4.35 SHEAR STRENGTH AND JOINT EFFICIENCY OF SCOTCHPLY XP-251S BONDED WITH METLBOND 400, t = 0.10 in.

Table 4.24

SHEAR STRENGTH OF DOUBLE OVERLAP JOINTS OF SCOTCHPLY XP-251S BONDED WITH METLBOND 400, ADHEREND THICKNESS 0.20 IN.

Specimen Number	Length of Overlap (in.)	Width of Joint (in.)	Load at Failure (lb)	Adherend Stress (ksi)	Shear Strength (psi)	Joint Efficiency (%)	Joint Parameter (L/t)
1090-26-1	1.0	0.481	4160	36.5	4320	33.2	5
1090-26-2	1.0	0.507	4600	38.3	4550	34.8	5
1090-26-3	1.0	0.494	3830	32.7	3880	29.8	5
1090-26-4	1.0	0.502	3590	30.4	3590	27.6	5
1090-26-5	1.0	0.528	4420	35.4	4210	32.2	5
1090-26-6	1.0	0.451	3690	33.6	4090	30.6	5
				Average	4100	31.3	
1090-26-7	1.5	0.463	3050	28.5	2190	25.9	7.5
1090-26-8	1.5	0.507	4050	34.6	3660	31.4	7.5
1090-26-9	1.5	0.505	5060	43.6	3330	39.6	7.5
1090-26-10	1.5	0.512	5180	45.4	3360	41.2	7.5
1090-26-11	1.5	0.513	6310	53.9	4100	49.0	7.5
1090-26-12	1.5	0.530	4290	35.8	2700	32.5	7.5
				Average	3060	36.6	
1090-26-13	2.0	0.465	5300	48.6	2850	44.1	10
1090-26-14	2.0	0.503	5600	47.4	2730	43.0	10
1090-26-15	2.0	0.513	7360	60.9	3590	55.4	10
1090-26-16	2.0	0.498	6160	52.7	3100	47.9	10
1090-26-17	2.0	0.490	6820	59.3	3480	53.8	10
1090-26-18	2.0	0.481	5660	50.1	2950	45.5	10
				Average	3100	48.3	

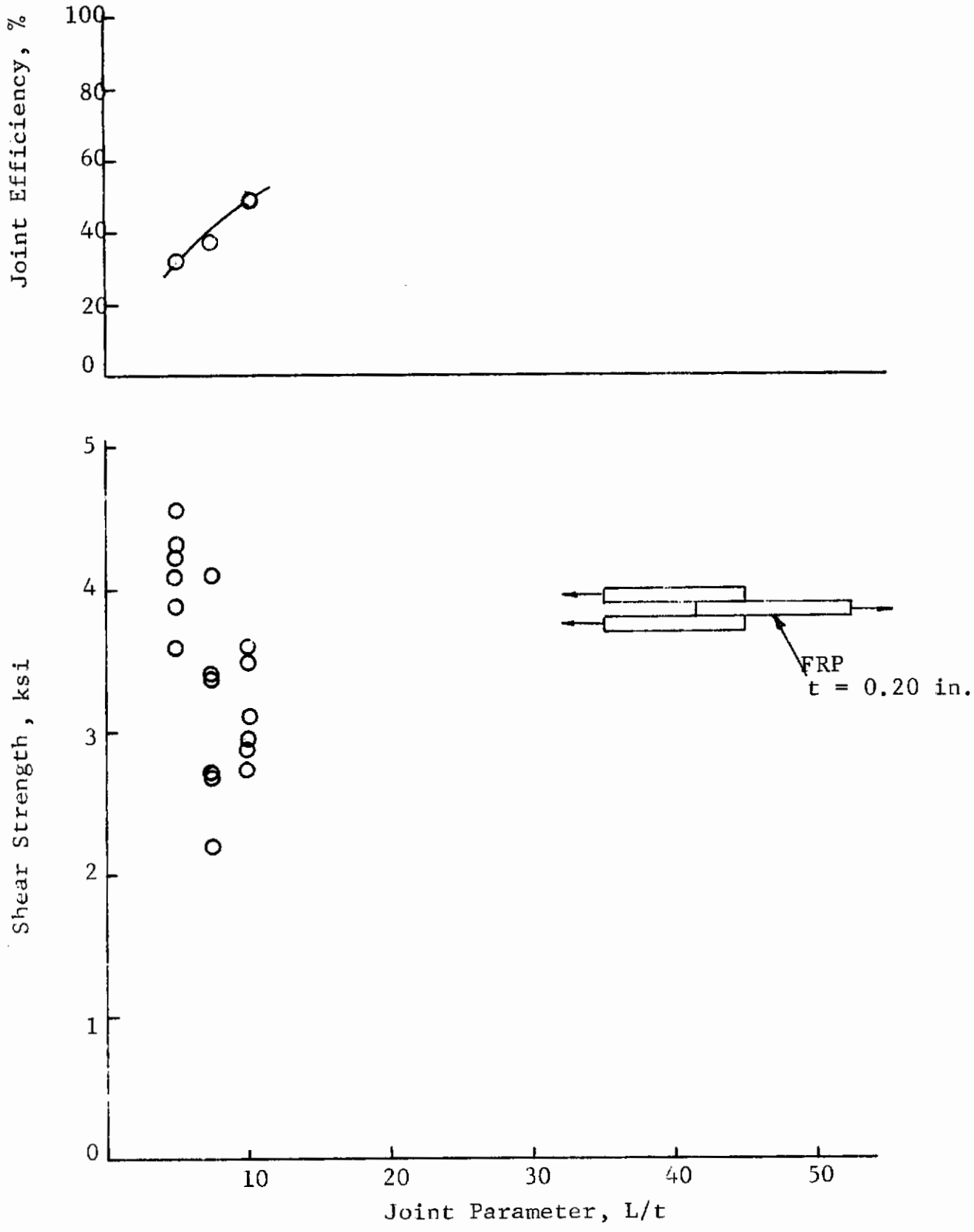

Fig. 4.36 SHEAR STRENGTH AND JOINT EFFICIENCY FOR SCOTCHPLY XP-251S BONDED WITH METLBOND 400, t = 0.20 in.

Table 4.25

SHEAR STRENGTH OF DOUBLE OVERLAP JOINTS OF SCOTCHPLY XP-251S BONDED WITH FM-47, TYPE 2 ADHEREND THICKNESS, 0.05 IN.

Specimen Number	Length of Overlap (in.)	Width of Joint (in.)	Load at Failure (lb)	Adherend Stress (ksi)	Shear Strength (psi)	Joint Efficiency (%)	Joint Parameter (L/t)
1080-35-1	0.5	0.509	870	30.0	1710	27.3	10
1080-35-2	0.5	0.514	980	33.6	1910	30.6	10
1080-35-3	0.5	0.513	920	31.5	1790	28.6	10
1080-35-4	0.5	0.514	940	32.6	1830	29.6	10
1080-35-5	0.5	0.512	940	32.2	1840	29.2	10
1080-35-6	0.5	0.513	920	31.6	1790	28.8	10
				Average	1810	29.0	
1081-35-7	1.0	0.516	1120	41.8	1090	38.0	20
1081-35-8	1.0	0.515	1140	42.5	1110	38.6	20
1081-35-9	1.0	0.514	1100	42.0	1070	38.2	20
1081-35-10	1.0	0.515	1210	46.2	1170	42.0	20
1081-35-11	1.0	0.516	980	36.6	950	33.3	20
1081-35-12	1.0	0.516	1190	44.4	1150	40.4	20
				Average	1090	38.4	
1081-35-13	1.5	0.515	1220	45.5	785	41.4	30
1081-35-14	1.5	0.514	1310	49.0	850	44.5	30
1081-35-15	1.5	0.514	1120	42.0	730	38.2	30
1081-35-16	1.5	0.512	1160	43.6	750	39.7	30
1081-35-17	1.5	0.514	1220	45.7	790	41.6	30
1081-35-18	1.5	0.514	1030	38.6	670	35.1	30
				Average	760	40.1	
1081-35-19	2.0	0.508	1200	47.2	590	42.9	40
1081-35-20	2.0	0.513	1320	52.6	640	47.9	40
1081-35-21	2.0	0.511	1340	52.3	660	47.5	40
1081-35-22	2.0	0.514	1340	53.1	650	48.3	40
1081-35-23	2.0	0.511	1360	54.1	670	49.2	40
1081-35-24	2.0	0.506	1460	57.6	720	52.5	40
				Average	660	48.0	

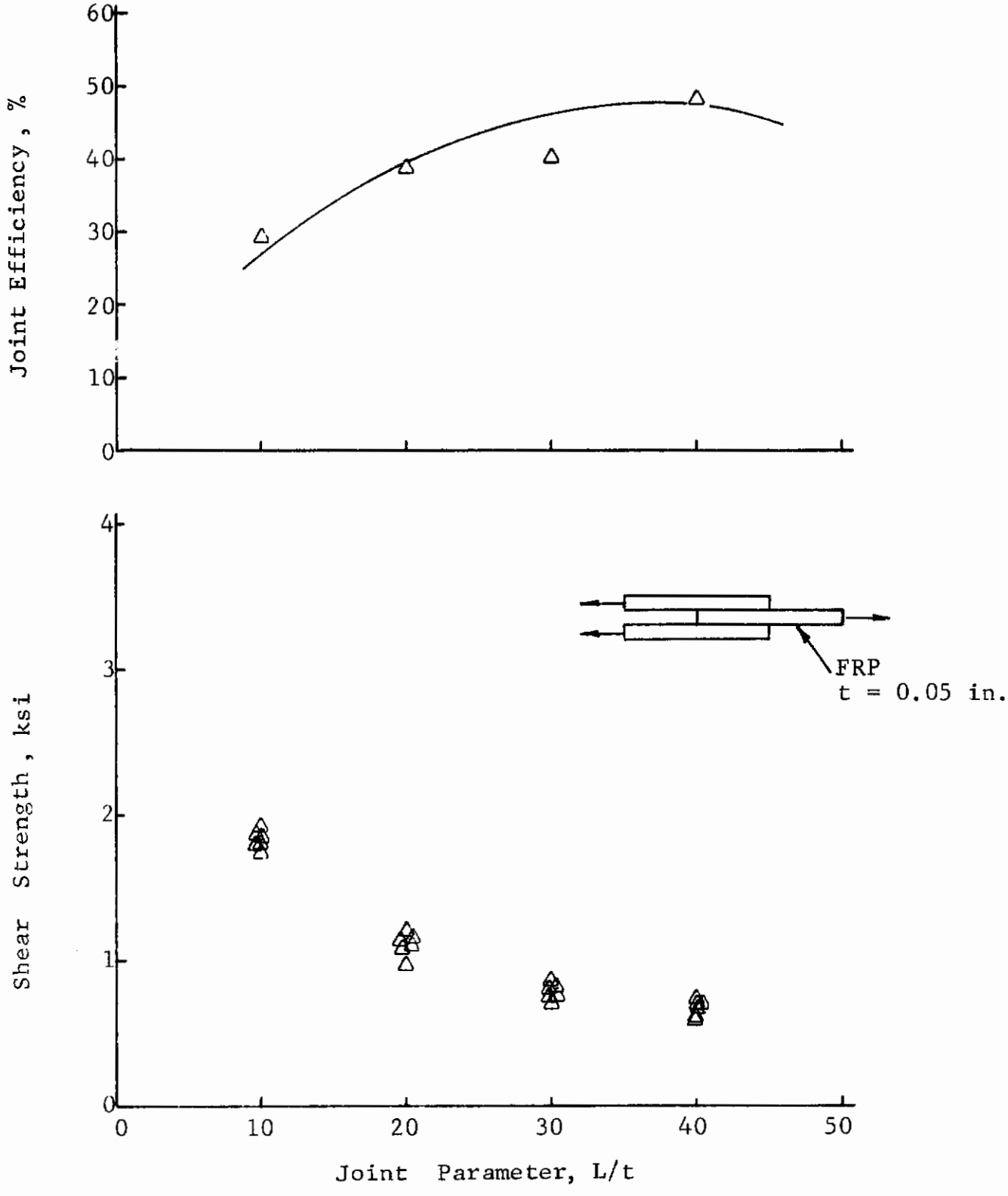

Fig. 4.37 SHEAR STRENGTH AND JOINT EFFICIENCY OF SCOTCHPLY XP-251S BONDED WITH FM-47, t = 0.05 in.

Table 4.26

SHEAR STRENGTH OF DOUBLE OVERLAP JOINTS OF SCOTCHPLY XP-251S
BONDED WITH FM-47 TYPE 2 ADHEREND THICKNESS 0.05 IN.

Specimen Number	Length of Overlap (in.)	Width of Joint (in.)	Load at Failure (lb)	Adherend Stress (ksi)	Shear Strength (psi)	Joint Efficiency (%)	Joint Parameter (L/t)
1081-70-1	2.0	0.558	1580	53.4	710	48.5	40
1081-70-2	2.0	0.551	2120	71.1	960	64.6	40
1081-70-3	2.0	0.562	1350	45.3	600	41.2	40
1081-70-4	2.0	0.546	1370	48.2	630	43.8	40
1081-70-5	2.0	0.553	1600	55.6	720	50.5	40
1081-70-6	2.0	0.363	1140	61.6	780	56.0	40
				Average	730	50.8	

This lot of FM-47 was received early in the program and film deterioration suspected. This is a repeat test. Results of the first test on fresh adhesive were:

Shear Strength (psi) 660
Joint Efficiency (%) 48.0

No apparent, deterioration of the film. Failures essentially cohesive within the adhesive layer.

Table 4.27

SHEAR STRENGTH OF DOUBLE OVERLAP JOINTS OF SCOTCHPLY XP-251S BONDED WITH FM-47, TYPE 2 ADHEREND THICKNESS, 0.10 IN.

Specimen Number	Length of Overlap (in.)	Width of Joint (in.)	Load at Failure (lb)	Adherend Stress (ksi)	Shear Strength (psi)	Joint Efficiency (%)	Joint Parameter (L/t)
1081-25-3	1.0	0.496	1500	26.8	1510	24.4	10
1081-25-4	1.0	0.496	1580	28.9	1590	26.3	10
1081-25-5	1.0	0.496	1270	23.1	1280	21.0	10
1081-25-6	1.0	0.496	1590	28.4	1600	25.8	10
				Average	1500	24.4	
1081-25-7	1.5	0.555	1190	18.5	717*	16.8*	15
1081-25-8	1.5	0.557	2260	35.0	1350	31.8	15
1081-25-9	1.5	0.561	1780	27.3	1070	24.8	15
1081-25-10	1.5	0.558	1970	30.4	1180	27.6	15
1081-25-11	1.5	0.561	2120	32.6	1260	29.6	15
				Average	1220	28.4	
1081-25-12	2.0	0.537	2160	35.9	1000	32.6	20
1081-25-13	2.0	0.556	2730	43.8	1230	39.8	20
1081-25-14	2.0	0.558	2610	41.8	1170	38.0	20
1081-25-15	2.0	0.558	2700	43.2	1210	39.3	20
1081-25-16	2.0	0.558	2660	42.6	1190	38.8	20
				Average	1160	37.7	

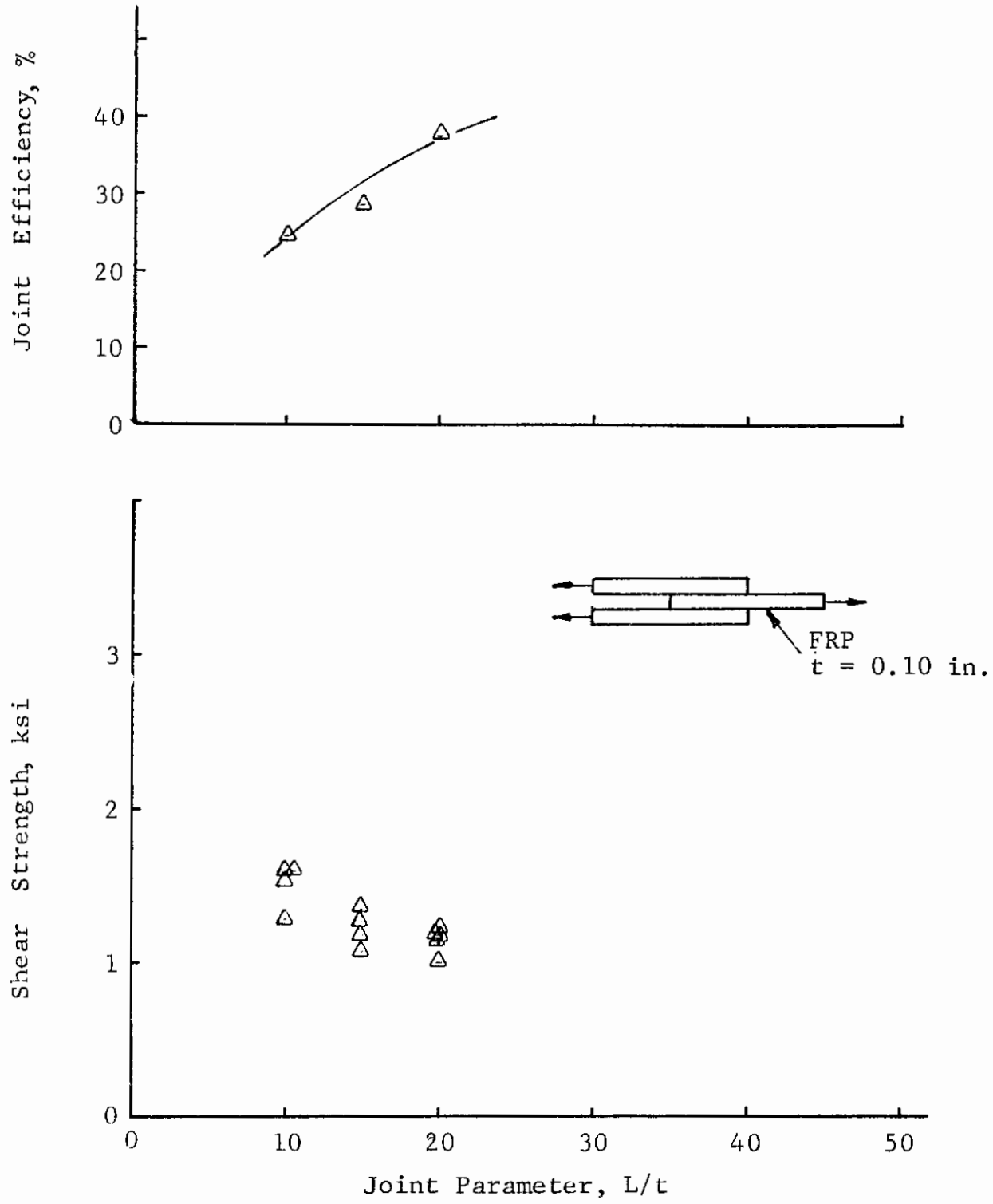

Fig. 4.38 SHEAR STRENGTH AND JOINT EFFICIENCY OF SCOTCHPLY XP-251S BONDED WITH FM-47, t = 0.10 in.

4.5.2 Strength of FRP-FRP Bonded Scarf Joints

This section contains the static strength results for the double-overlap scarfed joints bonded with FM-1000 and FM-47 adhesives. For each length of overlap (L) the outer two adherends are scarfed uniformly from the full thickness (t) to zero thickness at the end of the overlap.

Each table of data is followed by a graph of joint strength and joint efficiency as a function of the joint parameter (L/t).

Table 4.28

SHEAR STRENGTH OF SCARFED DOUBLE OVERLAP JOINTS OF SCOTCHPLY XP-251S BONDED WITH FM-1000, ADHEREND THICKNESS 0.05 IN.

Specimen Number	Length of Overlap (in.)	Width of Joint (in.)	Load at Failure (lb)	Adherend Stress (ksi)	Shear Strength (psi)	Joint Efficiency (%)	Joint Parameter (L/t)
1080-56-1	0.5	0.483	1920	73.6	3980	66.9	10
1080-56-2	0.5	0.481	1680	67.2	3490	61.1	10
1080-56-3	0.5	0.485	1820	70.3	3750	63.9	10
1080-56-4	0.5	0.485	1940	77.0	4000	70.0	10
1080-56-5	0.5	0.485	1840	71.0	3790	63.7	10
1080-56-6	0.5	0.485	1860	73.8	3840	67.1	10
				Avg.	3810	65.4	
1080-56-7	1.0	0.487	2300	92.7	2360	84.3	20
1080-56-8	1.0	0.484	2080	84.2	2150	76.5	20
1080-56-9	1.0	0.488	2190	86.2	2240	78.4	20
1080-56-10	1.0	0.488	2220	89.2	2270	81.1[a]	20
1080-56-11	1.0	0.488	2100	84.3	2150	76.7	20
1080-56-12	1.0	0.490	1950	79.6	1990	72.4	20
				Avg.	2190	78.2	
1080-56-13	1.5	0.488	2310	94.7	1580	86.1[a]	30
1080-56-14	1.5	0.485	2230	92.1	1550	83.7[a]	30
1080-56-15	1.5	0.486	2610	107.4	1790	97.6	30
1080-56-16	1.5	0.487	2470	101.2	1690	92.0[a]	30
1080-56-17	1.5	0.487	2840	116.4	1940	105.8[a]	30
1080-56-18	1.5	0.486	2470	101.6	1690	92.4	30
				Avg.	1710	92.9	
1080-56-19	2.0	0.489	2460	96.8	1260	88.0[a]	40
1080-56-20	2.0	0.488	2520	99.2	1290	90.2	40
1080-56-21	2.0	0.488	2610	102.8	1340	93.4[a]	40
1080-56-22	2.0	0.488	2710	104.6	1390	95.1[a]	40
1080-56-23	2.0	0.489	2620	103.1	1340	93.7	40
1080-56-24	2.0	0.488	2630	101.9	1350	92.6[a]	40
				Avg.	1330	92.2	

a. Composite failure near the grip area.

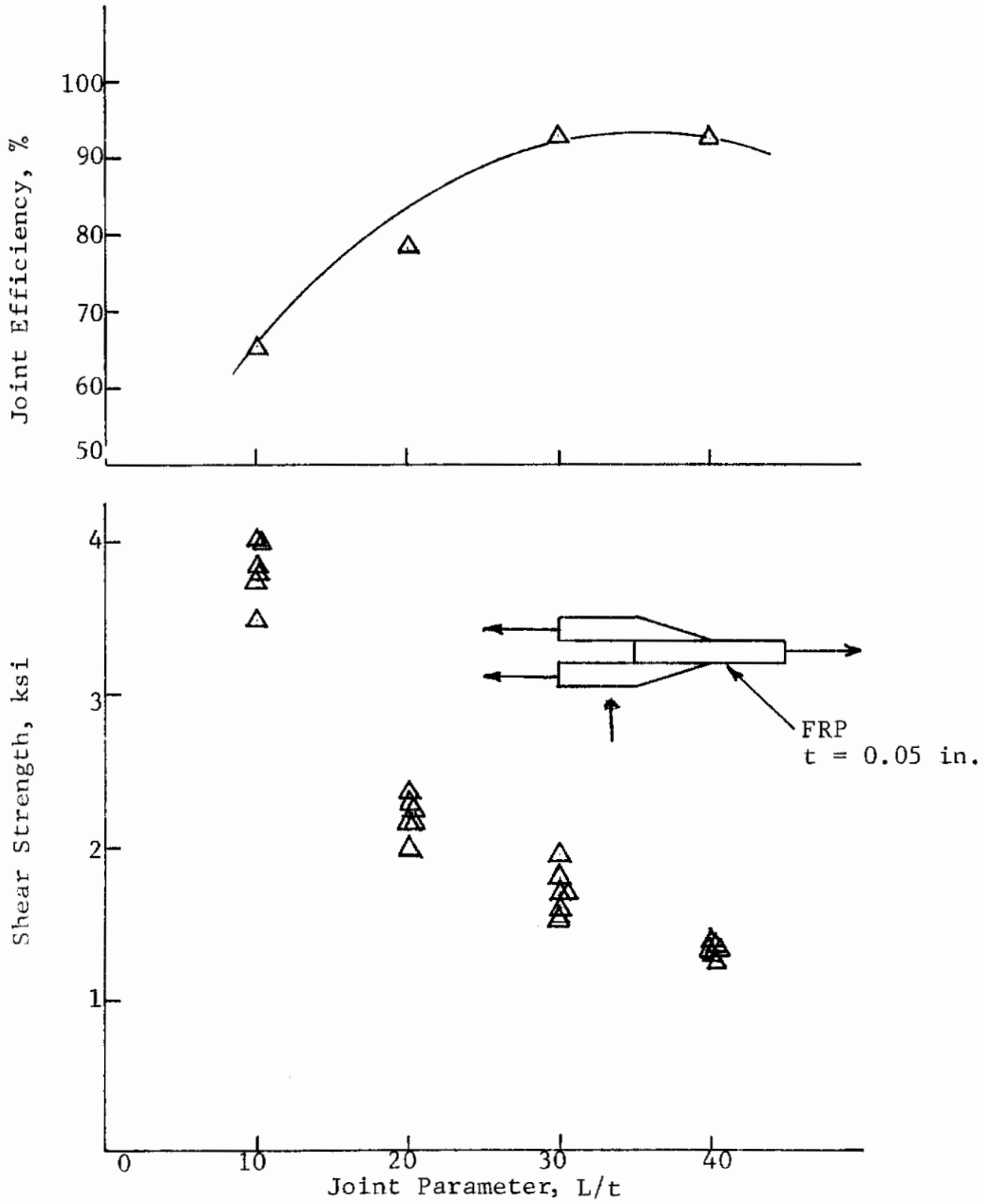

Fig. 4.39 SHEAR STRENGTH AND JOINT EFFICIENCY OF SCOTCHPLY XP-251S BONDED WITH FM-1000, t = 0.05 in. SCARFED JOINT

Table 4.29

SHEAR STRENGTH OF SCARFED DOUBLE OVERLAP JOINTS OF SCOTCHPLY XP-251S BONDED WITH FM-1000, ADHEREND THICKNESS 0.10 IN.

Specimen Number	Length of Overlap (in.)	Width of Joint (in.)	Load at Failure (lb)	Adherend Stress (ksi)	Shear Strength (psi)	Joint Efficiency (%)	Joint Parameter (L/t)
1080-55-1	0.5	0.493	3460	63.8	7020	58.0	5
1080-55-2	0.5	0.484	2880	54.5	5950	49.5	5
1080-55-3	0.5	0.489	2700	50.2	5520	45.6	5
1080-55-4	0.5	0.486	2960	55.3	6090	50.3	5
1080-55-5	0.5	0.482	2480	46.4	5140	42.2	5
1080-55-6	0.5	0.490	2470	45.8	5040	41.6	5
				Avg.	5790	47.9	
1080-55-7	1.0	0.489	4070	75.6	4160	68.7	10
1080-55-8	1.0	0.487	3240	61.0	3330	55.4	10
1080-55-9	1.0	0.489	4340	80.7	4440	73.4	10
1080-55-10	1.0	0.487	3580	68.1	3680	61.9	10
1080-55-11	1.0	0.487	3830	72.1	3930	65.6	10
1080-55-12	1.0	0.485	3420	65.3	3520	59.4	10
				Avg.	3840	64.0	
1080-55-13	1.5	0.487	4250	78.0	2910	70.9	15
1080-55-14	1.5	0.489	4450	82.0	3030	74.5	15
1080-55-15	1.5	0.486	4190	77.7	2870	70.6	15
1080-55-16	1.5	0.488	4300	80.1	2940	72.8	15
1080-55-17	1.5	0.487	4070	76.0	2790	69.1	15
1080-55-18	1.5	0.488	3520	65.5	2410	59.5	15
				Avg.	2820	69.6	
1080-54-1	2.0	0.490	3430	72.2	2000	65.6	20
1080-54-2	2.0	0.489	3870	71.3	1970	64.8	20
1080-54-3	2.0	0.490	3810	70.7	1940	64.3	20
1080-54-4	2.0	0.491	4200	77.8	2140	70.7	20
1080-54-5	2.0	0.488	4450	81.5	2280	74.1	20
1080-54-6	2.0	0.491	3770	69.2	1920	62.9	20
				Avg.	2040	67.1	

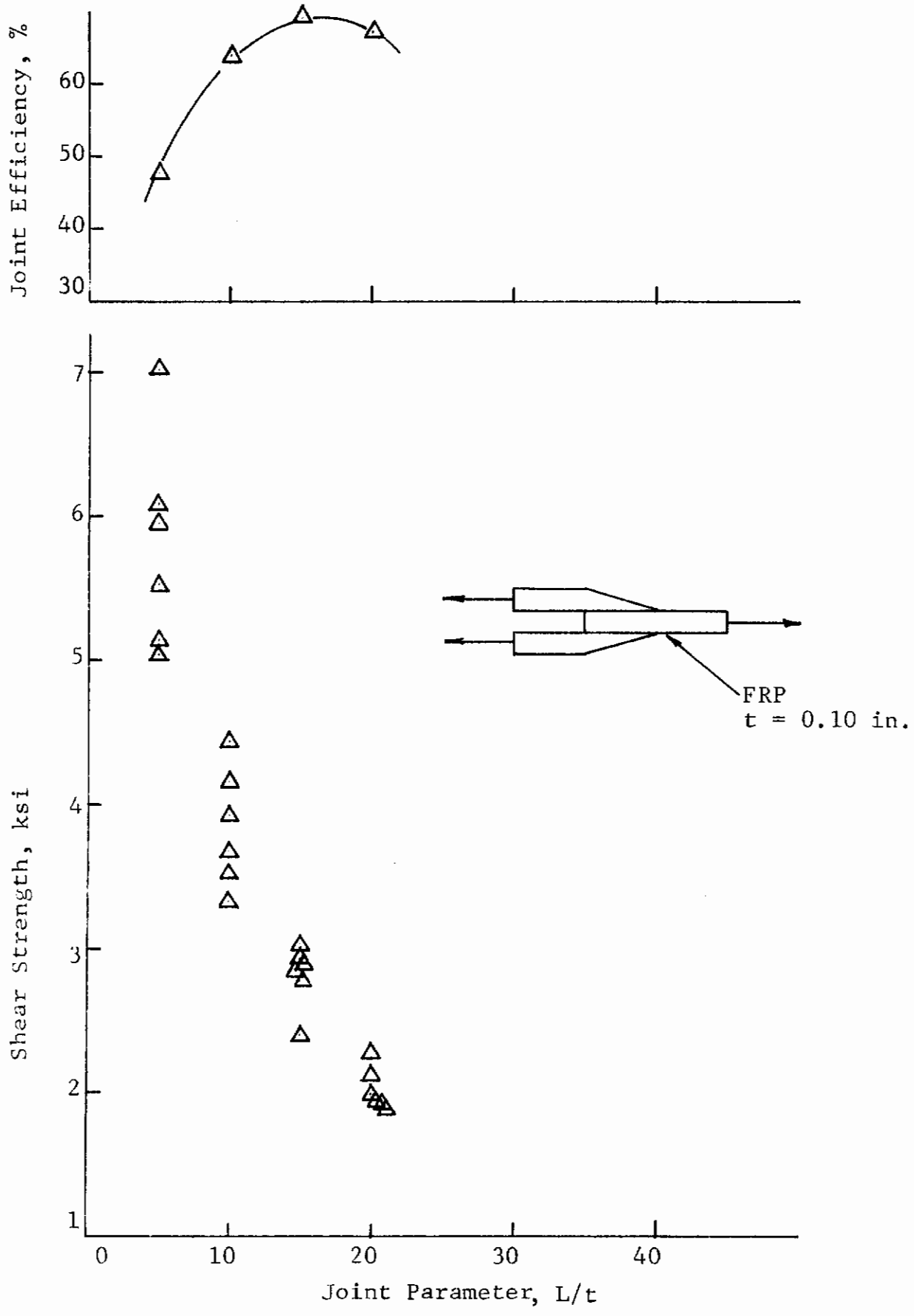

Fig. 4.40 SHEAR STRENGTH AND JOINT EFFICIENCY OF SCOTCHPLY XP-251S BONDED WITH FM-1000, t = 0.10 in. SCARFED JOINT

Table 4.30

SHEAR STRENGTH OF SCARFED DOUBLE OVERLAP JOINTS OF SCOTCHPLY XP-251S BONDED WITH FM-1000, ADHEREND THICKNESS 0.20 IN.

Specimen Number	Length of Overlap (in.)	Width of Joint (in.)	Load at Failure (lb)	Adherend Stress (ksi)	Shear Strength (psi)	Joint Efficiency (%)	Joint Parameter (L/t)
1080-57-1	1.0	0.487	5320	54.6	5460	49.6	5
1080-57-2	1.0	0.469	4370	47.3	4660	43.0	5
1080-57-3	1.0	0.486	4460	46.1	4590	41.9	5
1080-57-4	1.0	0.487	4070	42.2	4180	38.4	5
1080-57-5	1.0	0.486	4610	48.2	4740	43.8	5
1080-57-6	1.0	0.487	4050	41.8	4160	38.0	5
				Avg.	4630	42.5	
1080-57-7	2.0	0.483	5480	57.2	2840	52.1	10
1080-57-8	2.0	0.481	5640	58.9	2940	53.6	10
1080-57-9	2.0	0.483	5820	60.7	3020	55.2	10
1080-57-10	2.0	0.471	5970	63.9	3180	58.1	10
1080-57-11	2.0	0.486	5370	56.4	2770	51.3	10
1080-57-12	2.0	0.490	5780	60.2	3000	54.7	10
				Avg.	2960	54.2	

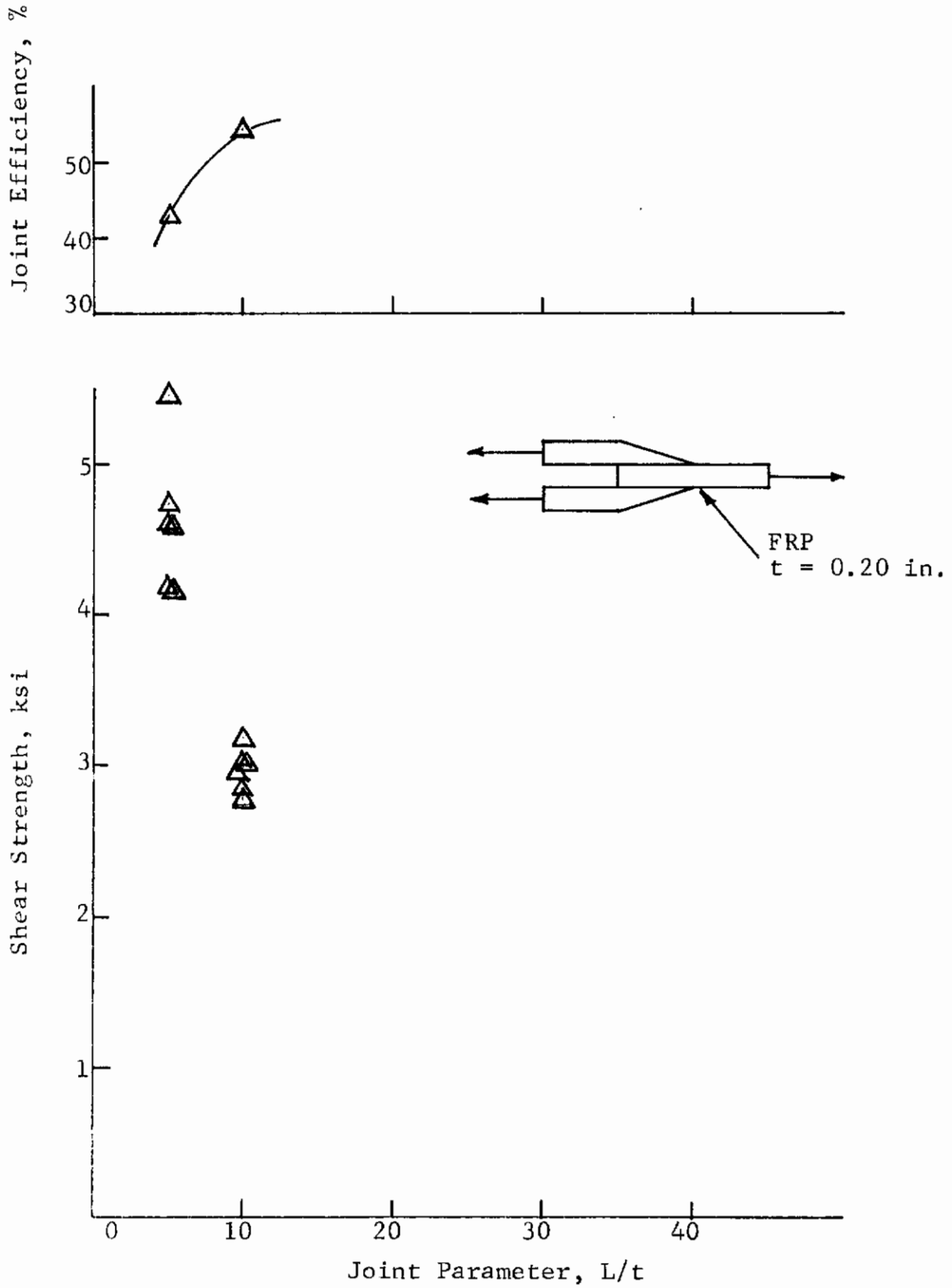

Fig. 4.41 SHEAR STRENGTH AND JOINT EFFICIENCY OF SCOTCHPLY XP-251S BONDED WITH FM-1000, t = 0.20 in. SCARFED JOINT

Table 4.31

SHEAR STRENGTH OF SCARFED DOUBLE OVERLAP JOINTS OF SCOTCHPLY XP 251S BONDED WITH FM-47, TYPE 2, ADHEREND THICKNESS 0.05 IN.

Specimen Number	Length of Overlap (in.)	Width of Joint (in.)	Load at Failure (lb)	Adherend Stress (ksi)	Shear Strength (psi)	Joint Efficiency (%)	Joint Parameter (L/t)
1081-59-1	1.0	0.500	1170	44.2	1170	40.3	20
1081-59-2	1.0	0.499	1600	63.0	1600	57.3	20
1081-59-3	1.0	0.498	1270	50.0	1280	45.4	20
1081-59-4	1.0	0.499	1000	37.9	1000	34.4	20
1081-59-5	1.0	0.501	1280	47.4	1280	43.1	20
1081-59-6	1.0	0.487	1230	50.0	1260	45.5	20
				Avg.	1260	44.3	
1081-59-7	2.0	0.498	1170	44.4	587	40.3	40
1081-59-8	2.0	0.499	1770	65.8	887	59.8	40
1081-59-9	2.0	0.500	1510	57.0	755	51.8	40
1081-59-10	2.0	0.483	1540	61.3	797	55.8	40
1081-59-11	2.0	0.497	1820	69.2	915	62.9	40
1081-59-12	2.0	0.498	1070	40.5	537	36.8	40
				Avg.	750	51.2	

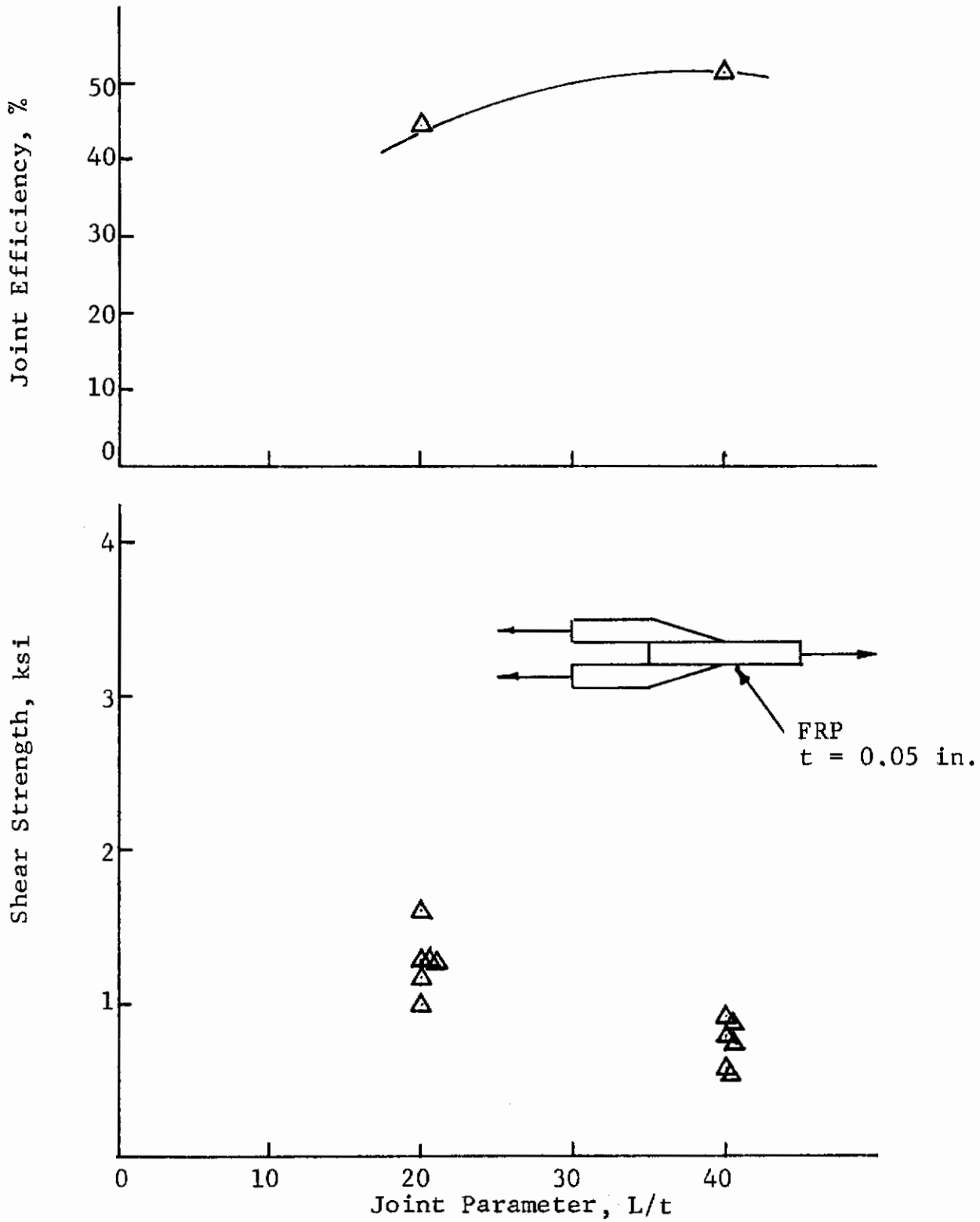

Fig. 4.42 SHEAR STRENGTH AND JOINT EFFICIENCY OF SCOTCHPLY XP-251S BONDED WITH FM-47, TYPE 2, t = 0.05 in. SCARFED JOINT

Table 4.32

SHEAR STRENGTH OF SCARFED DOUBLE OVERLAP JOINTS OF SCOTCHPLY XP-251S BONDED WITH FM-47, TYPE 2, ADHEREND THICKNESS 0.1 IN.

Specimen Number	Length of Overlap (in.)	Width of Joint (in.)	Load at Failure (lb)	Adherend Stress (ksi)	Shear Strength (psi)	Joint Efficiency (%)	Joint Parameter (L/t)
1081-58-1	1.0	0.490	900	15.8	918	14.4	10
1081-58-2	1.0	0.490	1370	24.3	1400	22.1	10
1081-58-3	1.0	0.493	1170	20.2	1190	18.4	10
1081-58-4	1.0	0.488	720	12.8	738	11.6	10
1081-58-5	1.0	0.490	1420	25.2	1450	22.9	10
1081-58-6	1.0	0.494	580	10.1	587	9.2	10
				Avg.	1050	16.4	
1081-58-7	2.0	0.493	1580	28.9	802	26.3	20
1081-58-8	2.0	0.494	2200	39.8	1110	36.2	20
1081-58-9	2.0	0.490	2070	37.4	1060	34.0	20
1081-58-10	2.0	0.490	1720	30.8	869	28.0	20
1081-58-11	2.0	0.492	1850	33.3	939	30.3	20
1081-58-12	2.0	0.489	1890	34.2	964	31.1	20
				Avg.	960	31.0	

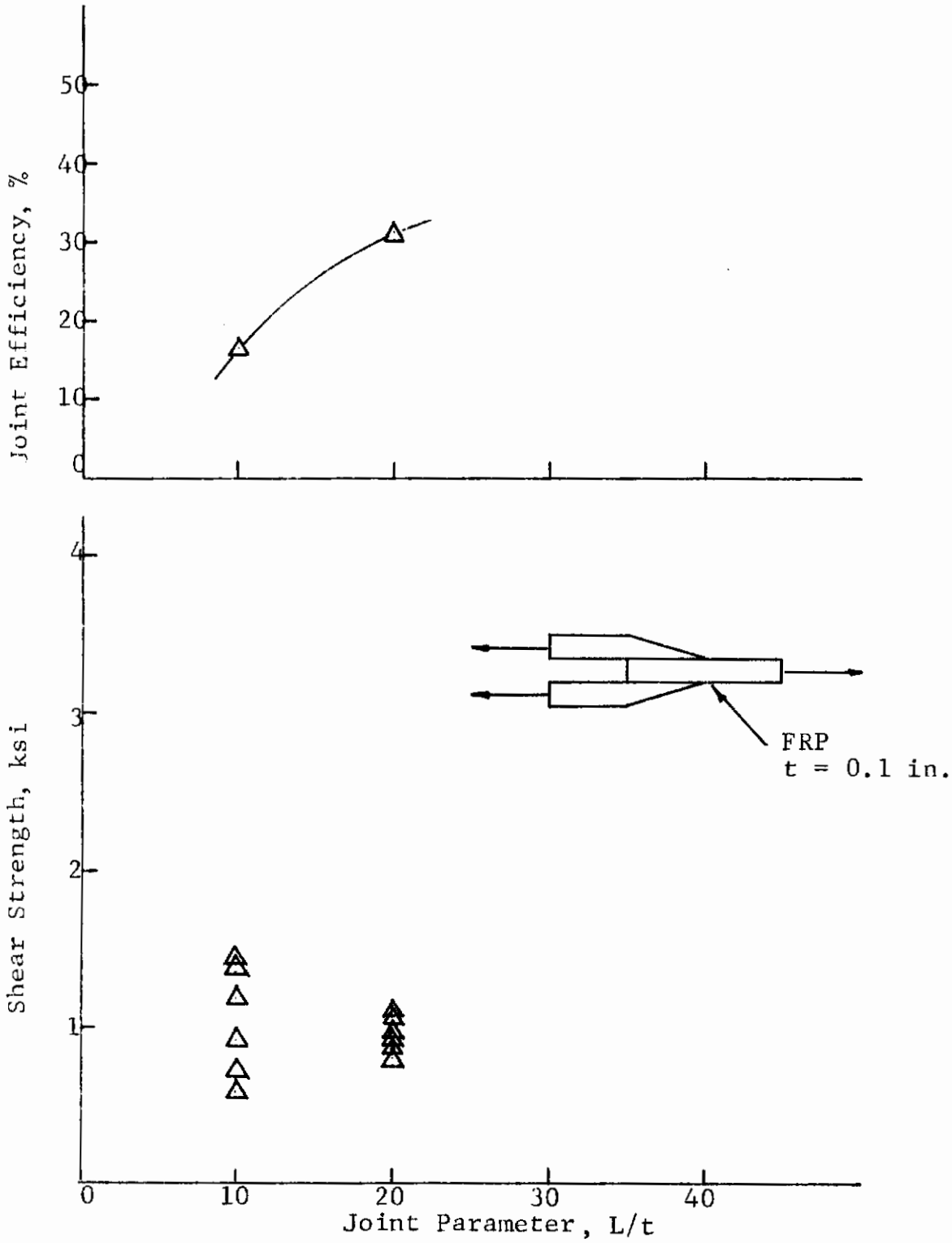

Fig. 4.43 SHEAR STRENGTH AND JOINT EFFICIENCY OF SCOTCHPLY XP-251S BONDED WITH FM-47, TYPE 2, t = 0.10 in, SCARFED JOINT

4.5.3 Strength of FRP to Metal Bonded Joints

This section contains the static strength results for the double overlap Scotchply to steel and Scotchply to titanium joints bonded with FM-1000 and Fm-47 adhesives.

Each table of data is followed by a graph of joint strength and joint efficiency as a function of the joint parameter (L/t).

Table 4.33

SHEAR STRENGTH OF DOUBLE OVERLAP JOINTS OF SCOTCHPLY XP-251S BONDED WITH FM-1000, ADHEREND THICKNESS, 0.10/0.05/0.10 IN. STEEL-FRP-STEEL

Specimen Number	Length of Overlap (in.)	Width of Joint (in.)	Load at Failure (lb)	Adherend Stress (ksi)	Shear Strength (psi)	Joint Efficiency (%)	Joint Parameter (L/t)
1080-66-1	1.0	0.521	1910	66.6	1830	60.5	20
1080-66-2	1.0	0.527	1730	59.7	1641	54.3	20
1080-66-3	1.0	0.534	1970	67.0	1840	60.9	20
1080-66-4	1.0	0.531	1880	64.4	1770	58.5	20
1080-66-5	1.0	0.510	1750	62.5	1720	56.8	20
1080-66-6	1.0	0.530	1750	60.0	1650	54.5	20
				Average	1740	57.6	
1080-66-7	1.5	0.527	1950	72.5	1230	65.9	30
1080-66-8	1.5	0.522	1770	66.5	1130	60.5	30
1080-66-9	1.5	0.525	2030	75.7	1290	68.8	30
1080-66-10	1.5	0.499	1820	71.7	1210	65.2	30
1080-66-11	1.5	0.538	2010	73.4	1250	66.7	30
1080-66-12	1.5	0.550	2110	75.4	1280	68.5	30
				Average	1230	65.9	
1080-66-13	2.0	0.521	2710	100.0	1300	90.0	40
1080-66-14	2.0	0.511	1990	74.8	970	68.0	40
1080-66-15	2.0	0.527	1990	72.7	940	66.1	40
1080-66-16	2.0	0.505	1960	74.6	970	67.8	40
1080-66-17	2.0	0.532	2550	92.2	1200	83.8	40
1080-66-18	2.0	0.533	2420	87.3	1140	79.4	40
				Average	1090	76.0	

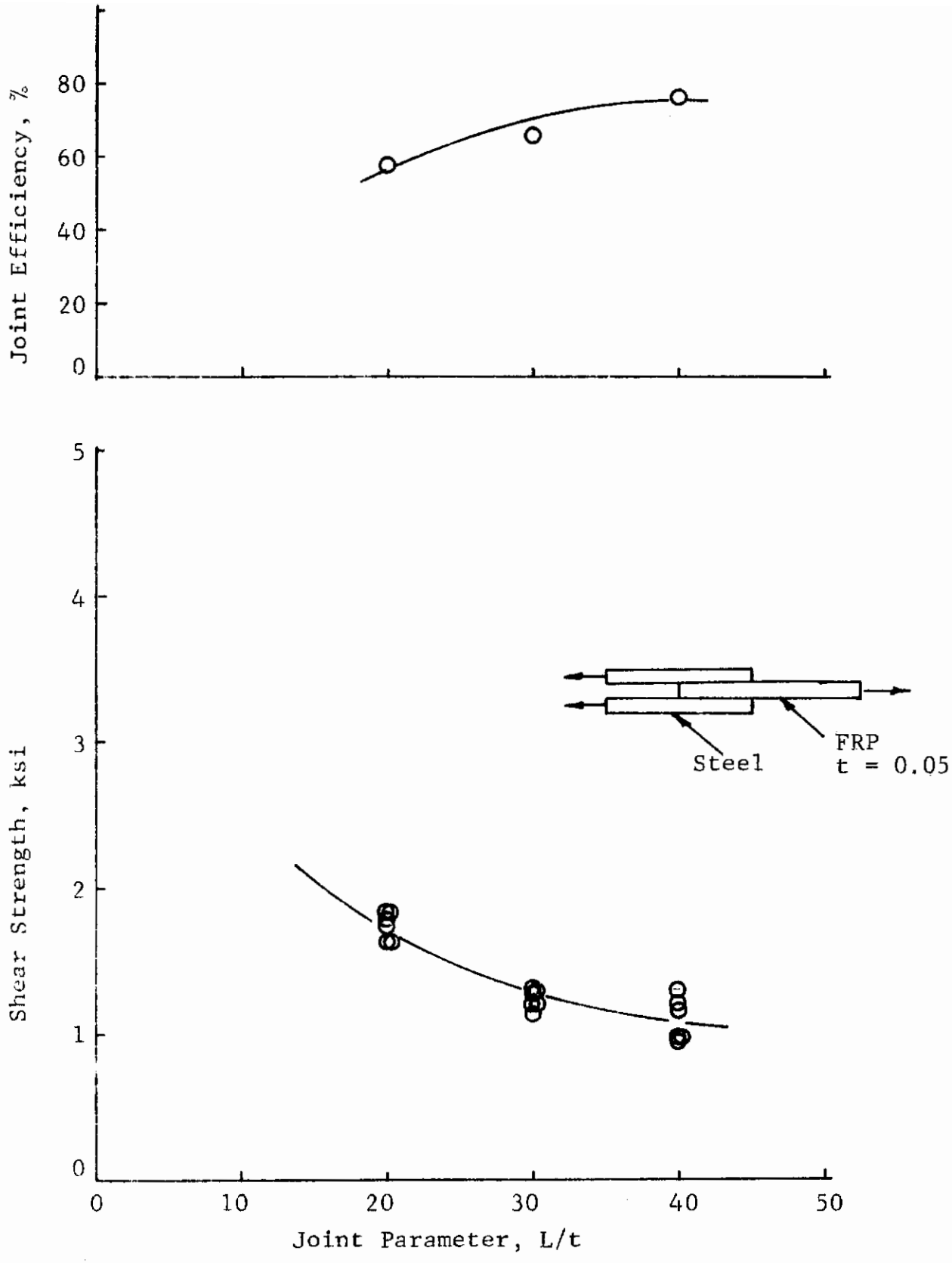

Fig. 4.44 SHEAR STRENGTH AND JOINT EFFICIENCY OF STEEL BONDED TO SCOTCHPLY XP-251S WITH FM-1000, t = 0.10/0.05/0.10 IN.

Table 4.34

SHEAR STRENGTH OF DOUBLE OVERLAP JOINTS OF SCOTCHPLY XP-251S AND STEEL BONDED WITH FM-1000, ADHEREND THICKNESS 0.10/0.10/0.10 IN. STEEL-FRP-STEEL

Specimen Number	Length of Overlap (in.)	Width of Joint (in.)	Load at Failure (lb)	Adherend* Stress (ksi)	Shear Strength (psi)	Joint Efficiency (%)	Joint Parameter (L/t)
1080-67-1	1.0	0.514	2220	41.5	2160	37.7	10
1080-67-2	1.0	0.545	2540	44.8	2330	40.7	10
1080-67-3	1.0	0.520	2000	37.0	1920	33.6	10
1080-67-4	1.0	0.530	2170	39.4	2050	35.8	10
1080-67-5	1.0	0.513	2350	44.0	2290	40.0	10
1080-67-6	1.0	0.497	2430	47.0	2440	42.7	10
				Average	2200	38.4	
1080-65-1	2.0	0.514	3560	59.2	1730	53.8	20
1080-65-2	2.0	0.535	2980	47.6	1390	43.3	20
1080-65-3	2.0	0.513	3470	58.3	1690	53.0	20
1080-65-4	2.0	0.525	3020	49.2	1440	44.7	20
1080-65-5	2.0	0.525	3400	55.4	1620	50.4	20
1080-65-6	2.0	0.522	2800	46.2	1340	42.0	20
				Average	1530	48.0	

* Stress in scotchply member

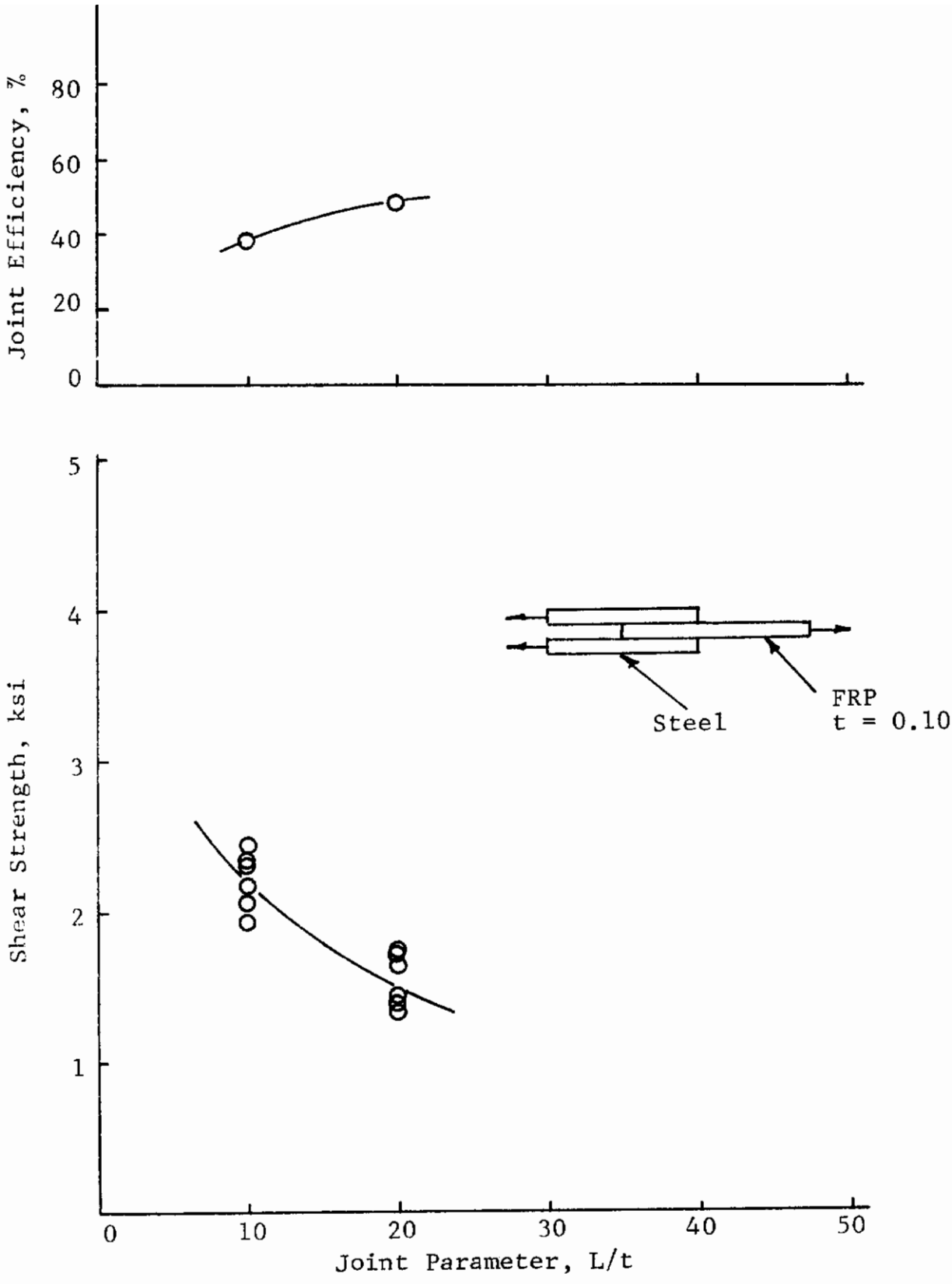

Fig. 4.45 SHEAR STRENGTH AND JOINT EFFICIENCY OF STEEL BONDED TO SCOTCHPLY XP-251S WITH FM-1000, t = 0.10/0.10/0.10 IN.

Table 4.35

SHEAR STRENGTH OF DOUBLE OVERLAP JOINTS OF SCOTCHPLY XP-251S BONDED TO STEEL[a] WITH FM 1000, ADHEREND THICKNESS 0.10/0.10/0.10 IN. FRP-STEEL-FRP

Specimen Number	Length of Overlap (in.)	Width of Joint (in.)	Load at Failure (lb)	Adherend Stress (ksi)	Shear Strength (psi)	Joint Efficiency (%)	Joint Parameter (L/t)
1080-64-1	1.25	0.516	2530	45.0	1960[b]	150	12.5
1080-64-2	1.25	0.515	2560	45.6	1990[b]	152	12.5
1080-64-3	1.25	0.535	2575	44.2	1920[c]	147	12.5
1080-64-4	1.25	0.518	2650	46.9	2050[b]	156	12.5
1080-64-5	1.25	0.520	2700	47.6	2080[c]	159	12.5
1080-64-6	1.25	0.526	2780	48.5	2110[c]	162	12.5
				Average	2020	100[d]	

a. Single steel adherend 0.109 inch thick between double Scotchply 0.10 inch thick adherends.

b. Failure was 100% cohesive in scotchply adherend.

c. Joint did not fail; steel adherend yielded excessively as evidenced by necking. Shear strength of 2020 psi reported as a minimum value.

d. Joint efficiency was arbitrarily set at 100% since the yield point graphed on the Instron recorder indicated from 20 to 22 ksi and the efficiency was set at 30 ksi σ_y for steel adherend.

Table 4.36

SHEAR STRENGTH OF DOUBLE OVERLAP JOINTS OF SCOTCHPLY XP-251S BONDED TO STEEL WITH FM-1000, ADHEREND THICKNESS 0.10/0.20/0.10 IN. STEEL-FRP-STEEL

Specimen Number	Length of Overlap (in.)	Width of Joint (in.)	Load at Failure (lb)	Adherend Stress (ksi)	Shear Strength (psi)	Joint Efficiency (%)	Joint Parameter (L/t)
1080-68-1	1.0	0.497	3400	36.6	3420	33.3	5.0
1080-68-2	1.0	0.499	2990	31.9	3000	29.0	5.0
1080-68-3	1.0	0.503	3780	40.2	3760	36.5	5.0
1080-68-4	1.0	0.494	3870	41.9	3920	38.1	5.0
1080-68-5	1.0	0.504	4240	45.1	4210	41.0	5.0
1080-68-6	1.0	0.504	4250	45.1	4220	41.0	5.0
				Average	3760	36.5	
1080-68-7	1.5	0.491	4470	49.1	3040	44.6	7.5
1080-68-8	1.5	0.530	Adherend (steel) failure				7.5
1080-68-9	1.5	0.496	3850	42.1	2590	38.3	7.5
1080-68-10	1.5	0.512	5260	54.5	3420	49.5	7.5
1080-68-11	1.5	0.488	5280	57.6	3610	52.4	7.5
1080-68-12	1.5	0.483	4090	46.1	2820	41.9	7.5
				Average	3100	45.3	
1080-68-13	2.0	0.493	2560	27.6	1300*	25.1*	10.0
1080-68-14	2.0	0.506	4200	43.5	2080	39.5	10.0
1080-68-15	2.0	0.479	4750	52.5	2480	47.7	10.0
1080-68-16	2.0	0.507	4370	45.6	2150	41.5	10.0
1080-68-17	2.0	0.481	4710	51.3	2450	46.6	10.0
1080-68-18	2.0	0.508	2330	24.3	1150*	22.1*	10.0
				Average	2291	43.8	

* a. Failure principally in Scotchply throughout except for some specimens in the 2.0 in. overlap. Asterisks denote data reflecting incomplete bonds which were not included in the averages.

b. Specimens were single adherend Scotchply, double adherend steel.

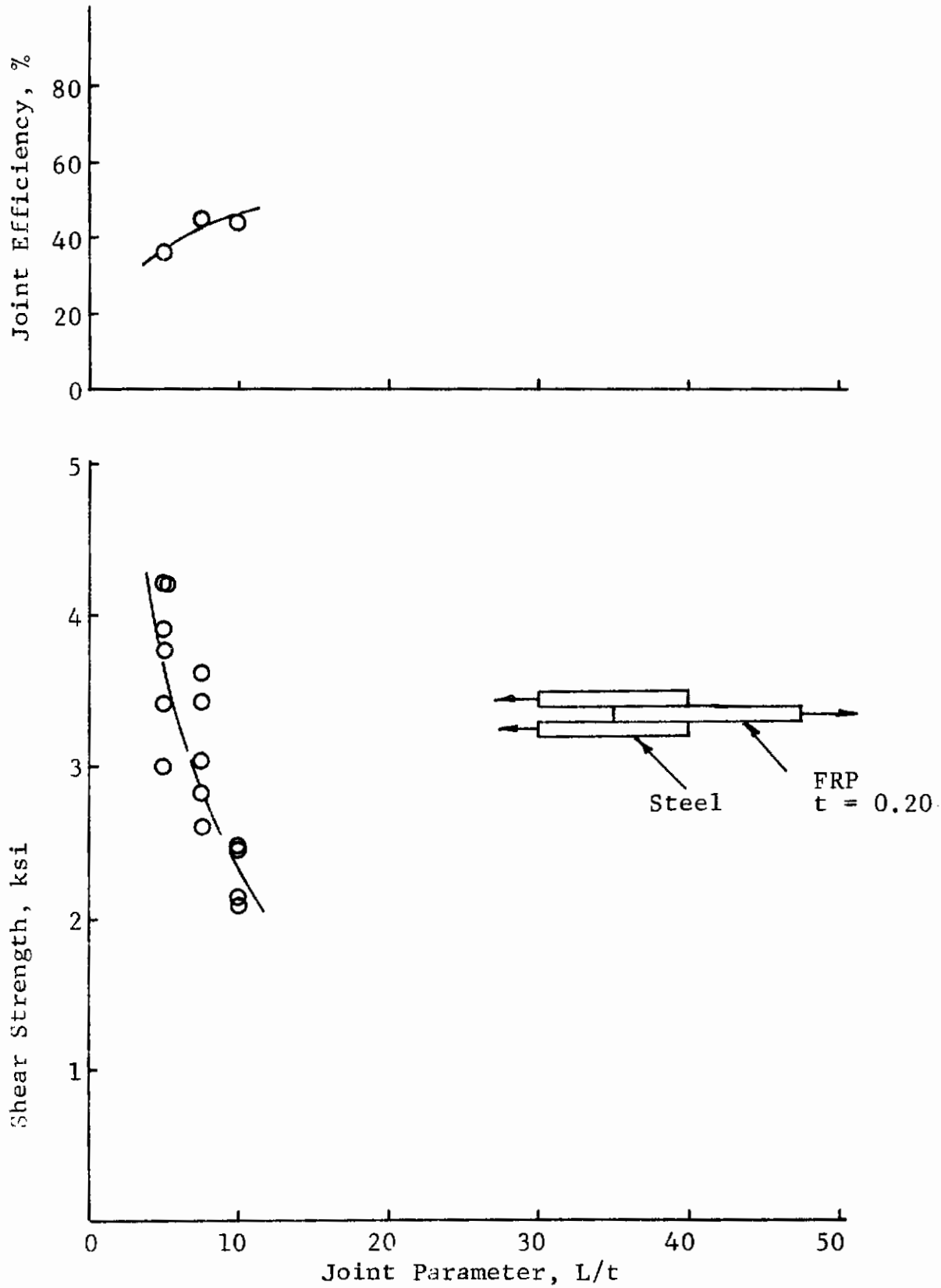

Fig. 4.46 SHEAR STRENGTH AND JOINT EFFICIENCY OF STEEL BONDED TO SCOTCHPLY XP-251S WITH FM-1000, t = 0.10/0.20/0.10 IN.

Table 4.37

SHEAR STRENGTH OF DOUBLE OVERLAP JOINTS OF SCOTCHPLY XP-251S AND STEEL BONDED WITH FM 47-TYPE 2, ADHEREND THICKNESS 0.10/0.05/0.10 IN. STEEL-FRP-STEEL

Specimen Number	Length of Overlap (in.)	Width of Joint (in.)	Load at Failure (lb)	Adherend Stress (ksi)	Shear Strength (psi)	Joint Efficiency (%)	Joint Parameter (L/t)
1081-77-1	1.0	0.536	2020	68.8	1880	62.5	20
1081-77-2	1.0	0.529	1630	57.1	1540	51.9	20
1081-77-3	1.0	0.496	1860	68.2	1880	62.0	20
1081-77-4	1.0	0.538	1620	56.8	1510	51.6	20
1081-77-5	1.0	0.513	1470	54.1	1430	49.2	20
1081-77-6	1.0	0.550	1700	58.3	1550	53.0	20
				Average	1630	55.0	
1081-77-7	1.5	0.498	1710	66.0	1140	60.0	30
1081-77-8	1.5	0.522	1960	72.2	1250	65.6	30
1081-77-9	1.5	0.551	1830	63.9	1110	58.1	30
1081-77-10	1.5	0.538	1850	66.1	1150	60.1	30
1081-77-11	1.5	0.550	2220	77.6	1330	70.5	30
1081-77-12	1.5	0.501	1980	76.0	1320	69.1	30
				Average	1220	63.9	
1081-77-13	2.0	0.548	1880	67.3	860	61.2	40
1081-77-14	2.0	0.510	1800	67.2	880	61.1	40
1081-77-15	2.0	0.530	1670	60.6	790	55.1	40
1081-77-16	2.0	0.532	1800	66.5	840	60.5	40
1081-77-17	2.0	0.490	1830	73.2	930	66.5	40
1081-77-18	2.0	0.536	1810	63.7	840	57.9	40
				Average	860	60.4	

Scotchply was between two adherends.

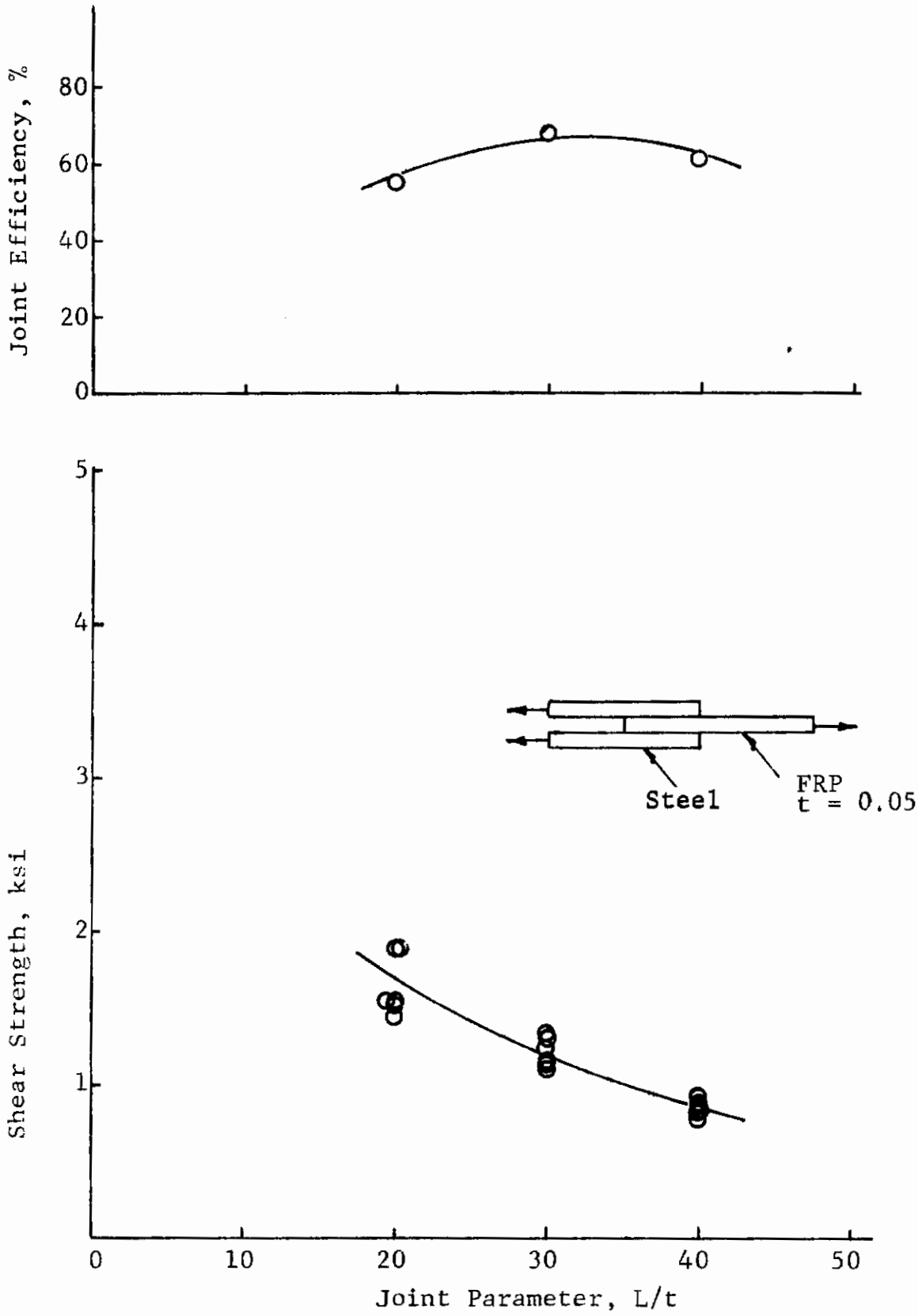

Fig. 4.47 SHEAR STRENGTH AND JOINT EFFICIENCY OF STEEL BONDED TO SCOTCHPLY XP-251S WITH FM-47, t = 0.10/0.05/0.10 IN.

Table 4.38

SHEAR STRENGTH OF DOUBLE OVERLAP JOINTS OF SCOTCHPLY XP-275 AND STEEL BONDED WITH FM-47 ADHESIVE FILM, ADHEREND THICKNESS 0.10/0.10/0.10 IN. STEEL-FRP-STEEL

Specimen Number	Length of Overlap (in.)	Width of Joint (in.)	Load at Failure (lb)	Adherend Stress (ksi)	Shear Strength (psi)	Joint Efficiency (%)	Joint Parameter (L/t)
1081-87-1	1.0	0.596	2370	37.2	1990	33.8	10
1081-87-2	1.0	0.503	2680	49.8	2660	45.3	10
1081-87-3	1.0	0.500	2150	40.2	2150	36.5	10
1081-87-4	1.0	0.503	2590	48.1	2570	43.7	10
1081-87-5	1.0	0.491	2050	39.0	2090	35.5	10
			Average	42.9	2290	39.0	
1081-78-1	1.5	0.512	2950	49.7	1920	45.3	15
1081-78-2	1.5	0.530	2000	32.7	1260	29.7	15
1081-78-3	1.5	0.537	2600	41.9	1610	38.1	15
1081-78-4	1.5	0.525	2610	43.0	1660	39.1	15
1081-78-5	1.5	0.552	3120	48.9	1880	44.5	15
1081-78-6	1.5	0.510	2340	39.9	1530	36.3	15
				Average	1640	38.8	
1081-78-7	2.0	0.536	2490	39.6	1160	36.0	20
1081-78-8	2.0	0.564	3450	52.0	1530	47.3	20
1081-78-9	2.0	0.522	3460	56.4	1660	51.3	20
1081-78-10	2.0	0.528	3050	55.8	1440	50.7	20
1081-78-11	2.0	0.526	3030	49.0	1440	44.5	20
1081-78-12	2.0	0.518	3270	53.7	1580	53.7	20
				Average	1470	47.3	

a. Mode of failure was from 50 to 75% cohesive (adhesive film) in the 1.5 inch overlap joint and ca. 100% cohesive (adhesive film in the 2.0 inch overlap).

b. Single Scotchply laminate adherend between two steel adherends.

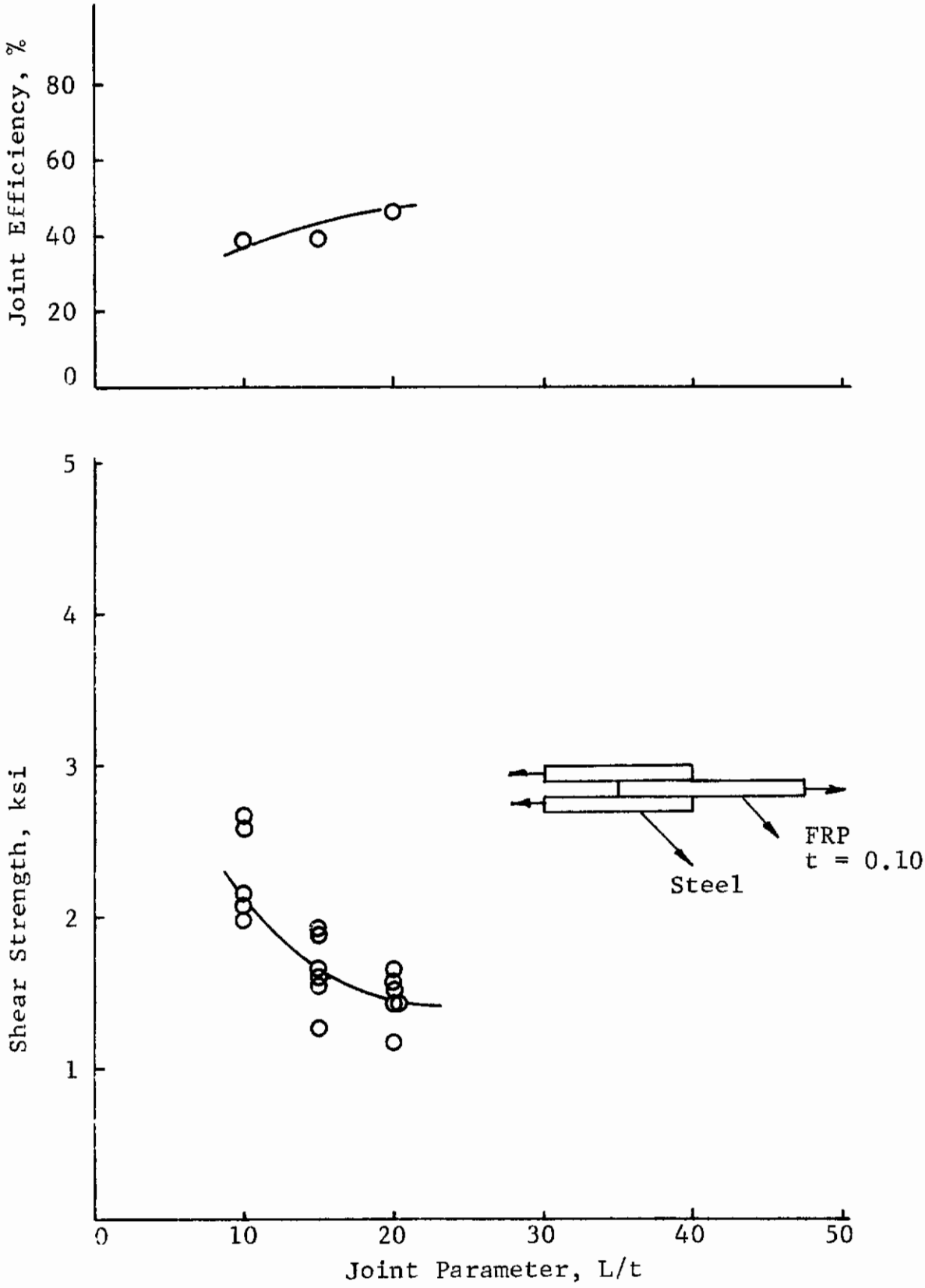

Fig. 4.48 SHEAR STRENGTH AND JOINT EFFICIENCY OF STEEL BONDED TO SCOTCHPLY XP-251S WITH FM-47, t = 0.10/0.10/0.10 IN.

Table 4.39

SHEAR STRENGTH OF DOUBLE OVERLAP JOINTS OF SCOTCHPLY XP-251S AND STEEL BONDED WITH FM-47 FILM, ADHEREND THICKNESS 0.10/0.20/0.10 IN. STEEL-FRP-STEEL

Specimen Number	Length of Overlap (in.)	Width of Joint (in.)	Load at Failure (lb)	Adherend Stress (ksi)	Shear Strength (psi)	Joint Efficiency (%)	Joint Parameter (L/t)
1081-76-2	1.0	0.501	2490	27.0	2490	24.5	5
1081-76-3	1.0	0.506	3260	35.0	3220	31.8	5
1081-76-4	1.0	0.507	2380	25.5	2350	23.2	5
1081-76-5	1.0	0.506	2030	21.8	2010	19.8	5
1081-76-2	1.0	0.509	2660	28.4	2610	25.8	5
			Average	27.5	2340	25.0	
1081-76-7	1.5	0.510	2550	26.0	1670	23.6	7.5
1081-76-8	1.5	0.502	2620	27.0	1740	24.5	7.5
1081-76-9	1.5	0.511	2490	25.2	1620	22.9	7.5
1081-76-10	1.5	0.503	2310	23.9	1530	21.7	7.5
1081-76-11	1.5	0.500	2300	23.8	1530	21.6	7.5
1081-76-12	1.5	0.503	2530	26.1	1680	23.7	7.5
			Average	25.3	1630	23.0	
1081-76-13	2.0	0.502	2830	30.5	1410	27.7	10
1081-76-14	2.0	0.509	2660	28.4	1210	25.8	10
1081-76-15	2.0	0.500	3250	35.5	1630	32.2	10
1081-76-16	2.0	0.511	3150	33.7	1540	30.6	10
1081-76-17	2.0	0.501	3020	33.1	1510	30.1	10
1081-76-18	2.0	0.497	2430	26.9	1220	24.4	10
			Average	31.4	1440	28.5	

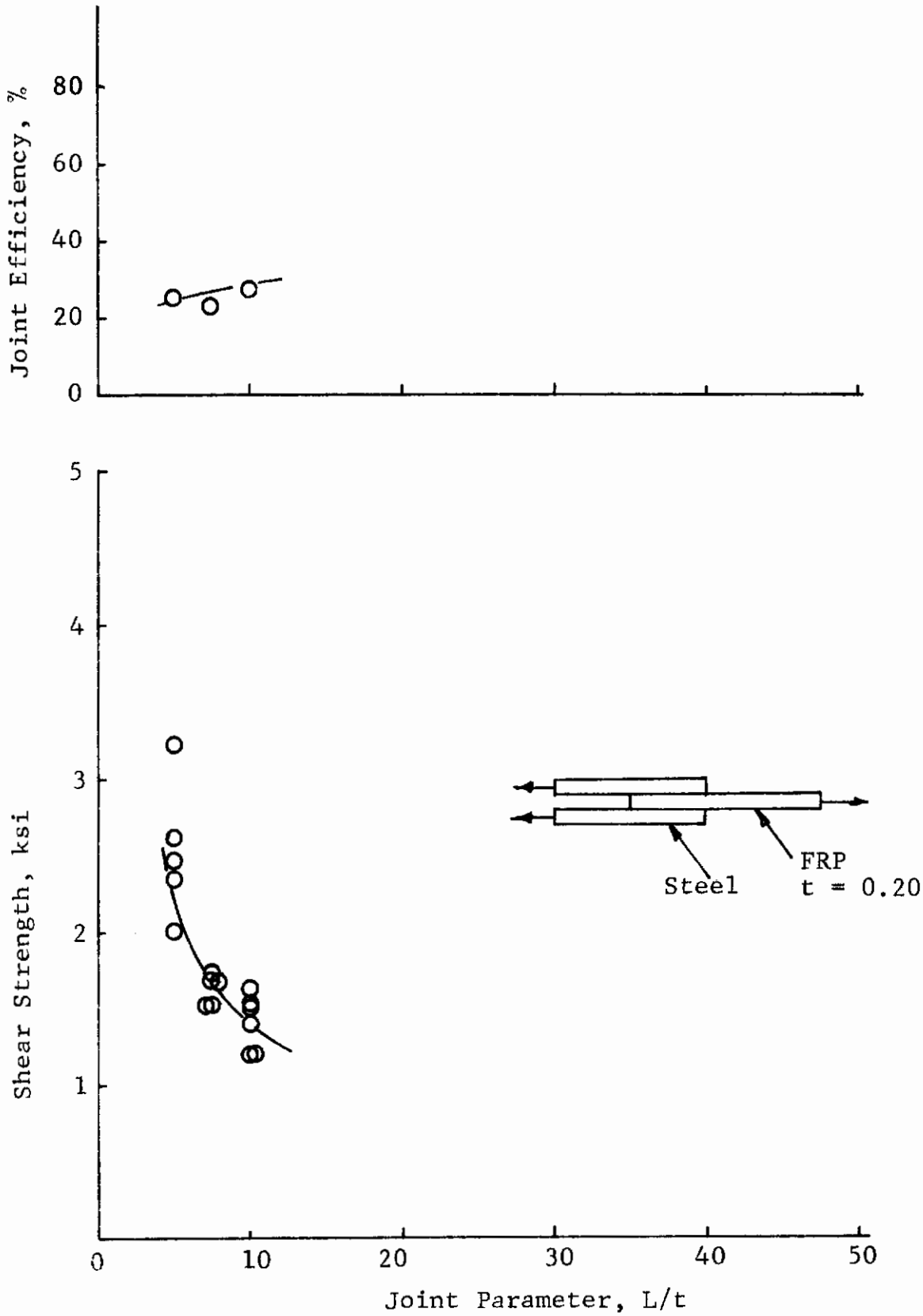

Fig. 4.49 SHEAR STRENGTH AND JOINT EFFICIENCY OF STEEL BONDED TO SCOTCHPLY XP-251S WITH FM-47, t = 0.10/0.20/0.10 IN.

Table 4.40

SHEAR STRENGTH OF DOUBLE OVERLAP JOINTS OF SCOTCHPLY XP-251S AND TITANIUM BONDED WITH FM-1000 FILM, ADHEREND THICKNESS 0.05/0.10/0.05 IN. FRP-TITANIUM-FRP

Specimen Number	Length of Overlap (in.)	Width of Joint (in.)	Load at Failure (lb)	Adherend Stress (ksi)	Shear Strength (psi)	Joint Efficiency (%)	Joint Parameter (L/t)
1080-71-1	1.0	0.489	4430	90.6	4530	69.6	20
1080-71-2	1.0	0.509	4380	86.1	4300	66.3	20
1080-71-3	1.0	0.510	4200	82.3	4120	63.4	20
1080-71-4	1.0	0.491	4310	87.8	4390	67.5	20
1080-71-5	1.0	0.512	3220	63.0	3140	48.4	20
1080-71-6	1.0	0.495	4450	90.0	4500	69.2	20
				Average	4160	64.1	
1080-71-7	1.5	0.507	5020	100.0	3300	76.9	30
1080-71-8	1.5	0.497	5120	104.0	3430	79.6	30
1080-71-9	1.5	0.497	4620	93.9	3100	72.3	30
1080-71-10	1.5	0.493	4590	94.0	3100	72.3	30
1080-71-11	1.5	0.503	4550	91.4	3020	70.2	30
1080-71-12	1.5	0.516	4970	97.3	3210	74.8	30
				Average	3190	74.3	
1080-71-13	2.0	0.496	5150	106.0	2600	81.4	40
1080-71-14	2.0	0.508	4620	92.8	2270	71.4	40
1080-71-15	2.0	0.499	5260	108.0	2640	83.0	40
1080-71-16	2.0	0.506	5060	102.0	2500	78.5	40
1080-71-17	2.0	0.502	5150	105.0	2560	80.6	40
1080-71-18	2.0	0.490	5430	113.0	2770	86.9	40

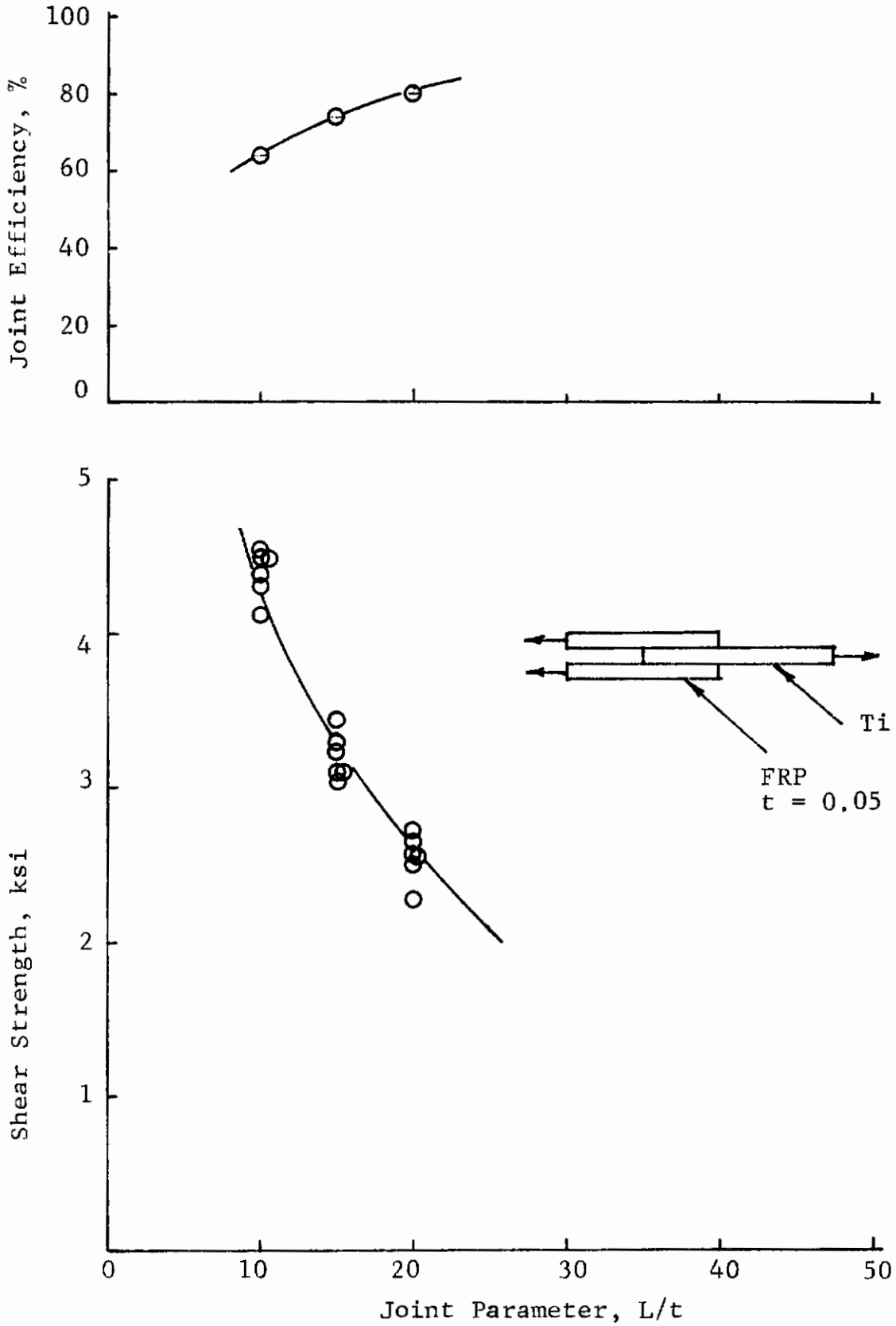

Fig. 4.50 SHEAR STRENGTH AND JOINT EFFICIENCY OF TITANIUM BONDED TO SCOTCHPLY XP-251S WITH FM-1000, t = 0.05/0.10/0.05 IN.

Table 4.41

SHEAR STRENGTH OF DOUBLE OVERLAP JOINTS OF SCOTCHPLY XP-251S AND TITANIUM BONDED WITH FM-1000 ADHESIVE FILM, ADHEREND THICKNESS 0.10/0.10/0.10 IN. FRP-TITANIUM-FRP

Specimen Number	Length of Overlap (in.)	Width of Joint (in.)	Load at Failure (lb)	Adherend Stress (ksi)	Shear Strength (psi)	Joint Efficiency (%)	Joint Parameter (L/t)
1080-83-1	1.0	0.508	3900	78.3	3840	60.2	10
1080-83-2	1.0	0.515	4900	96.6	4760	74.4	10
1080-83-3	1.0	0.515	4460	87.9	4330	67.5	10
1080-83-4	1.0	0.511	3300	65.9	3230	50.6	10
1080-83-5	1.0	0.505	4080	82.1	4040	63.2	10
1080-83-6	1.0	0.505	4100	82.4	4060	63.3	10
				Average	4040	63.4	
1080-72-1	1.5	0.499	6740	138.0	4500	100.0	15
1080-72-2	1.5	0.499	4220	86.3	2820	66.4	15
1080-72-3	1.5	0.502	6800	138.0	*	100.0	15
1080-72-4	1.5	0.499	4680	95.7	3130	73.6	15
1080-72-5	1.5	0.516	7000	138.3	*	100.0	15
1080-72-6	1.5	0.497	6830	140.0	4580	100.0	15
				Average	3760	100.0	
1080-69-1	2.0	0.552	5100	03.3	2310	79.3	20
1080-69-2	2.0	0.509	6970	138.0	3420	100.0	20
1080-69-3	2.0	0.553	7270	133.0	3290	100.0	20
1080-69-4	2.0	0.494	6940	142.0	3510	100.0	20
1080-69-5	2.0	0.523	7130	138.0	3410	100.0	20
1080-69-6	2.0	0.521	7100	138.0	3410	100.0	20
				Average	3230	100.0	

* Titanium adherend failed.

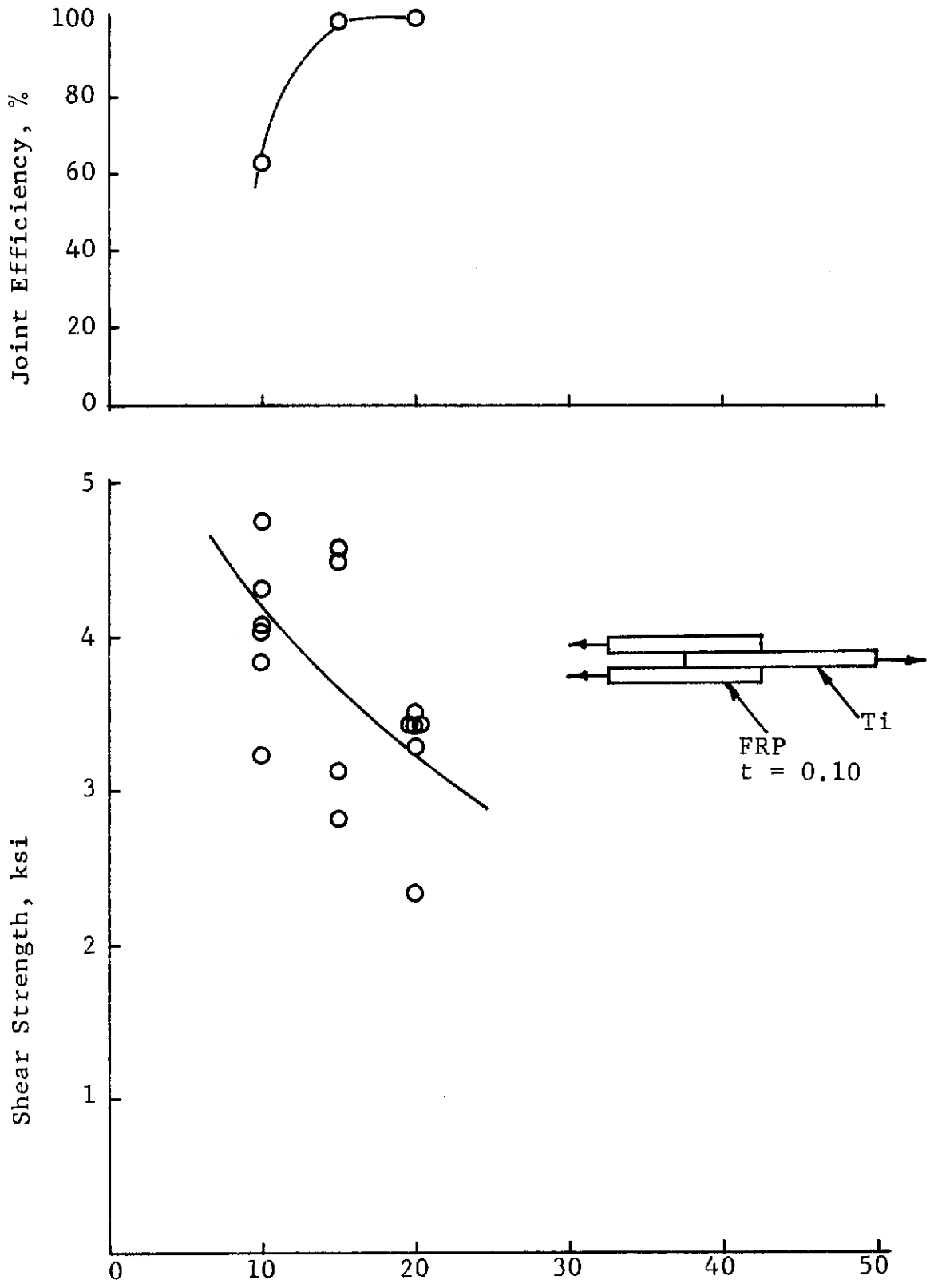

Fig. 4.51 SHEAR STRENGTH AND JOINT EFFICIENCY OF TITANIUM BONDED TO SCOTCHPLY XP-251S WITH FM-1000, t = 0.10/0.10/0.10 IN.

Table 4.42

SHEAR STRENGTH OF DOUBLE OVERLAP JOINTS OF SCOTCHPLY XP-251S BONDED TO TITANIUM WITH FM 1000, ADHEREND THICKNESS 0.20/0.10/0.20 IN. FRP-TITANIUM-FRP

Specimen Number	Length of Overlap (in.)	Width of Joint (in.)	Load at Failure (lb)	Adherend Stress (ksi)	Shear Strength (psi)	Joint Efficiency (%)	Joint Parameter (L/t)
1080-82-1	1.0	0.504	4280	85.9	4250	60.2	5
1080-82-2	1.0	0.505	2850	57.0	2820[a]	43.7	5
1080-82-3	1.0	0.502	5530	111.0	5510	85.6	5
1080-82-4	1.0	0.503	5620	113.0	5590	86.9	5
1080-82-5	1.0	0.506	5460	109.0	5400	83.9	5
1080-82-6	1.0	0.484	5370	112.0	5500	83.6	5
				Average	5250	74.0	
1080-82-7	1.5	0.498	3210	65.1	2150	50.1	7.5
1080-82-8	1.5	0.510	2230	44.2	1460	34.0	7.5
1080-82-9	1.5	0.505	3650	73.0	2410	56.1	7.5
1080-82-10	1.5	0.504	4240	85.0	2800	65.4	7.5
1080-82-11	1.5	0.504	3010	60.3	1990	46.4	7.5
1080-82-12	1.5	0.503	3330	67.0	2210	51.6	7.5
				Average	2170[a]	50.6	
1080-82-13	2.0	0.491	6370	128.0	3240	98.6	10
1080-82-14	2.0	0.508	5980	118.0	2940	90.8	10
1080-82-15	2.0	0.505	4950	99.0	2450	76.2	10
1080-82-16	2.0	0.509	6310	123.0	3100	94.6	10
1080-82-17	2.0	0.488	5210	106.0	2670	81.5	10
1080-82-18	2.0	0.496	5930	119.0	2990	91.6	10
				Average	2900	88.8	

a Low results from poor adhesion to one side of the titanium.

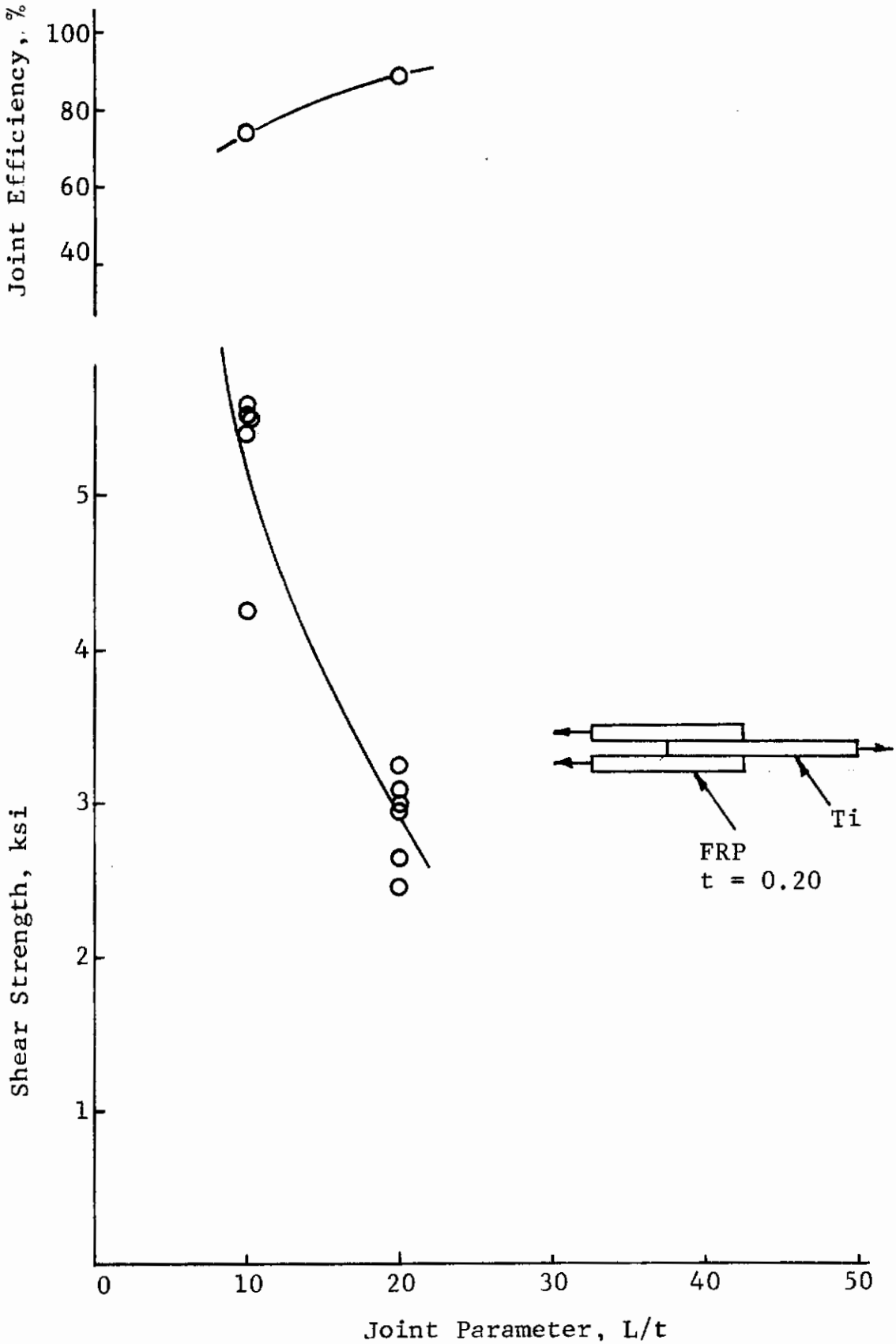

Fig. 4.52 SHEAR STRENGTH AND JOINT EFFICIENCY OF TITANIMUM BONDED TO SCOTCHPLY XP-251S WITH FM-1000, t = 0.20/0.10/0.20 IN.

Table 4.43

SHEAR STRENGTH OF DOUBLE OVERLAP JOINTS OF SCOTCHPLY XP-251S BONDED TO TITANIUM WITH FM-47 FILM, ADHEREND THICKNESS 0.10/0.10/0.10 IN. FRP-TITANIUM-FRP

Specimen Number	Length of Overlap (in.)	Width of Joint (in.)	Load at Failure (lb)	Adherend[a] Stress (ksi)	Shear Strength (psi)	Joint[b] Efficiency (%)	Joint Parameter (L/t)
1081-86-1	1.0	0.515	2810	54.6	2730	42.1	10
1081-86-2	1.0	0.506	2810	55.5	2780	42.7	10
1081-86-3	1.0	0.503	2900	58.2	2880	44.8	10
1081-86-4	1.0	0.511	2380	46.8	2330	36.0	10
1081-86-5	1.0	0.511	2810	55.5	2750	42.7	10
1081-86-6	1.0	0.501	2450	49.1	2450	37.8	10
				Average	2650	41.0	
1081-81-7	1.5	0.500	4320	86.2	2880	66.4	15
1081-81-8	1.5	0.504	3490	70.6	2310	54.4	15
1081-81-9	1.5	0.505	3750	75.8	2480	58.4	15
1081-81-10	1.5	0.504	3630	73.5	2400	56.5	15
1081-81-11	1.5	0.505	3700	74.8	2440	57.5	15
1081-81-12	1.5	0.502	4200	85.4	2790	65.6	15
				Average	2560	59.8	
1081-81-1	2.0	0.503	1810	36.0	900	27.8	20
1081-81-2	2.0	0.523	1920	36.7	920	28.2	20
1081-81-5	2.0	0.526	1690	32.3	805	24.8	20
1081-81-6	2.0	0.508	1430	28.3	705	21.8	20
				Average	830[c]	25.6	

a. Stress in the titanium.
b. Based on titanium allowable stresses.
c. Poor adhesion for this group, all strengths are low.

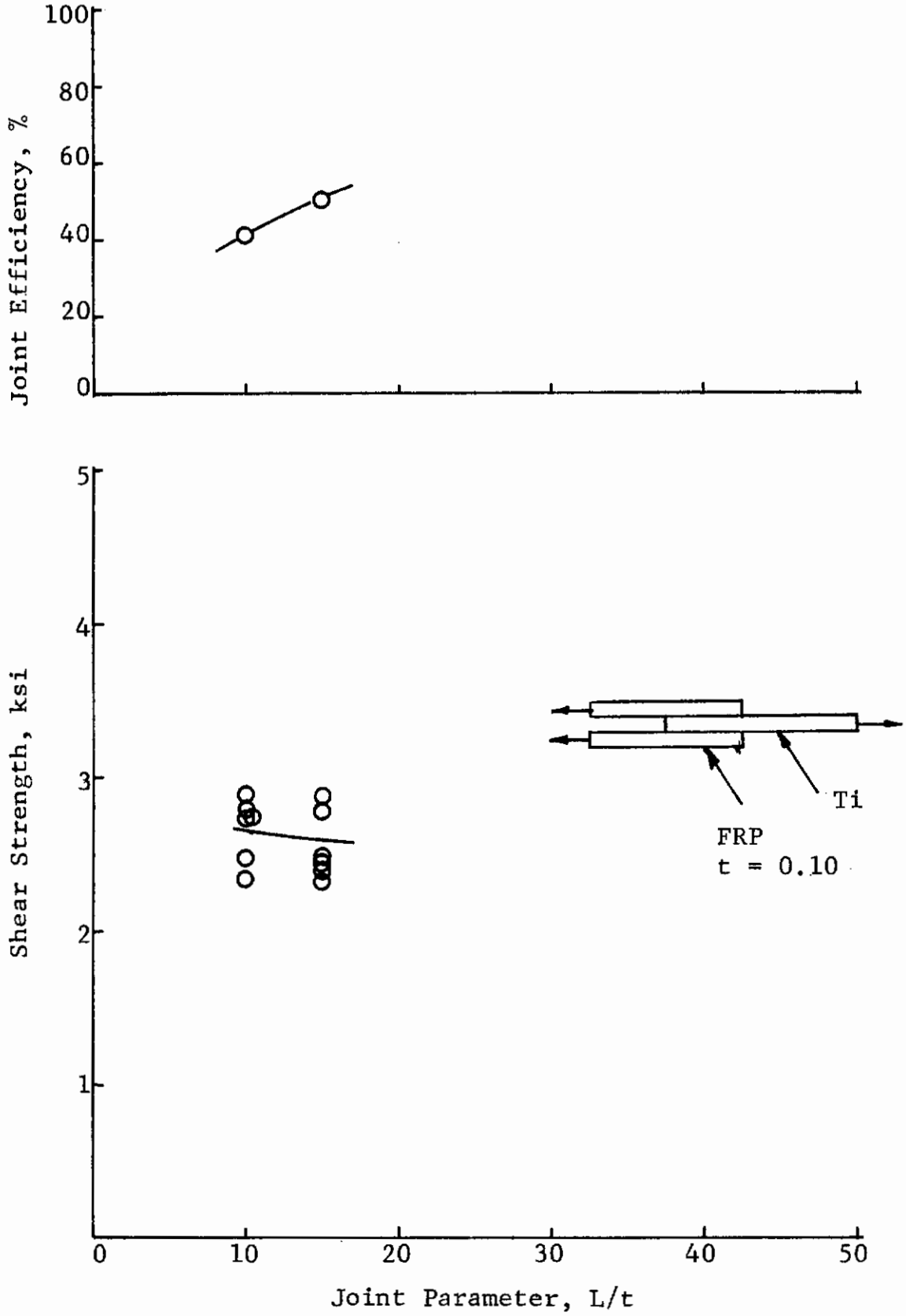

Fig. 4.53 SHEAR STRENGTH AND JOINT EFFICIENCY OF TITANIUM BONDED TO SCOTCHPLY XP-251S WITH FM-47, t = 0.10/0.10/0.10 IN.

Table 4.44

SHEAR STRENGTH OF DOUBLE OVERLAP JOINTS OF SCOTCHPLY XP-251S AND TITANIUM BONDED WITH FM-47 FILM, ADHEREND THICKNESS 0.20/0.10/0.20 IN. FRP-TITANIUM-FRP

Specimen Number	Length of Overlap (in.)	Width of Joint (in.)	Load at Failure (lb)	Adherend[a] Stress (ksi)	Shear Strength (psi)	Joint[b] Efficiency (%)	Joint Parameter (L/t)
1081-79-1	1.0	0.513	1500	29.7	1460	22.8	10
1081-79-2	1.0	0.503	1730	34.7	1720	26.7	10
1081-79-3	1.0	0.502	1600	32.4	1590	24.9	10
1081-79-4	1.0	0.491	1520	31.4	1550	24.2	10
1081-79-5	1.0	0.473	1345	28.9	1420	22.2	10
1081-79-6	1.0	0.434	1345	31.5	1550	24.2	10
			Average	31.4	1550[c]	24.1	
1081-79-7	1.5	0.509	2890	57.7	1890	44.4	15
1081-79-8	1.5	0.504	3300	66.5	2180	51.3	15
1081-79-9	1.5	0.502	3170	64.2	2100	49.4	15
1081-79-10	1.5	0.505	3330	66.9	2200	51.4	15
1081-79-11	1.5	0.504	4060	81.8	2690	63.0	15
1081-79-12	1.5	0.502	3030	61.3	2010	47.3	15
			Average	66.4	2180	51.3	
1081-79-13	2.0	0.540	3580	66.0	1660	50.7	20
1081-79-14	2.0	0.516	3210	62.0	1560	47.7	20
1081-79-15	2.0	0.512	3400	66.1	1660	51.0	20
1081-79-16	2.0	0.514	3170	61.4	1540	47.2	20
1081-79-17	2.0	0.501	3270	64.9	1630	49.9	20
1081-79-18	2.0	0.498	3340	66.4	1680	51.1	20
			Average	64.5	1620	49.6	

a. Stress in titanium.
b. Based on titanium allowable stresses.
c. Poor adhesion gave low results.

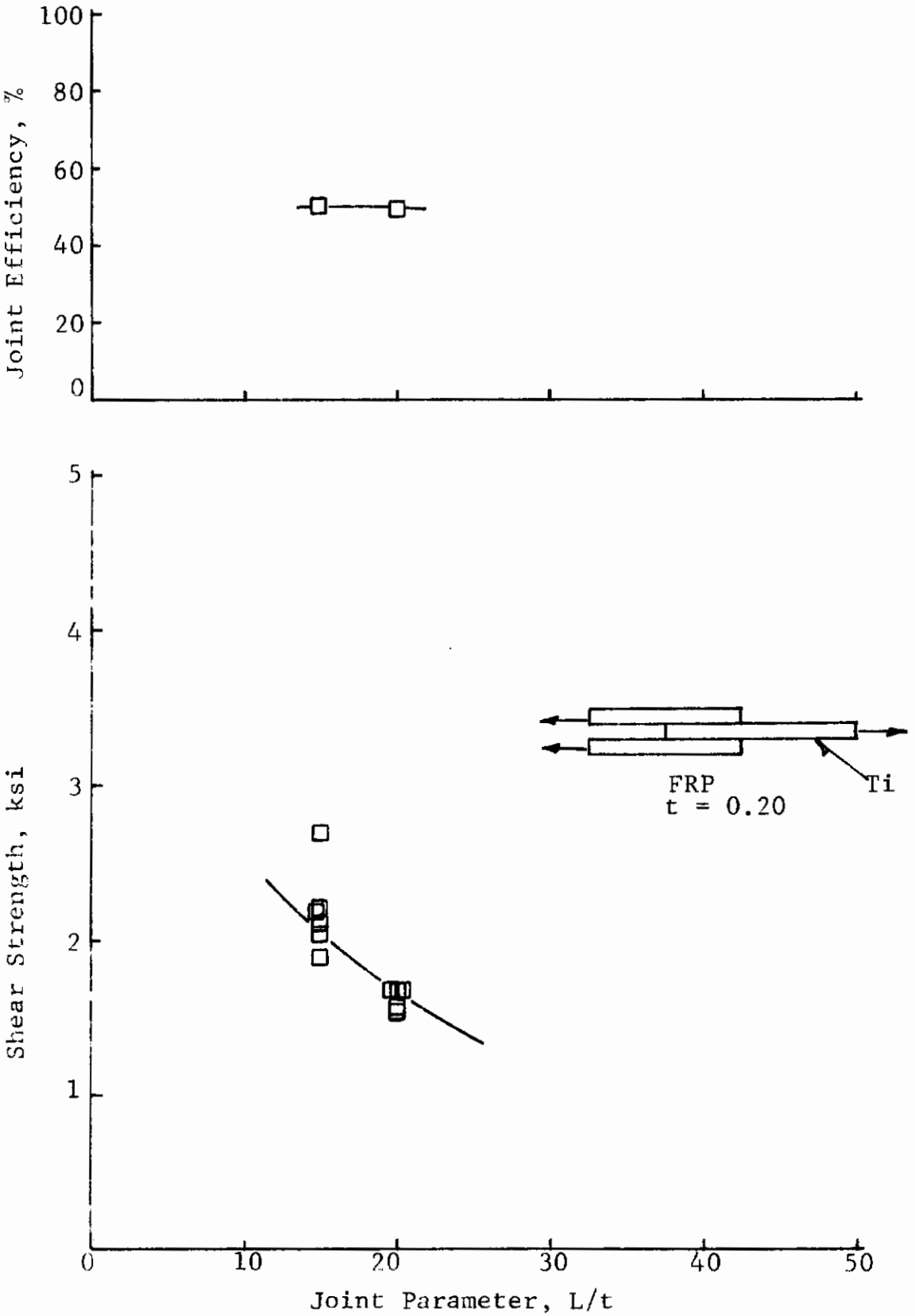

Fig. 4.54 SHEAR STRENGTH AND JOINT EFFICIENCY OF TITANIUM BONDED TO SCOTCHPLY XP-251S WITH FM-47, t = 0.20/0.10/0.20 IN.

4.5.4 Fatigue Strength of FRP-FRP Double Overlap Joints

This section contains the fatigue strength results for the double overlap joints of Scotchply XP-251S bonded with Metlbond 400, FM-1000 and FM-47 adhesives. All these joints were tested by the U.S.D.A. Forest Products Laboratory.

Table 4.45

FATIGUE STRENGTH OF DOUBLE OVERLAP JOINTS OF XP-251S BONDED WITH FM-1000. TESTED AT 900 CYCLES PER MIN AND LOAD RANGE OF 0.1

Specimen Number	Length of Lap	Maximum Shear Stress (psi)	Cycles to Failure	Location of Failure
1080-73-12	0.5	1,664	57,200	Bond
1080-73-11	0.5	1,664	82,400	Bond
1080-73-10	0.5	1,456	278,000	Bond
1080-73- 9	0.5	1,456	229,200	Bond
1080-73- 8	0.5	1,248	1,578,200	Bond
1080-73- 7	0.5	1,248	421,400	Bond
1080-73- 6	0.5	1,144	4,044,000	Bond
1080-73- 5	0.5	1,144	1,097,900	Bond
1080-73- 4	0.5	1,144	10,934,100	Bond
1080-73- 3	0.5	1,040	5,837,300	Laminate
1080-73- 2	0.5	4,120	1/4	Bond
1080-73- 1	0.5	3,390	1/4	Bond
1080-73-20	1.5	828	24,500	Laminate
1080-73-19	1.5	828	4,000	Bond
1080-73-18	1.5	724	219,200	Bond
1080-73-17	1.5	724	14,900	Laminate
1080-73-15	1.5	621	112,100	Laminate
1080-73-16	1.5	621	2,372,100	Laminate
1080-73-23	1.5	569	49,900	Laminate
1080-73-24	1.5	569	68,700	Laminate
1080-73-22	1.5	517	2,539,300	Laminate
1080-73-21	1.5	518	1,663,200	Laminate
1080-73-13	1.5	1,976	1/4	Bond
1080-73-14	1.5	2,211	1/4	Bond

Table 4.46

FATIGUE STRENGTH OF DOUBLE OVERLAP JOINTS OF XP-251S BONDED WITH METLBOND 400. TESTED AT 900 CYCLES PER MIN AND LOAD RANGE OF 0.1

Specimen Number	Length of Lap	Maximum Shear Stress (psi)	Cycles to Failure	Location of Failure
1090-74- 9	0.5	2,100	4,100	Bond
1090-74- 6	0.5	2,100	34,400	Bond
1090-74- 5	0.5	1,750	359,000	Bond
1090-74- 8	0.5	1,750	131,300	Bond
1090-74-11	0.5	1,575	838,200	Bond
1090-74- 7	0.5	1,400	350,600	Bond
1090-74- 3	0.5	1,400	3,283,800	Bond
1090-74- 4	0.5	1,050	4,364,300	Laminate
1090-74-10	0.5	1,050	7,151,400	Laminate
1090-74-12	0.5	1,225	>11,000,000	--
1090-74- 1	0.5	4,239	1/4	Bond
1090-74- 2	0.5	3,438	1/4	Bond
1090-74-17	1.5	918	43,900	Laminate
1090-74-18	1.5	918	14,200	Laminate
1090-74-15	1.5	765	701,200	Laminate
1090-74-19	1.5	765	158,100	Laminate
1090-74-16	1.5	612	952,400	Laminate
1090-74-20	1.5	612	1,440,500	Laminate
1090-74-21	1.5	536	712,400	Laminate
1090-74-22	1.5	536	981,400	Laminate
1090-74-23	1.5	459	1,626,500	Laminate
1090-74-24	1.5	655	3,044,400	Laminate
1090-74-13	1.5	2,320	1/4	Laminate
1090-74-14	1.5	1,743	1/4	Laminate

Table 4.47

FATIGUE STRENGTH OF DOUBLE OVERLAP JOINTS OF XP-251S BONDED WITH FM-47. TESTED AT 900 CYCLES PER MIN AND LOAD RANGE OF 0.1

Specimen Number	Length of Lap	Maximum Shear Stress (psi)	Cycles to Failure	Location of Failure
1081-75-10	0.5	905	187,300	Bond
1081-75-11	0.5	814	20,700	Bond
1081-75-12	0.5	724	2,151,000	Bond
1081-75- 9	0.5	814	275,700	Bond
1081-75- 8	0.5	724	>11,075,000	--
1081-75- 7	0.5	634	10,423,600	Bond
1081-75- 6	0.5	634	1,539,000	Bond
1081-75- 5	0.5	543	>10,000,000	--
1081-75- 3	0.5	498	>17,000,000	--
1081-75- 4	0.5	452	>11,000,000	--
1081-75- 2	0.5	1,790	1/4	Bond
1081-75- 1	0.5	1,820	1/4	Bond
1081-75-16	1.5	390	82,700	Bond
1081-75-15	1.5	390	27,800	Bond
1081-75-17	1.5	312	1,403,400	Bond
1081-75-18	1.5	312	1,236,300	Bond
1081-75-19	1.5	351	1,806,000	Bond
1081-75-20	1.5	351	797,500	Bond
1081-75-23	1.5	429	57,200	Bond
1081-75-24	1.5	429	108,500	Bond
1081-75-21	1.5	273	2,060,900	Bond
1081-75-22	1.5	234	>10,100,000	--
1081-75-13	1.5	831	1/4	Bond
1081-75-14	1.5	861	1/4	Bond

REFERENCES

4.1 Kuenzi, E. and Stevens, G. H. "Determination of Mechanical Properties of Adhesives for Use in the Design of Bonded Joints," U.S. FPL Research, Note FPL-011.

4.2 Noyes, J. V. and Jones, B. H. "Crazing and Yielding of Reinforced Composites," Third Quarterly Progress Report, Contract No. AF-33(615)-3931, March 1967.

5.0 DESIGN OF BONDED JOINTS

A design procedure for any structure is the result of a combination of analysis and experiment to develop a predictive scheme, which will cover a larger class of structures than that from which the original experimental data was obtained. For bonded joints the objective is to make the transition from strength data on simple single or double overlap joints to a more complex bonded structure. The problem is to scale data from one half or one inch overlap joints to a complex component.

Inherent in this process is the assumption that the original experimental joint data can be predicted by the analysis, and if the results do not fit, how great a correction factor must be employed to fit the data. If the simple joint results cannot be predicted, then results for larger structures will certainly be more in error since the details of load distribution on the joints are less well understood in the larger components.

Two comparisons of analysis and experiment were made. First the results of the Volkersen analysis were used to compare shear stress concentration factors with experimental values. Since the relationship of this analysis with the others studied was established in the parametric studies, qualitative comparisons could also be made with these analyses.

Secondly, the experimental results were compared to relative adherend stiffness for each joint since this stiffness will affect the adhesive deformations and subsequent stresses in the adhesive. This relative adherend stiffness - shear strain behavior is common to all the joints analyses; therefore, its comparison with experimental data is important to all the present analyses and others to be developed.

Based on the results of these two comparisons, predictions are made for the feasibility of design methods for more complex parts.

5.1 ANALYTICAL-EXPERIMENTAL COMPARISON

The analysis which most closely fits the double overlap joint geometry tested experimentally in this program is the Volkersen analysis. Sufficient parametric studies were made such that predictions could be made for a series of the joints tested. The comparison of the analysis and experiment was made on the basis of shear stress concentration factor (n) and the joint parameter (Δ).

Note that the stress concentration factor at the end of the overlap is as follows:

$$n = \frac{\tau(x = L)}{\tau_{avg.}}$$

$$\tau_{avg.} = \frac{P}{wL}$$

$$\tau(x = L) = \frac{P}{wL} \quad (\Delta/2)^{1/2} \cdot \coth (\Delta/2)^{1/2}$$

$$\Delta = \frac{GL^2}{Ett_a}$$

therefore

$$n = f(\Delta)$$

where the symbols are defined as in section 3.2.

The function $n = f(\Delta)$ was computed directly from the analysis with the following data as input.

The length of overlap (L), adherend thickness (t) and adhesive thickness (t_a) were measured experimentally for each joint. The adherend modulus (E) was obtained experimentally for the Scotchply XP-251S and handbook values are used for the metal adherends. The value for adhesive modulus (G) was calculated for the experimental value of tensile modulus (E) obtained from the adhesive film tests and an assumed value of

Poisson's ratio. Poisson's ratio ($\mu = 0.45$) was used for all three adhesives. This value has been obtained in measurements of Poisson's ratio for other epoxy materials and similar resins and is felt to be a good approximation for use in this work.

The experimental value of stress concentration (n) was calculated from the observed average shear strength (τ_{avg}) at any (Δ) and the shear strength extrapolated to zero overlap which was assumed to be the shear strength of the material. The strength at zero overlap is considered to be a good measure of the shear strength of the material since as overlap decreases the shear stress becomes more uniform.

5.1.1 FM-1000 Adhesive

The comparison of shear stress concentration for FM-1000 fiberglass to fiberglass bonded joints is shown in Fig. 5.1. The following data were used in the analysis:

Adhesive - FM-1000	Adherend - Scotchply XP-251S
t_a = 0.008 in.	t = 0.050 in.
E = 160,000 psi	E = 4.1×10^6 psi
μ = 0.45	
G = 55,000 psi	
τ_{ult} = 6,800 psi	

The general shape of both the predicted and experimental curves are the same, but the analysis predicts significantly higher stresses than those observed experimentally. At $\Delta = 10$, the analysis predicts n = 2.3, while n = 1.8 was observed experimentally. At higher (Δ) the difference becomes more marked.

If the value of shear strength of the adhesive were actually higher, (for example, 10,000 psi) there would be a better fit to the data at higher values of (Δ).

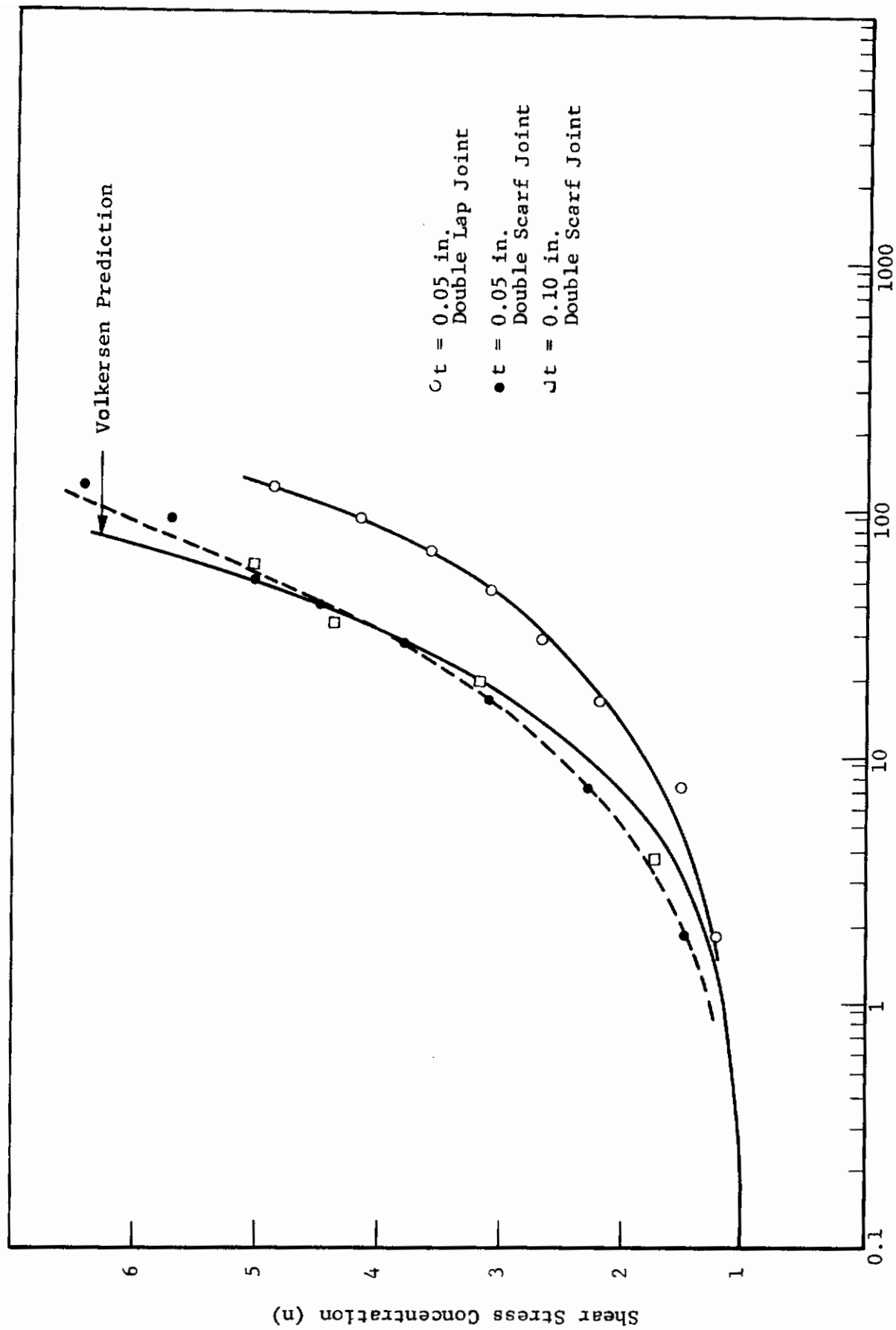

Fig. 5.1 COMPARISON OF VOLKERSEN ANALYSIS AND DATA FOR FM-1000 ADHESIVE

No analysis was made for the scarfed joints at this same adherend thickness of t = 0.05, but theoretically, the shear stress in these joints should be uniform; i.e., n = 1.0 should hold true for all the joints and shear strength should have been constant with change in the joint parameter (L/t). Since this was not true as was observed in section 4.3.2 and the joints behaved more as full thickness lap joints, the experimental results for (n) for these joints were plotted in Fig. 5.1. Also note that the shear strength of the adhesive τ_{ult} = 8500 was higher for the scarf joints.

The scarf joint results were almost a perfect fit to the Volkersen prediction for this adherend thickness. This would indicate that the scarf joint is behaving more like a homogeneous adherend than a composite material adherend.

Figure 5.1 also shows the experimental results for the 0.10 in. thick composite adherend joints. These data also fall very close to the predictions of the analysis. These results are anomalous since one would intuitively postulate that the results for the scarf joints and thinnest adherends would fall together rather than the scarf joints and the thicker adherend joint.

One possible explanation is that the failure modes of the scarfed and 0.10 in. joints are more alike. It was observed that the 0.10 in. and 0.20 in. thick joints contained shear failures three to four lamina away from the bonded area, with the load never reaching the outer plies. In the 0.05 in. thick joints the load was carried further into the composite, but scarfing apparently increased the local sites for shear failure inducing shallow failures and behavior more like the 0.10 in. thick adherend joints.

5.1.2 Metlbond 400 Adhesive

The analytical and experimental comparison for Metlbond 400 is shown in Fig. 5.2. The following data was used for the analysis:

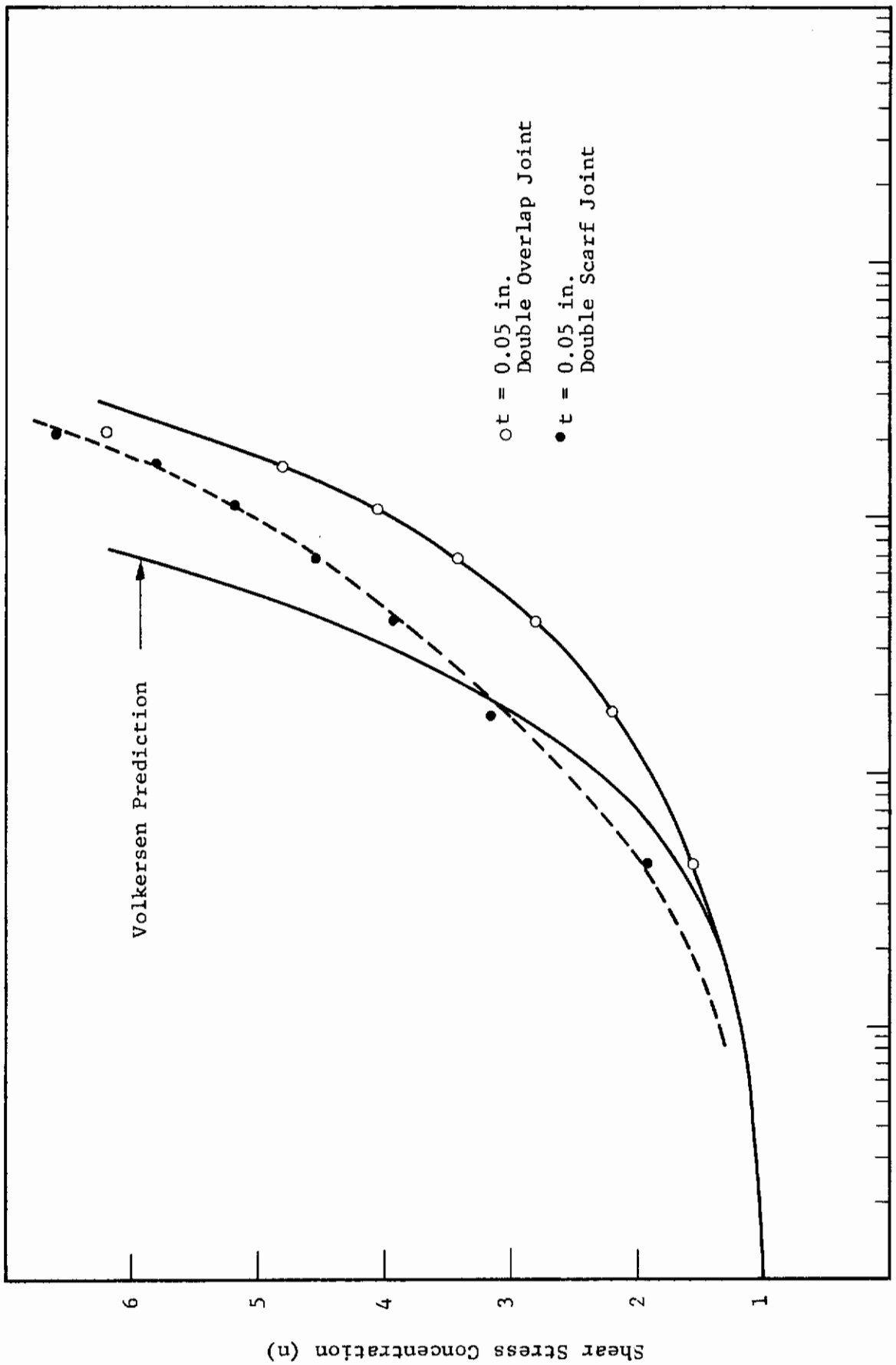

Fig. 5.2 COMPARISON OF VOLKERSEN ANALYSIS AND DATA FOR METLBOND 400 ADHESIVE

Adhesive - Metlbond 400	Adherend - Scotchply XP-251S
t_a = 0.007 in.	t = 0.050 in.
E = 292,000 psi	E = 4.1 x 10^6 psi
μ = 0.45	
G = 100,000 psi	
τ_{ult} = 6,500 psi	

The analysis again predicts higher stress concentrations than those observed analytically and similarly the scarf joint data shows a better fit to the results than the full thickness joints. The scarf joint fit is not as close as with the FM-1000 adhesive.

Up to (Δ) = 50 the experimental results for Metlbond 400 are almost identical but at values greater than this the stress concentration for FM-100 are increased. For both of these materials, if the adhesive were exhibiting plastic behavior, the experimental (n) should be lower since τ_{ult} would remain the same but τ_{avg} would be higher at failure than if the behavior was all elastic.

5.1.3 FM-47 Adhesive

Figure 5.3 shows the analytical and experimental results for FM-47, the stiffest brittle adhesive. The input data for the analysis was as follows:

Adhesive - FM-47	Adherend - Scotchply XP-251S
t_a = 0.008 in.	t = 0.050 in.
E = 621,000 psi	E = 4.1 x 10^6 psi
μ = 0.45	
G = 214,000 psi	
τ_{ult} = 3,300 psi	

The data for this adhesive shows the poorest fit with the analysis. Also, the scarf joint results are very close to the data for the full thickness adherend joints. In one respect this adhesive provides the best model to the Volkersen

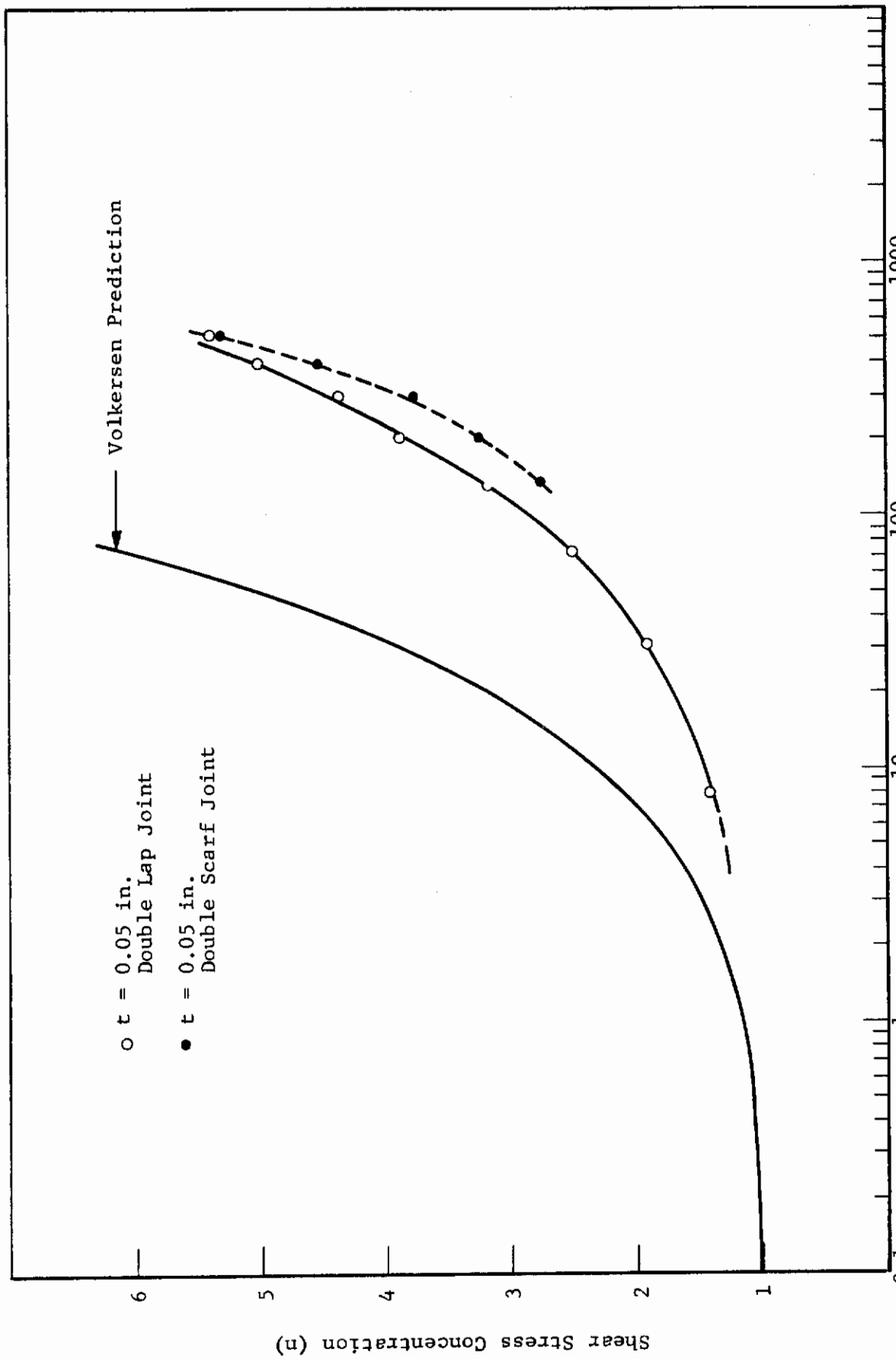

Fig. 5.3 COMPARISON OF VOLKERSEN ANALYSIS AND DATA FOR FM-47 ADHESIVE

analysis because all of the joint failures did occur in the adhesive. It is further disappointing, then, that the results are not closer to the analytical predictions.

The factors which influence the data fit are the input values for shear strength, modulus and adhesive thickness. Assuming the maximum possible error for any of these data, a maximum change of 20 to 30 percent in stress concentration would be obtained which is still insufficient to account for the difference between analysis and experiment.

5.2 EMPIRICAL METHODS

The one basic assumption inherent in all the joints analyses is that the primary source of shear stress variation is due to the differential straining in each adherend. The differential straining is due to two factors:

a) The load distribution along the bonded area is not uniform, the load is maximum at the point of entry into the bonded length and then decreases to zero at the other end of the overlap.

b) There can exist a difference in relative stiffness of the adherends. This stiffness difference combined with load variation will induce further differential straining.

One of the reasons for including the bonded metal adherends in this study was to obtain as wide a variation in relative variation as possible. The range of relative deformations obtained is shown in Table 5.1, along with the resultant joint strengths for FM-1000 and FM-47 bonded with a 1.0 in. overlap.

The stiffness ($Et = 2.0 \times 10^5$ lb/in) of the 0.05 in. fiberglass adherend was assigned a relative stiffness equal to one. This was shown in section 4.2.1. All other adherends are related to this unit value. The relative deformation is obtained by dividing load by the stiffness. For the double overlap configuration the outer two adherends only carry one half the load of the inner member.

Figure 5.4 shows the graphical results for this data. For the FRP to metal bonded joints, shear strength definitely decreases as relative adherend deformation increases. The greater the deformation between the adherends the weaker the joint. This holds true for both adhesives.

Table 5.1

SHEAR STRENGTH AND RELATIVE STIFFNESS OF DOUBLE OVERLAP JOINTS
FM-1000 AND FM-47 ADHESIVES, 1.00 IN. OVERLAP

Adherend Combination	Thickness (t) (in.)	Adherend Stiffness Et (lb/in.)	Adherend Deflection P/Et (in.)	Relative Deflection	FM-1000 Shear Strength τ (psi)	FM-47 Shear Strength τ (psi)
FRP/FRP/FRP	0.05/0.05/0.05	1 / 1 / 1	1 / 2 / 1	2	2600	1100
FRP/FRP/FRP	0.10/0.10/0.10	1 / 1 / 1	1 / 2 / 1	2	2000	1500
FRP/FRP/FRP	0.20/0.20/0.20	1 / 1 / 1	1 / 2 / 1	2	4100	
FRP/Ti/FRP	0.05/0.10/0.05	1 / 8 / 1	4 / 1 / 4	4	4160	
FRP/Ti/FRP	0.10/0.10/0.10	2 / 8 / 2	2 / 1 / 2	2	4040	2600
FRP/Ti/FRP	0.20/0.10/0.20	4 / 8 / 4	1 / 1 / 1	1	5250	
Steel/FRP/Steel	0.10/0.05/0.10	13 / 1 /13	1 /26 / 1	26	1600	1650
Steel/FRP/Steel	0.10/0.10/0.10	13 / 2 /13	1 /13 / 1	13	2250	2300
Steel/FRP/Steel	0.10/0.20/0.10	13 / 4 /13	1 / 6.5 / 1	6.5	3750	2250

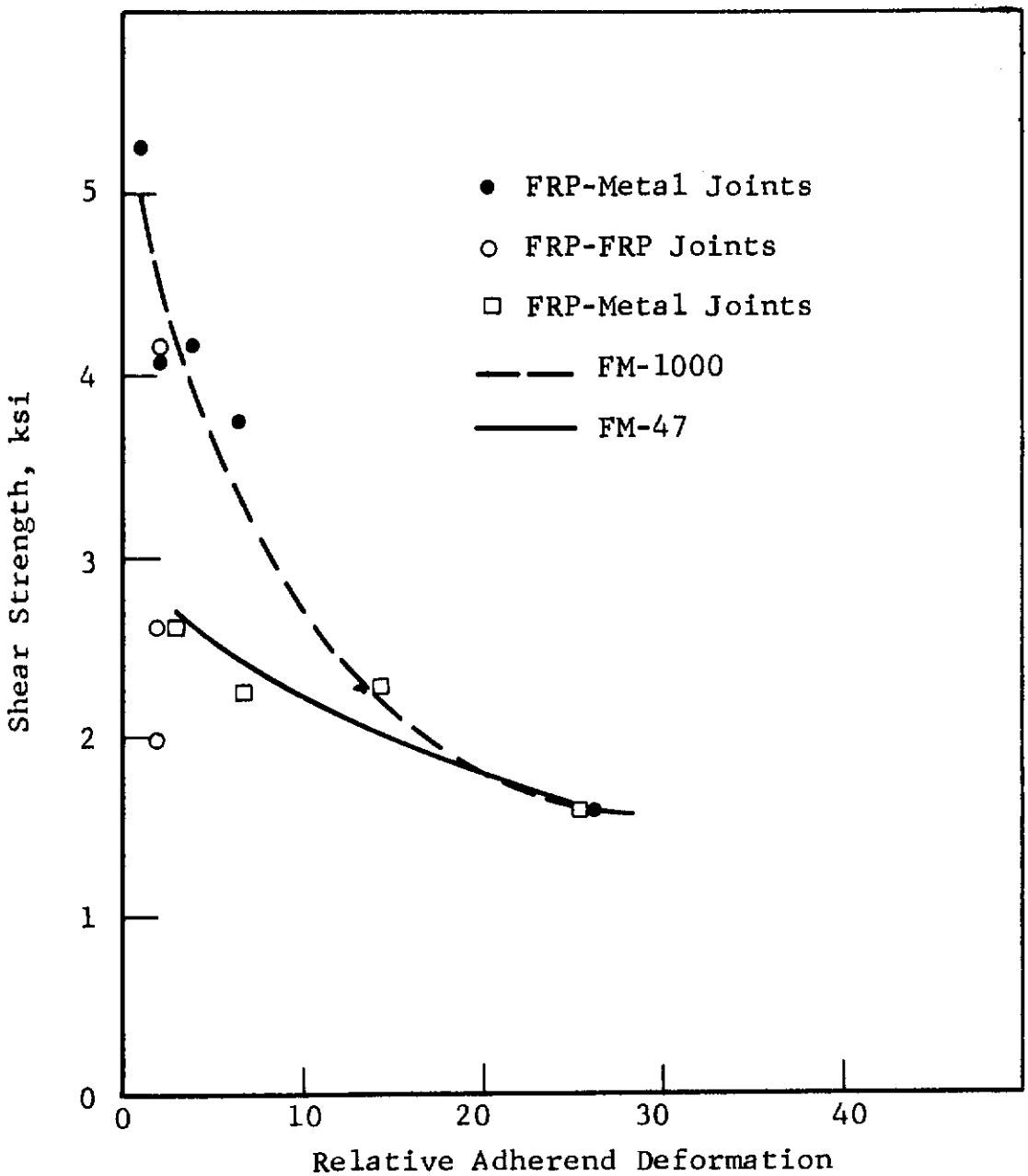

Fig. 5.4 JOINT SHEAR STRENGTH VS RELATIVE ADHEREND DEFORMATION

5.3 CONCLUSIONS

The main conclusion concerning the feasibility of a rational design procedure for bonded joints is that at present there is none available for composite joints. The Volkersen analysis consistently predicted higher stress concentrations than those observed experimentally, and even if the stresses are reduced 25 percent to bring them in line with the finite element analysis, this does not provide sufficient improvement.

The real failing of present analyses is that they do not consider the detailed behavior of the composite adherend. This is the one area where composite joints are markedly different from metal joints. In bonded metal joints shear failure in the adherend near the bonded area is unknown, in the composite joints studied in this program it was a common mode of failure.

It is clearly evident then that successful composite joint design must combine failure criteria and analysis for the composite adherend with failure criteria and analysis with the adhesive. The finite element method provides the analysis technique this must now be supplemented with materials data and failure criteria as input.

At present, the best design technique appears to be the empirical one of developing shear strength-joint parameter data, using this as a guide for gross adhesive selection and overlap design, then building a part and testing it.

6.0 MECHANICS OF BOLTED AND RIVETED JOINTS: SURVEY AND REVIEW

6.1 INTRODUCTION

6.1.1 Purpose

The purpose of this study was to provide a review of the state-of-the-art of riveted and bolted joint design with a specific goal of determining rational joint design procedures for reinforced plastic materials. Where papers dealt specifically with the particular material behavior of other classes of joined materials, such as steel, only the portions which could be applied to reinforced plastic joint design were considered in this review. Only open literature and government reports were reviewed and individual procedures from closed company files or engineering practices were not considered.

Rational joint design implies that a means of analyzing the stresses in the joined plates and in the fasteners is available. To this must be added the requirement for the existence of failure laws for the materials. Because a wide variety of failure laws exist for various orientations of fibrous reinforced plastics, the reader should apply those failure criteria to the analyses for the particular joint application of interest. The literature on failure laws for composites was not reviewed here.

6.1.2 Description of Joint Geometry

It is important at the outset of this review to clearly define the joint geometry and the attendant parameters which might vary for any individual joint. In Fig. 6.1 a single lap joint is shown with a single row of bolts or rivets. In the literature, this type of joint is most frequently referred to simply as a lap joint. Figure 6.2 shows a double lap joint. This type of layout occurs frequently in what is referred to as a butt joint where two plates are joined together by two "cover" or "splice" plates. The combined thickness of the splice plates may be less than, equal to, or greater than the thickness of the "main" plate.

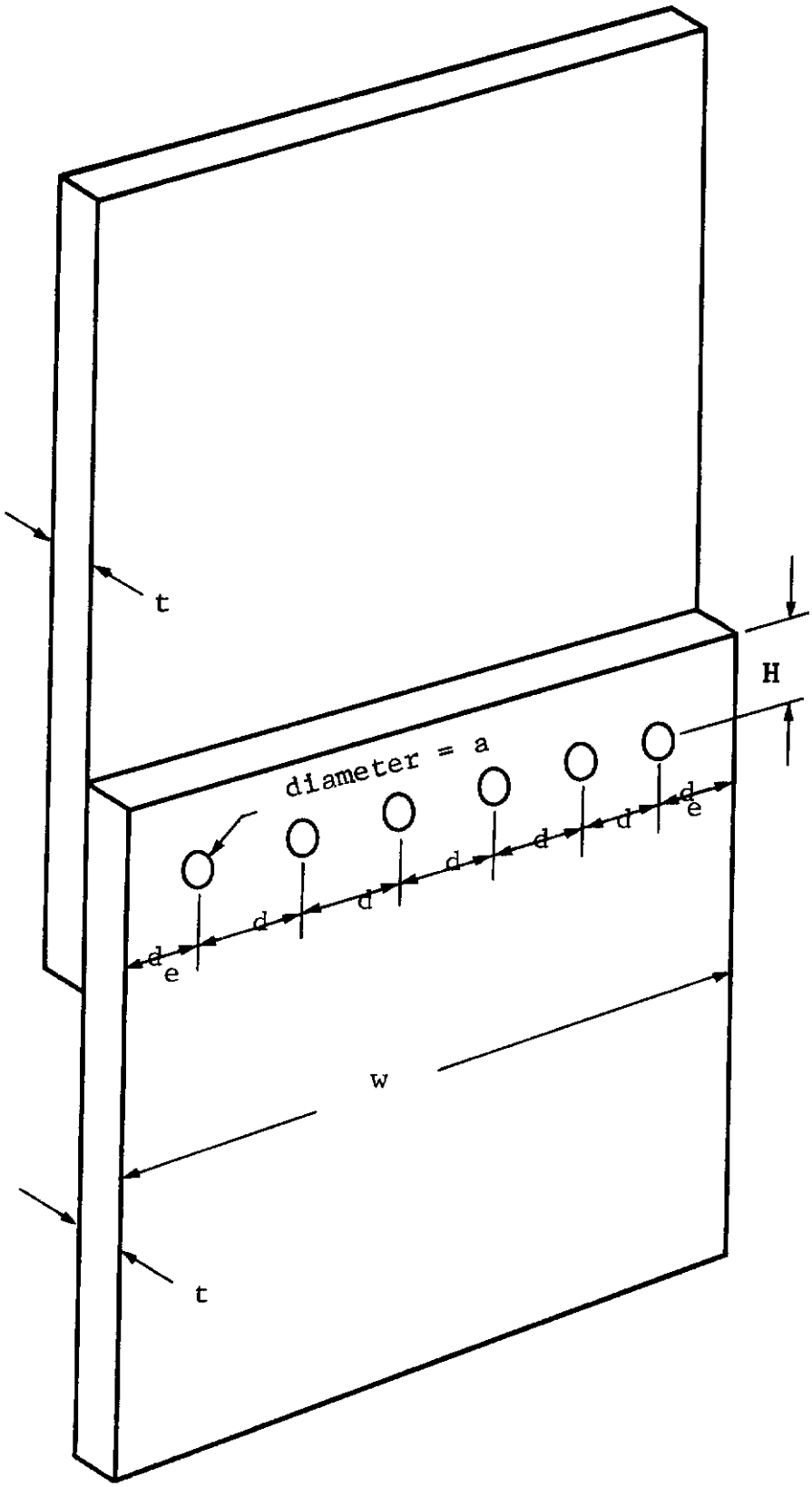

Fig. 6.1 TYPICAL BOLTED OR RIVETED SINGLE-LAP JOINT

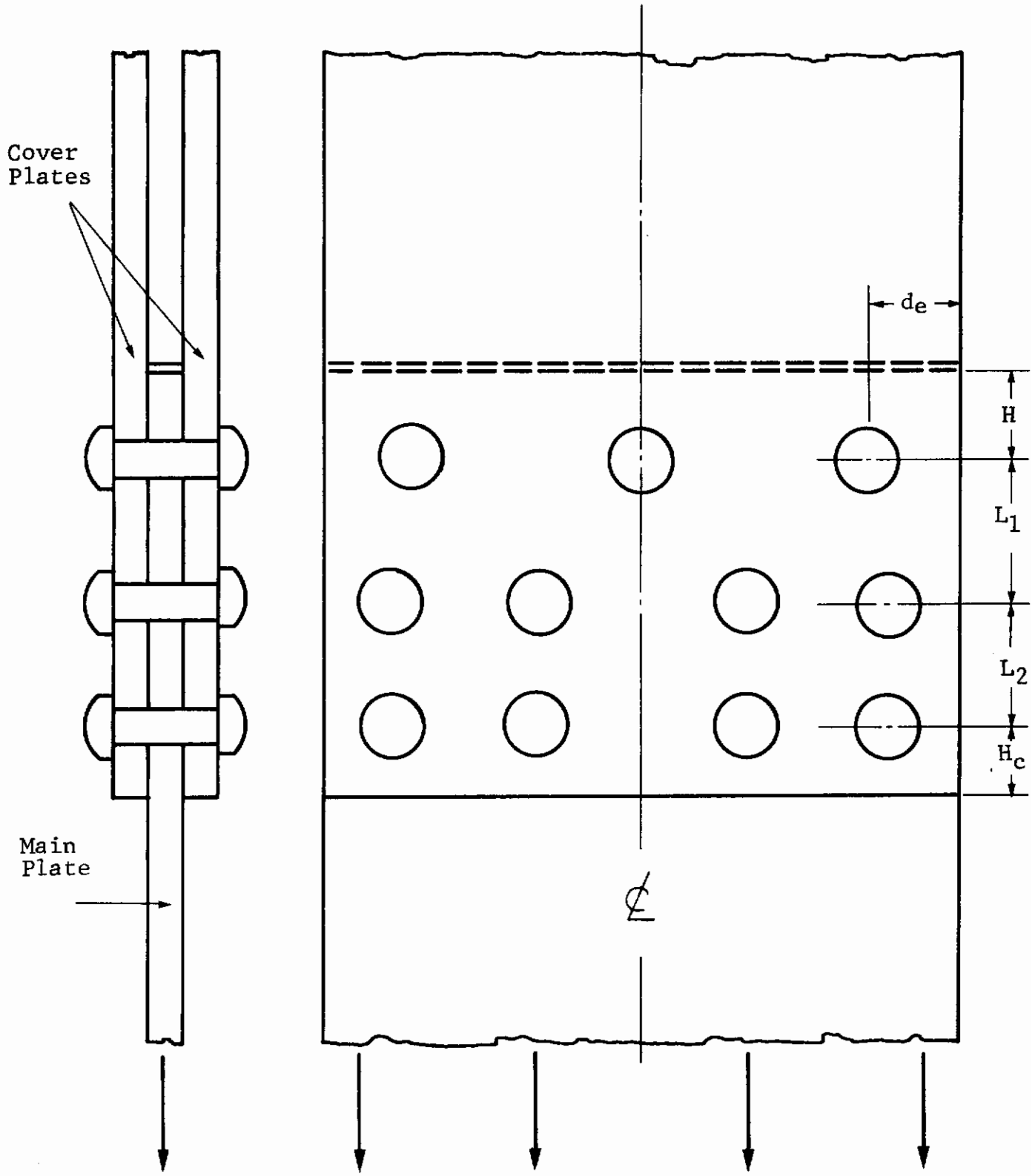

Fig. 6.2 MULTI-ROW RIVETED OR BOLTED JOINT (ROWS 1 AND 2 ARE STAGGERED, ROWS 3 AND 4 ARE IN UNIFORM RECTANGULAR PATTERN)

A group of rivets or bolts arranged in a straight line is termed a row if they are at right angles to load direction and a line if they are parallel to the load direction. Fig. 6.1 illustrates a single row of rivets or bolts. In multiple row joints, the rivets may be "staggered"; i.e., arranged so that the blank spaces in the forward row are backed up by rivets in the second row and the rivets in the forward row are backed up by blank spaces in the second row, or the rivets may appear on a uniform rectangular pattern. Each row of rivets or bolts may have a different number of rivets.

In general, however, most analyses have assumed that for finite width joints, the rows are each symmetric about the centerline of the joint which is coincident with the centerline of the plates in the direction of the loads.

The width of the plates is taken alawys to be w, the pitch of the rivets in any row as d, the rivet or bolt diameter as a, and the distance from the transverse centerline of the first rivet row to the end of the plate as H. Spacing or pitch of the various rows is L_i which occurs between the ith and the (i + 1)th rows.

6.2 STRESS ANALYSIS OF BOLTED AND RIVETED JOINTS

6.2.1 Problems of Theoretical Analysis

6.2.1.1 Fundamental Considerations

The bolted and riveted lap joint structure contains almost all of the problems associated with adhesive lap joints plus several additional complicating factors. In an adhesive joint there is a continuous mechanism of stress distribution along the entire length of the joint, whereas bolted or riveted joints possess discrete points of stress concentration over the surface of the joint. The complexity of both types of joints usually require two dimensionalization in the design procedure but the adhesive joint generally is approached by studying the joint sideways (from the edge) while the bolted or pinned joint is approached from the surface normal to the plane of the joint. This is not to say that the joints are really two-dimensional, but rather that in the opinion of their investigators to date, the simplification of two-dimensional analysis has been along these separate routes. It will become patently clear in this review that while two-dimensionalization of the adhesive joint may be appropriate, the same simplification does not hold true for riveted or bolted joints. It will be clear that the additional problem of stress distribution through the "sheet" thickness must eventually also be investigated for discrete point joints as well. The review of the literature indicated that this level of sophistication, however, is almost completely lacking.

The delineation of the problems associated with an analysis of riveted and bolted joints includes the following major steps:

1. A knowledge of the stress distribution around a single hole due to the load induced by the fastener in the hole.

2. A knowledge of the displacement field around this hole.

3. The stress and displacement interaction of one loaded hole with the stresses and displacements of a neighboring loaded hole.

4. The influence of the mapping of the fasteners on the load distribution to the fasteners.

5. The interaction between fastener parameters (E_f, σ_y, σ_{ult}, etc.,) plate parameters (E_a, t_a, σ_{yield}, σ_{ult}, etc.,) and surface geometry of the joint as well as their interrelationship with general field stresses at infinity since these stresses could also vary along the length of the joint.

The parameters which are generally accepted as contributing to the stress distribution over the joint are:

1. Elastic deformation of the plates and holes.

2. Elastic deformation of the fastener.

3. Plastic deformation, locally, in the vicinity of the hole.

4. Plastic deformation of the fastener.

5. Mechanical slip (friction) between plates.

6. Bending due to unsymmetrical loading in the two planes of the plates.

To attack these problems, investigators cannot simply limit their approach to elastic, isotropic and homogeneous

analyses because load distribution among the discrete fasteners must involve inelastic plate properties.

Most investigators have limited their studies to Item 1 if they attempted to produce mathematically exact stress solutions. Investigators following empirical methods have attempted to combine Steps 1, 2, 3, 4 and 5 to obtain load distributions among fasteners and then have used various means of identifying stress maximums for the most heavily loaded hole in the overall joint. Therein lies an anomaly: having permitted inelastic strains to produce a given load distribution, a return to elastic deformation theory to obtain the stresses around individual holes is no longer acceptable and most available analyses are inaccurate in the inelastic zone. Indeed, most joint designers rely on some plasticity around the initially highly loaded holes to permit the initially lower loaded holes to assume greater loads and thus "work" all the fasteners equally hard. On the surface it would appear that under fatigue or repeated loading conditions such a philosophy would be unacceptable. It is also known that the damping characteristics of this class of discrete point fasteners has been of considerable assistance in moderating high cyclic stresses at the joint because of an other nonlinear phenomenom, "slip", thus leading to an attenuation of the stresses across the joint.

6.2.1.2 General Approaches

The objectives of a rational analysis of a joint are to determine:

1. The ultimate strength of the joint.
2. The load-deformation characteristics of the joint.

While it is generally acknowledged that the ultimate strength of the joint may be predicted within a few percent, an accurate prediction of the load-deformation characteristics of the joint

is less reliable. The following discussion was gained principally from the summary of behavior given by Schenker (6.58).

Examination of a typical joint such as is shown in Fig. 6.3 will illustrate the fundamental parameters and behavior of joints. The joint illustrated is a double lap joint with two rows. Moving from left to right, the load is transferred out of the inner plate to the outer plates. Row 1 total force removal is R_1 and load removed by Row 2 is R_2. From statics we have

$$R_1 + R_2 = P$$

Since the joint is symmetrical, the solution is trivial and $R_1 = R_2$. Thus the load carried by the inner plate is reduced from P to P/2 at 0, the first row.

Deformations relative to 0 are shown in Fig. 6.3c. AD represents the deformation of the inner plate relative to 0. ABE represents the deformation of the outer plates relative to 0. The difference

$$\delta_i - \delta_o$$

represents the slip between the inner and outer plates at any point. In the case shown the slip is constant and equal to the relative movement between plates at the first row. The elongation between Rows 1 and 2 is given by CE, which is the sum of the slip AB and the stretch of the plates CD. Ignoring local hole deformations, the elastic deformation CD is given by

$$CD = PL_1/2wtE$$

where

E = modulus of elasticity of the plate.

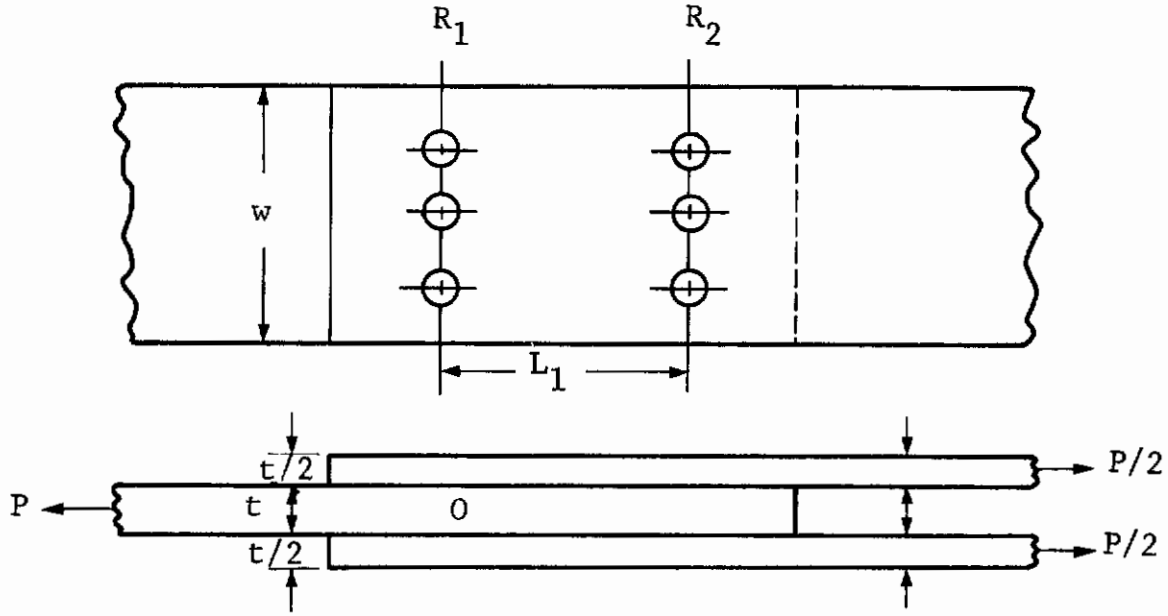

(a) Joint

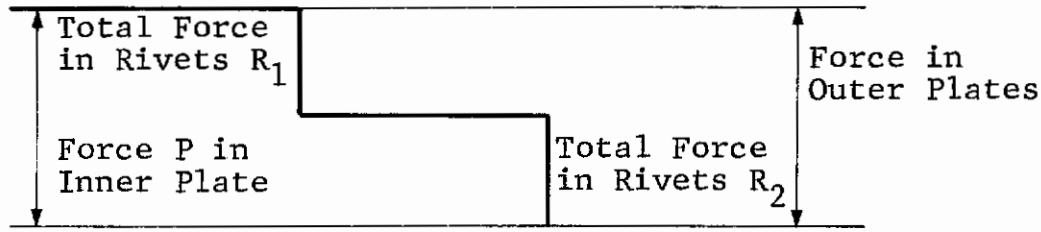

(b) Forces

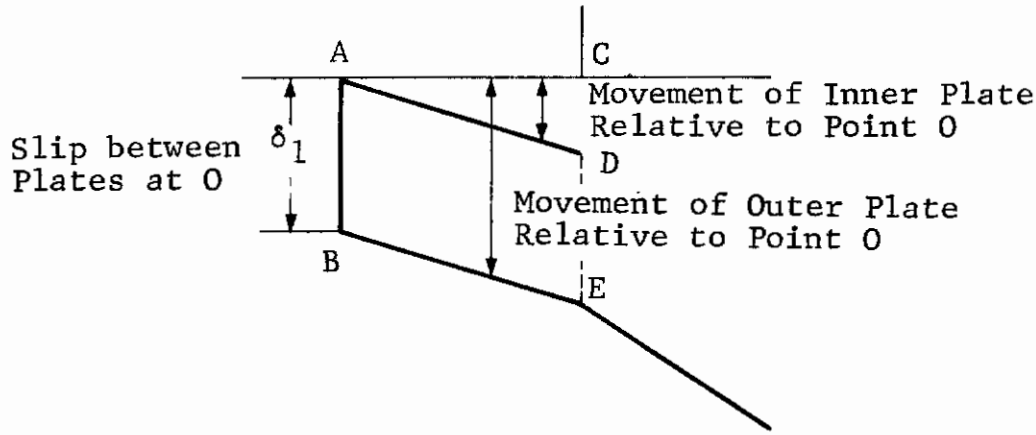

(c) Deformation

Fig. 6.3 GEOMETRY, FORCE DISTRIBUTION, AND DEFORMATION OF TYPICAL JOINT, AFTER SCHENKER (6.58)

The total deformation of the joint in the elastic range is at least

$$\delta_1 = PL_1/2wtE$$

but may exceed this amount if "slop" on hole clearance is present in the rivet holes, or other complications occur. Most authors include various specialized conditions which lead to deformations greater than this absolute minimum. The importance of δ_1 may be adjudged from the fact that it includes clearance take up, rivet deformations, and local plate deformations around the rivet due to bearing of the rivet on the plate.

In a two row joint the stresses may be considered statically determinate and thus the deformations δ_1 may be experimentally determined. An average load per rivet, P/n, then may be plotted against δ_1. This gives rise to various possibilities, as described by Schenker (6.58) and Wilson (6.74) shown in Fig. 6.4, where a modulus, H, for the P/n-slip curves may be established in the linear elastic regime. H is generally smaller for larger grip/diameter ratios because larger rivets have a reduced stiffness and larger clearance. Local plate deformation is a very significant factor, as is rivet deformation. The effect of grip length on H is also significant. Joints of the single lap type appear to give smaller values of H than do double-lap joints.

Rivet yielding is generally based on the assumption of an elastic-perfectly plastic rivet material behavior. For a joint with 2r identical rivet rows and an elastic-perfectly plastic rivet material, the outer rivet inelastic deformation must be

$$r(r-1)R_yL/EA$$

where R_y = yield load of one rivet row if all rivets are to assume equal loads. As the plates begin to deform inelastically,

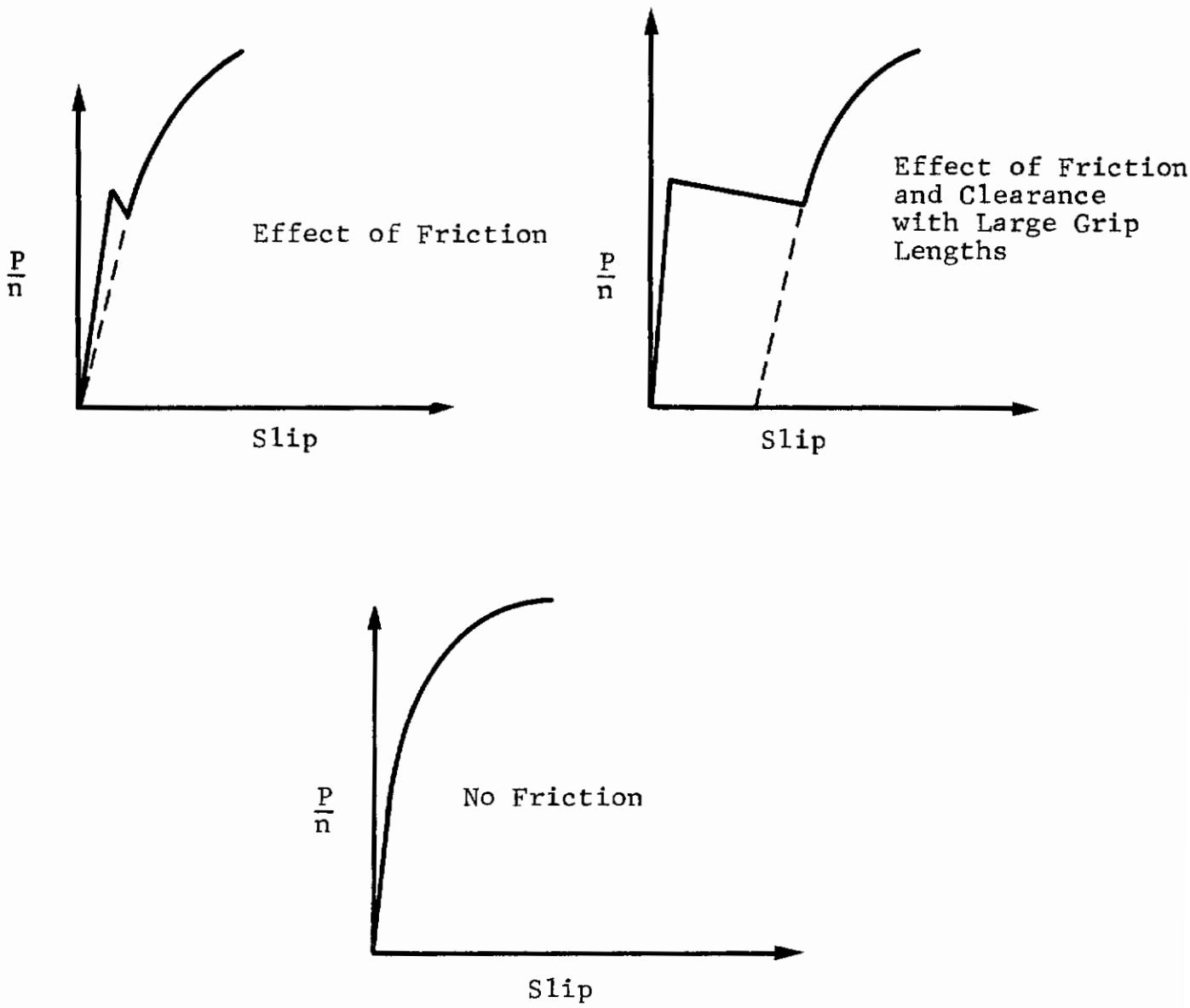

Fig. 6.4 LOAD-DEFORMATION BEHAVIOR OF JOINTS

the plate modulus, E, decreases and $R_y L/EA$ increases. A relationship for an inelastic load-end slip can be determined experimentally from a two row joint similar to the determination of H and used as a constant for multi-row joints. This leads to the empirical type behavior described in Section 6.3 or provides constants for the analytical processes described in many of the papers in this Section.

Plate deformations already described in this section for the case of no friction can also include gradual load transfer when friction is present as it almost always is. Figure 6.5b (for a two row joint) shows this friction type load transfer. The load transfer across the plate-friction zone is gradual rather than steep through the rivet zone. Slip, which takes place at the end of the joint, occurs immediately as represented by AB and DE. When the static friction is finally overcome, relative slip may take place at the center of the joint. Until then, however, the movements of the inner and outer plates at the center must coincide; i.e., be in contact. However, once slip has occurred, the movements digress from each other as shown in Fig. 6.5d. Total joint elongation is given by

$$\Delta = \delta_1 + PL/2wtE$$

in the elastic range.

After sufficient slip, there is a sharing of the load transfer between friction and rivet shear. The load transfer then again assumes some steep (vertical) position as in Fig. 6.3 and the deformations assume the previous appearance (see Fig. 6.3).

For multi-row joints total elongation, Δ, must be determined from statically indeterminate analyses. The load assumed by each row is not constant and inelasticity complicates the matter severely.

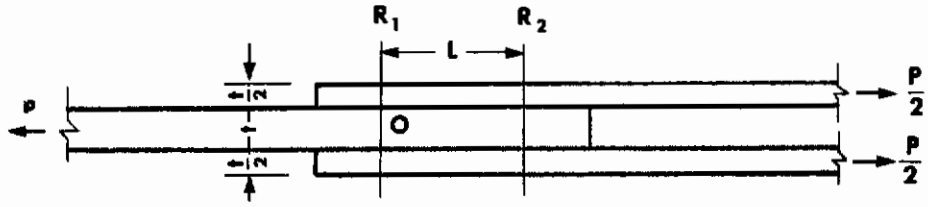

(a) Tension Connection

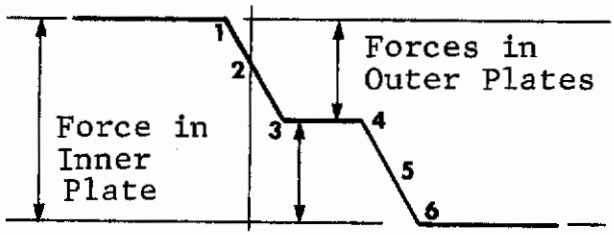

b) Forces Transferred by Friction

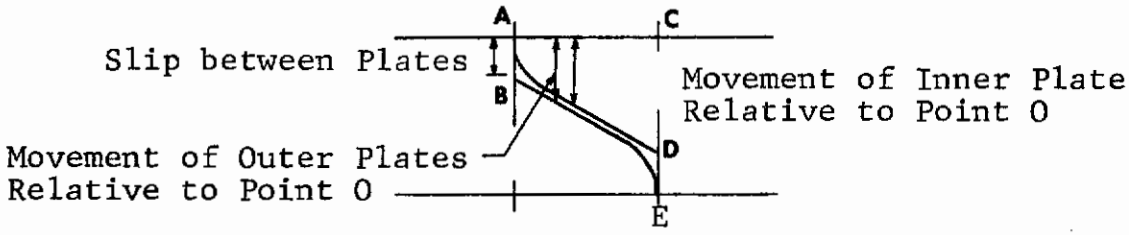

(c) Deformation before Static Friction is Overcome

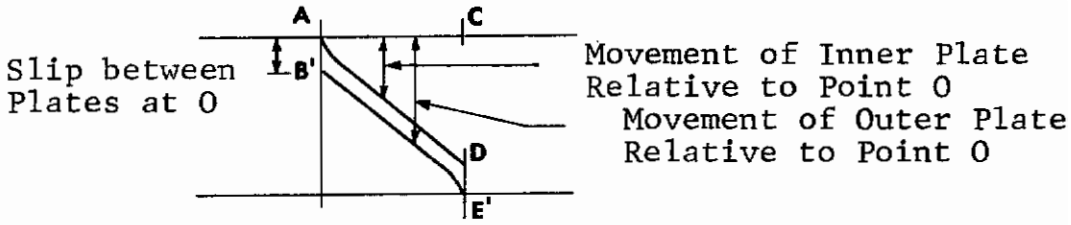

(d) Deformation after Static Friction is Overcome

Fig. 6.5 LOAD TRANSFER AND JOINT DEFORMATION WITH FRICTION BETWEEN PLATES, AFTER SCHENKER (6.58)

The joint total elongation (see Fig. 6.6) in the elastic range is given by

$$\Delta = \sigma_1 + \frac{mPL}{2wtE}$$

where m is the number of spaces between rows. As demonstrated by Schenker and is independent of friction or load distribution in the rivets. This expression can be modified to account for the presence of holes (which reduce the cross-sectional area). Two offsetting effects occur simultaneously: (1) The presence of holes should increase the total deformation and (2) The rivet heads bridge the holes and thus decrease the effect of the holes reducing the plate width. A modified expression is thus possible of the form

$$\Delta = \sigma_1 \, r\frac{kmPL}{2EA_g}$$

where k = constant

A_g = Gross Area of Section

Inelastic joint deformations as approached by Koegler and Schnitt (6.38) involve "equivalent plate" dimensions to account for the hole local deformations. Others have utilized various experimentally determined constants to establish inelastic joint parameters.

Joint efficiences, η_G, for both yield strength and ultimate strength are of importance to the joint designer. Several relationships for the joint efficiency, η_G, have been proposed. Let the strength of the plate material be given by σ_{ult} and the average gross section stress at joint failure be $\sigma_{G,ult}$; then η_G is defined as $\sigma_{G,ult}/\sigma_{ult}$. Schutz (6.61) has proposed the "Relative Gage Method" relationship for drilled plates as:

$$\left[68 + S\,\frac{w}{a}\right] \left[1 - \frac{a}{w}^2\right] \quad \% = \eta_G \leq 87\%$$

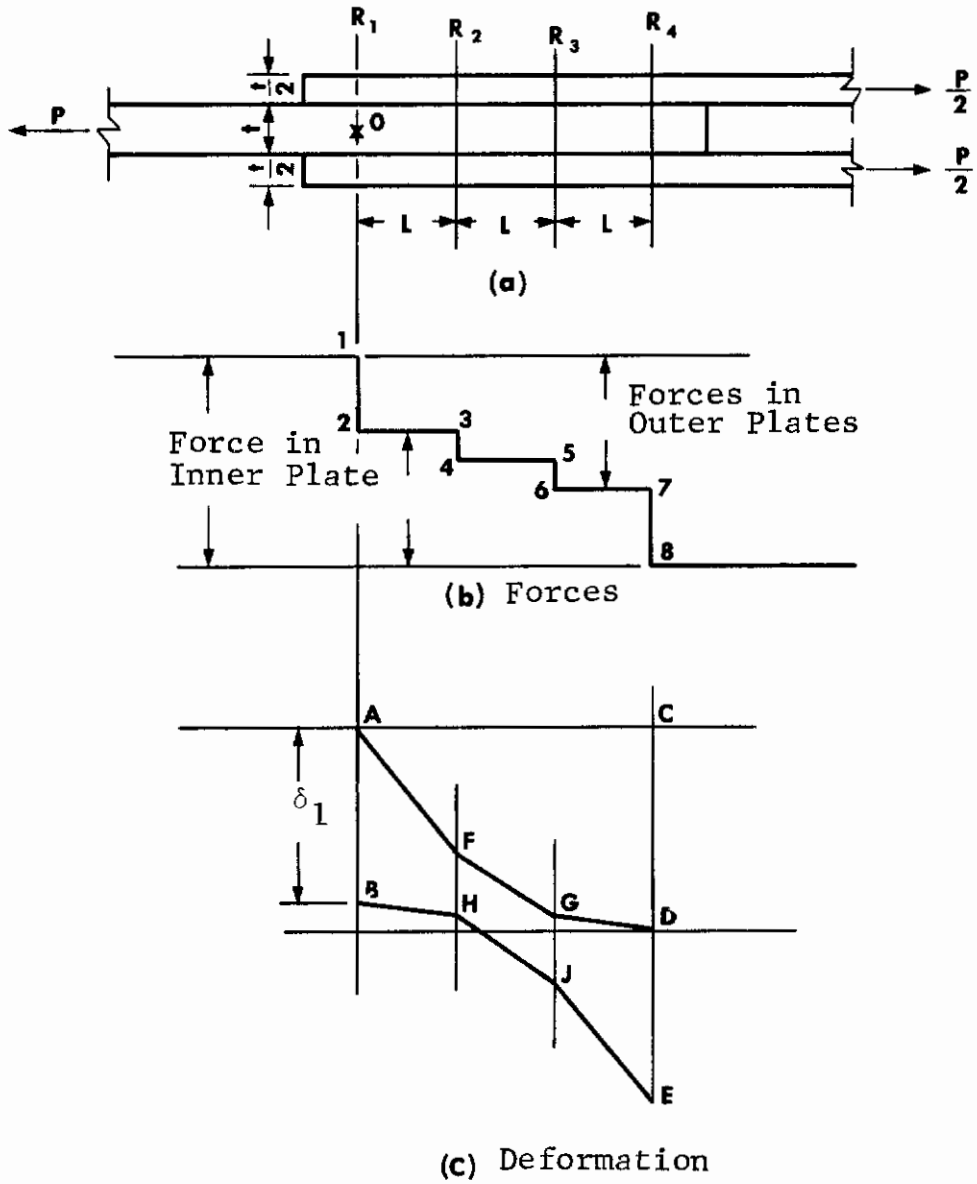

Fig. 6.6 MULTI-ROW JOINT LOAD TRANSFER AND DEFORMATION, AFTER SCHENKER (6.58)

The AREA method gives

$$\eta_G = \left[1 - \frac{a}{w}\right] \left[100\right] \%$$

Problems in the analysis were discussed earlier. (See Section 6.2.2. Problems in the experimental analysis are discussed in Section II B. The remaining sections cover the various analyses, assumptions and ranges of coverage given by the various authors, whose individual papers are discussed in the annotated bibliographies. It is most probable that the composite joint designer will have to use both experimental and analytical results to define his assumptions; thus, a careful review of this literature, particularly that of Vogt (6.71) will give, it is hoped, appropriate means to do so.

6.2.2 Problems of Experimental Analysis

The most commonly employed experimental method of studying the stress distribution in bolted or riveted joint is the method of photoelasticity. The method employs models made of a birefringent plastic. The differences between the large deformations in a plastic material and the smaller deformations in a metal or composite are readily evident. Furthermore, photoelasticity implies that the behavior is represented only within the elastic region for the material. Inelastic stress analyses are not easily performed using photoelasticity since scaling of the material properties is difficult to achieve. The more recent technique of photoelastic coatings has been applied to bolted joint analysis by some individuals but the cases are rare in the literature to date. The older work was performed largely as a substantiation of analytical procedures and is primarily based on the use of electrical resistance strain gages.

6.2.3 Elastic Behavior

Several of the analyses made followed the assumption of linear elastic theory. Where feasible, the generalized three-dimensional state of stress was reduced to an engineering strength

of materials approach and the employment of minimum energy principles was made. Idealized models set up under those conditions also called for special assumptions to resolve the special problems attacked by individual authors. Much of the experimental work also required the assumption of elastic behavior. Those assumptions are delineated in the annotated bibliographies which follow.

6.2.4 Inelastic Problems

In both the analysis and experimental papers a heavy concentration of effort on elastic (and linear) behavior was evident. However, almost all authors agreed that the inelastic mechanisms were equally, if not more, important in the study of the behavior of joints. Most authors assumed sufficient plasticity occurred even at early stages in the deformation to permit load distribution in accordance with the condition of localized yielding at the bolt or riveted holes.

For bolted or riveted joints another phenomenom is also possible; i.e., the mechanism of slip of the rivets or bolts. Most bolts are produced with diameters slightly smaller that the holes in which they are inserted. Then the bolt heads bear against the surfaces of the plates which are being joined and the relative positions of the bolts are largely determined by the friction between plates and bolts. This mechanism is, however, subject to instantaneous and permanent change during the course of loading. The deformation of "slip" then must be added to deformations arising from distortion to yield the total deformation in the load-displacement diagram.

Finally, the process of residual deformation can be utilized to improve fatigue life where a residual compressive state (due to interference fit bolts) added to a cyclic joint tensile load results in a shift in the nature of the S-N curve (i.e., a shift in the R ratio). This phenomenom manifests itself in a distinctly nonlinear load-deformation curve even in the elastic or recoverable region.

A combination of these three mechanisms may be present in any joint and it is the incorporation of the appropriate expressions of this nonlinear behavior into joint behavioral equations which permits closer and closer agreement between theory and experiment.

6.2.5 Stress Distribution around Individual Bolt Holes

The behavior of large joints with multiple fasteners depends to a large extent on the mechanical behavior of individually loaded fastener-hole systems. Indeed, the deformation component δ_1 is critically dependent on this parameter. The elastic state of stress around a hole has been studied analytically by Bickley (6.6), Knight (6.37), Theocaris (6.70), and Chi and Irwin (6.11) and experimentally by Coker and Scoble (6.12), Hennig (6.27), Frocht and Hill (6.23), Jessop (6.39, 6.40). A summary of work on elastic stress concentration factors around holes appears in a paper by Cox (6.13). Plastic deformation around individual holes was treated analytically by Koegler and Schnitt (6.38), and for creep deformations analytically by Marin (6.46). Experimentally plastic deformations around individual holes has been treated by Bodine (6.7), Mead (6.47), and by Lambert and Snell (6.41).

6.2.6 Distribution of Load among Several Fasteners

The distribution of load among several fasteners in a joint is statically indeterminate problem. Here the problem is to identify individual fastener loadings so as to identify the most heavily loaded fastener. Elastic theories are postulated by Batho (6.4), Hovgaard (6.30), Tate and Rosenfield (6.38), Vogt (6.71), Rosenfield (6.54), Muckle (6.50), Budiansky (6.3), Deneff (6.17), Lobbett and Robb (6.45), Switsky, Forray, and Newman (6.67) and Owen (6.52). Experimentally some work was performed by Bollenrath (6.8). Analytical work which incorporated plastic deformation into the analysis was performed by

Koegler and Schnitt (6.38), and an excellent work by Vogt (6.71). Other work included that by Deneff (6.17) and Fischer and Rumpf (6.21).

The problem of "slop" in the fasteners was treated by Batho (6.3), Switsky (6.67), and Fischer and Rumpf (6.21).

6.2.7 Annotated Bibliography: Theoretical Analyses

Batho, C. (6.3)

"The Partition of Load In Riveted Joints," J. Franklin Institute, v 182, Nov. 1916, pp. 553-604.

This paper describes a method of load partitioning among rivets in a joint. The analysis is based on the principle of least work. Batho assumes that the stresses between rivet rows is uniform. The work stored in the rivets themselves is assumed proportional to the square of the load (spring); therefore, the system must be linearly elastic.

The first joint type studied by Batho is a single line of rivets in a double lap joint. Batho obtains a set of linear simultaneous equations in the bolt load unknowns, R_1, R_2, etc. Batho shows that the load proportion on the first rivet in the line is as shown in Fig. 6.7.

Batho then analyzed the case where a nonuniform distribution of stress exists between any two rows of rivets. He next attacked the problem of the unequal load partitioning among the two cover plates in the double lap joint. Other problems attacked included:

1. The main plate (center plate) and two cover plates having different moduli of elasticity.
2. A variable width center plate in the double lap joint.
3. Multiple rivets in each row and different numbers of rivets in each row.

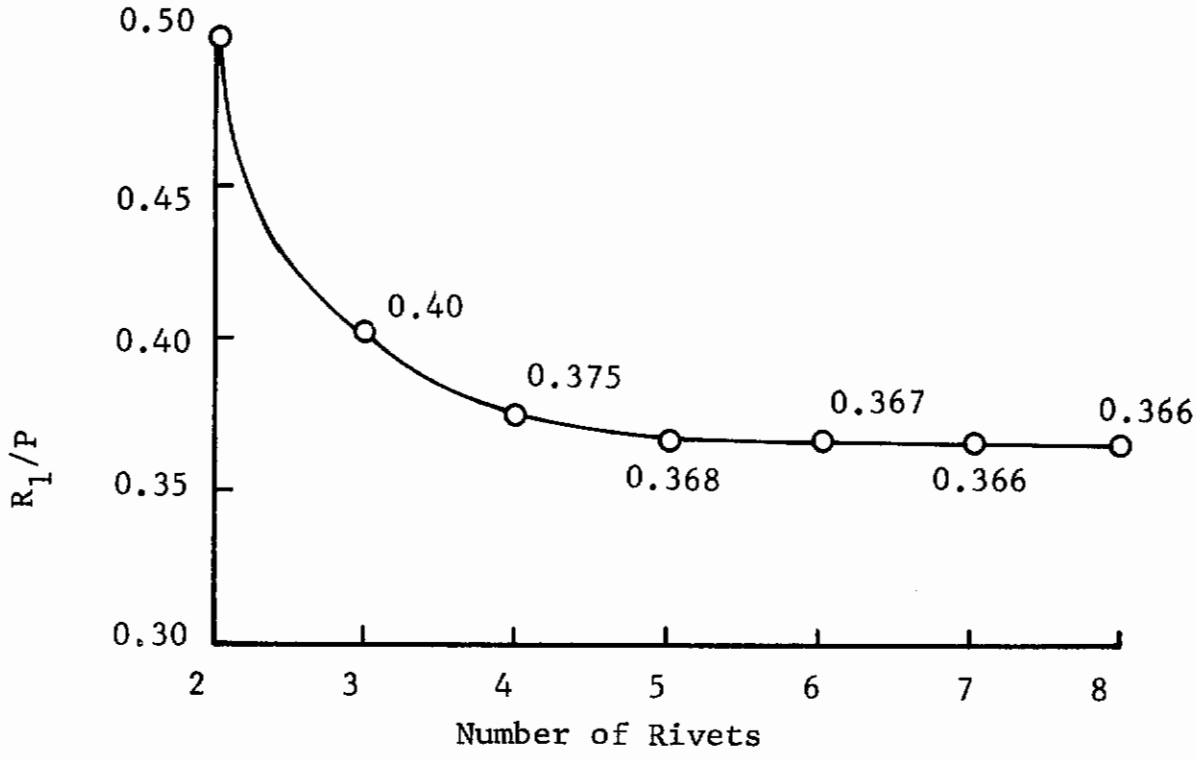

Fig. 6.7 MAXIMUM LOAD (ON FIRST RIVET) AS A FUNCTION OF THE NUMBER OF RIVETS, AFTER BATHO (6.3)

4. Joints with rivets of different sizes so that the rivet constants of proportionality are different.

5. Single Lap Joints.

Batho then manufactured and tested several steel joints to evaluate his analysis. The experimental methods were very primitive using mirror extensometers. The results agreed well with the theory up to the elastic limit of the material.

Bickley, W. (6.6)

"The Distributions of Stress Round a Circular Hole in a Plate," Phil. Trans. Roy. Soc., (London) Vol 227A, 1928, pp. 383

Bickley first turned his attention to solving the problem of the stress distributions around holes in tension members where the load was applied to the circular boundary. His interest had been stimulated by Coker's initial work in (Ref. 6.12).

Bickley attacked the problem of determining a general solution using the Airy Stress Function for the loaded circular hole in an infinite plate and applies the general solution to several special cases of loads applied to the boundary of the hole. These solutions are those which Bickley ascribes to the various conditions of a rivet on a hole in the plate, namely a normal pressure varying as cos θ over the internal circular boundary of an otherwise infinite plate. Bickley also finds the general solution for the stresses in the plate due to any force system acting on the periphery of the hole. Included are:

1. Single concentrated force.

2. Uniform radial pressure along an arc.

3. Normal pressure proportional to cos θ=acting over half the boundary.

4. Stresses around a hole due to an undersized rivet bearing on the hole

$$p = \sqrt{1 - \theta^2/\alpha^2}$$

where

$$|\theta| < \alpha$$

5. Friction on rivet producing tangential tractions of the magnitude $\sin^3 \theta \cos \theta$.

The importance of these solutions can be adjudged when it is realized that most subsequent analytical efforts for rivet type problems drew heavily on Bickley's solution. The individual solutions require the solution of additional problems which account for finite boundaries to produce useful solutions to commonly encountered rivet-load situations.

The general Bickley stresses for a loaded circular boundary are too long to be reproduced here, but a summary of the solutions (1 through 5 above) are shown in Fig. 6.8.

Howland, R.C.J. (6.32)

"On Stresses in Flat Plates Containing Rivet Holes," Proc. 3rd Int. Congr. Appl. Mech., 1930, Vol II, pp. 74

Howland obtains the generalized plane stress solution for stresses around a hole in a finite width plate loaded by a rivet-like distribution of force varying as the cos θ. See Bickley (Ref. 6.6). The hole diameter to plate width ratio is a/w = 0.5. Using a converging approximation (each successive approximation introducing residual tractions) alternately on the interior and external boundaries, Howland finds the stresses σ_{rr}, $\tau_{r\theta}$, $\sigma_{\theta\theta}$ at the rim of the hole to be given as shown in Table 6.1.

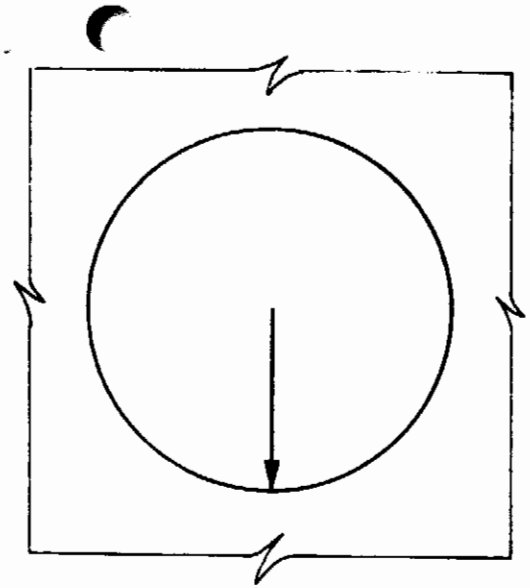

a) Single Concentrated Force

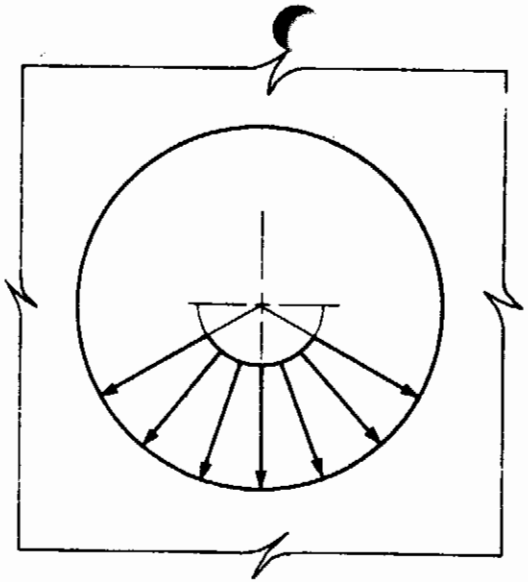

b) Uniform Normal Pressure over Arc

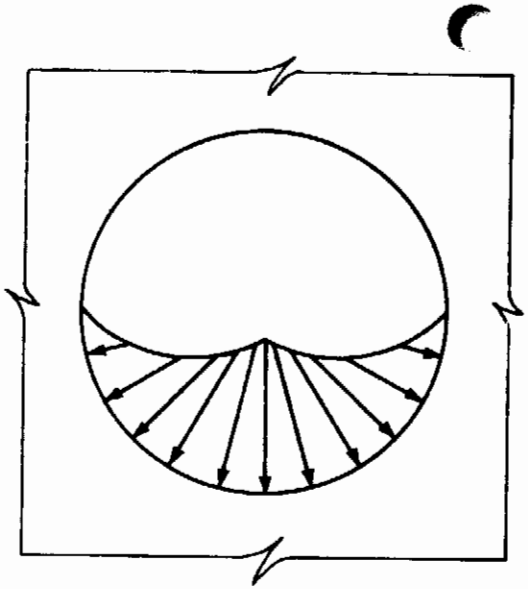

c) Normal Force Varying as Cosine over Half Circumference

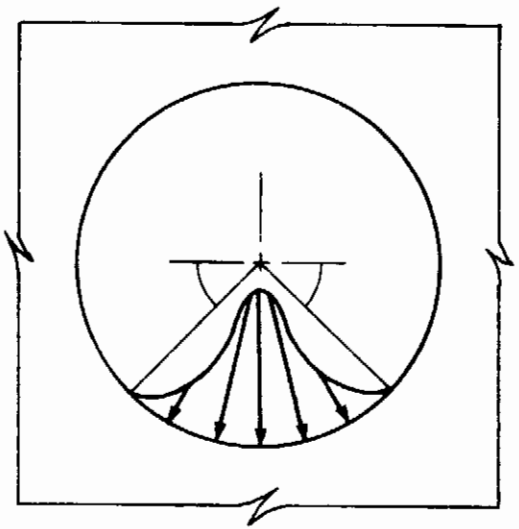

d) Stress around Hole Due to Undersized Rivet

$p = 1-\theta^2/\alpha^2$

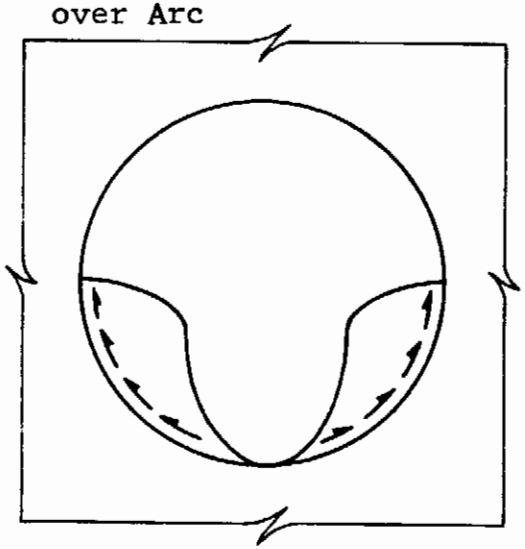

e) Stresses Due to Friction

Shear Traction = $\sin^3 \theta \cos \theta$

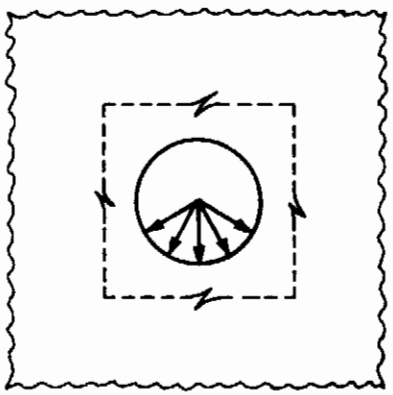

General Infinite Sheet

Fig. 6.8 RIVET SOLUTIONS OBTAINED IN SERIES FORM BY BICKLEY((6.6) FOR LOADED HOLES IN INFINITE SHEET

Table 6.1

STRESS PRODUCED AT THE RIM OF A HOLE FOR a/w = 0.5
PULLED WITH A FORCE P IN THE DIRECTION θ = 90°

θ (deg)	$\frac{\sigma_{rr}}{\sigma_m}$	$\frac{\tau_{r\theta}}{\sigma_m}$	$\frac{\sigma_{\theta\theta}}{\sigma_m}$
-90	-	-	-2.61
-75	-	-	-1.35
-60	-	-	-0.31
-45	-	-	0.92
-30	-	-	2.88
-15	-	-	4.45
0	0	-0.24	5.54
15	-0.40	-0.29	4.43
30	-0.87	-0.38	2.92
45	-1.38	-0.43	1.12
60	-1.85	-0.38	0.07
75	-2.17	-0.22	-0.83
90	-2.28	0	-2.05

It is thus seen that the maximum tensile stress occurs at $\theta = 90°$ and is 5.52 times the gross section tensile stress $\sigma_m = P/wt$. If the gross section shear stress τ_m is given by

$$\tau_m = \frac{\sigma_1 - \sigma_2}{2} = \frac{P}{2wt}$$

Then $\tau_{r\theta} = -0.86$ appears to be the maximum shear at the rim of the hole and this occurs at $\theta = 45°$. The maximum compressive stress at the rim of the hole is given by:

$$\sigma_{\theta,max} = -2.28\ \sigma_m$$

Batho, C. (6.4)

"Experimental and Theoretical Investigations on Riveted and Bolted Joints, with the Application of the Theory to Welded Joints," First Report of the Steel Structures Research Committee (London, H.M.S.O.) 1931, pp. 100-179.

Since a riveted joint is a form of a statically indeterminate structure, if all components obey Hooke's Law, the stresses will be distributed in accordance with the principle of least work from Castigliano's Theorem. This paper uses this principle to produce an analytical method for partitioning load in an overall riveted joint to first the rows of rivets and secondly, individual rivets in each row. The form of the equations purportedly is simplified from a previous paper. In addition, Batho also attempts to find the optimum solution; i.e., uniform load partition over all the rivets. In this particular paper, the solution is also extended to the case of a welded joint. Finally, the results of experiments performed years earlier by the author and several other individuals, as well as some planned specifically for the purpose of proving the theory, are used as a criterion of test for this load partitioning theory.

Batho first attacked the problem of a double lap butt joint with the combined thickness of the two cover plates equal to that of the center plate. The center plate is of uniform thickness while cover plates are of uniform or variable width and thickness; there are any number of rivets in a row. (See Fig. 6.9.)

The partitioning of load among the rows is accomplished by making the following assumptions:

1. Each rivet in the row takes the same proportion of the load.
2. The plate sections between the rows carry a uniform load distribution across the section.
3. The parts of the plate cut out by the rivet holes are neglected.

The results are in the form of a set of linear equations in the unknown loads X_1, X_2, etc. The first is of the form:

$$\left[(n-1)+\sum_{1}^{n-1}\alpha+\left(\frac{1}{m_1}+\frac{1}{m_n}\right)\frac{Ak}{L}\right]X_1+$$

$$\left[(n-2)+\sum_{2}^{n-1}\alpha+\frac{Ak}{m_nL}\right]X_2+\ldots.=\left[(n-1+\frac{Ak}{Lm_n}\right]P$$

Where $\alpha_1=\eta_1\frac{A_1}{A_1}$, etc. and $\sum\alpha=\alpha_1+\alpha_2\ldots.$

here η_1 = ratio of the strain energy in the cover plate between the first and second rivet rows to the strain energy in a plate of the same length, of uniform cross-section $A1_1/2$, at a given load η_2 = ...

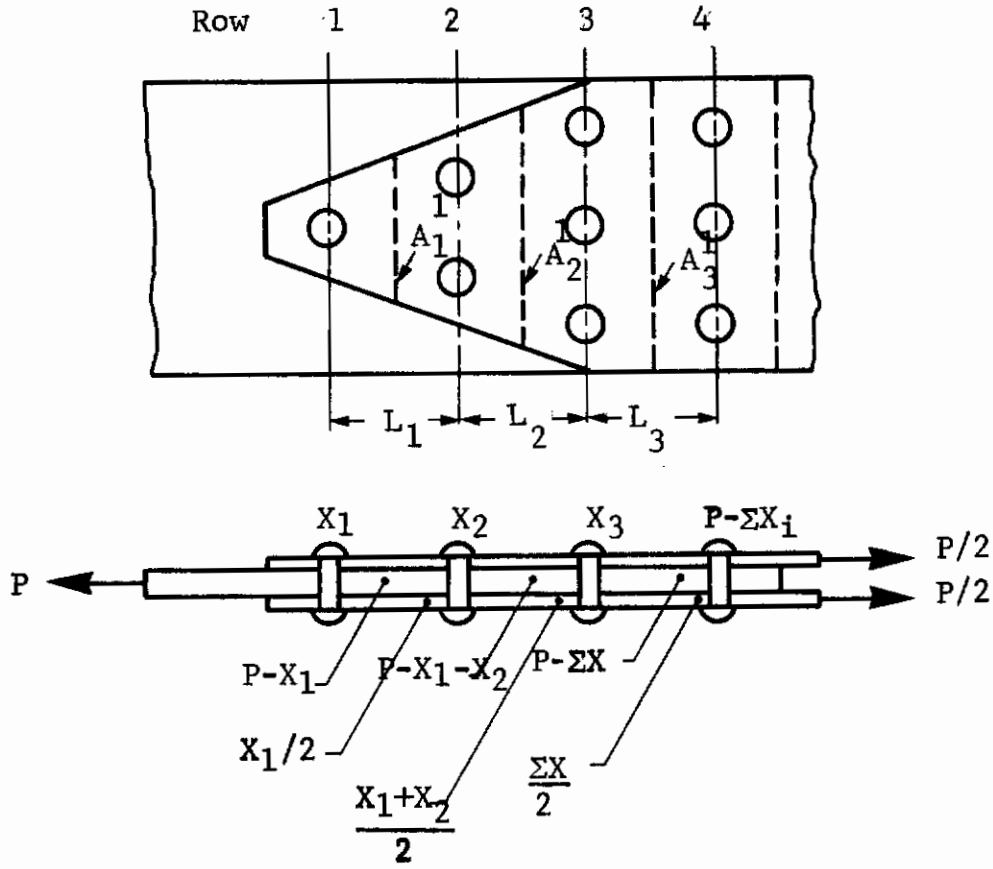

P	=	load on joint
n	=	number of rows of rivets
m_1	=	number of rivets in first row
m_2	=	number of rivets in second row, etc.
m_n	=	number of rivets in last row
L_i	=	pitch of rows
A_1	=	area of cross-section of middle plate
$A_1/2$	=	mean area of cross-section of cover plate between first and second rows of rivets, etc.
X_1	=	load transferred by first row of rivets, etc.

Fig. 6.9 DOUBLE LAP MULTI-RIVET BUTT JOINT STUDIED BY BATHO (6.4)

The author also gives the other equations in tabular form but the reader is referred to the original paper. There are therefore n-1 equations for the n-1 inknown forces X_1, etc.

Batho discusses several important subcases:

1. Completely flexible rivets.

   Here $\frac{Ak}{L} = \infty$

2. Completely rigid rivets.

   Here $\frac{Ak}{L} = 0$

For the first case $Ak/L = \infty$, all terms in the equations vanish in comparison to the terms carrying Ak/L. This yields load transfer to a rivet row in proportion to the number of rivets in the row. If all rows have the same number of rivets, each row gets an equal amount of load. (This is in substantial agreement with many of the empirical and conventional assumptions.)

For the second case, $Ak/L = 0$, the solution becomes independent of the number of rivets in each row and indeed only the first and last rows carry the load for the special case where the cover plates are of uniform section throughout. If the cover plates are of exactly one-half the thickness of the middle plate each, then the first and last rows of rivets carry equal load between them. If the cover plates are of greater cross section, then the first row carries more load than the last. If the cover plates are of smaller cross section, the last row carries more load than the first.

Batho also solves as a special case the geometry of the splice plates required to equally partition the load among the rivets. Another special case is a joint having cover plates of uniform cross section and only one row of rivets.

To confirm the theory, Batho conducted several experiments on riveted joints. Load partition to a row of rivets was determined by measuring the strains across a section between two successive rows of rivets and calculating total stress

transmitted. Row by row the agreement with his theory was substantially excellent (the error varying from 0.19 to 2.62 percent from the theory). The partition of load among individual rivets in a row was also in fairly close agreement with the theory. The theory is primarily applied to the symmetrical case (double overlap joint).

Experiments were also carried out with splice plate double overlap joints using both riveted and bolted joints in steel plates (four rows of rivets varying from 1 to 3 rivets per row were involved). The experiments, although extremely limited in scope, were copiously studied at several load levels and much behavioral type information was obtained.

Several parameters were also introduced which appear to have significant influence on the load carrying capacity of joints but which have not been investigated by subsequent investigators. These include friction between plates, cover plate sizing, load deformation curves for a given rivet in an overall joint, slip between rivets in joints, etc., etc.

The experiments on the bolted joints in particular, pointed up a problem (that of slip) which is not encountered in riveted joints. In Fig. 6.10, a comparison of the deformation load curves for riveted and bolted joints are shown. There is always a loop formed in riveted joints which represents some storage of energy during loadings subsequent to the first. If no loop were present then the value of Ak/L would remain constant from loading to loading and the action of the rivet would follow Hooke's Law exactly; i.e., work = kx^2. The actual work stored is proportional to the shaded area in Fig. 6.10 and as can be seen since the loop for bolted specimens is wider than for riveted specimens. The value Ak/L will increase at a faster rate for bolted specimens than for riveted specimens.

Finally, Batho conducted a large number of slip experiments on bolted specimens, to determine load redistribution with slip.

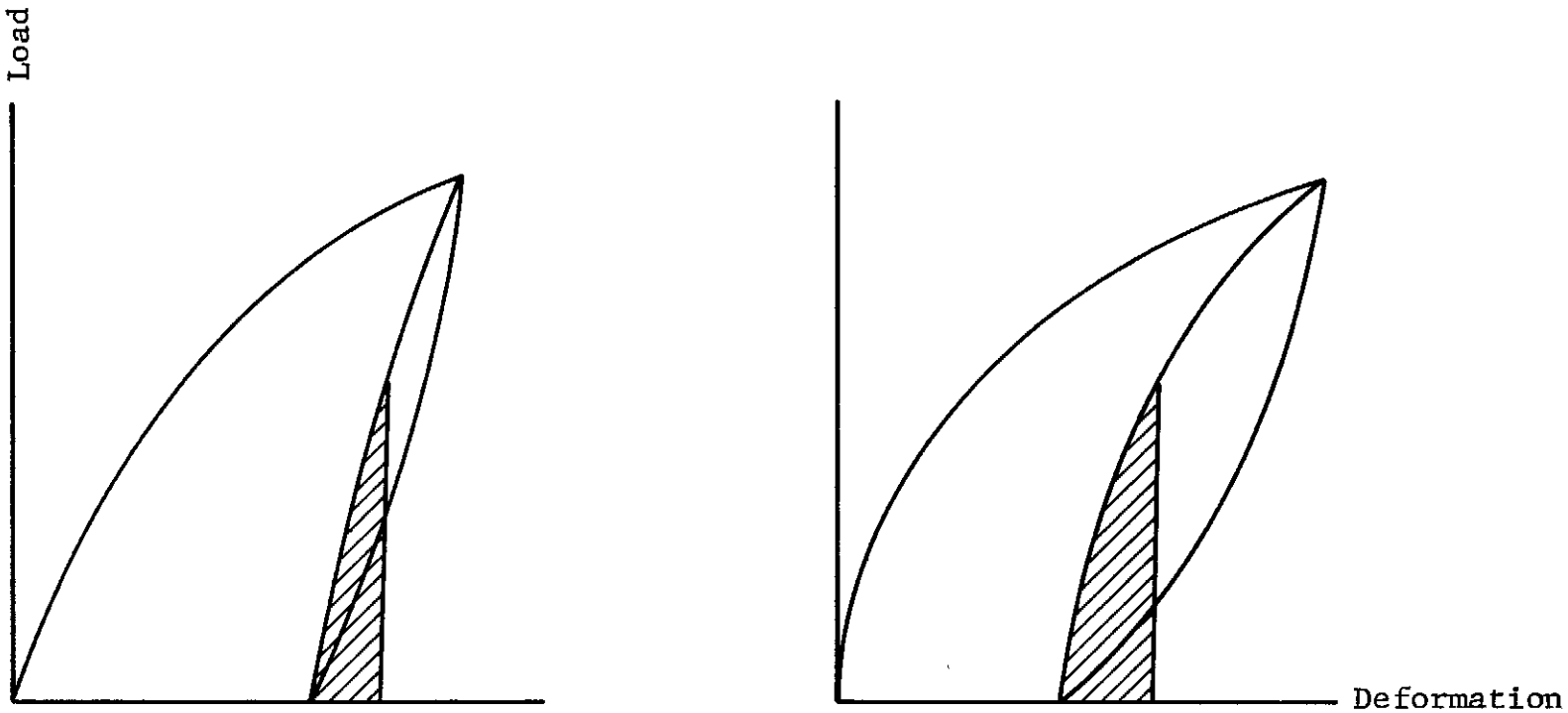

a) Riveted Joint

b) Bolted Joint

Fig. 6.10 ASYMPTOTIC LOAD DEFORMATION CURVES FOR RIVETED AND BOLTED JOINTS, AFTER BATHO (6.4)

Hovgaard, W. (6.30)

"A New Theory of the Distribution of Shearing Stresses in Riveted and Welded Connections and Its Application to Discontinuities in the Structure of a Ship," Trans. Inst. of Naval Arch., 1031, pp. 108-138.

The theory developed by Hovgaard in this paper assumes that a riveted joint with a large number of fasteners can be treated as a continuous lap joint. The intermittent shear areas are spread out over the length of the joint. The method is, of course, limited to within elastic behavior.

Knight, R. C. (6.23)

"The Action of a Rivet in a Plate of Finite Breadth," Philosophical Magazine, Series 7, Vol 19, No. 127 March 1935, pp. 517-540.

This paper is an excellent theoretical work using the theory of elasticity to determine the stress distribution around a hole in a plate for various a/w ratios and is similar to earlier studies by Bickley (Ref. 6.6). The solution contains results for rivets pulled both in the longitudinal direction of the plate and transverse to the plate. The ratio a/w was held at $a/w = 0.5$. Poisson's ratio of the plate was set at $\nu = 0.25$. The results given correspond to those shown also in Ref. 6.70.

Koegler, R. K., and Schnitt, A. (6.38)

"Effects of Yielding and Perforation on a Wing Tension Surface," J. Aero. Sciences, Vol 10, 1943. pp.273-284.

This paper is frequently referred to in later publications because of its nearly unique approach in describing the inelastic behavior of multi-fastener riveted or bolted joints. The authors recommend approaching the problem by assuming that the holes be replaced by rectangular slots (see Figs. 6.11 and 6.12). For studying the effects on a transverse section, a rectangle, a_T by a, is to be employed. For studying the effects

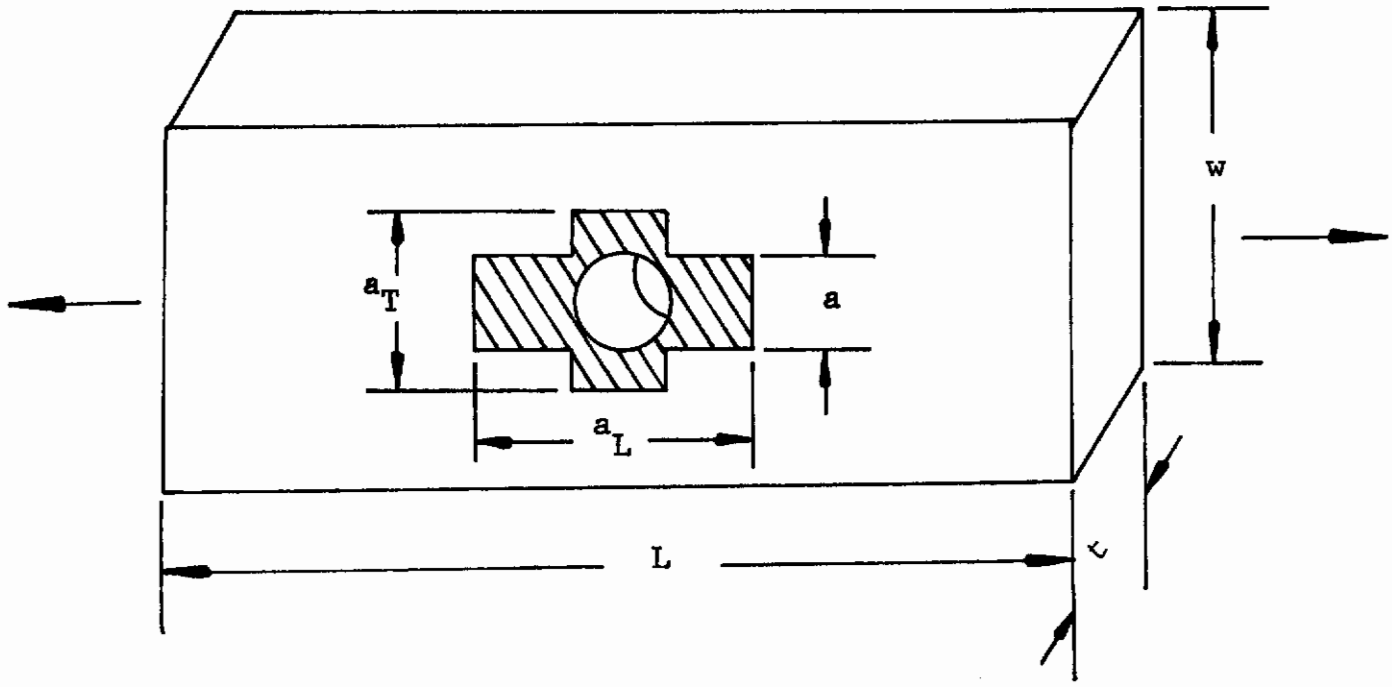

Fig. 6.11 RECTANGULAR EQUIVALENTS OF CIRCULAR RIVET HOLES, AFTER KOEGLER AND SCHNITT (6.38)--SINGLE HOLE

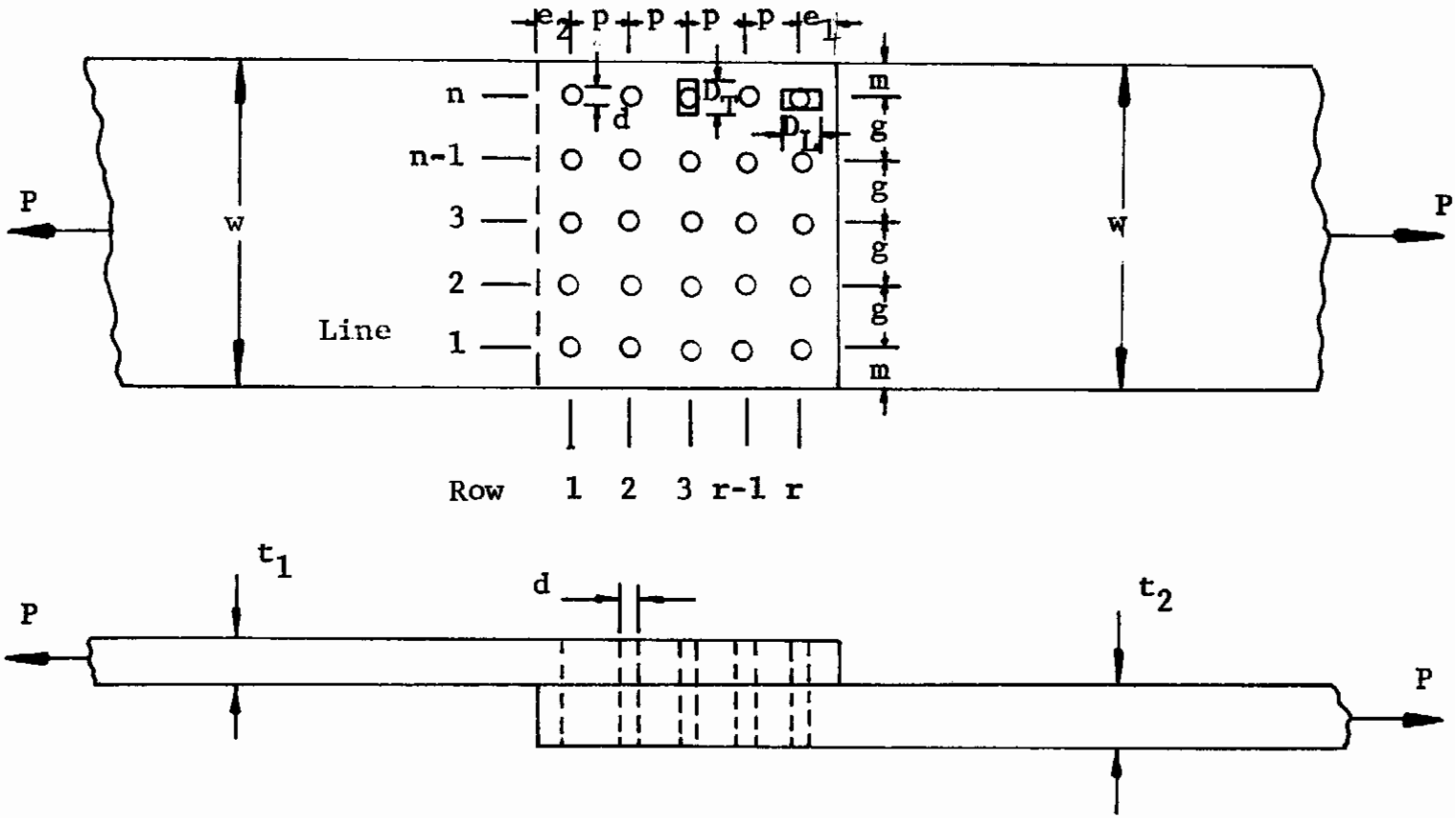

Fig. 6.12 RECTANGULAR EQUIVALENTS OF CIRCULAR RIVET HOLES, AFTER KOEGLER AND SCHNITT (6.38)--MULTIPLE HOLES

on a longitudinal section, a rectangle, a_L by a, is to be employed. Data for aluminum alloy (Alclad 24ST) indicate relationships of the form:

$$a_T = a + (0.09)(d - 3a)$$

and

$$a_L = 0.54d - 1.12a$$

where

a = hole diameter

and

d = pitch distance in a row

For n lines of holes and assuming

$$w = nd$$

the area of the net section becomes

$$A_{net} = 0.91\ wt - 0.73\ nat$$

The deformation of the plate can be considered equal to the deformation of an equivalent solid plate part of which is stressed at the gross section stress σ_G and part at the net section stress ($\sigma_N = P/(w - a)t$, for a single hole. Thus, the equivalent length of the plate at the higher stress becomes $\bar{L}$ and the strains due to the net and gross stresses are:

$$\varepsilon_N \text{ and } \varepsilon_G$$

Thus, the total deformation becomes

$$\Delta' = (L - \bar{L})\ \varepsilon_G + \bar{L}\ \varepsilon_N$$

or

$$\Delta' = L\ \varepsilon_G + \bar{L}\ (\varepsilon_N - \varepsilon_G)$$

for the length L.

To determine $\bar{L}$ we must know the stress-strain curve of the material, and have the results of at least one test on a specimen with a hole to determine Δ'. Although $\bar{L}$ can be calculated from the data on a load-displacement curve, the approach falls apart if the $\bar{L}$ is not constant in the plastic range.

Jenkins, E. S. (6.33)

"Rational Design of Fastenings," SAE Journal, Sept. 1944, pp. 421-429.

This paper is a review of design methods in use at the time of the writing of this paper in the aircraft industry.

Tate, M. B. and Rosenfeld, S. J. (6.68)

"Preliminary Investigation of the Loads Carried by Individual Bolts in Bolted Joints," NACA TN 1051, May 1946, pp. 70.

This report describes an analytical method for determining the distribution of load among individual rivets or bolts in symmetrical butt joints. The solution can be readily carried out numerically. The solution is satisfactory for several combinations of materials common in aircraft construction. The solution is satisfactory only in the elastic range of behavior for the materials.

In addition to the analytical procedures, several tests were conducted on 24S-T aluminum alloy plate fastened by two or three bolts. Agreement between the theory and experiment fell within 10 percent.

The assumptions upon which the theory were based are:

1. The ratio of stress to strain is constant (linear elasticity).
2. The stress is uniformly distributed over the cross section of the plate and butt straps.

3. Friction is negligible.

4. Bolts fit the holes initially and material of the plates in the immediate vicinity of holes is not damaged or stressed in making the holes or inserting the bolts.

5. Bolt deflection and bolt load are linearly elastically related.

On the basis of these assumptions, the relationship between loads on any two successive bolts (in a line) is

$$R_{i+1} = \frac{C_i}{C_{i+1}} R_i + \frac{2K_p + K_s}{C_{i+1}} R_i - \frac{2K_p}{C_{i+1}} p + \frac{2K_p + K_s}{C_{i+1}} \sum_{1}^{i-1} R_i$$

where

R_i = Load on ith bolt in line ~ lbs

C_i = ith bolt constant dependent on elastic properties, geometric shape, dimensions and manner of loading of bolts, and upon the bearing properties and thickness of plates ~ in./lb

K_p = Plate constant for tension or compression loads, dependent on geometric shape, dimensions elastic properties of plates and the assumed stress distribution ~ in./lb

K_s = Strap constant (see K_p) ~ in./lb

p = Pitch in.

In our defined geometries, K becomes

$$K = \frac{L_i}{wtE}$$

and the linear relation between bolt load and displacement becomes

$$\delta = \frac{CR}{2}$$

Vogt, F. (6.71)

"The Load Distribution in Bolted or Riveted Joints in Light Alloy Structures," NACA TM-1135, April 1947 pp. 51

This report, which is a reprint of an English report,* describes analytical rpocedures for determining the load distribution in riveted and bolted joints in light alloy (aluminum, magnesium materials. The theory includes both double and single lap joint analyses. The theory involves a set of simultaneous equations such as

$$c_1R_1 + a_1R_1 = b_1(P - R_1) + c_2R_2$$

$$c_2R_2 + a_2(R_1 + R_2) = b_2(P - R_1 - R_2) + c_3R_3 \text{ etc.}$$

and the equilibrium equations

$$P = R_1 + R_2 \ldots + R_n$$

where a_i, b_i, c_i are relative stiffnesses of the joint parts, P is the applied load and R_i are the bolt loads.

The quantities a_i, b_i, and c_i are constants below the proportional limit and functions of the load above the proportional limit.

The theory above is for a single line of bolts but can be modified for several rows normal to the tensile load where each row contains a number of bolts. If the number of bolts in the ith row is m_i and R_i is the total load on these bolts

* Report No. SME 3300 Oct. 1944, R.A.E. Farnsborough, England

then the load is assumed to be uniformly distributed over the bolts so that each bolt carries R_i/m_i load. The terms c_iR_i in the previous equation are then replaced by c_iR_i/m_i.

Several examples are solved by Vogt, such as:

1. Relatively Stiff Bolts in Plate

   (Here the well known result that an increase in the number of bolts does not substantially decrease the stress on the highest stressed bolt).

2. Very Flexible Bolts $(c \rightarrow \infty)$

   $R_i \rightarrow P/m$ as $C \rightarrow \infty$

3. Tapered Plates

4. Large Diameter Bolts $(a/t > 1)$

5. Small Diameter Bolts $(a/t \ll 1)$

Vogt presents a review of the literature which permits a designer to estimate the theoretical behavior laws for the quantities a_i, b_i and c_i both below and above yield.

Vogt also rewrites his equations for the case where the loads are above the limit of proportionality. He does this because the simultaneous set of equations becomes nonlinear.

For the case of symmetrical joints, Vogt rewrites his equations so that $c_i = c$ and some simplifications are possible.

Vogt also solves the following specific problems:

1. Reinforcement of the main plate by side plates.

2. Single lap joints with some bending of the plates out of plane permitted. For this case the following results are of interest:
   a. "The load-distribution in the joint is dependent on the total load, even below the proportional limit (instead of being independent as for double lap joints)."

b. "For the same value of c, the load distribution at small loads show greater non-uniformity than that for double shear joints."

c. "The load distribution becomes more uniform as the loads are increased and in some cases is better than that for the double lap joints even below the limit of proportionality."

d. "At higher loads, the load distribution approximates that for double lap joints provided the elastic limit or ultimate strength has not been reached."

e. "The results for double lap joints are therefore recommended for design because only the load distribution at the highest allowable loads are of interest and this will usually be a safe approximation."

Rosenfeld, S. J. (6.54)

"Analytical and Experimental Investigation of Bolted Joints," NACA TN 1458, July 1947, pp. 48.

This report describes an analytical and experimental investigation of stresses in a symmetrical butt (double lap) joint. The analyses were described in Ref. 6.68. A recurrence formula for the bolt loads used in conjunction with appropriate boundary conditions is developed in this paper to produce sets of simultaneous linear equations which can be solved for the bolt loads.

An approximate analysis based on shear-lag methods is presented which has some gain in speed of calculation at only a small loss in accuracy.

Additional electrical resistance strain gage tests were performed to compare the results of those experiments with the theory.

Muckle, W. (6.50)

"The Distribution of Load in Riveted Joints," Shipbuilder and Marine Engine Builder, April 1949, pp. 225-228.

Muckle employs the principle of minimum strain energy to determine the loads taken by various rows of rivets in a joint. Since the cases of one and two rows of rivets are obvious for equal plate thicknesses, Muckle solves the problem for 3, 4 and 5 rows of rivets. He adds the strain energy in the plates between the first and last rows of rivets to the strain energy (due to shear) in the rivets and minimizes the sum, thus apportioning the load. He makes the following assumptions:

1. The holes are rectangular.
2. The plate between the rivet rows is in uniform tension.
3. The rivet or some portion of it is in uniform shear.
4. The system behaves linear elastically.
5. The joint is a balanced (equal thickness cover plates of half center plate thickness) double lap joint.
6. Friction can be ignored.

Muckle concludes that the first and last rows of the joint assume most of the load.

Langhaar, H. L. (6.42)

"Dimensional Analysis and Theory of Models, Sec. 40, Dimensionless Plotting of Test Data for Riveted Joints," J. Wiley & Sons, pp. 87-91.

This chapter summarizes two papers by Holbach (6.28)

and Fefferman Ref. 6.18. In general, this rivet bearing stress at joint failure is a function as

$$\sigma_B = f(\sigma_{ult}, a, t, H)$$

which can be rewritten in nondimensional form

$$\sigma_B = \sigma_u f\left[\frac{a}{t}, \frac{H}{a}\right]$$

By plotting in nondimensional form as shown in Fig. 6.13, the ultimate bearing and shear stresses can be obtained for a given rivet type.

Langhaar also discusses a single-lap multifastener riveted joints.

Here the nondimensional expression becomes

$$\sigma_m = \sigma_u f\left[\frac{a}{d}, \frac{a}{t}\right]$$

or

$$\sigma_m = \sigma_u f\left[\frac{w - na}{w}, \frac{a}{t}\right]$$

A typical plot of joint efficiency, N_a vs $(w - na)/w$, is shown in Fig. 6.14. It is clear that for maximum joint efficiency there exists some value of w - na/w to do this. The analysis, although not really pertinent to joint design, is of sufficient interest to be utilized when selecting rivet types or in analyzing the results of testing.

Theocaris, P.(6.70)

"The Stress Distribution in a Strip Loaded in Tension by Means of a Central Pin," ASME J. A. M. Paper No. 55-A-34, 1955.

This paper presents the stress distribution around a pinned hole which is attained by superposing the solution for

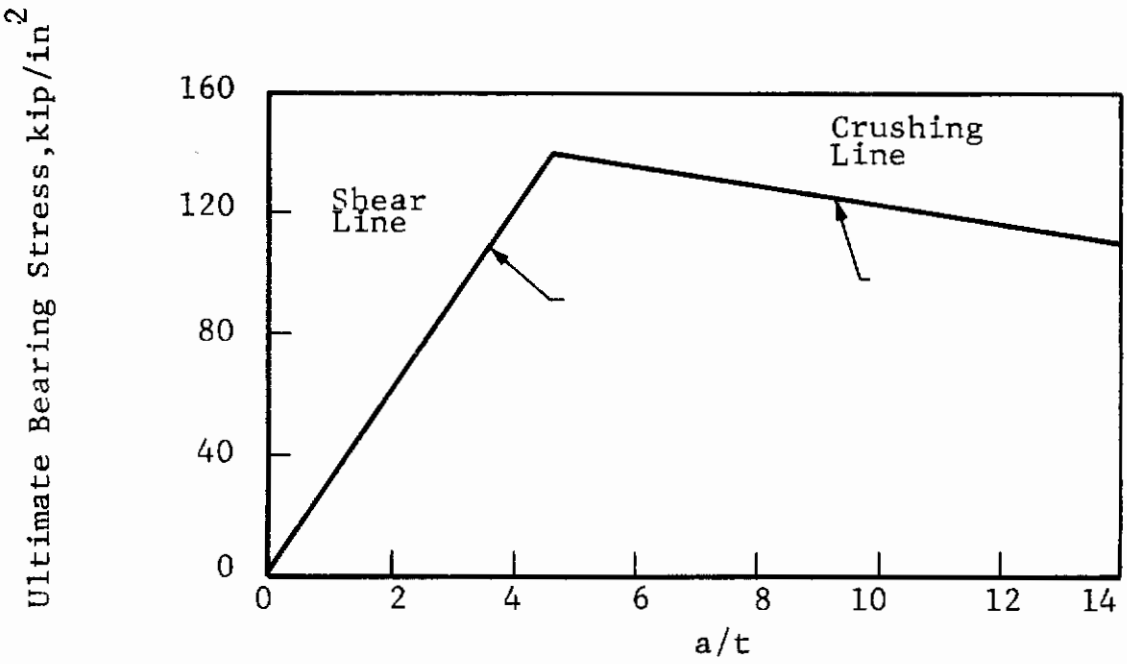

Fig. 6.13 EXPERIMENTAL CHART SHOWING ULTIMATE BEARING STRESS FOR 17S-T PROTRUDING HEAD RIVETS IN UNCLAD 24S-T SHEETS, AFTER LANGHAAR (6.42)

Crushing line applies for joints with edge distance equal to two rivet diameters.

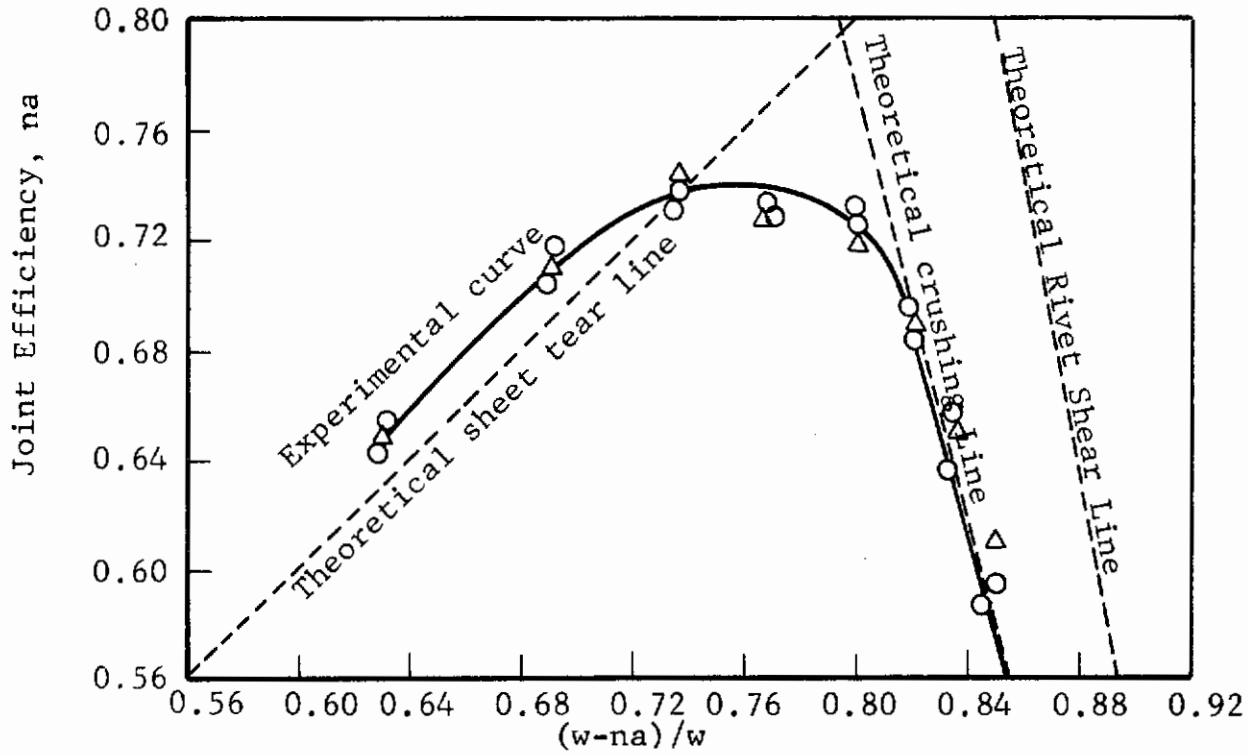

Fig. 6.14 EFFICIENCIES OF 2-ROW RANDOM RIVETED 25S-T LAP JOINTS WITH PROTRUDING HEAD 17S-T RIVETS, AFTER LANGHAAR (6.42)

two subproblems: 1) The problem of a strip with a hole loaded in tension and 2) the problem of a strip loaded through a pin where the pin thrust is equilibrated by a uniform thrust and a uniform tension on the short edges of the strip respectively. Two of Howland's papers are used to furnish solutions to the subproblems. The solution is obtained by convergency of the process of alternating successive approximations to the solution. The principal contribution of Theocaris is to produce a solution for various values of the ratio a/w which he calls λ. He finds an optimum value of λ that is the value of a/w for which the load transmission is the greatest. This maximum load carrying capacity (for the finite width plate) occurs for a/w between $\lambda = 0.4$ and $\lambda = 0.5$. The region of influence of the hole is limited to a circle of diameter, d = 1.5 times the strip width.

The mean stress at infinity in the plate is taken as $\sigma_m = P/wt$ where P is the load on the strip.

The expressions which delineate the stresses for the second subproblem are too lengthy to write down here and the reader is referred to the paper instead. The values of the principal stresses at the rim of the hole are shown in Table 6.2 and are plotted in Figs. 6.15 and 6.16 for various ratios of $\lambda = a/w$. The principal stresses are also shown plotted in Figs. 6.17 and 6.18 across the width of plate through the center of the hole (η axis) and the maximum stresses along the centerline of the strip (ξ axis) in Fig. 6.19 and Table 6.3. Figure 6.20 shows the maximum tensile stress at the edge of the hole as a function of the ratio a/w. Figure 6.21 shows the minimum compressive stress at the bottom of the hole as a function of the ratio a/w.

The wide applicability of the Theocaris solution is due to the generality of the expressions for any ratio of a/w.

Table 6.2

PRINCIPAL STRESSES AT THE RING OF THE HOLE ACCORDING TO THEOCARIS (6.70)
$K_1 = \sigma_1/\sigma_m$, $K_2 = \sigma_2/\sigma_m$, $\sigma_m = P/tw$

	a/w=0.2		a/w=0.3		a/w=0.4		a/w=0.5	
θ	K_1	K_2	K_1	K_2	K_1	K_2	K_1	K_2
90°	-0.13	-5.27	-0.50	-3.65	-0.96	-2.80	-1.21	-2.32
75°	0.14	-5.24	-0.28	-3.52	-0.64	-2.70	-0.95	-2.21
60°	1.01	-4.75	0.58	-3.12	0.22	-2.38	-0.10	-1.92
45°	2.31	-3.83	1.82	-2.50	1.45	-1.87	1.16	-1.46
30°	3.73	-2.69	3.05	-1.75	2.86	-1.26	2.73	-0.91
15°	5.44	-1.44	4.36	-0.94	4.18	-0.60	4.26	-0.42
0°	6.62	0	5.26	0	4.84	0	5.10	0
-15°	5.00	0	4.13	0	4.03	0	4.19	0
-30°	3.11	0	2.66	0	2.60	0	2.55	0
-45°	1.53	0	1.30	0	1.06	0	0.86	0
-60°	0.07	0	-0.04	0	-0.27	0	-0.48	0
-75°	-0.85	0	-0.93	0	-1.16	0	-1.31	0
-90°	-1.14	0	-1.17	0	-1.47	0	-1.63	0

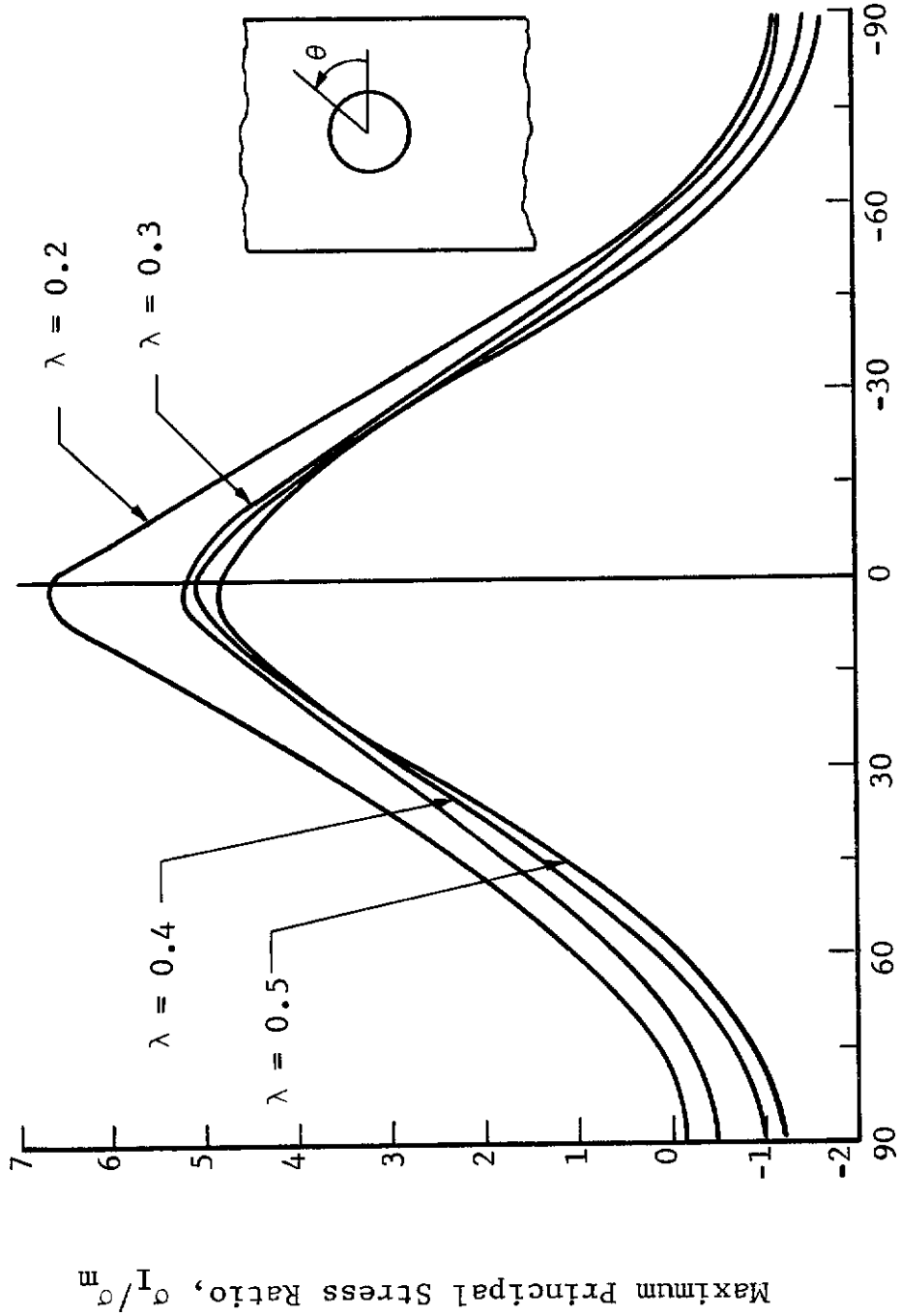

Fig. 6.15 MAXIMUM PRINCIPAL STRESSES σ_I AT THE RIM OF THE HOLE VERSUS ANGULAR POSITION AS A FUNCTION OF THE RATIO $\lambda = a/w$

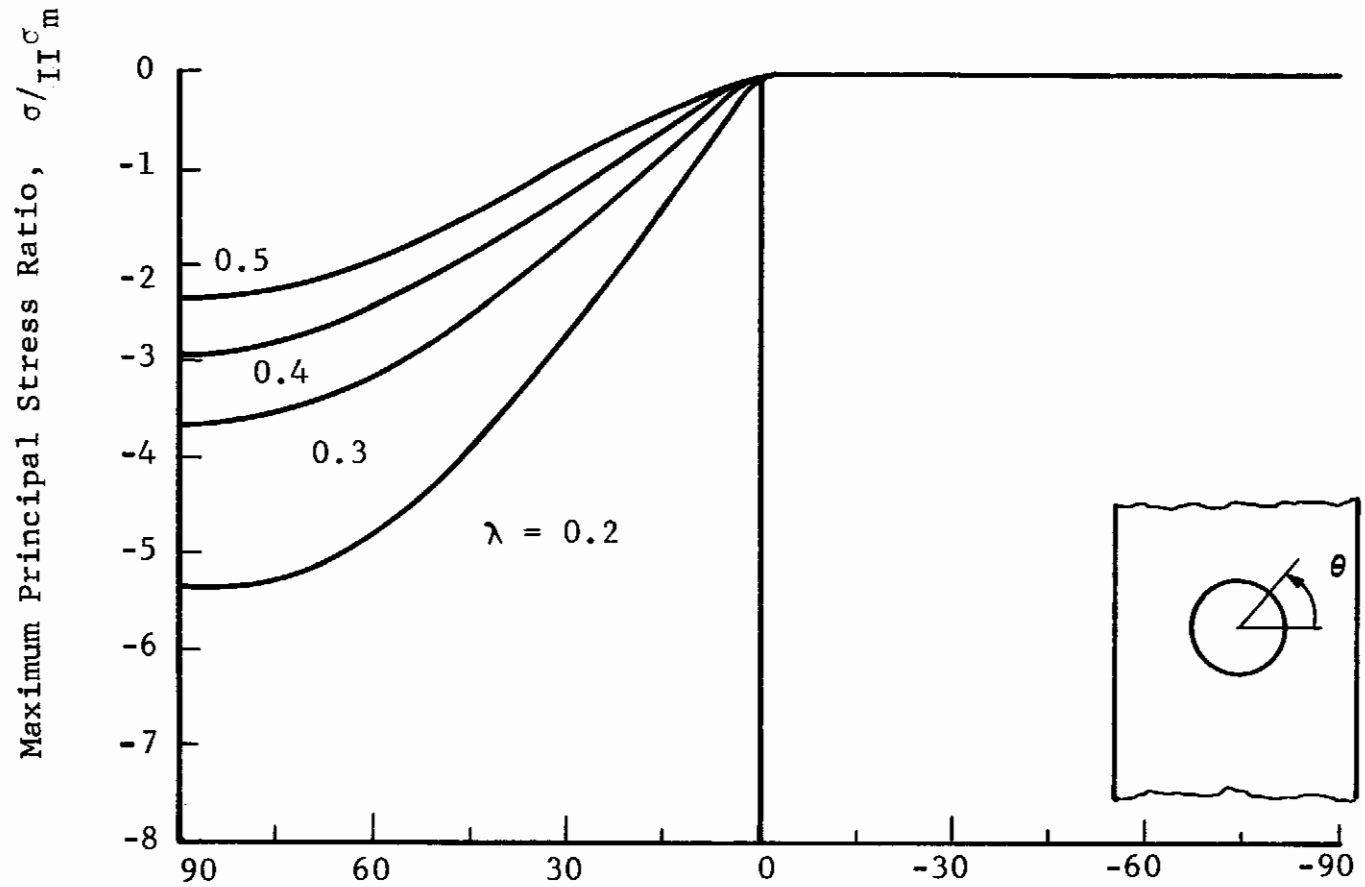

Fig. 6.16 MINIMUM PRINCIPAL COMPRESSIVE STRESSES σ_{II} AT THE RIM OF THE HOLE VERSUS ANGULAR POSITION AS A FUNCTION OF THE RATIO $\lambda = a/w$

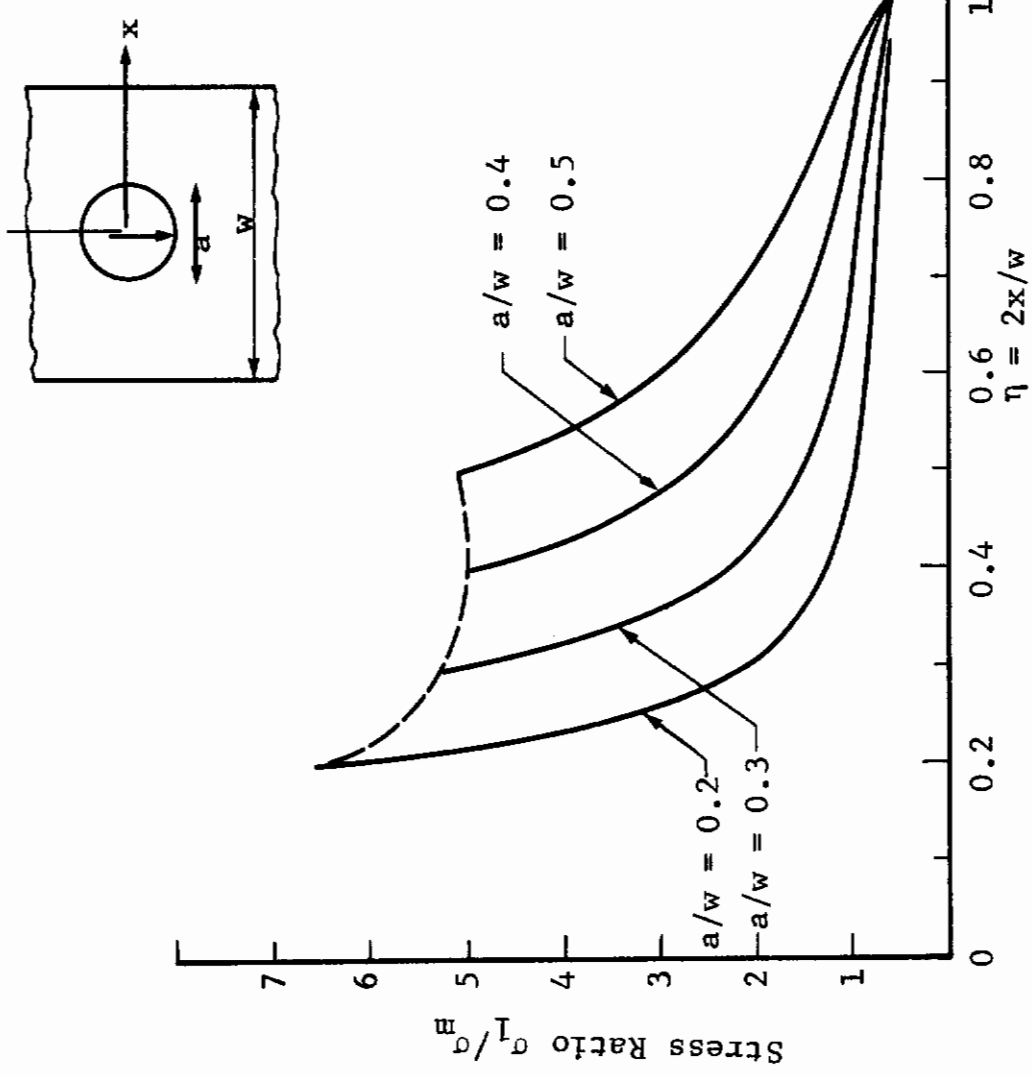

Fig. 6.17 MAXIMUM PRINCIPAL STRESS, σ_1, ACROSS THE WIDTH OF THE STRIP

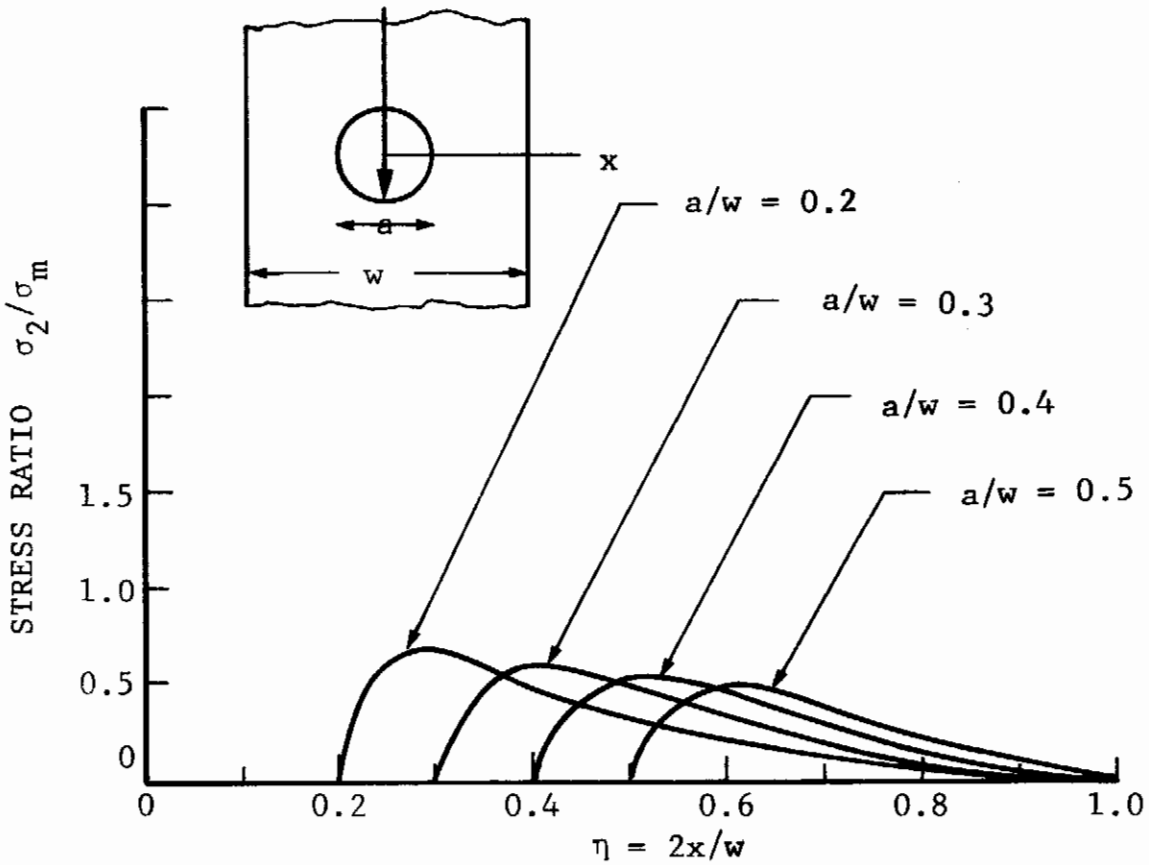

Fig. 6.18 MINIMUM PRINCIPAL STRESSES, σ_2 ACROSS THE WIDTH OF THE STRIP

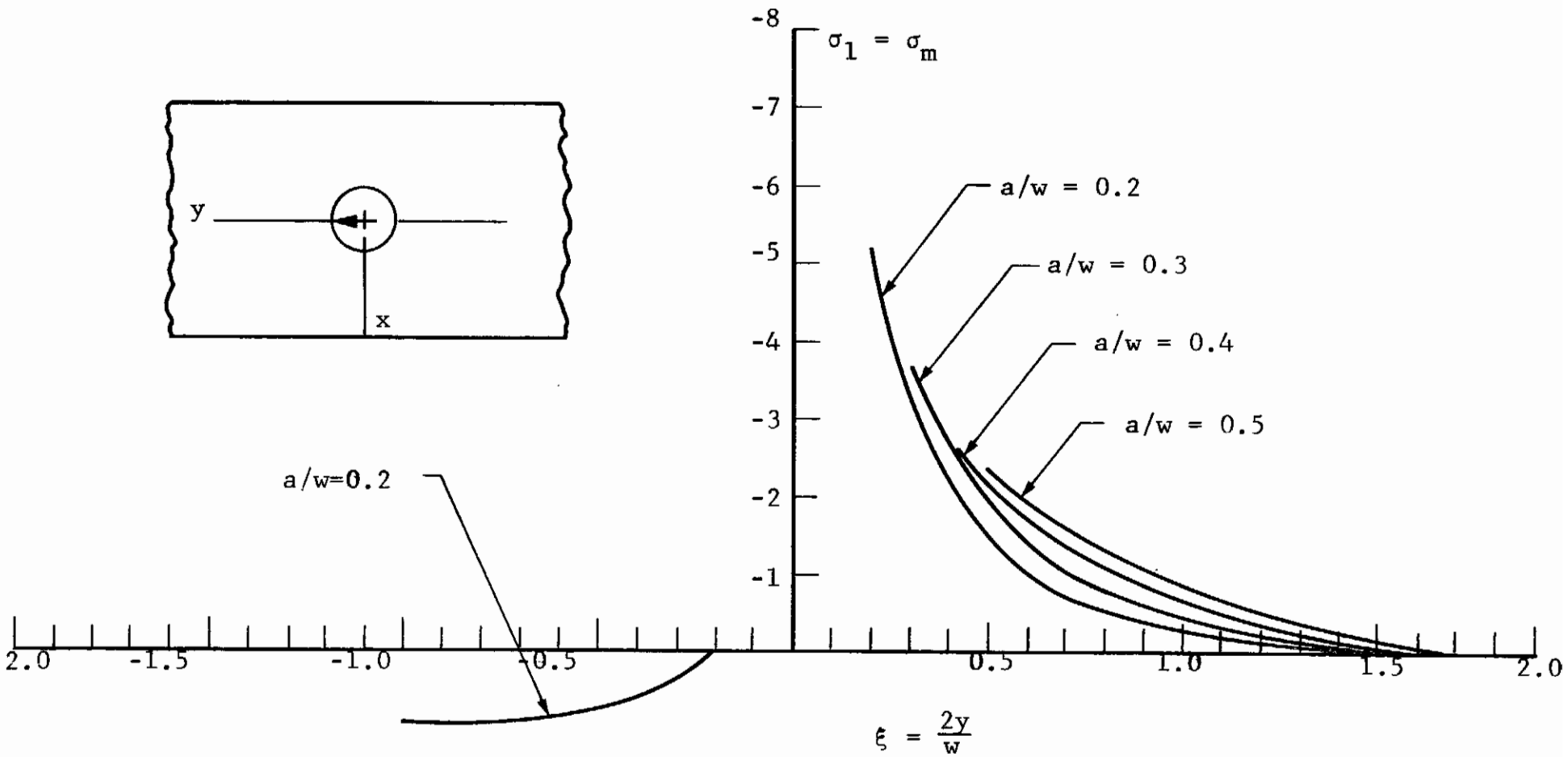

Fig. 6.19 VALUES OF THE MAXIMUM PRINCIPAL STRESSES ALONG THE CENTERLINE OF THE STRIP THROUGH THE LOADED HOLE FOR THE VALUES OF σ_2/σ_m

Table 6.3

VALUES OF THE PRINCIPAL STRESSES ALONG THE CENTERLINE OF THE STRIP (PARALLEL TO THE PIN LOAD)
$K_1 = \sigma_1/\sigma_m$, $K_2 = \sigma_2/\sigma_m$, $\sigma_m = P/wt$

$\xi=zy/w$	a/w=0.2		a/w=0.3		a/w=0.4		a/w=0.5	
	K_1	K_2	K_1	K_2	K_1	K_2	K_1	K_1
0.2	-5.21	-0.15						
0.3	-3.38	0.34	-3.67	-0.51				
0.4	-2.18	0.55	-2.73	0.28	-2.76	-0.96		
0.5	-1.50	0.48	-1.97	0.39	-2.32	-0.10	-2.31	-1.21
0.6	-1.05	0.37	-1.42	0.38	-1.78	0.17	-1.98	-0.33
0.7	-0.77	0.31	-1.05	0.35	-1.37	0.22	-1.67	-0.02
0.8	-0.55	0.25	-0.78	0.30	-1.04	0.22	-1.34	0.17
0.9	-0.45	0.21	-0.61	0.27	-0.82	0.19	-1.10	0.16
1.0	-0.32	0.15	-0.43	0.20	-0.61	0.10	-0.84	0.12
1.4	-0.07		-0.10		-0.21		-0.32	
1.57	-0.01		-0.04		-0.11		-0.10	
-0.2	0	-1.17						
-0.3	0.28	-0.34	0	-1.19				
-0.4	0.62	0.03	0.07	-0.24	-0.04	-1.48		
-0.5	0.80	0.02	0.33	-0.03	-0.02	-0.52	-0.01	-1.63
-0.6	0.87	-0.01	0.50	0	+0.14	-0.21	-0.12	-0.71
-0.7	0.91	-0.01	0.63	0.03	0.31	-0.10	0.01	-0.34
-0.8	0.93	-0.03	0.70	0.03	0.44	-0.06	0.14	-0.11
-0.9	0.93	-0.03	0.77	0.03	0.56	-0.05	0.28	-0.08
-1.0	0.95	-0.05	0.83	0	0.65	-0.04	0.42	-0.06

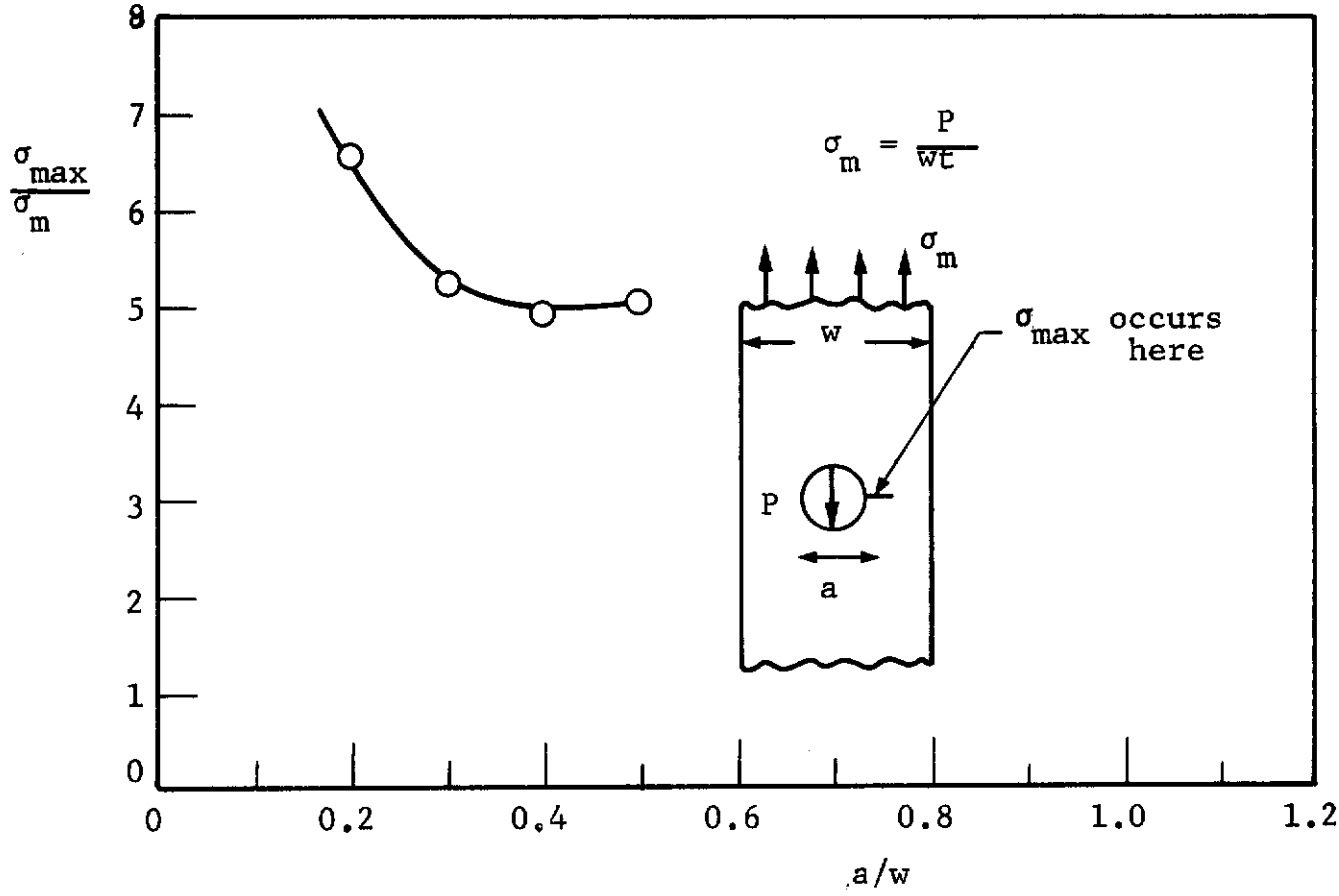

Fig. 6.20 MAXIMUM TENSILE STRESSES AT THE EDGE OF THE PINNED HOLE AS A FUNCTION OF THE RATIO a/w

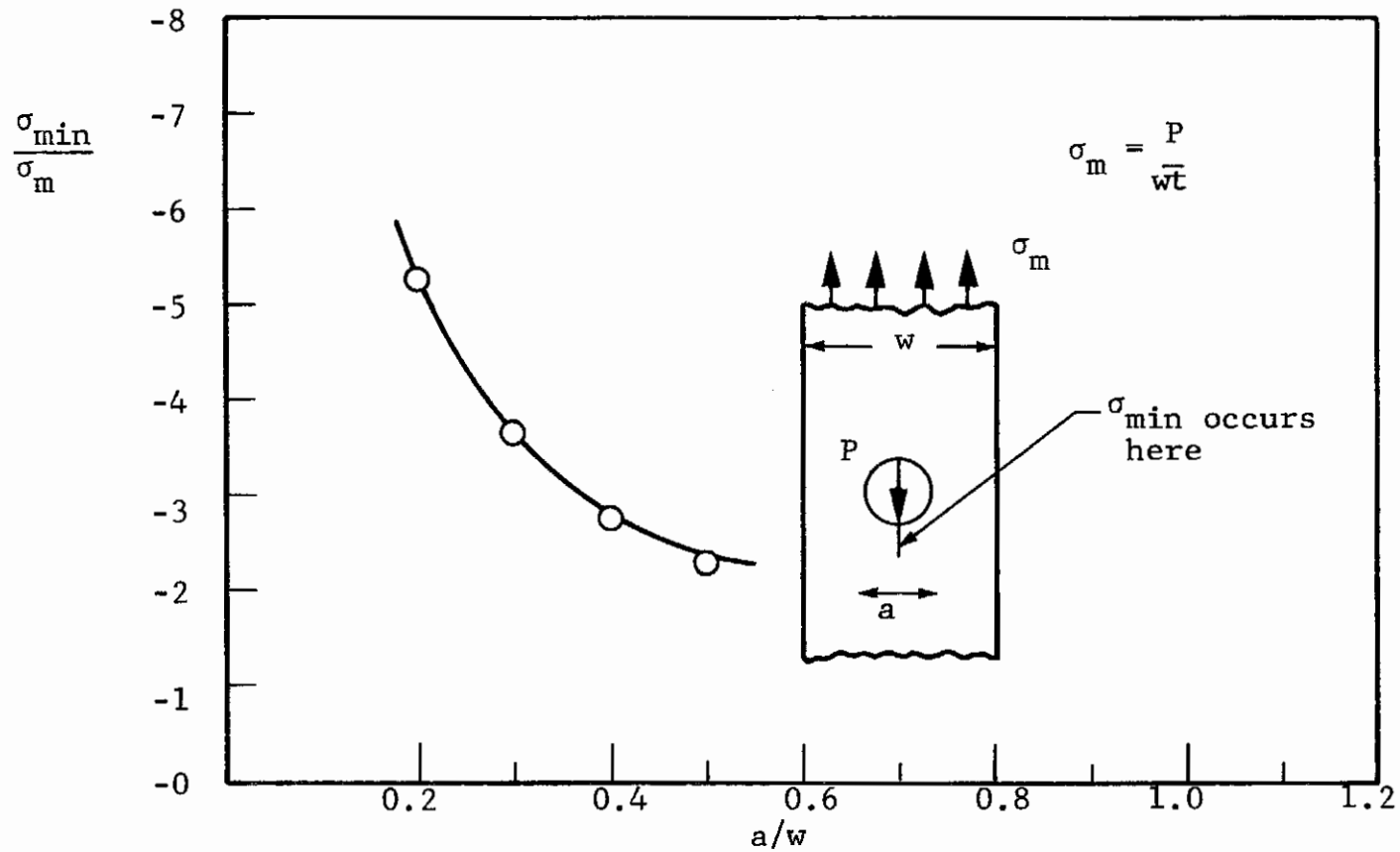

Fig. 6.21 MINIMUM COMPRESSIVE STRESSES AT THE BOTTOM OF THE PINNED HOLE AS A FUNCTION OF THE RATIO a/w

Chi, M. and Irwin, L. K. (6.11)

"Deformation in Strips with Holes Loaded through Pins," BuWeps Report No. RAAE-343-60-16, July 1958.

The authors use the Bickley Airy Stress function for an infinite plate loaded by a rigid pin plus Bickley's assumption of the cosine function distribution of forces on the hole to determine the displacements in the strip. To this they add the Kirsch solution displacements to obtain the deformations in a strip loaded by a pin and a uniform stress at infinity. Using this solution plus a conclusion of Atsumi, the authors derive relative displacements for two holes in series along the centerline of the strip. The equations for the raidal and tangential displacements for a single loaded hole are given as

$$u_r = \frac{2P}{\pi te}\left[\frac{1 + \nu'}{\pi} \left[\frac{a}{2r}\right] + \frac{3 + 2\nu' - (\nu')^2}{} \left[\log_e \frac{a}{2r}\right] \cos\theta \right.$$

$$+ \frac{1 - (\nu')^2}{} \frac{a^2}{r^2} \cos\theta$$

$$+ \sum_{2,4,6}^{\infty} \frac{1}{\pi} \left[\frac{a}{2r}\right]^{m-1} \left\{ \frac{\sin \frac{m-1}{2}\pi}{m-1} + \frac{\sin \frac{m+1}{2}\pi}{m+1} \right\} \cdot$$

$$\left. \left\{ \frac{\frac{m}{2} + 1 + \left[\frac{m}{2} - 1\right]\nu'}{m-1} - \frac{\frac{m}{8}\ 1+\nu'}{m+1} \frac{a^2}{r^2} \right\} \cos m\theta \right]$$

$$+ \frac{\pi (1-\nu')}{256} \frac{r}{a} + \frac{\pi (1+\nu')}{256} \frac{a}{r} + \left[\frac{\pi}{64} \frac{a}{r} + \right.$$

$$\left. + \frac{\pi (1+\nu')}{256} \frac{r}{a} - \frac{\pi}{1024} (1+\nu') \frac{a^3}{r^3} \right] \cos 2\theta \Bigg]$$

$$u_\theta = \frac{2P}{\pi te} \left[\frac{1+2\nu'+(\nu')^2}{8} \sin\theta - \frac{3+2\nu'-(\nu')^2}{8} \left[\log_e \frac{a}{2r} \right] \sin\theta \right.$$

$$+ \frac{1-(\nu')^2}{64} \frac{a^2}{r^2} \sin\theta + \sum_{2,4,6}^{\infty} \frac{1}{\pi} \left[\frac{a}{2r} \right]^{m-1} \left(\frac{\sin \frac{m-1}{2} \pi}{m-1} \right.$$

$$\left. + \frac{\sin \frac{m+1}{2} \pi}{m+1} \right) \cdot \left(\frac{-2+\frac{m}{2}(1+\nu')}{m-1} - \right.$$

$$\left. - \frac{\frac{m}{8}(1+\nu')}{m+1} \frac{a^2}{r^2} \right) \sin m\theta -$$

$$- \left(\frac{\pi}{128} (1-\nu') \frac{a}{r} + \frac{\pi}{256} \frac{r}{a} (1+\nu') \right.$$

$$+ \frac{\pi}{1024} (1+\nu') \frac{a^3}{r^3} \Bigg) \sin 2\theta \Bigg]$$

where

a = hole diameter

ν' = ν/ + ν

ν = Poisson's ratio

P = load on pin

t = adherend thickness

E = modulus of adherend

r = coordinate measured from hole center

θ = coordinate measured from bottom of the hole (center of pin load)

Figure 6.22 shows the relative displacements for two holes along the longitudinal centerline of the strip for several spacings of the two holes.

Marin, J. (6.46)

"Determination of Creep of Structural Joints from Simple Tensile Creep," ASTM (1961) Preprint, Presented at 64th Annual Meeting of the Society, June 1961.

This paper outlines an approximate analytical method for the determination of creep deformations in a structural joint based upon simple stress-strain time relation in tension for the material. The problem treated is shown in Fig. 6.23.

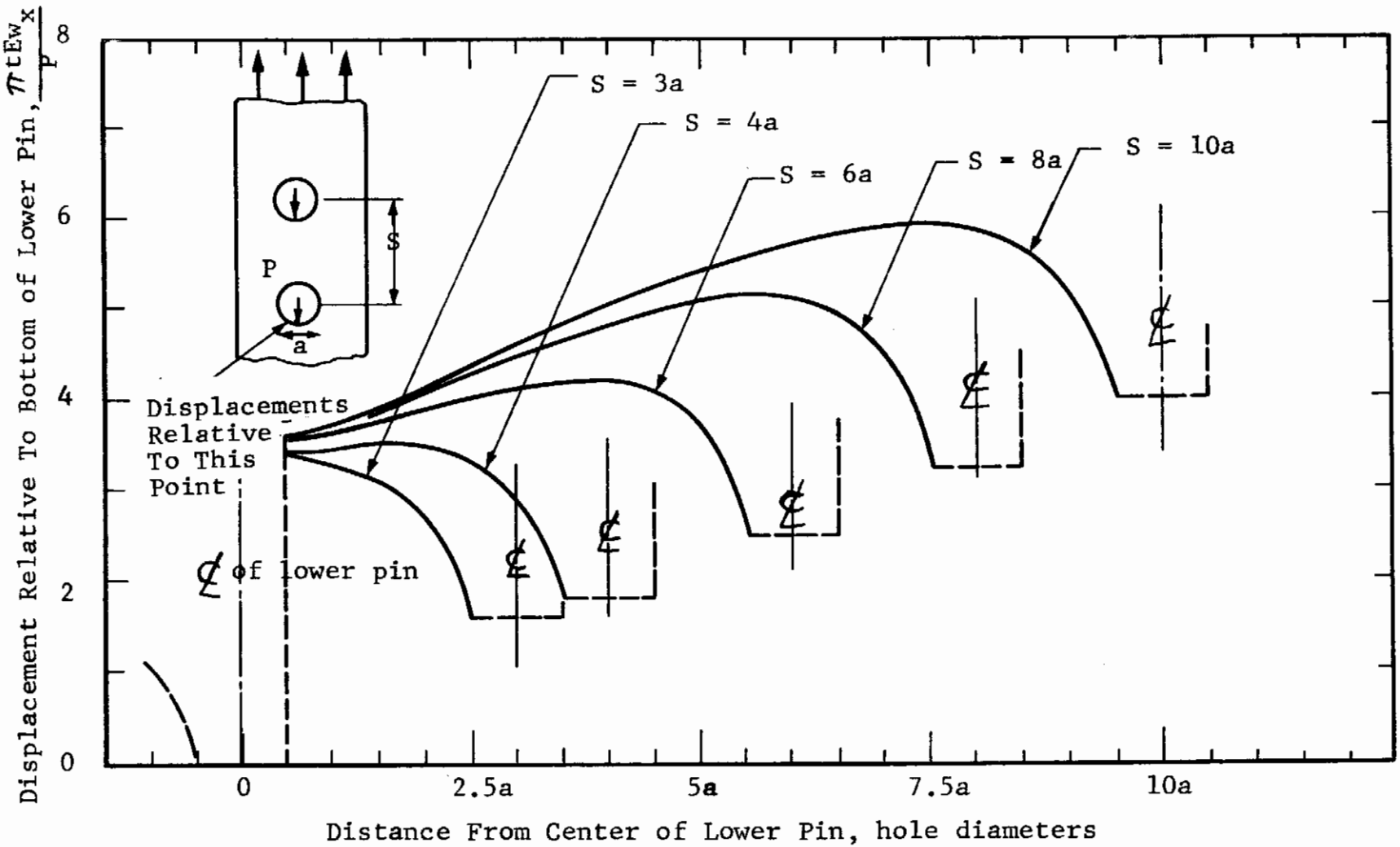

Fig. 6.22 RELATIVE DISPLACEMENTS ALONG THE LONGITUDINAL BETWEEN TWO PINS FOR VARIOUS SPACINGS OF THE TWO PINS

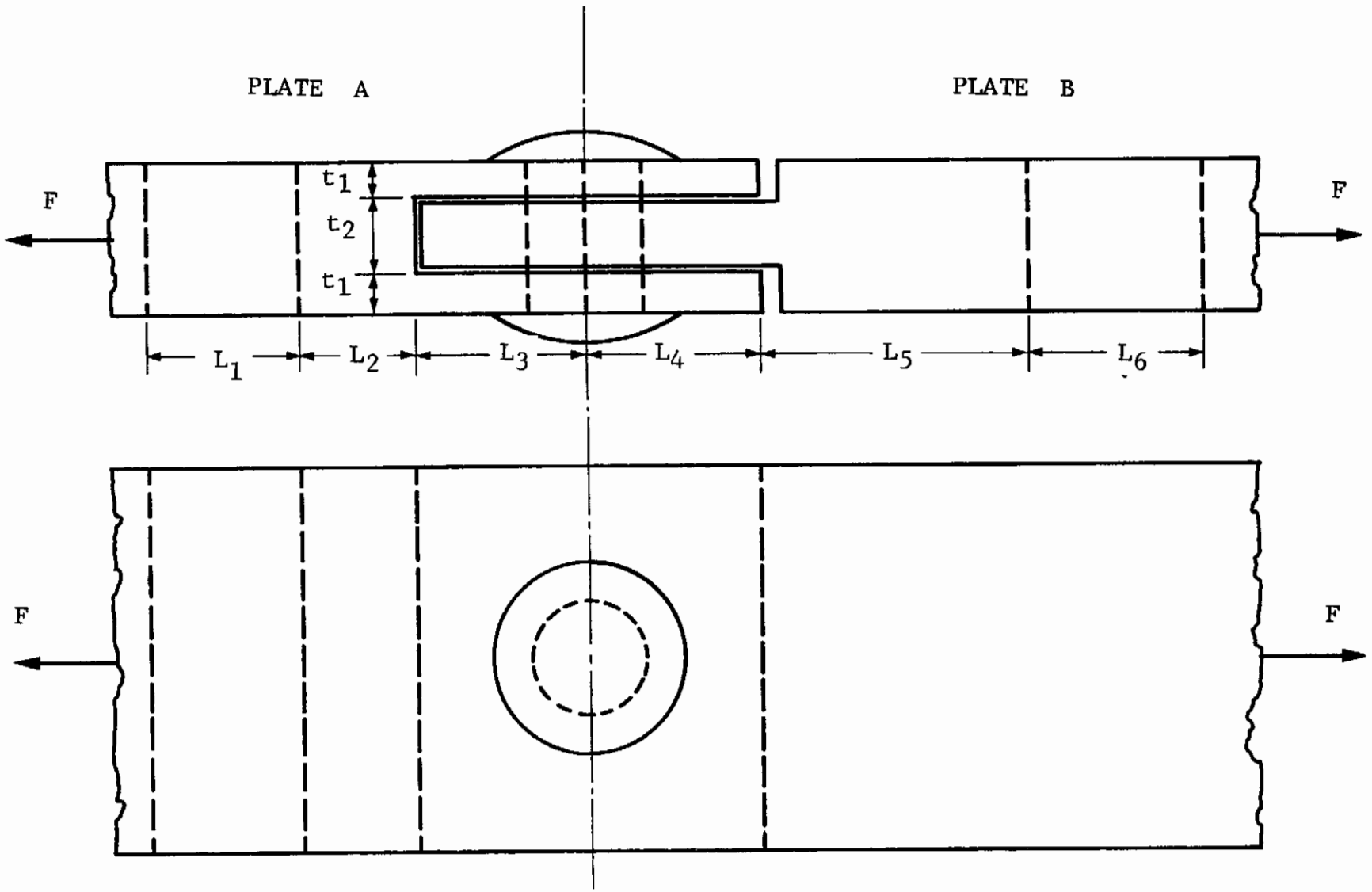

Fig. 6.23 JOINT CONFIGURATION AND DIMENSIONS ASSOCIATED WITH CREEP ANAYSIS BY MARIN (6.46)

The total creep is made up of:

1. Deformation e_1 for the length of the plate L_1.
2. Deformation e_2 for the length of the plate L_2.
3. Deformation e_3 for the length of plate L_3.
4. Deflection e_R of the rivet.
5. Deformation e_4 for the length of plate L_4.
6. Deformation e_5 for the length of plate L_5.
7. Deformation e_6 for the length of plate L_6.

In the lengths L_1 and L_6 creep deformation is essentially uniform across the plate. The total deformation of the bolted joint is:

$$e = \sum_{i=1}^{6} e_i + e_R$$

The expressions for e_2, e_3, e_4 and e_5 are more complicated and are based on tensile creep behavior under uniform load. The expressions for e_2, e_3, e_4 and e_5 are more complicated and are based on experiment and previous analyses by the author, Marin.

Marin makes one calculation example for the ratio of creep deformation in the joint, e, to that of a nonriveted member e_T and obtains

$$e/e_T = 48$$

Budiansky, B. and Wu, T. T. (6.9)

"Transfer of Load to a Sheet from a Rivet Attached Stiffener," J. Math Phys., Vol 40, July 1961, pp. 142-162.

This paper describes a shear-lag analysis within the limits of elastic behavior of the stress transfer between a

flat sheet and a discrete point rivet-attached stringer (see Fig. 6.24). The assumptions made are:

1. Frictional forces between stringer and sheet can be ignored.
2. The loss of stringer area due to rivet holes can be ignored.
3. The rivets themselves behave as rigid inclusions in the sheet. This implies continuity of contact at all times between rivet and sheet.
4. The interaction between individual rivets in the sheet is largely ignored.

Influence coefficients for each fastener, are determined from the Muckhelishivili complex potential. This coefficient describes the elongation of the mth interval due a limit load on the nth fastener.

The problem then sets up as a simultaneous set of difference equations and results in an equation in kernal form. The parameters in the problem depend primarily on the ratio, L_i/a and vary only slightly with Poisson's ratio, ν. Numerical calculations are made for various numbers of rivets up to five as a function of the two principal parameters. A comparison is made with another solution for continuous load transfer such as occurs in a welded or bonded joint.

As a special case the problem, where a broken stringer exists, is treated using the analysis developed. The loads on the rivet adjacent to the break are calculated.

Deneff, G. V. (6.17)

"Fatigue Prediction Study," WADD TR 153, Jan. 1962, pp. 207.

This report is primarily aimed at the prediction of fatigue life from the stress state, the fatigue data, and the

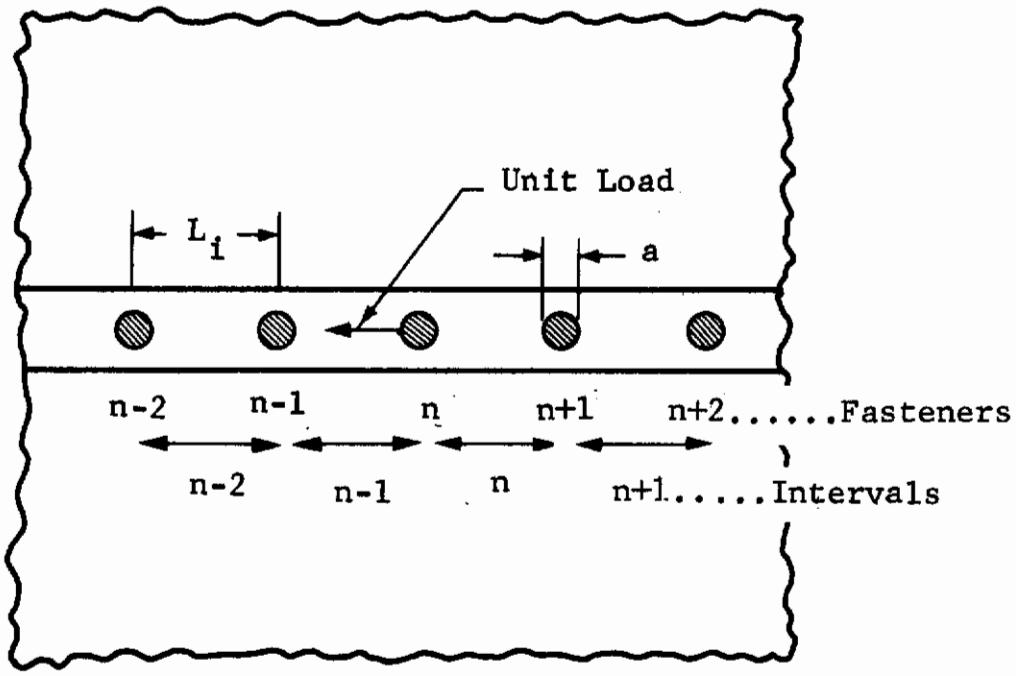

Fig. 6.24 RIVET ATTACHED STIFFENER AND RIVET NUMBERING STUDIED BY BUDIANSKY AN WU (6.9)

theory of cumulative fatigue damage. The general methods are applied to a structural joint. The fatigue data may be in several forms.

Deneff first points out that life predictions are basically the problem of 1) defining local stresses, 2) defining material strength properties, and 3) combining the local stresses and the material strength through the medium of some cumulative damage theory.

The analysis method used was numerical (employing an IBM 709 digital computer) and is given the name programmed force method.

The p.f.m. requires that the actual joint be reduced to an idealized structure of discrete bar and panel elements. The bar elements are capable of carrying axial loads, shear, torsion, and bending. The panel elements support shear loads. The solution is exact for the idealized structure, hence the closer the representation, the more realistic the solution. Each attachment becomes a bar element and the deformation can be separated into linear and nonlinear components in the analysis.

Deneff also performed several experiments to check the theory using strain gages and photoelasticity. The cumulative fatigue damage theories checked by Deneff were:

1. Miner
2. Corten-Dolen
3. Shanley
4. Freudenthal
5. Marco and Starkey
6. Richart and Newmark
7. Henry

The report is well written and is certainly a must for all joint designers who wish to utilize rational joint design methods.

Lobbett, J. W. and Robb, E. A. (6.45)

"Thermomechanical Analysis of Structural Joint Study," WADD TR-61-151, January 1962, pp. 172.

This report is an extensive study employing an analysis method called the Redundant Force Method which is used for continuous type joints for various combinations of load and temperature. Comparisons are made with analyses by means of the Minimum Complementary Energy Method and the experimental method of photoelasticity. Finally, several tests to ultimate strength were conducted on spotwelded, bolted and brazed single and double lap joints.

Conclusions reached were:

1. In the analysis of a bolted joint, the bolt installation torque is of primary importance. As the torque increases, the friction between plates increases. This then decreases the shear load on the bolts in a multi-row joint. Figure 6.25 shows the relationships a 5-bolt joint (5 bolts in a line). Figure 6.26 shows a much smaller effect of temperature.

2. Two plates fastened together (single lap) at their overlap bow in the presence of a thickness-wise temperature gradient. Due to this bowing, the bolt axial loads increase as the plate thickness increases.

   The report contains several summary charts and graphs which describe the behavior of bolted or riveted joints as indicated from the analysis presented in this report.

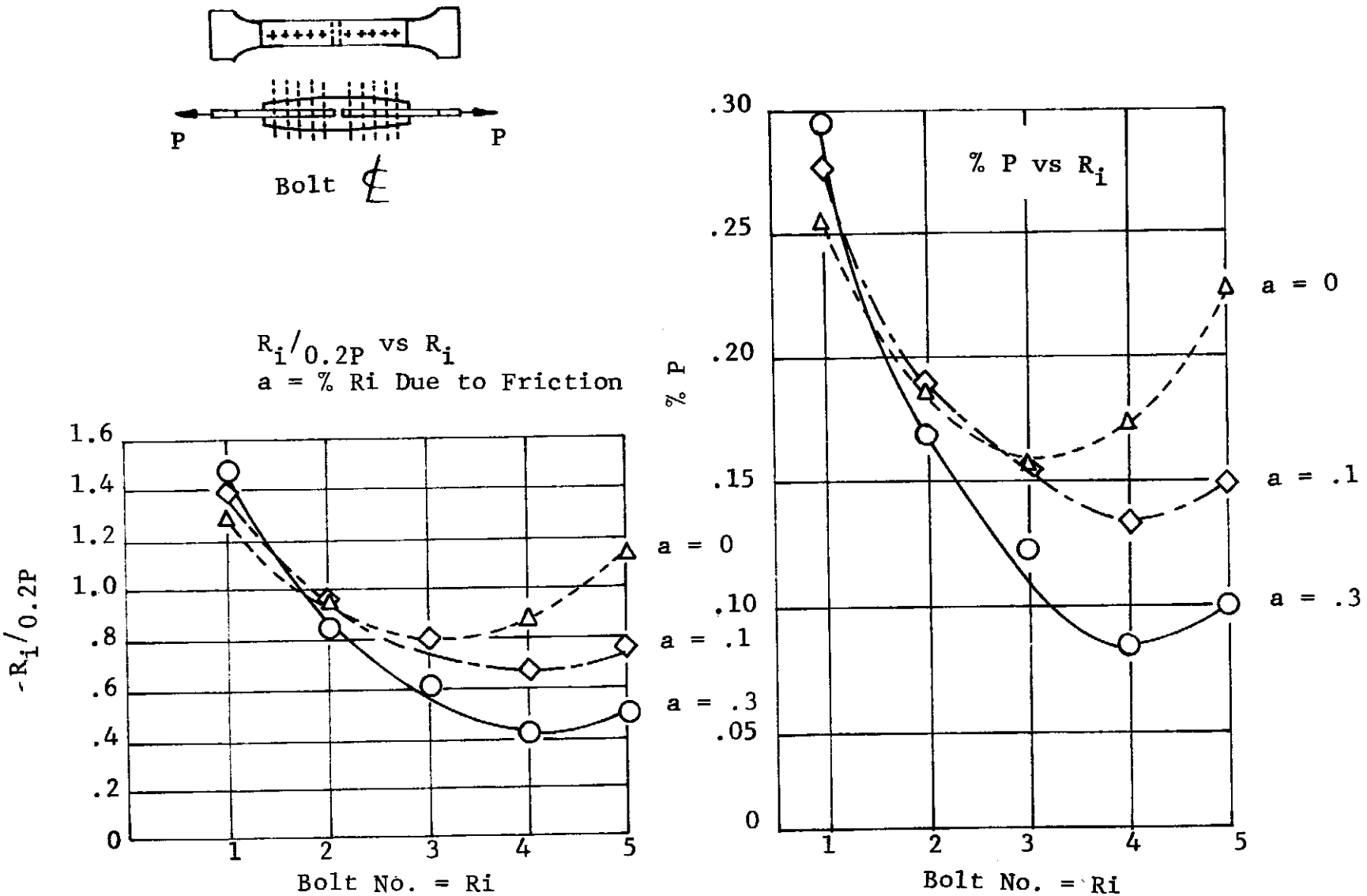

Fig. 6.25 EFFECT OF LOAD CARRIED BY FRICTION FOR A 5 BOLT JOINT (5 BOLTS IN A LINE), AFTER LOBBETT (6.45)

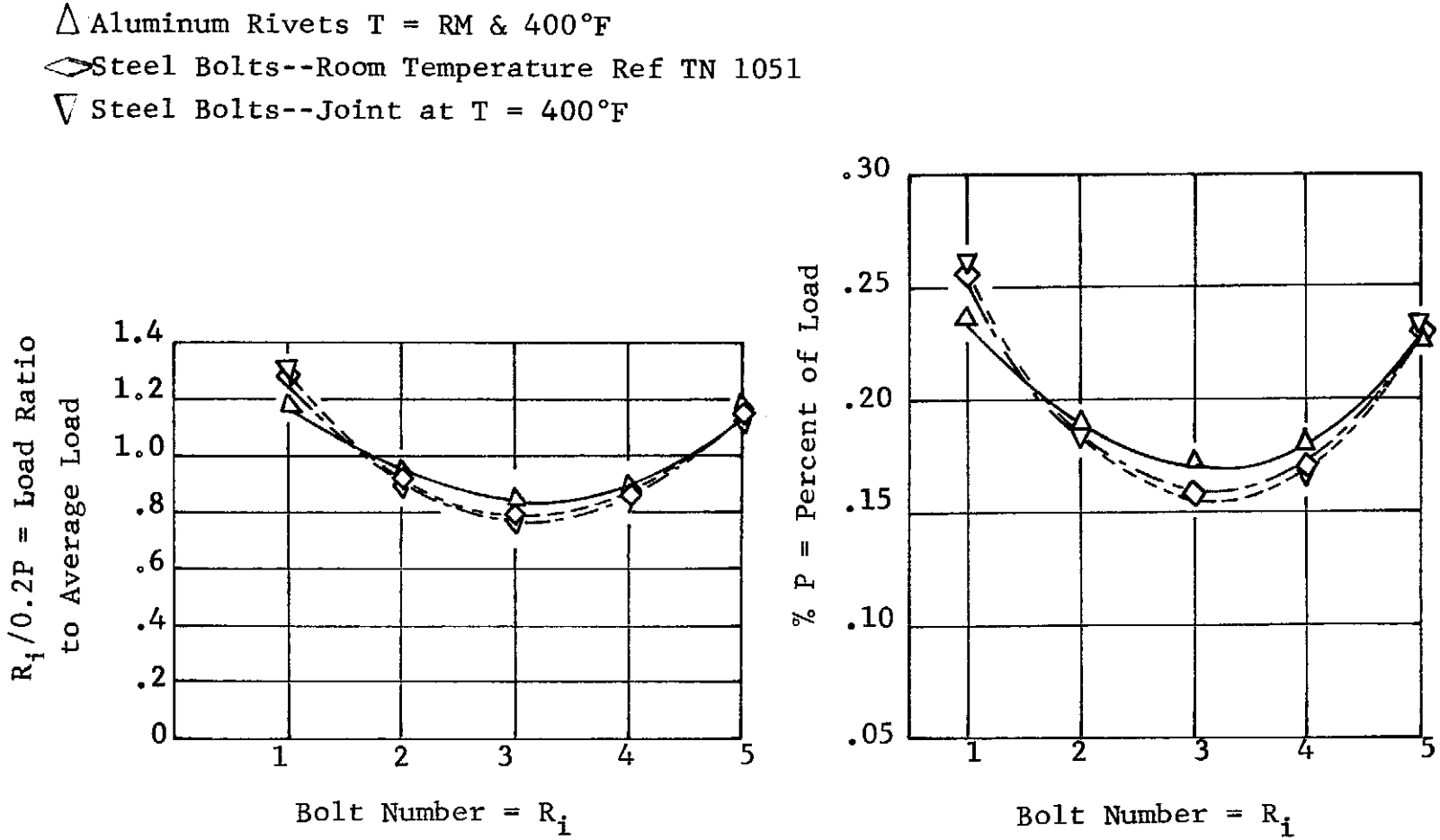

Fig. 6.26 LOAD DISTRIBUTION OF 5 BOLT OR RIVETED JOINT (5 BOLTS IN A LINE) AT ROOM AND ELEVATED TEMPERATURE, AFTER LOBBETT (6.45)

Switsky, H., Forray, M. J. and Newman, M. (6.67)

"Thermostructural Analysis Manual, Section 5-Thermoelastic Analysis of Joints," Vol I, WADD TR 60-517, August 1962.

This report is designed to attack the specific problem of analysis of bolted or riveted joints under combined mechanical and thermal loadings. The generalized joint is simplified to a single line of discrete fasteners. Single lap joints only are shown but the authors' "one-dimensional" case is more representative (for mechanical loads) of the double lap joint. In this "one-dimensional" case, the joint does not bend out of plane, and hence, distortions depend only on the axial flexibilities of the joint components in the direction of the applied external loading.

The method used by Switsky to obtain the load partitioning is to satisfy 1) the compatibility conditions for the joint displacements and 2) equilibrium equations. These are illustrated in Fig. 6.27. The adherends may be of different materials. The first type of solution made was to assume the fasteners filled the holes and that the combination distorted elastically. An alteration was then made to this solution to account for "slop" in the holes arising from both manufacturer's tolerances and differential thermal expansions.

The deformation has two contributing components. The first portion of the deformation is due to uniaxial stretching of the sheets due to the combined effects of temperature and mechanical loading. The second component is due to local distortions of the holes and attachments. These components add to produce the total (elastic) deformation. N-1 equations are obtained from the compatibility equations and one equation from equilibrium. This yields N equation in the N unknown loads P_j. These compatibility equations are expressible in terms of a single "recurrence" equation. In general, no simple relationships exist between successive P_j's. This occurs because the

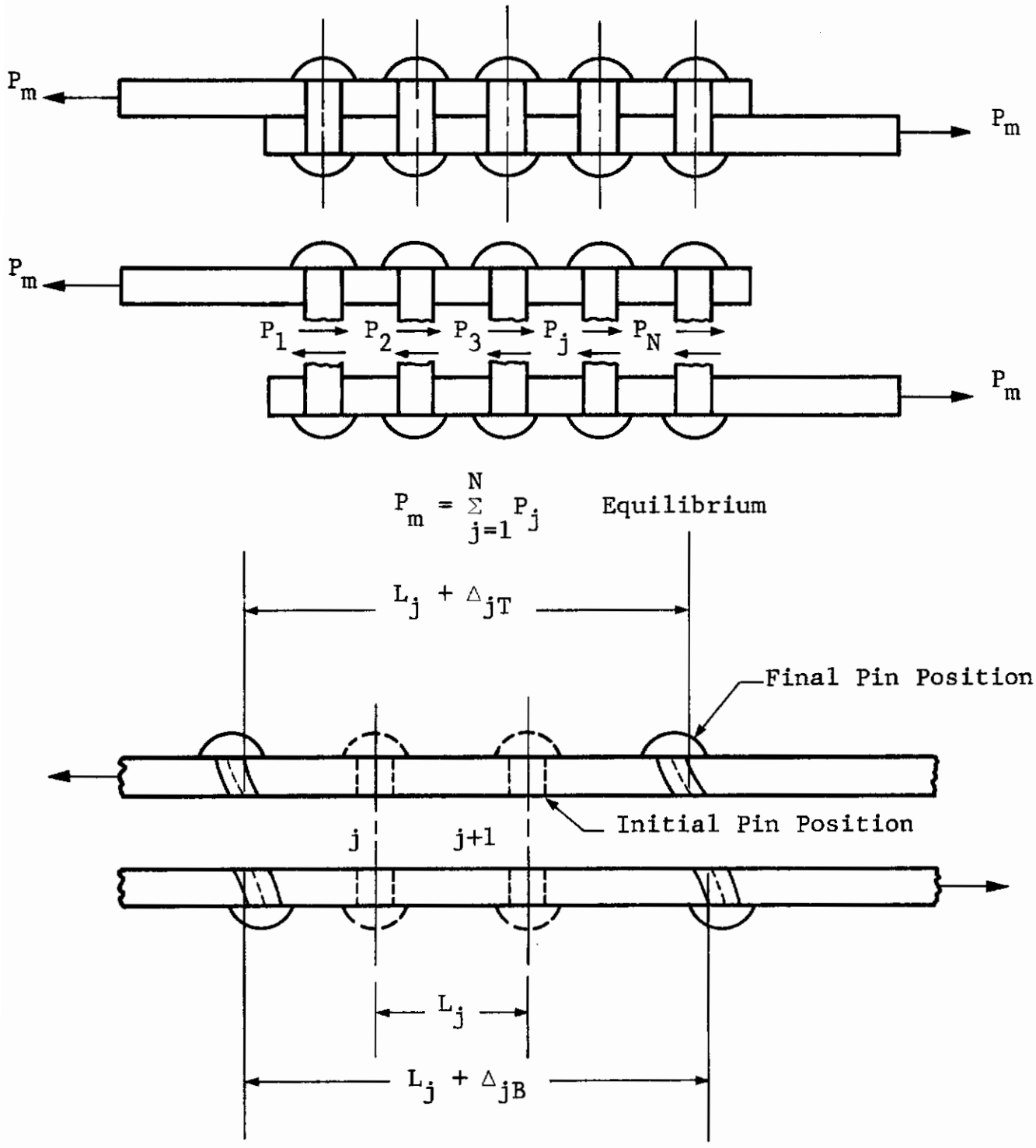

Fig. 6.27 EQUILIBRIUM AND COMPATIBILITY FOR ONE-DIMENSIONAL JOINT, AFTER SWITSKY (6.67)

coefficients in the equations are functions of the flexibilities and of the temperature distribution.

Following presentation of the general solution, Switsky then considered the special case where the flexibilities of the sheets and attachments are the same from row to row. Switsky states this condition is realized when

1. Sheet thicknesses are constant.
2. Fasteners are the same size and shape.
3. Spacing between rows is the same.
4. Temperature variation through the splice thickness does not vary appreciably in the direction of the mechanical loading.

The reader is referred to the report for the solution to this special case. Switsky presents curves for the coefficients in these equations which permit the numerical calculation of the rivet loads for up to ten rows of rivets. When the number of rows exceeds ten, the curves give the loads in the first five attachments from either end of the joint.

The equation is separated into two superimposable terms representing respectively the contributions from 1) the mechanical loads, and 2) the thermal loading. For an odd number of fasteners (rows), the central fastener must have zero contribution from the thermal loading (from a symmetry argument). For constant "bay" (space between individual adjacent fasteners) properties, the attachment loads due to thermal loading alone are symmetrical about the center of the joint.

Switsky then attacks the problem of the very stiff plates, where the fastener and hole distortions predominate, Switsky states that this condition occurs for very thick plates with small diameter fasteners or in the case of local yielding. Another relationship is derived for the load partitioning. In this solution, the mechanical contribution to the loads distributes

rather uniformly while the thermal contributions vary symmetrically about the center fastener. For the case of large local deformation, the effective hole flexibility coefficient increases and the sheet flexibility coefficient may become negligible in comparison. For this case, the contribution of the thermal loading is very nearly eliminated.

Switsky next attacks the problem of very rigid attachments and flexible sheets. Switsky states that this occurs when the sheets consist of soft materials and the fasteners are housed in large diameter bushings. The appropriate equations are then derived for this limiting case.

Switsky also derives equations appropriate to the influence of "slop" in the fastener on the load distribution. This set of equations assumes the "slop", e, is always given by $e \geq 0$. The equations, however, are not in readily solvable form (they are not simultaneous linear algebraic equations) involving unknowns as coefficients which require perturbational techniques to solve them. Switsky outlines the following recommended process for their solution:

1. Assume a set of directions for the attachment loads.
2. Determining the differential displacements between adjacent fasteners from one equation and solve simultaneous compatibility and equilibrium equations.
3. If the directions agree with the assumed directions, the solution is correct.
4. If the directions disagree, a new set of assumptions must be made preferably with the derived set.

The correct solution is obtained when the assumed set matches the derived set. An example involving a scarfed joint with three rows is then given.

Finally, Switsky gives an approximate approach to the "two-dimensional" (single lap) joint. The following simplifying assumptions are made:

1. Constant bay properties
   a. sheet thickness
   b. fastener size, stiffness, etc.
   c. fastener spacing
2. Thermal loads are assumed to be constant in the direction of the loads but can vary through the thickness.
3. Vertical out-of-plane deflections and clamping loads have a negligible effect on the load distribution (little beam column effect).
4. Moments at the attachments have a negligible effect on or are included in the attachment hole flexibility.
5. Contact faces of the top and bottom plates are initially plane and the external load is applied parallel to this plane.
6. The deformations are elastic with these assumptions. Switsky derives a new set of compatibility equations for the joint. The equilibrium equation remains the same.

Switsky concludes by stating the importance of determining accurately the load-flexibility diagram for a given fastener-hole combination. By using the initial flexibility slope, the loads on the individual fasteners will be predicted larger than actual at the higher load levels. When load deformation data is available and the joint analysis shows loads corresponding more closely to secant flexibilities then the flexibilities should be corrected and the analysis repeated. Switsky claims this process will converge. Switsky also presents

a method to be used if no data is available and how data in Mil-Handbook-5 can be used advantageously here.

Owen, J. B. B. (6.52)

"Design of Bolted Joints for Uniform Mean Stresses" Aero. Research Council Rept. No ARC 26, 153 STRUT 2647, August 1964.

This report utilizes the Batho Ref. 6.4 solution in an attempt to illustrate a means of designing bolted joints to produce equal bolt loads or constant mean stress in the plates. Owen's assumptions are:

1. Only average strains in the cover plates (outer and inner plates of a doublelap joint) are kept constant. Stress concentrations are neglected.
2. Friction in the joints is neglected.
3. Bolts are idealized into lines or shown in Fig. 6.28 according to their idealized distortion patterns.

Owen uses a form of Hooke's Law to construct an effective modulus E for the stretch ν and thus

$$\frac{np}{aE} = \frac{(N-n)p}{AE}$$

and therefore

$$\frac{A}{a} = \frac{N}{n} - 1$$

To effect equal bolt load partition all the ν must be equal. Owen concluded that this could be effected by changing 1) the cover plate geometry, 2) the bolt diameter or stiffeners, and 3) a combination of both. Owen constructed a joint and experimentally tested it. His results were inconclusive.

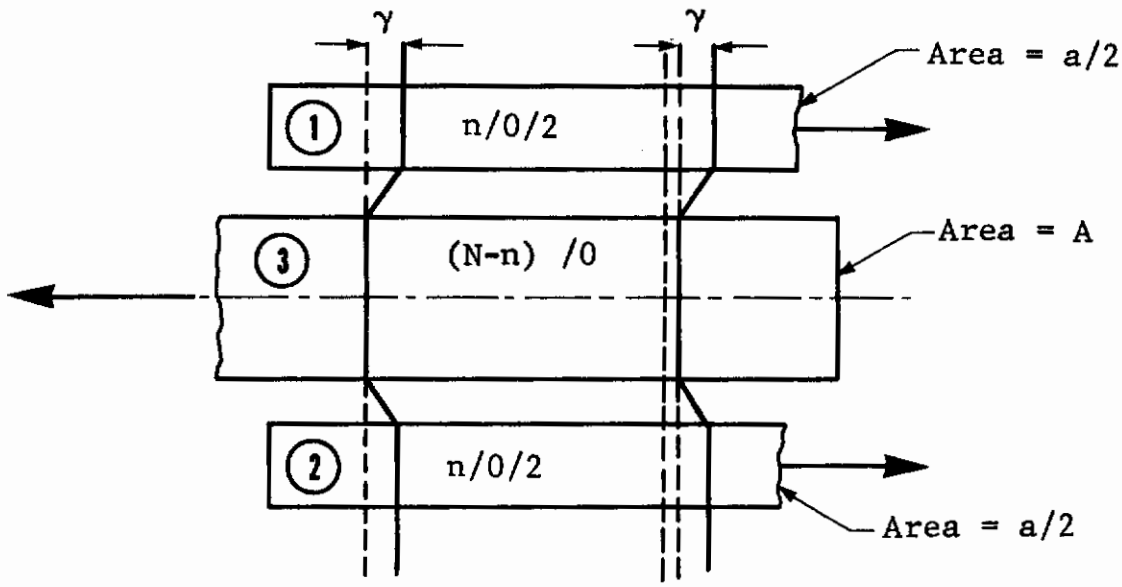

Fig. 6.28 IDEALIZED RIVETS OR BOLTS FOR DOUBLE LAP RIVETED JOINT

Fisher, J. W. and Rumpf, J. L. (6.21)

"Analysis of Bolted Butt Joints," J. Structural Div., Proc. ASCE, October 1965, pp. 181-203.

This paper presents an analytical technique developed by Francis in England for a double lap joint with both of the outer plates of equal thickness and made of the same material. The inner plate may be of any thickness and of a material different from that of the two outer plates. The joint is divided into equal gage strips (gage is the transverse space between holes) so that a single gage strip can be handled more or less independently. (See also Schenker Ref. 6.58). The theory is based on the assumptions that:

1. The fasteners transmit all applied load by shear and bearing once major slip has occurred (see Fig. 6.29).
2. The frictional forces may be neglected in the region for which the solution is intended, the region between major slip and ultimate load.

Equilibrium relations are developed which account for shear at all rivets. A second set of relationships are then developed in the nonlinear range which account for compatability of displacements between the two outer plates and the inner plate. Very sophisticated analyses are developed for the deformations locally in the neighborhood of the holes. These relationships include the effects of shear, bending and bearing on the fastener and localized effect of bearing on the plates.

Fisher finds that he can handle the problem semi-empirically if he knows the load-deformation behavior of "standard coupons," i.e., a plate with holes and the fastener itself. He also develops analytical models for these quantities, i.e., plates with holes and fasteners.

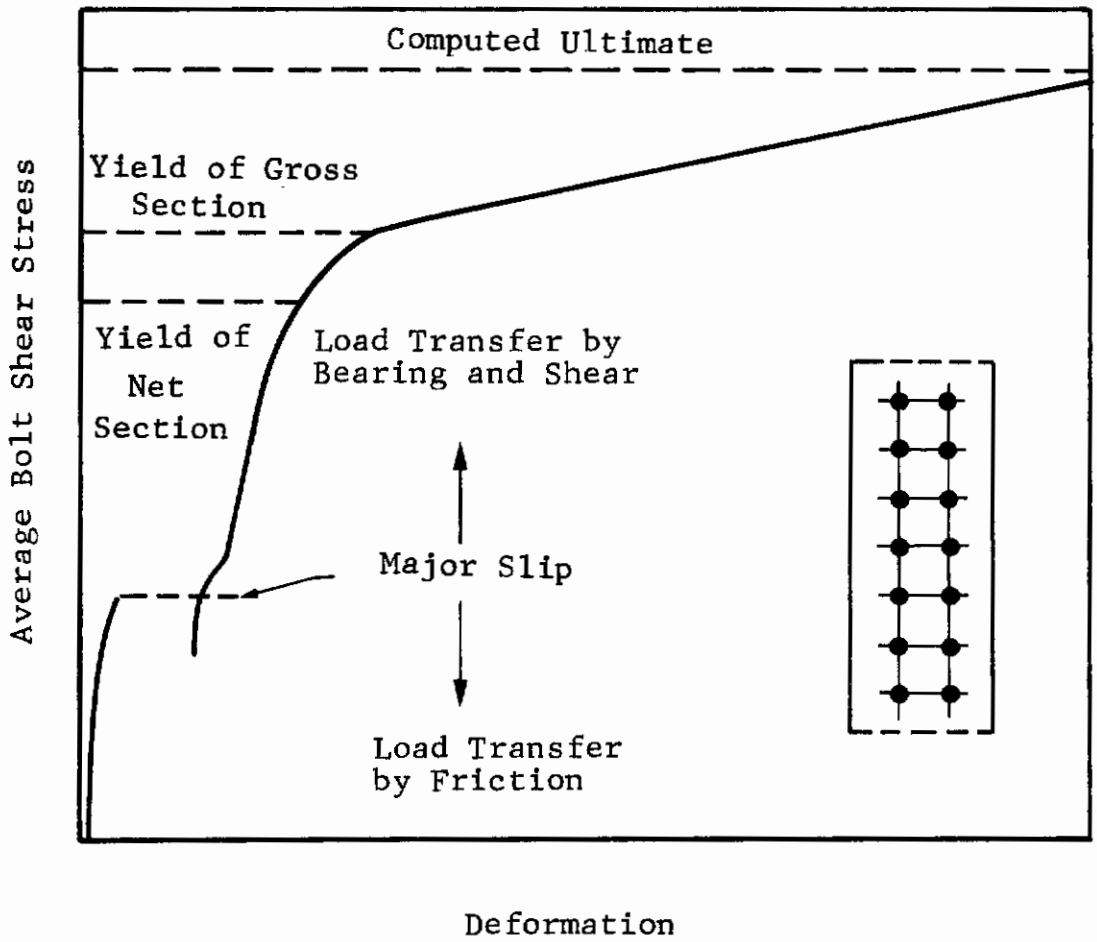

Fig. 6.29 LOAD-DEFORMATION BEHAVIOR OF JOINT STUDIED BY FISHER (6.21)

Fisher then attempts a general solution of the equilibrium and compatability equations derived earlier using both his experimental and analytical models for the standard coupon behavior. The following assumptions were used by Fisher to facilitate the solution:

1. Fasteners transmit all load once slip has occurred.
2. The analytical expressions are applicable to the component elements of the connection. (This is equivalent to the assumption that the load-deformation relationships for the strip between successives rows of fasteners is essentially identical).
3. All fasteners are the same diameter.

An iterative process based on a trial solution for the fastener loads was used and it was checked by equilibrium. Digital computer techniques facilitated the lengthy computations.

Differences in the experimental methods used to obtain the fastener-deformation relationships for a single fastener gave rise to three computational methods for predicting joint ultimate loads. These three methods were:

Method 1

All bolts were assumed to behave the same as a single bolt loaded in a tension jig. The maximum load and deformation in the end fasteners of the joint correspond to the ultimate load and deformation of a single fastener in a tension jig.

Method 2

All bolts were assumed to behave the same as a single bolt loaded in a tension jig. The failure load and deformation of the end fasteners

of the joint correspond to the rupture load and deformation of a single fastener in a tension jig.

Method 3

All bolts are assumed to behave the same as a single bolt loaded in a compression jig. The maximum load and deformation of the end fasteners of the joint correspond to the ultimate load and deformation of a single fastener in a compression jig.

Comparison of the results of a series of tests as shown in Table 6.4 for A440 steel show the acceptability of the three methods for predicting ultimate joint loads.

The paper is well written and provides a methodology for extending the joint analysis into the nonlinear behavioral range.

6.2.8 Annotated Biblography: Experimental Analyses

Coker, E. G. and W. A. Scoble (6.12)

"The Distribution of Stresses Due to a Rivet in a Plate," Trans. Inst. Naval Architects, 1913, pp. 207-218.

This paper contains a discussion of the stress distribution in plates with holes. The stress distributions are obtained by the methods of photoelasticity (which gives the sum of the principal stresses). After checking the accuracy of the experimental techniques on the case of the unloaded hole in a strip, Coker applied the methods to a tension member with a rivet in a hole.

His first solution was for an "idle" (not loaded) rivet in an infinite plate stretched in tension. If the gross section stress (at infinity here) is σ_m, then the values of σ_1 and σ_2 are given in Table 6.5.

Table 6.4

COMPUTED AND TEST ULTIMATE STRENGTHS OF BOLTED JOINTS, AFTER FISCHER AND RUMPF (6.21)

Joint Number	Load at Failure (kips)	Computed Ultimate Strength (kips)				
		Method 1	Method 1 Computer / Observed	Method 2	Method 3	Method 3 Computed / Observed
1	728	730	1.003	699	800	1.099
2	727	730	1.003	699	800	1.099
3	767	767	1.000	757	798	1.040
4	1188	1209	1.018	1193	1320	1.111
5	1610	1604	0.996	1596	1720	1.068
6	2125	2062	0.970	2074	2155	1.014
7	2545	2425	0.953	2446	2526	0.993
8	1070	1086	1.015	1075	1147	1.017
9	2180	2080	0.954	2094	2164	0.993
10	1270	1268	0.998	1224	1392	1.096
11	2785	2720	0.977	2726	2842	1.020

Table 6.5

PRINCIPAL STRESSES ALONG TRANSVERSE AXIS THROUGH CENTER OF IDLE RIVET IN PLATE

2x/a	$\frac{\sigma_1}{\sigma_m}$	$\frac{\sigma_2}{\sigma_m}$
1.12	2.20	-0.60
1.16	2.24	-0.31
1.20	2.05	-0.20
1.60	1.45	0.06
2.00	1.28	0.07
2.40	1.19	0.03
3.20	1.04	-0.04
4.00	0.93	-0.09

Next Coker examined the case of a force applied to the plate through a rivet. Table 6.6 shows the principal stresses along the transverse axis through the rivet (perpendicular to the rivet force) and along the longitudinal axis through the rivet (parallel to the rivet load). Although Coker could not measure σ_1/σ_m at $2r/a = 1$ on the side of the rivet, his estimate was that the tension stress was "very high, probably of the order of 5 σ_m". This case involved the following parameters: $a/w = 0.25$ and $a/H = 0.286$, where H is the distance from the center of the hole to the end of the plate.

Coker also examined the case where $a/w = 0.5$ and $a/H = 1.0$ see Table 6.7).

Templin, R. L. (6.69)

"Aluminum Connecting Rods, An Investigation of the Stress Distribution," Mechanical Engineering, Vol 58, March 1936, pp. 169-170.

This paper presents the results of a mechanical strain gage investigation of the stresses in a connecting rod. The ratio a/w was held to

$$a/w = 0.485$$

Three levels of interference including zero were investigated. The maximum stress concentrations (tensile) were found to act at the edge of the hole across the pine and the stresses were determined to vary from 1.20 to 2.68 σ_{nom} where

$$\sigma_{nom} = \frac{P}{(w-a)t}$$

Table 6.6

PRINCIPAL STRESSES FOR LOADED RIVET (a/w = 0.25)

2r/a	σ_1/σ_m	σ_2/σ_m	σ_1/σ_m	σ_2/σ_m
1.32	2.03	0.23	--	--
1.40	1.35	0.45	--	--
1.60	--	--	0.025	-2.52
1.80	1.02	0.38	0.255	-1.445
2.20	0.90	0.25	--	--
2.60	0.72	0.22	0.205	0.625
3.00	0.60	0.145	--	--
3.16	0.535	0.125	--	--
3.40	--	--	0.185	0.185
3.72	0.375	0.00	--	--
4.40	--	--	0.2	0.00
5.00	--	--	0.34	0.00

Table 6.7

PRINCIPAL STRESSES FOR LOADED RIVET WITH a/w = 0.33 AND a/H = 1.0

2 r/a	Stresses across Section σ_1/σ_m	Stresses across Section σ_2/σ_m	Stresses below Rivet σ_1/σ_m	Stresses below Rivet σ_2/σ_m
1.20	2.68	0.125	--	--
1.40	--	--	-3.44	-0.88
1.45	1.90	0.30	---	--
1.72	--	--	--	--
1.80	1.42	0.42	--	--
2.00	--	--	-1.39	0.49
2.20	1.11	0.35	--	--
2.32	--	--	-0.93	0.55
2.60	0.42	0.31	-0.41	0.84
2.84	0.02	--	-0.025	1.30
2.90	--	0.30	--	--
Edge of plate = 3.0		0.195	0.225	1.82

Hennig, A. (6.27)

"Polarized Light Stress Investigations on Tensile Bar with Holes and on a Rivet Hole," Trans. from Z. Tech. Mech. and Thermo. Forschung auf dem Gebiete des Ingeneir, v 4, n 2, 1933, pp. 63-63.

This paper is an early attempt at a photoelastic solution for the stress distribution around unloaded holes in finite width strips. Despite the fact that Hennig placed a great deal of emphasis on obtaining very accurate measurements of the photoelastic isoclinics, his solution for the unloaded hole is incorrect. The solution is obtained for several ratios of hole diameter to plate width. Hennig obtains the empirical relationship for a/w from 1 to 1.5:

$$\sigma_T = \sigma_m \left[3 - 4\frac{r}{a} + 6.4\left(\frac{r}{a}\right)^3\right]$$

where

σ_T = maximum normal stress at hole periphery

σ_m = nominal stress at infinity

r = distance from hole center

a = hole diameter

w = width of strip

This relationship indicates stresses of far lower magnitude than those obtained theoretically later by Howland but are also lower than those obtained much earlier by Coker (6.12).

Hennig also attacked the multiply connected problem of a rivet in the hole by photoelasticity. First he established the isoclinics (constant stress directions) for two types of material using Sonntag's eqn and was convinced that the stress directions, φ, did not change substantially for the different Poisson ratios encountered (ν = 0.3 for iron and ν = 0.22 for flint glass).

Hennig obtained results corresponding to (his titles are shown in parenthesis)

1. Loose fitting rivet (single force).
2. Tight fitting rivet (ground rivet).
3. Rivet bearing at 2 points on side of hole.
4. Rivet close to edge of plate.
5. Rivet at center of infinite sheet.

Henning, after integrating the stresses across various sections to obtain the load, claimed good agreement with the known applied load. He concluded, however, that the experiments would be open to doubt for the following reasons:

1. Mode of force introduction is critical.
2. Contact surfaces may influence the stress state considerably (friction, etc.).
3. Possibility of plastic flow occurring in the contact region.
4. Influence of the a/H ratio and of the a/w ratio.

This paper contains a review of the German literature until 1933.

Bollenrath, F. (6.8)

"About the Stress Distribution in Electric Resistance Welding Joints in Thin Sheet Metals," Redstone Scientific Information Center, Report No. RSIC-297, October 7, 1964, Trans. from January 1937 Article.

This report examines the case of spot-welded joints in single lap and double lap joints. Although the simulated spot weld area appears continuous with the parent adherend material, the value of the paper is that it is practically unique since it describes the stress distribution through the thickness.

The method used to determine the stresses is that of photoelasticity. Stresses are separated only along the boundaries of the specimen where one of the principal stresses is zero. The maximum tensile stresses are of the order of 5.43 times the gross section stress $\sigma_m = P/wt$ for $a/w = 0.5$.

The cases studied by Bollenrath are shown in Fig. 6.30. These cases essentially involve 1) a single-lap single weld, 2) a double-lap single-weld and 3) a single-lap double-weld. Since the examination is through the thickness no a/w ratios are available, the a/t ratio was held at a/t = 3.0 as shown in Fig. 6.31 (the single-lap single weld). The maximum tensile stress due to the bending in the adherends next to the rivet or weld was 3.42 times the average gross stress of $\sigma_{T',max} = 3.42\ \sigma_m$. (For spot welded joints, the maximum stress occurred at the center of curvature in the weld between the two adherends and was equal to $5.43\ \sigma_m$.) The surface compressive stress on the outside at B was $\sigma_{C',max} = 1.42\ \sigma_m$.

As shown in Fig. 6.32 (the double-lap single-weld), we have

$$\sigma_{T,max} = 1.40\ \sigma_m$$

$$\sigma_{C,max} = 1.43\ \sigma_m$$

As shown is Fig. 33 (the single lap, double weld), we have

$$\sigma_{T,max} = 3.0\ \sigma_m$$

$$\sigma_{C,max} = 0.8\ \sigma_m$$

In this last case, the compressive stress which occurs at the weld interface falls off rapidly and becomes tensile between the two welds.

Bollenrath points out that the peak tensile stresses for spot weld ($5.43\ \sigma_m$) are the same as those for rivets ($5.4\ \sigma_m$).

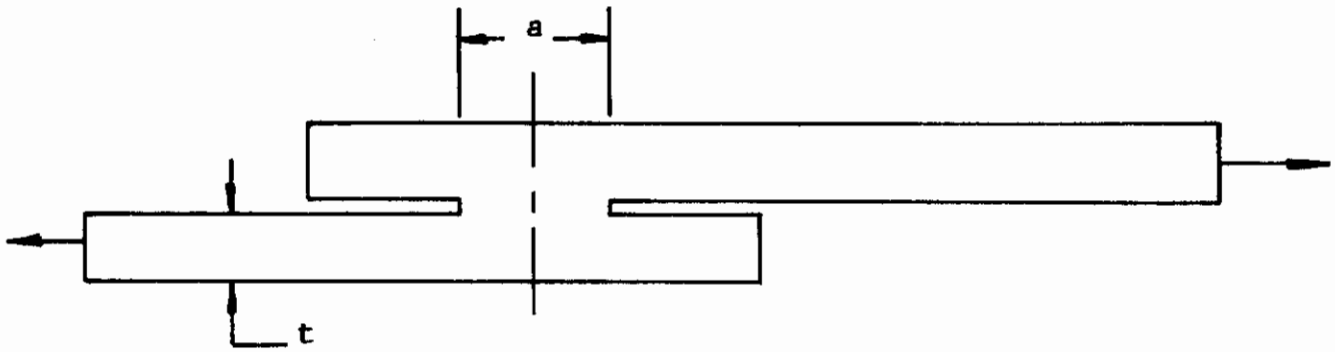

a) Single-Lap Single-Weld Joint

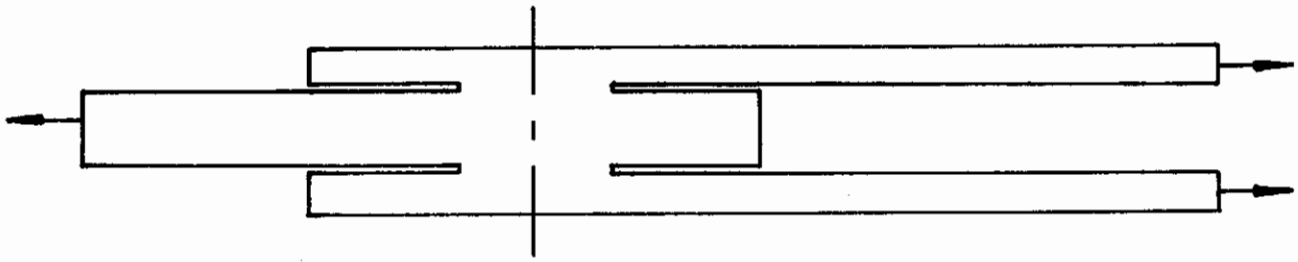

b) Double-Lap Single-Weld Joint

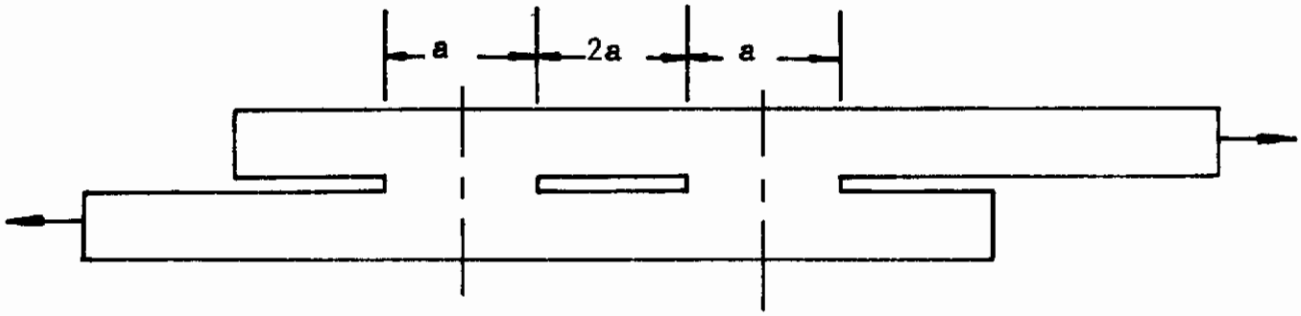

c) Single-Lap Double Weld Joint

Fig. 6.30 JOINT TYPES STUDIED BY BOLLENRATH (6.8)

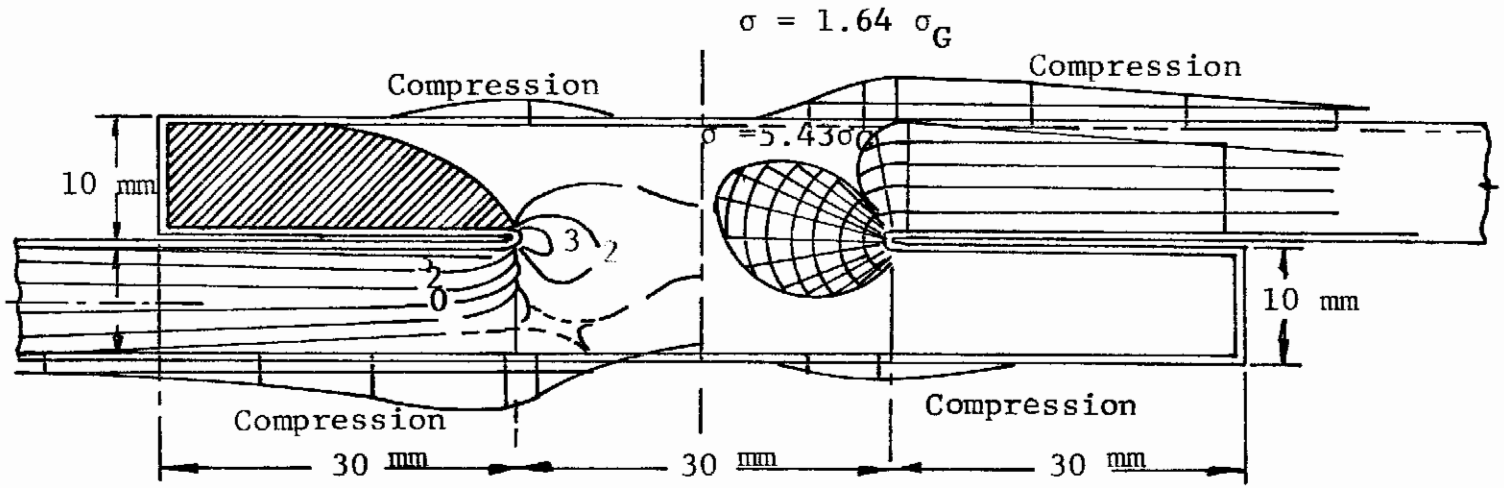

Fig. 6.31 ACROSS THE THICKNESS STRESSES FOR SINGLE-LAP, SINGLE WELD JOINT (6.8)

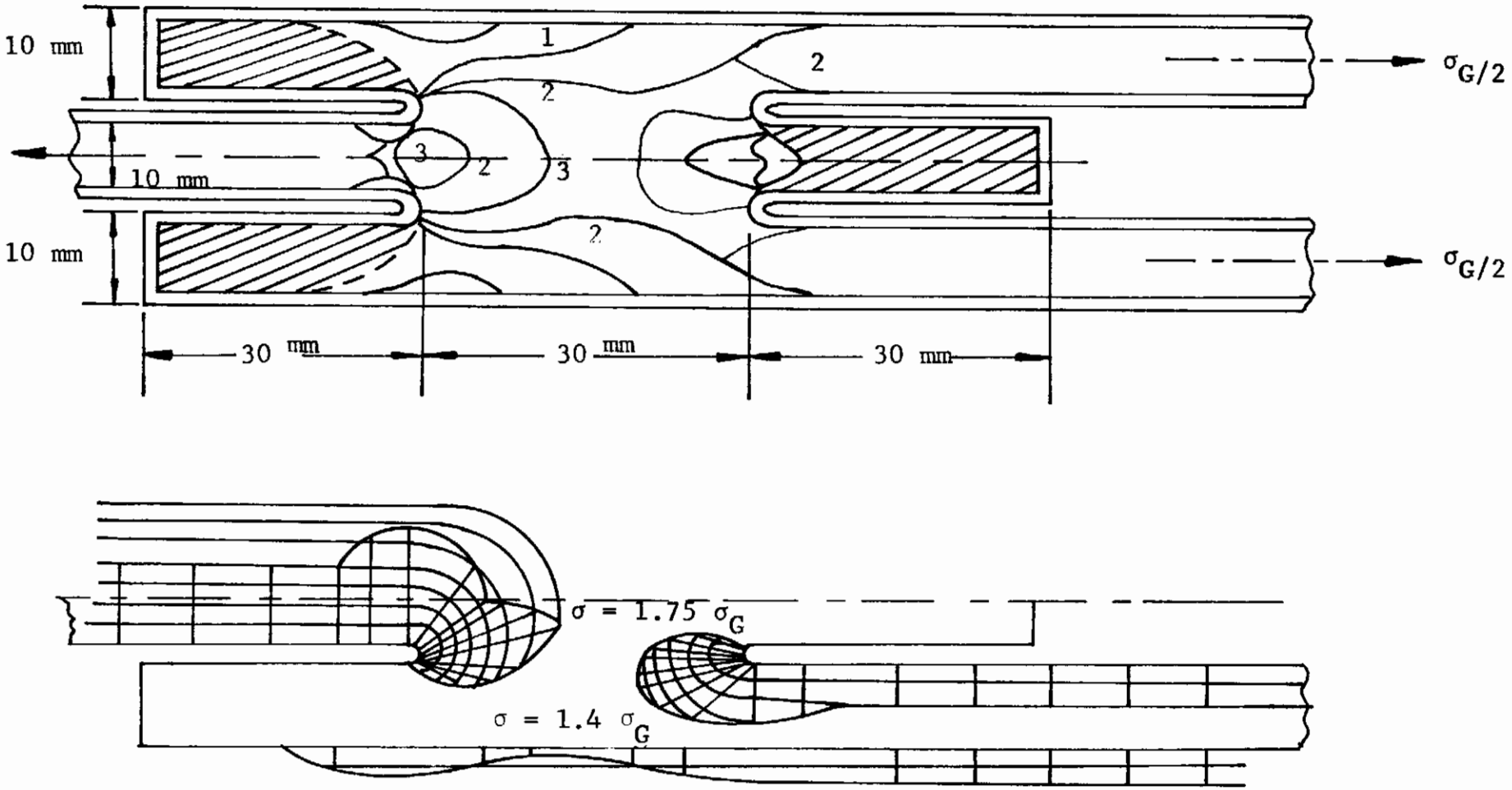

Fig. 6.32 ACROSS THE THICKNESS STRESSES FOR DOUBLE-LAP, SINGLE-WELD JOINT

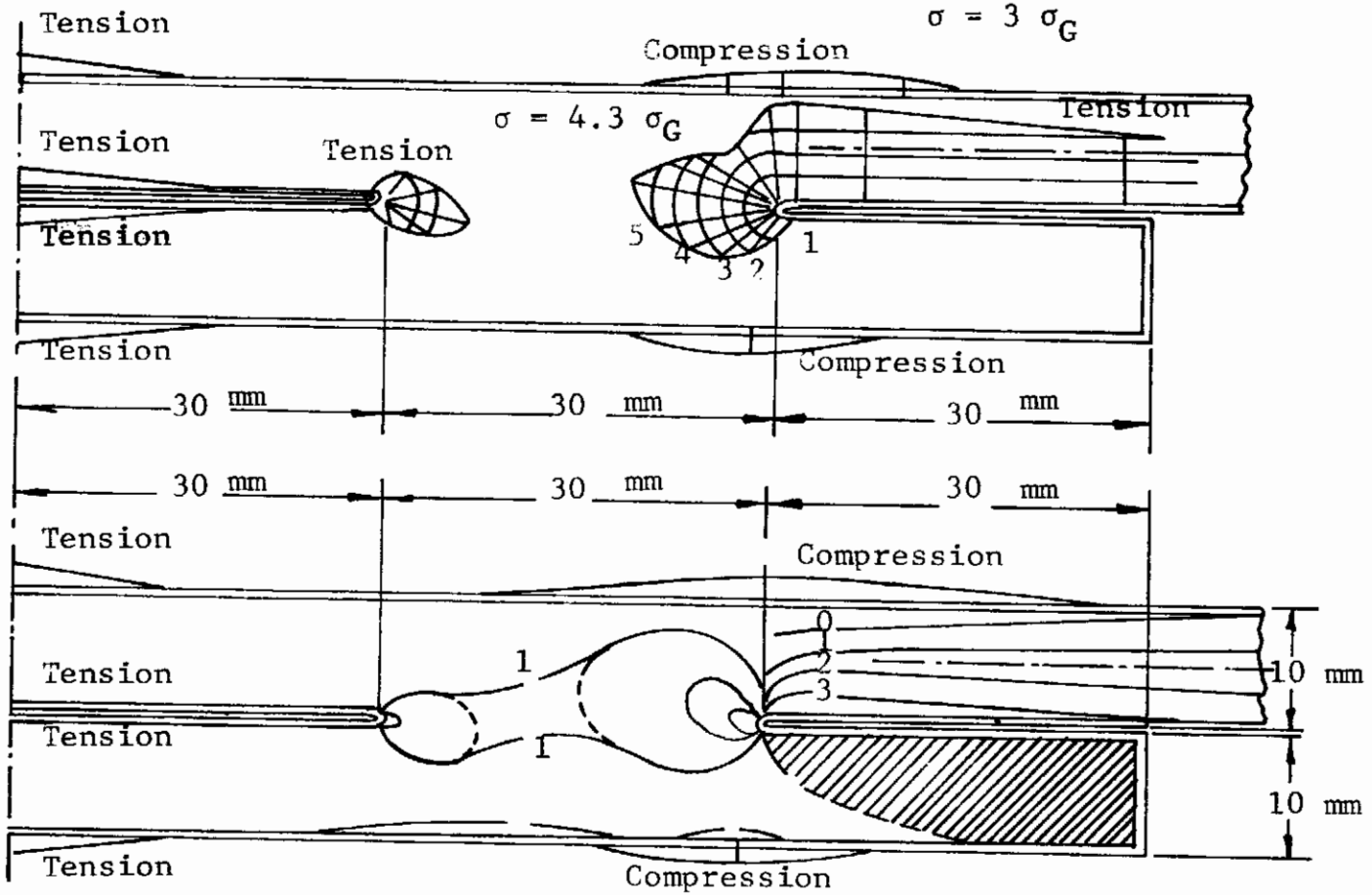

Fig. 6.33 ACROSS THE THICKNESS STRESSES FOR SINGLE-LAP, DOUBLE-WELD JOINT

Although this is so, it is not a problem for single cycle tests to destruction since flow will occur and attenuate the stress levels. However, it is problematical in fatigue loading. Several examples are cited to prove this point.

It is also interesting to note that the results are also applicable to adhesive joints containing a non-glue area crack since the peak stresses ($5.43\ \sigma_m$) occur at the crack tip. Such a condition could, indeed, be a limiting factor in adhesive joint design.

Frocht, M. and Hill, H. (6.23)

"Stress Concentration Factors Around a Central Circular Hole in a Plate Loaded Through a Pin in the Hole," Trans. ASME Vol 62, 1940, pp. A-5.

Frocht employed two experimental methods in this investigation. The first utilizing electrical resistance strain gages and Huggenberger mechanical gages together with aluminum models determined the maximum stresses at the edge of a hole loaded by means of a pin in the hole. By starting with a very wide plate (55 in.) and conducting successive tests on decreasing plate widths (to 12 in.), Frocht was able to cover the range of $0.146 \leq a/w \leq 0.66$ for a single pin. The hole center to plate end distance, H, (see Fig. 6.34) was maintained at $a/H = 0.4$ until the final test at which time the ratio was changed to $a/H = 0.67$. In this range, Frocht examined the stress concentrations for various classes of pin fit. The results are shown in Fig. 6.34. Remember when using these results that $\bar{\sigma} = P/(w-a)t$.

The second class of solutions were obtained using the method of photoelasticity. Here shaving of the edge was also employed to present similar curves for the range $0.086 \leq a/w \leq 0.76$. During the course of these investigations, Frocht was forced to vary H/w so that his final curves shown in Fig. 6.35 are parametric in H/w. In this investigation, Frocht also studied various fits and came to the conclusion that neat-fitting

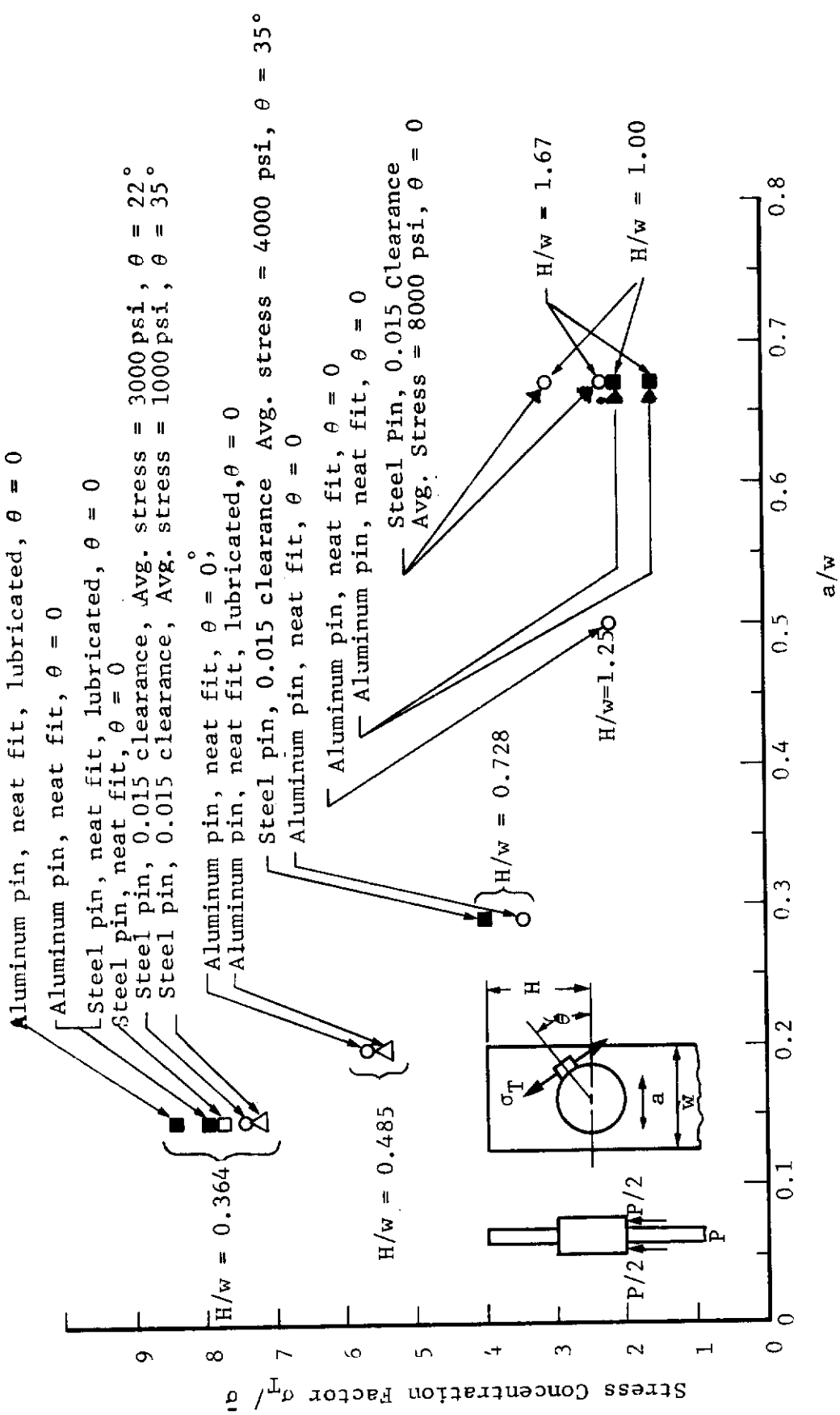

Fig. 6.34 STRESS CONCENTRATION FACTORS FOR VARIOUS a/w RATIOS AND SEVERAL PIN-FIT CONDITIONS

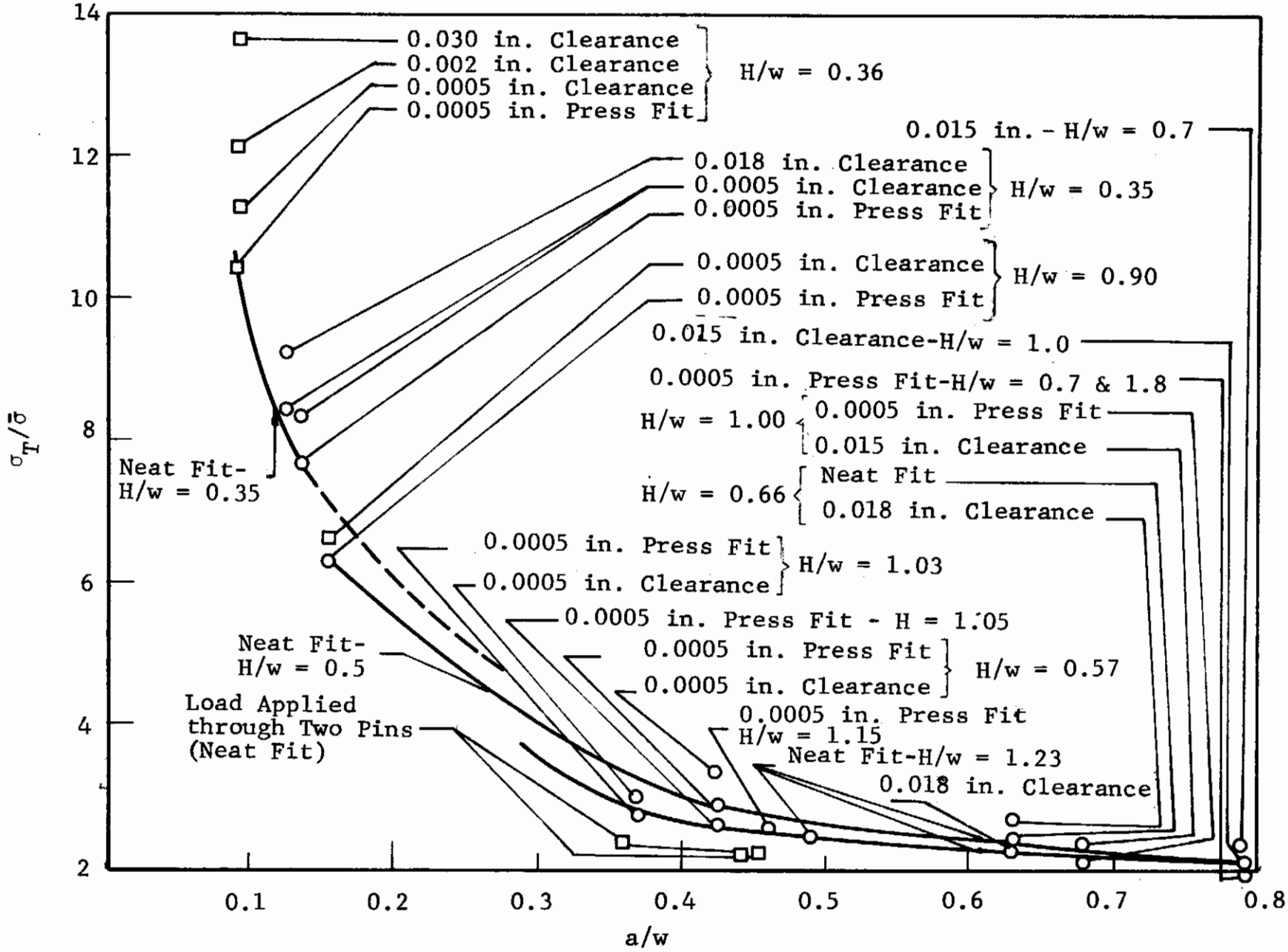

Fig. 6.35 STRESS CONCENTRATION FACTORS DETERMINED PHOTOELASTICALLY, AFTER FROCHT (6.23)

pins give lower stress concentrations than loose or clearance type pins. For this reason he also plotted a composite curve shown in Fig. 6.36 for neat-fitting pins only. This curve contains several points from other solutions found in this review and some points which this author was unable to locate in open literature. (Frocht obtained some data by private communications.) It is also important to note that Frocht was aware of the potential difference in the several classes of solutions since the theory of elasticity tells us, that, for multiply-connected regions, the solution depends on Poisson's ratio, ν. Frocht also presented a curve compositing all the results from both strain gages on aluminum models (ν = 0.3) and the photoelastic bakelite resins models (ν = 0.45). These results are also shown in Fig. 6.37.

Frocht also conducted tests where two pins spaced equidistant about the centerline were used to carry the load instead of a single pin. For this case a/w took the values a/w = 0.18 and a/2 = 0.225. These are plotted in Fig. 6.35 for the case where the combined length of the two diameters is equal to that for a single pin, i.e., at a/w = 0.36 and a/w = 0.45. It is interesting to note that Frocht found from several tests where the center to center distance of the two holes was varied that no effect on the stress concentration factors was observed.

Wilkins, E. W. C. and Jessop, H. T. (6.73)

"A Photoelastic-Fatigue Programm in Connection with Bolted Joints," J. Roy. Aero. Soc., Vol 58, June 1954, pp. 435-438.

This paper describes a planned combined photoelastic experiment and fatigue tests for a double-lap single-rivet hole configuration with the following parameters varied

$$a/w,\ \nu_{pin}/\nu_{plate},\ \ a_{pin}/a_{plate}$$

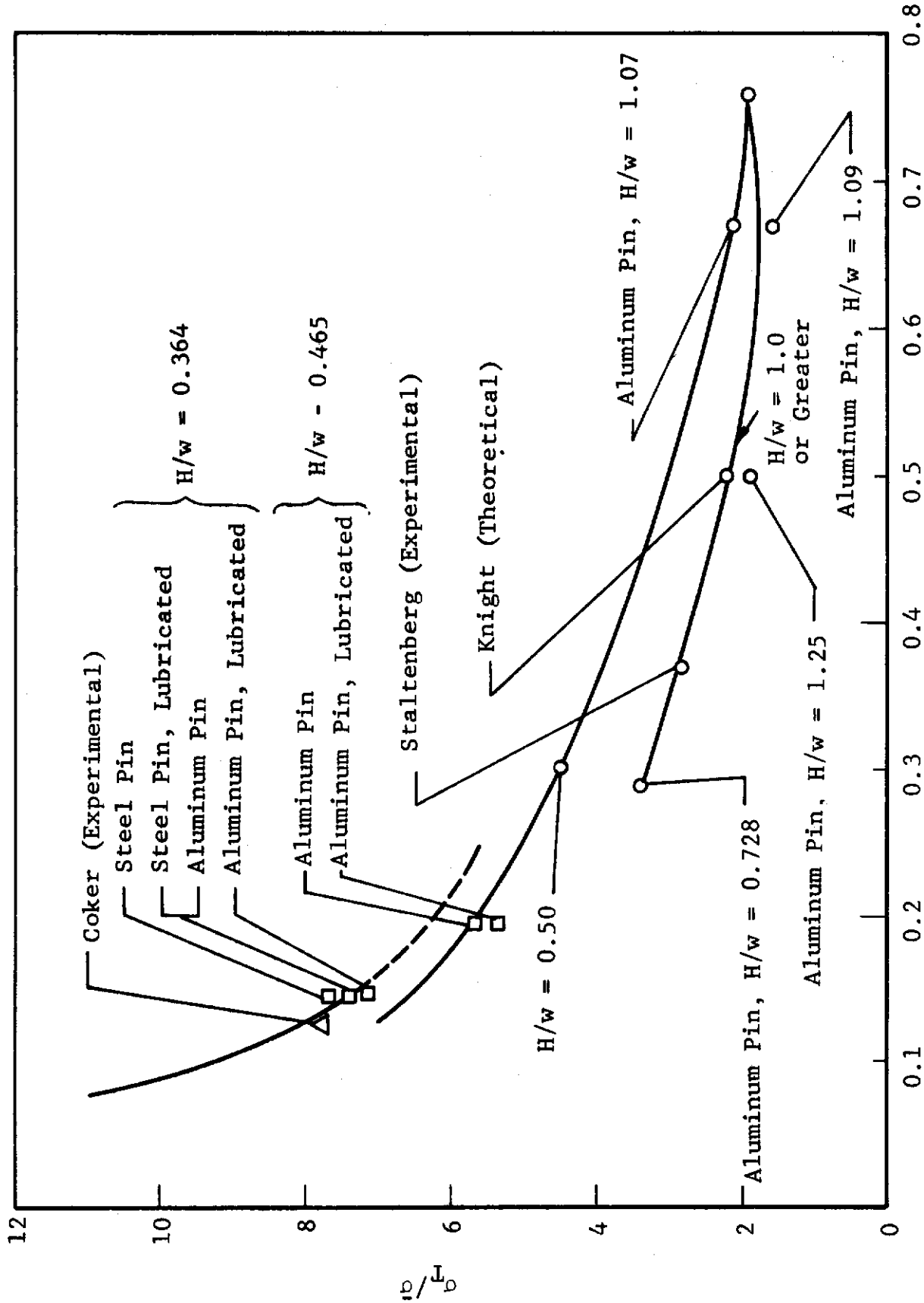

Fig. 6.36 STRESS CONCENTRATION FACTORS FOR NEAT-FITTING PINS, AFTER FROCHT (6.23)

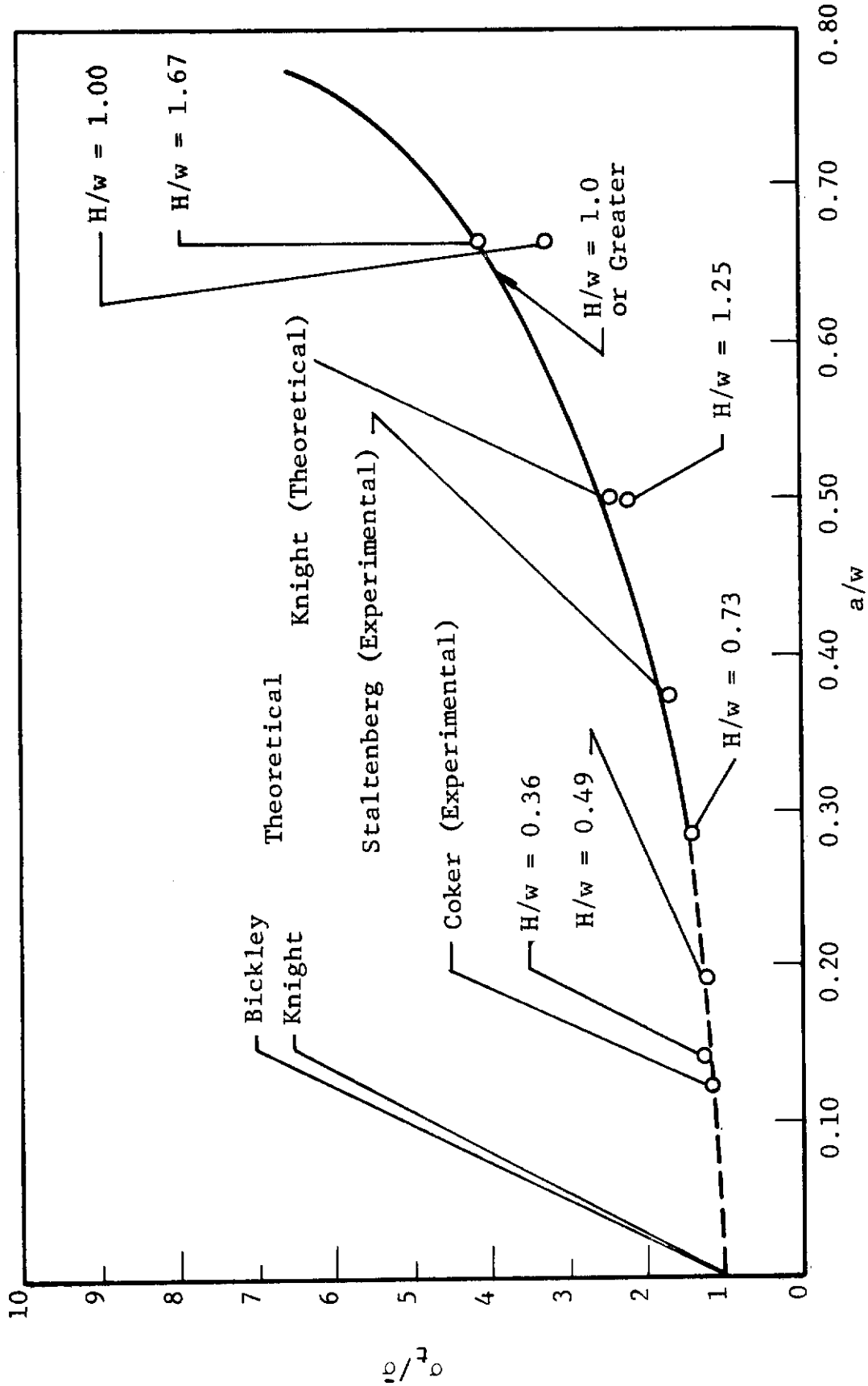

Fig. 6.37 STRESS CONCENTRATION FACTORS BASED ON AVERAGE BEARING STRESS, AFTER FROCHT (6.23)

a/t was to vary from 0.125 to 0.50 E_{pin}/E_{plate} was to vary from 1 to 100. No results are presented.

Jessop, H. T., Snell, C., and Hollister, G. S. (6.34)

"Photoelastic Investigation in Connection with the Fatigue Strength of Bolted Joints," The Aero. Quarterly, August 1955, pp. 230-239.

This paper describes a photoelastic investigation of the stresses surrounding an idle rivet or bolt in a hole in a strip. Hole diameter to plate width ratios investigated were a/w = 0.5, 0.375, 0.25 and 0.125. Extensive measurements were made of the zone about the rivets where contact between the rivet and hole was eliminated. This zone was defined by some angle called the lift angle (see Fig. 6.38). Stresses along the horizontal axes across the hole and along the vertical axis below the hole were determined for each of the four a/w ratios listed above.

The general conclusions reached by Jessop were:

1. The maximum shear stresses on the hole periphery were not substantially different from those around an unfilled hole in a tension plate.
2. The peak tensile stresses on the hole boundary were in all cases reduced by the presence of the tightly fitting pin.
3. Small variations in pin fit affect the stresses far more significantly than wide variations in the elastic modulus.
4. The angle of lift appears to be insensitive to load level and the stress distributions are not appreciably affected by load level.

These qualitative observations by Jessop may contribute substantially to any design approach involving loaded rivets.

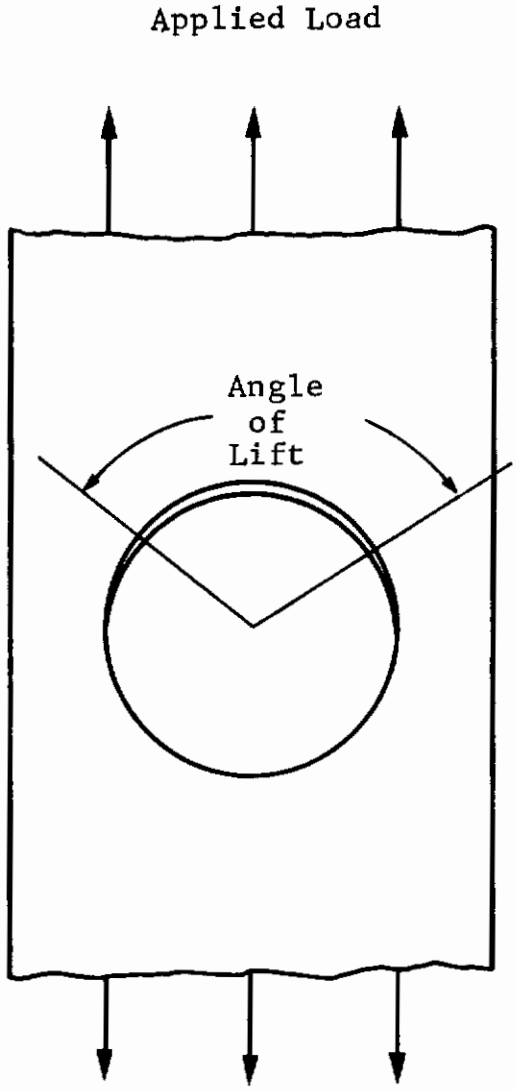

Fig. 6.38 ANGLE OF LIFT, AFTER JESSOP (6.34)

Many more solutions exist for the stresses around unfilled multiple holes in plates than for loaded or filled holes. The shear stresses for such configurations are well established in the literature. For materials which may fail in shear, the utilization of these solutions would be helpful. It also appears that the pin diameter to hole diameter becomes a critical parameter.

Figure 6.39 shows the plot of the maximum tensile and minimum compressive stresses across the hole perpendicular to the load direction as a function of a/w. Figure 6.40 shows the plot of the maximum and minimum stresses along the vertical axis as a function of a/w. Figure 6.41 is a comparison of the maximum tensile stresses at the side of the hole for the filled and unfilled holes.

Jessop, H. T., Snell, C., and Holister, G. S. (6.35)

"Photoelastic Investigation on Plates with Single Interference - Fit Pins with Load Applied to Plate Only," The Aeronautical Quarterly, Nov. 1956, pp. 297-314.

This paper describes a photoelastic investigation of the influence of an interference type pin on the stress concentration factor around the pin in a plate loaded in tension. No load is applied directly to the pin (see Fig. 6.42). Two levels of interference and several classes of pin material were studied. In general, the stress concentration factor decreased with increasing levels of interference. No differences were found for different ratios of Young's modulus of pin and plate.

Bodine, E. G., et al (6.7)

"Creep Deformation Patterns of Joints Under Bearing and Tensile Loads," NACA TN 4138 December 1957, pp. 36.

This report describes an experimental study of creep deformations in a model (oversize) of a riveted joint. The permanent deformations which occurred in the model were measured

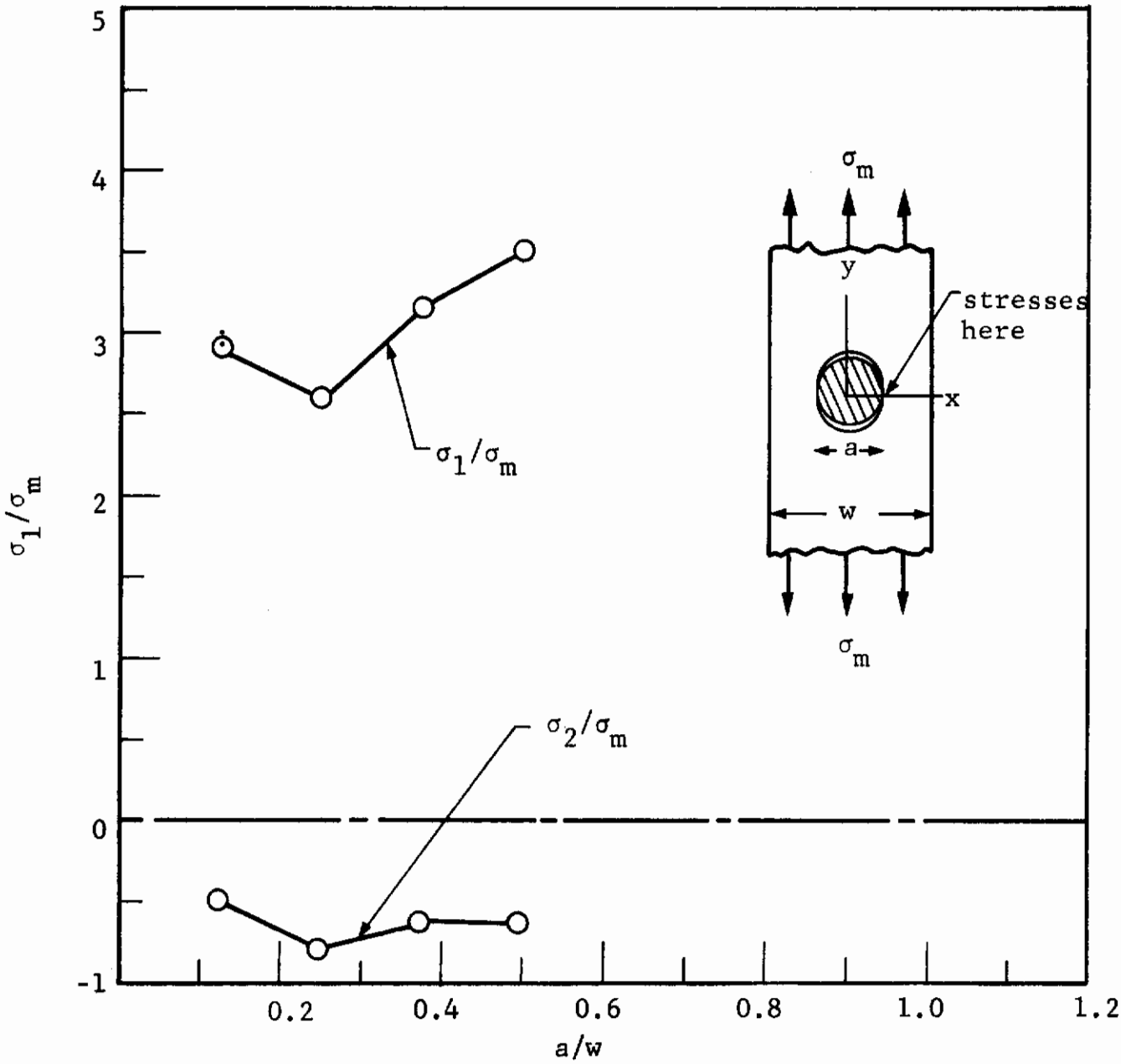

Fig. 6.39 PRINCIPAL STRESSES AT THE EDGE OF THE HOLE FOR VARIOUS a/w RATIOS ACCORDING TO JESSOP (6.34)

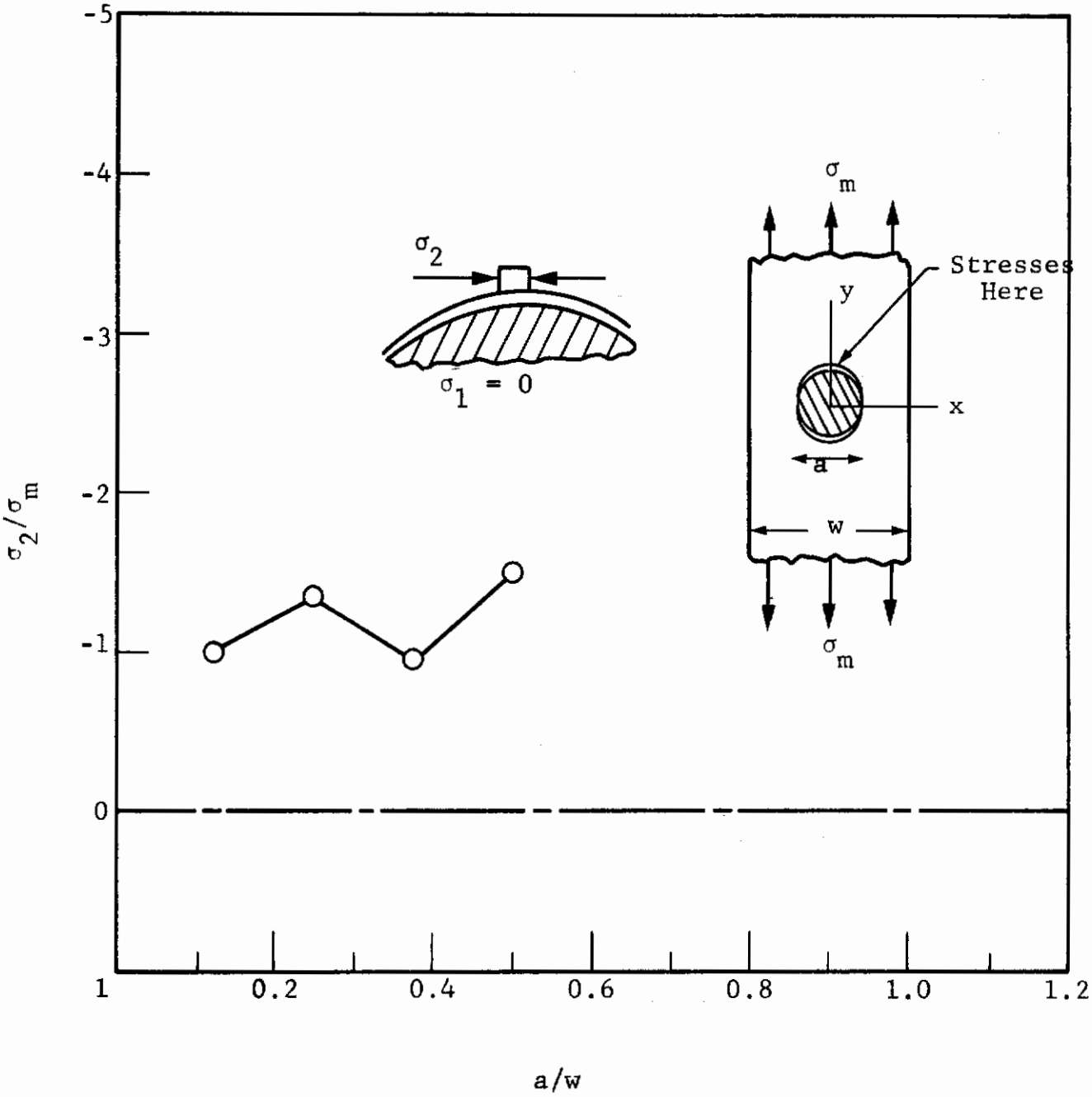

Fig. 6.40 PRINCIPAL STRESS, σ_2, AT THE TOP OF THE HOLE FOR VARIOUS a/w RATIOS ACCORDING TO JESSOP (6.34)

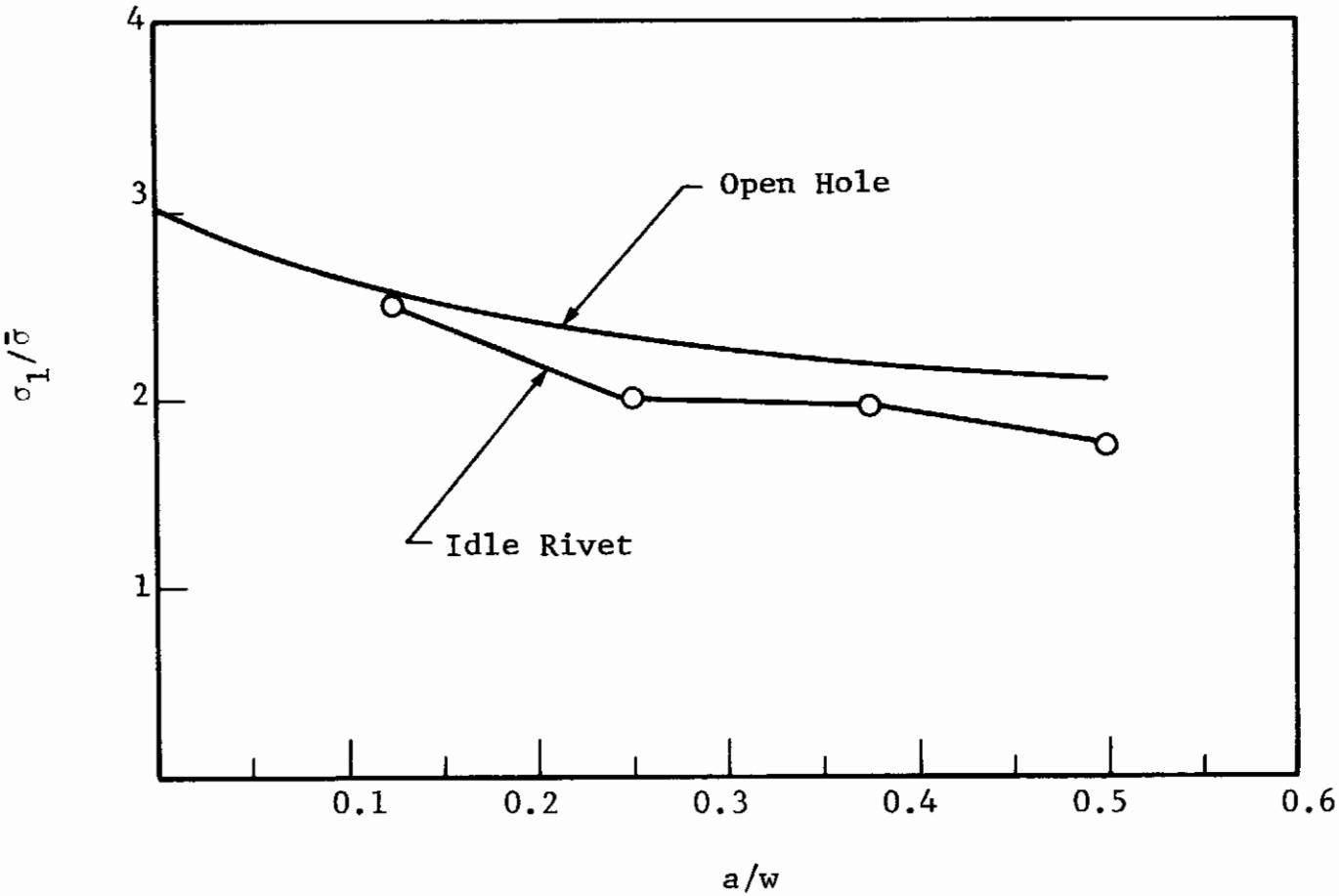

Fig. 6.41 STRESS CONCENTRATION AT THE EDGE OF THE HOLE WITH IDLE RIVET COMPARED TO THAT FOR UNFILLED HOLE, $\bar{\sigma}$ = MEAN TENSILE STRESS ACROSS SECTION THROUGH HOLE CENTER, ACCORDING TO JESSOP (6.34)

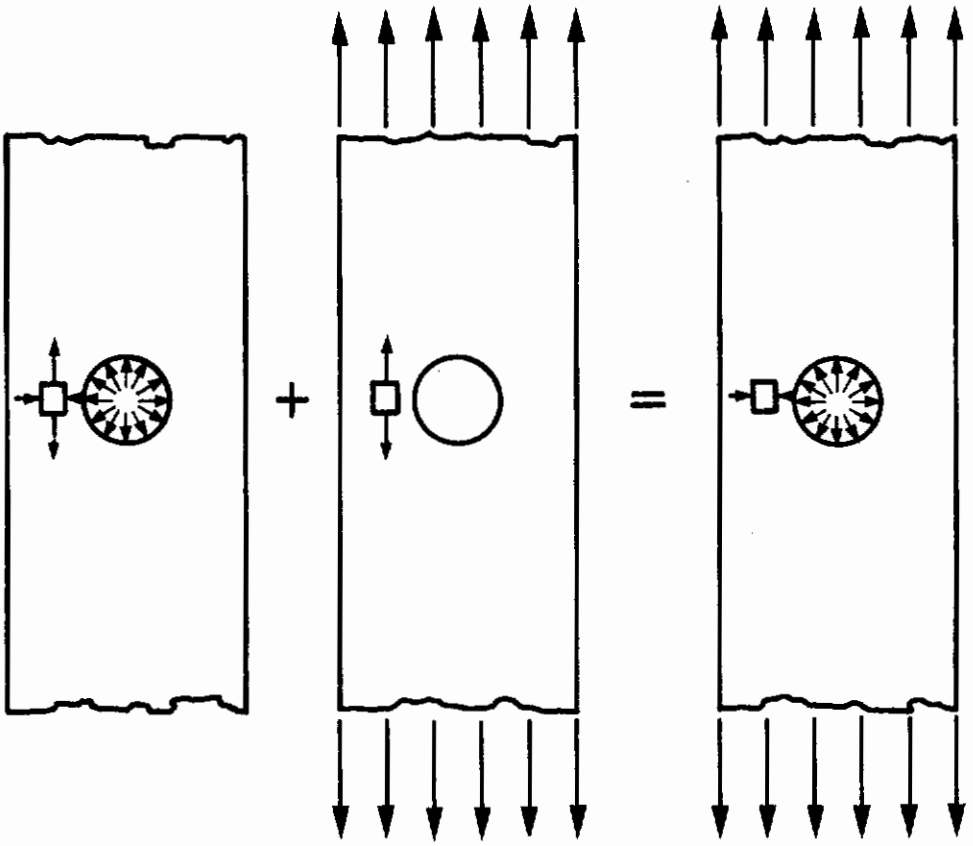

a. Pin Interference b. Tension c. Plate with Interference Pin in Tension

Fig. 6.42 PLATE WITH INTERFERENCE PIN IN TENSION STUDIED BY JESSOP

after testing through the use of a photogrid applied to one face of each specimen. Specimens were of aluminum and were tested at elevated temperature (400°F). They were subjected to combined tension and rivet bearing loads.

Conclusions obtained from the tests were that:

1. A reduction in life will occur for a given constant total load as the bearing portion of the load is increased.

2. Analysis of the deformation in the area of the rivet holes show that after an initial transient period, a steady-state stress-distribution occurs until fracture becomes imminent.

3. From conclusion 2 and uniform tensile creep data stress distributions across the minimum section are calculated. Stress concentrations derived from these results indicate that significant stress relief due to creep occurs. The strain concentrations continue to increase with time.

4. The total deformation of the joint can be broken down into a plate deformation component and a hole deformation component. The plate deformation component is relatively independent of the ratio of total load to bearing load. The hole deformation component is sensitive, however, to this ratio, particularly at high bearing loads.

5. To obtain a balanced design, the ratio of total load to bearing load in highly stressed regions should be kept as high as possible.

Reliance of stress redistribution as an alternative to balanced design may lead to excessive deformation or premature failure.

Jessop, H. T., Snell C., and Holister, G. S. (6.36)

"Photoelastic Investigation on Plates with Single Interference-Fit Pins with Load Applied (a) to Pin Only and (b) to Pin and Plate Simultaneously," The Aero. Quarterly, May 1958, pp. 147-163.

This paper is part of the continuing study by Jessop, et al,on the effects of pin interference on the stress concentration factors around pinned holes. This investigation also was performed by the method of photoelasticity. The load was applied a) through the pin and reacted by the plate at infinity; and b) through the pin with a superposed tensile stress on the plate.

Three levels of pin interference were employed "Lift" occurred at all load levels when the load was applied to the pin only.

The results are applicable only within an elastic state of stress.

Mead, D. J. (6.47)

"The Internal Damping Due to Structural Joints and Techniques for General Damping Measurement," ARC Technical Dept., Current Papers, C.P. No. 452, 1959, pp. 43.

This paper describes a method of obtaining, from simple experimental observations, the structural damping coefficients of a riveted or bolted joint vibrating in a known mode and at a given frequency when subjected to harmonically varying loads. Because of the complicated nature of the loading, analytical expressions provided can only be general.

Mead attributes damping at a riveted or bolted joint to three distinct mechanisms.

1. In the elastic range, to elastic hysteresis.

2. In the plastic range, to plastic deformation.

3. In the slipping range, to dynamic friction.

In the first range, the energy lost will approximate that in a structure of similar dimensions with no joint. The loss is proportional to the stress amplitude squared and is independent of frequency.

In the plastic range, the energy loss will depend upon the stress distribution over contact areas and on the material stress-strain curve. Due to complexities of the stress distribution and nature of the contact areas, a theoretical expression of the energy loss in this regime is not feasible.

In the third range the energy loss depends on the coefficient of sliding friction, on the normal pressure between plates, and on the amplitude of relative displacement. The normal pressure between plates is the hardest variable to measure or control.

General expressions are obtained for the energy loss including as much as possible from the three ranges above. The paper provides an excellent starting point for individuals interested in measuring or calculating damping in structural joints.

Fessler, H. and Haines, D. J. (6.19)

"Photoelastic Stress Distributions in Lugs,"
the Aero. Quarterly, August 1959, pp. 230-24.

This paper describes a photoelastic coating analysis of the stress distribution beyond the yield point in a circular ended lug (see Fig. 6.43). The photoelastic coating was bonded to an aluminum alloy lug and the strain distribution determined by a reflection type polariscope. The lug was loaded by a neat-fitting pin.

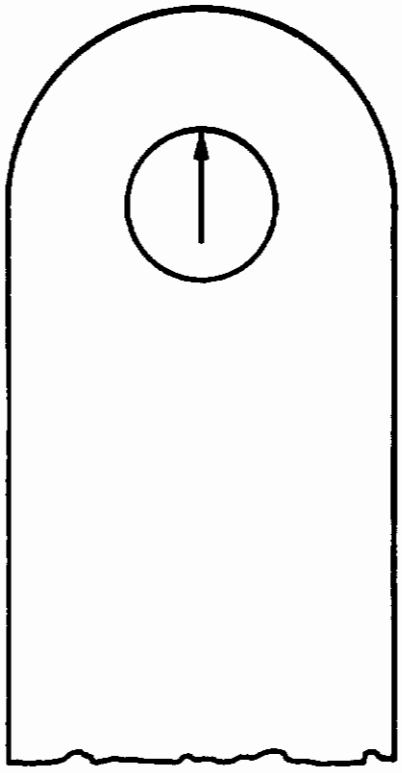

Fig. 6.43 SINGLE HOLE LUG STUDIED BY FESSLER (6.19)

Fessler used the maximum shear stress criterion of yield to determine the elasto-plastic boundary under different load levels from the photoelastic coating data. Four ratios of a/w were studied. The extent of yield across the section normal to the direction of loading was measured at different loads and it was found that the progress of yield across the section was independent of the a/w ratio.

Residual stresses after unloading were also measured. The elasto-plastic contours for a/w = 0.5 are shown in Fig. 6.44.

Lambert, T. H. and Brailey, R. J. (6.39)

"The Influence of the Coefficient of Friction on the Elastic Stress Concentration Factor for a Pin-Jointed Connection," the Aero. Quarterly, February 1962, pp. 17-29.

This paper is an experimental investigation employing the method of photoelasticity to explain an apparent anomoly in the work of Jessop, et al, Ref. 6.36. Apparently, a non-linear relationship between interference fit and maximum shear stress appears at higher loads in the Jessop tests. Lambert explains the difference by an apparent change in the load transfer mechanism which occurs when the ratio of tangential shear stresses to normal stresses at the hole periphery exceed the limiting coefficient of friction, micro-slip occur and a change in the mechanism of load transference occurs.

Lambert uses Araldite plates and various pins similar to the Jessop work to study the effects of slip. Repeated loading tests were also conducted. A copper contact on the base of the pin in the hole was used to determine the load at which contact was severed and hence the change in load transfer had occurred.

Lambert, T. H. and Brailey, R. J. (6.40)

"The Use of An Interference-Fit Bush to Improve the Fatigue Life of a Pin-Jointed Connection,"

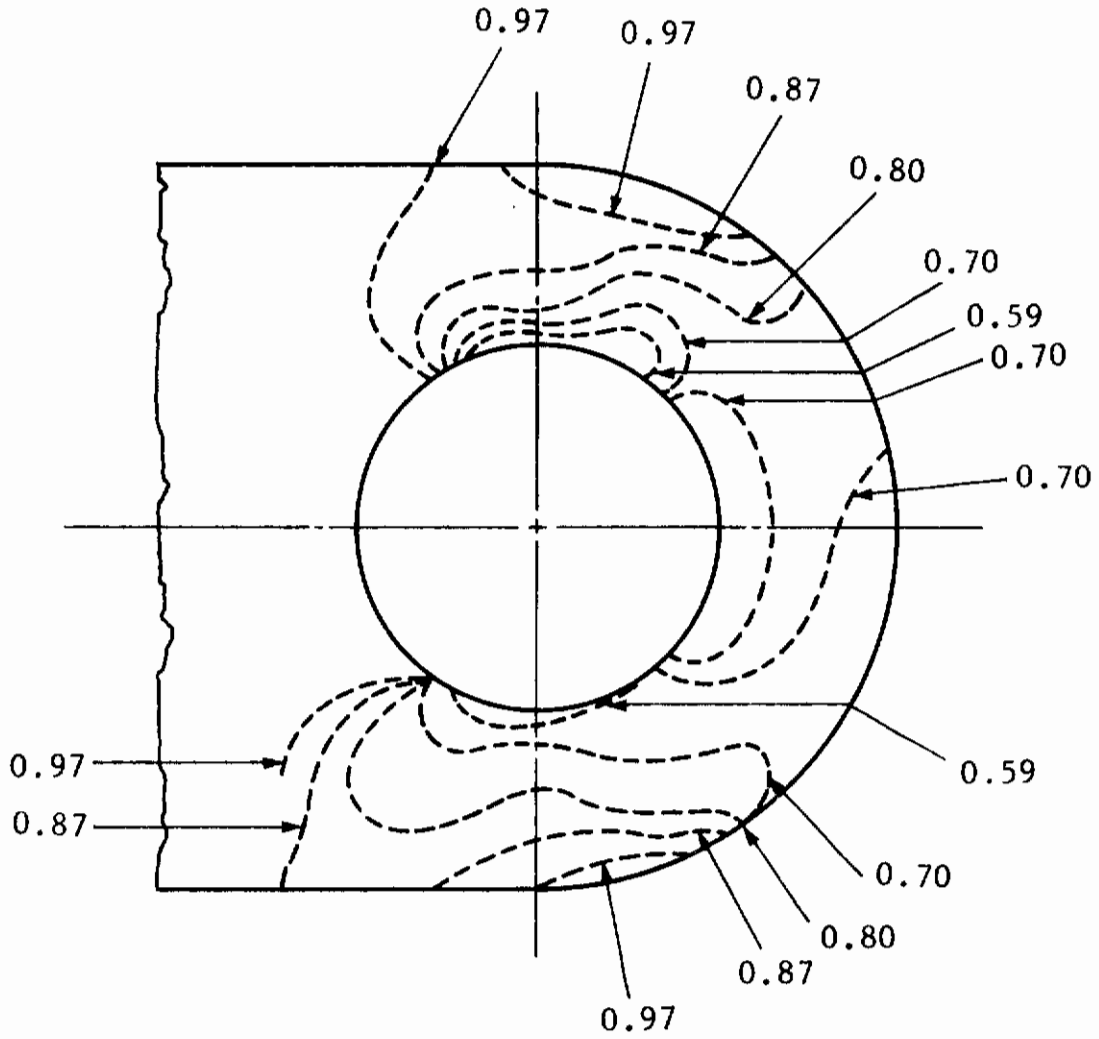

Fig. 6.44 YIELD CONTOURS SHOWING THE EXTENT OF YIELD FOR THE STATED FRACTION OF THE ULTIMATE LOAD OF THE LUG, AFTER FESSLER (6.19)

Aero. Quarterly, August 1962, pp. 275-284.

This paper describes a photoelastic and analytical study of interference fit bushes on the stress concentration factor around pinned holes in plates. The benefits from interference-fit pins in plates are well known; the possibility of using interference bushes instead of interference pins was not explored yet. This paper describes a study designed to fill that gap.

Ligenza, S. J. (6.44)

"Cyclic Stress Reduction Within Pin-Loaded Lugs Resulting from Optimum Interference Fits, Experimental Mechanics," January 1963, pp. 21-28.

This paper presents the results of a photoelastic study of stresses arising from combined interference fit and applied tension. The stress conditions arising from cyclic tension type loads are shown in Fig. 6.45. It can easily be seen that the stress excursions $\Delta \sigma_{max}$ is smaller for interference $\delta/b \neq 0$ than is the stress excursions for no interference, $\delta/b = 0$. Thus the fatigue loading of the interference fit riveted lug moves from an R ratio of R = -1 or 0 to $R > 0$ and hence the life at peak stress moves to the right thus providing longer lives for the same load excursions.

The paper is not as well written as it might be but contains much valuable information on interference-fit rivet type problems.

Cox, H. L. and Brown, A. F. C. (6.13)

"Stresses Round Pins in Holes," the Aero. Quarterly, November 1964, pp. 357-372.

This paper is a summary of work performed in England and the United States on the stress concentration factors around pin-loaded lugs. Some new photoelastic studies were performed in the nature of supplementary data gathering. Data on interference fit stress-concentration factors are also presented.

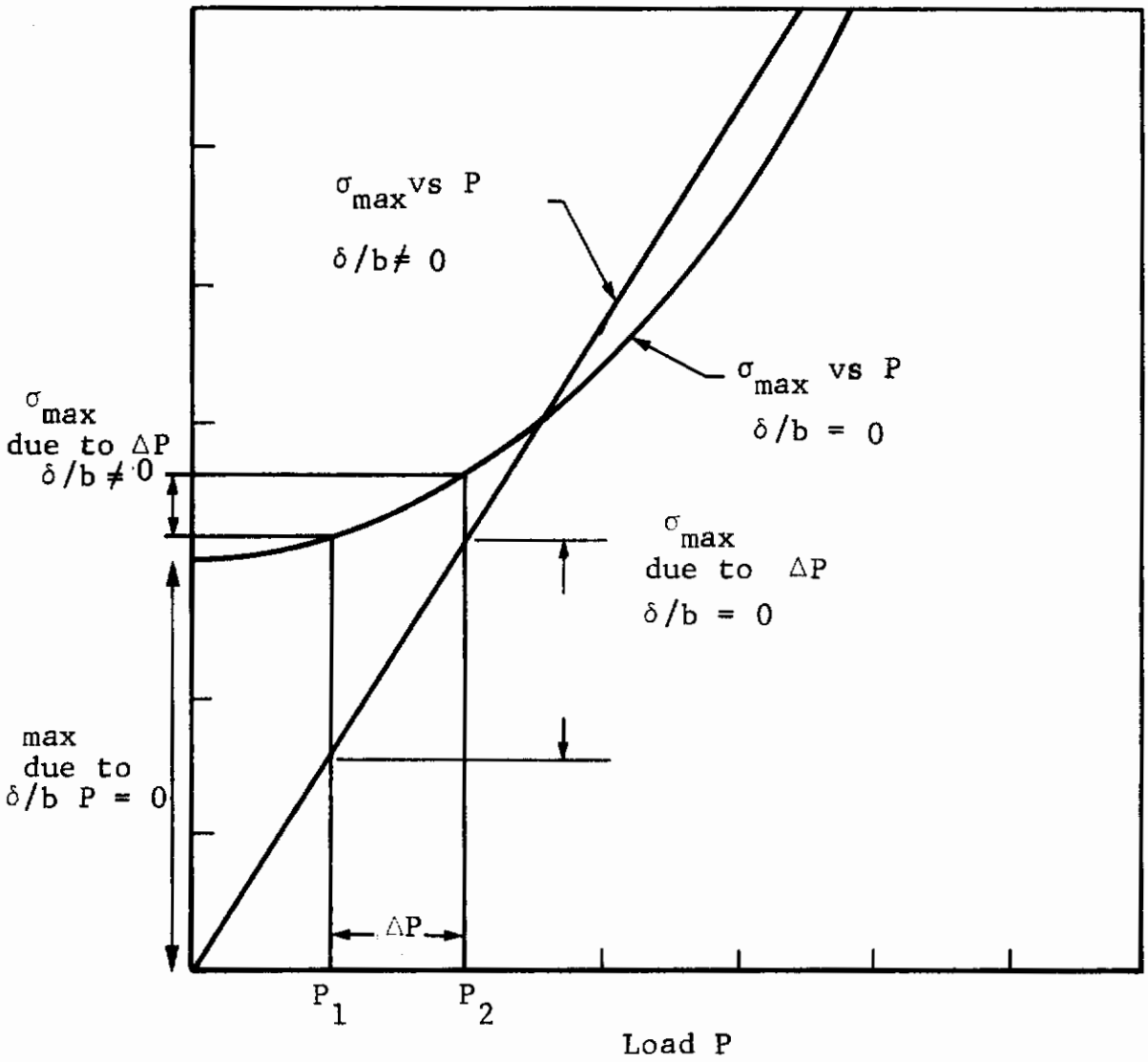

Fig. 6.45 VARIATION OF MAXIMUM STRESS WITH APPLIED LOAD FOR TWO CONDITIONS: 1) NO INTERFERENCE $\delta/b = 0$, and, 2) WITH INTERFERENCE, $\delta/b \neq 0$

Lambert, T. H. and Snell, C. (6.41)

"Effect of Yield on the Interference between a Pin and a Plate," J. Mech. Eng. Sci., Vol 6, 1964, pp. 38-43.

This paper describes an experimental investigation using Araldite photoelastic coatings to determine the reduction in stress concentration factors possible when the interference fit produces stresses beyond yield. The material used was HS30WP aluminum alloy which has a stress-strain curve approximating elastic-perfectly plastic behavior. A simple plasticity analysis is also presented which employs the maximum shear criterion of plastic flow without work hardening.

6.3 EMPIRICAL BOLTED AND RIVETED JOINT DESIGN

6.3.1 Summary

The ideal in empirical joint design is to have an equation relating the strength of a joint to joint parameters. For bolted and riveted joints, where the mapping of the joint is generally complex, a fairly complicated relationship would be required. About the closest that this has been approached is the work of Holbach Ref. 6.28 and Fefferman and Langhaar Ref. 6.18. In general the majority of authors surveyed merely produced a set of conclusions which could be utilized by joint designers. In this regard it is of interest to also consult the reference works of Fisher and Beedle Ref 6.20 and Fisher and Kormanek Ref. 6.22. Very few references on the behavior of bolted or riveted joints in GRP were located. The work at USDA Forest Products Laboratory Refs. 6.72, 6.75, 6.76,6.77, Strauss Refs. 6.65, 6.66, Ruffalo Refs. 6.55, 6.56, 6.57, Abel Ref. 6.1, Carylon 6.10 and Prokhorov 6.53 were the only literature located in this field.

6.3.2 Annotated Bibliography: Noncomposite Adherends

Schaechterle, K. (6.60)

"On the Fatigue Strength of Riveted and Welded Joints and the Design of Dynamically Stressed Structural Members Based on Conclusions Drawn from Fatigue Tests," Int. Assoc. for Bridge and Structures Engineering, Vol 2, 1934, pp. 312-379.

This German paper describes the results of an extensive fatigue study on riveted and welded joints in steel. Material notch toughness is taken into account.

Wilson, W. M. and Thomas, F. P. (6.74)

"Fatigue Tests of Riveted Joints," U. of Ill. Engrg. Exper. Station Bulletin No. 302, 1938.

This engineering station report deals with the fatigue strength of riveted joints connecting structural steel plate.

The joints were all double overlap and rivets were all nominal one inch in diameter. Static tests were performed as well as the fatigue tests although much of the report deals with fatigue aspects and a great deal of information obtained has to do with the rivets including material variations of the rivets, the report also contains test results on the following aspects of general interest:

1. The spacing of the rivets in a row.
2. The contribution of friction.
3. Initial tension along the axis of the rivets.

The tests on the rivets included work on the initial tension in the rivets. This was then supplemented by tensile tests on the rivets made after driving, through the use of the fixture shown in Fig. 6.46.

A correlation was also made between slip, between plates and shear on the rivet. The specimens studied were single overlap multi-rivet configurations. These configurations are described in Table 6.8. Load slip diagrams were prepared for the specimen using various grip areas and using various rivet materials.

Fatigue tests were performed on a $\pm$200,000 lb walking beam fatigue machine at 33 cpm. Most tests were performed in the modes $0 \leq R \leq 0.5$ but several tests were performed at R = -1. All fatigue tests were performed on joints with two rows of two holes each. a/w was held at either 0.0837 or 0.111. Row spacing, s/w, was held at 0.33. d_e/w was either 0.250 or 0.125. a/H was held constant at 0.575.

A second series of fatigue tests were performed on two double overlap joint types described below:

Joint 1: Single Line of 4 Rivets

a/w = 0.132

a/H = 0.445

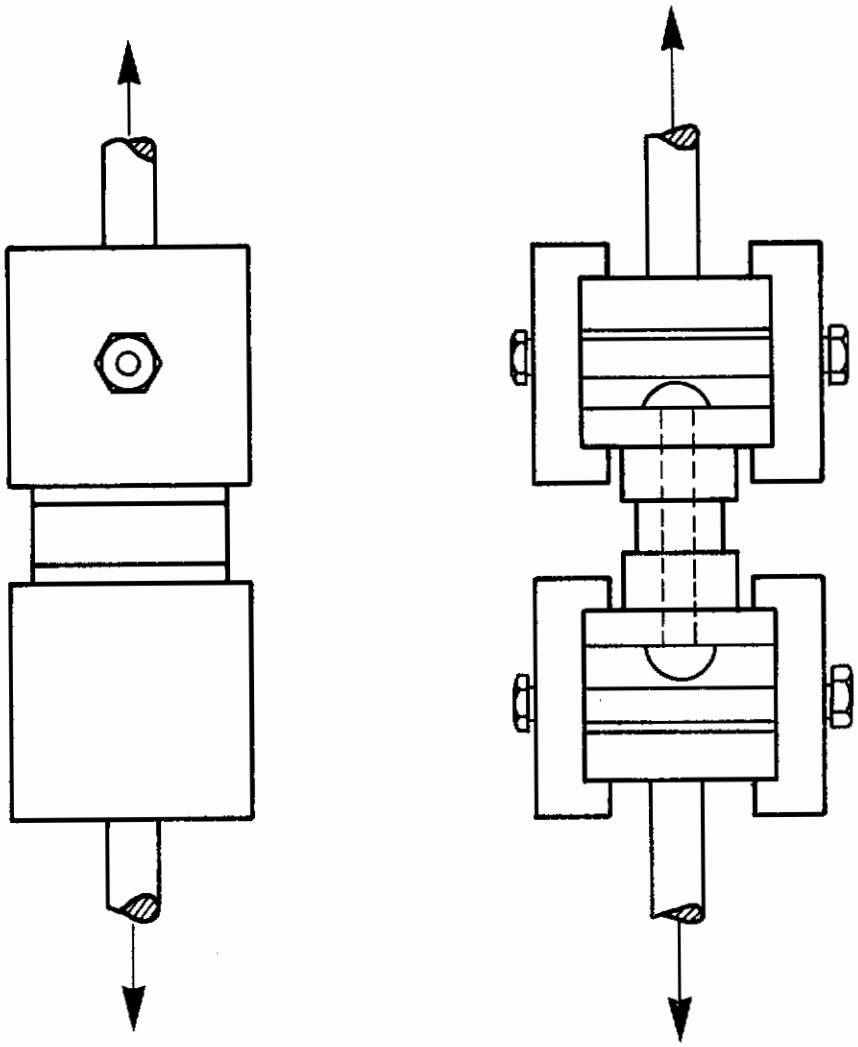

Fig. 6.46 TEST FIXTURE USED BY WILSON (6.74) FOR STUDYING INITIAL TENSION IN RIVETS

Table 6.8

TYPES OF JOINTS STUDIED BY WILSON (6.74) IN FRICTION EXPERIMENTS

Joint Number	Number of Rows	Number of Rivets in Each Row	a/w	de/w	d/w	a/H
1	2	2, 1	0.125	0.250	0.5	0.250
2	2	2, 2	0.125	0.250	0.5	0.250
3	3	2, 2, 2	0.125	0.250	0.5	0.250
4	2	1, 1	0.570	0.500	--	0.250
5	2	1, 1	0.445	0.500	--	0.250

$s/a = 4.0$

Joint 2: Single Rivet

$a/w = 0.0832$

$a/H = 0.148$

Other types of joints tested by Wilson included joints with fills (metal plates between the main adherends).

Finally, Wilson tested several joints designed to fail in the plates. The tension:shear:bearing ratio (T:S:B) was 1.0:0.60:1.26. The conclusions reached were that by increasing the nominal unit bearing to unit tension ratio from 1.17 to 2.35 did not affect the fatigue strength of the plates in riveted joints for which the tension in the rivets was so great that the plates did not slip enough to bring the rivets into bearing. This indicates that a plateau in the joint efficiency exists for which small variations in other parameters could be made to increase the joint efficiency.

Experiments were also made to determine the effect of transverse spacing on joint strength. The joint configurations are presented in Table 6.9 in accordance with the symbols defined in Figs. 1 and 2. Wilson also investigated the influence of method of hole manufacture on the fatigue strengths. Since this is related in total to the material (mild steel), the results are not of sufficient general interest here to be reviewed. The same is true for Wilson's extensive studies on the differences in fatigue strength for carbon and silicon steel plates.

Wilson also studied the effects of a/H on joint strength for the joints described in Table 6.8, Specimen 3. The a/h ratio was varied from $0.40 \leq a/H \leq 0.57$. Another double overlap riveted joint with $a/H = 0.4$ to 0.5 for a single row of two rivets ($a/w = 0.084$, $d_e/w = 0.25$, $d/w = 0.5$) was also studied. The results indicated no influence of a/H within the range tested on the fatigue strengths of the joint.

Table 6.9

JOINTS TESTED BY WILSON FOR EFFECT OF TRANSVERSE RIVET SPACING ON JOINT STRENGTH

Joint Number	Number of Rows	Number of Rivets in Each Row	a/w	de/w	d/w	a/H
1	6	1, 1, 1, 1, 1, 1	0.143	0.500	--	0.57
2	3	2, 2, 2	0.123	0.202	0.60	0.57
3	2	3, 3	0.098	0.146	0.35	0.57

Wilson also studied the effect of surface conditions on the fatigue strength of the riveted joints.

In conclusion, the vast array of data obtained by Wilson can be used as a good yardstick to test theories which purport to give the strengths of riveted or bolted joints. The important conclusions reached by Wilson are:

1. Decreasing the spacing of rivets (i.e., decrease d/w) will increase the fatigue resistance.
2. Method of manufacture of holes (for steel) does not alter fatigue resistance.

Davis, R. E., Woodruff, G. B., and Davis, H. E. (6.15)

"Tension Tests of Large Riveted Joints," ASCE Trans., Paper No. 2084, May 1939, pp. 1193-1245.

This paper presents the results of extensive testing on large riveted joints. Joint length (no. of rows), splice plate geometry, pitch (d/w), and pattern geometry were variables. In general, equal load distribution was determined to be satisfactory for most design purposes. Also joints with as many rivets in the end rows as in the interior rows behaved as well as those with fewer rivets in the end rows. The plates and rivets were steel.

The joints tested by Davis were designed to determine

1. Strength of long joints.
2. Relative behavior of joints for different rivet materials.
3. Relative behavior of joints for different plate materials.
4. Difference between butt and splice joints.
5. Partition of load among rows.
6. Effective net section of riveted plates.

7. Slip phenomena.

8. Proper design relationship between tension in plates and shear in rivets.

Davis describes what he calls perfect fabrication of riveted joints and the behavior of such a perfectly fabricated joint under load. Take as an example the joint shown in Fig. 6.47. For perfect fabrication, the following conditions result:

1. Plates absolutely flat.

2. Faying surfaces in contact at time or riveting.

3. Holes matched perfectly.

4. Rivets concentric with holes after driving with uniform annular space around each rivet.

5. For hot-driven rivets Davis states that during driving the rivets should completely fill the hole.

The behavior under load of this perfectly fabricated joint is illustrated in Fig. 6.48. The behavior is broken into four stages as described below:

Stage I — Static friction prevents slip.

Stage II — Load greater than static friction and joint slips until rivets come into bearing.

Stage III — Plates and rivets deform elastically so that load slip relation is linear.

Stage IV — Yielding of plates or rivets or both occurs and nonlinear behavior is observed to fracture of plate or shear in rivet.

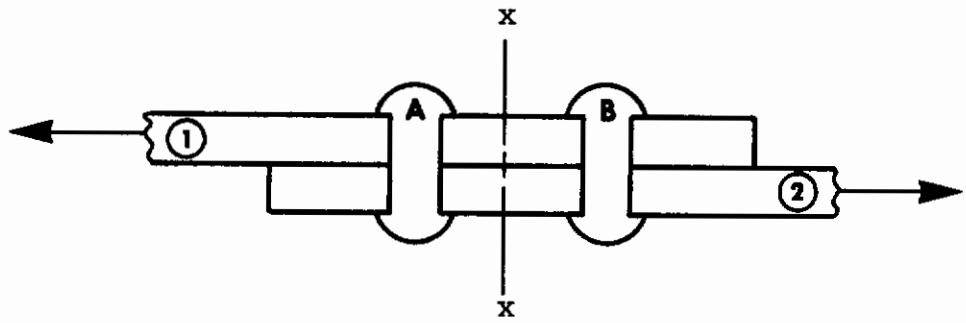

Fig. 6.47 EXAMPLE OF TWO RIVETS (IN A LINE JOINT) USED FOR PURPOSES OF EXPLAINING PERFECT JOINT BEHAVIOR BY DAVIS (6.15)

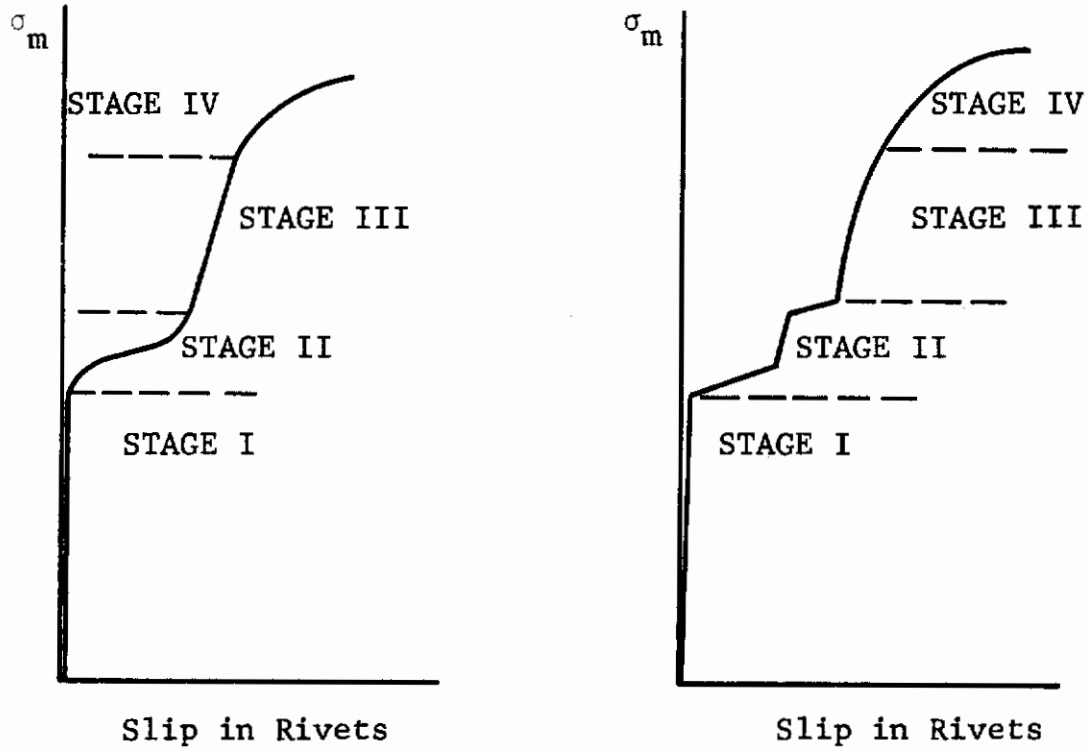

Fig. 6.48 BEHAVIOR OF PERFECTLY FABRICATED TWO-RIVET JOINT , AFTER DAVIS (6.15)

During Stage II, the rivets tilt and increase the pressure between adherends. This increases resistance to movement. In single lap joints, the bending due to eccentricity causes the plates to peel apart at the ends and reduces friction. This plus nonuniform clearance around holes, rivet bending, local rivet distortions at contact points causes the load-slip relationship in Stage II to assume various forms.

Davis tested forty different geometries of joints of the single lap type. Using strain gages and dial gages, Davis measured the load transfer between rows and slip along the joints. Semi-autographic records of the load-displacements were obtained and plotted (slip of the joint was recorded in a log). The descriptions of the specific joints and results are described in detail in the paper and are not repeated. Joint efficiences (σ_m/σ_{ult}) for joints designed to fail in the plates varied from 67.5 percent to 93.8 percent. (Joint yield efficiences (σ_m/σ_{yield}) were closer and varied from (82.5 to 91.4 percent) although it must be more difficult to ascertain this point exactly.

Among Davis' extensive conclusions, we have

1. Length of Joint

   Longer joints (no. of rows) are lower in efficiency and fail essentially in the rivets.

2. Rivet Pitch (d/w)

   Small variations in the (d/w) ratio give relatively small variation in efficiency. a/d varied from 0.167 to a/d = 0.333. Best efficiencies were obtained for a/d = 0.22.

3. Single lap joints produced higher ultimates than double lap joints.

4. Strength of plates in a riveted joint is not proportional to the area of the net sections. The use of fewer rivets in the end sections is ineffective. Wide spacing of the end row rivets is undesirable since premature rivet failures occur.

5. Butt and shingle joints perform essentially the same.

6. Slip

   Studies of slip are important. The rivets cannot develop full resistance to shear until after slip has occurred. Depending on specific joint geometry, the load-slip relationship may assume many forms.

7. At low loads (Stage I), the load partitioning may be largely controlled by joint conditions such as plate warpage, tension in rivets, faying surface characteristics.

   During Stage II, when slip is general, the shear stresses become equalized among the rivets although uniform partitioning is improbable.

   In Stage III, the end rivets assume greater loads.

   In early Stage IV, rivets tend to assume uniform load partitioning.

   In later Stage IV, the amount of plastic flow in the plate is sufficient to cause detrusion of the end rivets.

Davis concludes by presenting an interesting table shown here as Table 6.10.

Table 6.10

RECOMMENDATIONS FOR JOINT DESIGN BY DAVIS

Ratio	Tension in Plate Cross Section	Single Shear in Rivets
$\frac{\text{Useful Limit Point for a Joint}}{\text{Yield Strength of Mill Coupons}}$	0.72	--
$\frac{\text{Useful Limit Point for a Joint}}{\text{Ultimate Strength of Mill Coupons}}$	0.42	--
$\frac{\text{Ultimate Joint Strength}}{\text{Ultimate Strength of Mill Coupons}}$	0.75	0.88
$\frac{\text{Effective Rivet Yield for Joint}}{\text{Yield Strength of Mill Coupons}}$	--	0.83
$\frac{\text{Effective Rivet Yield for Joint}}{\text{Ultimate Strength of Mill Coupons}}$	--	0.55

Holleman, C. H. (6.29)

"Tension Joints in Aircraft," J. Aero. Sci., October 1943, pp. 295-302.

This paper discusses the applicability of conventional riveted joint design assumptions made for use with steel to joints in aluminum alloys. A description of several series of tests of these assumptions is presented. The paper is sufficiently general in approach so that the same questions can be asked for reinforced composite materials as well. Holleman's conclusion for the applicability of the assumptions to aluminum was that 80 percent overall efficiency of the joint was the highest that could be obtained if the following suggestions were observed.

1. Design for about 10 percent holes out in the outer row.
2. Make the outer rivets as large as is consistent with the dimensional limitations of the structure, i.e., avoid extremely small rivets.
3. Avoid staggering rivets particularly in the two outer rows.
4. Keep spacing between rows of rivets as low as possible and still provide against shearing out between rows.
5. Make thickness of butt plates as near to that of main plate as possible. (This will reduce differential elongation between rows of rivets.)
6. Assume 90 percent net area efficiency at all rivet rows when selecting rivet size and pitch.

Holbach, G. E. (6.28)

"The Structural Analysis and Significance of Rivet Shear Tests," Proc. Soc. Exper. Stress Anal. Vol 3, No. 1, 1945, pp. 131-154.

This paper describes a means of analyzing rivet shear data to determine the local geometry efficiency; i.e., dimpling, hole shape, contact geometry, etc., for riveted joints. Variables include:

1. Rivet Diameter
2. Sheet Thickness
3. Rivet Material
4. Adherend Material
5. Stability of Adherend (against buckling)
6. Type of Rivet Head
7. Fixity Afforded by Head
8. Induced Loads
9. Hole Preparation
10. Tolerances
11. Workmanship
12. Joint Deflection (bending)
13. Premanent Set (slip)

A single-lap two rivet (in a line) joint was used to test these local variables. The maximum load and an arbitrary deflection criterion (see MIL-HDBK-5) were used to evaluate joint effectiveness. Two parameters, P/a^2 and t/a, were set up as the unit strength and nondimensional geometry parameters respectively. They were related to a rivet coefficient, K, in accordance with the expression

$$P/a^2 = K_r \; t/a$$

By plotting the test results of P/a^2 versus t/a, the coefficients K_r were determined for various rivet joint shapes. For constant K_r, the data was plotted as a straight line with the slope equal to the bearing strength. In point of fact, actual test data showed that an effective bearing strength was not constant but decreased with a decrease in t/a. Thus, the importance of buckling in thin sheets is evidenced.

Holbach makes several conclusions on the basis of his test work for the various fastener types. All tests were performed on aluminum.

The paper is well written and should be used as a guide in selecting rivet details for a joint design from test data.

Fefferman, R. L. and Langhaar, H. L. (6.18)

"Investigations of 245-T Riveted Tension Joints,"
J. Aero. Sciences, Vol 14, No. 3, 1947, pp. 133-147.

This paper describes the results of extensive testing on several geometries of riveted joints in 245-T Aluminum. This paper is a real classic in that it illustrates an excellent blend of analytical, experimental and empirical design of a joint.

A series of tests of 110 tension joints was designed to explore the feasibility of optimizing joints in 245T Aluminum plate using protruding head rivets. Initially several pilot tests were performed in order to properly design the test program. These tests included:

1. Tests of the Principle of Similitude

   Because of the complicated nature of a riveted joint and local nature of strain concentrations and the relative inflexibility of some parameters such as grain size, a series of scaling tests were performed. The results indicated that the principle of similitude held for the joints, provided that geometric apportioning was maintained (i.e., the

a/t, d/a, L/d ratios were maintained). This implied that the joint efficiencies were identical.

2. Sheet Thickness Tests

A series of tests were performed to ascertain whether or not sheet thickness influenced the joint efficiency. The results indicated that the sheet thickness has no influence upon the efficiency of a joint unless the rivets become ciritcal in shear, thus, substantiating a generalized assumption of plane stress.

3. Effect of d_e/a ratio

The margin distance d_e have a significant influence on joint efficiency. In general, the results of pilot tests indicated that the joints benefit by large margin distance if the bearing stresses are low but joint efficiencies may decrease as margin distances increase if the bearing stresses are high. For joints with staggered rivet patterns, the larger margin distances give substantially lower joint efficiencies.

4. Effect of Joint Width

Results of preliminary testing indicated that infinitely wide joints could be satisfactorily represented by 5-rivet rows and that no changes in the efficiencies for up to 10 rivets in a row, were evident.

5. Lap or Butt Joints

Mathematically, there should be no differences in the behavior of lap or butt type joints. Within the scope of the joint types studied by P. Fefferman, there appeared to be no significant difference in the test results.

Fefferman then designed and conducted the main test program. He plotted the results in nondimensional form, i.e., joint efficiency versus a/d (for an infinite width joint) for the first row. The theoretical rivet shear and crushing lines were superposed on the chart as well as sheet tear lines in that the displayed data indicated the agreement between the various experimental joint efficiencies and the theoretical predicted values. The results followed the former two lines fairly closely. Fefferman then examines the test results in comparison with elementary joint theory and presents several conclusions based on tearing in successive rivet rows.

Finally, Fefferman presents the following general method for computing the efficiency of a riveted joint.

1. Calculate the rivet factors, $(d-a)/d$, for all rows.
2. Obtain the maximum bearing stress, σ_B, for rivets in the front row.
3. Calculate the joint parameter $\lambda = \sigma_B/\sigma_{ult}$ (where σ_{ult} = ultimate tensile strength of sheet material).
4. Determine the factor $R_o\ C_n$
   where R_o = empirical efficiency correction factor for perforated sheet
   $C_n = (d_n - a_n)/d_n$
   d_n = pitch of rivets in nth row
   a_n = diameter of rivets in nth row
   from empirical data
5. Calculate the factor

$$\varphi = \frac{\sigma_{ult}\ R_o C_n}{\sigma_B \sum_{i=1}^{n} (1-C_i)}$$

and obtain $K = R/R_o$. (where R = empirical connection factor for joint) from empirical data).

6. Determine the efficiency for front row tear by the formula

$$E = KR_oC_n$$

7. Determine the efficiencies corresponding to other types of failures through the equation

$$E_t = C_\alpha + \lambda \sum_{k=\alpha+1}^{n} (1-C_k)$$

where α takes the values 0, 1, 2, ..., n-1. The most important case is that in which failure results by shearing or crushing of all rivets ($\alpha = o$)

8. The actual joint efficiency is the smallest value obtained from steps 6 and 7.

Details of the appropriate empirical data to obtain are given in the paper.

Fefferman also presents a detailed procedure for determining the optimum joint geometry for maximum joint efficiency.

The paper is well written and is an absolute must for all joint designers.

Howard, D. M. and Smith, F. C. (6.31)

"Fatigue and Static Tests of Flush Riveted Joints," NACA-TN 2709, June 1952.

This report describes the results of 190 tests on multiple-rivet single-lap joints. The tests were conducted for two types of joint topography: Type 1 a/d = 0.250, a/w = 0.0417
Type 2 a/d = 0.125, a/w = 0.0417

All tests were performed on aluminum or aluminum alloy plates.

Among the conclusions reached were:

1. Flush riveted joints with dimpled holes have greater joint efficiency than machine countersunk holes.
2. Lap joints are superior under fatigue loads to butt (spliced) joints using machine countersunk holes.
3. No single relationship between static and fatigue properties for riveted joints is possible.

Schutz, F. W. Jr. (6.61)

"The Efficiency of Riveted Structural Joints," Publication No. 4478, U. of Illinois, 1952.

This PhD thesis is an attempt to predict with greater accuracy the maximum load-carrying capacity of large riveted structural joints. During the experimental phase of the thesis, 130 tests on structural joints were performed. All joints were designed to fail in the main structural plates. On analyzing these results, a new method of predicting joint strengths was developed. This method is called the "relative gage" method. The method is capable of predicting the relationship between joint efficiency and joint geometry better than previous methods The method provides for the effects of three other variables on joint efficiency. These are 1) material ductility, 2) method of forming holes, and 3) ratio of bearing stress to tensile stress on holes.

The method was then applied to the results of 1025 tests on structural riveted joints. The results were also predicted by two other methods: the AREA Method and the Wilson Rule. The study showed that, for the overall variety of joints studied, the relative gage method was the best. Of all test results 87 percent fell with 4.5 percent of the relative gage method,

while the AREA specification predicted 40 percent and the Wilson Rule method predicted 65 percent to fall within 4.5 percent of the actual values. A possible specification governing the net section of tension members is given in the conclusions.

The thesis was unavailable for this review but the results were summarized in the University of Illinois summary of publications.

Baron, F. and Larson, E. W. (6.2)

"Comparison of Bolted and Riveted Joints,"
ASCE Transactions, Vol 120, 1955, pp. 1322-1334.

This paper is essentially an empirical test comparing bolted and riveted joints subjected to static and fatigue loads. The paper is concerned only with double overlap joints (see Fig. 6.49). The slip at each rivet was measured for loading and unloading cycles at the beginning and at some periodic times throughout the repeated load applications. The results indicated that:

1. The fatigue strengths of joints using high strength bolts were considerably higher than similar joints with hot-driven or cold-driven rivets.
2. The clamping force of a bolt on the joint may decrease slightly during cyclic loading but the nuts do not necessarily turn.
3. The cyclic slip of joints hardened with bolts is negligible, although slip during the first load application can equal the clearance in the bolt hole.
4. The shear stress of the first major slip of the joint depends on:
   a. the clamping force
   b. the degree of bolt hole filled
   c. the condition of contact at the surface interface.

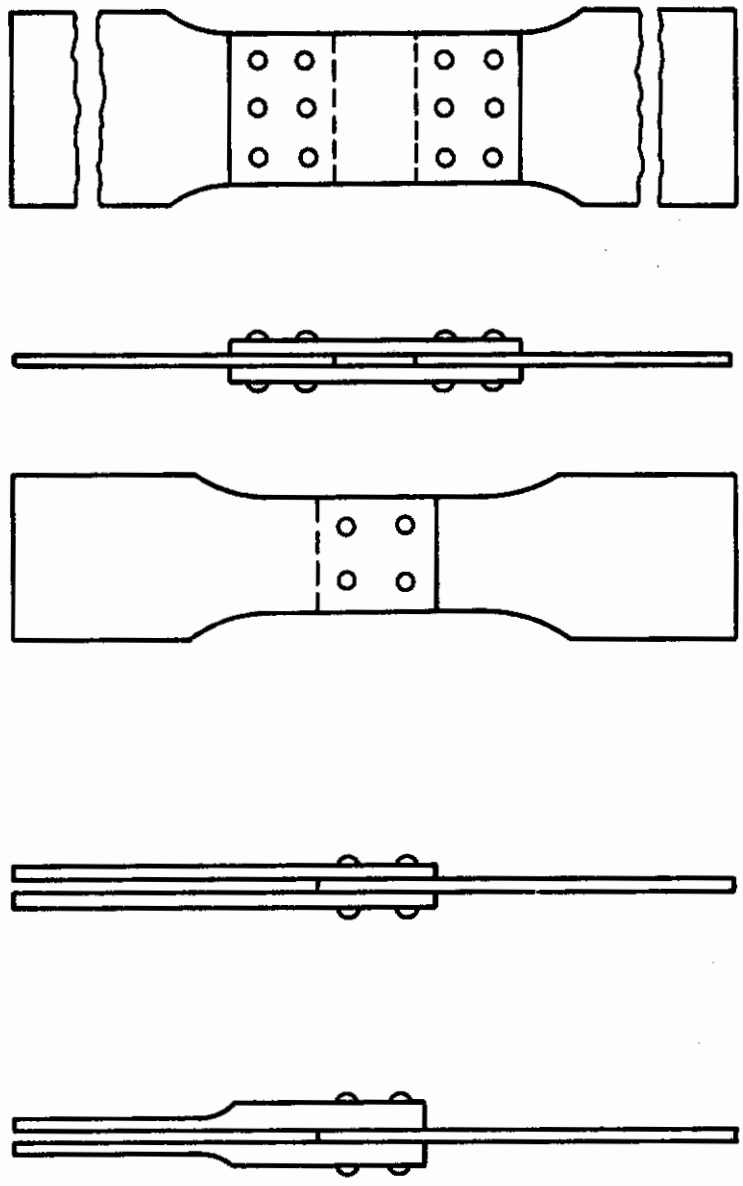

Fig. 6.49 JOINTS STUDIED BY BARON AND LARSON (6.2)

There is an indication of a strong degree of frictional correlation to slip.

Mordfin, L., and Legate, A. (6.49)

"Creep Behavior of Structural Joints of Aircraft Materials under Constant Loads and Temperatures," NACA TN 3842, Jan. 1957. pp. 53.

This report describes the results of 55 creep and creep-rupture tests on structural joints. A simple strength of materials type approach for predicting the time to failure and mode of failure of a structural joint knowing the temperature, gross section tensile stress, properties of the base material was used.

Smith, C. R. (6.63)

"Influence of Residual Stresses and Stiffness Factors on Fatigue Strength of Metals and Structures," General Dynamics Convair Report No. G.D./C 62-55, March 1962, A.D. 274656.

This report was intended to determine the fatigue life of pin loaded lugs with varying amounts of bushing interferences. The emphasis is on the fatigue failure mechanism on a local level (at the pin) rather than on the overall joint failure. The fatigue failure criterion used is the Smith Method for estimating fatigue life. Recommendations are made for specific ways in which the fatigue life of such lugs can be increased using 1) interference bushings, 2) tapered bolts, 3) thin auxilliary doublers, 4) tightly driven rivets, and 5) edge driven rivets. Emphasis is placed on aluminum alloys.

Starting with stress-strain and fatigue S-N curves for various axially loaded R ratios, Smith determines that a residual compressive state of stress on the lug hole will permit increased life where the failure occurs through the hole by preventing the return of stress to zero. Figure 6.50 shows this effectiveness for an 0.003 in. interference. Various special cases are treated to show how the mechanism works. Both the

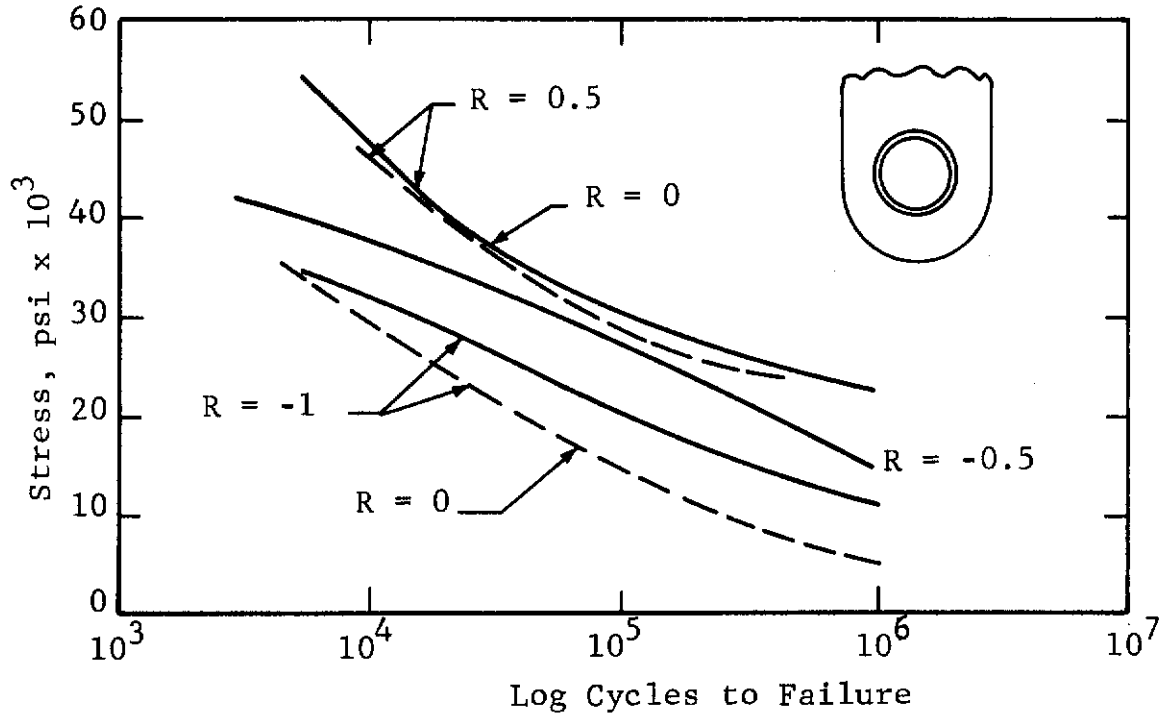

Fig. 6.50 EFFECT OF INTERFERENCE = 0.003 IN. ON S-N CURVES FOR 7075 LUG, SOLID LINES WITH INTERFERENCE, DASHED LINES WITHOUT INTERFERENCE, AFTER SMITH (6.63)

tapered bolt (drawn up to some interference) and the press-fit bushing appear to yield similar results.

Smith also discusses some of the aspects associated with cumulative fatigue with underloading and overloading cycles. Smith conducted a photoelastic study to verify the amount of the predicted residual stresses obtained in interference fits.

Smith's conclusions are:

1. Fatigue failures are caused by localized stresses.
2. Since the failure are local, the stresses can be adjusted so as to be different from those around a hole with no bushing.
3. Local stresses are limited by the yield stress of the material.
4. Limiting the local stresses to the yield of the material will permit elastic determination for the stress cycles.
5. Residual stresses may influence fatigue life more than any other variable.
6. Long time loading where heat is concerned can limit the applicability of the technique since heating reduces residual stresses.

Bendigo, R. A., Hansen, R. M. and Rumf, J. L. (6.5)

"Long Bolted Joints," F. Struct. Div., Proc. ASCE Dec. 1963, pp. 187-213.

This paper presents the results of 23 tests on long structural joints, A7 steel connected by means of high strength bolts. The influence of joint length (no. of rows) on the ultimate strength of bearing type connections is established. Data are also obtained on slip resistance for design of friction-type connections.

Mittenbergs, A. A. and Beall, L. G. (6.48)

"Effects of Pin Interference and Bolt Torque on Fatigue Strength of Lug Joints," ASTM Proc., Vol 63, 1963, pp. 671-683.

This paper describes an empirical investigation of the effect of pin interference on the fatigue life of lugs under combined loadings. In general, the fatigue life increased for a given stress level as pin interference was increased. Investigations also showed that an increase in bolt torque beyond a certain required minimum value resulted in a small improvement in the load carrying capacity of shear joints.

Schijve, J. and Jacobs, F. A. (6.59)

"Programmed Fatigue Tests on Aluminum Alloy Lug Specimens with Slotted Holes and Expanded Holes," National Lucht-En Ruimtevaartlaboratorium, Amsterdam, NLR-TN-M.2139, Nov. 1964.

This report describes an empirical investigation of constant amplitude and programmed amplitude fatigue tests on aluminum alloy lugs. Cumulative fatigue damage theories were employed in the analysis of the data.

Hartman, A, Jacobs, F. A. and Van der Vet, W. J. (6.26)

"Constant Load Amplitude and Programme Fatigue Tests on Single-Lap Joints in Clad 2024T3 and 7075-T6 Aluminum Alloy with Two Rows of Rivets or Huckbolts" National Lucht-en Ruimtevaart-laboratorium, NLR-TN-M.2147, July 1965.

This report deals with an investigation of the fatigue resistance of riveted joints. The specimens were double row single-lap joints in two types of aluminum. The variables were the type of rivet. Conclusions reached were

1. Under spectrum type fatigue loading, the Palmgren-Miner Law

$$\Sigma \frac{n}{N} = 1$$

yields a conservative estimate of the fatigue life.

2. Fractographic studies indicate that the number of fatigue cracks generated under spectrum loading of joints is less than the number generated at high stress level constant amplitude tests but greater than the number generated at low stress level constant amplitude tests and is closer to the number generated at the high stress levels.

3. The ultimate strength of the joint is a combination of two mechanisms 1) a loaded hole, and 2) a clamped joint. As a loaded hole, the fatigue strength is affected by all the factors for lugs. As a clamped joint, its fatigue strength is affected by other variables such as pressure exerted by rivets, welding, and fretting in clamped area, presence of coatings, sealants, cladding layer, etc.

4. For rivets and similar bolts of the same diameter, the fatigue strengths are almost equivalent.

All details of the test work are included in the report.

6.3.3 Annotated Bibliography: Composite Adherends

Werren, F. (6.72)

"Bolt Bearing Properties of Glass-Fabrics Base Plastic Laminates," FPL Report No. 1824, June 1951.

The report contains the results of approximately 400 tests on 112, 181 and 143 glass cloth polyester resin composites. The specimens were tested with the load at several angles to the warp, for two plate thicknesses, various hole diameters, and both wet and dry. The tabular data present both proportional

limit and ultimate load, and mode of failure. The data as presented is rather complete and will remain a valuable source of invormation.

The specific data sought by Werren was the bearing or "crushing" strength ahead of the rivet rather than the strength of joints and it is important to remember this when interpreting Werren's results for an actual joint design. For single-lap single-rivet joints, Werren varied both the a/w ratio and the a/H ratio. Werren calculated both the bearing strength

$$\sigma_B = \frac{P}{t(w-a)}$$

for each test performed. The nominal stress at a substantial distance from the hole which is truly reflective of joint efficiency is given by

$$\sigma_m = \frac{P}{tw}$$

and can be calculated as follows from Werren's results

$$\sigma_m = \frac{w-a}{w} \quad \sigma_{net} = \frac{a}{w} \sigma_B$$

Werren examined all the failures obtained and excluded both edge failures (tearing from the side of the hole to the edge of the plate) and shear tearout failures (failures propagating at some angle to the corners, side or bottom of the plate). The remainder which were crushing failures below the rivet yielded the desired bearing strength information. Conclusions were then made as to the necessary end distances (a/H ratio) and the edge distances (a/w ratio) to insure crushing failure at the rivet.

If one calculates the value σ_m for each joint, however, the joint efficiencies may be higher for some of the tearing or shear tear out failures. As an example see Table 6.11 and a

Table 6.11

RESULTS OF BOLT BEARING TESTS FOR PARALLEL LAMINATED 181 COMPOSITES, AFTER WERREN (6.72)
(Bolt and Hole Diameter Were 1/4 In., Load Applied at 0° to Warp)

Specimen Number	Plate Width w (in.)	End Distance H-a/2 (in.)	Edge Distance $\frac{w-a}{2}$ (in.)	Bearing* Strength σ_B (psi)	σ_{net} (psi)	Failure Type**	σ_m (psi)	a/w
0-24-1	0.511	0.75	0.13	--	32,590	E	16,600	0.49
0-24-3	0.504	0.75	0.13	--	43,620	E	17,400	0.495
0-24-5	0.508	0.75	0.13	--	33,770	E	17,200	0.49
0-24-7	0.508	0.75	0.13	--	34,290	E	17,400	0.49
0-24-11	0.698	0.75	0.22	38,670	27,790	E	17,800	0.36
0-24-13	0.696	0.75	0.22	37,770	27,620	C	17,700	0.36
0-24-15	0.698	0.75	0.22	42,250	28,800	C	18,500	0.36
0-24-17	0.692	0.75	0.22	39,740	28,670	C	18,300	0.36
0-24-21	0.881	0.75	0.32	--	18,900	C	13,600	0.285
0-24-23	0.880	0.75	0.31	35,600	18,850	C	13,500	0.285
0-24-25	0.874	0.75	0.31	37,580	19,770	C	14,100	0.285
0-24-27	0.878	0.75	0.31	--	19,820	C	14,200	0.285

* Bearing Stress at a Deformation of 0.01 in.

** C = Crushing under Rivet
E = Failure to Edge

comparison with Theocaris' (Ref. 6.70) theory in Fig. 6.51. Comparison is, of course, difficult since the Werren data represents actual test data for failure and the Theocaris theory is for the elastic stresses and only for the tensile stress at the side of the hole. A true comparison would require a complete stress distribution and a complete failure envelope for the material at all a/w ratios to correctly plot the Theocaris predicted load dropoff. Furthermore, it is to be noted that if the theoretical stress concentration, K = 5.2, at a/w = 0.4 is used, then the predicted strength based on tensile data for the same material (σ_T = 49,100 psi) is σ_m = 9,600 psi and it is clear that the actual joint strength level attained was σ_m approximately 17,000 psi, which is almost twice the theoretical.

Werren concluded that (considering bearing strength only)

1. The stresses at proportional limit and maximum load are approximately the same for 45° loading as well as for 0° and 90° loading.
2. The bearing proportional limit and strength are reduced for wet laminates from those obtained for dry laminates similarly loaded.
3. The σ_B values decrease as a/t increases.
4. σ_B decreases in the wet condition for all a/w and a/H ratios.
5. The a/w and a/H required to prevent tensile tear-out and shear vary with laminate, conditioning, loading angle, and a/t ratio. Also that a/H = 0.22 and a/w = 0.168 are adequate to prevent edge tensile or shear tear out.
6. Smaller a/w and a/H ratios are required for 112-114 laminates than for the others tested.

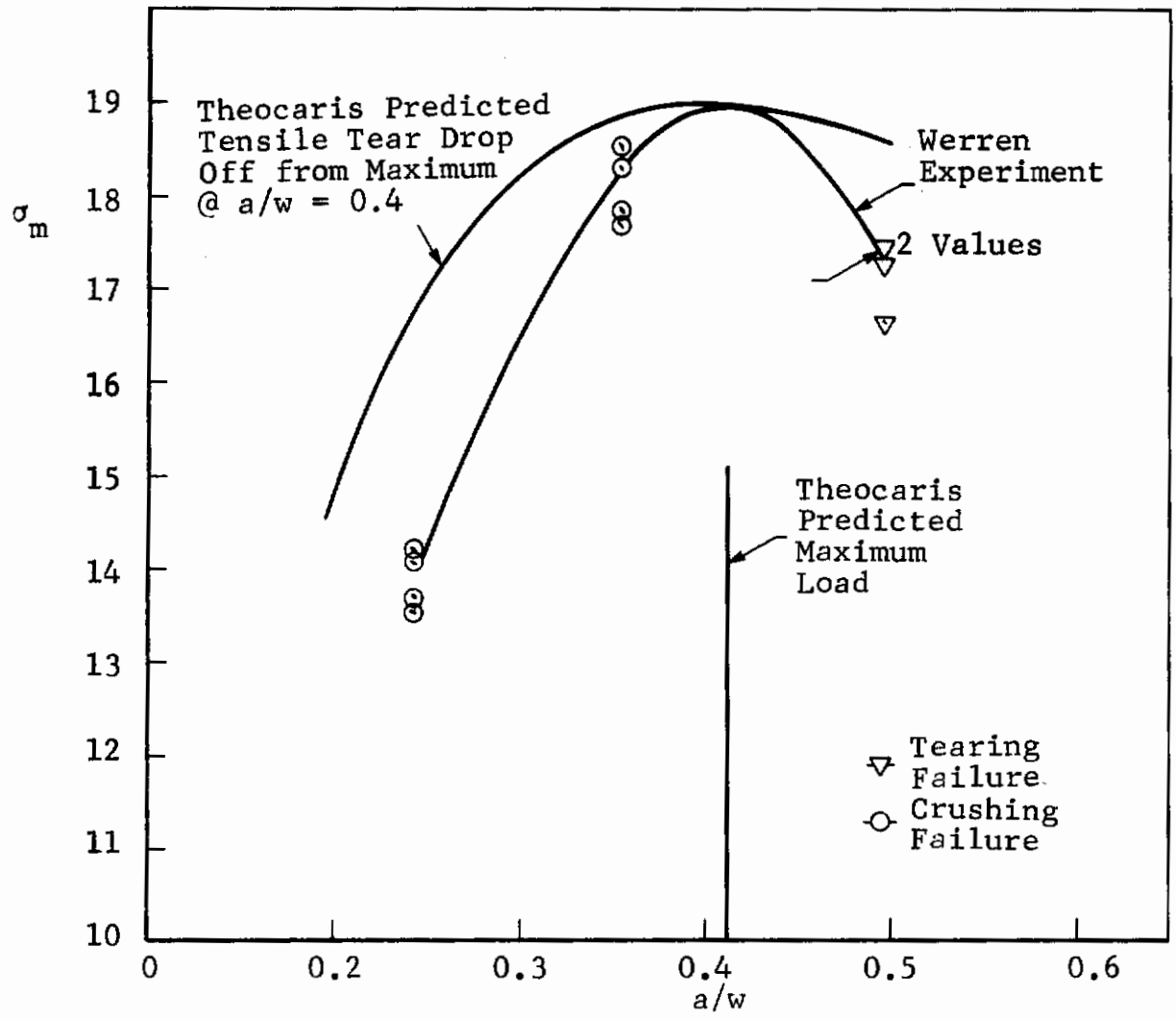

Fig. 6.51 COMPARISON OF WERREN (6.72) DATA FOR PARALLEL PLIED LAMINATE WITH SINGLE-LAP SINGLE RIVET FAILURE DATA WITH THEOCARIS (6.70) PREDICTED MAXIMUM LOAD TRANSMISSION

(Author's Comment)

It is worthwile to note that misinterpretation of Comments 5 and 6 could lead to joint design heavier than optimum since stronger joints might fail by tensile or shear tear-out instead of by bearing failures under the rivets.

Young, R. (6.75)

"Supplement to Bolt-Bearing Properties of Glass-Fabric Base Plastic Laminates," FPL Report No. 1824A, Oct. 1955.

This report is a continuation of the Werren 72 work and covers bolt bearing tests on four glass fiber reinforced polyester composites. The four systems of reinforcement tested were:

1. 162 glass fabric with Volan A finish
2. 120 glass fabric with Volan A finish
3. 184 glass fabric with Volan A finish
4. Resin sized, mechanically bonded glass fiber material

The presentation of results is similar to that in the Werren report.

Young, R. (6.76)

"Supplement to Bolt-Bearing Properties of Glass-Fabric Base Plastic Laminates," Report No. 1824 B, October, 1955.

This is a continuation of earlier studies. See (Ref. 6.72) and (Ref. 6.75). This report presents the results of 75 tests on 181 glass cloth-polyester composites. The thickness of the laminate was varied from 0.020 to 0.115 in. A marked effect on the bearing stress was evidenced for laminates whose thicknesses were less than 0.06 in. or approximately 1/16 in.

Young, R. (6.77)

"Supplement to Bolt-Bearing Properties of Glass-Fabric Base Plastic Laminates," FPL Report No. 1824 C, February 1957.

This is another continuation of studies in (Ref. 6.72, 6.75 and 6.76). This report presents the results of additional tests on two new composites: 112 and 181 glass cloth based epoxy resins. The results are handled similar to those in the previous three reports.

Strauss, E. L. (6.65)

"Mechanical Joints in Reinforced Plastic Structures," Machine Design, March 17, 1960, pp. 197-201.

In this paper Strauss first examines the failure types which occur when a riveted joint in a laminate is loaded. His conclusions based on these results were:

1. Tensile failures occur by propagation of a crack from the edge of the sheet.
2. Shear tear-out failures occur by shearing-out a plug from the hole to the end of the plate or by pulling the head of the fastener through the laminate.
3. Bearing failures occur by crushing of the laminate between the rivet and the end of the plate.

Strauss then concludes that bearing failures are best because they are noncatastrophic. From this he concludes that the number of fasteners, fastener size and spacing should be selected so that the joint is critical in bearing, that is, as the joint is loaded, the bearing strength of the laminate is exceeded before the load reaches the tensile strength of the laminate or the shear strength of the plastic or fastener.

The sufficiency of this criterion is based on qualitative reasons (such as, "when a joint is stressed to its ultimate bearing stress, the material is still able to sustain stress") rather than quantitative rationale such as a plot of σ_m versus a/w, a/H, etc.

Ruffalo, A. (6.55)

"Design Manual for Joining of Glass Reinforced Structural Plastics," Naval Material Laboratory. Report on Laboratory Project 6066-1, Bureau ID No. 16-1009-2, Navships 250-634-1, Aug. 1961.

This report is a catalog of properties and techniques for applying adhesives, bolts, screws, rivets and special fasteners in reinforced plastic materials applications. Properties of the individual mechanical fasteners are presented as well. Reinforced plastic laminates are divided in this report into six grades with various ultimate flexural, tensile and compressive properties. For each of these grades, the following characteristics are described:

1. Screw pullout force for various thread depth engagement. This includes machine screws, self-tapping screws (thread cutting and thread forming).
2. Transverse capabilities for screw fasteners for various thread depth engagements.
3. Advantages and disadvantages of various fastener application techniques such as resin dipping, eccentric loading, head configuration and machining practices for screws and bolts.
4. General designs considerations for screws, bolts and rivets.
5. Sizes and types of rivets for reinforced plastics.

6. End and edge distances to prevent tear-out (see also Werren (Ref. 6.72) for appropriate comments).

7. Sleeves, collars, inserts for special type fasteners.

8. Effects of dynamic loading.

9. Empirically obtained data on multifastener joints for various edge and end distances. Since the basic grade type material properties are in terms of material minimums, it is not clear whether or not the recommended values include a safety factor or not. For example, it is stated that 100 percent of the material strength is available for a double row of rivets where the edge distance is equal to 3a and the end distance is equal to 3a. It is a certainty that 100 percent of the base strength could not be obtained in practice and hence the recommended procedure might prove unsafe where the base material just passes the minimum grade strengths. It is particularly important since Ruffalo recommends using actual material strengths obtained from tests on procured materials as the base for the joint design loads.

10. Row spacing.

11. Fastener head pullthrough.

12. Examples of typical joint designs.

The basis of the design manual includes work conducted at Naval Material Laboratory and USDA Forest Products Laboratory.

Strauss, E. L. (6.66)

"How to Design Mechanical Joints," Materials in Design Engineering, Feb. 1963, pp. 86-94.

This paper is a review of work by the author and based on philosophies established earlier by the author (Ref. 6.65). It contains methodologies for designing joints such as single lap, offset lap, single shear butt joints and double shear butt joints (see Fig. 6.52). Strauss bases his strength retention factors for various a/w ratios on unloaded hole stress concentration factors. This results in a substantial decrease in design efficiency when loaded holes are actually designed.

Ruffalo, A. (6.56)

"How to Evaluate and Select Mechanical Fasteners," Materials in Design Engineering, Feb. 1963, pp. 95-100.

This paper is a review for the open literature of the work found by that author in (Ref. 6.55).

Abel, K. B. (6.1)

"Feasibility of Reinforced Plastics for Primary Structures of Army Aircraft," U.S. Army Transportation Command, TRECOM Technical Report 63-15, March 1963, pp. 201-218.

A variety of joints with rivets, screws and bolts combined with four types of glass reinforced epoxy were tested to destruction. Rational design techniques were not used to design the joints which were the single lap, single fastener and double lap, single fastener types. One hundred fifteen combinations of reinforced plastic materials, plies, rivets, bolts, and screws were tested (a total of 311 specimens). The article, similar to many extensive testing program reports on the same subject, includes the type of failure reported on a specimen by specimen basis. Therefore, it is possible to summarize the number of

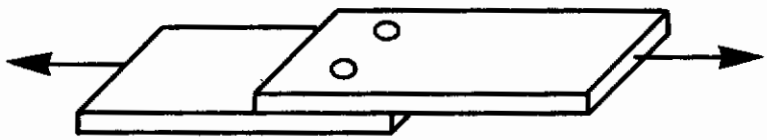

Single Lap Joint

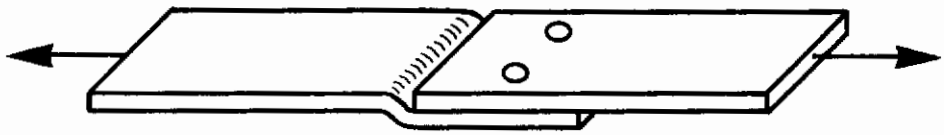

Offsett Single Lap Joint

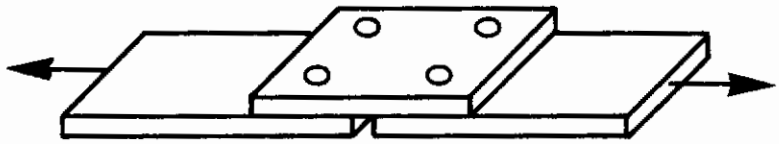

Single Shear Butt Joint

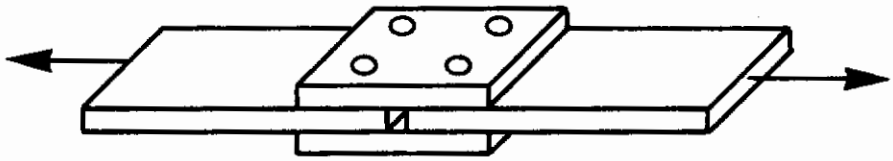

Double Lap Joint

Fig. 6.52 JOINT TYPES DESCRIBED FOR DESIGN PROCEDURE BY STRAUSS (6.66)

failures which occur in a fairly large sample. The summary of all failure types is:

Tension: 5.5%

Shear Tear-out: 30.5%

Combined Bearing Shear and Tearout: 4%

Bearing: 44.5%

Combined Bearing and Shear: 19%

Bolt or Rivet Shear: 8%

Tension and Delamination: 1%

The type of fasteners studied included:

1. Flush-headed rivets
   $0.067 \leq a/w \leq 0.094$
   $a/H = 0.40$
2. Protruding head rivets
   $0.067 \leq a/w \leq 0.094$
   $a/H = 0.40$
3. Flush head screws
   $0.094 \leq a/w \leq 0.125$
   $a/H = 0.40$
4. Protruding head bolts
   $0.067 \leq a/w \leq 0.094$

General trends indicated were:

1. σ_m increases as a/w increases.
2. σ_m decreases at t/a increases for constant a/w.
3. Flush head rivets deliver about the same σ_m for constant a/w at all t/a ratios.
4. Bolted joints represent a substantial increase in σ_m over either flush riveted or protruding head rivets for the same a/w and t/a ratios.

5. The advantages of single or double lap joints are not clearly demonstrated.

Ruffalo, A. (6.57)

"Research and Development Report on Joint Design Data for High Strength Plastics," Final Report, Lab. Project 6066-1 Suppl. 2, September 16, 1963, U.S. Naval Applied Science Laboratory, Brooklyn, N. Y.

This report describes fastener pullout studies for a two to one 0°-90° fiber orientation. The types of failures were examined by an ultrasonic flaw detection technique of the pulse-echo type and compared against "standard flaws." The effect on fastener pullout strength of panel stiffener plates and counterboring was also investigated. The joint parameter (a/w) was practically zero and a/t varied between

$$0.25 \leqq a/t \leqq 0.5$$

Depth of penetration (DOP) varied from

$$0.25 \leqq \frac{DOP}{t} \leqq 0.88$$

Nominal plate thickness was 1 in.

Carylon, G. (6.10)

"Fasteners and Adhesives in Joining Plastics," Plastics Handbook, 1963.

This brief review describes some techniques for joining plastics and a review of the types of fasteners available for composite joining.

Prokhorov, B. F. (6.53)

"Joints Used in Plastic and Composite Shipboard Superstructures, Deck Houses, Light Bulkheads and Enclosures," Trans. from the Russian, 1965, Dept. of Navy, A.D. 629509.

This translated document treats plastic and composite joints in various ship components in the Soviet Union. Analysis is also available for the design of mechanical joints provided the following information is available:

1. Bearing and shear strengths of material.
2. Data on strength of plates with holes.
3. Experimental data on the joints.

These are sufficient to determine t, a, d, H, and L_i.

6.4 ANNOTATED BIBLIOGRAPHIES: GENERAL REFERENCES

DeJonge, A. E. R. (6.16)

"Riveted Joints: A Critical Review of the Literature Covering Their Development," ASME, New York, 1945, 250 pp.

This is, of course, the most extensive survey ever made of riveted joints and was performed for the ASME by DeJonge It contains some 1364 references, all annotated. A review of this extensive literature is also made prior to the annotated bibliographies. The review tends to be primarily a documentation of historical precedence rather than a technical evaluation of the articles.

Giddings, H. (6.24)

"Aircraft Riveting," J. Roy. Aero. Soc., v 4, 1950 pp. 753-778.

This paper is an excellent review of riveting practices in England at the time of writing of the paper. The discussion covers the following topics:

1. Static Load Requirements
2. Repeated Load Requirements
3. Fatigue Load Requirements
4. Materials to Be Joined
5. Rivet Materials
6. Rivet Manufacturing Processes
7. General Rivet Characteristics, Geometry, etc.
8. Sheet Preparation
9. Riveting Practices
10. Strength of Multifastener Riveted Joints and Design
11. Strength Test Results
12. Fatigue Test Results
13. Sealing Practices
14. Joint Finishing Techniques

These techniques, practices and processes constitute a very practical aircraft riveting design manual. The tables and data presented are excellent and will provide an analysis of riveted joints with a great deal of practical information on the rivet stiffnesses which are so important in calculating joint displacements and strengths by any of the methods described earlier in this report.

Schenker, L., Salmon, C. G., and Johnston, B. G. (6.58)

"Structural Steel Connections," U. of Mich., AFSWP, Rept. No. 352, prepared for Bureau of Yds. and Docks, U.S. Navy Dept. Contract No. 74521, June 1954.

This report, prepared for the Bureau of Yards and Docks, U.S. Navy Department, was directed primarily toward a review of the literature for suitable joint design under transient dynamic joint conditions.

The report chapters include two general reviews of interest here, however, and which are exclusively concerned with static tension type joints. The first chapter presents analytical, experimental and empirical studies reviews on the fasteners themselves. This chapter contains sections on the strengths of rivets and the strengths of bolts, on the deformation and energy absorbtion of rivets and bolts and finally a section on the properties of welded connections.

A second chapter on tension connections directly has the following sections and subsections:

Riveted Tension Connections

- Load Deformation Relations
- Effect of Rivet Pattern on Plate Strength
- Effect of Rivet Pattern on Rivet Strength

Bolted Tension Connections

- Load Deformation Relations
- Ultimate Strength of Bolted Connections

Pinned Connections

The Strength of Pin-Connected Plate Links
The Strength of Eye Bars

This second chapter deals extensively with analytical procedures for including, for the elastic (linear) and inelastic (plastic flow plus slip), portions of the load-displacement relations for a riveted joint. A generalized expression for this total elongation of the joint is given from Batho (Ref. 6.3, 6.4) as

$$\Delta = \delta_1 + K \frac{nPL}{2wtE}$$

where

δ_1 = displacement of the first rivet row
n = number of spaces between rows
P = load
L = pitch between rows
w = width of plate
t = thickness of plate
E = modulus of plate material

and K is an empirical constant derived from tests on the joint.

This expression is good only within the elastic range. For the inelastic range up to $P = nA_g\sigma_y$ where n = predicted ultimate efficiency and σ_y = yield strength of the plate material, the expression becomes

$$\Delta = \delta + K \frac{nPL}{2EA_G}$$

where A_G is the gross section area.

Similar deformation expressions from Koegler and Schmidt (Ref. 6.38), and others are also summarized nicely. Schenker then summarizes some of the work performed on the effect of rivet pattern on strength. Ratios are developed for proportioning of load

among rivet rows and failure predictions there from. Schenker describes and summarizes work done where the plates are partitioned into several strips of equal width (see Fig. 6.53) and strip contains a hole at the center. The plate width is W_G and, thus, where the strength of the metal is unaffected by the holes at the center, the ultimate net strength of the plate becomes

$$(w_G - \alpha)/w_G$$

times the gross strength of the plate, i.e.,

$$\bar{E} = (1 - \alpha/w_G)$$

where E_G is the gross efficiency of the perforated plate. Schutz (Ref. 6.61) also performed much work on this concept. Schenker summarized the feelings of many investigators, that the joint efficiency, $\bar{E}$, is usually less than $\bar{E}_G$ for large values of w_G/α, but for small values of w_G/α, the true joint efficiency is greater than $\bar{E}_G$.

The strength of pin-connected plate links and eye bars is also covered.

Smith, C. R. and Lindeneau, G. (6.64)

"Riveted Joints Fatigue Strength," ASTM STP-203, 1956, pp. 10-23.

This paper is a review of techniques for improving the fatigue life of riveted joints. One of the most beneficial methods appears to be the prestressing caused by driving the rivet into the hole in such a manner as to cause initial interference between hole in the plate and the rivet. A large number of practical suggestions are presented in this review paper.

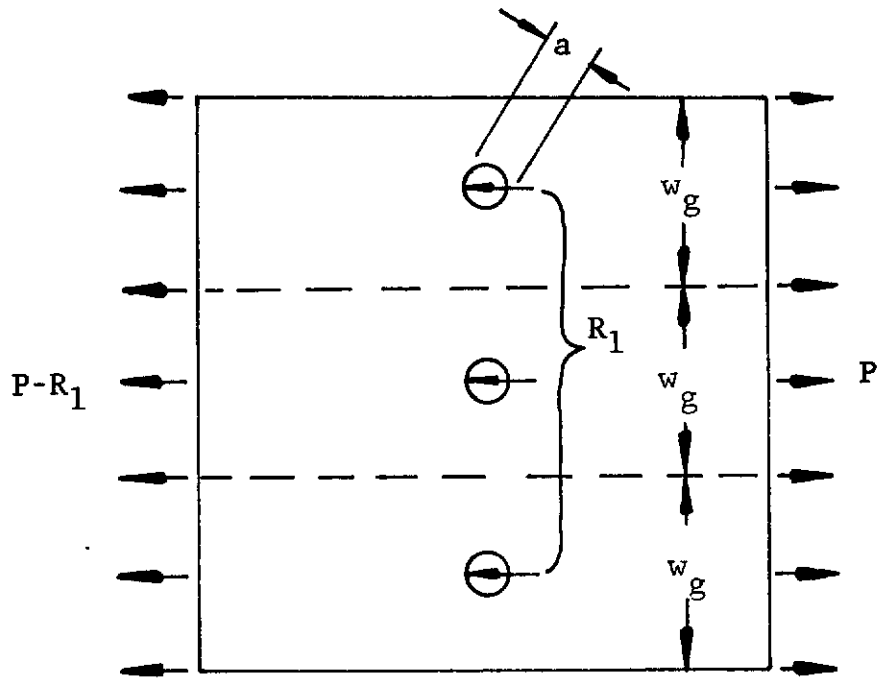

Fig. 6.53 STRIP METHOD OF RIVETED OR BOLTED PLATE JOINT ANALYSIS, AFTER SCHENKER (6.58)

Grover, H. J. (6.25)

"Estimation of Fatigue Life of Welded, Riveted and Bolted Structures," In Metal Fatigue by Sines and Waisman, McGraw-Hill, N.Y., 1959, pp. 307-324.

This paper is a summary of results obtained from fatigue investigations on various types of joints. Chapters appear on fusion welds, riveted joints, spot welded joints, bolted joints, screws and bolts, fatigue behavior of composite structures, and estimation of fatigue life times of joints.

Niles, S. and Newell, J. S. (6.51)

"Airplane Structures," Chapter 13, Connections, John Wiley & Sons, 1961, pp. 462-500.

This chapter in an aircraft design reference book is valuable as a summary of bolted and riveted joints design procedures. Also included are design procedures for cemented and brazed joints, fuzed (welded) joints and spot-welded joints design analyses.

Some of the design "rules" by Niles and Newell include some which may be expressed mathematically for a specific problem.

1. Riveted and bolted joints should be geometrically arranged so that the rivets do not transmit tension across a faying surface.
2. Bolting should be avoided when both tension and shear are to be transmitted.

The test results and theories postulated by other aircraft joint designers such as Koegler and Schnitt (Ref. 6.38), Fefferman and Langhaar (Ref. 6.18), Templin and Hartman (Ref. 6.69) Holleman (Ref. 6.29), Muckle (Ref. 6.50) and Giddings (Ref. 6.24). were reviewed.

Another chapter is presented on design of eccentrically loaded joints where bending and/or torsion is transmitted as well as tension. The final section which appears is on the rather specialized subject of design of stepped tapered splice plates.

Crum, R. (6.14)

"Fatigue of Metal Joints," Machine Design, March 30, 1961, pp. 108-113.

This paper presents scattered bits and pieces of information regarding joint design techniques for fatigue resistance.

Levitt, C. W., et al (6.43)

"Riveted and Bolted Joints: Fatigue of Bolted Structural Connections," J. Struct. Div., Proc. ASCE, Feb. 1963, pp. 49-65.

This paper is a review of the technology for high-strength bolting practices and techniques. It contains many practical suggestions on the utilization of high-strength bolts for increasing the fatigue resistance of structural joints.

Fisher, J. W., and Beedle, L. S. (6.20)

"Bibliography on Bolted and Riveted Structural Joints," Lehigh Univ. Institute of Research, Fritz Engrg. Lab. Report No. 302.1, Dec. 1964, 152 pp.

This report was part of work carried out for the Research Council on Riveted and Bolted Structural Joints. The majority of the papers reviewed were written in the period between 1944 and June 1964. Papers written before that period were reviewed by DeJonge (Ref. 6.16) and were not included in this review. A historical review of the studies on bolted joints is first presented, then a set of annotated bibliographies in Index-card format is presented. Finally, a set of tables for all references is presented which contains a brief description of

the fastener (bolt or rivet type, size, etc.) a brief description of the joint type (splice, single lap, etc.), a sketch of the types of joints investigated (stress range, bolt size, joint size, grip length, pre-tension, etc.), a description of the test conditions, (static, fatigue, ultimate, displacements, etc.) and a description of the analytical procedures associated with the particular reference joints.

Two hundred forty-one reference abstracts are included.

Smith, C. R. (6.62)

"Interference Fasteners for Fatigue Life Improvement," Experimental Mechanics, Vol. 5, Aug. 1965, pp. 19A-23A.

This paper is a condensation of prior work by the author on the mechanism of fatigue life improvements for lugs through the use of interference type fasteners. See also Refs. 6.73, 6.34, 6.35, 6.7, 6.36, 6.19, 6.39, 6.40, 6.44, 6.13, and 6.41.

Fisher, J. W., Kormanik, R., and Allan, R. N. (6.22)

"Supplement to Bibliography on Bolted and Riveted Structural Joints," Fritz Engrg. Lab., Rpt. No. 302.2 Feb. 1966, 173 pp.

This report continues the work described in Ref. 6.20 from June 1964 to Dec. 1965. Two hundred forty-nine abstracts were prepared for this report.

REFERENCES

6.1 Abel, K. B., "Feasibility of Reinforced Plastics for Primary Structures of Army Aircraft," U.S. Army Transportation Command, TRECOM Tech. Report 63-15 March, 1963, pp. 201-218.

6.2 Baron, F., and Larson, E.W., "Comparison of Bolted and Riveted Joints," ASCE, Transactions, Vol. 120, 1955 pp. 1322-1334.

6.3 Batho, C., "The Partition of Load in Riveted Joints," J. Franklin Institute, Vol. 182, Nov. 1916, pp. 553-604.

6.4 Batho, C., "Experimental and Theoretical Investigation on Riveted and Bolted Joints, With the Application of the Theory to Welded Joints," First Report of the Steel Structures Research Committee London, H.M.S.O., 1931, pp. 100-179.

6.5 Bendigo, R. A., Hansen, R. M., and Rumpf, J. L., "Long Bolted Joints," Proc. American Soc. Civil Eng., J. Structural Div., Dec. 1963, pp. 187-213.

6.6 Bickley, W. G., "The Distribution of Stress around a Circular Hole in a Plate," Phil. Trans. Roy Soc., London, Vol. 227A, 1928, pp. 383-415.

6.7 Bodine, E. G., Carlson, R. L., and Manning, G. K., "Creep Deformation Patterns of Joints under Bearing and Tensile Loads," NACA TN 4138, Dec. 1957.

6.8 Bollenrath, F., "About the Stress Distribution in Elastic Welding Joints in Thin Sheet Metals," Redstone Scientific Information Center, Report No. RSIC-297, Oct. 7, 1964.

6.9 Budiansky, B., and Wu, T. T., "Transfer of Load to a Sheet from a Rivet-Attached Stiffener," J. Math. and Physics, Vol. 40, July 1961, pp. 142-162.

6.10 Carylon, G., "Fasteners and Adhesives in Joining Plastics," Plastics Handbook, 1963.

6.11 Chi, M., and Irwin, L. K., "Deformation in Strips with Holes Loaded through Pins," BuWeps Rept. No. RAAE - 343-60-16, July 1958.

6.12 Coker, E. G. and W. A. Scoble, "The Distribution of Stresses Due to a Rivet in a Plate," Trans. Instn. of Naval Architects, 1913, pp. 207-218.

6.13 Cox, H. L., and Brown, A. F. C., "Stresses Round Pins in Holes," The Aero Quarterly, Nov. 1964, pp. 357-372.

6.14 Crum, R. G., "Fatigue in Metal Joints," Machine Design, Part I, Mechanical Joints, March 30, 1961, pp. 108-113.

6.15 Davis, R. E., Woodruff, G. B. and Davis, H. E., "Tension Tests of Large Riveted Joints," ASCE, Transactions, Paper No. 2084, May 1939, pp. 1193-1245.

6.16 DeJonge, A. E. R., "Riveted Joints: A Critical Review of the Literature Covering Their Development," ASME N. Y., 1945.

6.17 Deneff, G. V., "Fatigue Prediction Study," WADD TR-153, January 1962.

6.18 Fefferman, R. L., and Langhaar, H. L., "Investigations of 24S-T Riveted Tension Joints," J. Aero. Sciences, Vol. 14, No. 3, 1947, pp. 133-147.

6.19 Fessler, H., and Haines, D. J., "Plasto-Elastic Stress Distribution in Lugs," The Aero. Quarterly, Aug. 1959, pp. 230-246.

6.20 Fisher, J. W. and Beedle, L. S., "Bibliography on Bolted and Riveted Structural Joints," Lehigh University Inst. of Research, Fritz Engrg. Lab. Report No. 302.1, Dec. 1964.

6.21 Fisher, J. W., "Analysis of Bolted Butt Joints," J. Structural Division, Proc. Am. Soc. Civ. Eng., Oct. 1965, pp. 181-203.

6.22 Fisher, J. W., Kormanik, R. and Allan, R. N., "Supplement to Bibliography on Bolted and Riveted Structural Joints," Fritz Engineering Laboratory Reports No. 302.2, Feb. 1966.

6.23 Frocht, M. M. and Hill, H. N., "Stress Concentration Factors around a Central Circular Hole in a Plate Loaded through Pin in the Hole," Trans. ASME, Vol. 62, 1940 pp. A-5.

6.24 Giddings, H., "Aircraft Riveting," J. Roy. Aero. Soc., Vol. 54, 1950, pp. 753-778.

6.25 Grover, H. J., "Estimation of Fatigue Life of Welded, Riveted and Bolted Structures," in "Metal Fatigue," by Sines and Waisman, McGraw Hill, 1959, pp. 307-324.

6.26 Hartman, A., Jacobs, F. A., and Van Der Vet, W. J., "Constant Load Amplitude and Programme Fatigue Tests on Single-Lap Joints in Clad 2024-T3 and 7075-T6 Aluminum Alloy with Two Rows of Rivets or Huckbolts," National Lucht-En Ruimtevaartlaboratorium, NLR-TN-M.2147, July 1965.

6.27 Hennig, A., "Polarized Light Stress Investigations on Tensile Bar with Holes and on a Rivet Hole," Trans. from Z. Tech. Mech. and Thermo. Forschung auf dem Gebiete des Ingeniur, Vol. 4, No. 2, 1933, pp. 52-63.

6.28 Holbach, G. E., "The Structural Analysis and Significance of Rivet Shear Tests," Proc. Soc. Exp. Stress Analysis, Vol. 3, No. 1, 1954, pp. 131-154.

6.29 Holleman, C. H., "Tension Joints in Aircraft Structures, Jour. Aero. Sci., Vol. 10, 1943, pp. 295.

6.30 Hovgaard, W., "A New Theory of The Distributions of Shearing Stresses in Riveted and Welded Connections and Its Application to Discontinuities in the Structure of a Ship," Trans. Inst. Naval Architects, 1931, pp. 108-138.

6.31 Howard, D. M., and Smith, F. C., "Fatigue and Static Tests of Flush Riveted Joints," NACA TN 2709, June 1952.

6.32 Howland, R. C. J., "On Stresses in Flat Plates Containing Rivet Holes," Proceedings 3rd International Congress Appl. Mech., 1930, Vol. II, pp. 74-79.

6.33 Jenkins, E. S., "Rational Design of Fastenings," SAE Journal, Sept. 1944, pp. 421-429.

6.34 Jessop, H. T., Snell, C., and Hollister, G. S., "Photo-elastic Investigation in Connection with the Fatigue Strength of Bolted Joints," The Aero. Quarterly, Aug. 1955, pp. 230-239.

6.35 Jessop, H. T., Snell, C. and Holister, G. S., "Photoelastic Investigation on Plates with Single Interference-Fit Pins with Load Applied to Plate Only," Aero.Quarterly, Vol. 7, Nov. 1956, pp. 297-314.

6.36 Jessop, H. T., Snell, C. and Hollister, G. S., "Photoelastic Investigation on Plates with Single Interference-Fit Pins with Load Applied a) to Pin Only, and b) to Pin and Plate Simultaneously," The Aero. Quarterly, May 1958, pp. 147-163.

6.37 Knight, R. C., "The Action of a Rivet in a Plate of Finite Breadth," Philosophical Magazine, Series 7, Vol. 19, No. 127, March 1935, pp. 517-540.

6.38 Koegler, R. K., and Schnitt, A., "Effects of Yielding and Perforations on a Wing Tension Surface," J. Aero. Sciences, Vol. 10, 1943, pp. 273-284.

6.39 Lambert, T. H. and Brailey, R. J., "The Influence of the Coefficient of Friction on the Elastic Stress Concentration Factor for a Pin-Jointed Connection," Aero. Quarterly, Vol. 13, Feb. 1962, pp. 17-29.

6.40 Lambert, T. H., and Brailey, R. J., "The Use of an Interference-Fit Bushing to Improve the Fatigue Life of a Pin-Jointed Connection," Aero. Quarterly, Vol. 13, Aug. 1962, pp. 275-284.

6.41 Lambert, R. H., and Snell, C., "Effect of Yield on the Interference between a Pin and a Plate," J. Mech. Engr. Sci., Vol. 6, No. 1, 1964, pp. 38-43.

6.42 Langhaar, H. L., "Dimensional Analysis, Problems of Stress and Strain," Section 40; "Dimensionless Plotting of Test Data for Riveted Joints."

6.43 Levitt, C. W., Chesson, E., and Munse, W. H., "Riveted and Bolted Joints: Fatigue of Bolted Structural Connections," Proc. ASCE, Feb. 1963, pp. 49-65.

6.44 Ligenza, S. J., "Cyclic Stress Reduction within Pin-Loaded Lugs Resulting from Optimum Interference Fits," Experimental Mechanics, Vol. 3, 1963, pp. 21-28.

6.45 Lobbett, J. W., and Robb, E. A., "Thermo-Mechanical Analysis of Structural Joint Study," WADD TR-61-151, January 1962.

6.46 Marin, J., "Determination of Creep of Structural Joints from Simple Tensile Creep," ASTM, 1961 Preprint, presented at 64th Annual Meeting of the Society, June 1961.

6.47 Mead, D. J., "The Internal Damping Due to Structural Joints and Techniques for General Damping Measurements," Aero. Res. Council, London, Current Papers, C. P. No. 452, 1959.

6.48 Mittenbury, A. A., and Beall, L. G., "Effects of Pin Interference and Bolt Torque on Fatigue Strength of Lug Joints," ASTM Proc., Vol. 63, 1963, pp. 671-683.

6.49 Mordfin, L. and Legate, A. C., "Creep Behavior of Structural Joints of Aircraft Materials under Constant Loads and Temperatures," NAXA TN 3842, Jan. 1957.

6.50 Muckle, W., "Distribution of Load in Riveted Joints," Shipbuilder and Marine Engine Builder, April 1949, pp. 225.

6.51 Niles, S., and Newell, J. S., "Airplane Structures," Chapter 13, Connections, J. Wiley and Sons, 1954, pp. 462-500.

6.52 Owen, J. B. B., "Design of Bolted Joints for Uniform Mean Stresses," Aero. Research Council, Report No. ARC 26, 153 Strut. 2647, August 28, 1964.

6.53 Prokhorov, B. F., "Joints Used in Plastic and Composite Shipboard Superstructures, Deckhouses, Light Bulkheads and Enclosures," Translated from the Russian, Dept. of the Navy, 1965, A. D. 629 509.

6.54 Rosenfield, S. J., "Analytical and Experimental Investigation of Bolted Joints," NACA TN 1458.

6.55 Ruffalo, A., "Design Manual For Joining Glass Reinforced Structural Plastics," Naval Material Laboratory, Report on Laboratory Project 6066-1, Bureau ID No. 16-1009-2, Navships 250-634-1, August 1961.

6.56 Ruffalo, A., "How to Evaluate and Select Mechanical Fasteners," Materials in Design Engineering, Feb. 1963, pp. 95-100.

6.57 Ruffalo, A., Research and Development Report on Joint Design Data for High Strength Plastics," Final Report Lab. Project 6066-1, Suppl. 2, Sept. 16, 1963, U.S. Naval Applied Science Lab.

6.58 Schenker, L., Salmon, C. G., and Johnston, B. G., "Structural Steel Connections," University of Michigan, AFSWP, Report No. 352, prepared for Bureau of Yards and Docks, U.S. Navy Dept., Contract No. 74521, June 1954.

6.59 Schijve, J., And Jacobs, F. A., "Programme Fatigue Tests on Aluminum Alloy Lug Specimens with Slotted Holes and Expanded Holes," National Lucht-En Ruimtevaartlaboratorium Amsterdam, NLR-TN-M.2139, Nov. 1964.

6.60 Schuechterle, K., "On the Fatigue Strength of Riveted and Welded Joints and the Design of Dynamically Stressed Structural Members Based on Conclusions Drawn from Fatigue Tests," Int. Assoc. for Bridge and Structures Engineering, Vol. 2, 1934, pp. 312-379.

6.61 Schutz, F. W. Jr., "The Efficiency of Riveted Structural Joints," Publication No. 4478, U. of Ill., 1952.

6.62 Smith, C. R., "Interference Fasteners for Fatigue Life Improvement," Exp. Mech., Vol. 5, August 1965, pp. 19A-23A.

6.63 Smith, C. R., "Influence of Residual Stresses and Stiffness Factors on Fatigue Strength of Metals and Structures," G. D. Convair Rept. No. G.D/C62-55, March 1962, A. D. 274656.

6.64 Smith, C. R. and Lindeneau, G. D., "Riveted Joints Fatigue Strength," ASTM-STP-203, 1956, pp. 10-28.

6.65 Strauss, E. L., "Mechanical Joints in Reinforced Plastic Structures," Machine Design, March 17, 1960, pp. 197-201.

6.66 Strauss, E. L., "How to Design Mechanical Joints," Materials in Design Engineering, Feb 1963, pp. 86-94.

6.67 Switsky, H., Forray, M. J., and Newman, M., "Thermo-Structural Analysis Manual," Section 5; "Thermo-Elastic Analysis of Joints," Vol. 1, WADD TR-60-517, August 1962.

6.68 Tate, M. B., and Rosenfeld, S. J., "Preliminary Investigation of the Loads Carried by Individual Bolts in Bolted Joints," NACA TN 1051, May 1946.

6.69 Templin, R. L., "Aluminum Connecting Rods, An Investigation of the Stress Distribution," Mechanical Engineering Vol. 58, March 1936, pp. 169-170.

6.70 Theocaris, P., "The Stress Distribution in a Strip Loaded in Tension by Means of a Central Pin," ASME J. Appl. Mech., Paper No. 55-A-34.

6.71 Vogt, F., "The Load Distribution in Bolted or Riveted Joints in Light Alloy Structures," NACA TM 1135, April 1947.

6.72 Werren, F., "Bolt Bearing Properties of Glass Fabric Base Plastic Laminates," FPL Report No. 1824, June 1951.

6.73 Wilkins, E. W. C. and Jessop, H. T., "A Photoelastic Fatigue Programme of Experimental Research in Connection with Bolted Joints," J. Royal Aeronautical Society, Vol. 58, June 1954, pp. 435-438.

6.74 Wilson, W. M., and Thomas, F. P. "Fatigue Tests of Riveted Joints," U. of Ill., Engl Exp. Stat. Bulletin No. 302.

6.75 Young, R., "Supplement to Bolt Bearing Properties of Glass-Fabric Base Plastic Laminates," FPL Report No. 1824A, Oct. 1955.

6.76 Young, R., "Supplement to Bolt Bearing Properties of Glass-Fabric Base Plastic Laminates," FPL Report No. 1824B, Oct. 1955.

6.77 Young, R., "Supplement to Bolt Bearing Properties of Glass-Fabric Base Plastic Laminates," FPL Report No. 1824C, Feb. 1957.

7.0 STATIC STRENGTH OF MECHANICAL JOINTS

The purpose of this study was to establish the efficacy of several of the theories described in Section 6.0 for predicting the strength of mechanical joints. This series of tests was intended to:

- Establish parameters and constants for some of the analyses for a glass reinforced plastic of current interest.
- Provide load distribution data for a multi-fastener joint in a glass reinforced plastic.
- Provide datum from which a comparison of analyses could be made.

7.1 COMPOSITE TEST MATERIAL

The composite material for the mechanical joint studies was the 3M XP-251S roving prepreg tape laminated in an orthogonal (0°-90°) fiber layup. Individual composite plates were press fabricated in 13 ply thicknesses (0°-90°-0°....90°-0°) with successive layers "cross-plied." The plate sizes were 12 in. by 14 in. This was the same material was was used in the bonded joint studies.

The per-ply thicknesses in the pressed form were 0.0082 in. and hence reasonably close to the manufacturers specified thickness of 0.0075 in./ply. The plates were cured for 30 minutes at 300°F followed by a 4-hour post-cure at 350°F. A separate measure of tensile strengths was made for the material for the results are shown in Table 7.1. These are approximately the same as the manufacturers' stated values of 130 ksi prorated for the greater thicknesses.

7.2 PINNED JOINT PARAMETERS

7.2.1 Single-Pin Tests

Six single-pin specimens such as are shown in Figure 7.1 were prepared from the Scotchply XP-251S prepreg material described

Table 7.1

TENSILE STRENGTHS OF SCOTCHPLY XP-251S USED IN JOINT TESTS

Specimen Number	Width (in.)	Thickness (in.)	Ultimate Strength (ksi)
1	0.339	0.053	110
2	0.339	0.053	103
3	0.339	0.103	118
4	0.339	0.103	132
5	0.339	0.053	101.5
Average	--	--	112.9

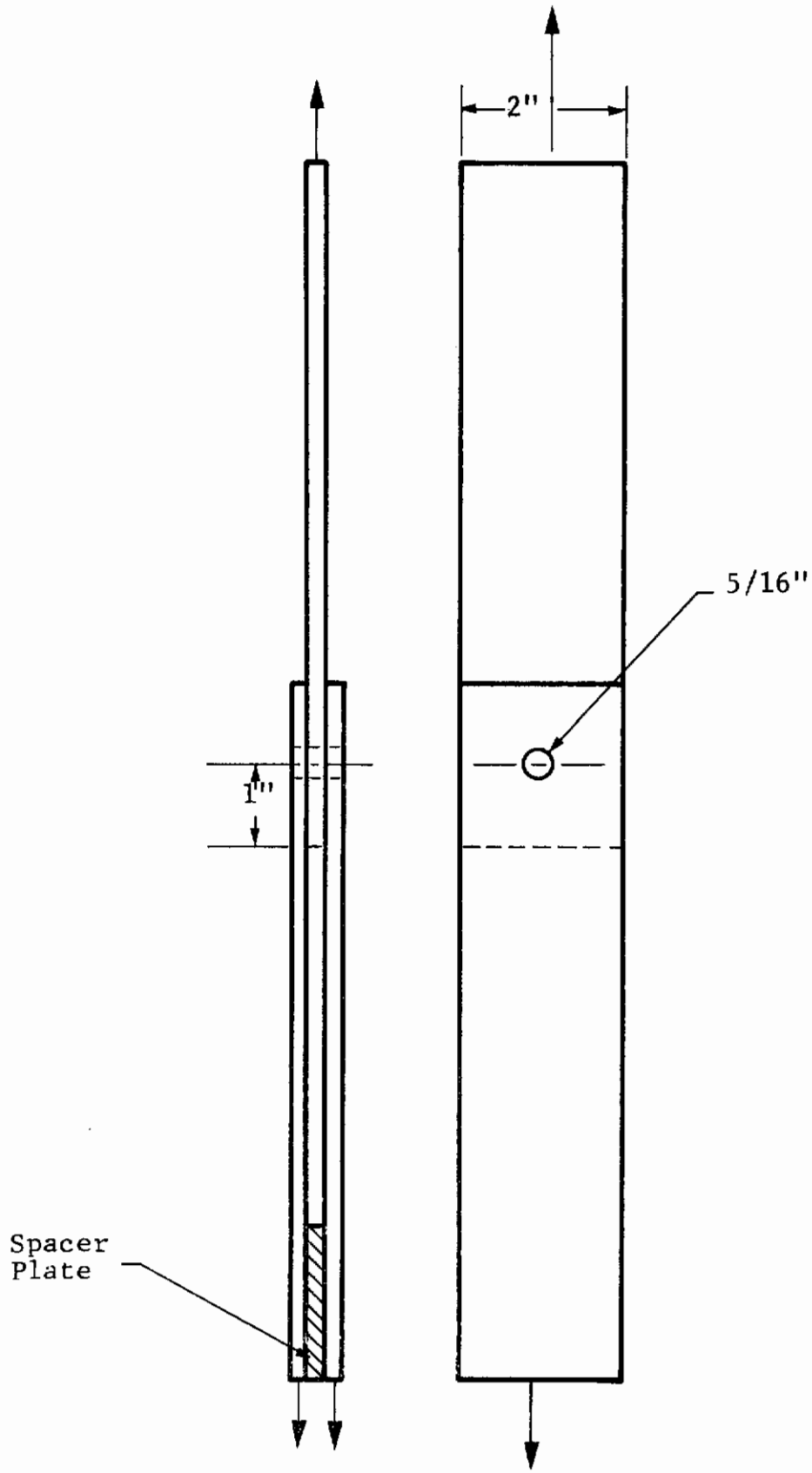

Fig. 7.1 SINGLE PIN DOUBLE OVERLAP SPECIMEN (1/2 Scale)

above. The specimens were double overlap, therefore they provided symmetric loading to the pin joint. Each of the main plates and the splice plates was approximately 9 in. long by 2 in. wide by 0.100 in. thick. Steel dowel pins were used as the load transfer mechanism. Test results are shown in Table 7.2.

- For a/w ratios less than 0.15, the Bickley (7.2) solution shows that the stresses are not sensitive to the presence of the edges.
- The Ruffulo (7.3) manual recommends the use of a minimum of 3 hole diameters to the edge and ends of the strip from the hole center; 3 by 5/16 is less than 1 in., therefore the edge and end distances are approximately designed according to this manual.

Although the Theocaris' (7.6) solution applies strictly to the elastic case, the maximum elastic compressive stress is approximately -5.6 times the gross section tensile stress. The compressive strength of the material is approximately 100 ksi thus permitting a gross section tensile stress of approximately 17.9 ksi. Since the gross section tensile stress at failure for the joints was approximately 10.45 ksi, the joint clearly did not carry the Theocaris (7.6) theoretically predicted strength.

7.2.2 Two-Pin Tests

Specimens with two pins in a line were also prepared and tested. The specimen configuration is shown in Figure 7.2.

When several pins in a line are employed, the theoretical load-carrying capacity of the joint depends upon the distribution of load between the several rivets. For pins spaced some distance apart little interaction between the two stress distributions will be present and the stress distribution around a single hole "prorated" for the load delivered to that pin will apply. Thus if 75 percent of the load is applied to a single pin, then the load-carrying capacity of the joint is enhanced by [(1/0.75)-1]

Table 7.2

TEST RESULTS FOR SINGLE PIN (a/w = 0.187), DOUBLE OVERLAP JOINTS IN SCOTCHPLY

Specimen Number	Load @ First Yield (lb)	Gross Section Stress @ First Yield (ksi)	Ultimate Load (lb)	Gross Section Stress @ Ultimate (ksi)
1-1PJ-1	2140	9.40	2220	9.75
1-1PJ-4	2180	9.55	2400	10.50
1-1PJ-5	2200	8.80	2640	10.55
1-1PJ-6	2160	9.00	2580	10.75
2-1PJ-1	2140	9.37	2480	10.85
2-1PJ-2	2020	8.70	2380	10.25
Average	--	--	--	10.44

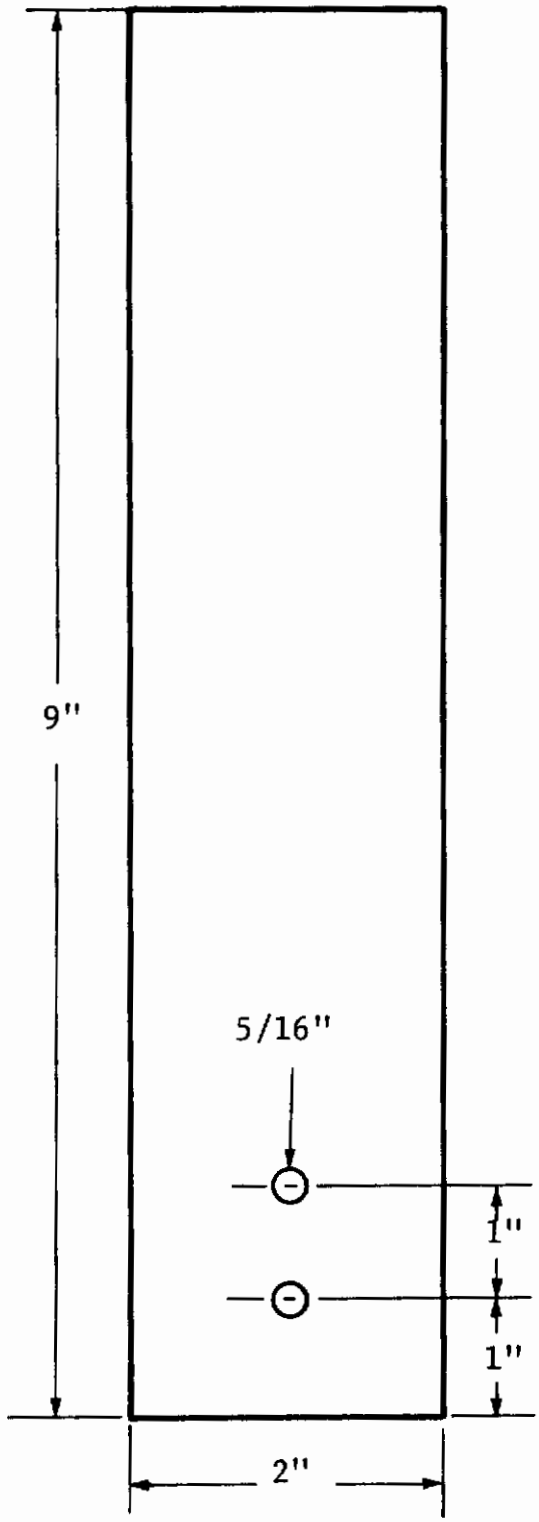

Fig. 7.2 TWO PINS IN A LINE, DOUBLE OVERLAP SPECIMEN

or 33 1/3 percent. Since the two-pin joint is symmetric about a transverse line located midway between the two pins, the load should be distributed equally between the two pins. Therefore, each pin carries 50 percent of the load and the total joint efficiency is enhanced by [(1/0.50)-1] or 100 percent.

A second set of two-pinned specimens was tested in tension. A double overlap, equal-coverplate-thickness specimen was selected. Pins were located as shown in Figure 7.2. The test results are shown in Table 7.3. Although in this case it would not be expected that the load would be equally distributed among the two pins, the load carrying capacity of the joint was approximately double and approached the theoretical limit of 17.9 ksi gross section stress for a single rivet. For a perfectly designed single-lap two-pin joint, the gross section stress should approach 35.8 ksi based on the Theocaris (7.6) solution. Since this joint configuration did not sustain the theoretical gross section stress either, it is apparent that the Theocaris (7.6) solution does not apply to pinned joints.

During the test it become evident, even in the double-overlap case, that the joint was deforming "out-of-plane" and hence either (1) the "out-of-plane" deformations introduce stresses substantially higher than those predicted by simple theory or (2) the low-modulus composite coupled with eccentricities introduced during the loading give rise to a local buckling phenomenom directly under the bearing of the pin.

7.3 MULTIPLE BOLT TESTS

7.3.1 Specimen Geometries and Test Procedures

Multiple bolt joint tests were conducted on specimens with the configurations shown in Figures 7.3 through 7.6. The specimens were loaded to destruction in an Instron Universal Testing Machine. The specimens were gripped on composite tabs which had been affixed by adhesive bonding to the main plates of the specimens.

Table 7.3

RESULTS OF TWO-PINS-IN-A-LINE JOINT TESTS IN SCOTCHPLY XP-251S

Specimen Number	Load @ First Yield (lb)	Gross Section Yield Stress (ksi)	Ultimate Load (lb)	Gross Section Ultimate Stress (ksi)
2-2PJ-7	3500	15.20	4100	17.80
2-2PJ-5	3400	14.80	3900	17.00
3-2PJ-2	3480	14.15	4060	16.50
3-2PJ-5	3560	15.60	4220	18.50
4-2PJ-2	3540	15.40	4460	19.45
5-2PJ-2	3580	16.40	4380	20.05
Average	--	--	--	18.21

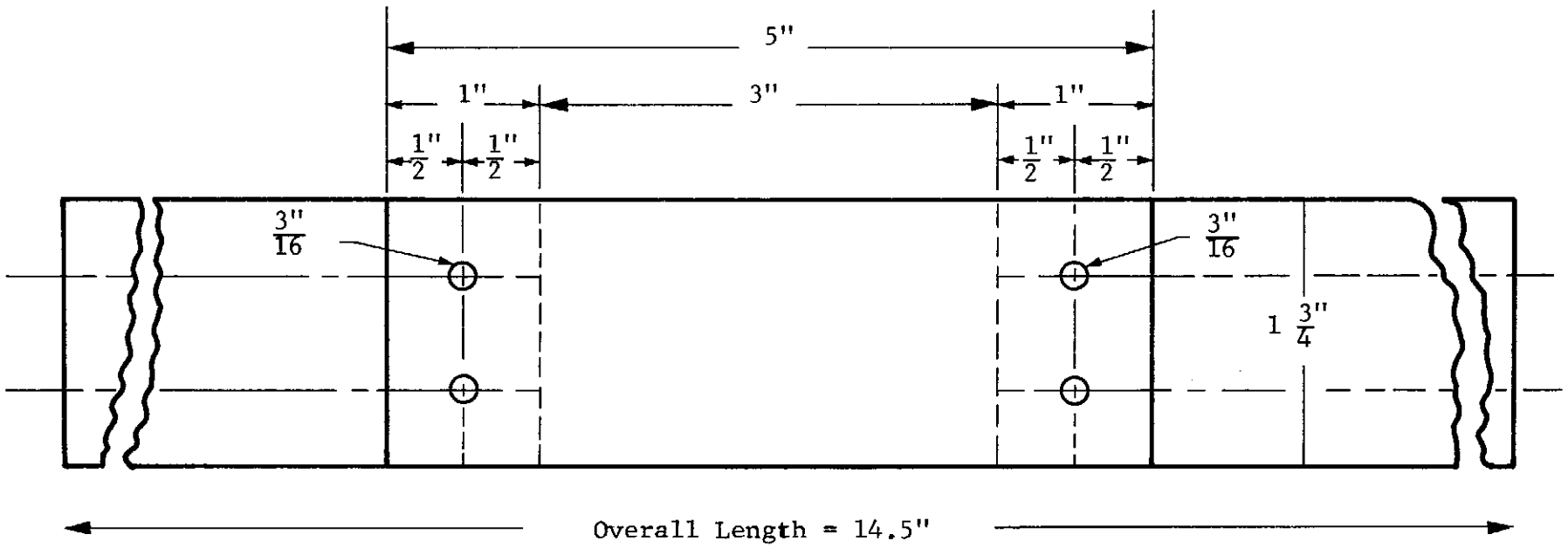

Fig. 7.3 DIMENSIONS OF SINGLE-ROW DOUBLE-LINE BOLTED SPECIMEN

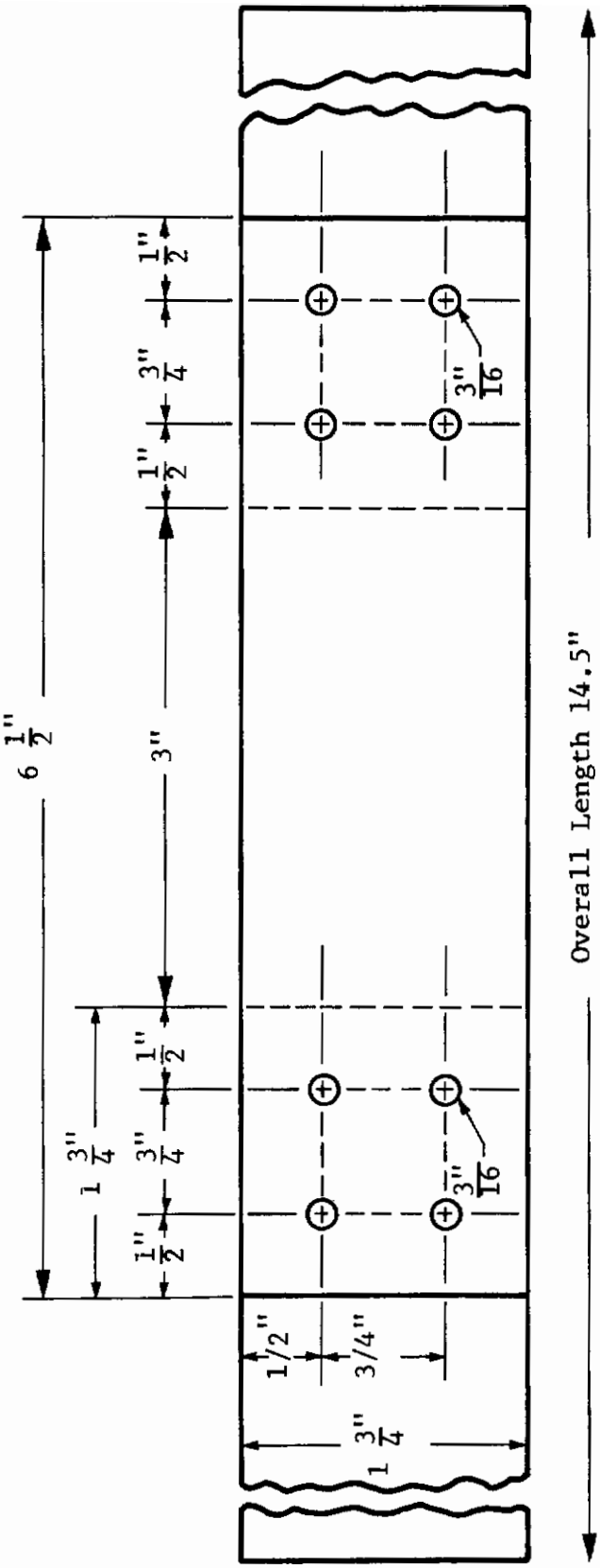

Fig. 7.4 DIMENSIONS OF DOUBLE-ROW DOUBLE-LINE BOLTED JOINT SPECIMEN

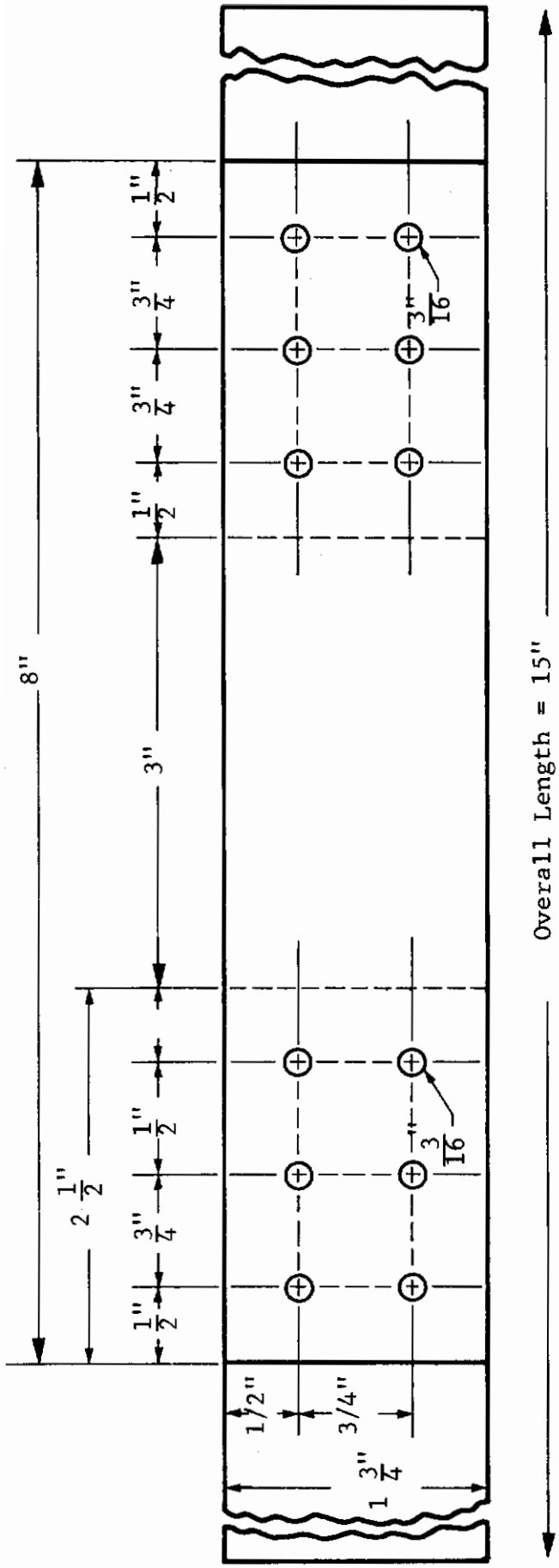

Fig. 7.5 DIMENSIONS OF TRIPLE-ROW DOUBLE-LINE BOLTED JOINT SPECIMEN

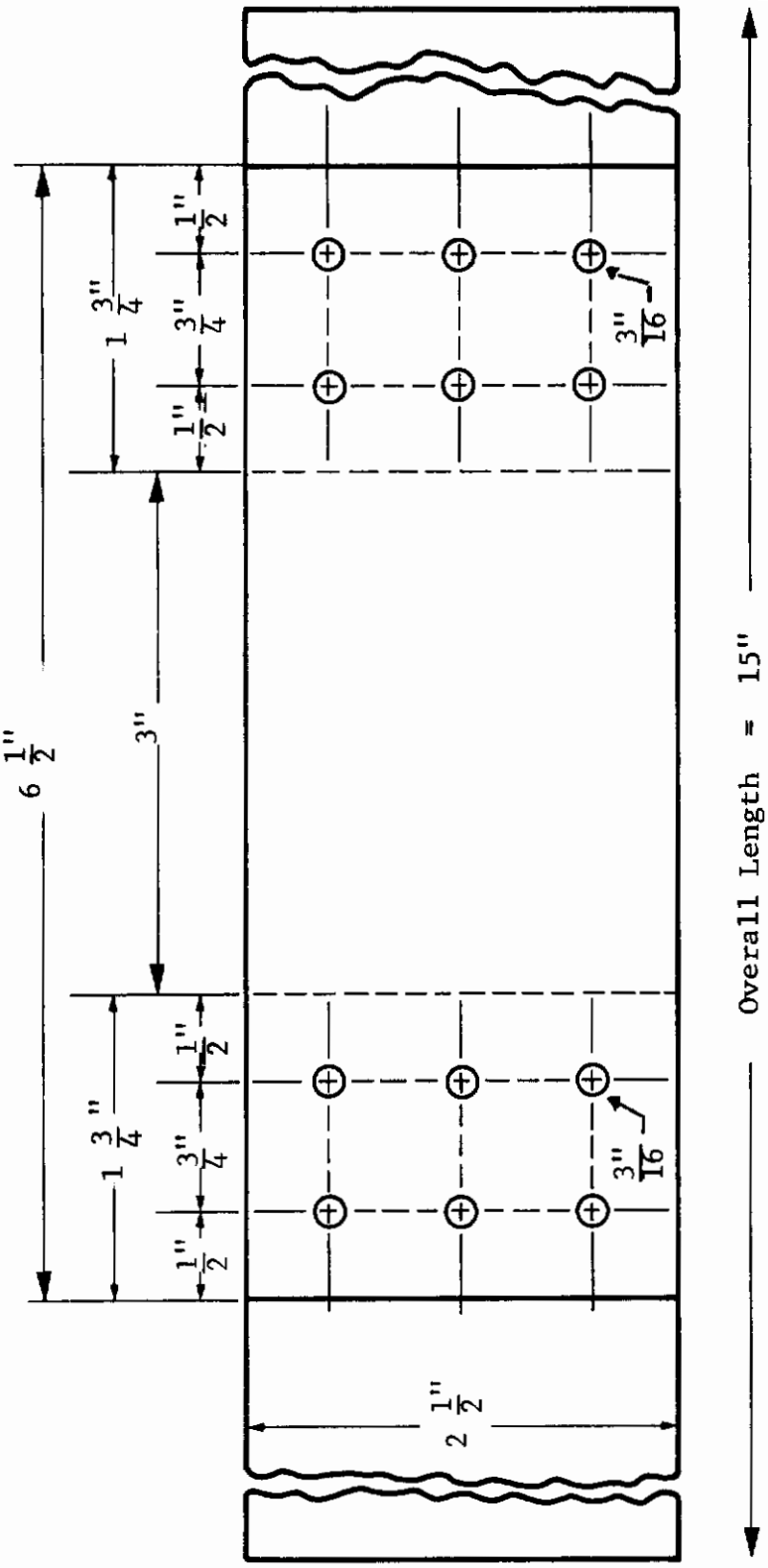

Fig. 7.6 DIMENSIONS OF DOUBLE-ROW TRIPLE-LINE BOLTED JOINT SPECIMEN

Specimen 8-T-2 was fitted with electrical resistance foil gages prior to testing. The gages were located between the rows of bolts and were on both splice plates. Gage locations are shown schematically in Figure 7.7.

The tensile strengths of the joints are shown in Table 7.4, Figure 7.8 illustrates typical specimens before and after testing.

7.3.2 Load-Distribution Among Multiple-Fastener Joints

Specimen 8-T-2 was instrumented as described above and tested incrementally to failure. At each increment of load, the strain was measured by the strain gages at the separate locations on the splice plates (Figure 7 7). The strains were plotted against gross section stress and then averaged over the separate splice plates at each gage location. The averaged stress at each gage location was then determined across the sections of the splice plates between the rows of bolts for four gross section stress levels. The load per unit thickness was plotted across the three sections as shown in Figures 7.9 through 7.11 for the same four gross section stress levels. Figure 7.12 shows schematically the load transfer from main plates to splice plates. A comparison of the actual load, recorded from the testing machine and the integrated load, $F_1 + F_2 + F_3$ gives an indication of the accuracy of the experiment. Table 7.5 summarizes the results.

7.3.3 Comparison with Tate-Rosenfeld Load Distribution

The Tate-Rosenfeld (7.5) equations for load per row of bolts is given by

$$F_{i+i} = \frac{C_i}{C_{i+i}} F_i + \frac{2k_m + k_s}{C_{i+i}} F_i - \frac{2k_m}{C_{i+i}} F_g + \frac{2k_m + k_s}{C_{i+i}} \sum_{1}^{i-1} F_g$$

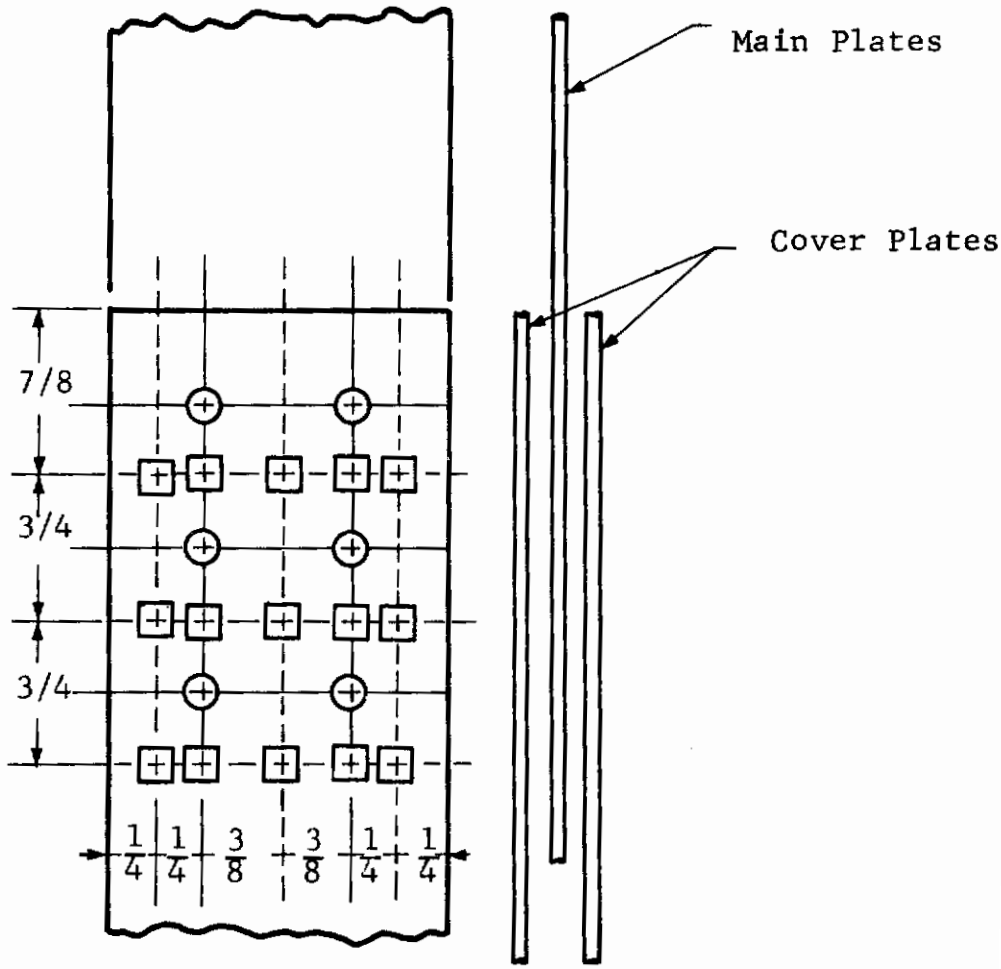

Fig. 7.7 LOCATION OF ELECTRICAL RESISTANCE FOIL STRAIN GAGES ON SPECIMEN 8-T-2

Table 7.4

RESULTS OF MULTIPLE FASTENER STRENGTH TESTS

Specimen Number	Number of Lines	Number of Rows	Number of Bolts	Combined Splice Plate Thickness (in.)	Main Plate Thickness (in.)	Specimen Width (in.)	Failure Load (lb)	Ultimate Stress In Main Plate (ksi)
1-T-1	2	1	2	0.067	0.068	1.738	2450	21.0
2-T-2	2	1	2	0.070	0.068	1.741	2500	20.5
Avg.	2	1	2	--	--	--	--	20.7
3-T-1	2	2	4	0.069	0.069	1.735	5100	42.6
4-T-2	2	2	4	0.066	0.069	1.748	4400	38.1
Avg.	2	2	4	--	--	--	--	40.3
5-T-1	3	2	6	0.078	0.069	2.493	7000	36.0
6-T-2	3	2	6	0.063	0.070	2.498	6800	43.2
Avg.	3	2	6	--	--	--	--	39.6
7-T-1	2	3	6	0.069	0.070	1.746	6600	54.8
8-T-2	2	3	6	0.068	0.069	1.743	6250	52.7
Avg.	2	3	6	--	--	--	--	53.7

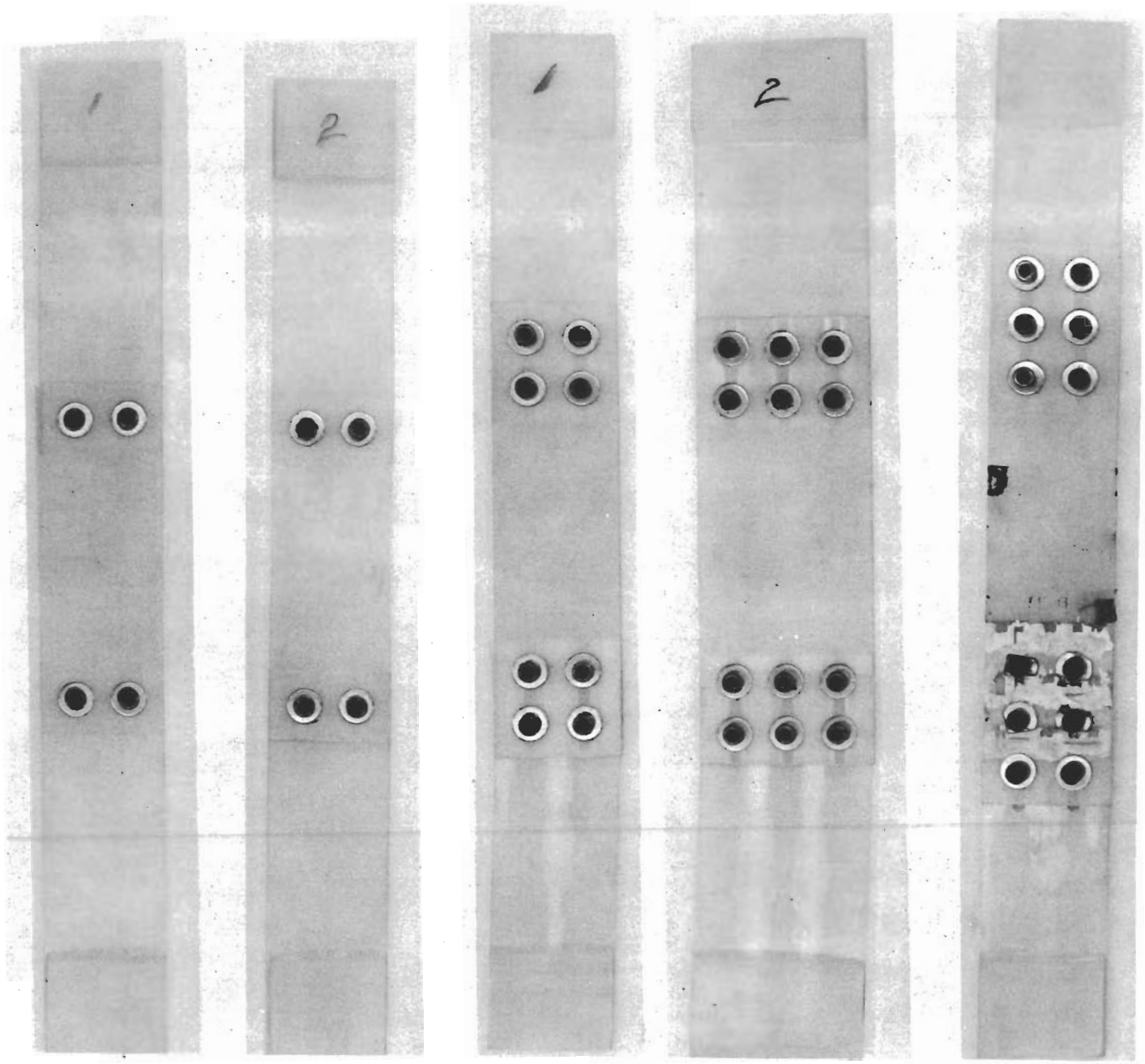

a. 1-T-1 2-T-1 Untested Specimens

b. 3-T-1 After Test

c. 6-T-2 After Test

d. 8-T-2 After Test

Fig. 7.8 TYPICAL MULTI-FASTENER JOINT TEST SPECIMENS

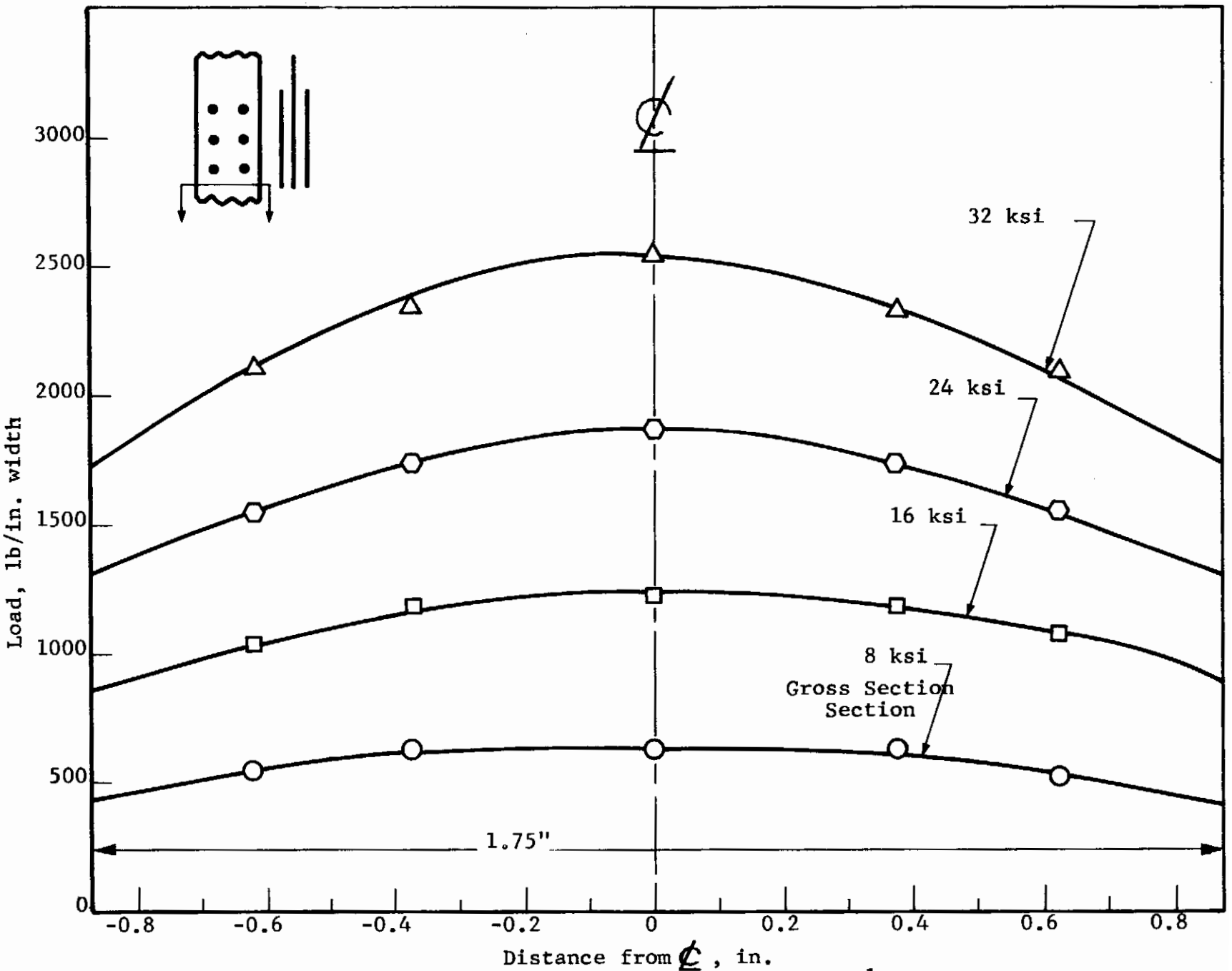

Fig. 7.9 LOAD DISTRIBUTION ACROSS SECTION AA[1] (See Insert)

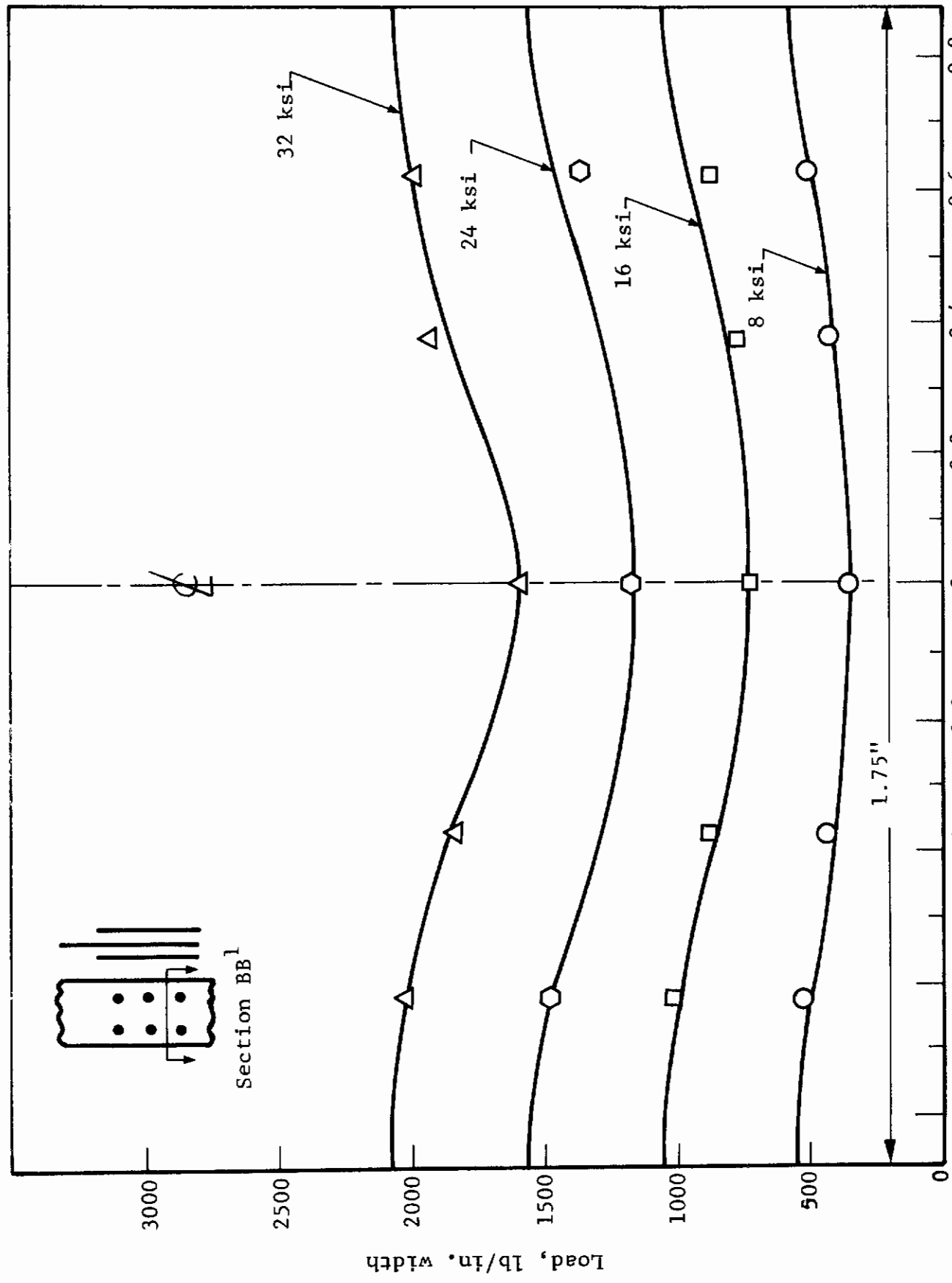

Fig. 7.10 LOAD DISTRIBUTION ACROSS SECTION BB[1] (See Insert)

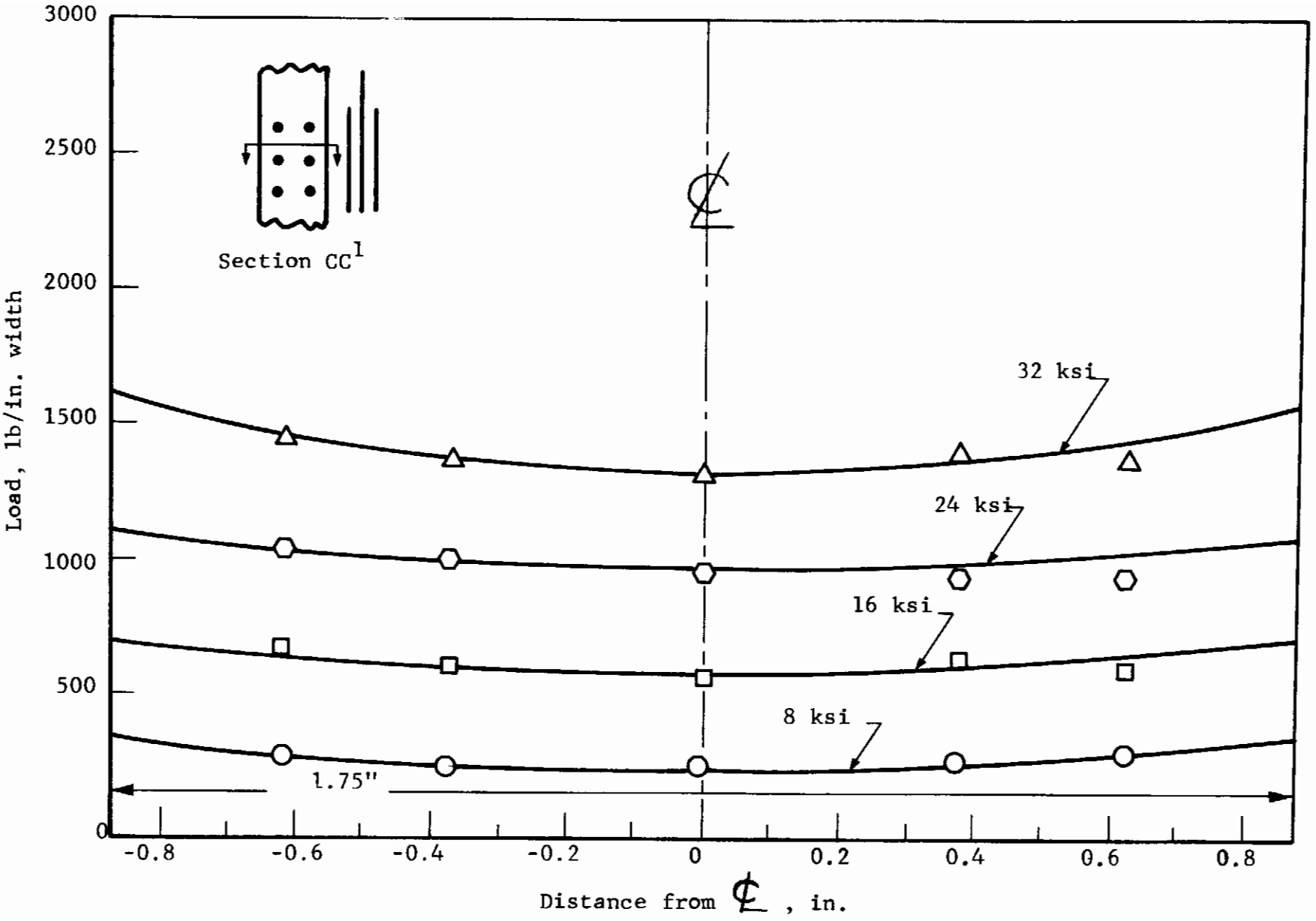

Fig. 7.11 LOAD DISTRIBUTION ACROSS SECTION CC[1] (See Insert)

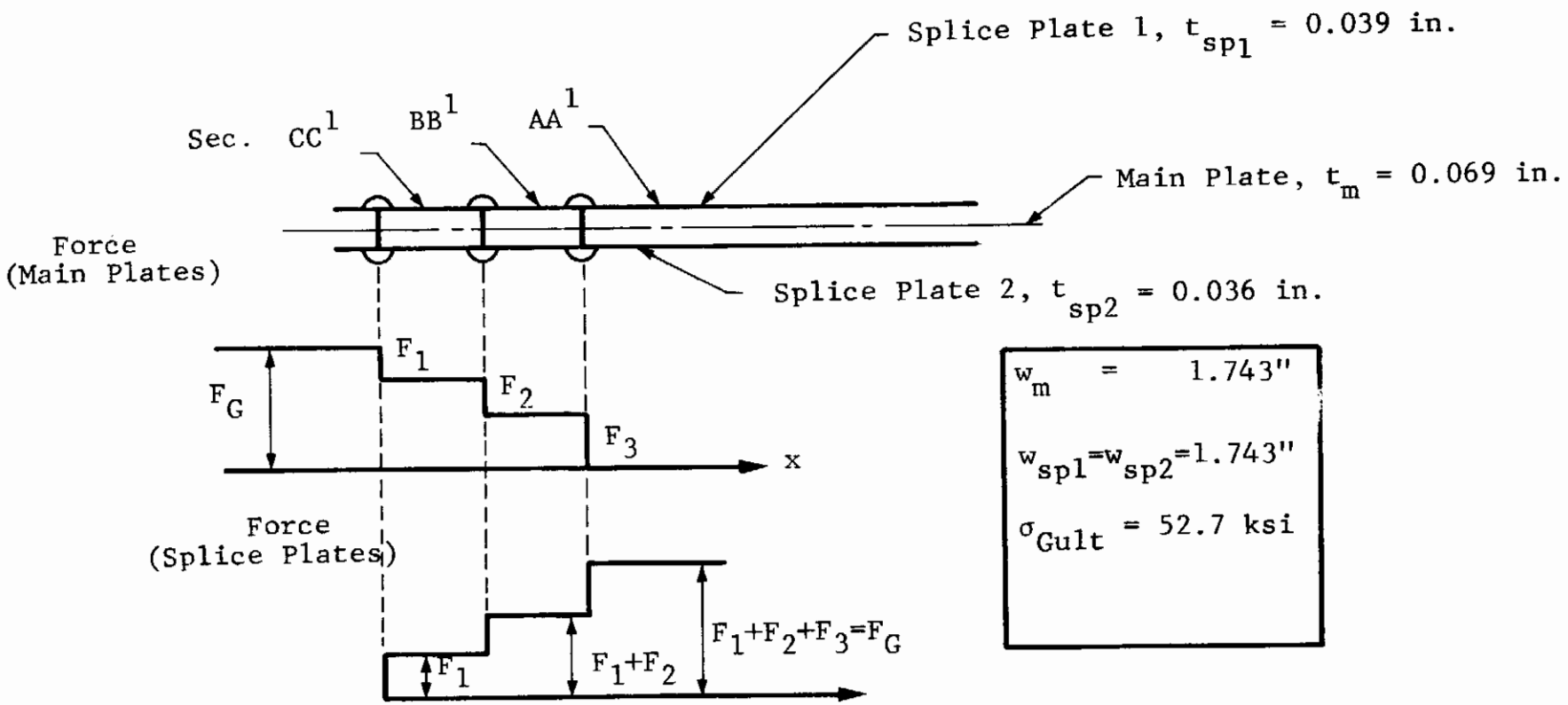

Section AA^1 records double splice plates total load
Section BB^1 records F_1+F_2
Section CC^1 records F_1

Fig. 7.12 LOAD TRANSFER FOR TRIPLE ROW DOUBLE-LINE BOLTED JOINT (SPECIMEN 8-T-2)

Table 7.5

SUMMARY OF LOAD TRANSFER FOR JOINT 8-T-2
AT FOUR GROSS SECTION STRESS LEVELS

Gross Section Stress Level (ksi)	Actual Load (lb)	$F_1 + F_2 + F_3$ (lb)	$F_1 + F_2$ (lb)	F_1 (lb)	F_2 (lb)	F_3 (lb)
8	951	962	788	525	263	174
6	1900	1924	1540	1137	403	384
24	2950	2886	2360	1790	570	526
32	3800	3890	3240	2540	700	650

where

$$k_m = \frac{P}{w_m t_m E_m}$$

$$k_s = \frac{P}{w_s t_s E_s}$$

p = pitch of bolts in a row

For the joint 8-T-2

$$k_m = (0.75)/(1.75)(0.069)(3.5 \times 10^6) = 1.78 \times 10^{-6} \text{ in. per lb.}$$

And therefore the predicted loads become, since all the C_i are equal,

$$F_1 = \frac{-2k_m}{C_{Av}} F_G$$

The first estimate for C_i given by Tate (7.5) was the general expression:

$$C = \frac{2}{t_m E_{bb}} \left[\frac{4}{3\pi} \left[\frac{t_m}{D} \right]^2 \left[k_1 + 5/4 \ (t_m/D)^2 \right] + 2k_2 + k_3 + k_4 \right]$$

An average value of C is obtained by replacing t_m by the expression

$$t_{av} = \frac{t_{s1} + t_{s2} + t_m}{2}$$

Also

$$k_1 = E_{bb}/G_b$$

$$k_2 = E_{bb}/D_{bbr}$$

$$k_3 = E_{bb}/E_{sbr}$$

$$k_4 = E_{bb}/E_{mbr}$$

E_{bb} = bolt bending modulus = 29×10^6 psi

G_b = shear modulus of bolt = 11×10^6 psi

E_{bbr} = bolt shearing modulus = 29×10^6 psi

E_{sbr} = splice plate bearing modulus = 3.5×10^6 psi

E_{mbr} = main plate bearing modulus = 3.5×10^6 psi

therefore

$k_1 = 2.64$

$k_2 = 1.0$

$k_3 = 8.3$

$k_4 = 8.3$

and hence

$$C_{av} = \frac{2}{(0.069)(29 \times 10^6)} \left[\frac{4}{3\pi} \left[\frac{0.069}{0.087} \right]^2 \left[2.64 + \frac{5}{4} \left[\frac{0.069}{0.087} \right]^2 \right] + 2\,(1) + 8.3 + 8.3 \right]$$

$C_{av} = 19.5 \times 10^{-6}$ in./lb.

The general expression is rewritten

$$F_{i+i} = F_i + \frac{2k_m + k_s}{C_{av}} F_i - \frac{2k_p}{C_{av}} F_G + \frac{2k_p + k_s}{C_{av}} \sum_{1}^{i-1} F_j$$

$k_s = 1.76 \times 10^{-6}$ in./lb., $k_m = 1.78 \times 10^{-6}$ in./lb.,

$C_{av} = 19.5 \times 10^{-6}$ in./lb.

$$\frac{2k_m + k_s}{C_{av}} = \frac{3.52 + 1.78}{19.5} \text{ in./lb.} = 0.272 \text{ in./lb.}$$

$$\frac{2k_m}{C_{av}} = 0.181 \text{ in./lb.}$$

Starting with the second bolt successive F_i are determined as follows:

$$F_1 = F_1 = 1.00\ F_1$$

$$F_2 = 1.272\ F_1 - 0.181\ F_G$$

$$F_3 = 1.272\ (F_2) - 0.181\ F_G + 0.272\ F_1$$

$$= 1.272\ (1.272\ F_1 - 0.181\ F_G) - 0.181\ F_G + 0.272\ F_1$$

$$= (1.62 + 0.27)\ F_1 - (0.23 + 0.18)\ F_G$$

$$F_3 = 1.89\ F_1 - 0.41\ F_G$$

From equilibrium we have $F_G = \sum F_i$

and therefore

$$F_G = (1.000 + 1.27 + 1.89)\ F_1 - (0.18 + 0.41)\ F_G$$

$$F_G = 4.16\ F_1 - 0.59\ F_G$$

Hence

$$F_1 = \frac{1.59}{4.16}\ F_G = 0.381\ F_G$$

$$F_2 = 1.485\ F_G - 0\ 181\ F_G = 0.30\ F_G$$

$$F_3 = 0.72\ F_G - 0.41\ F_G = 0.31\ F_G$$

The theory indicates that in the elastic region the first row should take approximately 38 percent of the load, the second row 30 percent and the third row 31 percent of the load. A comparison with the experiment for the lowest load level (presumably elastic) shows that the first row took 55 percent

of the load, the second row took 27.3 percent of the load and the third row only took 18.1 percent of the load.

A comparison was not made with the other theories but the symmetry of the joint would indicate that the Batho (7.1) expressions, the Vogt (7.7) equations, Switsky's (7.4) analysis and others would also give a distribution of load similar to the Rosenfield-Tate (7.5) theory. Since the experiment indicated that a significant difference exists between analysis and experiment and that the first row assumed such a large proportion of the load, further sophistication in the analyses will be required.

References (Section 7.0)

7.1 Batho, C., "The Partition of Load in Riveted Joints", J. Franklin Institute, Vol. 182, Nov. 1916, pp. 553-604.

7.2 Bickley, W. G., "The Distribution of Stress Around a Circular Hole in a Plate", Phil. Trans. Roy. Soc. (Lond.), Vol. 227@, 1928, pp. 383-415.

7.3 Ruffalo, A., "How to Evaluate and Select Mechanical Fasteners", Materials in Design Engineering, Feb. 1963, pp. 95-100.

7.4 Switsky, H., Forray, M. J., and Newman, M., "Thermostructural Analysis Manual", WADD TR-60-517, August 1962.

7.5 Tate, M. B., and Rosenfeld, S. J., "Preliminary Investigation of the Loads Carried by Individual Bolts in Bolted Joints", NACA TN 1051, May 1946.

7.6 Theocaris, P. S., "The Stress Distribution in a Strip Loaded in Tension by Means of a Central Pin", ASME J. Appl. Mech., paper No. 55-A-34.

7.7 Vogt, F., "The Load Distribution in Bolted or Riveted Joints in Light Alloy Structures", NACA TM 1135, April 1947.

8.0 CONCLUSIONS AND RECOMMENDATIONS FOR FURTHER STUDY

8.1 ADHESIVE BONDED JOINTS

8.1.2 Conclusions

The major conclusion in the area of bonded composite joints is that the feasibility of using a rational engineering procedure remains to be demonstrated. The available stress analyses for these joints are inadequate and there still remains a lack of materials property data for the composites as well as for the adhesives. At present, the best design method available is to treat each specific joint as an individual structure, use average shear strength data for the particular adherends involved, build a part and test it. This technique will gradually improve as the general analysis of composites continues to develop and design procedures for the composite adherends improve. Bonded joint design will be a logical extension of this work.

Specific results leading to this overall general conclusion are as follows:

1. From the comparison of results of the stress analyses, the Volkersen, Goland and Reissner, and numerical shear lag methods all predict higher stresses than those obtained from the finite element analysis. The finite element analysis is assumed to predict the most reasonable elastic stresses and these stresses are lower by a factor of at least one half than the other analytical results. This follows the same trend observed by AVCO (2.2) in comparing their finite element analysis to Volkersen.

2. The comparison of analysis and experimental results for joints strength showed that the analytical predictions were conservative in predicting strength. The analyses predicted higher stress concentration factors than those observed experimentally.

3. Static joint strength and fatigue strength were a strong function of adhesive modulus. The lower modulus, more plastic adhesive, gave higher strengths than the stiff brittle material. The lower modulus adhesive developed a higher percentage of composite failure than the brittle stiff adhesive.

4. In the thinnest joints, it was possible to develop full composite strength with almost all composite failure. In the thicker adherends load transfer occurred only through the first three to four lamina next to the bonded area. At this point composite shear failure occurred, usually in a cross ply lamina. This means the joints were shear critical in the composite not in the adhesive.

5. Static joint strength was graphed as a function of the joint parameter (L/t). For each adherend thickness (t), a separate curve was obtained which is contrary to the predictions of the Volkersen and Goland and Reissner analyses.

6. The work on determination of mechanical properties demonstrated that adhesives could be characterized from free film tests and it also provided a measure of the variability in these properties. These results must be taken into account when examining data from torsion-shear tests which involve a much smaller sample of material.

7. Joint strengths obtained for composite to metal bonds were as strong as those for composite to composite joints. In the composite to metal joints, the strength decreased as relative stiffness between the two adherends increased.

8. Scarfing the bonded area did not significantly increase joint strength in composite to composite bonds.

9. The assumption of joint failure occurring only in the adhesive was inadequate for joints analysis. This assumption is basic to most bonded joint analysis. In a composite joint, shear strength of the adhesive is close to that of the

composite; therefore, the joint behaves more as a monolithic structure of a single anisotropic material, than in a metal joint where the adhesive is a true subunit of the structure with markedly different properties.

8.1.3 Recommendations

The following studies are suggested as logical extensions for further work in joint mechanics:

1. More mechanical property data is required for common structural adhesives. This should include quasi-static and time dependent properties and a specific comparison should be made of results obtained from free film and in joint properties.

2. Shear modulus should be obtained and compared by torsion of a bonded circular cylinder, torsion of a circular cylinder of bulk material, from calculation of a tensile modulus and Poisson's ratio from a free film tensile test, and torsion of a bulk plate in saddle shear.

3. Further work in analysis of joints must study the whole joint as a total structure. The state of stress in the adhesive and adherend must be combined with failure criteria for both materials in order to predict joint behavior. This will require that a failure criteria for the composite must be available.

4. An experimental study should be made of the residual stresses in the adhesive and how these stresses relax with time.

5. The specific load distribution should be measured through the thickness of the adherend and along its bonded length. Experimentally, this would be less difficult than instrumenting the adhesive and from this data the actual strain distribution in the adhesive could be obtained.

6. Joints analysis should be extended to include general non-linear material behavior with further inclusion of time dependent material properties. Again this can only be successfull if these data are available for the materials in question.

8.2 MECHANICALLY FASTENED JOINTS

8.2.1 Conclusions

The major conclusion for mechanical joints is similar to that as for bonded structures. At present, the detailed understanding of how the load is distributed to several fasteners in isotropic, homogeneous materials needs further development, and as a result, the most effective way to rationally deal with bolted joints is to employ semi-empirical methods in their design. The problem lies in making the transition from an isotropic, homogeneous material to a composite material. The problem is not that the stress analysis is more complicated at the semi-empirical level, but it is because the failure mode is so different for composites that a complete stress analysis and failure envelope (in four dimensions) will be required to even develop the semi-empirical method for a given class of joints. The failure modes for composite bolted joints may be tensile, compressive, shear, buckling or mixed in any combination at the optimum joint efficiency.

8.2.2 Recommendations

The following suggestions for further work are made for bolted joints:

1. Analysis for out-of-plane single pin stresses should be developed so that the effect of the third dimension, thickness which plays an important role in load distribution per fastener can be ascertained for composites.

2. Buckling as a failure mode directly under the fastener should be investigated. A coupled post buckling eccentric analysis, based on this and item one, would then yield a new failure criterion for bolted joints which do not now use buckling as a possible means of bolted joint failure.

3. Other tests which determine the Vogt coefficients, the Koegler and Schmitt factors for effective hole width, the Budiansky inelastic influence coefficients, the Rosenfeld and Tate coefficients, etc., are necessary. With these empirically determined constants available, for a variety of composite materials, a more sophisticated analysis will be possible.

4. Wider joints of larger than actual size should be prepared and a detailed stress analysis mapped over the plane of the joint should be undertaken. This analysis should employ photostress as the experimental technique due to the fact that whole-field stress-determinations are of interest in determining the load distribution to each fastener.

5. The gross deformation of the joint versus load should be obtained for two or three classes of joints and a wide variety of matrix material-fiber material-fiber orientation combinations.

6. Finally, the most glaring deficiency in trying to apply the rational stress analysis methods to composite material bolted joints is that failure envelopes for any matrix-fiber combination do not exist for various orientations of the fibers even when the relative orientation percentages are known. Therefore, the point in the stress field where the stresses fall outside the envelope are unknown and hence the failure stresses, yield stresses, etc., cannot be predicted.

DISTRIBUTION LIST

MAA (2 cys)
MAT
MAN
MAY
MAM
MAC
MAX
AVTM
APFT
API (3 cys)
APT
FDFM
FDTS

Air University Library
Maxwell AFB Ala 36112

AFRPL (RPRPT)
Edwards AFB Calif 93523

HQ USAF (AFCSAI)
Washington, D. C. 20330

MAAM (Library)
ASNPD30 (1 cy)
ASBED-50 (1 cy)
ASBO
ASNF
ASNP
MAAE
FOTC
ASNFL
ASNFS
ASNNYQ
ASNNXL

USAF (AFXSAI)
Air Battle Analysis Center
Deputy Director of Plans for War
Directorate of Plans, DC5/P&O
Washington, D. C. 20330

Dept of the Navy
Naval Air Systems Command
Attn: Max Stander (RRMA-32)
21st & Const Ave, N.W.
Washington, D. C. 20025

Dept of the Navy
Naval Ships Systems Command
Attn: Code P 346
Washington, D. C. 20025

Dept of the Navy
Office of Naval Research
Attn: J. M. Crowley
Structural Mechanics Br
Washington, D. C. 20025

Dept of the Navy
Naval Air Engineering Center
Attn: T. Manno (ASL)
Philadelphia, Pa. 19112

David Taylor Model Basin
U.S. Navy, Code 761
Attn: P. Posniak
Washington, D. C. 20007

Navy Department
Chief of Naval Operations
Washington, D. C. 20350

Navy Department
Chief of Naval Research
Code (ONR-740)
Washington, D. C. 20360

Navy Department
Chief of Naval Material
Code NSP43
Washington, D. C. 20360

Commander
Naval Air Systems Command
HQS (AIR-604)
Washington, D. C. 20360

Commander
Naval Air Systems Command
HQS (AIR-320)
Washington, D. C. 20360

Commander (2cys)
Naval Air Systems Command
HQS (AIR-5203/AIR-52032E-Sid Weiss)
Washington, D. C. 20360

Commander
Naval Ship Systems Command
HQS (Code 2052)
Washington, D. C. 20360

Commanding Officer
Naval Air Development Center
(Aero Materials Dept)
Johnsville
Warminster, Pa. 18974

Commanding Officer
Naval Air Development Center
(Aero Structures Dept)
Johnsville
Warminster, Pa. 18974

Director
Naval Research Lab
(Code 2020)
Washington, D. C. 20390

Commander
Naval Ordance Lab
Silver Spring, Md. 20910

Commander
Naval Weapons Lab
Dahlgren, Va. 22448

Commanding Officer & Director
Naval Applied Science Lab
Flushing & Washington Aves
Brooklyn, New York 11251

Naval Plant Representative
Naval Plant Rep Office
Applied Physics Lab
John Hopkins University
8621 Georgia Ave
Silver Spring, Md. 20910

AEDC (Dr. H.K. Doetsch)
Arnold AFS Tenn. 37389

AF Special Weapons Center
Attn: SWOI
Kirtland AFB, NM 87117

APGC (PGTRI/Tech Library)
Eglin AFB, Fla. 32542

ASD (ASLSS)
WPAFB O 45433

Army Rocket & Guided Missile Agency
Attn: Tech Library
Redstone Arsenal, Ala. 36000

Dept of the Army
Ordnance Corps
Springfield Arsenal
Attn: R&D Div.
Springfield, Mass. 01100

Dept of the Army
Office, Chief of Ordnance (ORDTB)
Washington, D. C. 20025

Dept of the Army
Office of Quartermaster General
Attn: R&D Branch
Military Planning Div.
Washington, D. C. 20025

AFLC Maintenance Technology Office (2 cys)
Chemical Engineering Div.
Attn: OCRC/Mr. H. Karimi/R.H. Jungers
Tinker AFB, Okla. 73145

Apollo Spacecraft Program Office
Officer Symbol "PE"
Manned Spacecraft Center
Houston, Texas 77000

U.S. Army Missile Command
Army Propulsion Lab & Center (REDD)
AMSMI-RKB, Bldg. 7120
Attn: W.S. Crownover
Redstone Arsenal, Ala 35809

DDC (20 cys)
Cameron Station
Alexandria, Va. 22314

Adhesives Engineering Co.
Div of Heller Helicopter Corp
Attn: Dr. D.W. Elam
1411 Industrial Rd
San Carlos, Calif. 94070

Aerojet General Corp
Electronics Div
Structural Materials Gp
Attn: Mr. I. Petker
Azusa, California 91702

Aerojet General Corp
Attn: Mr. A. V. Levy
Sacramento, Calif. 95809

Aeronca Mfg Co
Attn: Harry Pratt
1712 Germantown Rd
Middletown, Ohio 45042

Aeronutronic Division
Philco Ford
Applied Mechanics Staff
Attn: Mr. A.V. Gentile
Ford Rd.
Newport Beach, Calif. 92600

Aerospace Corp
Materials Lab
2400 E. El Segundo Blvd
El Segundo, Calif. 90245

Aerospace Corp
San Bernardino Ops
Attn: Dr. L. Rubin
1111 East Mill St.
San Bernardino, Calif 92408

Aerospace Corp
Div. of Gen. Dynamics Corp
International Airport
Los Angeles, Calif 90000

Aerospace Industrial Assoc.
Attn: J.P. Reese, Tech Services
1725 DeSales St. NW, Ste 600
Washington, D. C. 20036

Aerospace Industries Assoc of Am Inc
Attn: Tech Library
610 Shoreham Bldg.
Washington, D. C. 20005

Allison Div.
General Motors Corp
Attn: Tech Library
Indianapolis, Ind. 46200

American Brake Shoe Co
Research Center
Attn: W. F. Smith
Mahwah, New Jersey 07430

American Cyanamid Co (2 cys)
Bloomingdale Dept
Plastics & Resins Div
Attn: R. B. Krieger Jr/Dr. H.C. Engel
Havre DeGrace, Md. 21078

Avco Corporation
Attn: H. E. Beatty
Aerostructures Div.
Dept 520, Bush Rd
P. O. Box 210
Nashville, Tenn. 37202

Avco Corporation
Research & Development Div
Wilmington, Mass 01887

Avco Corporation (2 cys)
Attn: R. Timmons/Dr. E.M. Lenoe
Lowell Industrial Park
Wilmington, Mass 01851

Avco Research & Development
Attn: Tech Library
Wilmington, Mass. 01851

The Babcock & Wilcox Co
Research & Dev Div
Research Center
1562 Beeson St.
Alliance, Ohio 44601

Beech Aircraft Corp
Attn: C. A. Rembleske
Wichita, Kansas 67201

Bendix Corporation (2 cys)
Aerospace Div
Attn: R. V. Cervelli/A. Courtney
South Bend, Ind. 46620

Bendix Aviation Corp
Pacific Div
Attn: J. A. Merrill
11700 Sherman Way
North Hollywood, Calif. 91605

The Boeing Company
SST Division
Attn: G. F. Harbord
D-9-3200/MS 49-02
P. O. Box 3733
Seattle, Wash. 98124

The Boeing Company (4 cys)
Aerospace Div
Attn: E. C. Bovee/M. Kushner
G. E. Hughes/W. Symonds
P. O. Box 3707
Seattle, Washington 98124

The Boeing Company
New Products Dept
Attn: H. E. Hightchew
Box 707
Mail Stop 59-89
Renton, Washington 98055

The Boeing Company
Attn: R. J. Hilton
Box 77-44
Renton, Washington 98055

The Boeing Company (2 cys)
Attn: C. Johnson/Al Paxhia
Wichita, Kansas 67210

The Boeing Company
Vertol Div
Attn: R. Pinckney
1000 Woodlawn Ave
Morton, Pa. 19070

Bostrom-Amalga Corp
Attn: J. L. McLarty
W137 N5500 Williams Pl
Menomonee Falls, Wisc 53051

Brunswick Corp
Defense Products
Attn: R. Copeland
Marion, Va. 24354

California Institute of Technology
Jet Propulsion Lab
Attn: Mr. H. Martina
4800 Oak Grove Dr.
Pasadena, Calif. 91103

Case Institute of Technology
Attn: Prof. L. A. Schmit
University Circle
Cleveland, Ohio 44106

Chance Vought Aircraft Co
Attn: Tech Library
P. O. Box 5907
Dallas, Texas 75222

Chance Vought Aircraft Co.
Vought Astronautics Div
Attn: B. Forcht
P. O. Box 5987
Dallas, Texas 75222

Convair
Div/General Dynamics Corp
Mail Zone 6-181
P. O. Box 1950
San Diego, Calif 92112

Convair
Div of General Dynamics Corp
Attn: Tech Library
Ft Worth, Texas 76101

Curtiss Wright Corp
Curtiss Div
Attn: H. Robbins
Caldwell, New Jersey 07006

Chrysler Corp
Missile Div
Attn: H. W. Haugen
16 Mile Rd at Van Dyke
Detroit, Mich. 48200

Ferro Corporation
Attn: R. W. Pelz
4150 East 56th St
Cleveland, Ohio 44105

Federal Aviation Agency
Engr & Mfg Div, FS-120
Attn: B. Grochal
Washington, D. C. 20025

General American Trans Corp
Plastics Div
Compton, Calif 90224

General American Trans Corp
Attn: G. Engholm
7501 N. Natchez Ave.
Niles, Illinois 60648

General Electric Co
Aerosciences Lab
Attn: I. J. Grunfest
D Street
Philadelphia, Pa 19104

General Electric Company
Attn: Tech Library
Evendale, Ohio 45200

General Electric Co
Attn: Tech Library
1 Plastics Avenue
Pittsfield, Mass. 01201

General Electric Co
Attn: Tech Library
Waterford, New York 12188

General Electric Co
Attn: H. A. Galpern
Materials & Processes Lab
1100 Western Ave
West Lynn, Mass 01905

General Electric Co
Advanced Design Engrg
Attn: R. S. Shane
901 Broad Street
Utica, New York 13501

General Electric Co.
Materials & Processes Lab
Large Steam Turbine-Generator Dept
Attn: A. F. Zavist
Bldg 55, Rm 119
Schenectady, New York 12305

General Electric Co
Valley Forge Sta. Rm M 2112
M&P Technologies
Attn: Dr. A. A. Watts
P. O. Box 8555
Philadelphia, Pa 19101

General Electric Co.
Advanced Engine & Tech Dept
Attn: Mr. C. Conliffe
Evendale, Ohio 45215

General Electric Co
Attn: V. N. Saffire
P. O. Box 8555
Philadelphia, Pa. 19101

General Electric Company (3 cys)
Space Sciences Lab
Attn: Dr. Wendl/L. McCreight/
J. V. Mullin
P. O. Box 8555
Philadelphia, Pa 19101

General Electric Co/Missile &
Space Div.
Re-entry Systems Dept
Attn: Wm Postelnek
Valley Forge Space Tech Center
P. O. Box 8555
Philadelphia, Pa. 19101

General Dynamics
Attn: C. W. Rogers
Mail Zone C-68, P. O. Box 74B
Ft. Worth, Texas 76101

General Dynamics/Convair
P. O. Box 1128
Attn: R. T. Sullins
San Diego, Calif 92112

General Dynamics
Attn: P. R. deTonnancour
P. O. Box 748, E87
Ft. Worth, Texas 76101

General Dynamics-Astronautics
Materials Research Group
Attn: T. T. Tanalski
Mail Zone 592-10
P. O. Box 166
San Diego, Calif 92112

General Dynamics-Pomona
Attn: H. A. Swift
Chief of Structures & Matls
Mail Zone 6-56
Pomona, Calif 91769

General Motors Corp
General Motors Tech Center
Attn: E. B. Jackson/Librarian
Research Labs
12 Mile & Mound Rds
Warren, Michigan 48000

General Motors Res Labs
Met Engrg Dept
12 Mile & Mound Rds
Warren, Michigan 48000

General Motors Corp
Allison Div
Attn: Plastics Engrg
Indianapolis, Ind. 46200

Goodyear Aerospace Co. (2 cys)
Attn: L. Toth/B. F. Martin
1210 Massillon Rd
Akron, Ohio 44315

Goodyear Aerospace Corp (3cys)
Attn: R. Burckley/C. A. Haudenchild/
B. D. Raffel
Akron, Ohio 44315

Goodyear Aircraft Co
Arizona Div
Attn: G. Wintermute
Plastics Engrg
Dept 452A
Litchfield Park, Arizona 85340

Grumman Aircraft Corp (2 cys)
Attn: W. B. Atcheson/F. J. Turek
Bethpage, L. I., New York 11714

Grumman Aircraft Engrg Corp (2cys)
Attn: G. Lubin/A. August
Bethpage, L. I., New York 11714

B. F. Goodrich Co (2 cys)
Aerospace & Defense Products Div
Attn: E. M. Tatarzycki/
H. W. Stevenson
500 S. Main Street
Akron, Ohio 44318

Hamilton Standard
Attn: E. T. Trace
Rm 625, Hulman Bldg
Dayton, Ohio

Hayes International Corp
Attn: B. A. Reymann
P. O. Box 1568
Huntsville, Ala 35800

Hercules Powder Co (2 cys)
Attn: R. E. Randolph/J. A. Kerns
P. O. Box 210
Cumberland, Md. 21502

Hercules Powder Co.
Attn: J. T. Paul
Research Center
Wilmington, Deleware 19899

Hexcel Products Inc. (2 cys)
Attn: A. C. Marshall/R.C. Steele
2332 Fourth St.
Berkeley, Calif. 94710

Honeycomb Co of America Inc
Attn: J. Hutchins
1225 Connecticut Ave
Bridgeport, Conn 06600

Hughes Aircraft Co. (3 cys)
Attn: Dr. Colner/L. B. Keller/
N. I. Hall
Culver City, Calif 90230

Hughes Tool Co.
Aircraft Div
Attn: H. Ney
Culver City, Calif 90230

I.I.T. Resrarch Institute
Attn: Dr. Cornish
10 West 35th Street
Chicago, Ill. 60616

International Harvester Co
Solar Div
Attn: J. V. Long
San Diego, Calif 92112

Johns-Manville Co.
Plastics Development
Attn: J. Parkinson
Manville, New Jersey 08835

Kaman Aircraft Corp
Attn: Tech Library
Bloomfield, Conn 06002

Lamtex Industries
Attn: O. Marcus/W. E. Poneman
Motor Avenue
Farmingdale, New York 11735

Lawrence Radiation Lab (2cys)
Attn: B. L. Garner/P. G. Fleming
Livermore, Calif 94550

Lockheed Aircraft Corp
Attn: Plastics Dept
2555 N. Hollywood Way
Burbank, Calif 91502

Lockheed Aircraft Corp
Attn: Structures Dept
7701 Woodley Ave
Van Nuys, Calif 91406

Lockheed Aircraft Corp
Calif Div
Attn: Librarian
Burbank, Calif 91500

Lockheed Aircraft Corp
Missiles & Space Div
Tech Info Center
3251 Hanover St
Palo Alto, Calif 94304

Lockheed-Georgia Corp (3 cys)
Attn: H. P. Gilpin/M. L. McIntyre/A. C. Fehrle
Marietta, Ga 30060

Lockheed Aircraft Corp
Attn: W. J. Critchlow
Dept 74-44, Bldg 170
Plant B-1
Burbank, Calif 91503

Lockheed Missile & Space Div
Attn: J. E. Gaughan
Dept 83-31, Box 504
Sunnyvale, Calif 94086

Lockheed Missile & Space Co
Materials Sciences Lab
Attn: J. B. Rittenhouse
Dept 52-30, Bldg 201
3251 Hanover St.
Palo Alto, Calif 94304

Lockheed Missiles & Space Co.
Attn: L. R. Lunsofrd
1111 Lockheed Way
Sunnyvale, Calif 94016

Lockheed Missiles & Space Co.
Palo Alto Research Labs
Attn: D. O. Hoffman
Palo Alto, Calif 94301

Long Sault Woodcraft Limited
Attn: G. Escher
St. Andrews East, Quebec, Canada

Lord Mfg Co
1635 West 12th St
Erie, Pa. 16511

LTV
Attn: K. R. Marsh
P. O. Box 5907
Dallas, Texas 75222

LTV
Aeronautics & Missiles Div
Attn: J. E. Martin
P. O. Box 5907
Dallas, Texas 75222

LTV
Vought Astronautics Div
Attn: B. Forcht
P. O. Box 5897
Dallas, Texas 75222

Lunn Laminated Inc
Attn: H. T. Douglas
Huntington Station, New York
11746

Lycoming Div
Avco Corp
Stratford, Conn 06497

Martin Co (2 cys)
Attn: G. Holback/Dr. I. Pincus
Baltimore, Md 21203

Martin Company
Attn: Tech Library
Box 179, No. L-8
Denver, Colorado 80201

Martin Marietta Corp
Attn: Tech Library
Orlando, Florida 32800

Martin Marietta Corp
Attn: Mr. N. Chessin
Advanced Materials R&D
MP-105
Orlando, Fla 32805

Martin Marietta Corp
Attn: N. Miller
Baltimore, Md 21503

Martin Company
Attn: E. R. Jones
Orlando, Fla 32805

Massachusetts Institute
of Technology
Dept of Civil Engrg
Attn: Prof. F. J. McGarry
Cambridge, Mass 02139

McDonnell Douglas Corp
Douglas Aircraft Co
Product Development
Attn: H. E. Felix, Dir.
2000 N. Memorial Dr.
Tulsa, Oklahoma 74115

McDonnell Douglas Corp
Douglas Aircraft Co.
Attn: Tech Library
El Segundo, Calif 90245

McDonnell Douglas Corp
Douglas Aircraft Co
Attn: Tech Library
3000 Ocean Park Blvd
Santa Monica, Calif 90405

McDonnell Douglas Corp
Douglas Aircraft Co.
Attn: Dr. S. Yurenka/E.P. Troeger
300 Ocean Park Blvd.
Santa Monica, Calif. 90405

McDonnell Douglas Corp.
Douglas Aircraft Co.
Missiles & Space Systems Div
Attn: L.B. Greszczuk/D.E.Harbaugh
3000 Ocean Park Blvd
Santa Monica, Calif 90406

McDonnell Douglas Corp
Douglas Aircraft Co.
Attn: H. Schgelderup/C-251
3855 Lakewood Blvd
Long Beach, Calif 90803

McDonnell Aircraft Corp
Attn: Mr. E.G. Szabo
Municipal Airport - Box 516
St. Louis, Mo. 63103

McDonnell Aircraft Corp
Attn: Tech Library
P.O. Box 516
St. Louis, Mo. 63166

Minneapolis-Honeywell Reg Co
Materials Engrg
Attn: K.C. Cummings
2600 Ridgway Rd
Minneapolis, Minn 55440

Minnesota Mining & Mfg
Attn: J. N. Schurb
1210 University Ave.
St. Paul, Minn. 55106

Minnesota Mining & Mfg Co.
Attn: J. W. Davis
1210 University Ave
St. Paul, Minn. 55106

Minnesota Mining & Mfg Co
Attn: R. H. Lamb
49 Park Ave.
Dayton, Ohio 45419

Monsanto Co.
Attn: J. M. Trice
800 N. Lindberg
St. Louis, Mo. 63100

Narmco R&D
Div of Whittaker Corp
Attn: B. Levinetz
3540 Aero Court
San Diego, Calif 92123

National Aeronautical Establishment
National Research Council
Structures & Materials Lab
Attn: Mr. Paul McLean
Ottawa, Canada

NASA
Lewis Research Center
Attn: D. Morris/Librarian
21000 Brookpark Rd
Cleveland, Ohio 44135

NASA
Flight Research Center
Attn: J. Jones/Librarian
P. O. Box 273
Edwards, Calif 93523

NASA
Lewis Research Center
Attn: M. Hansen/Mail 49-1
21000 Brookpark Rd
Cleveland, Ohio 44135

North American Rockwell
Rocketdyne Div
D 596-109 Z4
Attn: T. Moyer
6633 Canoga Ave
Canoga Park, Calif 91303

North American Rockwell Corp
Structural and Ablative Plastics
Attn: C.I. Yates, Dept 939
2000 North Memorial Drive
Tulsa, Oklahoma 74151

North American Rockwell
Attn: E. Dickerson
International Airport
Los Angeles, Calif 90009

North American Rockwell (3 cys)
Attn: L. Hackman/G. Clark/
Dr. R. Foye
4300 E. Fifth Avenue
Columbus, Ohio 43216

North American Rockwell (2 cys)
Attn: Dr. L. A. Harris/
R. W. Spencer
12214 Lakewood Blvd.
Downey, Calif 90241

North American Rockwell
Attn: LAD Library, Dept. 262
International Airport
Los Angeles, Calif 90009

Northrop Aircraft Corp
Norair Div
Attn: R. D. Hayes
3901 W. Broadway
Hawthorne, Calif 90250

Northrop Aircraft Corp
Norair Div
Attn: Tech Library
Hawthorne, Calif 90250

Owens-Corning Fiberglas
Aerospace Div
Attn: D. Mettes
Granville, Ohio 43023

Owens-Corning Fiberglas
Attn: R. J. Weaver
900 17th St, Suite 508
Washington, D. C. 20006

Parsons Corporation
Aircraft Div
Attn: J. O'Hara
Traverse City, Mich. 49684

Prewitt Aircraft Co.
Attn: R. H. Prewitt
410 South Springfield Rd.
Clifton Heights, Pa. 19018

Picatinny Arsenal (2 cys)
Attn: G. R. Rugger/J. Scavuzzo
Dover, New Jersey 07801

Republic Aviation
Fairchild Hiller Div
Attn: H. Gaebe
Haggerstown, Md. 21740

Rocketdyne
Div of NAR
Attn: Tech Library
6633 Canoga Ave
Canoga Park, Calif 91303

Rocketdyne
Attn: R. R. Moran
Solid Rocket Div
6633 Canoga Ave
Canoga Park, Calif. 91303

Mr. E. K. Rishel
Plastic Consultant
382 Fairfax Rd
Drexel Hill, Pa. 19026

Rocketdyne (2 cys)
Div of NAR
Attn: E. L. Hawkinson/
W. Greenway
6633 Canoga Ave.
Canoga Park, Calif 91303

Rohr Aircraft Co.
Attn: Librarian
Chula Vista, Calif. 92012

Rohr Aircraft Co.
Attn: Mr. J. Schell
Riverside, Calif.

Rubber & Asbestos Corp
225 Bellville Ave
Bloomfield, New Jersey 07003

Ryan Aeronautical Co.
Lindberg Field
Attn: Mr. N. Brink
San Diego, Calif. 92112

Sikorsky Aircraft
Engrg Dept.
Attn: G. A. Dmitroff
Main Street
Stratford, Conn. 06497

Sikorsky Aircraft (2 cys)
Div of United Aircraft Corp.
Attn: R. M. Kee/T. D. Johnson
Bridgeport, Conn. 06600

Solar Aircraft Co.
Attn: John V. Long
San Diego Plant
San Diego, Calif 92112

Southern Research Institute
2000 Ninth Avenue South
Birmingham, Ala. 36605

Southwest Research Institute
Attn: G. Grimes
8500 Culebra Rd
San Antonio, Texas 78208

A. O. Smith
Research Div
Milwaukee, Wisc. 53200

Space Technology Lab Inc.
Attn: W. W. Wood
P. O. Box 95001 Airport Station
Los Angeles, Calif 90045

Sandia Corp
Sandia Base
Attn: Tech Library
Albuquerque, New Mexico 87115

Shell Chemical Co.
Attn: Adhesives/Resins Dept
1120 Commerce Ave.
Union, New Jersey 07083

Texas A&M College
Aerospace Engrg Dept
Attn: Prof. C.A. Rodenberger
College Station, Texas 77843

Thiokol Chemical Corp
Wasatch Div
Attn: C. Vogt
Brigham City, Utah 84302

TRW Inc
Attn: J. N. McCarthy
23555 Euclid Ave.
Cleveland, Ohio 44117

Union Carbide Corp.
Carbon Products Div.
Parma Tech Center
Tech Info Service
Attn: Dr. T. L. Weng
P. O. Box 6116
Cleveland, Ohio 44101

Union Carbide Corp
Carbon Products Div
Attn: G. B. Spence
Parma, Ohio 44130

Union Carbide Plastics Co.
Attn: Dr. F. Rugg
River Rd
Boundbrook, New Jersey 08805

United Aircraft Corp
Research Labs
Attn: Pete Borie
East Hartford, Conn 06108

University of Dayton Research Institute
Attn: Mr. Wm Mahieu
300 College Park
Dayton, Ohio 45409

Unclassified

Security Classification

DOCUMENT CONTROL DATA - R & D

(Security classification of title, body of abstract and indexing annotation must be entered when the overall report is classified)

1. ORIGINATING ACTIVITY *(Corporate author)*
IIT Research Institute

2a. REPORT SECURITY CLASSIFICATION
Unclassified

2b. GROUP
NA

3. REPORT TITLE
Feasibility of Joining Advanced Composite Flight Vehicle Structures

4. DESCRIPTIVE NOTES *(Type of report and inclusive dates)*
Final Report, May 1, 1966 through July 1, 1967

5. AUTHOR(S) *(First name, middle initial, last name)*
Kutscha, D. and Hofer, K. E.

6. REPORT DATE	7a. TOTAL NO. OF PAGES	7b. NO. OF REFS
January 1969	457	110

8a. CONTRACT OR GRANT NO.	9a. ORIGINATOR'S REPORT NUMBER(S)
AF33(615)-3962	AFML-TR-68-391
b. PROJECT NO.	
c.	9b. OTHER REPORT NO(S) *(Any other numbers that may be assigned this report)*
d.	

10. DISTRIBUTION STATEMENT
This document has been approved for public release and sale; its distribution is unlimited.

11. SUPPLEMENTARY NOTES	12. SPONSORING MILITARY ACTIVITY
	Air Force Materials Laboratory

13. ABSTRACT

A combined analytical-experimental study was carried out to establish the feasibility of developing rational design techniques for bonded and mechanical joints in advanced composite structures. Available stress analyses were compared for their predictions of maximum stresses in joints and these results were compared to experimental data.

The static strengths were measured for three adhesives bonded to fiberglass, steel, and titanium, and the fatigue strengths were measured for the optimum joint designs. A direct relationship was shown between joint behavior and adhesive modulus.

The load distribution and joint strength was studied for fiberglass bolted joints. These results were also compared to analytical predictions. An extensive literature survey was made for design procedures in mechanical joints.

Recommendations were made for specific additional work required both in joints analysis and characterization of materials.

DD FORM 1 NOV 65 1473

Unclassified

Security Classification

14. KEY WORDS	LINK A		LINK B		LINK C	
	ROLE	WT	ROLE	WT	ROLE	WT
Adhesives, joints, bonded joints, mechanical joints, fastener theory, composite materials, joint theory and design, bolted joints, riveted joints.						